ISSN 0289-842X

RIKEN Accelerator Progress Report

1993

vol. 27

理化学研究所
The Institute of Physical and Chemical Research (RIKEN)

RIKEN Accelerator Progress Report
January-December 1993

理化学研究所
The Institute of Physical and Chemical Research (RIKEN)
Wako-shi, Saitama, 351-01 JAPAN

CONTENTS

Page

I. **PREFACE** 1

II. **OPERATION OF ACCELERATORS**

RRC Operation 3

RILAC Operation 5

AVF Cyclotron Operation 6

Tandetron Operation 8

III. **RESEARCH ACTIVITIES**

1. Nuclear Physics

Theory

Reaction Cross Sections of Light Isobars (A = 17) in the Glauber Model 9

Multistep Process in the ^{14}O Dissociation Reaction 10

E1 Giant Resonance in ^{22}O 11

Isoscalar Monopole Vibrations around Thermal Equilibrium 12

Classical Quantization of γ-Soft Rotor 13

Tilted Axis Rotating States in ^{182}Os Yrast 14

Asymmetric Nuclear Matter and Finite Nuclei 15

Neutron-Skin and Proton-Skin Formations in Exotic Nuclei Far from Stability 16

How Many Nuclides Do Exist? 17

Systematics of Alpha Q-values: Potential Dependence of the Alpha Decay Life Time 18

Relativistic Density Dependent Hartree Approach for ^{16}O, ^{40}Ca, and ^{208}Pb 19

Systematic Study of Sr Isotopes in the Relativistic Mean Field Theory 20

Relativistic Mean Field Theory for the Isotope Shifts of Ba, Cs, and Xe 21

Instability of the Degenerate Electron Gas 22

Quasiparticle Properties and the Dynamics of High-Density Nuclear Matter 23

General Formula of the Coalescence Model 24

Nuclear Recoil Effects in e^+-e^- Pair Production through 0^+-0^+ Transition 25

Distribution of Perturbative Gluon in the MIT Bag Model 26

Momentum Evolution of the Twist-three Part of the Spin-dependent Structure Function 27

Color Confinement, Quark-Pair Creation and Dynamical Chiral-Symmetry Breaking in the Dual Ginzburg-Landau Theory 28

First-Order Phase Transition with Global Z_3 and Z_4 Symmetry 29

Experiment

Study of α Decays Following ^{40}Ar Bombardment on ^{238}U 30

Production of High-Spin Isomer Beam 31

High-Spin States of ^{144}Pm 32

High-Spin States of ^{145}Sm 33

Coincidence Measurements for Neutrons and α Particles from the Fragmentation of ^{6}He at 800 A MeV 34

Measurement of Light Charged Particle Emission in Coincidence with Fission Fragments from ^{84}Kr + ^{27}Al, ^{56}Fe at 10.5A MeV 35

Neutron Emission in the ^{40}Ar + ^{116}Sn Reactions at E/A = 30, 37 MeV/u 36

Charged Particle Emission in ^{40}Ar + ^{nat}Ni Reactions at E/A = 30 MeV 37

Spin-Isospin Excitation in sd-Shell Nuclei Studied by (d,^{2}He) Reactions 38

Measurement of Analyzing Powers for the d + p Elastic Scattering at E_d = 270 MeV 39

Measurements of the Tensor Analyzing Power Axx* for Deuteron Elastic Scattering from ^{12}C, ^{40}Ca, and ^{208}Pb at Ed = 270 MeV 40

(^{12}C,^{12}N) Charge-Exchange Reaction at E/A = 135 MeV 41

Measurement of Quadrupole Moments for the Neutron-rich Nuclei ^{14}B and ^{15}B 42

The Solar Neutrino Production Reaction ^{7}Be(p, γ)^{8}B Studied by the Coulomb Dissociation Method 43

Interaction Cross Sections and Radii of Mass Number A = 17 Isobars (^{17}N, ^{17}F, and ^{17}Ne) 44

Beta-delayed Neutron Decay of ^{19}C and Its Astrophysical Implications 45

The Decay of ^{14}Be 46

Coulomb Dissociation of ^{11}Be 47

Mass Dependence of Pion Production in Heavy Ion Collisions Near but Below Threshold 48

Are All Dripline Nuclei Spherical? 49

Experimental Study of the ^{8}He + p Elastic and Inelastic Scattering 50

Observation of ^{10}He 51

Project at GSI "Determination of Neutron Skin Thicknesses for Na Isotopes" 52

2. Atomic and Solid-State Physics

Theory

Charge Asymmetry of Ionization Cross Sections of Atomic Hydrogen by Antiproton and Proton Impact 53

Double Excitation of H^- by Fast Proton and Anti-Proton Impact II. Spectral Line-profile of an Ejected Electron from $2s2p\ ^1P^o$ Shape Resonance 54

Photodetachment Spectra of H^- 55

Double Ionization of Helium by Compton Scattering 56

Energy Shift in the Molecules $[(dd\mu)\text{-}d]ee$ and $[(dt\mu)\text{-}d]ee$ 57

Auger Monopole de-Excitation of the Muonic Molecule $[(dd\mu)_{1,1}\ dee]_{K,\nu}$ 58

Experiment

Experimental and Theoretical Study of Multiple Ionization Probabilities in 26 MeV Ne^{4+} + Ne Collisions 59

Energetic Electron Production in 20 MeV/u N^{q+} and Ta^{q+} Bombarding Cu and Fe Thin Foils 60

Double and Single Ionization of Helium at Impact Parameter 0 61

Target Ionization in 42 MeV Ar^{12+}-Ar Collisions 62

Measurement of Radiative Electron Rearrangement X Rays from 0.8 MeV/amu Ti Ions Excited by Carbon Foil 63

Binary Encounter Peaks for 0° Electrons in Collisions of Bi^{q+} 64

Beam-Foil Experiment of Neonlike Iron 65

Ejected Electron Spectra from $O^{4+**}(1s^2 3l3l')$ 66

Multiply Charged and Cluster Ions Produced from Gaseous and Frozen CF_4 under Energetic Heavy Ion Impact 67

Ions from C_{60}/C_{70} Fullerenes Deposited on Metallic Foil under Energetic, Heavy Ion Impact 68

Muon Catalyzed Fusion in Thin Solid D_2 Layer 69

Resonance Ionization Spectroscopy of Fe 70

Laser Spectroscopy of Implanted Trace Atoms on a Metal Substrate: Application of Laser Ablation Ion Trap Method 71

^{57}Fe Mössbauer Studies of $YBa_2Cu_{3.928}Fe_{0.072}O_8$ Oriented along the C Axis 72

Charge State and Diffusivity of Hydrogenic Atom in GaAs with Si Donors 73

Annealing Behaviour of Kr Atoms in Kr-Implanted Aluminium 74

High Energy Heavy Ion Irradiation of Superconductor $La_{2-x}Sr_xCuO_4$ 75

Single Event Effect in Power MOSFETs and CMOS ICs by High-Energy Heavy Ion 76

3. Radiochemistry and Nuclear Chemistry

Preparation of a Radioactive Multitracer Solution from Iron Foil Irradiated by 80 MeV/nucleon ^{16}O Ions 77

Observation of Complex Formation of a Number of Metal Ions with Tea Extracts 78

Production of Multitracer Nuclides by Irradiation with a ^{84}Kr Beam 79

Transport of Tc(VII) and Re(VII) through a Supported Liquid Membrane 80

Determination of Stability Constants of Lanthanide-Humate Complexes with Multitracer Technique 81

Utilization of Multitracer Solutions for Studies on the Ion Exchange Behavior of a Strongly Acidic Resin NAFION 82

Adsorption Behavior of Various Elements in Chloride Solutions on Activated Carbon Fiber and Non-ionic Macro-reticular Copolymer Using Multitracer 83

Study of the Solvent Extraction of Various Elements with Diphosphine Dioxide (DPDO) by Use of the Multitracer 84

Yield Distributions of Hf Isotopes from the Reactions of Heavy Ions on W Target 85

Study on the Nuclear Reactions of ^{93}Nb, ^{181}Ta, and ^{197}Au Induced by Secondary Neutrons in 40 MeV/nucleon ^{40}Ar Ion Collisions 86

Limiting Behavior of the Recoil Velocities in the Heavy-Ion Reactions 87

Dependence of Mass Transfer in the Heavy Ion Reaction on the Mass Asymmetry at Entrance Channel 88

Competition between Fission and Spallation in the Reaction Induced by Intermediate Energy Heavy Ions 89

Time-Differential Perturbed-Angular-Correlation (TDPAC) of γ-Rays of ^{99}Ru in $YBa_2Cu_3O_{7-x}$ Using ^{99}Rh as a Source Nuclide 90

Slow Positron Beam Production Using AVF Cyclotron 91

Positronium Formation and Annihilation in Porous Silicon 92

Heavy Ion Beam Analysis for H-D Isotope Exchange in Glass Surface Layers 93

4. Radiation Chemistry and Radiation Biology

Time and Depth Resolved Dynamics of Excited States in Ion Track in Condensed Matter 95

Beam End Point Measurement with Positron Emitting Secondary Beams 96

Initial Recombination in a Parallel Plate Ionization Chamber Exposed to Heavy-ion Beams 97

Ionization Tracks Produced by Ar (95 MeV/u) Ions and their *Core-Penumbra* Structure 98

Calibration of CR-39 Track Detector for Space Radiobiological Studies and LET Measurements of Cosmic Ray Nuclei 99

Radiation Effects of Ion-particles on Various DNA Structures 100

Studies on Induced Mutations by Ion Beam in Plants
Induced Mutants of Rice Resistant to Bacterial Leaf Blight 101

Effect of HZE Particles (Ar, N) on Hatching Rate and Occurrence of Pycnosis of *Artemia salina* 102

Chromosome Aberrations Induced by 135 MeV Carbon and Neon Beams of RIKEN Ring Cyclotron in Human Blood Cells 103

Molecular Characterization of Mutations in Human Cells Irradiated with Carbon Ions 104

RBEs of Various Human Monolayer Cells Irradiated with Carbon Beams 105

Sensitivity of ts85 Mutant Strain from Mouse FM3A Cells to Heavy Ions 106

PLD Repair in Tumor Cells after Carbon Beam Irradiation 107

The Early Skin Reaction after Carbon Ion Slit-Beam Irradiation 108

5. Instrumentation

Computing Environment around the Accelerator Facility 109

A GAL16V8A Programming Equipment 110

In-beam Mössbauer Spectroscopy in RILAC (1) 111

Development of Low Energy Unstable Nuclear Beam Channel "SLOW" 112

New Detector System for the First Focal Plane of SMART 113

Measurement of the Fusion Cross Section of $^{27}Al + ^{197}Au$ Using MWPC and Multi-target System 114

First Laser-rf Double Resonance Spectroscopy of Refractory Elements 115

Measurement of Attenuation Length of Scintillation Photons in Liquid Xenon Due to Heavy Ions 116

Measurement of Response Functions of Organic Liquid Scintillator for Neutrons up to 133 MeV 117

Test of Inorganic Scintillators Using RIKEN Ring Cyclotron 118

A New Method of Pulse Shape Discrimination for BaF_2 Scintillators 119

Development of Radiation Monitor in Space 120

Segmented Germanium Detector 121

6. Material Analysis

In-situ Analysis of Liquid Samples by PIXE 123

Hydrogen Depth Profile of Al-alloy Vacuum Chamber Exposed to Synchrotron Radiation 124

Simultaneous Depth Analysis of Deuterium and Helium in He^+-implanted YIG Annealed in D_2 125

IV. NUCLEAR DATA

Status Report of the Nuclear Data Group 127

Production Cross Sections of Radioxenon Isotopes 128

V. DEVELOPMENT OF ACCELERATOR FACILITIES

1. Ion Accelerator Development

Status of the RIKEN 10 GHz ECR Ion Source 129

Development of the RIKEN Polarized Ion Source 130

Basic Study of Polarized He-3 Ion Source for the RIKEN AVF Cyclotron 131

Development of a New Type of Single-Bunch Selector 133

Development of a Beam Phase Monitor with a Micro-Channel Plate 135

Development of the Second-Harmonic Buncher for the RILAC 137

Design of a Variable Frequency RFQ Linac for RILAC 139
Construction of RIKEN-RAL Muon Research Facility 141
Theoretical Study of the Relativistic Cyclotron Maser Cooling 142

2. Synchrotron Radiation Source Development

Correction of Emittance Modulation by Linear Coupling 143
Survey for SPring-8 Storage Ring 144
Field Measurements of SPring-8 Dipole Magnets 145
Field Measurements of SPring-8 Quadrupole Magnets 146
Construction of Power Supplies for SPring-8 SR Magnet 147
Preliminary Network for SPring-8 Machine Group 149
Measurement of Temperature Dependence of HOM Frequencies in a Bell-shaped Cavity 150
Test of Dummy Loads 151
Test of 1.2 MW Circulator 153
A Phase Lock System of 508.58 MHz Reference Line 155
A Direct Counter of 508.58 MHz 157
Transmission Test of the Timing Signal for the SPring-8 158
Control of SPring-8 SR Klystron Test Bench 160
Performance Test of Energy Analyzer for Photoelectrons Produced by SR Irradiation 161
Outgassing Rate Measurement of Braided Wire 163
Design of Beam Position Feedback Systems for SPring-8 Storage Ring 164

VI. RADIATION MONITORING

Measurement of Activities Induced by 135 MeV/u ^{20}Ne Incident on an Iron Target with the Activation Method 165
γ-ray Spectrum from Iron Targets Bombarded by Accerelated Ions 166
Shielding Effect of the Concrete Wall between E1 and E2 Rooms 167
Leakage Radiation Measurements in the Ring Cyclotron Facility 168
Residual Activities in the Ring Cyclotron Facility 169

VII. LIST OF PUBLICATIONS 171
VIII. LIST OF PREPRINTS 176
IX. PAPERS PRESENTED AT MEETINGS 178
X. LIST OF SYMPOSIA 187
XI. LIST OF SEMINARS 188
XII. LIST OF PERSONNEL 190

AUTHOR INDEX

I. PREFACE

This report illustrates research activities at the RIKEN Accelerator Research Facility for the year of 1993. The research program has been coordinated in the framework of the project entitled Multidisciplinary Researches on Heavy Ion Science. It covers a variety of research fields; nuclear physics, atomic physics, nuclear chemistry, radiation biology, condensed matter physics in terms of accelerator or radiation, basic studies on energy production, basic studies on accelerator cancer therapy, material characterization, application to space science, accelerator engineering, laser technology and computational technology.

The major facility involved is the RIKEN Ring Cyclotron (RRC) which is a K = 540 separate-sector cyclotron providing intermediate-energy heavy ions over a broad range of elements. Two injector accelerators, i.e., an energy-variable heavy ion linear accelerator (RILAC) and a K = 70 AVF cyclotron, are alternatively operational in a stand-alone mode. The accelerators were constructed in series and the whole complex has been operational since 1988. In addition there exists a 1.5 UD Tandetron, which has been renewed this year. For this year the RRC alone has delivered the beam time (on the target) of about 5000 hours.

The research program is carried out by researchers from 14 RIKEN laboratories among about 50 in total. A large number of outside researchers and students from universities or other research institutions have also participated in our activities. Domestically the number of the participants amounts to about 300, while international collaboration is extended over about 30 institutions. Besides the activities at home international cooperative programs located at foreign facilities are being undertaken. A major program at present is on muon science, for which installation of a muon beam facility is in progress at Rutherford-Appleton Laboratory.

The heavy ion research program at the Facility has enjoyed another year of steady development. A special emphasis at RRC has been continuously placed on the development and application of a variety of types of radioactive isotope beams (RIB): Firstly intermediate-energy RIB by means of the projectile fragmentation (PF) have been most frequently used by accounting for about 40% of the whole RRC beam time. To ease the heavy interference among the experimental setups a beam distributing magnet to switch beams into three different channels has been newly installed. The beams have been useful particularly for studies on neutron-rich nuclei and nuclear astrophysics: ^{10}He has been identified; structure and dynamics of neutron halos or skins have been studied in terms of Coulomb dissociation and direct nuclear reaction processes; Coulomb excitation of ^{32}Mg has been observed; delayed neutron spectroscopy has been initiated, a study on sub-barrier fusion reactions involving extremely neutron-rich nuclei is in progress; and finally the Coulomb dissociation cross section of ^{8}B has been successfully measured in relation to the solar neutrino problem.

The second type of RIB is the spin-polarized beam which is also produced via the PF process covering a wide range of nuclear species. The beam has been primarily used to determine nuclear moments of unstable nuclei including exotic nuclei such as ^{17}B. The third type of RIB is the high-spin isomer beam which is produced via a reverse-kinematics fusion reaction. Beams of heavy isomers with spins close to 30 h are obtained with considerable intensities. In an attempt to reach extremely high spin states the beams have been applied to Coulomb excitation to populate states on top of the isomeric states.

Heavy unstable nuclei have also been studied using a gas-filled type recoil separator (GARIS). Here a major program aims at developing a new scheme of synthesizing very heavy elements. A method in terms of (Heavy ion, αxn) reactions has been tested. So far an encouraging indication has been obtained for the synthesis of an isotope in the region of Z = 108. It has been realized that the separator is also powerful for the study of other trans-uranium isotopes and a related project has been initiated.

In the context of nuclear physics spin-isospin response is another major subject, where reactions (d,^{2}He) and (d,d(0^{+})) are primarily concerned. The main apparatus for this research is a high-resolution particle analyzer (SMART) which has a Q-Q-D-D magnetic configuration with wide angular and momentum acceptance. A spin-polarized ion source for deuteron has been also developed, which has so far achieved a beam intensity of about 100 μA at the source exit. The spin-isospin response has been as well studied via heavy-ion exchange reactions. These reactions at high energies have been proved to provide useful spectroscopic probes.

The heavy ion research activities have covered a variety of domains beside nuclear physics. Among them studies on atomic physics have been pursued, enjoying an extremely wide energy range of heavy ions provided by the ECR ion source, RILAC and RRC. Ionization processes in hard collisions between heavy ions and atoms are studied by measuring slow recoil ions and fast electron ejectiles. Beam foil spectroscopy of highly charged heavy ions in the region of VUV photons has been extended to Fe and Nb ions. Basic information

for laser and plasma applications is gained.

In the field of nuclear chemistry significant development has continued on the methodology of multi-tracer. Formula using different target and projectile combinations at RRC have been newly established to prepare mixtures of a variety of radioactive isotopes. Sets of multi-tracers thus obtained have been extensively utilized for chemical, environmental and biological systems to trace the circulation behavior of different elements simultaneously. For instance studies on rats have been started. Radioactive isotopes are as well used for other methodologies such as Mössbauer spectroscopy and TDPAC, which are applied to high-Tc superconductors and magnetic materials. On the other hand in-beam Mössbauer spectroscopy using Coulomb excited ^{57}Fe is in progress at RILAC.

Heavy ion beams have offered a variety of means for material characterization such as PIXE, Rutherford scattering and channeling effects. Recently a project on slow positron spectroscopy using short lived isotopes was started at the AVF cyclotron. Heavy-ion beams are also useful to improve the property of material. In this context a new project on high-Tc superconducting materials has been started. It has been found that the critical current density increases significantly after irradiation of high-energy Xe ions.

Studies on irradiation effects with heavy-ion beams are directed to two major fields. One is the domain of radiation biology. Effects of high LET are studied for a variety of biological samples. In particular the study on DNA damages is continued by incorporating mutation analysis. Basic studies for heavy-ion-beam cancer therapy are carried out in collaboration with National Institute of Radiological Science. Studies of curing probability are extensively performed with tumor-bearing mice. Recently an intriguing application of radioactive beam was tested in relation to the cancer therapy. Use of a radioactive beam may offer a possibility to gain real-time information on the range of the ions shooting the body, where the location of the stopped isotopes may be spotted by means of positron tomography. A simulation experiment using a radioactive beam of ^{11}C was performed, demonstrating an encouraging perspective.

Another important domain on irradiation effects concerns the space technology. High-energy heavy ions from RRC serve as a good simulator of cosmic rays in space. Thus a broad range of samples, including detectors and biological samples are irradiated to study characteristic damages. In particular studies on electronic devices are made in collaboration with National Space Development Agency of Japan.

Concerning the muon program the primary effort has been made to complete a muon beam facility at the proton synchrotron ISIS of the Rutherford-Appleton Laboratory. It is expected to be finished in 1994. At home the production of negative muon beams is studied using high-energy heavy ions.

In summary the year of 1993 has marked a steady and continuous development of the Facility. In view of the ever growing demands for the Facility we have started an intensive study for a next-generation accelerator to be installed at the Facility. A broader use of radioactive beams will be pursued. An energy booster in terms of super-conducting separate-sector cyclotron is considered as a possible candidate.

Masayasu Ishihara
Director
RIKEN Accelerator Research Facility

II. OPERATION OF ACCELERATORS

RRC Operation

A. Goto, M. Kase, N. Inabe, T. Kageyama, I. Yokoyama, M. Nagase, S. Kohara, T. Nakagawa, K. Ikegami, O. Kamigaito, J. Fujita, H. Isshiki,* H. Akagi,* R. Ichikawa,* N. Tsukiori,* R. Abe,* K. Takahashi,* S. Otsuka,* T. Maie,* T. Kawama,* T. Honma,* and Y. Yano

Table 1 lists the ions that were served to users from November 1992 to October 1993. We delivered 24 kinds of ion species for the last one year in a total beam time of 184 days. Of those days, the AVF-RRC operation was performed for 143 days (78%) and the RILAC-RRC operation for 40 days (22%). The beam time of 135.5 days (74%) was devoted to nuclear physics experiments and that of 48.5 days (26%) to non-nuclear physics experiments. Experiments using secondary beams with RIPS (68.5 days) and biological irradiation experiments (31.5 days) have the majority in nuclear physics and non-nuclear physics study, respectively. The AVF-RRC complex has been able to routinely provide, e.g., over 200 pnA of 135 MeV/nucleon light ions and over 60 pnA of 95 MeV/nucleon ^{40}Ar ions. We accelerated 21 MeV/nucleon ^{181}Ta ions, which are the heaviest ever accelerated with RRC. Figure 1 shows the plots of the ions accelerated so far in the available region of energy-mass space.

Regular long-term overhauls were carried out for 3 weeks in the winter and for 6 weeks in the summer. In the summer overhaul, the following irregular maintenace was made: replacement of the MDC2 with a new one, shift of the phase probe assembly upward by 5 mm, and replacement of the slide-contacts for the movable short of the 3 kW rebuncher resonator. The shift of the phase probe assembly was made because we had such a trouble that in April and May the upper electrodes of the two outermost phase probes got out of place due to melt-down of their supports hit by beams.

Table 1. RRC beams accelerated during November 1992 – October 1993.

Particle	Charge	RF F (MHz)	h	Injector	Energy (MeV/nucleon)	Beam time (days)
H_2	1	24.6	5	AVF	70	2.5
	1	32.6	5	AVF	135	4.5
d	1	24.6	5	AVF	70	3
	1	32.6	5	AVF	135	6
pol. d	1	32.6	5	AVF	135	11
^{11}B	5	24.6	5	AVF	70†	3.5
^{12}C	6	32.6	5	AVF	135	28
^{13}C	6	24.6	5	AVF	70†	5.5
^{14}N	4	25.4	9	RILAC	21†	1.5
	7	32.6	5	AVF	135	1.5
^{16}O	8	26.2	5	AVF	80	5
^{18}O	8	24.6	5	AVF	70	9
	8	29.0	5	AVF	100	32.5
^{20}Ne	10	32.6	5	AVF	135	10
^{22}Ne	10	30.1	5	AVF	110†	8.5
^{40}Ar	5	18.0	11	RILAC	7†	3.5
	14	30.0	9	RILAC	30	4
	14	33.0	9	RILAC	37	3.5
	14,15	34.4	9	RILAC	40†	4.5
	17	28.1	5	AVF	95	12.5
^{58}Ni	9	19.5	10	RILAC	10†	3
^{84}Kr	13	20.0	10	RILAC	10.5	5.5
^{136}Xe	23	18.6	10	RILAC	9†	11.5
^{181}Ta	37	25.4	9	RILAC	21†	4
					Total	184

† New beams

* Sumijyu Accelerator Service, Ltd.

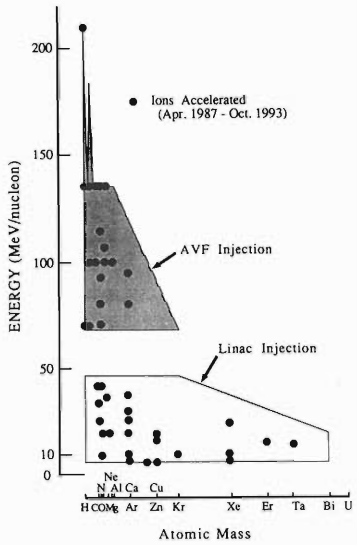

Fig. 1. RRC beams accelerated during April 1987–October 1993.

We had the following big machine troubles in September after the summer-overhaul period: the newly installed MDC2 was found to be mis-manufactured for the production of magnetic field and had to be repaired, the final RF amplifier of the RRC stopped operating four times due to the trouble of cooling water for the plate electrode, and the power-feed part of the 3 kW rebuncher resonator was burnt. Because of those troubles, 11 days of the scheduled machine time had to be cancelled.

This year, several R&D's have been made: installation of a second-harmonic buncher on the injection beam line of the RILAC,[1] development of a new beam detector with a micro-channel plate (MCP),[2] development of a single-bunch selector for use on the injection beam line of the AVF cyclotron,[3] and installation of an ExB spin rotator immediately downstream of the polarized p/d ion source.[4] By the installation of the second-harmonic buncher next to the existing fundamental-frequency buncher, the output beam intensities from the RILAC have been improved by a factor of 1.5, and those from the RRC by a factor of 2–3. Time structures of the AVF cyclotron and RRC beams were measured with the new beam detector. The detector has been found to work not only as a phase monitor for stabilizing the magnetic fields of the cyclotrons, but also as a monitor for single-turn extraction or a measuring instrument of turn number inside the cyclotrons. The single-bunch selector is very compact and cost-saving because it is operated in the low energy section before the AVF cyclotron. It was used for a calibration experiment of a neutron counter with 135 MeV/nucleon H_2^+ beam. We plan to increase the repetition rate from 20 kHz up to as high as 1 MHz using a higher-speed semi-conductor device. The installation of the spin rotator, taking advantage of the single turn extraction available for both the AVF cyclotron and the RRC, has allowed us to freely control the spin direction of polarized deuterons without reducing the polarization or the intensity.

Design of a new injector system of the RILAC has also progressed, aiming to increase beam intensities of heavy ions by one or two orders of magnitude. It consists of a single-stage high-field 18 GHz ECR ion source[5] and a variable-frequency RFQ linac.[6] Both of them have already been preliminarily designed. The RFQ linac is characteristic of its "folded coaxial" structure, which has the advantages of the compactness of the cavity even for the low frequency and the wide frequency-tunable range of the cavity. A half-scaled model for the cold test of the cavity is now under fabrication for completion by the end of this year.

Stand-alone use of the AVF cyclotron, which is made while the RRC is operated with the RILAC beam injection, started in June of this year. The total beam time was 8 days. For the details, see Ref. 7.

References

1) S. Kohara et al.: This report, p. 137.
2) M. Kase et al.: Proc. 9th Symp. on Accel. Sci. and Technol., Tsukuba, p. 474 (1993).
3) N. Inabe et al.: This report, p. 133.
4) H. Okamura et al.: This report, p. 130.
5) T. Nakagawa et al.: Proc. 9th Symp. on Accel. Sci. and Technol., Tsukuba, p. 98 (1993).
6) O. Kamigaito et al.: This report, p. 139.
7) A. Goto et al.: This report, p. 6.

RILAC Operation

E. Ikezawa, M. Hemmi, T. Chiba, Y. Chiba, T. Aihara,* T. Ohki,*
H. Hasebe,* H. Yamauchi,* M. Kase, M. Yanokura, and Y. Miyazawa

RILAC has been in steady operation, and has supplied various kinds of ion beams for experiments. Table 1 gives the statistics of operation from Jan. through Dec. 1993. Table 2 summarizes the time sharing for individual research groups. The percentage of the beam time for RIKEN Ring Cyclotron (RRC) was about 41%; ions of ^{14}N, ^{36}Ar, ^{40}Ar, ^{58}Ni, ^{84}Kr, ^{136}Xe, and ^{181}Ta accelerated by RILAC were injected to RRC. Table 3 gives the statistics of ions used this year. We began accelerating B^{3+}, Ga^{11+}, and Nb^{12+} at the frequencies of 35, 30, and 32 MHz respectively. The beam time for metallic ions amounted to about 22%.

Table 1. Statistics of the operation from Jan. 1 through Dec. 31, 1993.

	Day	%
Beam time	170	46.6
Frequency change	20	5.5
Overhaul and improvement	33	9.0
Periodic inspection and repair	27	7.4
Machine trouble	2	0.5
Scheduled shut down	113	31.0
Total	365	100

Table 2. Beam time for individual research groups.

	Day	%
Atomic physics	41	24.1
Solid-state physics	12	7.1
Nuclear chemistry	19	11.2
Radiation chemistry	13	7.6
Accelerator research	16	9.4
Beam transportation to RRC	69	40.6
Total	170	100

Cancellation of the scheduled beam time due to machine troubles in RILAC totalled two days; one day due to a vacuum leak at a gate valve of the beam transport line and the other due to the end of life of the final vacuum tube which was used for the last thirteen years in the RF system of No. 1 resonator. Another three days of beam time were abandoned owing to trouble in RRC and another day in user side.

We carried out the following items in this year.

Preventative maintenance: 1) Because of deterioration of the optical fiber cables transmitting control signals to the injector high voltage station, the cables used for eight years were replaced with new ones. 2) The power supplies for the drift tube magnets used in the resonators No. 1 and 3 were remodeled by replacing the obsolete power transistors with the modern ones. 3) Three water pumps for the cooling tower water circuit, the ordinary water circuit, and the deionized water circuit were overhauled.

Table 3. List of ions used in this year.

Ion	Mass	Charge state	Day
He	4	1	10
B	11	3	1
C	12	2	2
N	14	3, 4	6
N	15	3	1
O	16	2	2
Ne	20	4	2
Ar	36	5, 6	6
Ar	40	4, 5, 6, 8	58
Ca	40	6, 7	3
Fe	56	6	13
Ni	58	9	5
Ga	69	11	2
Kr	84	11, 13	12
Nb	93	12	6
Mo	98	11	1
Xe	136	9, 15, 16	33
Ta	181	16	4
Bi	209	16	3

Improvement: 1) A carbon foils exchanger installed at the exit of No. 6 resonator was replaced with a new one; this unit can mount 40 carbon foils. 2) To feed enriched gas such as ^{36}Ar and ^{136}Xe in the ion source, we installed two more reservoirs. There are two feeding systems, each has two reservoirs. 3) In an electrostatic quadrupole lens installed at the beam exit of the ECR source, the surface insulation of high voltage connectors was deteriorated with sputtered metals; the shields from sputtering were fortified.

Development: 1) A second-harmonic buncher was installed in the injection beam line in this March.[1] Using both the fundamental-frequency and the second-harmonic bunchers, we got about 50% increase of beam intensity at the exit of RILAC compared to that with only the former. 2) We have tested to obtain metallic ions by use of a material such as BN, LiF, and Ga_2O_3. Ion currents with these compound rods except the BN case were very stable. At present we can supply ions of 10 gaseous and 37 solid elements.

References

1) S. Kohara et al.: This report, p. 137.

* Sumijyu Accelerator Service, Ltd.

AVF Cyclotron Operation

A. Goto, T. Kageyama, M. Kase, S. Kohara, M. Nagase, T. Nakagawa, K. Ikegami, O. Kamigaito, N. Inabe, I. Yokoyama, J. Fujita, H. Isshiki,* H. Akagi,* R. Ichikawa,* N. Tsukiori,* R. Abe,* K. Takahashi,* S. Otsuka,* T. Maie,* T. Kawama,* T. Honma,* and Y. Yano

Table 1 lists the ions accelerated by the AVF cyclotron in the past four years since the first beam was obtained. We have accelerated 16 kinds of ion species. Beam intensities of several eμA are routinely extracted in recent operation. The total beam time for the last one year was 143 days. The beam times for the following three kinds of ions exceeded 50% of the total beam time: 5.2 MeV/nucleon (95 MeV/nucleon from the RRC) $^{40}Ar^{11+}$ and 7 MeV/nucleon (135 MeV/nucleon) $^{12}C^{4+}$ and $^{18}O^{6+}$.

The beam extraction efficiency of over 75% (the maximum record is 90%) is routinely obtained. The beam transmission efficiency through the cyclotron is then typically about 20%, though it depends on the kind of accelerated ion and in some cases drops as low as about 5%. A single turn extraction can be achieved by carefully adjusting the first harmonic field near the extraction and the currents of the trim coils near the cyclotron center. One of the advantages of the single turn extraction available for both the AVF cyclotron and the RRC is that it allows us to freely control the spin direction of a polarized beam using an ExB spin rotator (a Wien filter) placed downstream of the polarized ion source, without reducing the polarization or the intensity.

Pulse width of the extracted beam was preliminarily measured with a new type of beam phase monitor.[1] The width (FWHM) of 5.5 MeV/nucleon $^{18}O^{6+}$ ion beam was 1.6 nsec corresponding to 8.4 RF degrees. Precise measurement with the monitor will be made.

A single-bunch selector has been successfully developed.[2] It is very compact and cost-saving because it is operated on the beam transport line between the ECR ion source and the AVF cyclotron. Performance study of the single-bunch selector was carried out for the 7.45 keV H_2^+ beam from the ECR ion source (the beam energy from the AVF cyclotron was 7 MeV/nucleon). The time spectrum obtained with the above beam phase monitor located immediately after the cyclotron showed that almost complete single-bunch selection was achieved. The repetition rate of the selector is now as low as 20 kHz. We plan to increase the repetition rate up to as high as 1 MHz using a higher-speed semi-conductor device.

This year, there have been serious troubles with respect to the following cyclotron components: a part of the RF slide-contacts of the movable shorting plate was burnt and melt; and the deflector became not to work due to its unendurable leak current. In the latter case, powder-like stuff containing very thin and short

Table 1. Ions accelerated with the AVF cyclotron during April 1989 – October 1993.

Particle	Charge	RF freq. (MHz)	Energy* (MeV/nucleon)	Intensity (eμA)	Particle	Charge	RF freq. (MHz)	Energy* (MeV/nucleon)	Intensity (eμA)
p	1	19.35	9.9 (210)	5.2	^{14}N	4	13.0	4.4 (80)	3.3
	1	21.1	11.8 (270)	0.07		5	16.3	7.0 (135)	12.0
H_2	1	12.3	4.0 (70)	3.1	^{15}N	4	12.3	4.0 (70)	2.6
	1	14.0	5.2	5.0		5	15.25	6.1 (115)	1.3
	1	16.3	7.0 (135)	5.4	^{16}O	5	13.1	4.4 (80)	7.8
d	1	12.3	4.0 (70)	1.4		6	16.3	7.0 (135)	3.3
	1	13.8	5.0	2.6	^{18}O	5	12.3	4.0 (70)	5.2
	1	14.5	5.5 (100)	0.6		6	14.5	5.5 (100)	12.0
	1	16.0	6.7 (130)	0.5	^{20}Ne	7	16.3	7.0 (135)	7.4
	1	16.3	7.0 (135)	3.4	^{22}Ne	6	12.3	4.0 (70)	5.9
pol. d	1	16.3	7.0 (135)	0.3		7	15.05	6.0 (110)	1.7
^{11}B	3	12.3	4.0 (70)	1.0	^{24}Mg	7	14.5	5.5 (100)	2.1
^{12}C	4	13.95	5.1 (92)	0.7	^{27}Al	8	14.5	5.5 (100)	0.3
	4	14.5	5.5 (100)	0.6		9	16.0	6.7	0.5
	4	16.3	7.0 (135)	7.3	^{40}Ar	11	13.0	4.4 (80)	0.4
^{13}C	4	12.3	4.0 (70)	2.0		11	14.05	5.2 (95)	4.6

* The values in the parentheses show the energies obtained by the coupled operation with the RRC.

* Sumijyu Accelerator Service, Ltd.

needle-like stuff adhered to the surfaces of the septum and the electrode along the median plane level. To remove the origin-unknown stuff, we had to disassemble the cyclotron five times during the past one year.

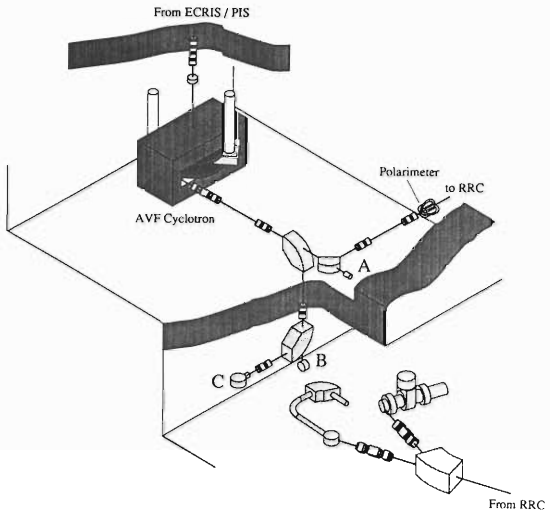

Fig. 1. Schematic drawing of the arrangement of experimental ports A–C in the AVF cyclotron vault and E7 experimental room. Port A: Radioisotope production; Port B: Slow-positron experiment; and Port C: Nuclear physics experiment.

Stand-alone use of the AVF cyclotron started in June of this year. For this use three experimental ports have been provided as shown in Fig. 1: at port A is installed a chamber for use in radioisotope production; at port B a scattering chamber for slow-positron experiments; at port C a scattering chamber for nuclear physics experiments. The port A is located at the end of the extraction straight line in the cyclotron vault, the port B at the end of the vertical line in E7 experimental room and the port C at the end of the horizontal line in E7. So far two experiments were made in a total beam time of 8 days: production test of slow-positrons using 5.2, 7 and 9.9 MeV/nucleon proton beams at the port B[3)] for 3.5 days and measurement of fusion cross sections using 6.7 MeV/nucleon ^{27}Al beam at the port C for 4.5 days. The stand-alone use is made while the RRC is operated with the RILAC beam injection.

References

1) M. Kase et al.: Proc. 9th Symp. on Accel. Sci. and Technol., Tsukuba, p. 474 (1993).
2) N. Inabe et al.: This report, p. 133.
3) Y. Itoh et al.: This report, p. 91.

Tandetron Operation

E. Yagi, T. Urai, and M. Iwaki

The Tandetron was operated for 60 days for experiments in the period from Nov. 1, 1992 to Oct. 31, 1993. In this period the beam time allotted to experiments was much reduced because of various troubles in the duoplasmatron ion source and the electric power supply for the switching magnet.

The experimental studies on the following subjects were made.

(1) Rutherford backscattering spectroscopy (RBS)

(a) Behaviour of Kr atoms implanted into aluminium by a channelling method (Metal Physics Lab.).

(b) Behaviour of Xe atoms implanted in iron (Metal Physics Lab.).

(c) Analysis of radiation damage in a Tb- and Eu-implanted CaF_2 (Semiconductor Lab. and Surface Characterization Center).

(d) Silicide formation in Ni-deposited silicon (Metal Physics Lab.).

(e) Characterization of Ni films grown on MgO by biased dc sputter deposition (Metal Physics Lab.).

(2) Radiation effects

(a) Radiation damage of diamond (Earth Sciences Lab.).

(3) Nuclear reaction analysis

(a) Lattice location of hydrogen in niobium alloys by a channelling method (Metal Physics Lab.).

(4) Particle induced X-ray emission

(a) Application of PIXE to biomedical and material sciences: Trace element analysis using energy-dispersive X-ray spectrometry, and chemical state analysis using wave-dispersive X-ray spectrometry (Inorganic Chemical Physics Lab.).

III. RESEARCH ACTIVITIES

1. Nuclear Physics

Reaction Cross Sections of Light Isobars (A = 17) in the Glauber Model

H. Kitagawa, A. Ozawa, and I. Tanihata

[Glauber model, A = 17 isobars.]

Measurement of reaction cross sections of A = 17 isobars (^{17}Ne, ^{17}F, ^{17}N, ^{17}B) at LBL (incident energy is 790 MeV/u)[1] revealed an anomaly in ^{17}Ne and ^{17}B. The measured cross sections of ^{17}Ne and ^{17}B are fairly larger than those of other isobars.

By considering the separation energies, we find that the structure of ^{17}Ne is similar to that of ^{11}Li. Two proton separation energy of ^{17}Ne is very small, 0.954 MeV, whereas one proton separation energy is larger than it, 1.489 MeV. Two neutron separation energy of ^{11}Li is 0.197 MeV, and one neutron separation energy is 1.001 MeV. We consider that ^{17}Ne may be a candidate of a "proton-halo" nucleus.

We calculate the reaction cross sections of ^{17}Ne, ^{17}F, ^{17}O and ^{17}N where the targets are ^{9}Be, ^{12}C and ^{27}Al respectively. We do not consider ^{17}B, because there is no data of ^{17}Na, the mirror partner of ^{17}B.

Density distributions are calculated by the Skyrme-Hartree-Fock (HF) method with the SGII interaction except for ^{17}Ne. Considering the structure of ^{17}Ne stated above as a system of ^{15}O core and the two valence protons, the wave function of the valence proton is obtained from the Woods-Saxon potential whose separation energy is fitted to be a half of two proton separation energy, i.e. 0.954 MeV/2. We make the ^{17}Ne density distribution by adding twice the density of the valence proton in the $1d_{5/2}$ orbit to that of the ^{15}O core which is obtained by the Skyrme-HF. We do not consider for simplicity the paring effect of the two valence protons, which play an important role to become a "halo" nuclei. The density distribution of ^{17}Ne is shown in Fig. 1.

We employ the Glauber model to calculate the reaction cross section from the density distribution of both projectile and target. The reaction cross section is calculated by the following equation,

$$\sigma_R = 2\pi \int_0^\infty (1 - T(b))\, b\, db$$

$$T(b) = \exp\left[-\bar{\sigma} \int dr_\perp \int \rho_T(r) dz \int \rho_P(|\mathbf{r}' - \mathbf{b}|)\, dz'\right]$$

$$\bar{\sigma} = \frac{1}{A_T A_P}((Z_T Z_P + N_T N_Z)\sigma_{pp} + (Z_T N_P + N_T Z_P)\sigma_{np})$$

where N_P, Z_P, A_P, and ρ_P are the neutron, proton, mass numbers and the total density of the projectile, respectively, and $\mathbf{r}' = (x, y, z')$ and $\mathbf{b} = (b, 0, 0)$.

The effect of the Pauli blocking[2] and the effect of bending the path due to the Coulomb force are included, but they contribute only 1% at most at this incident energy, 790 MeV/u.

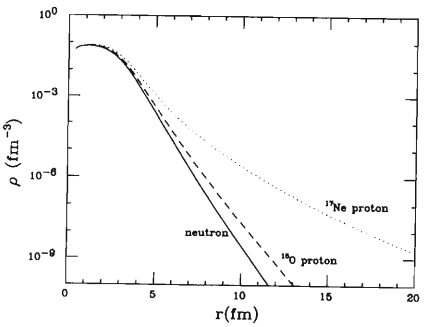

Fig. 1. Density distribution of ^{17}Ne is shown. The area between the ^{15}O proton and the ^{17}Ne proton shows the contribution of the two valence protons of ^{17}Ne.

Results of calculations of the ^{12}C-target case are shown in Fig. 2. For comparison we also show the results with the shell model-harmonic oscillator wave functions. We can see that the cross section of ^{17}Ne increases by including roughly the effect of the spatial expansion of the valence proton wave function due to the small separation energy.

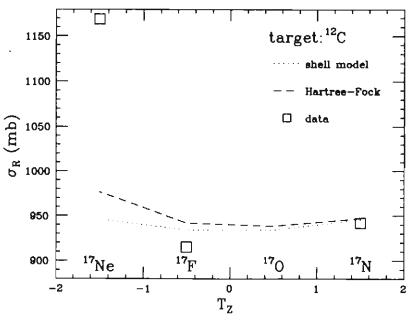

Fig. 2. Reaction cross section of A = 17 isobars at E_{inc}=790 MeV/u is shown. The target is ^{17}C. Dotted and dashed lines are the results of calculations of the shell model and the Hartree-Fock respectively. Squares are the observed values (Errors are not shown here).

Although the dependence on the isospin is qualitatively reproduced, the observed value of ^{17}Ne is not reproduced. If this rough estimation is reliable, we might be able to say that this discrepancy suggests an anomaly in ^{17}Ne such as a "proton-halo".

References

1) A. Ozawa et al.: RIKEN preprint, Nov. (1993).
2) H. Kitagawa: RCNP annual report, p. 95 (1992).

Multistep Process in the ^{14}O Dissociation Reaction

T. Motobayashi

[^{208}Pb(^{14}O,^{13}N p)^{208}Pb; Coulomb dissociation, coupled channel analysis.]

The Coulomb dissociation process can be a tool to study radiative capture processes exciting unbound states of astrophysical interest. This is based on the idea that the process is due to the absorption of a virtual photon and hence can simulate the photoabsorption process, the inverse reaction of the radiative capture.[1] The photoabsorption cross section is deduced by dividing the dissociation cross section by the virtual photon intensity, if one-step reaction mechanism is assumed.

A possible influence of the multistep Coulomb excitation on the results obtained for the ^{208}Pb(^{14}O,^{13}N p)^{208}Pb reaction has been discussed by Delbar.[2] This reaction is related to the ^{13}N(p,γ)^{14}O reaction, a key reaction igniting the hot-CNO cycle breaking out from the regular CNO cycle of hydrogen burning in massive stars. The process via the 1^- resonant state at E_{ex} = 5.17 MeV in ^{14}O almost determines the astrophysical reaction rate, and therefore the radiative width Γ_γ of this 1^- state is of crucial importance. Our Coulomb breakup experiment at E_{in} = 87.5 MeV at RIKEN reports Γ_γ= 3.1 $\pm$ 0.6 eV.[3] A direct measurement of ^{13}N(p,γ)^{14}O at Louvain La Neuve using a ^{13}N beam[4] gave a similar result Γ_γ= 3.8 $\pm$ 1.2 eV. Delbar argues in Ref. 2 that the excitation of the second 0^+ state at E_{ex} = 5.92 MeV via the 0^+-1^--0_2^+ two-step process affects the 0^+-1^- dissociation cross section. He gave an upper limit of the two-step contribution, which changes the value of Γ_γ from 3.1 eV obtained by Ref. 3 to 5.5 eV. He also proposed a possible explaination for the yield experimentally observed at a higher excitation energy of ^{14}O by this two-step Coulomb excitation to the 0_2^+ state.

The aim of the present report is to clarify the role of the multistep excitation mechanisms played in the breakup process ^{208}Pb(^{14}O,^{13}N p)^{208}Pb. A coupled channel calculation was performed by taking into account the ground state and four excited states, 1^- at 5.17 MeV, 0_2^+ at 5.92 MeV, 3^- at 6.27 MeV and 2^+ at 6.59 MeV of ^{14}O shown in Fig. 1. No experimental information is available for the transitions among them, except for the 0^+-1^- excitation. Some analogue transitions are known for ^{14}C, and they were used in the present calculation assuming the isospin symmetry.

An example of the results is shown in Fig. 2 for the

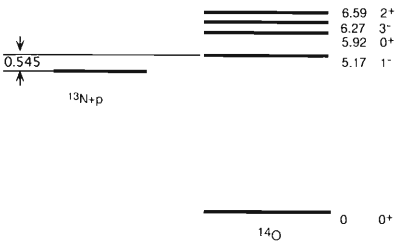

Fig. 1. Low lying states of ^{14}O.

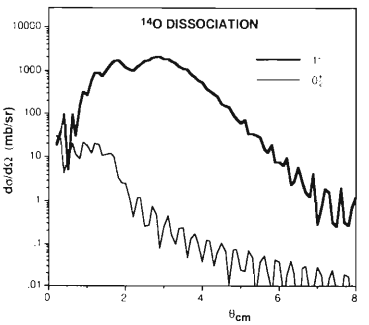

Fig. 2. Predictions of the coupled channel calculation for the reaction ^{208}Pb(^{14}O,^{13}N p)^{208}Pb exciting the 1^- and 0_2^+ states in ^{14}O.

case discussed by Delbar,[2] where the three states, 0^+, 1^- and 0_2^+, are taken into account. As seen in the figure, the two-step excitation to the second 0^+ state is very week and its effect is hardly seen in the 1^- excitation cross section. Therefore the multistep excitation is not likely to affect the ^{208}Pb(^{14}O,^{13}N p)^{208}Pb Coulomb dissociation result. The situation does not change when all the states in Fig. 1 are taken into account. The same coupled channel calculation suggests that the yield at above the 1^- state is due to the one-step nuclear excitation to the 2^+ and 3^- states.

References

1) G. Baur, C. A. Bertulani, and H. Rebel: *Nucl. Phys.*, **A458**, 188 (1986).
2) Th. Delbar: *Phys. Rev.*, **C47**, R14 (1993).
3) T. Motobayashi et al.: *Phys. Lett.*, **B264**, 259 (1991).
4) P. Decrock et al.: *Phys. Rev. Lett.*, **67**, 808 (1991).

E1 Giant Resonance in ^{22}O

M. Tohyama

[unstable nuclei, giant resonances, time-dependent density-matrix theory.]

We study the E1 giant resonance in ^{22}O as an example to understand the response of very neutron rich nuclei to external fields. We use a microscopic model called the time-dependent density-matrix theory (TDDM) which is a straight forward extension of the time-dependent Hartree-Fock (TDHF) theory so as to include the effects of nucleon-nucleon collisions. TDDM has been applied to the decay of giant resonances at zero[1] and finite temperatures[2] and to the mass fluctuations in low-energy heavy-ion collisions[3] and found to give reasonable dissipation-fluctuation properties. The E1 strength functions obtained are shown in Fig. 1. The TDHF strength function consists of two well separated components. One is the bump above 20 MeV and the other is the peaks seen below 15 MeV. The former may be associated with a core excitation mode because a similar bump is seen in the E1 strength function of ^{16}O. The latter is considered to originate in the excitation of the excess neutrons since there are no corresponding peaks in ^{16}O. The sharp peak at 20.4 MeV seen in the TDHF result is completely damped in TDDM and the TDDM strength distribution below 20 MeV becomes structureless. The strength distribution around 25 MeV and above, however, is not affected by the inclusion of two-body correlations. The effects of two-body correlations on the E1 mode in ^{22}O are quite different from those in closed shell nuclei like ^{16}O and ^{40}Ca, where the E1 strength distributions are not seriously affected by two-body correlations.[2]

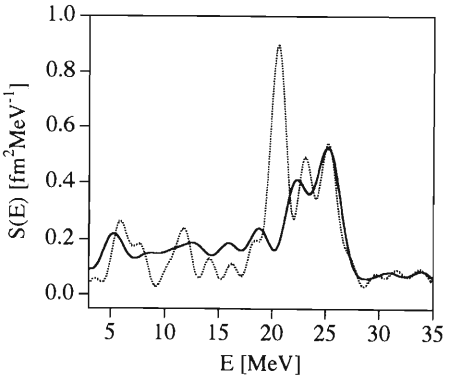

Fig. 1. E1 strength distributions in ^{22}O calculated in TDHF (dotted curve) and TDDM (solid curve).

References

1) M. Gong and M. Tohyama: *Z. Phys.*, **A335**, 153 (1990).
2) F. De Blasio et al.: *Phys. Rev. Lett.*, **68**, 1663 (1992).
3) M. Gong et al.: *Z. Phys.*, **A335**, 331 (1990).

Isoscalar Monopole Vibrations around Thermal Equilibrium

S. Yamaji, H. Hofmann,* and A. S. Jensen**

[Large scale collective motion, giant resonance, linear response theory.]

Dynamics of heated nuclei attracts a lot of attention because it is experimentally accessible and exhibits interesting features for systems of a finite number of particles both of quantal and statistical properties as well as the interplay between collective and single particle degrees of freedom. Commonly theoretical studies concentrate on thermodynamical features in the proper sense, such as the free energy, entropy or nuclear density. These quantities characterize static situations. Here, we want to discuss the temperature dependence of dynamical properties like positions and widths of specific excitations and their relative strength. Our approach[1] differs in two essential ways from the tranditional Hartree-Fock and RPA descriptions. First, the effective coupling constant depends both on deformation and on nuclear excitation energy. Secondly, we account for the temperature dependent additional incoherent coupling to residual degrees of freedom. The possible collective excitations may be parametrized conveniently in terms of the collective response function $\chi_{\rm coll}$. For one degree of freedom one obtains, by use of the assumption of proportionality between average potential and density variations

$$\chi_{\rm coll}(\omega) = \frac{\chi(\omega)}{1 + k\chi(\omega)} \tag{1}$$

where $\chi(\omega)$ is the intrinsic response function and $1/k$ is the coupling constant. The latter is given as,

$$\frac{1}{k} = -\frac{\partial^2 f}{\partial Q_0^2} - \chi \quad (\omega = 0) \tag{2}$$

where f is the free energy, $\chi(\omega = 0)$ is the static response and Q_0 is the equilibrium value of the collective coordinate Q which parametrizes the variation of the average potential. Both f and χ and therefore also $1/k$, depend on the temperature. We calculated the collective response function (1) for the typical isoscalar quadrupole vibration of the nucleus ^{208}Pb and found the usual low energy and giant resonance peaks at low temperatures whereas all the strength is concentrated in a low energy mode above a transition temperature of around 1.5 MeV.[2] In the present report we shall study the collective isoscalar monopole mode in addition to the quadrupole mode. The collective coordinate Q is assumed to be the scaling factor and relates to the density in the form of $Q^3 = n(Q)/n_0$, where n_0 is equilibrium density. The resulting stiffness $C(0) = d^2f/dQ^2$ in Eq. 2 is well approximated by[3]

$$C(0) = 216.7A(1 - 0.006T^2)\text{MeV}. \tag{3}$$

The collective response functin in Eq. 1 has been evaluated for ^{208}Pb. Its dissipative part is shown in Fig. 1 as a function of frequency for the temperatures of T = 0.5, 2.0, and 3.0 MeV. The pronounced resonance is well reproduced. Contrary to the quadrupole case, the resonance does not move to low frequency with increasing T. Only the width becomes broader, since the width of the intrinsic single particle states becomes broader as in the case of quadrupole vibration.

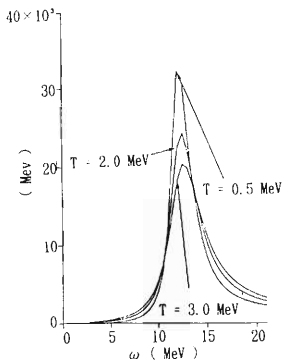

Fig. 1. The imaginary part of the collective response function for ^{208}Pb as a function frequency for T = 0.5, 2.0, and 3.0 MeV for the monopole vibration.

We can understand the reason why the quadrupole and monopole resonances behave so differently with increasing temperature. At zero temperature, our formalism can well reproduce the resonance energy for both the quadrupole and monopole vibrations. Even at a finite temperature the resonance energy is determined by the RPA dispersion equation[1]

$$\chi(\Omega_0) - \chi(0) = C(0). \tag{4}$$

As the stiffness $C(0)$ comes close to zero, the resonance energy Ω_0 comes close to zero-frequency. For the quadrupole vibration, the stiffness $C(0)$ is well estimated by the shell correction energy which disappears around T = 1.5 MeV, while the stiffness $C(0)$ for the monopole vibration weakly depends on the temperature (see Eq. 3).

References

1) S. Yamaji, H. Hofmann, and R. Samhammer: *Nucl. Phys.*, **A475**, 487 (1988).
2) H. Hofmann, S. Yamaji, and A. S. Jensen: *Phys. Lett.*, **B286**, 1 (1992).
3) C. Guet, E. Strumger, and M. Brack: *ibid.*, **B205**, 427 (1988).

* Physik-Department, Technischen Universität München
** Institute of Physics, University of Aarhus

Classical Quantization of γ-Soft Rotor

N. Onishi

[Classical Quantization, TDHF, Periodic orbits, γ-soft rotor, Geodesic in the four dimensional sphere.]

For highly non-linear quantum systems like nuclei, the time dependent Hartree-Fock (TDHF) theory is considered to be suitable.[1] This theory has a classical feature and therefore it is necessary to requantize the wave packets to obtain stationary states. To apply such a classical quantization as Bohr-Sommerfeld's quantization, one has to find periodic orbits in the solutions. Since no general methods finding the periodic solutions are available for the full-TDHF, one should try to find them case by case.

Another method to obtain stationary states is to truncate a subspace from the full-TDHF space. We applied this method to obtain the wobbling motion.[2] We learnt many aspects in the course of this study. In order to extend this method, especially to study a topological structure of the phase space, we tried a semi-classical treatment of the macroscopic model such as Bohr's hydrodynamical model.

As a simplest model in the framework of hydrodynamics, we take the γ-soft rotor which was studied intensively by Wilets-Jean,[3] intending to make a clear topological stucture of the classical orbits. This specific model has a nice feature of symmetry, O(5). The seniority is a good quantum number, which is the angular momentum of the five-dimensional space.[4] We solved a differential equation of the classical motion and found all classical orbits closed independently from the initial conditions. We calculated the action integral and quantized the states to obtain the energy spectra, which correspond completely to those obtained from the purely quantum mechanical procedure.[5] From the analysis, the topological structure is found interesting.

It is shown that the classical motion of a γ-soft rotor is reduced to the free motion in S^4 space. Therefore the trajectory is a geodesic in S^4 space forming closed orbits. Even if the orbits projected onto two dimensional space of γ and the conjugate mometum P_γ look rather complicated, it is clearly seen that all orbits are closed. It will be very interesting to see how the closed orbits distribute, if the S^4 space is deformed by the interaction which breaks O(5). Now the investigation is proceeding.

References

1) H. Reinhaldt: *Nucl. Phys.*, **A346**, 1 (1980).
2) N. Onishi: *ibid.*, **A456**, 279 (1986).
3) L. Wilets and M. Jean: *Phys. Rev.*, **102**, 788 (1956).
4) G. Rakavy: *Nucl. Phys.*, **4**, 289 (1957).
5) N. Onishi and Dong-il Chang: *ibid.*, **A557**, 301c (1993).

Tilted Axis Rotating States in ^{182}Os Yrast

T. Horibata and N. Onishi

[γ-deformation, Three-dimensional rotation, Wobbling motion.]

We found tilted axis rotating solutions in the yrast states of ^{182}Os by a self consistent three dimensional cranking calculations. Our method is based on the TD-HFB which is derived from the time dependent variational principle.[1] Since the method is free from the restrictions of the linear approximation, we can manipulate solutions in a region far from where such approximate methods could reach. Present solutions suggest a possible new interpretation for the backbending phenomena.

Chowdhury et al.[2] reported an observation of high-K isomers which decay abnormally fast into the yrast state in ^{182}Os. They claim that the large γ-deformation mixes the K-quantum number and prompts the penetration between the high-K isomeric deformation aligned prolate state and the well known rotation aligned state. On the other hand, the wobbling motion caused by the Coliolis interaction which is predicted to appear as a part of high spin survivals of γ-vibrational band is also predicted in this nucleus. Since the wobbling motion accompanies shape oscillations, the γ-deformation freedom is also expected to play a crucial role in the dynamics.

In this report we focus our discussion on the character of three dimensional potential surface of the nucleus. We employ the HFB space in order to take into account the pairing correlation. We truncate a model subspace from the full HFB space, in which wave functions are labeled by the three components of angular momentum referred to an intrinsic frame. The intrinsic frame of coordinate system is determined such that the principal axis (**PA**) of the mass quadrupole moment becomes the axis of coordinate system. Thus we obtain the variational equation with eight constraints. Those are the components of the angular momentum, the mass quadrupole moments and the particle numbers.

$$\delta\left\langle \Phi \middle| \left[\hat{H} - \sum_{k=1}^{3} \left(\mu_k \hat{J}_k + \xi_k \hat{B}_k \right) - \sum_{\tau=\mu}^{\nu} \lambda_\tau \hat{N}_\tau \right] \middle| \Phi \right\rangle = 0$$

The model hamiltonian employed in the present calculations is the pairing plus Q-Q force. First we performed the calculation for one dimensional rotation about the principal axis (**PAR**). The g-band crosses the s-band at $J = 14\hbar$. After constructing the **PAR**-yrast we launched off from the **PAR**-states to explore a vast unknown three dimensional potential field where any self consistent calculation has never been performed for the HFB-space. In Fig. 1 we show a potential surface obtained by the present calculation at $J = 15\hbar$. We found a local energy minimum at a distant point from the **PAR**-state. The energy of the point is about 0.3 MeV lower compared to that of the $J = 15\hbar$ **PAR**-state. The result suggests an existence of tilted axis rotating states (**TAR**) and the states possibly join the members of new yrast states.

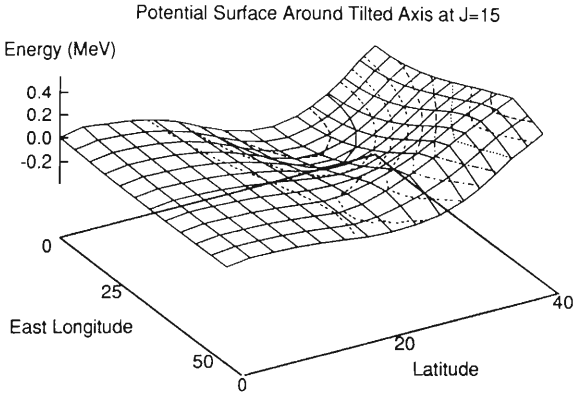

Fig. 1. The energy surface of $J = 15\hbar$ sphere. The direction of angular momentum vector is represented by east-longitude and latitude.

References

1) A. K. Kerman and N. Onishi: *Nucl. Phys.*, **A361**, 176 (1981); N. Onishi: *ibid.*, **A456**, 279 (1986).
2) P. Chowdhury et al.: *ibid.*, **A485**, 136 (1988).

Asymmetric Nuclear Matter and Finite Nuclei

N. Fukunishi

[Asymmetric nuclear matter.]

Discovery of the halo nucleus ^{11}Li[1] has made the study of neutron-rich nuclei one of the mainstreams of the nuclear physics. The binding mechanism of halo nuclei, two-neutron correlation in the halo part and its effects on the nuclear reactions attract much interest. Although the neutron halo is a very interesting phenomenon, it may be one of the interesting aspects of neutron-rich nuclei. The present status of the study of neutron-rich nuclei is restricted to light nuclei mainly because of experimental difficulties. We expect and believe that these experimental difficulties will be overcome in the near future.

Our purpose of this work is to investigate how the bulk properties of nuclei will change with many excess neutrons. Numerical calculations have not been finished. Thus, we will discuss briefly what we are interested in. First of all, we must investigate how far away from the β stability line the nucleus exists. The mass formula of Myers and Swiatecki[2] predicts that $N/Z = 2.25$ gives the neutron drip line for nuclei with $A = 40$–80. Here, N,Z, and A mean the neutron, the proton and the mass number, respectively. Note that this predicted value does not include the pairing and shell effects. Thus, a highly degenerate orbit near the drip line would allow the existence of more exotic nuclei, if the nuclear deformation does not take place in these nuclei. To investigate this possibility is one of our interests.

Weiss and Cameron discussed[3] that the saturation density changes in the neutron-rich nuclei. According to them, the saturation density is expected to be 15% smaller at $N/Z = 2.3$ than in the stable nuclei. It is a natural consequence of the Fermi-momentum dependence of the symmetry energy. It is very interesting that saturation properties may change with many excess neutrons.

The effective mass is one of the important quantities. In stable nuclei, the effective mass at the Fermi surface is nearly 1. On the other hand, it is predicted to be about 2/3 for occupied states away from the Fermi surface. Skyrme interactions, which are used widely, predict that the effective mass of the neutron becomes greater as the neutron number increases. On the other hand, that of the proton decreases with the neutron excess. The effective mass determines the density of states. Thus, it is one of the key ingredients when we discuss the possibility of the deformation in the neutron-rich nuclei.

We are also interested in the effective interaction in neutron-rich nuclei. Our approach which will be explained just below can answer how the pairing interaction, the quadrupole-quadrupole interaction and the spin-orbit interaction change with the neutron excess. With our best knowledge, fully microscopic investigation has been missing.

Microscopic calculations, which are based on the realistic nucleon-nucleon interaction and the non-relativistic Brueckner-Bethe-Goldstone[4] equation, are planned to investigate these quantities. The relativistic Brueckner-Hartree calculation[5] has been carried out for finite nuclei with many excess neutrons. On the other hand, neutron-rich nuclei are not enough investigated in terms of the non-relativistic many-body theory with the realistic nuclear force. Our approach is made of two steps. The first is the G-matrix calculation in the asymmetric nuclear matter. In this calculation, we treat the Pauli operator *exactly*,[6] and it is the most important difference between the calculation which we plan and many preceding calculations for the asymmetric nuclear matter.[7] Thus, we can discuss clearly effects of excess neutrons. The second step is application of the results in the asymmetric nuclear matter to finite nuclei using the Local Density Approximation (LDA) and the Density Matrix Expansion (DME).[8,9] This approach is used for stable nuclei by Negele et al. It is also effective for neutron-rich nuclei with the similar accuracy, because the short-range nature of the nuclear force justifies this approximate treatment for finite nuclei.

References

1) I. Tanihata et al.: *Phys. Lett.*, **160B**, 251 (1985); I. Tanihata et al.: *Phys. Rev. Lett.*, **55**, 2676 (1985).
2) W. D. Myers and W. J. Swiatecki: *Nucl. Phys.*, **81**, 1 (1966).
3) R. A. Weiss and A. G. W. Cameron: *Can. J. Phys.*, **47**, 2171; 2211 (1969).
4) K. A. Brueckner, C. A. Levinson, and H. M. Mahmoud: *Phys. Rev.*, **95**, 217 (1954); J. Goldstone: *Proc. Roy. Soc.*, **A239**, 267 (1957).
5) R. Brockmann and H. Toki: *Phys. Rev. Lett.*, **68**, 3408 (1992).
6) T. Cheon and E. F. Redish: *Phys. Rev.*, **C39**, 331 (1989).
7) For example, I. Bombaci and U. Lombardo: *ibid.*, **C44**, 1892 (1991).
8) J. W. Negele: *ibid.*, **C1**, 1260 (1970).
9) J. W. Negele and D. Vautherin: *ibid.*, **C5**, 1472 (1972).

Neutron-Skin and Proton-Skin Formations in Exotic Nuclei Far from Stability

N. Fukunishi, T. Otsuka, and I. Tanihata

[Neutron skin, Proton skin, Exotic nuclei.]

The neutron skin of the nucleus has been one of the central issues of nuclear structure.[1,2] The definition and presence of the neutron skin, however, have remained open problems for decades. It is only recent that thick neutron skins have been seen experimentally, although only quite light nuclei such as ^{6}He and ^{8}He were investigated.[3] We discuss the formation of the neutron skin and its physical importance briefly.

We employ the open-shell Hartree-Fock + BCS approach for several isotope chains, assuming the spherical equilibrium.[4] This treatment of the open-shell nucleus does not give the correct ground state properties, but gives average properties of low-lying states. However, it should be rather irrelevant to our major results, because we restrict ourselves to bulk properties such as densities which are rather common among those states.

To discuss the neutron skin, let us introduce a quantity, the "skin thickness". In the neutron skin, the neutron density $\rho_n(r)$ must be much greater than the proton density $\rho_p(r)$. In addition to it, the neutron density itself should not be too dilute. It is needed to distinguish the neutron skin from the neutron halo. These two conditions give the inner boundary R_1 and the outer boundary R_2 as follows;

$$\rho_n(r) \geq 4\rho_p(r) \quad \text{for } r \geq R_1$$
$$\rho_n(r) \geq \frac{1}{100}\rho_n(0) \quad \text{for } r \leq R_2.$$

The skin thickness is defined as $R_2 - R_1$. When R_2 is smaller than R_1, we set the skin thickness equal to zero.

Figure 1 shows the skin thickness as a function of the neutron number (N). We find the continuous growth of the skin thickness as N increases. It reaches more than $1fm$ for nuclei with $N/Z > 2$. It is surprising that the neutron number in the skin reaches about twelve for ^{181}Cs ($N = 126$).

Figure 1 suggests a strong correlation between the neutron skin and the stability of the nucleus. What is the key ingredient of the formation of the neutron skin? The answer is the difference of the Fermi energies between the proton (e_F^P) and the neutron (e_F^N). In stable nuclei, e_F^N is almost the same as e_F^P. The strong proton-neutron interaction violates this "balance" in the neutron-rich nuclei. As the neutron number increases, e_F^N goes up, which reaches nearly zero in the drip-line nucleus. The small Fermi energy of the neutron leads to slow fall off of the neutron density. On the other hand, excess neutrons give much attraction to protons, resulting in the deeper mean-potential

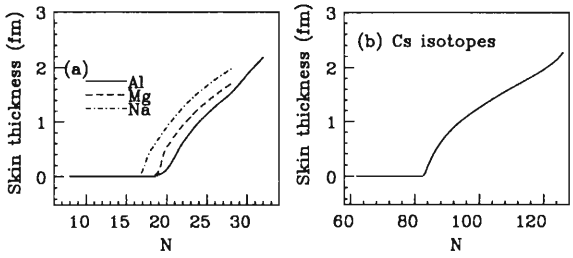

Fig. 1. (a) Skin thickness in fm for Na (dot-dashed line), Mg (dashed line) and Al (solid line) isotopes as a function of the neutron number, N. (b) Skin thickness in fm for Cs isotopes.

for protons. It causes stronger damping of the proton density, in addition to the existence of the Coulomb barrier. Thus, the shape proportionality between the proton and neutron densities is broken in the outer region of nuclei with $N \gg Z$, and the neutron skin emerges. This mechanism of the neutron skin formation is a general one, and indicates that the neutron skin should occur rather independently of minor details of calculations. One of the other Skyrme interactions (SGII)[5] gives basically the same results as shown in Fig. 1.

The neutron skin opens up new fields of interest. It is rather likely that the neutron skin affects the nuclear deformation and the giant resonance of the nucleus. A new type of deformation, in which the shape proportionality of the proton density and the neutron density is broken, or a new mode which is primarily comprised of the neutron particle-hole excitation is expected due to the fact that the neutron surface is away from the proton surface. The neutron skin is also expected to have a prominent effect on nuclear reactions. When an unstable nucleus with the neutron skin approaches a stable nucleus, neutrons in the skin can touch the other nucleus before protons can do so. The difference of e_F^N may behave as a driving force of the fast neutron flow from the neutron-rich to the stable nucleus.

References

1) A. Krasznahorkay et al.: *Phys. Rev. Lett.*, **66**, 1287 (1991).
2) W. D. Myers, W. J. Swiatecki, and C. S. Wang: *Nucl. Phys.*, **A436**, 185 (1985).
3) I. Tanihata, D. Hirata, T. Kobayashi, S. Shimoura, K. Sugimoto, and H. Toki: *Phys. Lett.*, **289B**, 261 (1992).
4) N. Fukunishi, T. Otsuka, and I. Tanihata: *Phys. Rev.*, **C48**, 1648 (1993).
5) N. Van Giai and H. Sagawa: *Phys. Lett.*, **106B**, 379 (1981).

How Many Nuclides Do Exist?

H. Sato and M. Uno

[Nuclear masses, α-, proton-, neutron-, β^--, and β^+-decays.]

"How many nuclides can exist as a compact system of proton number Z and neutron number N" is one of the intriguing and fundamental questions in nuclear physics. In this work, firstly we study the relationship between the history of the number of nuclides found and the half lives of those nuclides observed.[1] Next, we study the systematics of separation energies of the β^--, β^+-, proton-, neutron-, and α-emission decays of nuclides with both the mass observed experimentally and the realistic nuclear mass formula given by Tachibana, Uno, Yamada, and Yamada[2] (TUYY). Figure 1 shows the α separation energies of nuclides in the Z-N plane obtained with the TUYY mass formula. The effects of the closed shell are nicely observed. Then we perform the calculation of β^--, β^+-decay half lives with the nuclear gross theory and of proton-, neutron-, and α-emission decay half lives of nuclides with the R-matrix theory employing the separation energies obtained with the nuclear mass formula given by TUYY. And we study the systematics of those half lives in the Z-N plane. Furthermore, we study the half life dependence of the number of nuclides, and discuss the number of unstable nuclei possibly found experimentally.

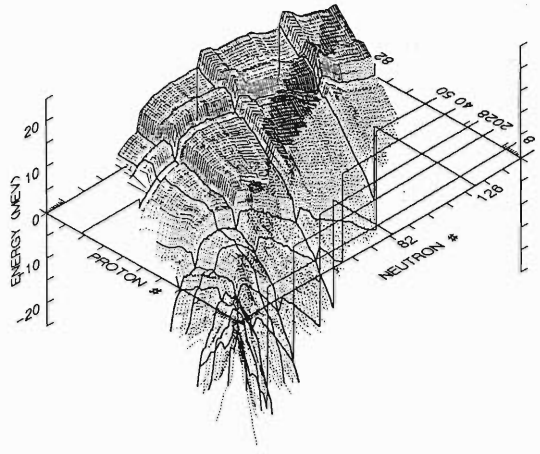

Fig. 1. The systematics of α Q values calculated with the TUYY mass formula.[2]

References

1) H. Sato and M. Uno: *Butsuri*, **39**, 892 (1984).
2) T. Tachibana, M. Uno, M. Yamada, and S. Yanada: *Atomic Data and Nuclear Data Tables*, **39**, 251 (1988).

Systematics of Alpha Q-values: Potential Dependence of the Alpha Decay Life Time

H. Sato

[α decay.]

We study the α decay half life of an even-even nucleus in terms of the α S-factor defined by the ratio of the experimental α decay life $t_{\rm exp}$ to the single α decay life t_α:[1] $S_\alpha = t_\alpha/t_{\rm exp} = \Gamma_\alpha/\Gamma_{\rm exp}$. Here $\Gamma_{\rm exp}$ is the experimental α decay width, and the single α width Γ_α is defined by: $\Gamma_\alpha = 2P\gamma^2$ with the penetrability P and the reduced width γ^2 given by

$$\gamma^2 = \frac{\hbar^2}{2\mu a_c} \frac{|u_{NL}(a_c)|^2}{\int_0^{a_c} |u_{NL}(r)|^2 \, dr},$$

where N is the node quantum number, and μ is the reduced mass. The channel radius a_c is chosen to be reasonably large. The wave function $u_{NL}(r)$ is a solution of the one body equation of the α-A relative motion given by

$$\left(\frac{P^2}{2\mu} + U_{\alpha A}\right) \frac{1}{r} u_{NL} Y_{Lm} = Q_{\alpha A} \frac{1}{r} u_{NL} Y_{Lm}$$
$$\text{with} \quad U_{\alpha A} = gU + U_C.$$

Here the α Q value $Q_{\alpha A}$ is taken from the compilation of Wapstra and Audi.[2] We employ the double folding potentials for U and U_C calculated by the M3Y and Coulomb interactions with the nuclear density distributions generated by the Density Dependent Hartree Fock type variational calculation including shell corrections[3] with the Skyrme III interaction. The parameter g is adjusted so as to reproduce $Q_{\alpha A}$ at each node quantum number N under the condition that the u_{NL} has a phase shift $\pi/2$ in the asymptotic region.

Choosing an appropriate node quantum number N, we calculate the S-factors and summarize those in Fig. 1. To make a quantitative discussion, we study

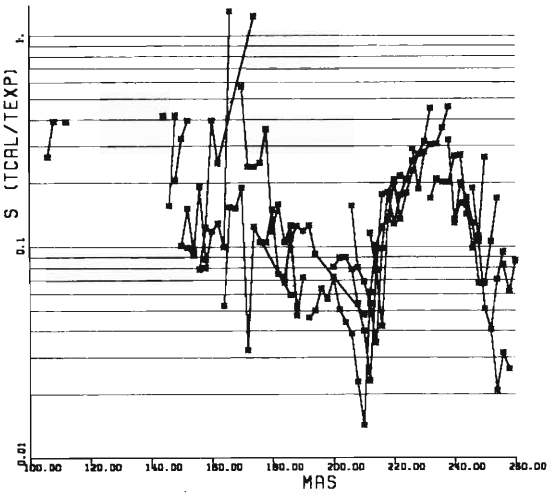

Fig. 1. S factors derived with M3Y folding potential.

decay half lives of 6^+ and 8^+ states of the ground band of ^{20}Ne and those of the ground and 18^+ states of ^{212}Po with theoretical S-factors (0.24 for ^{20}Ne and 0.061 for ^{212}Po[4]), and find nice agreements with experimental data except 18^+ of ^{212}Po.

The author would like to thank Professor M. Ishihara for his encouragement.

References

1) A. Arima and S. Yoshida: *Phys. Lett.*, **B40**, 15 (1974); *Nucl. Phys.*, **A219**, 475 (1974).
2) A. H. Wapstra and R. Hoekstra: *Atomic Data and Nuclear Data Tables*, **39**, 281 (1988).
3) K. Yazaki: *Nucl. Phys.*, **A277**, 189 (1977).
4) I. Tonozuka and A. Arima: *ibid.*, **A323**, 45 (1979).

Relativistic Density Dependent Hartree Approach for ^{16}O, ^{40}Ca, and ^{208}Pb

R. Brockmann and H. Toki

[Relativistic density dependent Hartree approach, rearrangement term, isovector interaction.]

The relativity has been demonstrated to be a key ingredient to describe the nuclear saturation property using the Relativistic-Brueckner-Hartree-Fock (RBHF) theory.[1] We have then developed a method to describe finite nuclei using the RBHF results of nuclear matter.[2] This new method, named as relativistic density dependent Hartree (RDDH) approach, is able to reproduce the binding energies and radii of ^{16}O and ^{40}Ca. As a next step, we study the effects of the rearrangement term and the isovector interaction for heavy nuclei.

The effect of the rearrangement term due to the density dependence of the effective interactions has been studied by many authors for the non-relativistic case. We can include this effect also for the relativistic case in the similar way. We will show the details of calculations in a future publication.[3] The calculated results are summarized in Table 1. As discussed in the previous publication for ^{16}O and ^{40}Ca, the RDDH results compare extremely well with experiment.[2] The binding energy per particle and the charge radius are slightly underestimated. The similar behavior is found also for the case of ^{208}Pb, where only the isoscalar interaction (sigma and omega mesons) is considered.

Table 1. Binding energy per particle and charge radius for various nuclei. RDDH and RDHR are the relativistic density dependent Hartree theory without and with the rearrangement term, respectively, which are compared with the experiment denoted by Exp.

	E/A [MeV]			R_c [fm]		
Nucl.	RDDH	RDHR	Exp	RDDH	RDHR	Exp
^{16}O	7.402	7.420	7.98	2.622	2.736	2.75
^{40}Ca	7.901	7.943	8.55	3.328	3.429	3.48
^{208}Pb	7.440	7.440	7.87	5.222	5.302	5.50

The results with the rearrangement term are depicted in the column headed by RDHR. The binding energy is not much influenced, while the radius is increased by about 0.1 fm. Hence, the radius is improved by introducing the rearrangement term.

We discuss now the inclusion of the isovector interaction (rho and delta mesons) for N/Z asymmetric nuclei. We extract the density dependent coupling constants for the rho and omega mesons from the RBHF results on both the nuclear matter and the neutron matter. Again the details of this extraction will be shown in a future publication.[3] The numerical results for ^{208}Pb are; B/A = 6.985 MeV and R_c = 5.214 fm. The isovector interaction acts repulsively for the binding energy and makes the agreement with the data worse. As the net effect, the binding energy is underestimated by about 1MeV for ^{208}Pb. Since the symmetry energy of the RBHF theory comes out reasonable, we believe this under binding originates from the isoscalar part. It would be very important to point out that the finite nuclei would be reproduced once the nuclear matter properties are reproduced.

In conclusion, we have now a many body theory to describe the saturation property of nuclear matter. With the use of this result, we find a straightforward approach as the RDDH can describe also finite nuclei. The relativity produces as very important effects the three body interaction and the spin-orbit interaction in the language of the non-relativistic framework.

References

1) R. Brockmann and R. Machleidt: *Phys. Rev.*, **C42**, 1965 (1990).
2) R. Brockmann and H. Toki: *Phys. Rev. Lett.*, **68**, 3408 (1992).
3) R. Brockmann and H. Toki: to be published.

Systematic Study of Sr Isotopes in the Relativistic Mean Field Theory

D. Hirata, H. Toki, I. Tanihata, and P. Ring*

[Nuclear Structure, binding energy, isotope shifts, deformation, relativistic mean field theory.]

Recently, using the nuclear radioactive beams, it becomes possible to study experimentally the unstable nuclei, in particular, those with large neutron excess. This technique enables us to study the structures of unstable nuclei and then find many interesting phenomena such as neutron halos and neutron skins.[1,2]

It is very interesting for theoreticians to study the structures of unstable nuclei with a reliable model. We choose the relativistic mean field theory (RMF) for this purpose. This is due to the recent success of the relativistic Brueckner-Hartree-Fock calculations on nuclear matter and we also found that the RMF theory using the NL1 parameter set describes spherical unstable nuclei well.[3]

The mean square nuclear charge radii $<\Delta r^2>$ in a long series of isotopes appear to be an important tool in the analysis of the structure of ground states of unstable nuclei because they give informations about new regions of deformation. The Sr ($Z = 38$) isotopes are particularly interesting, since an experiment performed by the ISOLDE group at CERN[4] provided systematically the $<\Delta r^2>$ from $A = 78$ to 100. The data show a large jump in the $<\Delta r^2>$ at A around 98 indicating that the nuclei in that region are strongly deformed. Hence, we calculated $<\Delta r^2>$ using the RMF theory with deformation using the NL1 parameter set and compare the results with the experimental data.[5]

We have performed constraint calculations to the quadrupole moment in order to obtain all local minima in the energy curve.

We show in Fig. 1 the binding energy per particle for all possible solutions, as a function of the mass number. The behavior of the E/A is reproduced quite well in the RMF theory, although we found a missing binding energy on the neutron rich side which we attribute to the strong ρ meson coupling strength in the NL1 parameter set.

Figure 2 shows the isotope shifts of Sr isotopes from $A = 78$ to 100 relative to $A = 88$ for all possible minima obtained and compared with the data. The small increase of the isotope shifts toward the proton rich side observed experimentally is not described well when the small deformation is chosen and the large deformation gives larger isotope shifts than the experimental values. The strong increase for the neutron rich side is well reproduced if the large oblate deformation is chosen, and the jump at $A = 98$ is also reproduced if the large prolate solution is selected.

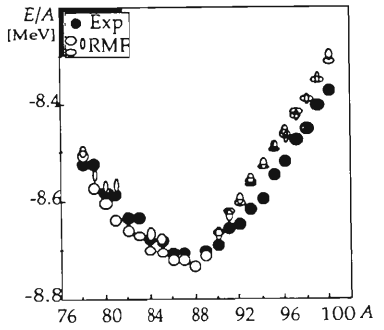

Fig. 1. The binding energy per particle E/A for Sr isotopes as a function of the mass number (A). The experimental data are shown by solid circles and the calculated ones by the open eliptics, indicating the shapes of the possible solutions.

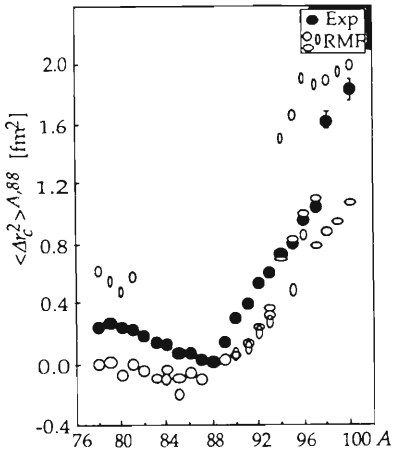

Fig. 2. The isotope shifts normalized to $A = 88$ for Sr isotopes as a function of A. The data are shown by solid circles and the calculated values by the open eliptics.

The discrepancies seen in Figs. 1 and 2 may be solved with the addition of the angular momentum projection and the triaxial deformation, but the present study is already able to explain the gross structure of the Sr isotopes.

References

1) I. Tanihata et al.: *Phys. Rev. Lett.*, **55**, 2676 (1985).
2) I. Tanihata et al.: *Phys. Lett.*, **B289**, 261 (1992).
3) D. Hirata et al.: *Phys. Rev.*, **C44**, 1467 (1991).
4) C. Thibault et al.: *ibid.*, **C12**, 644 (1975).
5) D. Hirata et al.: *Phys. Lett.*, **B314**, 168 (1993).

* Physik Department der Technischen Universität München

Relativistic Mean Field Theory for the Isotope Shifts of Ba, Cs, and Xe

D. Hirata, H. Toki, and I. Tanihata

[Nuclear Structure, isotope shift, deformation, relativistic mean field theory.]

There is an explosive interest in the study of unstable nuclei after the technical advance of unstable nuclear beams.[1] We are learning, in nuclei near the drip lines, many nuclear phenomena that have not been observed in stable nuclei.[2] One of the important systematic studies of unstable nuclei is pursued by the ISOLDE group at CERN using the laser spectroscopy. The measurement of the isotope shifts of $_{54}$Xe, $_{55}$Cs, and $_{56}$Ba shows a strong magic number effect at $N = 82$ in addition to some deviation of the isotope shifts from the systematics around $N = 64$ in Cs.[3] The non-relativistic Hartree-Fock theory provides the magic number effect at $N = 82$, but the effect is not so large as the data indicate.

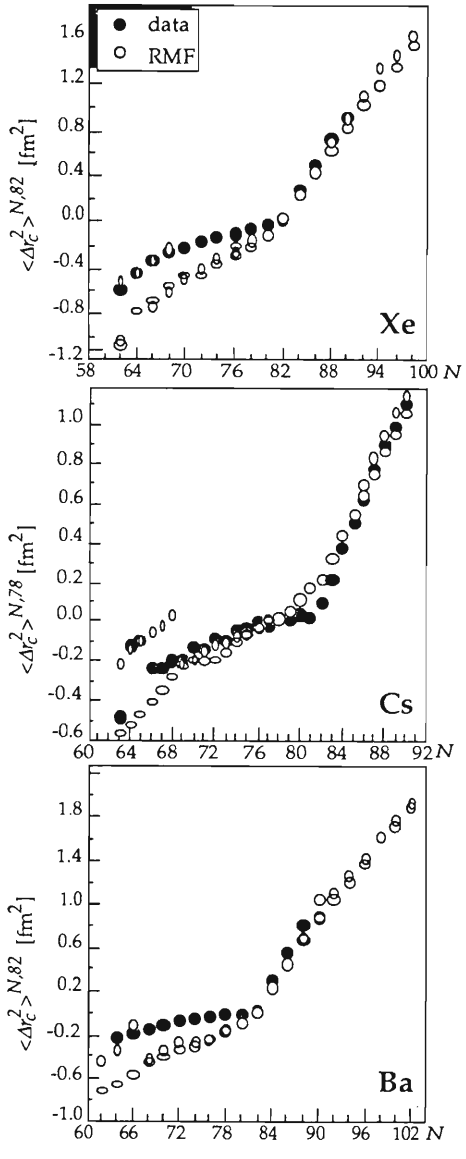

Fig. 1. The isotope shifts normalized to $N = 82$ for Xe and Ba isotopes and, to $N = 78$ for Cs isotopes, respectively, as a function of neutron number. The experimental data are indicated by solid circles and the calculated values by open eliptics denoting the shapes of the possible solutions.

On the other hand, the RMF theory has been demonstrated to work very well for unstable nuclei.[4] It is therefore very interesting to apply the RMF theory to these nuclei including the deformation degree of freedom. We use a newly obtained parameter set constructed by Sugahara and Toki, which includes the non-linear ω term.[5] We have performed constrained calculations to the quadrupole deformation and hence find several minima for each isotope.

We show in Fig. 1 the calculated results for isotope shifts of Xe, Cs, and Ba as a function of the neutron number. Nuclei Xe and Ba with an even proton number, show similar behavior for the isotope shifts. The change of the isotope shifts at $N = 82$ in calculation is not as drastic as the data show. The isotope shifts below $N = 82$ are underestimated significantly. However, the appearance of an energy minimum solution at large prolate deformation for several nuclei around $N = 66$ provides a good account of the data. The overall agreement is seen for the case of the Cs isotopes which have an odd proton number. The jump of the isotope shifts seen in the experiment around $N = 64$ may suggest the large prolate deformation, which is one of the energy minima for these nuclei. It would be important to accumulate the information for systematic understanding of unstable nuclei.

References

1) I. Tanihata: *Treatise on Heavy Ions Physics*, **8**, 443 (1989), and references therein.
2) I. Tanihata et al.: *Phys. Rev. Lett.*, **55**, 2676 (1985).
3) P. Aufmuth et al.: *At. Data Nucl. Data Tables*, **37**, 455 (1987).
4) D. Hirata et al.: *Phys. Rev.*, **C44**, 1467 (1991).
5) Y. Sugahara and H. Toki: TMU preprint (1993).

Instability of the Degenerate Electron Gas

K. Tanaka

[Instability, infrared divergence, electron gas.]

The degenerate electron gas is a classic model of the many-body problem. It is a system of interacting electrons placed in a positively charged uniform background to ensure the neutrality of the system, and is expected to serve as a model of electrons in metals or in astronomical objects like white dwarfs and neutron stars.

In the nonrelativistic (NR) case, the energy density[1] and the quasiparticle spectrum in the vicinity of the Fermi surface[2] were obtained as a high-density expansion, where the principal approximation is the RPA to sum up the dominant infrared-divergent terms, giving finally the finite results. Also, in the relativistic case, the resummation of the RPA series was required to obtain the finite result for the energy density.[3] In this paper, we investigate the quasiparticle spectrum in the relativistic RPA, corresponding to the energy density computation of Ref. 3. We employ a recently developed technique[4] to extract the dominant infrared singularities in the Fermi velocity, and investigate the behavior of the quasiparticle spectrum near the Fermi surface.

We find that the Fermi velocity suffers from the infrared divergence even in the RPA, in contrast to the NR case: If we include only the exchange self-energy correction, we obtain the result consistent with the NR case, i.e., the infinite positive slope of the quasiparticle spectrum at the Fermi surface due to the infrared divergence. This indicates the inadequacy of the approximation and suggests the resummation of the RPA series. By including further the RPA self-energy contribution, we find:

$$\delta v_{\mathrm{F}} = -\frac{1}{2}\left(\frac{e(p_{\mathrm{F}})}{2\pi}\right)^2 v_0^2 \left\{\ln\frac{p_{\mathrm{F}}^2}{\lambda^2} + O(1)\right\}, \qquad (1)$$

as the correction to the Fermi velocity of the free electron gas $v_0 = p_{\mathrm{F}}/\sqrt{p_{\mathrm{F}}^2 + M^2}$ (p_{F} the Fermi momentum and M the electron mass). $e(p_{\mathrm{F}})$ is the running coupling constant at the momentum scale p_{F}, and λ is the fictitious photon mass to cut-off the infrared divergence. The result indicates the infinite negative slope of the spectrum at the Fermi surface and therefore instability of the normal state for *any* density. Furthermore, this does not reduce to the corresponding (finite) result[2] in the NR limit.

The essential ingredient leading to the breakdown of the RPA in the relativistic case is the interactions via the exchange of the transverse photons. They have been neglected in the NR case as relativistically higher order effects of $O(v_0^2)$. However, as shown in Eq. 1, they give the infrared divergent contribution even after summing up the complete RPA series, due to the fact that the screening mass for the transverse modes is zero. This means that the NR treatment neglecting those degrees of freedom is illegitimate.

There has been no empirical indication of such instability of the Fermi surface as discussed above. In order to get the result consistent with the observation, one would at least have to include the higher order terms beyond the RPA. However, since it can be proved that the transverse screening mass is zero for the arbitrary order of perturbation theory, one might have to include nonperturbative effects beyond perturbation theory, or the degrees of freedom beyond the original model, e.g., phonons in the case of metals. We also note that the extension of our arguments would indicate the instability of the normal state for other gauge theories, e.g., for quark matter.

References

1) M. Gell-Mann and K. A. Brueckner: *Phys. Rev.*, **106**, 364 (1957).
2) M. Gell-Mann: ibid., p. 369.
3) I. A. Akhiezer and S. V. Peletminskii: *Sov. Phys. JETP*, **11**, 1316 (1960); B. Jancovici: *Nuovo Cimento*, **25**, 428 (1962).
4) K. Tanaka: RIKEN preprint, RIKEN-AF-NP-160 (1993).

Quasiparticle Properties and the Dynamics of High-Density Nuclear Matter

K. Tanaka

[Quasiparticle spectrum, high-density nuclear matter.]

One universal character shared by most normal Fermi liquids is the enhancement of the effective mass around the Fermi surface.[1] The relevant mechanism is the dynamics beyond the mean-field theory, i.e., the coupling of the single-particle motion to particle-hole (ph) excitations in the case of nuclear matter.

The investigation of the high-density behavior of the effective mass including those many-body correlations would be relevant to understand, e.g., stellar structure or evolution and high-energy heavy ion reactions. This requires a relativistic framework of Fermi liquids. In this paper[2] we compute the quasiparticle spectra employing the $1/N$ expansion method for the $\sigma\omega$ model.[3] (N is the extended number of nucleon species.) Based on the Landau theory of Fermi liquids,[4] the quasiparticle energy in nuclear matter, corresponding to the energy density up to the next-to-leading order, is obtained: This contains, in addition to the leading Hartree term of $O(1)$, the exchange and RPA self-energy terms of $O(1/N)$.

We find that, for high densities, the spectra show the "anomaly" around the Fermi surface, i.e., they are flat or decreasing due to the inclusion of the RPA self-energies. This anomaly corresponds to the effective mass enhancement discussed above, and the effect grows with increasing density. Figure 1 shows the real part of the quasiparticle energy for the "flat" case.

The growth of the anomaly can be understood by examining the high-density asymptotic behavior of the Fermi velocity $v_{\rm F}$. We obtain for $p_{\rm F} \to \infty$ ($p_{\rm F}$ the Fermi momentum):[2]

$$v_{\rm F} \to 1 - \frac{1}{2}\left(\frac{g_\omega(p_{\rm F})}{2\pi}\right)^2 \left\{\ln\frac{p_{\rm F}^2}{m_\omega^2} + O(1)\right\}, \qquad (1)$$

where m_ω is the ω-meson mass and $g_\omega(p_{\rm F})$ is the running coupling constant at the scale $p_{\rm F}$ for the nucleon-ω vertex. The first term ("1") is due to the Hartree term while the second term is the contribution due to the $O(1/N)$ self-energies. The result is governed by the infrared singularity for $m_\omega/p_{\rm F} \to 0$, and can be traced back to the fact that the the transverse screening mass of the vector bosons is zero, in contrast to a nonzero Debye screening mass for the longitudinal mode.

Thus, the anomaly in the spectra is due to the strong infrared behavior caused by the coupling of the ph excitation to the single-particle motion. Though a more realistic treatment would be required to fix the relevance to phenomenology, the universal character of this phenomenon already poses various interesting aspects for high-density matter, like the possibility of the new phase[5] above the critical $p_{\rm F}^{\rm c}$ where $v_{\rm F} = 0$, the thermodynamic properties and transport phenomena in this phase, and the extension to gauge theories.[6]

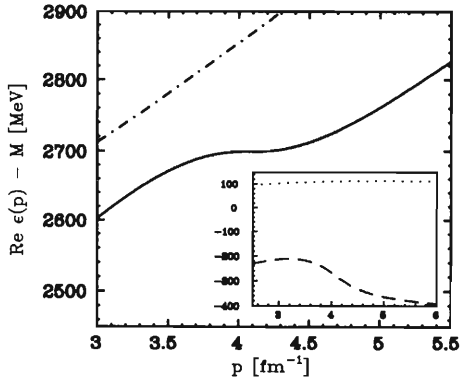

Fig. 1. The real part of the quasiparticle energy as a function of momentum for the case of $p_{\rm F} = 4.07$ fm^{-1}. The solid line shows the full result including the $O(1/N)$ self-energy contributions, while the dot-dashed line is the Hartree contribution contained in the full result. The insertion shows the $O(1/N)$ self-energy contributions as functions of momentum. The dotted and dashed lines are the exchange and RPA self-energy contributions, respectively.

References

1) C. Mahaux, P. F. Bortignon, R. A. Broglia, and C. H. Dasso: *Phys. Reports*, **120**, 1 (1985).
2) K. Tanaka: RIKEN preprint, RIKEN-AF-NP-160 (1993).
3) K. Tanaka, W. Bentz, and A. Arima: *Nucl. Phys.*, **A555**, 151 (1993).
4) L. D. Landau: *Sov. Phys. JETP*, **3**, 920 (1956).
5) C. J. Horowitz and B. D. Serot: *Phys. Lett.*, **B109**, 341 (1982).
6) K. Tanaka: This report, p. 22.

General Formula of the Coalescence Model

S. Hirenzaki, T. Suzuki, and I. Tanihata

[Coalescence model, Pi-neuts.]

The coalescence model has been widely used to calculate the formation cross sections of composite particles using the cross sections of constituent particles. In the model, particles in a coalescence phase volume are assumed to produce the composite particle. We have developed the general expression of the coalescence factor for the formation of arbitrary composite particles[1] using the density matrix formalism.[2] This expression is extremely useful and can be used to estimate the formation cross section of any kinds of composite particles such as hypernuclei, multi-hypernuclei, mesonic atoms, multi-mesonic atoms, pi-neuts, etc. As an example we have studied the formation cross section of the pi-neut and showed that the analysis using the recent data strongly denies the existence of πn^2.

In the coalescence model we can express the formation cross section of a composite particle "a" as follows;

$$\frac{\gamma_a}{\sigma_0}\frac{\mathrm{d}^3\sigma_a}{\mathrm{d}k_a^3} = F_c \prod_{i=1}^{A}\left[\frac{\gamma_i}{\sigma_0}\frac{\mathrm{d}^3\sigma_i}{\mathrm{d}k_i^3}\right], \tag{1}$$

where A is the total number of constituent particles that make "a" and the index i indicates an i-th particle. We denote the coalescence factor by F_c. To get the analytic expression of the coalescence factor F_c under the same assumptions as those in Ref. 2, we write the many body density matrix approximately as the product of the one body density matrix and assume the one body density matrix to have the following Gaussian form;

$$\rho_i(\mathbf{r},\mathbf{r}') = \frac{1}{(\pi\alpha_i^2)^{3/2}}\exp\left[-\frac{1}{\alpha_i^2}\left(\frac{\mathbf{r}+\mathbf{r}'}{2}\right)^2\right] \times C_i \exp\left[-\frac{1}{\beta_i^2}(\mathbf{r}-\mathbf{r}')^2\right], \tag{2}$$

where α_i determines the spatial distribution of particle i in the particle emission source that is formed in a reaction. For internal wavefunctions of the composite particle "a", we assume the Gaussian distribution for each particle;

$$\phi_i(\mathbf{r}) = \left[\frac{2}{\pi\delta_i^2}\right]^{3/4}\exp\left[-\mathbf{r}^2/\delta_i^2\right]. \tag{3}$$

We can get the general expression of F_c using these assumptions as follows;

$$F_c = S_p 2^{9(A-1)/2}\pi^{3(A-1)/2}\left[\prod_{i=1}^{A}\left(\frac{1}{2\alpha_i^2+\delta_i^2}\right)^{3/2}\right] \times \left[\sum_{i=1}^{A}\frac{1}{2\alpha_i^2+\delta_i^2}\right]^{-3/2}, \tag{4}$$

where S_p is the spin factor. As an example we apply our result (Eq. 4) to calculate the formation cross section of pi-neut (πn^2). The pi-neut was searched in different systems and the upper limits of the formation cross section were determined.[3,4] The upper limits of the formation cross section correspond to the upper limits of F_c and those in turn restrict α and δ parameters. Although the α and δ were not measured directly in these reactions, the restrictions are strong in these cases because α is not expected to be much larger than the size of colliding nuclei ($\leq$ 5 fm) and thus δ has to be larger than 28 fm.[4] On the other hand δ needs to be small in size to make the pi-neut to be a bound system.[5] We conclude that the existence of pi-neut (πn^2) is strongly denied by the recent data.

References

1) S. Hirenzaki, T. Suzuki, and I. Tanihata: *Phys. Rev.*, **C48**, 2403 (1993).
2) H. Sato and K. Yazaki: *Phys. Lett.*, **98B**, 153 (1981).
3) T. Suzuki et al.: *Phys. Rev.*, **C47**, 2673 (1993).
4) F. W. N. de Boer et al.: *ibid.*, **D43**, 3063 (1991).
5) H. Garcilazo: *Phys. Rev. Lett.*, **50**, 1567 (1983).

Nuclear Recoil Effects in e^+-e^- Pair Production through 0^+-0^+ Transition

H. Sato

[e^+-e^- production, 0^+-0^+ nuclear transition, recoil effect.]

The spontaneous and induced positron decay of the vacuum in a supercritical field is one of the production mechanisms of positrons (e^+s) through low energy nuclear phenomena. Instead of the e^+ from the spontaneous vacuum breakdown, however, anomalous peaks (80 keV width at around 350 keV kinetic energy) in the energy spectrum of e^+ have been reported in heavy ion scattering experiments with GSI-UNILAC. Moreover, electron (e^-) peaks, whose energy coincides with those of e^+s, were also observed. And a coincidence between e^+ and e^- in the peak energy region was claimed. The presence of such a coincidence excludes the spontaneous e^+ emission mechanism as a source of the e^+ peak. The observed coincidence intensity and the shape of the spectra eliminate the possibility of known internal conversion processes. It is also pointed out that the narrow peak in e^+ spectra cannot be explained with the QED plasma consisting of e^+s, e^-s, and photons. The production of a new neutral particle, whose main decay mode is the e^+e^- pair production, is also implausible.

In this work, we study the nuclear recoil effect on the e^+-e^- pair production through 0^+-0^+ transition in terms of the nuclear center of mass motion trapped in the crystal lattice. We study the e^+ spectrum obtained in connection with GSI experiments with special attention. The effects of the thermal motion and the vibrational motion in the lattice are studied as a nuclear recoil. Figure 1 shows a typical e^+ spectrum without Coulomb correction in the e^+-e^- pair production through 0^+-0^+ transition, whose nucleus is trapped in the crystal lattice at 300 K thermal motion. The Coulomb correction reproduces the asymmetric shape in the e^+ spectra. A division of peak is found to be a typical feature of the nuclear recoil effect. A study of the relationship with GSI experiments is in progress.

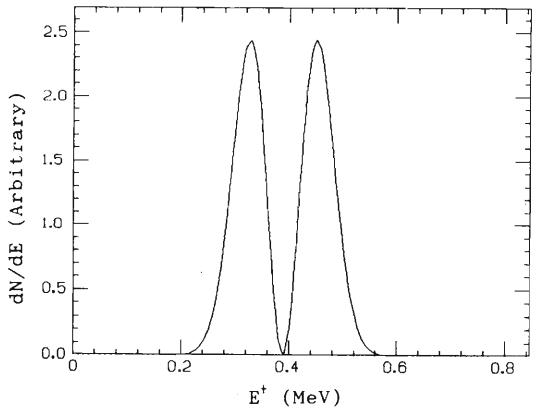

Fig. 1. Nuclear recoil effects on e^+ spectra in e^+-e^- pair production through 0^+-0^+ transition at temperature 300 K without Coulomb corrections.

Distribution of Perturbative Gluon in the MIT Bag Model

H. Kitagawa, Y. Nishino,* S. Tadokoro,** and T. Suzuki*

[perturbative gluon, MIT bag model, structure function.]

The structure function is one of the important observables to explore the properties of the nucleon. It can provide information of the nucleon from the data of the high energy lepton-nucleon deep inelastic scattering (DIS). The structure function is composed of two parts: the long-range part is assumed independent of the high momentum scale involved and is estimated using an effective model such as the bag models,[1] and the behavior of the short-range part is obtained by the perturbative QCD. By the QCD evolution to the relevant Q^2 scale, it is possible to compare the calculated structure function with the measured data. For this comparison, it is interesting to evaluate not only the non-singlet part which contains only the quark distribution, but also the singlet part in which both quark and gluon distributions are coupled. The gluon distribution has to be evaluated as the first step. We calculate it using the MIT bag model, and compare the result with the parametrization of Duke and Owens.[2]

We define the unpolarized gluon distribution assuming the light-cone dominance as

$$G(x) = -\frac{1}{2\pi Mx}\int d\xi^- \; e^{i\xi^- q^+} \left\langle p \left| F^{+\mu}(0) F^+_\mu(\xi^-) \right| p \right\rangle$$

where F is the color electro-magnetic tensor, q is the momentum transfer, M is the nucleon mass, and

$$\xi^- = \left(\xi^0 - \xi^3\right)/\sqrt{2}$$
$$q^+ = \left(q^0 + q^3\right)/\sqrt{2}.$$

It is possible to derive this expression by using the operator product expansion technique.[3] The product of the electro-magnetic current $J_\mu(\xi)$, whose Fourier transform is the hadronic tensor in the DIS, can be expanded in the operator product expansion as

$$\begin{aligned} J_\mu(\xi) J_\nu(0) &= \sum C \cdot \hat{\mathcal{O}}_{\mu\nu}\; \xi \cdots \xi \\ &= (\text{quark part}) + (\text{gluon part}) + \cdots \end{aligned}$$

where C and $\hat{\mathcal{O}}$ are the coefficient function and the operator respectively. By considering the gluon operator we can collect the gluon part, and obtain the above relation.

We estimate the expectation value of the gluon operator $\hat{\mathcal{O}}$ in the nucleon state, using gluon wave function of the MIT bag model,[4] which is obtained perturbatively from the quark wave function. For simplicity, we do not consider the momentum projection. The gluon distribution is calculated by the following equation,

$$G(r) = \frac{1}{4\pi Mx}\int dz \; \exp\left(\frac{iMxz}{\sqrt{2}}\right) \cdot \left\langle p \left| \sum_{i,j,a} B^a_i\left(-\frac{z}{2}\right) \cdot B^a_j\left(\frac{z}{2}\right) \right| \right\rangle$$

where B is the color magnetic field in the MIT bag model, and a is the color index.

Result of the calculation is shown in Fig. 1. Compared with the parametrization of Duke and Owens, our result of gluon distribution, $G(x)$, has strange oscillatory behavior and unphysical negative values. This oscillation is considered to reflect the feature peculiar to the MIT bag model, which has a rigid surface. It may be avoided by using other nucleon models, such as the soliton bag model, or by including the effect of the momentum projection.

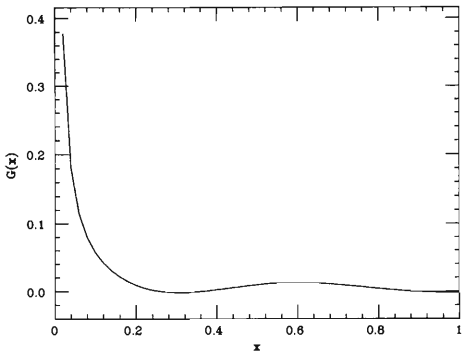

Fig. 1. Unpolarized gluon distribution, $G(x)$, calculated with the wave function in the MIT bag model is shown. The abscissa is the Bjorken variable, x, which represents the inelasticity of the scattering.

References

1) S. Tadokoro, H. Kitagawa, and T. Suzuki: *Phys. Rev.*, **D47**, 3045 (1993).
2) D. W. Duke and J. F. Owens: *ibid.*, **D30**, 49 (1984).
3) X. Ji: *Phys. Lett.*, **B289**, 137 (1992).
4) T. DeGrand, R. L. Jaffe, K. Johnson, and J. Kiskis: *Phys. Rev.*, **D12**, 2060 (1975).

* Research Center for Nuclear Physics, Osaka University
** Institute for Nuclear Study, University of Tokyo

Momentum Evolution of the Twist-three Part of the Spin-dependent Structure Function

H. Kitagawa, S. Tadokoro,* and T. Suzuki**

[structure function, momentum evolution, MIT bag model.]

It has become possible to investigate the structures of the nucleon by high energy lepton-nucleon deep inelastic scattering (DIS) experiments. By the recent developments of technology, the measurement becomes more precise, and we can discuss the observables which depend on the nucleon spin as well as fine structures of the nucleon. The observed asymmetry for scattering of polarized leptons off polarized nucleon target is expressed in terms of the structure functions by the following equation.

$$\left(d\sigma^{\uparrow\uparrow} - d\sigma^{\uparrow\downarrow}\right) / \left(d\sigma^{\uparrow\uparrow} + d\sigma^{\uparrow\downarrow}\right)$$
$$= D/W_1 \left[\left(M\nu G_1 - Q^2 G_2\right) + \eta\sqrt{Q^2}\left(MG_1 + \nu G_2\right)\right]$$

where D and η are kinematical factors, W_1 is the spin independent structure function, and G_1 and G_2 are the spin dependent structure functions. These structure functions almost scale in the Bjorken limit as

$$\begin{aligned} MW_1 &\rightarrow F_1 \\ \nu/M \cdot G_1 &\rightarrow g_1 \\ \nu^2/M^2 \cdot G_2 &\rightarrow g_2 \end{aligned}$$

aside from a small QCD scaling violation.

We have investivated the nucleon structure functions, whose low energy structures are estimated by the effective model of the nucleon, in particular, a bag model assuming the parton picture to hold.[1] In order to compare results of calculations with the observed values, these structure functions at low Q^2 have to be evolved to high momentum scales.

For the momentum evolution, we employ the renormalization-group equation, by which the Q^2 dependence of the perturbative parts is obtained. We assume that the remaining nonperturbative parts can be estimated by using the bag models. By the operator product expansion, these two parts are related with the moments which are obtained by the experiment, i.e.

$$\int x^n g_1(x,Q^2)dx = \frac{1}{2}a^n(\mu^2)F_2^n(Q^2,\mu^2)$$
$$\int x^n g_2(x,Q^2)dx = -\frac{n}{2(n+1)}$$
$$\cdot\left[a^n(\mu^2)F_2^n(Q^2,\mu^2) - d^n(\mu^2)F_3^n(Q^2,\mu^2)\right]$$

where $g_1(x,Q^2)$ and $g_2(x,Q^2)$ are the spin dependent structure functions, $a^n(\mu^2)$ and $d^n(\mu^2)$ are the low-momentum parts, and $F_2^n(Q^2,\mu^2)$ and $F_3^n(Q^2,\mu^2)$ are the twist-two and -three coefficient functions respectively, which are obtained by the perturbative QCD. The term "twist" is related to the dependence on Q^2 powers, and the "higher-twist" part can be obtained from the precise data. We investigate $g_2(x)$, observable of the transversely polarized spin state. This can be divided into two parts

$$g_2(x) = g_2^{WW}(x) + \bar{g}_2(x).$$

Since the twist-two part, $g_2^{WW}(x)$, is obtained directly from $g_1(x)$, whose behavior has been well investigated, we consider the remaining twist-three part, $\bar{g}_2(x)$. For simplicity, we calculate the second moment, whose momentum scale dependence has been given as,[2]

$$\int_0^1 x^2\bar{g}_2(x,Q^2)dx = -\frac{1}{3}d^2(\mu^2)\left[\frac{\alpha_s(Q^2)}{\alpha_s(\mu^2)}\right]^{77/81}.$$

We employ the MIT bag model,[3] then the nonperturbative part, $d^2(\mu^2)$, can be written analytically as,

$$d^2(\mu^2) = -\frac{1}{2M^2} < PS|\overline{\psi}(0)B\gamma\psi(0)|PS >$$

where M is the nucleon mass, ψ is the quark wave function, and B is the color magnetic field which is obtained perturbatively from the quark wave function. The final result is

$$d^2 = \frac{1}{2M^2V}\int d^3r\left[\left(R_1 + \frac{R_2}{3}\right)G^2 - \frac{1}{3}\left(R_1 - R_2\right)F^2\right]$$
$$R_1(r) = \left[2M(r) + \mu(R)/R^3 - \mu(r)/r^3\right]/4\pi$$
$$R_2(r) = 3\mu(r)/4\pi r^3$$
$$M(r) = \int_r^R dr'\ \mu'(r')/r'^3$$
$$\mu(r) = \int_0^r dr'\ \mu'(r')$$
$$\mu'(r) = 8\pi G(r)F(r)/3$$

where V is the bag volume, R is the bag radius, and $G(r)$ and $F(r)$ are the quark upper and lower components, respectively.

* Institute for Nuclear Study, University of Tokyo
** Research Center for Nuclear Physics, Osaka University

References
1) S. Tadokoro, H. Kitagawa, and T. Suzuki: *Phys. Rev.*, **D47**, 3045 (1993).
2) X. Ji and C. Chou: *ibid.*, **D42**, 3637 (1990).
3) T. DeGrand, R. L. Jaffe, K. Johnson, and J. Kiskis: *ibid.*, **D12**, 2060 (1975).

Color Confinement, Quark-Pair Creation and Dynamical Chiral-Symmetry Breaking in the Dual Ginzburg-Landau Theory

H. Suganuma, S. Sasaki,* and H. Toki

[color confinement, quark pair creation, chiral symmetry, abelian monopole condensation, dual Meissner effect, Schwinger mechanism.]

Recently, much attention has been paid on the dual Ginzburg-Landau theory[1] for the study of the color confinement of QCD. This theory is based on 'tHooft's idea,[2] that is, QCD is reduced to the abelian gauge theory with abelian monopoles in the abelian gauge. Like the superconductivity physics, condensation of such a monopole field leads to the dual Meissner effect, exclusion of the color-electric flux, which characterizes the color confinement.[1]

We study various features of nonperturbative QCD by using the dual Ginzburg-Landau Theory. To begin with, we derive the static potential between quark and antiquark with opposite color charge by considering the quark-current correlation,[1] in the pure-gauge case. The result of the quark potential is shown in Fig. 1. One finds good coincidence between our result and the Cornell potential, phenomenological one which reproduces the quarkonium data and lattice QCD data in the pure gauge.

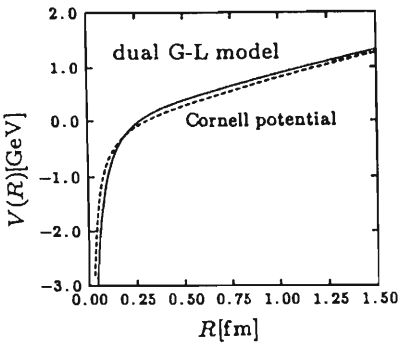

Fig. 1. The static quark potential in the quenched approximation. The dashed curve denotes the Cornell potential.

Thus the confinement for heavy quarks is shown in the dual Ginzburg-Landau theory. As for the string tension, we find that its expression corresponds to that of the energy per unit length of a vortex in the superconductivity physics.

Next, we study dynamical effects of light quarks. In particular, the quark-antiquark pair creation plays an important role in the screening effect of the confinement potential in the infrared region.[3] We estimate the quark-pair creation rate in the hadronic flux tubes by using the Schwinger formula,[4] and take account of the infrared screening effect for the confinement potential by introducing an infrared cutoff. Figure 2 shows the modification of the confinement potential, linear part of the quark potential, by the pair-creation effect. One finds the saturation of the confinement potential in a long-range region. Such a tendency has been found in the recent lattice QCD data with the dynamical quarks.[3]

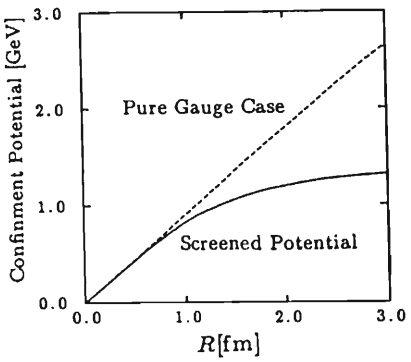

Fig. 2. The screening effect on the quark confinement potential. The dashed curve corresponds to the linear potential in the quenched approximation.

Finally, we study the dynamical chiral-symmetry breaking by solving the Schwinger-Dyson equation for the light quark field. We find that the dynamical chiral-symmetry breaking is largely enhanced by the abelian monopole condensation. The magnitude of the chiral-symmetry breaking, e.g. the pion decay constant or the chiral condensate, is well reproduced by using reasonable values for the gauge coupling constant and the QCD scale parameter in our case. (On the contrary, almost all studies have not been able to reproduce the enough amount of the dynamical chiral-symmetry breaking, unless a large gauge-coupling constant and a large QCD scale parameter are used.[5]) By extrapolating the dynamical mass to the time-like region, we find the absence of the physical poles in the quark propagator. Hence the confinement for light quarks is also shown as in the case of heavy quarks.

* Department of Physics, Faculty of Science, Tokyo Metropolitan University

References
1) T. Suzuki: *Prog. Theor. Phys.*, **80**, 929 (1988); **81**, 752 (1989).
2) G. 'tHooft: *Nucl. Phys.*, **B190**, 455 (1981).
3) L. I. Unger: *Phys. Rev.*, **D48**, 3319 (1993).
4) H. Suganuma and T. Tatsumi: *Prog. Theor. Phys.*, **90**, 379 (1993).
5) T. Kugo and M. Mitchard: *Phys. Lett.*, **B286**, 335 (1992).

First-Order Phase Transition with Global Z_3 and Z_4 Symmetry†

S. Ohta

[quantum chromodynamics, Potts model, first-order phase transition.]

Numerical calculation of pure-gauge lattice quantum chromodynamics (QCD) shows there is a weak first-order phase transition at a finite temperature. It is characterized by the global Z_3 symmetry of Polyakov lines and separates a low-temperature, color-confining and Z_3-disordered phase and a high-temperature, color-non-confining and Z_3-ordered phase. The existence of a first-order phase transition and its weakness are common to the systems with the global Z_3 symmetry such as the three-state Potts model. This work explains this weakness:[1–5)]

In the ordered phase, one of the three Z_3 spins is favored and dominates the volume. However, near the first-order phase transition, the other two Z_3 spins mix significantly into the system. In the three-state Potts model example, only about 60% of the volume is covered by the favored spin and the remaining 40% is evenly split between the two non-favored spins. These non-favored spins distribute in such a way that their neighborhoods are disordered, i.e. domains of disordered phase are mixed into the ordered phase. Such mixing leads to a small latent heat and weak phase transition.

Can we understand such mixing of disordered domains into the ordered phase? The two-point correlation functions, defined as the probability to find a pair of spin i and j separated by the distance r, provide the answer. The connected part of the correlation shows how the two spins interact: positive (or negative) connected part means attractive (or repulsive) interaction. It is found that most of the correlation functions are monotonous in the range r, either decreasing towards zero from above or increasing towards zero from below. Their asymptotic behavior is well described by single-component Yukawa forms, $\alpha \exp(-mr)/r$, in both ordered and disordered phases. A typical value of the correlation mass m near the phase transition is about 0.18, in accord with cluster sizes of several lattice spacings.

The only exception is the correlation between the two different non-favored spins in the ordered phase, which seems to have short-range repulsive and longer-range attractive components. The longer range should agree with the longest of the other correlation lengths, but is hard to confirm numerically. What is interesting is that their sum, the total connected correlation, is attractive in the relevant middle range of several lattice spacings and changes very slowly compared with the other correlation lengths. Indeed because this middle-range attraction lasts beyond the other correlations, its accumulated effect is at least comparable with those of the others and perhaps larger. Thus neighborhoods of the non-favored spins become disordered. This is also consistent with a vanishingly small surface tension at the ordered-disordered phase boundary which forbids formation of any spherical or convex cluster of like spins with a finite volume. Another calculation of mine suggests that the same mechanism works in pure-gauge lattice QCD thermodynamics.[4,5)]

Is this middle-range attraction unique to the systems with the global Z_3 symmetry? My numerical calculation of the two-point correlation functions in the four-state Potts model suggests it is. The model is governed by the global Z_4 symmetry, and has much stronger first-order phase transition separating ordered and disordered phases. In the ordered phase, the correlation among the different non-favored spins shows the same combination of short-range repulsion and longer-range attraction. But the sum dies out much more rapidly, within the ranges of the other correlations functions.[6)]

References

1) S. Ohta: Proc. Int. Symp. on Lattice '92, Amsterdam, 1992, eds. J. Smit and P. van Baal, *Nucl. Phys. B*, (Proc. Suppl.), **30**, 842 (1993).
2) S. Ohta: Proc. Int. Symp. on Computing in High Energy Physics '92, Annecy, 1992, eds. C. Verkerk and W. Wojcik, CERN Report, CERN, **92-07**, 361 (1992).
3) S. Ohta: *RIKEN Accel. Prog. Rep.*, **26**, 58 (1992).
4) S. Ohta: 48th Ann. Meet. Phys. Soc. Jpn., Sendai, Mar./Apr. (1993).
5) S. Ohta: preprint RIKEN-AF-NP-154; submitted for publication on *Phys. Rev. Lett.*
6) S. Ohta: Proc. Int. Symp. on Lattice '93, Dallas, Oct., 1993, *Nucl. Phys. B* (Proc. Suppl.) to be published.

† This work was supported in part by Parallel Computing Research Facility, Fujitsu Laboratory.

Study of α Decays Following ^{40}Ar Bombardment on ^{238}U

T. Nomura, M. Wada, N. Ikeda, S. Kubono, I. Katayama, Y. Pu, K. Morita, A. Yoshida, M. Kurokawa, T. Motobayashi, H. Murakami, Y. Nagai, H. Kudo, K. Sueki, M. Tanikawa,* I. Nishinaka, H. Nakahara, T. Shinozuka, M. Fujioka, H. Miyatake, Y. Fujita, T. Shimoda, and K. Tsukada**

[NUCLEAR REACTION, ^{238}U(^{40}Ar, α2n), E = 5.1 MeV/u; measured reaction products, α decays, spontaneous fission, time and position correlations; gas-filled separator.]

We performed an experiment on the ^{238}U(^{40}Ar, αxn) reaction using the RIKEN gas-filled separator (GARIS) to collect reaction products recoiling out of a thin target of ^{238}U. Their velocities and energies were measured by a time-of-flight system and a position-sensitive detector (PSD) placed before and at the focal plane of GARIS, respectively. Subsequent α decays and spontaneous fissions (SF) were also measured with the same PSD. The pulsed beam having the time structure of 10 ms beam-on and 10 ms beam-off was used. Details of the experimental set-up have been described in Ref. 1.

Based on the analysis of the time- and position-correlations as shown in Fig. 1, we have found a few α-decay events which have the following features: (1) α-decay energy is 9.37 ± 0.05 MeV; (2) they took place within 1 s after the recoil nuclei reached the PSD; (3) a few SF events occurred later at the same PSD position. These features are consistent with the theoretical prediction of decay properties of the yet unidentified nucleus ^{272}Hs, which was probably produced in the (^{40}Ar, α2n) reaction. However, its assignment is still indefinite because we are unable to find the expected α-decay of its daughter nucleus (^{268}Unh) because of its long half-life which is predicted to be around 1 h.

Improvement of the experimental set-up, such as that of position resolution of the PSD, is now in progress.

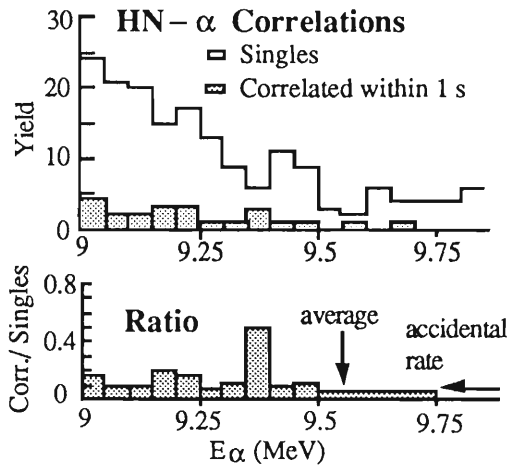

Fig. 1. (Upper) Singles and correlated α-decay spectra taken during the beam-off period of the pulsed beam. Only the heavy nuclei (HN) having the measured energies of less than 9 MeV are included in the HN-α correlations. (Lower) Ratios of the correlated events to singles events.

References

1) T. Nomura et al.: *RIKEN Accel. Prog. Rep.*, **26**, 9 (1992).

* Dept. of Chemistry, Univ. of Tokyo
** JAERI

Production of High-Spin Isomer Beam

T. Morikawa, Y. Gono, E. Ideguchi, A. Ferragut, Y. Zhang, T. Murakami, T. Kishida, K. Morita, A. Yoshida, H. Kumagai, M. Oshima, H. Kusakari, M. Sugawara, M. Ogawa, M. Nakajima, S. Mitarai, A. Odahara, T. Shizuma, M. Kidera, J. C. Kim, S. J. Chae, and B. J. Min

[Nuclear reactions, ^{24}Mg(^{136}Xe,$\alpha 9n$)^{147}Gd, ^{24}Mg(^{136}Xe,$11n$)^{149}Dy, ^{24}Mg(^{136}Xe,$10n$)^{150}Dy, E_p = 9 MeV/u, Recoil Separator, High-Spin Isomer Beams.]

We have developed a new experimental technique by utilizing the high-spin isomer beams produced via fusion-evaporation reactions. As reported in Refs. 1 and 2, it is possible to produce, via Xe-induced reactions of inverse kinematics, secondary beams consisting of the high-spin isomer. The unique character of this secondary beam is expected to enable us to study nuclear high-spin states of exotic condition. For the moment, the following experiments are being planned; a) Coulomb excitation for the search of off-yrast collective states built on the high-spin isomer. b) Secondary-fusion reactions for the efficient production of very high-spin states.

Since the cross section of the primary reaction is an order of 10^2 mb, the intensity of the secondary beam is very small as compared with that of the primary beam. For the utilization of the high-spin isomer beams for γ-ray spectroscopy, one needs the beam intensity of $> 10^5$ pps at least. In the beginning stage,[1] we have started with the beam-transport system with filling gases for charge equilibration. With this system, however, we could get the high-spin isomer beam of at most $\sim 10^4$ pps. This limitation came from both the poor transmission of $\sim$ 10% and the limit of the primary beam stably available below a few pnA.

In order to improve the transmission, we tried a new system without filling gases, since the numerical calculations of the beam optics predicted the transmission efficiency of $\sim$ 25% for the vacuum system by picking up the most probable three charge states. This predicted value is twice as large as the transmission for the gas-filled system.

As illustrated in Fig. 1, the new system has two focal planes, F1 and F2. A 3.6 mg/cm^2 ^{24}Mg target at F0 was bombarded by the primary beam of 9 MeV/u ^{136}Xe delivered from RIKEN Ring Cyclotron. The primary-beam intensity at F0 could be increased up to $\sim$ 10 pnA by the improvement in the RILAC injection system; in order to keep up with the large beam current, a new type of carbon stripper foil was used in the RILAC. The secondary beams of reaction products, mainly ^{147}Gd, ^{149}Dy, and ^{150}Dy, were electromagnetically separated from the primary beam, and focused on the PPAC at F1. A slit system just upstream of F1 was used for the elimination of both the primary beam and the stray beam. The reaction products were focused again by Q3 and Q4, and finally collected on the F2-focal plane where a plastic scintillator served as a catcher. A HP-Ge detector was set close to the catcher to detect the γ rays emitted from the reaction products.

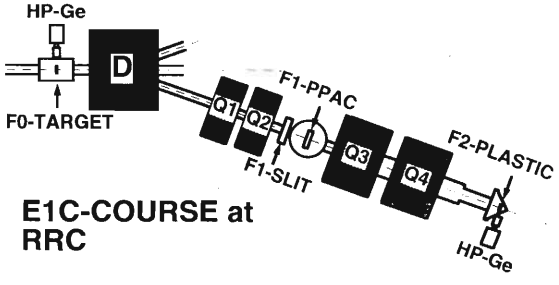

Fig. 1. Layout of the high-spin isomer beam facility at RIKEN RRC.

Optimization of the parameter setting for the magnets was made by monitoring a) the beam profile on the F1-PPAC, b) TOF spectrum between F1 and F2 and c) the γ-ray yield at F2. We obtained the best results with the parameters for the $B\rho$ value of ^{147}Gd 50$^+$ charge-state which corresponds to the fully stripped xenon ions. By using the catcher technique, we measured the transmission efficiency between F0 and F2 as well as the beam intensity at F2. As summarized in Table 1, the transmission of 20–30% was obtained for the reaction products of Xn channel, while the α channel marked a considerable drop of the transmission. This was due to the difference of angular spread caused by the particle emission. For ^{150}Dy produced via $10n$ channel, the intensity of 7×10^4 pps at F2 was realized with the primary beam intensity of $\sim$ 4 pnA. In addition, the beam-spot size was much reduced to 10$\sim$15 mmϕ as compared with 30$\sim$40 mmϕ of the gas-filled system.

Table 1. Transmission efficiency ε of the secondary beams with ^{147}Gd q = 50+ setting. The primary ^{136}Xe^{23+} beam was 9 MeV/u and 90 nA.

Nuclide		F0	F2	ε
^{147}Gd	$\alpha 9n$	5.9×10^4 pps	1.2×10^3 pps	2%
^{149}Dy	$11n$	1.6×10^4 pps	2.8×10^3 pps	18%
^{150}Dy	$10n$	2.2×10^5 pps	7.0×10^4 pps	32%

References

1) Y. Gono et al.: *RIKEN Accel. Prog. Rep.*, **26**, 12 (1992).
2) Y. Gono et al.: *Nucl. Phys.*, **A557**, 341c (1993).

High-Spin States of ^{144}Pm

Y. Zhang, Y. Gono, A. Ferragut, T. Morikawa, K. Morita, A. Yoshida, H. Kumagai, M. Oshima, H. Kusakari, M. Sugawara, M. Ogawa, K. Furuno,* T. Komatsubara,* J. Mukai,* J. Lu,* J. C. Kim, S. J. Chae, B. J. Min, and T. Murakami

[NUCLEAR REACTIONS ^{14}N(^{136}Xe,6n)^{144}Pm, 6.5 MeV/u, ^{138}Ba(^{10}B,4n)^{144}Pm, 42.5–55 MeV; Measured E_γ, I_γ, $\gamma\gamma$-coin, Excitation function, I_γ (θ).]

In a series of experiments searching for high-spin isomers in N = 82 region, a new isomer of a half life $T_{1/2} \sim 2.7$ μs with a probable spin value of 27$\hbar$ was found in ^{144}Pm.[1] Although a tentative decay scheme of this isomer was already reported,[2] a revised level scheme, which has been significantly extended, is given in this report.

Two experiments were performed. A nucleus ^{144}Pm was produced through a reaction ^{14}N(^{136}Xe,6n)^{144}Pm at a beam energy of 8.5 MeV/u which was provided by RIKEN Ring Cyclotron. Recoiled reaction products were collected on a catcher which was placed 6 m down stream from a target position. This distance corresponds to about 200 ns flight time. Gamma rays were detected by four HPGe detectors with BGO anti-Compton shields. $\gamma\gamma$-coincidence data were used to construct the level scheme.

An excitation function and γ-ray anisotropy were measured by using a reaction ^{138}Ba(^{10}B,4n)^{144}Pm with beam energies ranging from 42.5 to 55 MeV at Tandem Laboratory of Tsukuba University. The results of this experiments were also reported previously.[2]

Combining these experimental results, an extended level scheme of ^{144}Pm is proposed as shown in Fig. 1. Recently Glasmacher et al.[3] reported high spin states of ^{144}Pm studied by the ^{130}Te(^{19}F,5n)^{144}Pm reaction. They observed the levels up to the spin 20$\hbar$ state at 5.85 MeV. Most of the level structure is consistent with our results. However we could extend the level scheme up to the spin (27$\hbar$) state at 8.60 MeV.

In this level scheme, an 85.5 keV γ ray is placed to deexcite the isomeric state. Although this kind of low energy transition often causes isomerism, no such case has been observed in high-spin isomers of N = 83 isotones, ^{145}Sm, ^{147}Gd.

Systematic appearance of high-spin isomers at almost the same excitation energies in N = 83 isotones suggests that they originate from similar configurations. Probable configuration of the isomer of ^{144}Pm at 8.6 MeV may be obtained as $[\pi\{(h_{11/2})^2 d_{5/2}\}_{25/2^+}, \nu\{f_{7/2}h_{9/2}i_{13/2}\}_{29/2^+}]_{27^+}$ based on the deformed independent particle model.[4]

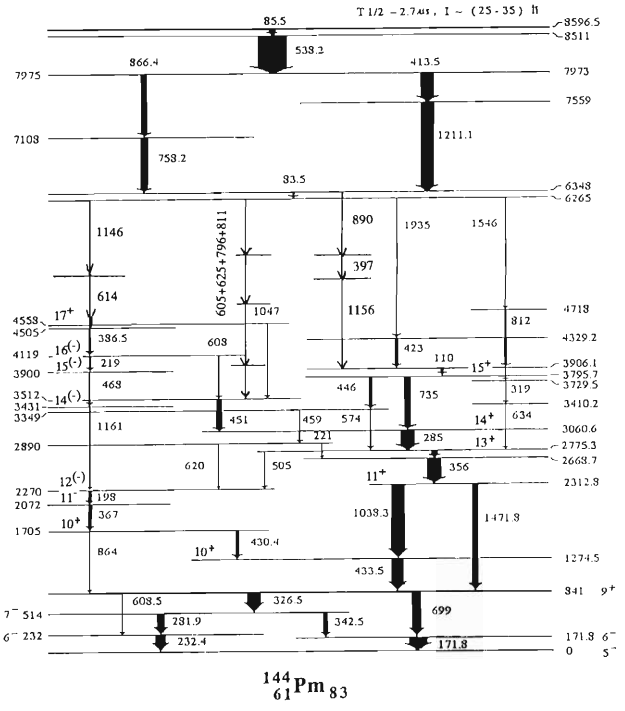

Fig. 1. Level scheme of ^{144}Pm.

References

1) T. Murakami et al.: *Z. Phys.*, **A345**, 123 (1993).
2) Y. H. Zhang et al.: *RIKEN Accel. Prog. Rep.*, **25**, 49 (1991).
3) T. Glasmacher et al.: *Z. Phys.*, **A345**, 119 (1993).
4) K. Matsuyanagi and H. Sagawa: Private communication.

* Tandem Accelerator Laboratory, University of Tsukuba

High-Spin States of ^{145}Sm

A. Odahara, Y. Gono, S. Mitarai, E. Ideguchi, M. Kidera, M. Shibata, T. Morikawa, K. Morita, A. Yoshida, H. Kumagai, A. Ferragut, Y. Zhang, M. Oshima, H. Kusakari, M. Sugawara, M. Ogawa, J. C. Kim, S. J. Chae, B. J. Min, and T. Murakami

[NUCLEAR REACTIONS ^{16}O(^{136}Xe,7n)^{145}Sm, 7.5 MeV/u, ^{20}Ne(^{136}Xe,α7n)^{145}Sm, 8.5 MeV/u, ^{139}La(^{10}B,4n)^{145}Sm, 47 MeV, ^{138}Ba(^{13}C,6n)^{145}Sm, 95 MeV; Measured E_γ, I_γ, I_γ (θ), $\gamma\gamma$-coin, Particle-γ coin, $T_{\gamma\text{-RF}}$.]

A new high-spin isomer was found in ^{145}Sm using the ^{16}O(^{136}Xe,7n)^{145}Sm reaction at the beam energy of 7.5 MeV/u.[1] To construct a decay scheme of the isomeric state, a $\gamma\gamma$-coincidence measurement was carried out by using the ^{20}Ne(^{136}Xe,α7n)^{145}Sm reaction at the beam energy of 8.5 MeV/u. The Xe beam was provided by RIKEN Ring Cyclotron. Since the decay scheme is too complicated to construct based solely on these data, the additional experiments were performed by using 5 or 6 sets of RIKEN BGOACS's and Tandem accelerators of Kyushu University and Japan Atomic Energy Research Institute. The 47 MeV ^{10}B beam was used at Kyushu University to make the ^{139}La(^{10}B,4n)^{145}Sm reaction. The 95 MeV ^{13}C beam was used to induce the ^{138}Ba(^{13}C,6n)^{145}Sm reaction.

Analyzing all these data, an extended decay scheme of the high-spin isomer of ^{145}Sm has been constructed as given in Fig. 1. The configuration of the isomer may be the same as that of ^{147}Gd,[2] i.e. $[\pi\{(h_{11/2})^2\}_{10^+}, \nu\{(h_{9/2})^{-1}i_{13/2}f_{7/2}\}_{29/2^+}]_{49/2^+}$. This assign-ment may be supported by the facts that the excitation energies of the isomers of ^{145}Sm and ^{147}Gd are about 8.5 MeV and the numbers of transitions de-exciting these isomers are roughly 50. The level scheme of ^{145}Sm was reported previously up to the $25/2^+$ state at the excitation energy of 3.48 MeV.[3] Although data analyses of the present results are still in progress, the angular distribution data indicated the spin assignments which are consistent with the reported ones.[3]

Interesting observation in the decay of the high-spin isomer is that there are some missing γ-ray intensities between about 3 and 6 MeV in the decay scheme. This fact was already pointed out in case of ^{147}Gd.[4] However the same was observed in ^{144}Pm[5] and also in

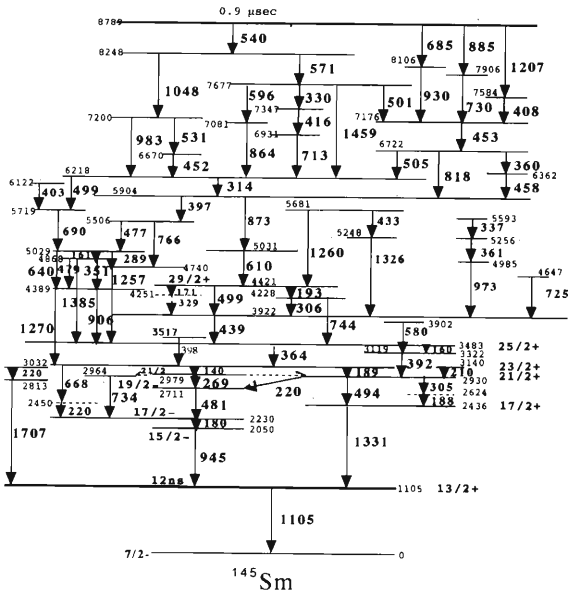

Fig. 1. Level scheme of ^{145}Sm.

^{182}Os.[6] So this phenomenon occurs rather commonly and seems to indicate that the decays of these high-spin isomers go through non-yrast states in these energy regions.

References

1) A. Ferragut et al.: *J. Phys. Soc. Jpn.*, **62**, 3343 (1993).
2) O. Häusser et al.: *Phys. Rev. Lett.*, **42**, 1451 (1979).
3) M. Piiparinen et al.: *Z. Phys.*, **A338**, 417 (1991).
4) R. Broda et al.: *ibid.*, **A305**, 281 (1982).
5) Y. H. Zhang et al.: This report, p. 32.
6) P. Chowdhury et al.: *Nucl. Phys.*, **A485**, 136 (1988).

Coincidence Measurements for Neutrons and α Particles from the Fragmentation of ^{6}He at 800A MeV

K. Yoshida, I. Tanihata, T. Kobayashi, T. Suzuki, S. Shimoura, K. Sugimoto,*
K. Matsuta,* S. Fukuda,* H. Wieman,** W. Christie,** and D. Olson**

[NUCLEAR REACTION ^{6}He(C, nα)X, E = 800A MeV; measured momentum distribution.]

Neutrons and α particles from the fragmentation of ^{6}He nuclei have been measured simultaneously at 800A MeV to study the structure of the halo nucleus ^{6}He. The ^{6}He nucleus is considered as a composite system with a core α particle and two valence neutrons that form the halo. Hence, the correlation between the neutron and the α particle is expected to have important information for the structure of the ^{6}He nucleus.[1)]

The experiment was carried out at the BEVATRON at Lawrence Berkeley Laboratory. Ions of ^{18}O were accelerated to 800A MeV and irradiated the Be target of 1″ in thickness to produce ^{6}He nuclei as the secondary beam. The secondary beam was purified by using the magnets of the transportation line B42 and was led to the reaction targets. The remaining contamination of the beam was identified and rejected by measuring the energy loss of a beam nucleus in a thin scintillator. The trajectory of a beam nucleus was also measured by three MWPC detectors. The reaction target was a carbon block of 5 g/cm^2 thickness. Charged particles from the fragmentation reaction of ^{6}He were measured by a HISS spectrometer and neutrons were detected by a plastic scintillator wall located at 10 m downstream of the reaction target.

The transverse-momentum distributions of neutrons and α particles show the two-Gaussian shape. The widths of the Gaussians are 40 and 110 MeV/c. Both widths are the same for neutrons and α particles. However, the distribution of neutrons has a larger contribution from the narrow component than that of α particles. The widths for α particles are consistent with the value obtained from the inclusive measurement at 400A MeV.[2)] In Fig. 1 shown is the momentum correlation function between the neutron and the α particle. The correlation function was deduced as $Y(P_n, P_\alpha)/\{\int Y(P_n, P_\alpha)dP_n \cdot \int Y(P_n, P_\alpha)dP_\alpha\}$, where $Y(P_n, P_\alpha)$ is the coincidence yield of the neutron and the α particle at momentums P_n and P_α, respectively. As seen in Fig. 1, the prominent feature of the correlation function is the two broad lines running parallel from the lower left to the upper right side of Fig. 1. A calculation with a simple kinematical model revealed that the lines can be reproduced with the assumption of the formation of the ^{5}He ground state. Thus the structure observed in the correlation function is due to the sequential decay of ^{6}He through the ^{5}He ground state and does not reflect the correlation between the neutron and the α particle in ^{6}He.

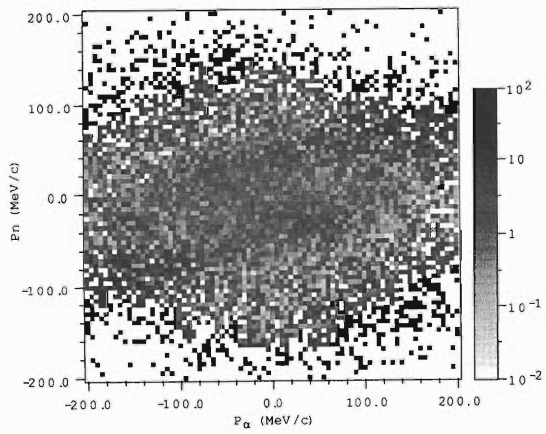

Fig. 1. Two dimensional plot of the correlation function of neutrons and α partilces from the fragmentation reaction of ^{6}He.

References

1) M. V. Zhukov, L. V. Chulkov, B. V. Danilin, and A. A. Korsheninnikov: *Nucl. Phys.*, **A533**, 428 (1991).
2) T. Kobayashi: *ibid.*, **A538**, 343c (1992).

* Osaka Univ.
** Lawrence Berkeley Laboratory, U.S.A.

Measurement of Light Charged Particle Emission in Coincidence with Fission Fragments from ^{84}Kr + ^{27}Al, ^{56}Fe at 10.5A MeV

Y. Futami, Y. Honjo, S. Tomita, T. Mizota, K. Yuasa-Nakagawa, H. Toyokawa, K. Furutaka, K. Matsuda, Y. Akeboshi, J. Kasagi, T. Nakagawa, S. M. Lee, and W. Shen*

[NUCLEAR REACTION ^{84}Kr + ^{27}Al, ^{84}Kr + ^{56}Fe, E(^{84}Kr) = 10.5 MeV/nucleon; measured light charged particle energy and angular distributions in coincidence with fission-like fragment.]

In a previous work,[1] we have studied the decay mechanisms of complex fragments from a hot compound nucleus (^{111}In, $E^* \approx 200$ MeV). These results (Z distribution of fragments, missing charge, etc.)[2] were compared with the theoretical calculations of the Extended Hauser-Feshbach method which considers all possible full statistical open channels giving binary divisions from the light particle emission to symmetric one in the highly excited compound nucleus.[3] It was concluded that the fission decays were dominant in the first-step calculation followed by post-evaporation. Data of the missing charges that correspond to total evaporated charged particles from a composite system were well reproduced by the calculations. The contribution to the predicted missing charge from pre-scission charged particle evaporation was calculated to be small compared to that from post-scission evaporation. Though the calculated results seem to be consistent with the observed data, there is a strong assumption embedded: the fission and the evaporation can compete equally even in the highly excited state of compound nucleus.

To verify this assumption and conclusion more directly, we performed a measurement of light charged particle multiplicity of pre- and post-scission evaporation. Multiplicity of protons and α particles was measured with coincident fission-like fragments for the reactions of ^{84}Kr + ^{27}Al, ^{84}Kr + ^{56}Fe at the incident energy of 10.5A MeV. The experiments were performed using the large cylindrical scattering chamber ASCHRA[4] of RIKEN Ring Cyclotron Facility. Heavy Fragments were detected by a time of flight counter telescope which consists of two channel-plate detectors and followed by an Si detector. This detection system was set at 10° with respect to the beam direction. Coincident light charged particles were observed using the 3π multi detector system that consists of 120 phoswich detectors and covers the angular range between 10° and 160°. The phoswich detector consists of thin plastic and thick BaF_2 scintillators that have good time response.[5] For each phoswich detector, the pulse shape discrimination technique was used, and it allowed us to identify γ-rays, neutrons, protons and α particles. To separate contributions of light particles from either prior to fission or after scission (fragment emission), it is quite powerful to use the correlation method between fission fragments and light charged particles using the characteristic difference of kinematics and source nature.[6,7] Energy spectra of protons and α particles were analyzed with a 3-source calculation[7] shown in Fig. 1. A pre-scission component from compound system and post-scission components from detected and undetected fragments of the charged particle multiplicity were extracted.

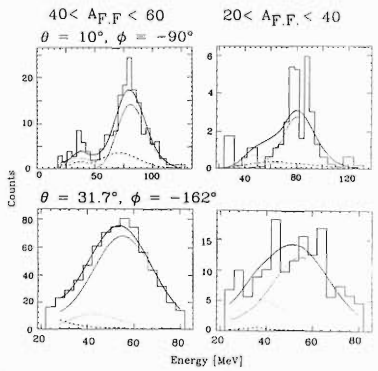

Fig. 1. Coincidence spectra (histograms) for α particle from the reaction 10.5A MeV ^{84}Kr + ^{27}Al overlaid by 3-source calculations (curves). The fitted post-scission, pre-scission and total spectra are shown by dashed, thin continuous and thick continuous lines respectively.

Contrary to the expectation, the experimental value of pre-scission charge multiplicity is 10 times as large as that calculated by the statistical model (GEMINI code[8]). This value corresponds to about 75% of total charge multiplicity. It may suggest that there is a hindrance effect of channels going to fission decays at first-step in the decay from a compound nucleus with high excitation energy and/or large angular momentum.

* Institute of Nuclear Research Academia Sinica, P. R. China

References

1) T. Nakagawa et al.: *RIKEN Accel. Prog. Rep.*, **26**, 14 (1992).
2) K. Yuasa-Nakagawa et al.: *Phys. Lett.*, **B283**, 185 (1992).
3) T. Matsuse et al.: Proc. Int. Symp. Nikko'91 (Nikko, June 1991) AIP Conf. Proc., **250**, 100 (1991).
4) T. Nakagawa et al.: *RIKEN Accel. Prog. Rep.*, **22**, 147 (1988).
5) Y. Futami et al.: *Nucl. Instr. Meth.*, **A326**, 513 (1993).
6) R. Lacey et al.: *Phys. Rev.*, **C37**, 2540 (1988).
7) L. Schad et al.: *Z. Phys.*, **A318**, 179 (1984).
8) R. J. Charity et al.: *Nucl. Phys.*, **A483**, 371 (1988).

Neutron Emission in the ^{40}Ar + ^{116}Sn Reactions at E/A = 30, 37 MeV/u

K. Furutaka, K. Yoshida, A. Yajima,* Y. Akeboshi,** K. Matsuda, T. Murakami, J. Kasagi, T. Nakagawa, K. Yuasa-Nakagawa, Y. Futami, A. Galonsky, and G. Bizard

[NUCLEAR REACTIONS: ^{40}Ar + ^{116}Sn at E/A = 30, 36.4 MeV; measured neutron energy spectra and angular distributions; moving source analysis.]

To study the properties of highly excited nuclei, we have measured energy spectra of neutrons emitted in ^{40}Ar + ^{116}Sn reactions at E/A = 30 and 36.4 MeV/u. Self-supporting foil of ^{116}Sn (about 1 mg/cm^2) was irradiated with 30 and 36.4 MeV/u ^{40}Ar beams of about 15 enA served from the RIKEN Ring Cyclotron. Neutrons emitted in these reactions were detected in coincidence with heavy evaporation residues (ER), with 22 liquid scintillation counters placed between 30 and 155 deg. with respect to the beam axis. Energies of neutron were measured through the Time-of-flight(TOF) method. TOF lengths ranged from 0.8 m to 2.4 m. Overall time resolution was about 1.5 ns (FWHM) for prompt γ-rays. Heavy residues were detected with 4 stacks of MCP-MCP-Si detector array and mass A_{ER} and velocity V_{ER} of evaporation residues were deduced. In off-line analysis, events were divided into 8 groups according to mass and velocity of heavy residues (2 mass bins $\times$ 4 velocity bins), and double-differential neutron energy spectra were obtained for each region.

The obtained spectra were analysed with the moving source model and multiplicity M, temperature parameter τ, and kinetic energy per nucleon ε were deduced. In the model, neutrons were assumed to be emitted isotropically from the sources. Two emission sources were needed to reproduce the spectra. One is a pre-equilibrium-like source whose velocity is roughly a half of the one for beam. The other is an equilibrium source moving with similar velocity to V_{ER}. Parameters obtained in the fitting are plotted in Fig. 1 against $R = V_{ER}/V_{FMT}$, where V_{FMT} is the velocity coresponding to the full momentum transfer. As seen in the figure, all parameters other than ε_{pre} are increasing functions of R. ε_{pre} is almost independent of R. No sizable increase is observed for M_{eq} by increasing incident energy, although apparent temperature τ_{eq} is increased. Detailed analyses are now under way.

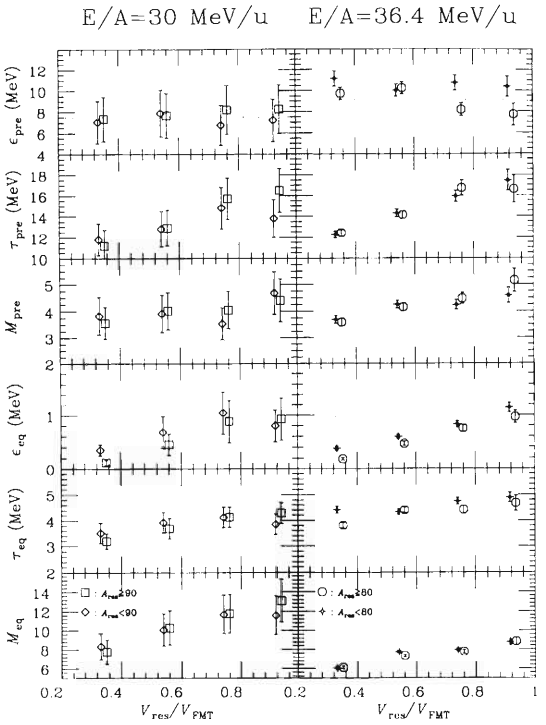

Fig. 1. Parameters obtained by the fit: M_{eq} (M_{pre}), τ_{eq} (τ_{pre}), and ε_{eq} (ε_{pre}) are multiplicity, temperature parameter, and kinetic energy per nucleon for an equilibrium (pre-equilibrium like) souce, respectively.

* Toshiba Electric, Co.
** Present Address: Mitsubishi Electric, Co.

Charged Particle Emission in ^{40}Ar + ^{nat}Ni Reactions at E/A = 30 MeV

K. Matsuda, Y. Akeboshi, K. Furutaka, J. Kasagi, T. Nakagawa,
K. Yuasa-Nakagawa, Y. Futami, and K. Yoshida

[NUCLEAR REACTIONS: ^{40}Ar + ^{nat}Ni at E/A = 30 MeV; measured charged particle energy spectra and angular distributions; moving source analysis.]

Properties of very hot nuclei have been studied through the heavy ion fusion reactions in intermediate-energy regions. In order to investigate the maximum excitation energy and the highest temperature that can be sustained by a nucleus, we measured charged particles in coincidence with heavy evaporation residues in the ^{40}Ar + ^{nat}Ni reaction at an incident energy of E/A = 30 MeV.

The experiment was performed in a large cylindrical scattering chamber ASCHRA and the beam was provided by RIKEN Ring Cyclotron. We constructed a 3π detector system consisting of 120 Phoswich Detectors (BaF_2 + Plastic scintillator) in order to detect and identify charged particles, neutrons and g-rays by this detector system.[1] This system gives us a unique method to determine the excitation energy of fusion products. The excitation energies can be extracted as a sum of kinetic energies of whole particles emitted from the excited nucleus in the reaction. The fusion residues were detected by four sets of telescopes placed at 10 degrees with respect to the beam axis. Each telescope consisted of two channel-plate detectors (CPD) and a silicon detector (SSD). The mass and the velocity of the residues were deduced from the time of flight and the total kinetic energies of residues which were measured by CPD's and SSD, respectively.

In the analysis, events were grouped into eight bins according to the mass of residues and the ratio $<R>$ between the residue velocities and those for the complete fusion residues. Figure 1 shows the obtained proton spectra in coincidence with residues in different velocities given by R and of mass = 45–60. The energy spectra were analyzed with the moving-source model. We assumed two sources, the fusion equilibrium source and the pre-equilibrium source, in this model since the spectra had two components and were not reproduced with one source. The results of moving-source fits were shown in Fig. 1 with solid lines. As seen, the observed spectra were well reproduced by the model. Further analysis is now in progress.

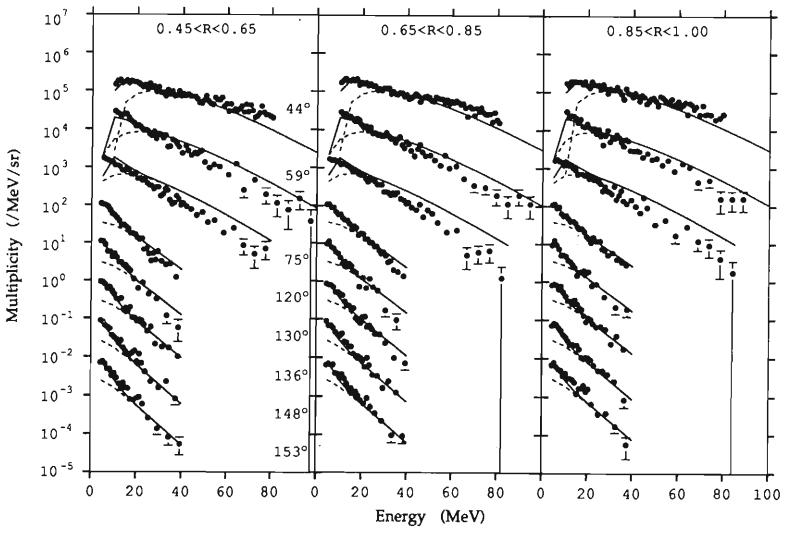

Fig. 1. Proton energy spectra observed in coincidence with residues in different velocities given by R and of mass = 45–60. Solid lines represent a moving-source fit with two sources, and dashed lines are contributions of pre-equilibrium emission. Note the change of ordinate scale by a factor of 10.

References

1) Y. Futami et al.: *Nucl. Instrum. Methods Phys. Res.*, **A326**, 513 (1993).

Spin-Isospin Excitation in sd-Shell Nuclei Studied by (d,^{2}He) Reactions

T. Niizeki, H. Ohnuma, T. Yamamoto, K. Katoh, T. Yamashita, H. Okamura, H. Sakai, S. Ishida, N. Sakamoto, H. Otsu, T. Wakasa, T. Uesaka, T. Ichihara, H. Orihara, H. Toyokawa, S. Kato, S. Kubono, and M. Yosoi

[NUCLEAR REACTION ^{28}Si, ^{26}Mg(d,^{2}He), E_d = 270 MeV.]

Gamow-Teller (GT) like transitions dominate small-angle spectra obtained in intermediate (p,n) reactions. The GT strength deduced from these reactions is roughly 2/3 of what one would expect from the sum-rule or from the most reliable shell-model calculations. The origin of such "missing strength" is the subject of many theoretical and experimental investigations at present. In order to obtain the GT strength corresponding to β^+ decays, it is necessary to study charge exchange reactions which increase T_z by one unit.

The (d,^{2}He) reaction is a unique tool for the study of spin-isospin excitation modes of nuclei, the GT strength in β^+ channel in particular, since ^{2}He particles are correlated proton pairs coupled to the singlet S state while the incident deuteron is in the triplet S state (with a small amount of triplet D mixture). Therefore, transitions with spin change of one unit is automatically selected, as well as the isospin change, in this reaction. The development of a large acceptance magnetic spectrometer SMART[1] at RIKEN has made it possible to study intermediate energy (d,^{2}He) reactions with good efficiency. It has been confirmed[2] that the (d,^{2}He) reactions on p-shell nuclei indeed excite selectively the GT-like states at small angles, and that the 0° (d,^{2}He) cross sections for such states are proportional to the GT strengths known from the β-decay measurements.

We have extended our study to sd-shell nuclei, and investigated the (d,^{2}He) reactions on ^{28}Si and ^{26}Mg. A comparison of the ^{28}Si(d,^{2}He)^{28}Al reaction with the ^{28}Si(p,n)^{28}P reaction will enable us to further establish the feasibility of using (d,^{2}He) reactions in the study of GT strength distributions in this mass region. Virtually nothing is known at present about ^{26}Na, the residual nucleus of the ^{26}Mg(d,^{2}He) reaction. A comparison of the spin strength distribution in such neutron-rich nuclei with shell model predictions will give us an important clue to explore the origin of missing strength problem.

A 270-MeV deuteron beam from the RIKEN Ring Cyclotron was led to the target located at the pivot of the beam swinger system in the E4 counting room. The targets were self-supporting foil of 50 mg/cm^2 thick ^{nat}Si and 2.6 mg/cm^2 thick ^{26}Mg enriched to 99%. The outgoing ^{2}He particles were analyzed by using a large solid angle magnetic spectrometer with wide momentum acceptance. Correlated proton pairs were detected in coincidence after the first dipole of the spectrometer. Two sets of multi-wire drift chambers (MWDC), each having six (X-X′-U-U′-V-V′) wire planes, and two sets of scintillation counter hodoscopes were used to identify protons and determine their trajectories. We have changed the counter gas for MWDC from Ar(70%) + iso-C_4H_{10}(30%) mixture previously used to Ne(20%) + C_2H_6(80%) mixture, and a helium bag was inserted between the exit window of the spectrometer and the counters, to reduce multiple scattering effects.

A sample spectrum from the ^{28}Si(d,^{2}He) reaction is shown in Fig. 1a. A strong peak at 2.0 MeV in ^{28}Al corresponds to the mirror state of the 2.1 MeV state in ^{28}P observed in the ^{28}Si(p,n)^{28}P reaction. The latter is reported[3] to have the GT strength B(GT) of 0.92. The (d,^{2}He) cross section at 0° observed in the present experiment is consistent with this B(GT) value. A 0° spectrum obtained for the ^{26}Mg(d,^{2}He) reaction is compared in Fig. 1b with the B(GT) strength distribution calculated with the shell-model wave functions.[4] The predicted distributions seem to be in good agreement with the present data. Further analysis of the experimental data is under way.

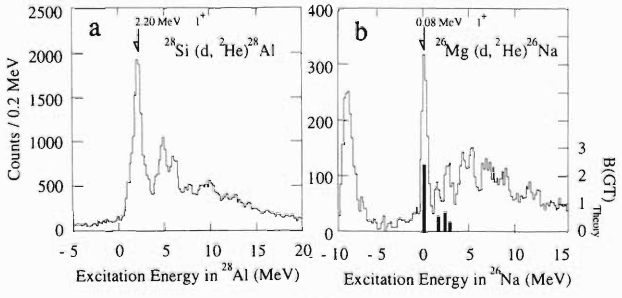

Fig. 1. Energy spectra of ^{2}He obtained at 0° for the ^{28}Si(d,^{2}He)^{28}Al and ^{26}Mg(d,^{2}He)^{26}Na reactions at E_d = 270 MeV. In Fig. 1b also shown the B(GT) distribution calculated from the shell-model wave function.

References

1) H. Ohnuma et al.: *RIKEN Accel. Prog. Rep.*, **21**, 164 (1987); **22**, 148 (1988); **24**, 108 (1990).
2) H. Ohnuma et al.: *Phys. Rev.*, **C47**, 648 (1993).
3) B. A. Anderson et al.: *ibid.*, **C43**, 50 (1991).
4) B. A. Brown et al.: Program OXBASH (unpublished).

Measurement of Analyzing Powers for the d + p Elastic Scattering at E_d = 270 MeV

N. Sakamoto, S. Ishida, H. Sakai, H. Okamura, H. Otsu, Y. Satou, T. Uesaka, T. Wakasa, K. Katoh, T. Niizeki, T. Yamashita, and K. Hatanaka

[NUCLEAR REACTIONS: d + p at E_d = 270 MeV; measured analyzing powers of A_y, A_{yy}, A_{xx}, A_{xz}.]

Complete set of analyzing powers A_y, A_{yy}, A_{xx}, and A_{xz} was measured for the d + p elastic scattering at E_d = 270 MeV. The angular distributions were obtained for the angles of the center of mass system from 57° to 138°. The vector and tensor polarized deuteron beams were provided by the RIKEN high intensity polarized ion source.

The measurement was carried out by using a scattering chamber installed in the beam transporting line of the Ring cyclotron. Four plastic scintillation counters ($\Delta\theta = 2.3°$) were placed at the same angles in the horizontal (left and right) and vertical (up and down) planes. In order to perform kinematically complete measurements, other four counters were placed at the angles for the recoil protons.

The target was a sheet of CH_2 with a thickness of 87 μm. The beam intensity on the target was 10–30 nA.

The tensor analyzing power A_{xz} measurement requires a polarized deuteron beam whose quantization axis lies in the scattering plane at a definite angle with respect to the incident beam direction. The spin axis was rotated into the horizontal plane, about 135° to the incident beam, by a "Wien-filter system" which is set at the exit of the ion source.

The beam polarizations were monitored continuously during the experiment by a polarization monitor system installed at the experimental room E3, downstream of the scattering chamber. Measured polarizations were typically 60–70% of the ideal values.

The result is shown in Fig. 1. The error bars include only statistical error. Theoretical analysis is now in progress.

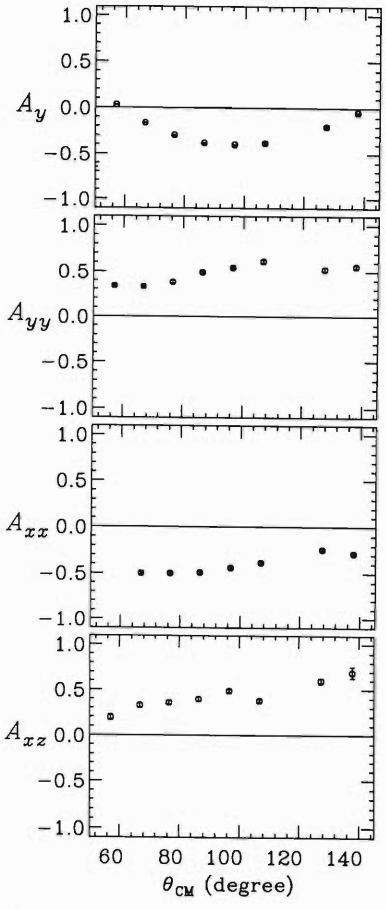

Fig. 1. Analyzing powers of the d + p elastic scattering at E_d = 270 MeV.

Measurements of the Tensor Analyzing Power Axx* for Deuteron Elastic Scattering from ^{12}C, ^{40}Ca, and ^{208}Pb at Ed = 270 MeV

T. Uesaka, K. Hatanaka, T. Ichihara, S. Ishida, T. Niizeki, H. Ohnuma, H. Okamura, H. Otsu, H. Sakai, N. Sakamoto, T. Wakasa, T. Yamamoto, and Y. Yano

[NUCLEAR REACTION ^{12}C, ^{40}Ca, and ^{208}Pb(d,d); tensor analyzing power.]

We measured the angular distributions of differential cross sections and Axx*'s for deuteron elastic scattering from ^{12}C, ^{40}Ca, and ^{208}Pb at Ed = 270 MeV using a polarized deuteron beam from the RIKEN High Intensity Polarized Ion Source. The beam polarization was measured at the AVF polarimeter and the D-room polarimeter and found to be about 50% of the maximum value.

Scattered deuterons were analyzed by the spectrograph SMART and detected at the secind focal plane F2. The detector system consisted of 8 MWDCs and trigger counters. The angular acceptance of F2 is about 8 degrees. We measured the angular distributions changing the incident beam angle with respect to the axis of the Analyzing Magnet by the Beam Swinger. The present data obtained with 5 separate Swinger angle settings cover from 5° to 37° in LAB-angle.

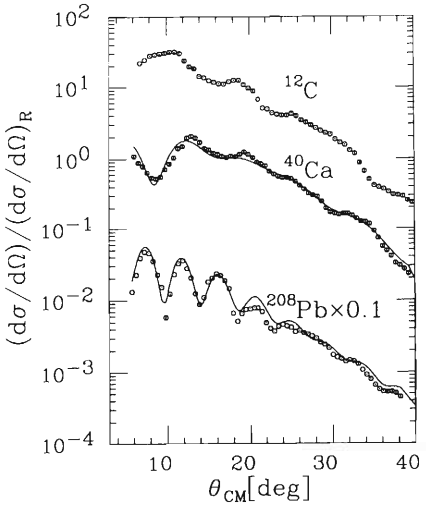

Fig. 1. Angular distributions of cross section for the deuteron elastic scattering from ^{12}C, ^{40}Ca, and ^{208}Pb at Ed = 270 MeV. The solid curves are the fits by the optical model calculation.

The angular distributions of differential cross sections are plotted as ratio-to-Rutherford in Fig. 1. The solid curves represent the fit by the optical model calculation. Figure 2 shows the tensor analyzing power Axx*, which is a combination of Axx, Ayy (, Azz), and Axz. (see Table 1)

Because deuteron spin precesses in the Swinger Magnet, the observed analyzing power depends on the Swinger angle. The error bars include the statistical errors and the errors of a beam polarization.

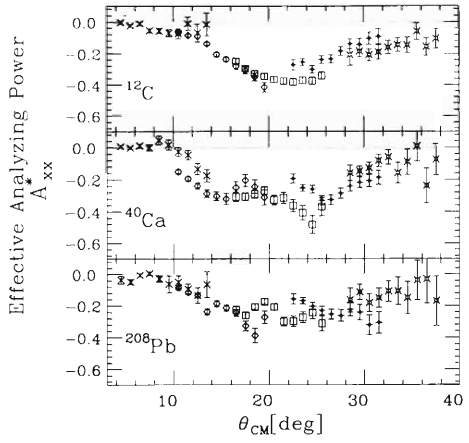

Fig. 2. Angular distributions of tensor analyzing power Axx*.

Table 1. Expressions of Axx*.

Swinger angle	Axx*
9°	0.90Axx + 0.030 (Ayy - Azz) - 0.13Axz
15°	0.80Axx + 0.056 (Ayy - Azz) - 0.17Axz
21°	0.70Axx + 0.090 (Ayy - Azz) - 0.20Axz
27°	0.56Axx + 0.13 (Ayy - Azz) - 0.24Axz
33°	0.40Axx + 0.17 (Ayy - Azz) - 0.24Axz

(^{12}C,^{12}N) Charge-Exchange Reaction at E/A = 135 MeV

T. Ichihara, T. Niizeki, Y. Fuchi,H. Okamura, H. Ohnuma, M. Hosaka, S. Ishida, K. Katoh, S. Kato, H. Kawashima, S. Kubono, S. Miyamoto, H. Orihara, N. Sakamoto, S. Takaku, Y. Tajima, M. Tanaka, H. Toyokawa, T. Uesaka, T. Yamamoto, T. Yamashita, M. Yosoi, and M. Ishihara

[NUCLEAR REACTION ^{12}C(^{12}C,^{12}N)^{12}B, E/A = 135 MeV.]

Charge-exchange reactions of the (n,p) type ($\Delta T_z = -1$) have recently attracted great interest because of their implications for astrophysical processes and for the quenching problem of the Gamow-Teller (GT) strength. Among a variety of charge-exchange reactions, heavy-ion induced reactions at intermediate energies would afford a unique means to study spin-isospin excitations. The applicability of the heavy-ion exchange reaction to the spectroscopy depends on whether it occurs via a direct one-step process.

One-step and two-step DWBA calculations show that in the E/A > 100 MeV region, a two-step process becomes negligible and a direct charge-exchange is dominant.[1,2]

The charge-exchange reaction of ^{12}C(^{12}C,^{12}N)^{12}B has been studied at E/A = 135 MeV using the spectrograph SMART at RIKEN.[3] Figure 1 shows the measured differential cross sections of the ^{12}C(^{12}C,^{12}N)^{12}B reaction leading to the ^{12}B (1^+) ground state. The differential cross sections of the elastic scattering of ^{12}C from ^{12}C were also measured to determine the optical potential parameters and they are plotted in Fig. 2.

Microscopic one-step DWBA calculations were performed with the code of Lenske et al.[1] by assuming the double folding model of the one-body transition density in the shell model and using the effective interaction of Franey and Love.[3]

The solid curve in Fig. 1 shows the result of the DWBA predictions. An excellent fit has been obtained for all the angle region. The dashed and dotted curves

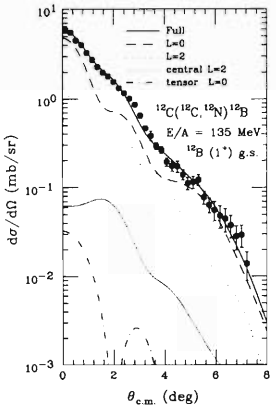

Fig. 1. Observed angular distributions of the ^{12}C(^{12}C, ^{12}N)^{12}B reaction.

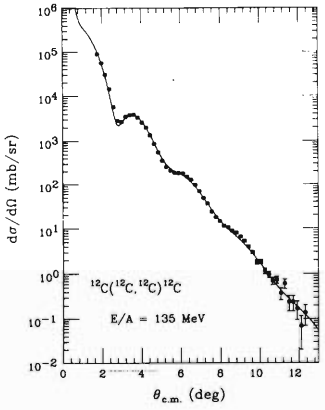

Fig. 2. Observed angular distributions of the ^{12}C(^{12}C, ^{12}C)^{12}C elastic scattering.

in Fig. 2 show the L = 0 and L = 2 components, respectively. The L = 0 component is mainly excited by the central part of the effective interaction, while the L = 2 component is mainly excited by the tensor part of the effective interaction.[2,4]

An intriguing observation in this figure is that the L = 0 component dominates over the L = 2 component. In particular the ratio of L = 0 to L = 2 is about 6 around 0°. This result differs significantly from that at E/A = 70 MeV,[1,2] where the contributions of the two components are comparable around 0° and a major fraction of the cross section is attributed to the L = 2 component (i.e. from the tensor interaction) for angles beyond 2°. This can be understood by the increased nuclear transparency at this energy region.[4]

The study of the ^{12}C(^{12}C,^{12}N)^{12}B charge-exchange reaction at E/A = 135 MeV shows that the cross sections for the $\Delta J\pi = 1^+$ transition can be quantitatively reproduced by the one-step DWBA calculation. This suggests that the heavy-ion charge-exchange reactions at this energy is dominantly the one-step process and a good spectroscopic tool for nuclear spin-isospin excitations.

References

1) H. Lenske et al.: *Phys. Rev. Lett.*, **1457**, 62 (1989).
2) N. Anantaraman et al.: *Phys. Rev.*, **C44**, 398 (1991).
3) M. A. Franey and W. G. Love: *ibid.*, **C31**, 448 (1985).
4) T. Ichihara et al.: *Phys. Lett. B*, to be published.

Measurement of Quadrupole Moments for the Neutron-rich Nuclei ^{14}B and ^{15}B

K. Asahi, H. Izumi, H. Ueno, K. Nagata, Y. Hori, H. Okuno, A. Yoshida,
T. Sekine, H. Sato, N. Aoi, G. Liu, M. Adachi, and M. Ishihara

[NUCLEAR REACTION ^{93}Nb(^{18}O, ^{14,15}B), $E/A = 70$ MeV/u, spin-polarized radioactive beams; measured β-NMR frequency; deduced quadrupole moments.]

The fragmentation of medium-energy heavy ions has been shown to be able to produce spin-polarized radioactive nuclear beams,[1] and in fact was utilized for measurements of magnetic moments of several nuclei.[2] In the present work we have applied this method to measurements of electric quadrupole moments for neutron-rich nuclei ^{14}B($I^\pi = 2^-$, $T_{1/2} = 12.8$ ms) and ^{15}B($I^\pi = 3/2^-$, $T_{1/2} = 10.3$ ms).

Experimental setup is similar to the previous experiment,[2] except for a part concerning the implantation and rf excitation for NMR. Fragments ^{14}B or ^{15}B emitted at $3.0° \pm 1.0°$ from an Nb target of 429 mg/cm^2 in thickness were accepted by the RIPS fragment separator.[3] The fragments were implanted in a stack of discs of single-crystal Mg placed at the final focus of the RIPS. An external field $B_0 = 30.6$ mT was applied in the z-direction defined normal to the reaction plane. After being stopped at a site in the crystal where an axially symmetric field gradient q was exerted, the fragment nuclei were exposed to an oscillating magnetic field. The up/down asymmetry of β-rays emitted from the stopper was observed in order to detect a spin flip transition induced by NMR.

The energy of a substate m of the nuclear spin I having the electric quadrupole moment eQ and the magnetic dipole moment $g\mu_N I$ is given by the first order perturbation theory as

$$E_m = -g\mu_N B_0 m + \frac{eqQ(3\cos^2\theta - 1)}{8I(2I-1)}[3m^2 - I(I+1)]$$

where θ denotes the angle of the principal axis of the field gradient relative to the z-axis. The transition between the states m and $m+1$ corresponds to the frequency $\nu_{m,m+1} = g\mu_N B_0/h - \nu_Q(3\cos^2\theta - 1)(2m+1)/4$, where ν_Q is defined as $\nu_Q = 3eqQ/[2I(2I-1)h]$. For a given ν_Q value, $\nu_{m,m+1}$ for all possible m can be calculated. In the present experiment, all these $2I$ different rf fields were simultaneously applied for each assumed value of ν_Q.

In Fig. 1 the observed β-ray up/down ratio with $\theta = 0°$ is plotted for fragments ^{14}B and ^{15}B, as a function of the assumed value for ν_Q, or eqQ/h. From the dip positions the quadrupole coupling constants were determined to be $|eqQ(^{14}\mathrm{B})| = 105.4 \pm 1.8$ kHz and $|eqQ(^{15}\mathrm{B})| = 134.5 \pm 2.7$ kHz. Taking the ratios to the ^{12}B result $|eqQ(^{12}\mathrm{B})| = 46.55 \pm 0.34$ kHz and using the reported values $|Q(^{12}\mathrm{B})| = 13.21 \pm 0.26$ mb,[4] the quadrupole moments were determined as $|Q(^{14}\mathrm{B})| = 29.9 \pm 1.0$ mb and $|Q(^{15}\mathrm{B})| = 38.1 \pm 1.3$ mb.

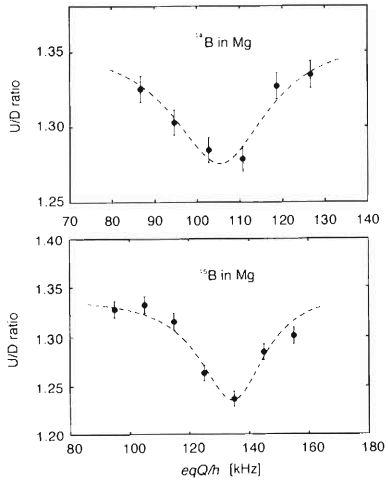

Fig. 1. Up/down ratio of the β-ray intensity as a function of the assumed value for eqQ/h, observed for ^{14}B (upper) and ^{15}B (lower) nuclei. The curves are results of the least-squares fitting with a Lorentzian function.

References

1) K. Asahi et al.: *Phys. Lett.*, **B251**, 488 (1990).
2) H. Okubo et al.: *Hyperfine Int.*, **78**, 97 (1993).
3) T. Kubo et al.: *Nucl. Instrum. Methods Phys. Res.*, **B70**, 309 (1992).
4) T. Minamisono et al.: *Phys. Rev. Lett.*, **69**, 2058 (1992).

The Solar Neutrino Production Reaction ^{7}Be(p, γ)^{8}B Studied by the Coulomb Dissociation Method

N. Iwasa, T. Motobayashi, M. Gai,[*1] S. Shimoura, T. Delbar,[*2] Y. Watanabe, T. Kubo, N. Inabe, Y. Futami, K. Furutaka, M. Kurokawa, H. Murakami, Y. Ando, T. Teranishi, K. I. Harn,[*3] Z. Zhao,[*4] R. H. France Jr.,[*1] T. Nakamura, S. Shirato, J. Z. Ruan (Gen), and M. Ishihara

[NUCLEAR REACTION ^{208}Pb(^{8}B,^{7}Be p)^{208}Pb, E = 47 A MeV.]

The low energy cross section for the ^{7}Be(p,γ)^{8}B reaction has been studied through the ^{8}B breakup process in the Coulomb field of ^{208}Pb at $E(^{8}\mathrm{B})$ = 47 A MeV. The cross section at E_{rel} = 0–20 keV is crucial in predicting the high-energy solar neutrino flux measured in the experiments of Davis et al.[1] and Kamiokande.[2]

An ^{8}B beam produced by the RIPS facility bombarded a ^{208}Pb target of 50 mg/cm^{2} thickness. The breakup products, ^{7}Be and proton, were detected in coincidence by a ΔE-E telescope of 1 m wide and 1 m height, set 5 m from the target with the symmetry axis along the beam line (Fig. 1). The ΔE-counter consisted of 10 plastic scintillators of 5 mm thickness and the E-counter consisted of 16 plastic scintillators of 6 cm thickness. At the center of the ΔE-counter an aluminum plate of 15 cm diameter and 4 mm thickness was settled to stop the beam. A helium-bag was set between the target and the detector to reduce multiple scattering and parasitic reactions.

The energies of the proton and ^{7}Be were determined by the TOF obtained by the signals from the telescope and a plastic scintillator placed at the second focal point in RIPS. The relative energy between the proton and ^{7}Be was obtained from their energies and positions of hit. The detection efficiency was calculated by a Monte Carlo simulation.

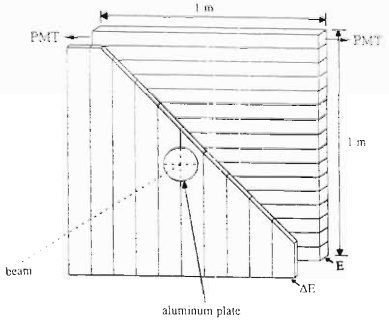

Fig. 1. Schematic view of the experimental setup.

*1 A. W. Wright Nucl. Struct. Lab., Phys. Dept., Yale Univ.
*2 Inst. Phys. Nucl. and Centre de Recherches du Cyclotron, Univ. Catholique de Louvain
*3 W. E. Kellogg Lab., California Inst. of Technol.
*4 Nucl. Phys. Lab. GL-10, Univ. of Washington

Figure 2 shows the astrophysical S-factor of the ^{7}Be(p,γ)^{8}B reaction obtained from the present experiment together with the existing (p,γ) data.[3] The present data are consistent with the data of Kavanagh, Vaughn et al. and Filippone et al. within the error. The extrapolation of the experimental S-factors to zero relative energy was performed with the help of an energy dependence proposed by Tombrello.[4] The result is slightly lower than the adopted value 22.4 ± 2.1 eV b of Bahcall et al.[5] and 21 ± 3 eV b of Turck-Chièze et al.[6]

The present data are limited in the energy range from 0.6 to 1.7 MeV. A measurement at lower relative energies with higher precision is under consideration.

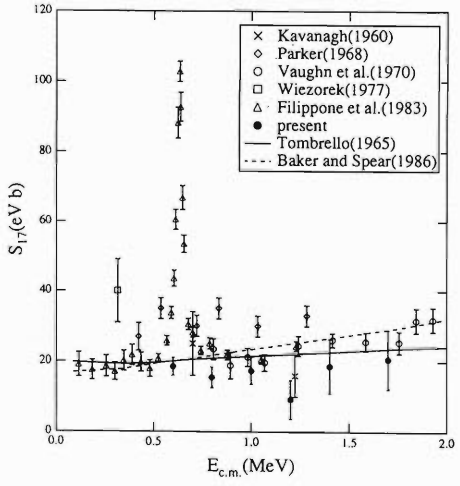

Fig. 2. The astrophysical S-factor for the ^{7}Be(p,γ)^{8}B as a function of relative energy.

References

1) R. Davis Jr. et al.: Proc. of the 21st Int. Cosmic Ray Conf., p. 143 (1990).
2) K. S. Hirata et al.: *Phys. Rev.*, **D44**, 2241 (1991).
3) B. W. Filippone: *Ann. Rev. Nucl. Part. Sci.*, **36**, 717 (1986).
4) T. A. Tombrello: *Nucl. Phys.*, **71**, 459 (1965).
5) J. N. Bahcall and R. K. Ulrich: *Rev. Mod. Phys.*, **60**, 297 (1988); J. N. Bahcall and M. H. Pinsonneault: *ibid.*, **64**, 885 (1992).
6) S. Turck-Chièze, S. Cahen, M. Cassé, and C. Doom: *Astrophys. J.*, **335**, 415 (1988).

Interaction Cross Sections and Radii of Mass Number A = 17 Isobars (^{17}N, ^{17}F, and ^{17}Ne)

A. Ozawa, T. Kobayashi, H. Sato, D. Hirata, I. Tanihata, O. Yamakawa,*1 K. Omata, K. Sugimoto,*2
N. Takahashi, T. Shimoda, D. Olson,*3 W. Christie,*3 and H. Wieman*3

[NUCLEAR REACTIONS Be,C,Al(^{17}N,^{17}N)X, Be,C,Al(^{17}F,^{17}F)X, Be,C,Al(^{17}Ne,^{17}Ne)X,
E/A = 700 MeV; measured interaction cross sections σ_1, deduced root mean square raii.]

Comparisons of radii between isobars have become possible with the use of radioactive nuclear beams. At relativistic and intermediate energies the isospin dependence of matter radii has been measured for light nuclei ($A < 20$) and strong isospin dependence has been shown.[1,2] With the exception of nuclei that have neutron halos, the observed global tendency was well reproduced by a Hartree-Fock (HF) model with a strong density-dependent interaction (Skyrme-III).[1] Isobars of mass number $A = 17$ provide a very wide span of $T_z = (N - Z)/2$ with 6 isobars. They include proton-halo candidates ^{17}Ne (S_{2p} ; separation-energy = 0.96 MeV) and ^{17}F (S_p = 0.60 MeV), and a neutron halo candidates ^{17}C (Sn = 0.73 MeV) and ^{17}B (S_{2n} = 1.21 MeV). Thus, these radii are interesting not only to see the isospin dependence in general, but also to search for halo nuclei.

The ^{17}Ne, ^{17}F, and ^{17}N secondary beams of about 700 A MeV were produced by projectile fragmentation of primary beam accelerated by the Bevalac at the Lawrence Berkeley Laboratory. The interaction cross section (σ_I) was measured by means of a transmission experiment with Be, C, and Al targets. Effective root mean square radii (RMS) are deduced from the σ_I's by a Glauber model calculation.[1]

The strong isospin dependence of RMS is seen in $A = 17$ isobars, as shown in Fig. 1. Steep increases of RMS at the proton-rich and neutron-rich sides are observed. To understand the reason for this increase, we performed the theoretical calculations for $A = 17$ isobars by using two microscopical models of the nucleus; the nonrelativistic HF model with a Skyrme-III potential[3] and the relativistic mean field model.[4] The results by these models reproduce the rough tendency of isospin dependence. However, at the proton-rich nucleus ^{17}Ne and the neutron-rich nucleus ^{17}B, the observed increases of radii are much stronger than the predicted ones. This anomalous enhancement of the radius in the same isobars suggests the existence of the proton halo in ^{17}Ne and the neutron halo in ^{17}B. However, our results show that RMS of ^{17}F is not larger than the systematics in $A = 17$ isobars. Thus, from the view point of matter size, no evidence is observed for a proton-halo in ^{17}F.

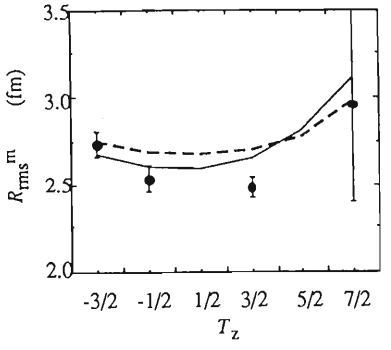

Fig. 1. The isospin dependence for RMS of mass number $A = 17$ isobars. The presently determined experimental values are shown by the closed circles. Dashed line shows RMS predicted by the nonrelativistic Hartree-Fock calculations with Skyrme-III potential. Predictions of the relativistic Mean Field calculations are shown by the solid line.

References
1) I. Tanihata et al.: *Phys. Lett.*, **B206**, 592 (1988).
2) A. C. C. Villari et al.: *ibid.*, **B268**, 345 (1991).
3) H. Sato and Y. Okuhara: *Phys. Rev.*, **C34**, 2171 (1986).
4) D. Hirata et al.: *ibid.*, **C44**, 1467 (1991).

*1 Fukui Univ.
*2 Osaka Univ.
*3 LBL, Berkeley, U.S.A.

Beta-delayed Neutron Decay of ^{19}C and Its Astrophysical Implications

A. Ozawa, R. N. Boyd, J. Kolata, F. Chloupek, G. Raimann, K. Yoshida, M. Fujimaki, T. Kobayashi, Y. Watanabe, I. Tanihata, S. Kubono, and K. Kimura

[RADIOACTIVITY ^{19}C(β^+ n); measured β-delayed E_n.]

In a recent study of inhomogeneous primordial nucleosynthesis models it was found that several critical points exist in the network of nuclides involved.[1] Specially, masses 15 and 18 are critical to synthesis of nuclides heavier than mass 20, as synthesis of either ^{15}N or ^{18}O will result in a cycling process which will preclude synthesis of heavier nuclides. ^{15}N is made by beta-decay of ^{15}C, so the strength of the ^{15}C(n, γ) reaction is crucial for regulating the synthesis of heavier nuclides. Similarly, ^{18}N is most likely to beta-decay to ^{18}O, from which it recycles back to ^{15}N, but the ^{18}N(n, γ) reaction could result in breakout from this lower mass cycle, creating heavier nuclides. Thus the latter reaction is also important in synthesis of heavy nuclides in the inhomogeneous models. Although some is known about the level structure in ^{16}C; this has allowed an estimate (actually a lower limit) to be made for the cross section, virtually nothing is known about levels above the n + ^{18}N threshold in ^{19}N. Thus, it is important to study such levels prior to attempting to measure cross section of the ^{18}N(n, γ) reaction. This can be done by measuring the energy of delayed neutron emission from the stopped ^{19}C nuclei, as shown in Fig. 1. We have measured the neutron energy by the time-of-flight (TOF) in the present experiment.

A ^{19}C beam of about 90 A MeV was produced by the projectile fragmentation of a primary beam ^{22}Ne accelerated by Ring Cyclotron and separated by the RIPS facility. The beam was stopped in a thin plastic scintillator ($\sim$ 10 mm) at the center of an array of neutron detectors. A beta ray emitted from stopped ^{19}C, which was a start signal for neutron TOF, was detected by triplet scintillators located up- and down-stream to the stopper. A delayed neutron emitted from levels above the n + ^{18}N threshold in ^{19}N was detected by the array of the neutron detectors that consist of three plastic walls ($100 \times 100 \times 6$ cm^3). The energy threshold

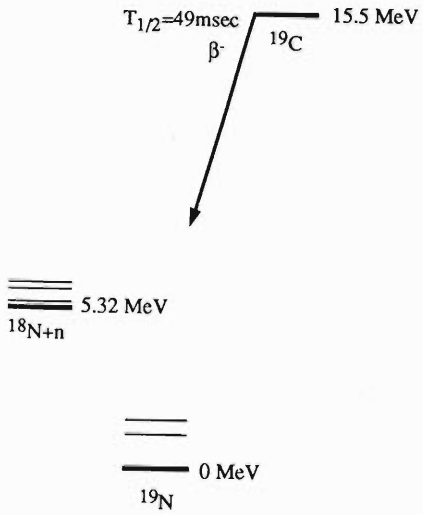

Fig. 1. Decay scheme of ^{19}C.[2]

for neutron in each neutron counters was set to be very low (around 200 keV). Neutron flight path was about 125 cm. For the calibration of neutron counters, beta delayed neutron emitted from ^{17}N was detected. Peak for 380 keV neutron was clearly shown on its TOF spectrum.

In order to assign levels above the n + ^{18}N threshold in ^{19}N, energies of gamma rays emitted from excited levels in ^{18}N and beta rays emitted from ^{19}C were also measured by two NaI scintillators (3″ ϕ) and a large ($10 \times 10 \times 10$ cm^3) plastic scintillator, respectively.

Analysis is now in progress.

References

1) F. K. Thielemann et al.: *Astrophys. J.*, (1994) to be published.
2) F. Ajzenberg-Selove: *Nucl. Phys.*, **A475**, 1 (1987).

The Decay of ^{14}Be

T. Kishida, T. Nakamura, G. Liu, Y. Watanabe, A. Yoshida, N. Aoi, M. Hirai, M. Ishihara, H. Okuno, H. Sakurai, T. Teranishi, H. Miyatake, T. Shirakura, E. Ideguchi, S. Shimoura, S. S. Yamamoto, M. D. Belbot, J. J. Kolata, and M. Zahar

[RADIOACTIVITY ^{9}Li(β^-); measured β-delayed neutron, triton, α and γ spectra; deduced logft. ^{14}B deduced level.]

In this report, we present the experimental arrangement and preliminary result of the recent experiment on the beta decay of ^{14}Be, which was performed using RIKEN Ring Cyclotron. The decay of ^{14}Be would be one of the promising processes in order to observe the super-allowed Gamow Teller (GT) beta-decay.[1)]

The super-allowed GT beta decays occur as beta decays to the GT giant resonance state. In our case, Sagawa estimated that the GT giant resonance state of ^{14}B would appear around 3 MeV lower than the ground state of ^{14}Be,[2)] which means that this excited state would be 13 MeV higher than the ground state of ^{14}B. This GT giant resonance state is unstable for particle decay; the kinematically possible final states are ^{13}B + n, ^{12}B + 2n, ^{11}B + 3n, ^{11}Be + t, ^{10}Be + t + n and ^{9}Li + α + n. We are, therefore, able to determine the energy level of the state by measuring the Q-value of the particle-decay modes listed above.

Figure 1 shows the arrangement of this experiment. Secondary beams of ^{14}Be were produced at the radioactive beam line RIPS from the fragmentation of 100 MeV/u ^{18}O primary beam by a Be target. These ^{14}Be's were transported to the experimental area and stopped in five-layers Si detectors which were placed at the final focus of the RIPS. The implanted ^{14}Be's decay with a life-time of 4.35 ms. The β rays from the decays were detected with scintillation counters. The beta-delayed charged particles were stopped in the same layer of Si where the mother ^{14}Be stopped. The kinetic energy of these charged particles were measured by the Si detectors. The beta-delayed neutrons were detected by three neutron counter walls which were placed 2 m apart from the final focus. The kinetic energy of neutrons was measured with the TOF method. Ge and NaI detectors were used to detect the beta-delayed γ emission.

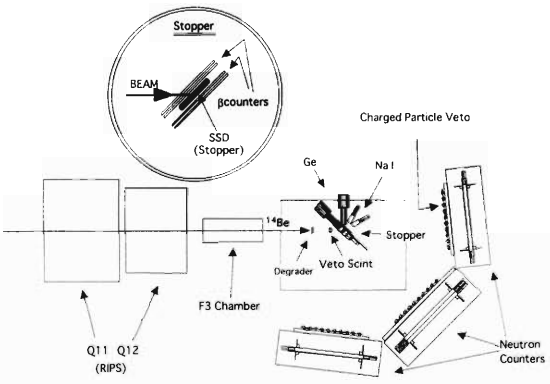

Fig. 1. Schematic diagram of the experimental arrangement.

The analysis of the data is now in progress. Figure 2 shows the TOF spectrum of a neutron counter. This spectrum contains information on the ^{14}B excited states via the reaction ^{14}B* $\rightarrow$ ^{13}B + n.

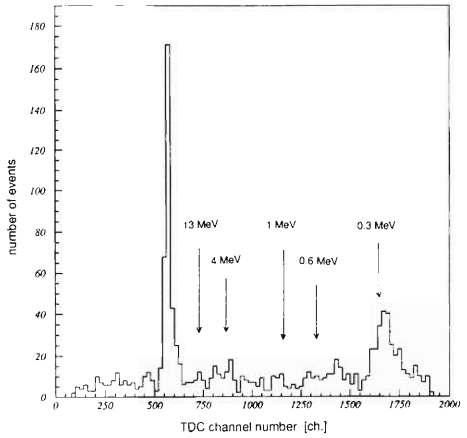

Fig. 2. TOF spectrum of a neutron counter. The values in the figure are the corresponding neutron kinetic energies.

References

1) H. Sagawa, I. Hamamoto, and M. Ishihara: *Phys. Lett.*, **B303**, 215 (1993).
2) Private communication.

Coulomb Dissociation of ^{11}Be

T. Nakamura, S. Shimoura, T. Kobayashi, T. Teranishi, N. Aoi, Y. Doki, M. Fujimaki, N. Inabe, N. Iwasa, K. Katori, T. Kubo, T. Suzuki, I. Tanihata, Y. Watanabe, A. Yoshida, and M. Ishihara

[NUCLEAR REACTION ^{11}Be + Pb, E(^{11}Be) = 72 MeV/nucleon,Coulomb dissociation, neutron halo; deduced dipole strength function dB (E1)/dE_x.]

One of the anomalous properties in halo nuclei is the low-lying dipole strength in the Coulomb dissociation. Earlier works on ^{11}Li[1-3] have shown that a peak appears at the excitation energy of about 1 MeV in the Coulomb dissociation energy spectrum. So far, however, the mechanism to yield such dipole strength has not been fully understood. One plausible mechanism is the excitation of a new collective mode, so called, the soft dipole resonance. The other is the direct breakup to continuum states. Here, we report results from a ^{11}Be + Pb reaction at 72 MeV/nucleon to disentangle the two possible mechanisms. The ^{11}Be nucleus was chosen for the sake of simplicity. Because ^{11}Be consists of a ^{10}Be core plus a single halo neutron, the excitation spectrum may be free from complication due to the two-neutron correlation expected in nuclei such as ^{11}Li.

The experiment was performed at the radioactive beam line RIPS at RIKEN Ring Cyclotron. The secondary ^{11}Be beam was produced and separated by the RIPS and was incident upon a Pb target. Two outgoing particles (n + ^{10}Be) from the dissociation process were measured in coincidence by using a system composed of a dipole magnet, a drift chamber, charged-particle hodoscopes and neutron counter walls. The excitation energy E_x was determined event-by-event by reconstructing the invariant mass of the excited ^{11}Be from the momentum vectors of detected particles.

Figure 1 shows the obtained excitation energy spectrum of Coulomb dissociation of ^{11}Be after efficiency correction and subtraction of the contribution from nuclear dissociation. The characteristic feature of the spectrum is a prominent peak which appears at E_x = 800 keV. The dipole strength function dB (E1)/dE_x was then deduced using the virtual photon theory,[4] as shown in Fig. 2. The deduced dipole strength function was analyzed in terms of the direct breakup of a halo nucleus, in which the dipole strength function for ^{11}Be is expressed in a simple analytical form as,[5]

$$dB(\mathrm{E1})/dE_x = N_S \times \mathrm{Const.} \times E_s^{1/2}(E_x - E_s)^{3/2}/E_x^4,$$

where N_S represents the spectroscopic factor for the $2s_{1/2}$ state and E_s represents the separation energy. We fitted the data with this function, taking N_S and E_s as free parameters. The effect of Coulomb post acceleration and the detector resolutions were evaluated

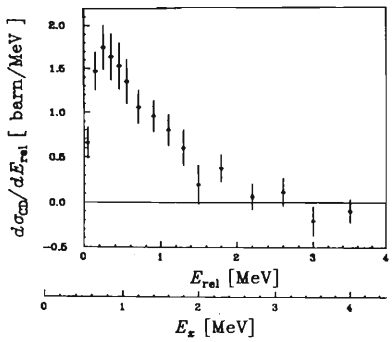

Fig. 1. The energy spectrum of Coulomb dissociation of ^{11}Be. $E_x = E_{rel} + E_s$.

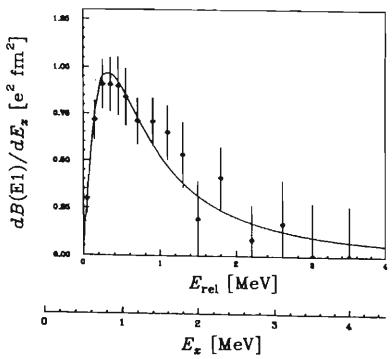

Fig. 2. Deduced B(E1) strength spectrum; open diamonds represent the B(E1) strength deduced from the data in Fig. 1. The solid line shows the dipole strength function analyzed based on the direct breakup picture (E_s = 540 ± 40 keV).

by Monte Carlo simulations and were incorporated in the fitting procedure. The solid curve corresponds to the E_s = 540±40 keV, where the best fit was obtained. The resultant value for E_s is in good agreement with the known separation energy of 504 ± 6 keV, which indicates that the direct breakup picture describes the Coulomb dissociation of ^{11}Be well.

References

1) S. Shimoura: Talk given at NFFS Conf. Bernkassel-Kues, Germany (1992).
2) K. Ieki et al.: *Phys. Rev. Lett.*, **70**, 6 (1993).
3) D. Sackett et al.: *Phys. Rev.*, **C48**, 118 (1993).
4) C.A. Bertulani and G. Baur: *Phys. Rep.*, **163**, 299 (1988).
5) G. Baur et al.: *Nucl. Phys.*, **A550**, 527 (1992).

Mass Dependence of Pion Production in Heavy Ion Collisions Near but Below Threshold†

J. Miller,*1 G. F. Krebs,*1 J. Panetta,*1 L. S. Schroeder,*1 P. N. Kirk,*2 Z. -F. Wang,*2 W. Bauer,*3 W. Benenson,*3 D. Cebra,*3 M. Cronqvist,*3 B. -A. Li, R. Pfaff,*3 T. Reposeur,*3 J. Stevenson,*3 A. V. Molen,*3 G. Westfall,*3 J. S. Winfield,*3 B. Young,*3 T. Murakami,*4 T. Suzuki, and I. Tanihata

[Nuclear reaction, subthreshold pion production, mass dependence.]

We have measured the inclusive cross section for production of negative pions near mid-rapidity in ^{20}Ne + NaF, ^{139}La + ^{139}La, and ^{197}Au + ^{197}Au collisions at $E = 183$ and $236A$ MeV. The reaction Au + Au is the heaviest system from which the subthreshold pion production has been measured to date. Primary beams were accelerated by the Bevalac at Lawrence Berkeley Laboratory and negative pions were detracted by a magnetic spectrometer.

Figure 1 shows the obtained inclusive cross sections of the negative pions. It shows an exponential dependence on pion energy that is typical of the pion production both above and below threshold. Also the other character shows no drastic change below and above the threshold.

The present data with other data at different energies give the almost constant yield ratio,

$$\frac{d\sigma}{d\Omega}(\mathrm{La} + \mathrm{La}) \Big/ \frac{d\sigma}{d\Omega}\ (\mathrm{Ne} + \mathrm{NaF}) = 20.$$

We compared these data with the results of two calculations based on the nuclear Boltzmann-Uehling-Uhlenbeck (BUU) equation. One is the perturbative calculation and the other is the non-perturbative calculation. We see that the perturbative BUU calculation gives better fit to the energy dependence of the ratio.

In conclusion, at these energies the pion production process is still dominated by nucleon-nucleon collisions.

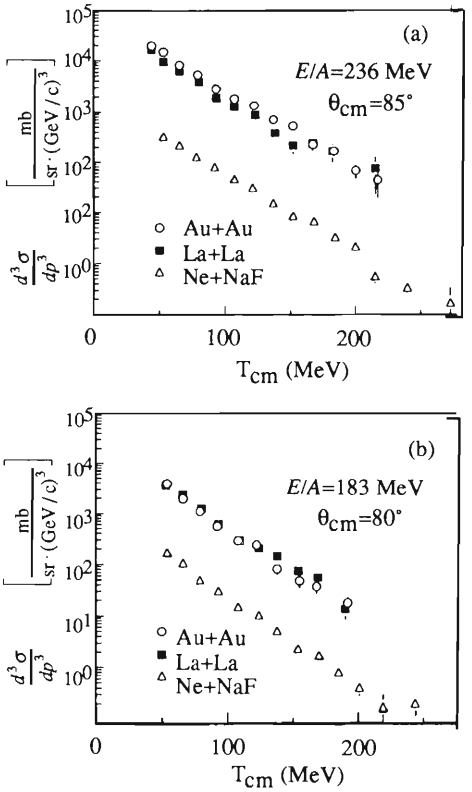

Fig. 1. Inclusive cross section versus pion kinetic energy in the center of mass for reactions at $E = 236$ A MeV (a) and at $E = 183$ A MeV (b).

† Extracted from Phys. Lett., **B314**, 7 (1993).

*1 LBL, Univ. of California
*2 Louisiana State Univ.
*3 NSCL, Michigan State Univ.
*4 Tokyo Institute of Technology

Are All Dripline Nuclei Spherical?

I. Tanihata

[Nuclear structure, Dripline nuclei.]

Recent development in high-intensity heavy ions at medium and high energies provided us explosive discoveries of new isotopes. As a result we now believe that the neutron drip line has been reached up to Z = 9 and the proton drip line has been reached up to Z = 18.[1] A pronounced systematics is seen in these driplines.

Let us consider adding two neutrons to a nucleus near the neutron drip line. When the two neutrons are added to a new orbital, it may form a bound or an unbound nucleus depending on the energy of the last orbitals. Suppose that the nucleus is bound and the last orbital has a degeneracy of more than two. Then the nucleus with two more neutrons is again bound because more binding energy is available. It is due to the increased number of two nucleon interaction chains and is seen in a relativistic mean field calculation.[2] This situation continues until this orbital is completely filled. The nucleus may become unbound only when two neutrons are added to a new orbital. The same is true for adding two protons to a nucleus near the proton drip line. The Coulomb repulsion may introduce a slight change but it is not seen in the following examination. Therefore the drip line indicates that the last orbital is completely filled there.

In the spherical shell model, an orbital has degeneracy of $2j + 1$. On the other hand the degeneracy is removed except for the nuclear spin in the deformed Nilsson orbitals and all of them have degeneracy of 2. As seen in Fig. 1, all dripline nuclei are consistent with the closure of spherical shell model orbitals in the order, except for the well known lowering of $2s_{1/2}$ for Be isotopes and probably the same effect for ^{17}Ne for the proton orbital.

It is found that the known drip lines can be understood as the closure of the spherical orbitals. It suggests that all known drip line nuclei are spherical. It would be interesting to see how it can be understood by a microscopic model of nuclei. This fact also gives the first visual effect of sub-shells to gross properties of nuclei. The changes of the order of shell orbitals are seen in the neutron drip line and possibly in the proton drip line. It is considered to be due to the character of a loosely bound orbital.

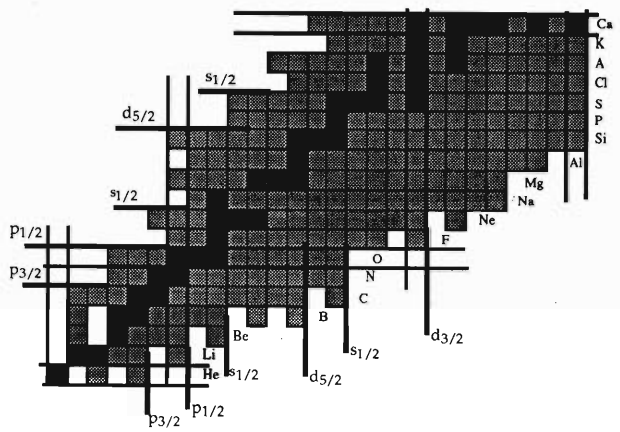

Fig. 1. A chart for light nuclei. Corresponding spherical shell model orbitals are shown by the thick lines. All dripline nuclei are consistent with the closure of the spherical orbitals.

References

1) A. C. Mueller and B. M. Sherrill: *Ann. Rev. of Nucl. and Part. Sci.*, **43**, in press.
2) D. Hirata, H. Toki, T. Watabe, I. Tanihata, and B. V. Carlson: *Phys. Rev.*, **C44**, 1467 (1991).

Experimental Study of the ^{8}He + p Elastic and Inelastic Scattering

A. A. Korsheninnikov, K. Yoshida, D. V. Aleksandrov, N. Aoi, Y. Doki, M. Fujimaki, N. Inabe, T. Kobayashi, H. Kumagai, C.-B. Moon, E. Yu. Nikolskii, M. M. Obuti, A. A. Ogloblin, A. Ozawa, S. Shimoura, T. Suzuki, I. Tanihata, Y. Watanabe, and M. Yanokura

[NUCLEAR REACTIONS, radioactive nuclar beam, p(^{8}He,p), p(^{8}He, p^{4,6,8}He), p(^{8}He,pn^{4,6}He), p(^{8}He,p2n^{4,6}He), p(^{8}He,2n^{4,6}He), p(^{8}He,n^{4,6}He), E/A = 72 MeV.]

The ^{8}He nucleus has the largest neutron to proton ratio among known bound nuclei and contains four valence neutrons, while neutron halo in ^{11}Li has two valence neutrons as well as in ^{6}He. To study structure of ^{8}He one needs data on the elastic scattering and excited states.

We studied the ^{8}He+p collisions using the ^{8}He beam produced by RIPS. The beam (72 ± 3 A MeV) hits targets CH_2 and C. Scattering angles and energies of recoil protons were determined by an SSD-telescope. Elastically scattered ^{8}He and ^{4,6}He from the ^{8}He decay were bent in a dipole magnet and measured by a drift chamber. To detect neutrons from the ^{8}He dissociation, we used 5 neutron walls.

Measured inclusive spectrum of protons is shown in Fig. 1A. A peak corresponding to the elastic scattering is clearly seen in the spectrum. The elastic scattering angular distribution is shown in Fig. 2A. Figure 1 shows also spectra for coincidences p+^{6}He, p+n, and p+^{6}He+n. Figure 1E shows the spectrum for coincidences p+^{7}He (^{7}He was selected from the invariant mass spectrum of ^{6}He+n). In all the spectra in Fig. 1B–E, a definite peak is observed at ~3.6 MeV. The ^{8}He excited state is also observed in the inclusive spectrum as shown in the inset in Fig. 1A. The observed

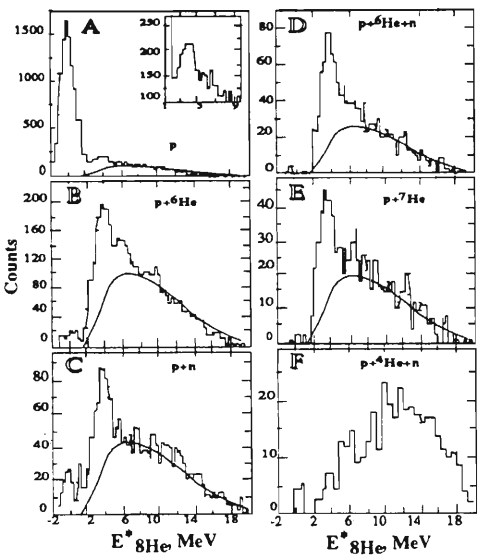

Fig. 1. Spectra of protons as a function of the ^{8}He excitation energy. Curves show calculations for final state interaction n+^{6}He at state ^{7}He.

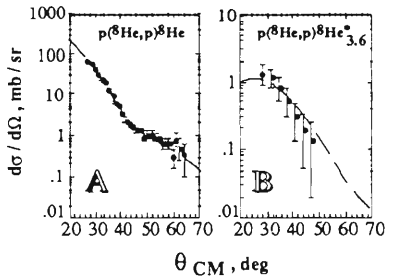

Fig. 2. Angular distributions for elastic (A) and inelastic (B) scattering ^{8}He+p. The curve in Fig. 2B shows the coupled channel calculation for $J^\pi = 2^+$ based on the elastic scattering calculation shown in Fig. 2A.

state ^{8}He* lies above thresholds ^{6}He+2n and ^{4}He+4n. The obtained parameters of the state are: $E^*_{^8\mathrm{He}} = 3.6 \pm 0.2$ MeV, $\Gamma < 1$ MeV, $\Gamma_{^4\mathrm{He}+4n}/\Gamma_{^6\mathrm{He}+2n} \leq 5\%$. The inelastic scattering angular distribution is shown in Fig. 2B. It is consistent with $J^\pi = 2^+$ for ^{8}He*.

We also applied invariant mass measurements and observed unstable states in ^{8}He, ^{7}He, ^{6}He, and ^{5}He. Figure 3 shows a spectrum for coincidences ^{6}He+n+n. In the spectrum, a definite peak is observed. Obtained parameters of the ^{8}He excited state are $E^*_{^8\mathrm{He}} = 3.55 \pm 0.15$ MeV, $\Gamma = 0.5 \pm 0.35$ MeV. They are in good agreement with the results obtained by the other method shown before and are colse to the results obtained in Ref. 1.

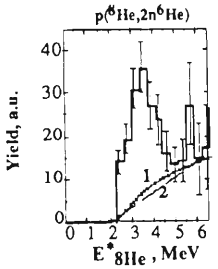

Fig. 3. Invariant mass spectra from reaction p(^{8}He, nn^{6}He). Curves show calculations for final state interactions ^{6}He+n (1) and n+n (2).

References

1) H. Bohlen et al.: Int. Conf. on Nuclei far from Stability, Bernkastel, Germany (1992).

Observation of ^{10}He

A. A. Korsheninnikov, K. Yoshida, D. V. Aleksandrov, N. Aoi, Y. Doki, M. Fujimaki, N. Inabe, T. Kobayashi, H. Kumagai, C.-B. Moon, E. Yu. Nikolskii, M. M. Obuti, A. A. Ogloblin, A. Ozawa, S. Shimoura, T. Suzuki, I. Tanihata, Y. Watanabe, and M. Yanokura

[NUCLEAR REACTIONS, radioactive nuclear beam, CD_2, C(^{11}Li, 2n^{8,6}He), CD_2, C(^{11}Li, n^{8,6}He), E/A = 60 MeV.]

We have carried out an experimental search for the superheavy helium isotope ^{10}He with taking into account the following two different mechanisms to produce ^{10}He: (1) The ^{10}He resonance can be manifested as a final state interaction of particles ^{8}He + n + n emitted in projectile fragmentation (e.g., in the ^{11}Li fragmentation). (2) One proton transfer reaction such as ^{11}Li + d $\rightarrow$ ^{10}He + ^{3}He can also produce ^{10}He.

The experiment was carried out using the secondary beam of ^{11}Li produced by RIPS. Invariant mass spectrum was measured for the ^{8}He + n + n and some other two and three particles in coincidence. The ^{11}Li beam with the energy 61 $\pm$ 3 A MeV hits thick targets CD_2 and C (390 mg/cm^2 and 280 mg/cm^2, respectively). Neutrons were detected by five layers of neutron walls. Charged particles were bent in a dipole magnet and then detected by a drift chamber and a scintillation counter hodoscope.

The resultant spectra are presented in Fig. 1 as a function of relative energy in the ^{8}He + n + n system, $E_{^{8}He-n-n}$. Figure 1A shows the distribution obtained with the CD_2 target. A strong peak is observed at $E_{^{8}He-n-n} \sim 1.2$ MeV. To see any possible target dependence of the spectrum, we show the corresponding spectrum for a deuteron target. As shown in Fig. 1B, a peak is seen at the same energy as in Fig. 1A. The corresponding spectrum of the C target also shows slight evidence of a peak at the same energy. Therefore it is considered that ^{10}He is produced in the projectile fragmentation of ^{11}Li nuclei.

We examined shapes of spectra from processes other then ^{10}He decay and considered different phase spaces and final state interactions between different particles. The results under various assumptions are shown by curves 1–5 in Fig. 1. They do not reproduce the observed peak.

Therefore the peak can be explained only as the ^{10}He resonance. The obtained parameters of the state

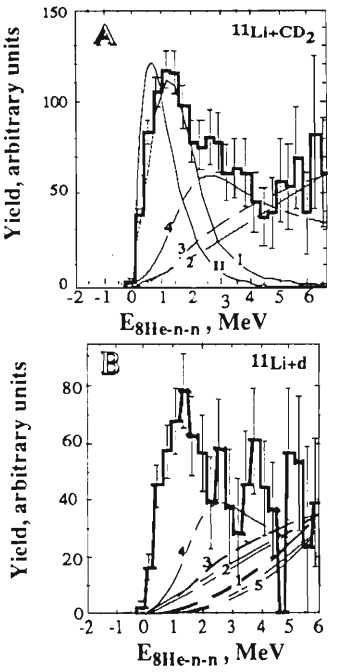

Fig. 1. Invariant mass spectra of ^{8}He + n + n from reactions: A, CD_2(^{11}Li, 2n^{8}He), B, d(^{11}Li, 2n^{8}He). Curves 1–5 show the phase space and final state interaction calculations under different conditions but without the ^{10}He resonance.

are: the energy above the ^{8}He + n + n threshold $E_{^{8}He-n-n} = 1.2 \pm 0.3$ MeV and the width $\Gamma \leq 1.2$ MeV. These parameters were found with taking into account uncertainty of the background subtraction (curves 1–5 in Fig. 1).

We also studied two particle coincidences ^{8}He + n. The main part of the ^{8}He + n spectrum is understood as a decay from the ^{10}He resonance. In the same experiment, we studied coincidences ^{6}He + n + n and ^{6}He + n and observed the known states ^{8}He* and ^{7}He.

Project at GSI "Determination of Neutron Skin Thicknesses for Na Isotopes"

T. Suzuki, T. Kobayashi, K. Yoshida, I. Tanihata, G. Münzenberg,* H. Geissel,*
K. Sümmerer,* F. Nickel,* W. Schwab,* H. Irnich,* K. H. Behr,* and K. Burkard*

[NUCLEAR REACTIONS; ^{40}Ar, ^{27}Al + Be, E = 1050 MeV/nucleon; Secondary beams; σ_I (^{A}Na + C, Al, Pb; A = 20–32); Density distribution; Relativistic Mean Field Theory.]

Recently, thick neutron skins are observed in ^{6,8}He, but extraction of the skin thickness is somewhat indirect because no information on radii of proton distribution is available.[1] However, for Na isotopes root-mean-square radii of the charge distribution were determined by the isotope shift measurements.[2] Therefore the measurement of the interaction cross sections σ_I, from which the matter radii are determined, provides the unique opportunity for direct comparison of difference between proton and neutron distributions.

For the measurement of the σ_I, we use the transmission method. For this method we identify and count the number of incident nuclei ($N_{\rm in}$) before the reaction target and then count the number of the same nuclei ($N_{\rm out}$), the nuclei without reaction, after the target. The σ_I can then be expressed as:

$$\sigma_I = \frac{1}{N_t} \ln\left(\frac{N_{\rm in}}{N_{\rm out}}\right).$$

The measurement of σ_I requires a separator of radioactive nuclei and a spectrometer after a reaction target. Although the FRS is designed for production of secondary radioactive beams, a large enough space is not yet available to put another spectrometer behind it. However, our study of its optics showed that a function of the FRS can be separated into two parts and we can use the FRS as the separator and the spectrometer simultaneously. Figure 1 shows this arrangement of the FRS.

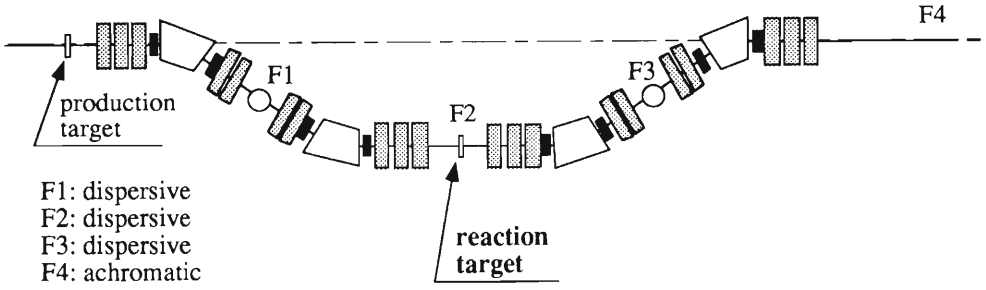

Fig. 1. The FRS separator and spectrometer at GSI for the interaction cross section measurement.

Radioactive nuclei produced via the projectile fragmentation are separated according to their A/Z at F1, then guided to the reaction target located at F2. Individual nucleus is identified by its TOF (between F1 and F2) and dE/dx. After the reaction target, non-interacted nuclei are guided through F3 to F4. These nuclei are identified again by their TOF (between F2 and F4) and dE/dx. The momentum and angular spreads of the incident beam to the reaction target can be adjusted so that all the non-interacted nuclei can reach F4. The momentum spread is restricted at F1 and F2 by selecting the beam position. The angular spread is selected by the incident angle of a nucleus into the reaction target. We can determine the σ_I with accuracy better than 1% unless counting statistics is limited due to the weak intensity of secondary beams.

Once this method is established, one can easily measure the σ_I of any secondary nuclei. Also the momentum distribution of the fragments from radioactive beams can be measured under the same geometry but changing the setting of magnets after F2.

The experimental system is now under construction. The first experiment is scheduled in coming spring.

References

1) I. Tanihata et al.: *Phys. Lett.*, **B289**, 261 (1992).
2) G. Hüber et al.: *Phys. Rev.*, **C18**, 2342 (1978).

* GSI, Darmstadt, Germany

2. Atomic and Solid-State Physics

Charge Asymmetry of Ionization Cross Sections of Atomic Hydrogen by Antiproton and Proton Impact

N. Toshima

The difference of the ionization cross sections of atomic hydrogen by antiproton and proton impact arises solely from higher-order perturbations since the first-order Born cross section does not depend on the sign of the projectile. Study of charge asymmetry of the ionization cross sections gives direct information of the effect of higher-order interactions. Ermolaev[1] calculated the ionization cross section of atomic hydrogen by antiproton impact by means of the coupled-channel method and compared the result with the ionization cross section by proton impact. The cross section ratio of the quantal calculation was different from the result of the CTMC (classical trajectory Monte Carlo) calculation.[2] The quantal ratio shows weaker energy-dependence than the classical one in the velocity range $1 < v < 5$ a.u., while the quantal ratio shows a broad maximum exceeding about 7% in the range $5 < v < 11$ a.u., where the classical ratio is almost constant and always smaller than unity. The structure of the quantal result in the higher-energy region was attributed to the Barkas effect which is by some reason missing in the classical description.

In this report we present the results of calculations by the coupled-channel method employing a large number of continuum states both on the target and on the projectile.[3] The eigenfunctions of each center are expanded further in terms of GTO basis functions generating the nonlinear parameters of the GTO as a modified geometrical progression. The expansion coefficients are determined so as to diagonalize the atomic Hamiltonian of the target and the projectile.[4] The GTO expansion method has the advantage that all the matrix elements can be evaluated analytically in contrast with the standard procedure based on the Slater-type orbital expansion, in which numerical integration is inevitable for two-center matrix elements.

The cross section ratios are plotted in Fig. 1. The present cross section ratio is closer to the classical value[2] than the result of Ermolaev.[1] The difference between the two quantal results arises mainly from the contribution of the projectile continuum states. The partial cross sections for the ionization into the target continuum states do not depend on the sign of the projectile charge strongly whereas the partial cross sections for the projectile continuum states do strikingly below 200 keV. We do not see a distinct Barkas effect around 1500 keV at variance with Ermolaev's result.

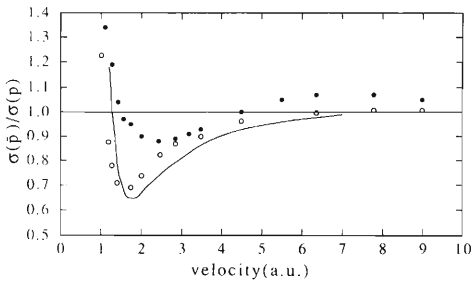

Fig. 1. The ratio of the ionization cross sections of atomic hydrogen by antiproton and proton impact. Open circles are present coupled-channel calculations and solid circles are from Ermolaev.[1] Solid line is the CTMC results of Schultz.[2]

The projectile continuum states are required even for the antiproton which interacts with the electron repulsively. They are necessary to make more complete the description of the electron-cloud distribution repelled by the antiproton. In this sense the ionization into the antiproton continuum is essentially different from the so-called capture to the continuum (CTC) component of positive ions.

References

1) A. M. Ermolaev: *Phys. Lett.*, **A149**, 151 (1990).
2) D. R. Schultz: *Phys. Rev.*, **A40**, 2330 (1989).
3) N. Toshima: *Phys. Lett.*, **A175**, 133 (1993).
4) N. Toshima and J. Eichler: *Phys. Rev. Lett.*, **66**, 1050 (1991); *Phys. Rev.*, **A46**, 2564 (1992); N. Toshima: *J. Phys.*, **B25**, L635 (1992).

Double Excitation of H^- by Fast Proton and Anti-Proton Impact II. Spectral Line-profile of an Ejected Electron from $2s2p\ ^1P^o$ Shape Resonance

K. Hino, M. Nagase,* H. Okamoto,** T. Morishita,** M. Matsuzawa, and M. Kimura

In a previous report,[1] we calculated the cross sections for the double electron excitation of H^- by the proton and anti-proton impact using the 67 state close-coupling (CC) calculation in comparison with experimental data.[2–4] Here we report the improved theoretical results within the same theoretical frame work.

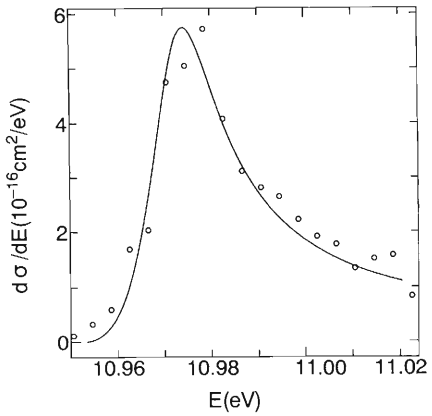

Fig. 1. Spectral line profile $d\sigma/dE$ of an electron ejected from the $2s2p\ ^1P^o$ state by proton impact at the incident energy of 1.5 MeV. open circle : experimental line profile obtained by Halka et al.[5] The excitation energy E is gauged from the ground state of H^- and calculated based on the Rydberg constant for the hydrogen atom $R_H = 13.59827$ eV.

To calculate the double electron excitation cross sections of H^- by the p and $\bar{p}$ impacts, we employ an improved basis set, *i.e.*, the 97 state one to expand the total wave function.

The set consists of the discrete $1s^2\ ^1S^e$, $2s^2\ ^1S^e$ and $2p^2\ ^1D^e$ states, the $2s2p\ ^1P^o$ shape resonance state and the $1skp\ ^1P^o$ continuum. These continua are properly discretized and incorporated into the CC calculation. Figure 1 shows the calculated line-profile of an ejected electron from the $2s2p\ ^1P^o$ shape resonance state by the p impact at 1.5 MeV/u in comparison with the data of the photodetachment of H^- observed by Halka et al.[5] for the decay into an H(N = 2) channel. (the experimental data are normalized to our theoretical results at the peak position.) The calculated results by the $\bar{p}$ impact are similar to those by the p impact. It is found that our calculated profile is in good agreement with the photodetachment data.

References

1) K. Hino et al.: *RIKEN Accel. Prog. Rep.*, **26**, 79 (1992).
2) P. W. Arcuni and D. Schneider: *Phys. Rev.*, **A36**, 3059 (1987).
3) J. O. Pedersen and P. Hvelplund: *Phys. Rev. Lett*, **62**, 2373 (1989).
4) J. P. Giese et al.: *Phys. Rev.*, **A42**, 1231 (1990).
5) M. Halka et al.: *ibid.*, **A46**, 6942 (1992).

* Berg Electronics
** Department of Applied Physics and Chemistry, University of Electro-Communications

Photodetachment Spectra of H^-

J. Tang, Y. Wakabayashi,* M. Matsuzawa, S. Watanabe, and I. Shimamura

Accurate *ab initio* calculations of the cross sections for photodetachment of H^- are few,[1] especially at photon energies near and above the threshold of the production of an H atom in an n=3 state. Discrepancy is found among these calculations, even for the broad shape resonance just above the $n = 2$ threshold. Only recently, the eigenchannel R-matrix method has been applied in a broader energy region ranging up to the $n = 4$ threshold.[1] We have recently proposed an accurate and powerful computational method, the hyperspherical close-coupling (HSCC) method, for two-electron atoms.[2] This method takes advantage of the hyperspherical coordinates, i.e., a pair of collective variables R and α, which replace the independent-electron radial coordinates r_1 and r_2. The hyperradius $R = \sqrt{r_1^2 + r_2^2}$ measures the 'size' of the electron pair and the hyperangle $\alpha = \arctan(r_2/r_1)$ describes the degree of radial electron-electron correlation. The accuracy and efficiency of the method have been demonstrated on various physical quantities of He.[3]

We apply the close-coupling method in terms of the hyperspherical coordinates to the two-electron system H^-. A two-dimensional matching procedure is used to connect the close-coupling wave function to an independent-electron wave function in the asymptotic region. The latter is described as the wave function of a detached electron moving in a dipole potential field of a neutral hydrogen atom. The total photodetachment cross sections and the partial cross sections for the production of H atoms in different states n are calculated up to the $n = 4$ hydrogenic threshold.

The quality of the wave function for the initial state of photodetachment of H^-, i.e., the ground ^1S state, is expected to be a decisive factor for the accuracy of the dipole matrix element. This is partly because the overlap integral between the initial and final states is small, and partly because the ground state of H^- is weakly bound. Using initial-state wave functions of varying degrees of accuracy, we found that the magnitude and shape of the $^1P^o$ shape resonance just above the $n = 2$ threshold depend sensitively on the initial-state wave function. This appears to be one of the reasons for the disparity among the cross sections in the literature.

Our calculated partial cross sections below the $n = 4$ threshold are substantially different from the results of eigenchannel R-matrix calculations.[1] In the R-matrix results, the partial cross section for the production of $H(n = 2)$ atoms is larger than that for the production of $H(n = 1)$ atoms at energies below the $n = 4$ threshold. This is difficult to understand in the nonresonant photodetachment, which is induced by a one-electron dipole operator. The $H(n = 1)$ production is a one-electron excitation process, while the $H(n = 2)$ production is a two-electron excitation process with one electron detached and the other excited; the latter process occurs only through the electron-electron correlation or configuration mixing. Our calculated results, as we expect, show that the $H(n = 1)$ partial cross section dominates over the $H(n = 2)$ partial cross section in the energy regions of nonresonant photodetachment, while the latter may be larger in some regions of resonances. In Fig. 1, the calculated total cross sections are compared with experimental spectra.[4,5] We see that the present results are in excellent agreement with experiments. Details of this work will be published elsewhere.[6]

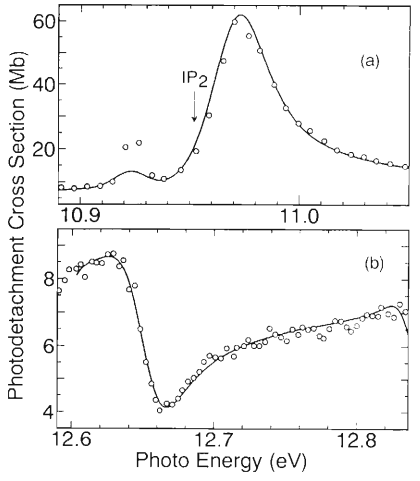

Fig. 1. Comparison of the calculated total photodetachment cross sections (solid lines) with experiments (circles) (a) near the $n = 2$ threshold and (b) below the $n = 3$ threshold.

References

1) H. R. Sadeghpour, C. H. Greene, and M. Cavagnero: *Phys. Rev.*, **A45**, 1587 (1992).
2) J.-Z. Tang, S. Watanabe, and M. Matsuzawa: *ibid.*, **A46**, 2437 (1992).
3) J.-Z. Tang, S. Watanabe, and M. Matsuzawa: *ibid.*, p. 3758; *ibid.*, **A48**, 841 (1993).
4) M. Halka et al.: *ibid.*, **A46**, 6942 (1992).
5) M. Halka et al.: *ibid.*, **A44**, 6127 (1991); M. Halka: Private communication.
6) J.-Z. Tang et al.: Accepted for publication in *Phys. Rev. A*.

* Dept. Appl. Phys. Chem., Univ. Electro-Commun.

Double Ionization of Helium by Compton Scattering

K. Hino, P. M. Bergstrom, Jr.,* and J. H. Macek*

Tunable, high intensity radiation from synchrotron sources has recently been applied to experiments measuring the ratio of double to single ionization of helium by photon impact, against which the current theoretical understanding of electron-electron interactions may be examined.[1] While the agreement between theory and experiment has been quite reasonable for photon energies from near threshold to 12 keV, Samson, Greene and Bartlett[2] have recently noted the importance of the Compton scattering process to the interpretation of these measurements. Indeed, most experiments have relied on measuring time of flight of residual ions, and have not yet been sensitive enough to discriminate ions produced by photoionization from those produced by Compton scattering. Here the ratio of double to single ionization for helium by photon impact reads

$$R = \frac{\sigma_{cs}^{2+} + \sigma_{ph}^{2+}}{\sigma_{cs}^{+} + \sigma_{ph}^{+}}, \qquad (1)$$

where σ_{cs}^{+} and σ_{cs}^{2+} are the single and double ionization cross sections by Compton scattering, and σ_{ph}^{+} and σ_{ph}^{2+} are counterparts by photoionization. The inability to distinguish between the two processes becomes problematic at high photon energies, where Compton scattering cross sections become comparable to photoionization cross sections at several keV and are dominant near 10 keV. Although the two distinct processes contribute to the overall ratio R of Eq. 1, experimental measurements for R above 6 keV take similar values to the theoretical asymptotic value of photoionization.

Here, we report the *ab initio* calculations of the double ionization of helium due to Compton scattering using the lowest-order many-body perturbation theory and the $\mathbf{A}^2$-approximation to the photon-electron interaction.[3] There exist substantial differences between Compton scattering and photoionization. (1) The most probable ejected energy of electrons, equivalent to the energy transfer of photons to an atom, by Compton scattering is significantly small relative to that of photoionized electrons.[2] (2) In photoionization, the non-relativistic dipole approximation to the photon-electron interaction is known to hold correctly to relatively high photon energy region due to a cancellation effect of relativistic and retardation effects. In contrast with that, the momentum transfer of photons to an atom is relatively large in Compton scattering and the dipole approximation is not valid.

We refer here to the contribution of Compton scattering to the ratio R of double to single ionization in helium at energies where this process is important. According to our calculations, Compton scattering dominates photoionization above 6 keV,[3] reflecting the importance of this process to the total ionization cross section at these energies. In Table 1 we tabulate our results for the overall ratio R as well as the individual ratios due to Compton scattering and photoionization at energies from 4 keV to 12 keV. Our overall ratio has a shallow dip structure around 6 keV, which corresponds to a transitional change of the dominant ionizing process from photoionization to Compton scattering. Furthermore, the Compton scattering ratio appears to be approaching to an asymptotic value of 1.66% at high energy, which is almost the same as the asymptote predicted for photoionization, despite the intrinsic differences between the two processes described above.

Table 1. Ratios (%) of double to single ionization cross sections of helium vs the incident photon energy ω (keV). R is the ratio defined in Eq. 1. R_{cs} and R_{ph} represent ratios due to Compton scattering and photoionization, that is $R_{cs} = \frac{\sigma_{cs}^{2+}}{\sigma_{cs}^{+}}$ and $R_{ph} = \frac{\sigma_{ph}^{2+}}{\sigma_{ph}^{+}}$, respectively.

ω	R	R_{cs}	R_{ph}
4.0	1.57	0.44	1.73
6.0	1.38	1.01	1.68
8.0	1.54	1.49	1.66
10.0	1.65	1.65	1.64
12.0	1.67	1.66	1.63

References

1) K. Hino et al.: *Phys. Rev.*, **A48**, 1271 (1993) and references therein.
2) J. A. R. Samson, C. H. Greene, and R. J. Bartlett: *Phys. Rev. Lett.*, **71**, 201 (1993).
3) K. Hino, P. M. Bergstrom, Jr., and J. H. Macek: *ibid.*, (submitted).

* Dept. of Phys. and Astronomy, Univ. of Tennessee, and Oak Ridge Nat'l. Lab.

Energy Shift in the Molecules $[(dd\mu)\text{-}d]ee$ and $[(dt\mu)\text{-}d]ee$

M. R. Harston, S. Hara, I. Shimaura, and M. Kamimura

Muon-catalyzed *d-t* fusion occurs within a molecule $[(dt\mu)\text{-}d]ee$, where d is a deuteron, t a triton, μ a negative muon, and e an electron. Therefore, the rate of the formation of this molecule in collisions of $t\mu$ with deuterium D_2 is crucial for determining the net rate of muon-catalyzed *d-t* fusion in D_2/T_2 mixtures. Similarly, the rate of the formation of the molecule $[(dd\mu)\text{-}d]ee$ in collisions of $d\mu$ with D_2 is crucial for determining the net rate of muon-catalyzed *d-d* fusion in D_2. These formation processes are resonance processes, and hence, the rates depend sensitively on the exact energy levels of the muonic molecules.

The sizes of the three-body systems $dt\mu$ and $dd\mu$ are much smaller than their distance from the other nucleus d and the size of the electronic orbitals. Hence, each of the muonic molecules may be approximated as consisting of two independent subsystems, namely the three-body system $dt\mu$ or $dd\mu$ and a deuterium-like molecule in which one of the d nuclei is replaced by a fictitious nucleus obtained by compressing $dt\mu$ or $dd\mu$ into a point charge.

The nonrelativistic energies of the isolated $dt\mu$ and $dd\mu$ were calculated accurately,[1] and were corrected for relativistic, hyperfine, finite-nuclear-size, vacuum-polarization, and other effects[2,3] as well as for the perturbation potential between the two subsystems.[2,4] The sum of these corrections agrees with experimental results for $[(dd\mu)\text{-}d]ee$ to within about 0.1 meV. However, this remarkable agreement must be fortuitous, since one of the corrections, at least, was not calculated to this high accuracy; a nonrelativistic perturbation correction of 1.0 meV was first calculated by use of the same method that led to a result 1.2 meV for $[(dt\mu)\text{-}d]ee$, which was proven later to be in error by a factor of 4.1,[4] and then scaled (without theoretical justification) by the same factor 4.1 to obtain a value 0.24 meV for $[(dd\mu)\text{-}d]ee$. Unfortunately, no calculations for $[(dd\mu)\text{-}d]ee$ of higher accuracy are found in the literature, and the error in the value 0.24 meV is difficult to assess. Here we intend to point out an effect that has been calculated by no other previous authors and that leads to a correction of the order of meV.

The perturbation potential may be divided into multipole interactions of $dt\mu$ or $dd\mu$ with the other deuteron and the electrons. The deuteron contribution to the first-order correction due to the monopole interaction V_0 is negligibly small. The first-order electron contribution due to V_0 scales in proportion to the electron density at and around the position of $dt\mu$ or $dd\mu$. In the literature, this contribution is calculated for a D-like atom model instead of the D_2-like subsystem in the unperturbed system, and is then scaled according to the electron-density ratio between these two cases.

The only big second-order term is the electron contribution that involves the dipole interaction V_1 twice. This term is calculated in the literature only for the D-like atom model and is scaled according to the electron-density ratio, although this scaling procedure is unjustified for this term. This term is fairly large and nearly cancels the first-order monopole term for the D-like atom model, as was predicted theoretically for this model.[5]

The first-order dipole correction vanishes exactly, and the largest contribution neglected so far is the first-order quadrupole contribution, which vanishes for the D-like atom model. We reported previously results for $[(dt\mu)\text{-}d]ee$ obtained by using an uncorrelated near-Hartree-Fock wave function for the D_2-like molecule.[6] In the present work, we have extended the calculations for $[(dd\mu)\text{-}d]ee$, using an elaborate configuration-interaction wave function.

A conspicuous aspect of the results for both $[(dt\mu)\text{-}d]ee$ and $[(dd\mu)\text{-}d]ee$ is that the quadrupole correction depends on the molecular rotational state and is as large as about 1 to 2 meV. Thus, the current excellent agreement between theory and experiment for $[(dd\mu)\text{-}d]ee$ is lost. This is in fact not surprising in view of the discussion in the third paragraph.

A question arises whether the first-order quadrupole term might be also canceled, to some extent, by the second-order dipole-dipole term if the latter is calculated accurately without making the usual scaling approximation. It is inconceivable, however, that this cancellation occurs for all important rotational states simultaneously, since these two kinds of terms depend on the rotational state in different ways. At any rate, the present work has proven definitely that the perturbation corrections found in the literature lack in a term, or perhaps terms, of the order of meV, whether or not they cancel each other to some extent.

References

1) M. Kamimura: *Phys. Rev.*, **A38**, 621 (1988).
2) D. Bakalov: *Muon Catal. Fus.*, **3**, 321 (1988).
3) K. S. Myint et al.: *Z. Phys.*, **A334**, 423 (1989).
4) A. Scrinzi and K. Szalewicz: *Phys. Rev.*, **A39**, 4983 (1989).
5) L. I. Menshikov: *Sov. J. Nucl. Phys.*, **42**, 918 (1985).
6) M. R. Harston, I. Shimamura, and M. Kamimura: *Phys. Rev.*, **A45**, 94 (1992).

Auger Monopole de-Excitation of the Muonic Molecule $[(dd\mu)_{1,1}dee]_{K,\nu}$

S. Hara, M. R. Harston, I. Shimamura, and M. Kamimura

The resonant formation of the muonic molecular ions $(dt\mu)_{1,1}$ and $(dd\mu)_{1,1}$ through reactions

$$t\mu + D_2 \rightarrow [(dt\mu)_{J=1,v=1}dee]_{K,\nu=2}, \quad (1)$$

$$d\mu + D_2 \rightarrow [(dd\mu)_{J=1,v=1}dee]_{K,\nu=7}, \quad (2)$$

plays an important role in the so-called muon catalyzed fusion processes in hydrogen isotope mixtures. In the above equations, J and v denote the rotational and vibrational quantum numbers of muonic molecular ions and K and ν, those of the muon molecular complexes $[(dt\mu)dee]$ and $[(dd\mu)dee]$, respectively. The direct fusion rate of the $(J = 1, v = 1)$ state of muonic molecular ions is small because of the large distance between two nuclei and the fusion mainly occurs in the lower (0,1), (0,0), and (1,0) states. Such lower states are formed by the Auger transitions

$$[(dt\mu)_{1,1}dee]_{K,2} \rightarrow [(dt\mu)_{J',v'}de]^{+}_{K',\nu'} + e, \quad (3)$$

and

$$[(dd\mu)_{1,1}dee]_{K,7} \rightarrow [(dd\mu)_{1,0}de]^{+}_{K',\nu'} + e. \quad (4)$$

So far, several authors[1-3] investigated the Auger dipole transition rate for reaction (3) in various approximations.

For $(dd\mu)_{1,1}$, the Auger dipole transition does not occur up to the first order since all the bound states of $(dd\mu)$ molecular ion have the same(gerade) parity under inversion of the muon coordinates. Therefore, the monopole transition (4) becomes the key reaction for the $(dd\mu)$ fusion. The monopole transition rate λ for reaction (4) is given, in the first order perturbation theory, as follows;

$$\lambda = 2\pi/\hbar\Sigma\, |< \Phi_{1,1}\Psi_i|\, V_m\, |\Phi_{1,0}\Psi_f >|^2, \quad (5)$$

where Φ and Ψ are the wave functions for the $(dd\mu)$ molecular ion and the molecule "D_2" (or "$D_2^+ + e$" for the final state), respectively, V_m is the monopole part of interaction potential V and Σ denotes the summation over K' and ν'. In Eq. 5, the "D_2" wave function is constructed regarding the $(dd\mu)$ molecular ion as a point nucleus positioned at the center of mass of the three particles. The interaction V is, therefore, the difference between the actual Coulomb interaction of the three particles with remaining d and two electrons (dee) and the Coulomb interaction of the "pseudo" point nucleus with (dee). A detailed explanation of the interaction is given in Ref. 4. The rotational and vibrational structure of the "D_2" molecule is properly taken into account in the frame of the adiabatic nuclei (Born-Oppenheimer) approximation.

In this research, we have calculated the Auger monopole transition rate of $[(dd\mu)_{1,1}dee]_{K,\nu=7}$ using accurate muonic wave functions.[4] For the initial molecular wave function Ψ_i, we have adopted the CI wave function[5] which includes 91% of correlation energy. The final state molecular wave function Ψ_f is obtained by the two-centre static exchange approximation.

We have also studied the transition rate for the process

$$(dd\mu)_{1,1}e \rightarrow (dd\mu)^{+}_{1,0} + e. \quad (6)$$

The present results are given and compared with Lane's result[6] in Table 1. The difference between the present result and that of Lane is mainly due to the poor $(dd\mu)$ wave function adopted by Lane. It should be noted that for $(dd\mu)e$ atom, only the continuum s-state contributes. On the other hand, for $[(dd\mu)dee]$ molecule, both the Σ_g and Σ_u continuum states give almost equal contributions.

Table 1. The Auger monopole transition rate (in 10^8/sec) for reactions (4) and (6) from various symmetries of the system.

	$[(dd\mu)_{1,1}dee]_{K,\nu=7}$	$(dd\mu)_{1,1}e$
Σ_g	1.0	
Σ_u	1.2	
Total	2.2	1.1
		2.4[6]

References

1) S. Hara: *RIKEN Accel. Prog. Rep.*, **25**, 63 (1991).
2) E. A. G. Armour, D. M. Lewis, and S. Hara: *Phys. Rev.*, **A46**, 6888 (1992).
3) A. Scrinzi and K. Szalewicz: *ibid.*, **A39**, 2855 (1989).
4) M. R. Harston, I. Shimamura, and M. Kamimura: *ibid.*, **A45**, 94 (1992).
5) S. Hara, H. Sato, S. Ogata, and N. Tamba: *J. Phys. B: Atom. Molec. Phys.*, **19**, 1177 (1986).
6) A. M. Lane: *Phys. Lett.*, **98A**, 337 (1983).

Experimental and Theoretical Study of Multiple Ionization Probabilities in 26 MeV Ne^{4+} + Ne Collisions

S. Lencinas, T. Kambara, S. Kravis, Y. Kanai, M. Oura,
Y. Awaya, M. Horbatsch,* and H. Schmidt-Böcking

We report experimental results of scattering-angle dependence of probabilities of target multiple ionization accompanied by projectile electron loss in Ne-Ne collisions and compare the results with semi-classical Vlasov-IPM (independent-particle model) calculations. We previously reported details of the experimental set-up and data reduction.[1)]

The Vlasov-IPM is based on a Vlasov equation

$$\partial_t f(r,p,t) + p \cdot \nabla_r f(r,p,t) - \nabla_r V_{eff}(r,t) \cdot \nabla_p f(r,p,t) = 0, \quad (1)$$

for a distribution function $f(r,p,t)$ which describes the motion in the phase space of a single-particle in an effective potential $V_{eff}(r,t)$. It is a semi-classical limit ($\hbar = 0$) of the quantum-mechanical Liouville equation. In the last decade, this method has been developed and applied successfully in the theoretical description of many-body problems of multiple ionization of a target in collisions with charged particles,[2)] where perturbative calculations should be invalid.

In the present calculation, the Vlasov equation has been solved to determine the impact parameter dependence of the charge transfer probability ($P_X(b)$), the one-particle ionization probabilities for the projectile ($P_L(b)$), and that for the target ($P_I(b)$) with a test-particle method which allows to incorporate dynamical changes of the binding energies of the target electrons during the collision. This model does not include ionization due to the interaction between electrons in the target and the projectile. However, the contribution of this effect to the total "loss" cross section should be smaller than 20% for the present collision system. If the ionization of the projectile, that of the target, and the electron transfer processes are independent single-electron processes, the probability for the n-fold electron loss of the projectile simultaneous with the production of a q-fold charged target ($P_{n,q}(b)$) is expressed with a statistical formula with the three parameters. When the electron transfer probability is small, it can be approximated by

$$P_{n,q}(b) = \left[\frac{4!}{n!(4-n)!} P_L^n (1-P_L)^{4-n}\right] \times \left[\frac{8!}{q!(8-q)!} P_I^q (1-P_I-P_X)^{8-q}\right], \quad (2)$$

where the first factor represents the projectile electron loss and the second one the target ionization.

Figure 1 shows the experimental probabilities of the target ionization in the single and double electron-loss channels of the projectile, compared with the Vlasov-IPM calculations. Excellent agreement between the calculation and the experiment in shape and magnitude of the probabilities $P_{n,q}(\theta)$ was found for the single electron-loss channel for the projectile and the triple ionization of the target ($n = 1, q = 3$). In the double electron-loss channel the shape of the probability is well reproduced, however, the absolute magnitude is overestimated by the model. The discrepancies observed in the small scattering angles below 0.2 mrad are attributed to the finite resolution of the measured scattering angle ($\Delta\theta = 0.15$ mrad) which is due to the beam-divergence and the angular resolution of the detector. The total ionization cross section integrated over the scattering angle shows a reasonable agreement with measurements of the total cross section[3)] within the experimental errors.

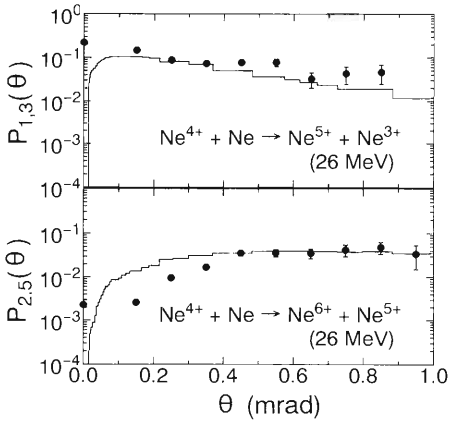

Fig. 1. Ionization probabilities $P_{n,q}(\theta)$. Filled circles: Experimental results, full line: Vlasov-IPM calculations.

References

1) S. Lencinas, Y. Awaya, and T. Kambara: *RIKEN Accel. Prog. Rep.*, **26**, 62 (1992).
2) M. Horbatsch: *J. Phys. B*, **25**, 3797 (1992).
3) H. Tawara, T. Tonuma, H. Kumagai, and T. Matsuo: *Phys. Rev.*, **A41**, 116 (1990).

* Dept. of Phys. and Astronomy, York Univ., Canada

Energetic Electron Production in 20 MeV/u N^{q+} and Ta^{q+} Bombarding Cu and Fe Thin Foils

Y. Yamazaki, K. Komaki, T. Azuma, K. Kuroki, N. Kakutani, K. Kawatsura, Y. Awaya, T. Kambara, Y. Kanai, M. Oura, and Y. Nakai

The energy and angular distributions of energetic electrons emitted in 21 MeV/u N^{4+} and Ta^{37+} ions bombarding Cu and Fe thin foils ($\sim$ 5000Å) have been measured with RIKEN Ring Cyclotron.

The final goal of the present experiment is to observe asymmetry of binary electron intensity for a magnetized (spin polarized) target like Fe. (A Cu target of a similar thickness is used as a reference to see the affects of stray magnetic field on the electron energy specta.)

In the present report, we discuss, as a first step, the general behaviour of the electron spectra from such energetic ion beams, where the binary electron energy amounts to several tens keV.

Figure 1 shows electron spectra $d^2I/dEd\Omega$ measured at 0° for 21 MeV/u N and Ta ions bombarding an Fe polycrystal foil ($\sim$ 5000Å). The ordinate is normalized per projectile assuming that average charge states of the projectile behind the target foil are around 60 and 7 for Ta and N ions, respectively. Each spectrum shows two peaks, the first one is called convoy electron peak, which appears at the velocity of the projectile, and the second one is called binary electrons which appears at energies about 4 times larger than the convoy electrons.

In general, the spectral shape is somewhat common to both ions except for an area around convoy electrons. (The spectra are not calibrated with respect to the electron detector (Micro Channel Plate) efficiency, i.e., the relative intensity between the convoy electron and the binary peak is not necessarily true.)

It is seen that the binary intensity for Ta ions is roughly 60 times as large as that for N ions, which is about a half of the prediction of a 1st Born calculation, where the binary electron intensity is proportional to the the square of the atomic number of the projectile.

On the other hand, the intensity ratio of convoy electrons between Ta and N ions are about 400, which is crudely the anticipated charge state ratio cubed.

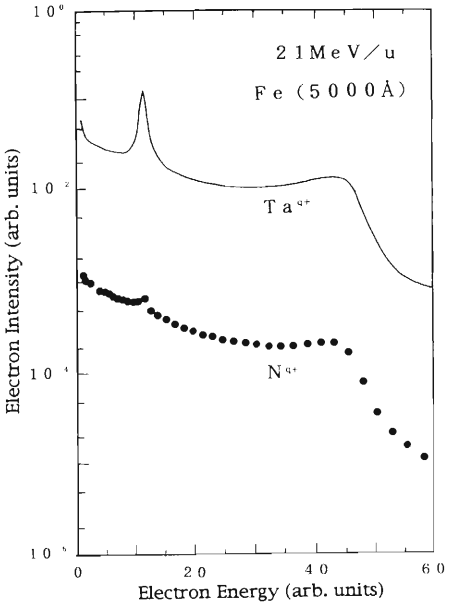

Fig. 1. The electron energy spectra measured at 0° for 21 MeV/u Ta and N ions bombarding a thin Fe foil ($\sim$ 5000Å).

Double and Single Ionization of Helium at Impact Parameter 0

L. Spielberger, T. Kambara, S. D. Kravis, M. Oura, Y. Kanai,
Y. Nakai, Y. Awaya, and H. Schmidt-Böcking

In ionic collisions the mechanisms leading to multiple target ionization are subject of great interest. To investigate these processes, helium is a well suited target because it is the simplest multiple-electron system. Several mechanisms are possible for the double ionization of a target He atom by a collision with an ion projectile: Independent multiple collisions between the projectile and the target electrons, a single collision between the projectile and a target electron followed by an electron-electron collision, and the emission of the second electron due to rearrangement effects in the target atom after a single ionization (shake off).

One of the main questions concerns the scaling of the ratio of the ionization probabilities

$$r(b) = P(\mathrm{He}^{2+}, b)/P(\mathrm{He}^{+}, b) \qquad (1)$$

with the charge q of the projectile at a given collision velocity, where $P(\mathrm{He}^{i+}, b)$ denotes the probability to produce He^{i+} ions in a collision at an impact parameter b. Recent investigations have shown that the q^2-scaling deduced from an independent-particle model can be disturbed by higher-order Born terms or dynamical correlation between both electrons. A theoretical study of the b dependence of this q-scaling shows that these effects have the strongest influence at small b.[1)]

In this work the probability ratio was studied in a collision system

$$\mathrm{O}^{6+}(1.05\ \mathrm{MeV/u}) + \mathrm{He} \rightarrow \mathrm{O}^{q'+} + \mathrm{He}^{i+}.$$

In the experiment at RILAC the ionized target He atoms (recoil ions) were detected in coincidence with the scattered projectiles. The charge state of the recoil ion was measured with a time-of-flight spectrometer. The projectile ions were charge-state analyzed in a magnet after the target and detected with a position-sensitive parallel-plate avalanche counter (PPAC), which provided the information on the scattering angle.[2)] Through the analyses of the charge state (q') of the projectile, we separately observed the channels of the target ionization ($q' = 6$), the electron loss ($q' = 7$) and the electron capture ($q' = 5$) for the projectile. Some of the projectile ions may get different charge states before the target through collisions with residual gas between the final analyzing magnet of RILAC and the target. These impurity ions were separated by a 'beam-cleaning' system, which consists of an electrostatic deflector placed just before the target. It produces a dispersion of the deflection angle among the different charge states which can be separated on the PPAC.

Unfortunately the scattering angle information could not be used in the present investigation due to poor statistics. Therefore we measured the ratio of the double- to single-ionization cross sections for a charge state channel q' of the projectile

$$R(q') = \sigma(\mathrm{He}^{2+}, q')/\sigma(\mathrm{He}^{+}, q') \qquad (2)$$

to get the information of the impact parameter. The values of $R(q')$ in the different channels are:

electron loss	$(q' = 7)$	$42\% \pm 2\%$
pure ionization	$(q' = 6)$	$5\% \pm 0.3\%$
electron capture	$(q' = 5)$	$62\% \pm 2.5\%$

Since a K-electron is lost in the electron loss channel, the electron loss is observed mainly in collisions with b smaller than the oxygen K-shell radius, whereas the pure ionization may come from collisions with much larger range of impact parameter. The values of $R(7)$ and $R(6)$, in the loss and pure ionization channels, are in a fair agreement with FIM (forced impulse method) calculations.[1)] Especially the ratio observed in the electron loss channel (mainly at small impact parameter b) is strongly enhanced compared to the ratio observed in the pure ionization (in a larger impact parameter region), as predicted by the calculations. The q^2-scaling is found to be valid for the present experimental results. The higher value of $R(5)$, in the capture channel, is not yet fully understood.

References

1) A. L. Ford and J. F. Reading: *J. Phys. B*, **23**, 2567 (1990).
2) T. Kambara et al.: This report, p. 62.

Target Ionization in 42 MeV Ar^{12+}-Ar Collisions

T. Kambara, Y. Kanai, S. Kravis, Y. Nakai, M. Oura, and Y. Awaya

The ionization processes in a fast heavy ion-atom collision have been experimentally studied through observation of the ionized target atoms (recoil ions).[1,2] When both the projectile and the target are multi-electron systems and the electronic orbits overlap significantly during the collision, the ionization processes are generally very complicated since they may include many elementary processes like direct ionization from the projectile and the target, electron transfer between them, and autoionization from their excited states after the collision.

We are interested in the inner-shell ionization and transfer processes in close collisions where the inner-shells of the projectile and the target overlap each other. We study a symmetric collision system:

$$Ar^{q+} + Ar \rightarrow Ar^{q'+} + Ar^{i+} \quad (q = 12) \qquad (1)$$

with 42 MeV Ar ions from the RILAC, by measurements of the charge state (i) distribution of the recoil as a function of the charge state (q') of the projectile after the collision and the scattering angle θ to get the impact parameter.

The experimental setup is shown in Fig. 1. The incident Ar^{12+} beam was collimated by a pair of slits with aperture of ± 0.3 mm and 4 m apart each other. The scattered ions from an Ar-gas target were charge-state selected with a dipole magnet and were counted with a two-dimensional position-sensitive parallel-plate avalanche counter (PPAC). By the charge-state analyses we observed the projectiles from one- and two-electron capture ($q' = 11$ and 10), pure ionization ($q' = 12$), and one-electron loss ($q' = 13$) processes separately. The scattering angle was deduced from the position of the scattered ion on the PPAC. The slow recoil ions were extracted from the target region at 90° to the beam direction by an electric field and charge-state analyzed by a time-of-flight spectrometer in coincidence with the scattered ions.

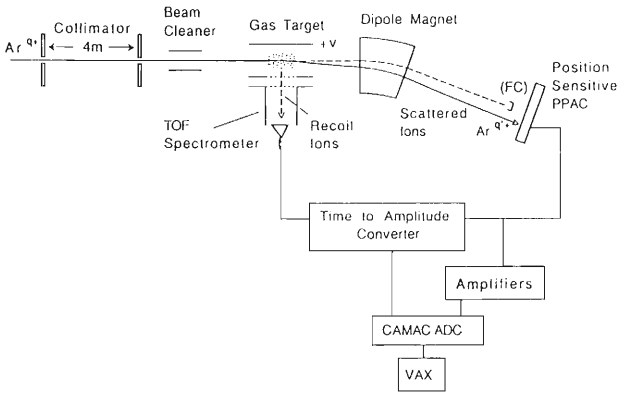

Fig. 1. Experimental setup.

Figure 2 shows the probabilities to produce recoil ions (i) and the projectile ions (q') simultaneously at scattering angle $\theta > 0.8$ mrad. In this range of the scattering angle, the projectile and the target undergo substantial overlap of the L-shells during the collision. The recoil charge (i) has a bell-shape distribution at $i \geq 8$ with a maximum at about $i = 11$ and the width of the distribution is almost independent of q'.

The high recoil-ion charge state ($i \geq 8$) in the close collisions indicates that almost all the M-electrons are ionized in the collision and the L-shell processes mainly determine the charge states of the collision partners. We compared the experimental results with an independent-electron model, in which the simultaneous charge state of the projectile and the recoil ions is determined by independent single L-electron processes, i.e., the L-ionization of the target, the L-electron loss of the projectile and the transfer of a target L-electron to a projectile L-vacancy. The lines in Fig. 2 show the results of the calculation. The calculation well agrees with the experimental results except for the case of a two-electron capture.

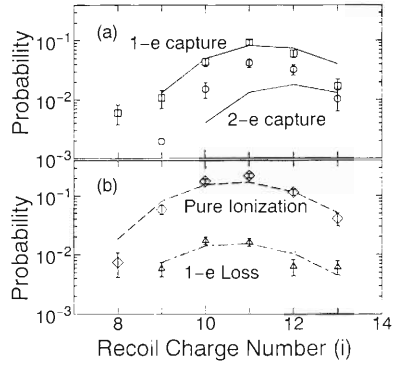

Fig. 2. Probabilities of target ionization simultaneous to (a) one- and two-electron capture and (b) pure ionization and one-electron loss by the projectile in close Ar^{12+}-Ar collisions.

References

1) C. L. Cocke and R. E. Olson: *Phys. Rep.*, **205**, 153 (1991).
2) T. Tonuma, H. Kumagai, T. Matsuo, and H. Tawara: *Phys. Rev.*, **A40**, 6238 (1989).

Measurement of Radiative Electron Rearrangement X Rays from 0.8 MeV/amu Ti Ions Excited by Carbon Foil

M. Oura, T. Kambara, Y. Kanai, S. Kravis, Y. Nakai, Y. Awaya, and B. DePaola

We have previously reported a measurement of the KL^3 RER (radiative electron rearrangement) x rays from 0.8 MeV/amu Ar ions excited by target foil.[1] The results have shown that the intensity ratios of KL^3 RER line to $K\alpha L^3$ line ($R_3 \equiv KL^3$ RER/$K\alpha L^3$) are smaller than the values obtained from x rays emitted by excited target atoms. The electronic configuration of L-subshells of fast ions in the foil is expected to be different from that of excited target atoms. Since the RER intensity is sensitive to the number of 2s electrons, it is expected that the different 2s-2p configuration between the excited projectile ions and the excited target atoms can be studied by the intensity ratio between the RER and satellite x rays.

In order to study the difference in the 2s-2p configuration between projectile ions and excited target atoms, we have performed two x-ray measurements at RILAC: one with 1.5 MeV/amu C^{2+}-Ti and the other with 0.8 MeV/amu Ti^{5+}-C collisions. Typical spectra of Ti K x rays are shown in Fig. 1. Figure 1(a) is the case of target atom excitation and clearly shows the KL^1-, KL^2-, and KL^3-RER lines in addition to the $K\alpha L^n$ satellite lines. Figure 1(b) is for projectile ions excited by the foil and only shows a small hump at 4.457 keV, which is close to the average energy of KL^3-RER transitions estimated to be 4.462 keV by theoretical calculation. We attributed the small hump at 4.457 keV to the KL^3-RER transition.

The intensities of the KL^3 RER and the $K\alpha L^3$ were estimated by fitting procedure in order to compare the intensity ratio for both projectile ions ($R_3^{Proj.}$) and excited target atoms ($R_3^{Tar.}$). The value of this ratio, ($R_3^{Proj.}/R_3^{Tar.}$), was 0.6 ± 0.25. This result shows the KL^n-RER x-ray emission probabilities relative to $K\alpha L^n$ x rays for excited projectile ions are smaller than those for excited target atoms.

In the case of target atom excitation, the multiple ionization is caused by a single collision, and a 2s vacancy produced can be filled by L_1-$L_{2,3}M$ Coster-Kronig transitions involving the excitation of M or valence electrons in the solid target before the KL^n-RER transition occurs. On the other hand, the projectile Ti ions in a target material quickly reach an equilibrium of charge state distribution through successive outer-shell collisions.[2] The mean number of the L-shell electrons is estimated to be 4.6 from relative intensities of each satellite lines. It is expected that such L-electrons are distributed statistically among the subshells, e.g. $2s^22p^3$-, $2s^12p^4$-, and $2s^02p^5$-configurations. In this case the 2s vacancy produced can be filled

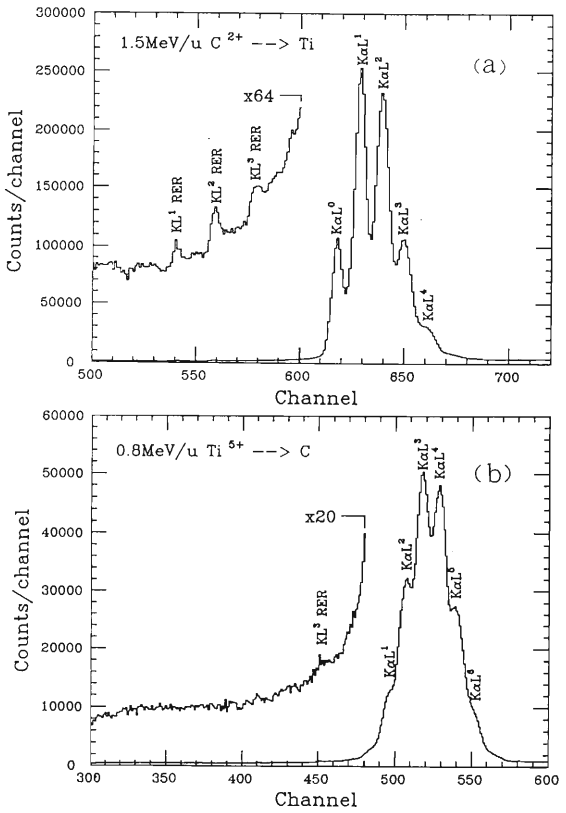

Fig. 1. Ti K x-ray spectra from (a) target atom excitation and (b) 0.8 MeV/amu Ti ions passing through the carbon foil.

only through the capture processes, because L_1-$L_{2,3}M$ Coster-Kronig transitions will not occur due to the missing of M-shell electrons. The probability to have two 2s electrons, i.e. $2s^22p^3$-configuration, at the emission of the x rays is roughly estimated to be 35% of possible electronic configurations of $2s^n2p^m$ (n+m = 5, $n \leq 2$). This probability, however, should be corrected because the ratio of the capture cross section to the ionization cross section for 2s can be estimated to be about twice that of 2p.

According to the above discussion, the value of ($R_3^{Proj.}/R_3^{Tar.}$) is expected to be larger than 0.35. This explains the experimental result (0.6 ± 0.25) within experimental uncertainty.

References

1) M. Ohura et al.: *RIKEN Accel. Prog. Rep.*, **25**, 70 (1991); M. Oura et al.: *ibid.*, **26**, 60 (1992).
2) T. Mizogawa et al.: *Phys. Rev.*, **A42**, 1275 (1990).

Binary Encounter Peaks for 0° Electrons in Collisions of Bi^{q+}

Y. Kanai, Y. Nakai, T. Kambara, M. Oura, S. Kravis, and Y. Awaya

We measured the binary encounter peaks in collisions of Bi^{q+} on H_2, He, and Ar at 0° with varying the incident charge state (16+ and 32+) and the incident energy (0.56, 0.8, and 1.2 MeV/nucleon). In this report, we present the incident charge state dependence of the binary encounter peak shift and the double differential cross sections of the binary encounter peaks including the $Bi^{10+,14+}$ data reported previously.[1)]

The beams of 0.56, 0.8, and 1.2 MeV/nucleon Bi^{q+} from RILAC were magnetically analyzed, collimated by two sets of four-jaw slits system and focused to the target gas cell. The target gas cell was 5 cm in length. Single collision conditions have verified experimentally.

Figure 1 shows the incident charge state dependence of the binary encounter peak shift ΔE_b (= $4 \times E_p \times (m/M)$-observed peak energy, where E_p is the projectile energy, m the electron mass, and M the projectile mass) for the 0.8 MeV/nucleon Bi^{q+} ($q = 10, 14, 16, 32$) on H_2. The values of the peak shifts for all collision systems are tabulated in Table 1. The calculated shift values by the Bohr-Lindhard model[1,2] ($\Delta E_b = 54.43 \times q^{1/2} \times (I_t/13.6)^{3/4} \times Z_{\rm eff}^{-1/6}$ eV), where q is the incident charge state, I_t the first ionization potential of the target, and $Z_{\rm eff}$ the effective nuclear charge of the target) are also shown in Table 1. Here, we use the value of (2 × (first ionization potential energy)/27.2)$^{1/2}$ as the value of $Z_{\rm eff}$. Absolute values of the peak shift and target dependence are qualitatively explained by the B-L model. But, the detail of the incident charge state dependence seems to be different from the $q^{1/2}$ dependence. From our results in Fig. 1, the peak shift seems to be independent of the incident charge state for $Bi^{10+,14+,16+}$ projectile ions. The B-L model is originary applied to the bare projectile ions. So, we have to apply this model to the (partially stripped) projectile ions with an ion radius which is much smaller than the release distance. The release distance is a characteristic distance in the B-L model. When the projectile ions come to this distance, target electrons are released from the target atoms because of the balance between the force from the projectile ions and the binding force to the target atoms. After that, released electrons collide with the projectile ions as free electrons. The release distance for the Bi^{32+} on H_2 is about 5.6 a.u., and the ion radius (mean radius of the outer electron orbit) of the Bi^{32+} is 0.5 a.u. On the other hand, the release distance for the $Bi^{10+,14+,16+}$ on H_2 is about 3.2–4 a.u., and the ion radius of $Bi^{10+,14+,16+}$ is about 1 a.u. and almost constant. From this, we may say that the B-L model is applicable to the Bi^{32+} on H_2, but is not applicable to the $Bi^{10+,14+,16+}$ on H_2.

The double differential cross sections of binary encounter electron for Bi^{q+} on H_2 and He targets at 0° and the peak energy are tabulated in Table 2. Absolute values are calibrated by using the He^{2+} collisions with the same collision velocity and the same targets. In our collision condition, the double differential cross section increases as the incident charge increases as reported previously.[1)]

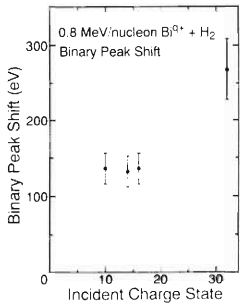

Fig. 1. The incident charge state dependence of the binary encounter peak shift.

Table 1. Binary encounter electron peak shifts at 0°.

	Binary Encounter Electron Peak Shift at 0°					
	H_2 target		He target		Ar target	
	Exp.	B-L.	Exp.	B-L.	Exp.	B-L.
0.8 MeV/u						
Bi^{10+}	136±20 eV	187 eV	216±40 eV	255 eV	-- eV	190 eV
Bi^{14+}	132 20	221	212 40	302	--	225
Bi^{16+}	136 20	237	219 40	323	184±40	240
Bi^{32+}	268 40	335	382 40	456	337 40	340
1.2 MeV/u						
Bi^{16+}	127 40	237	210 40	323	158 40	240
Bi^{32+}	230 40	335	397 40	456	315 40	340

$Z_{\rm eff}$ used are 1.065, 1.35, and 1.08, respectively, for H_2, He, and Ar.

Table 2. Double differential cross sections of ejected electrons at the binary encounter peak energy observed at 0°. Observed value has about 20% error.

		H_2 target	He target
0.56 MeV/u	Bi^{16+}	1.0 x 10^{-18} cm^2/eV sr	0.7 x 10^{-18} cm^2/eV sr
	Bi^{32+}	3.2	1.9
0.8 MeV/u	Bi^{10+}	0.5	0.32
	Bi^{14+}	0.7	0.42
	Bi^{16+}	0.8	0.45
	Bi^{32+}	2.4	1.4
1.2 MeV/u	Bi^{16+}	0.6	0.4
	Bi^{32+}	1.2	0.8

References

1) Y. Kanai et al.: *RIKEN Accel. Prog. Rep.*, **26**, 65 (1992).
2) J. O. P. Pedersen et al.: *J. Phys.*, **B24**, 4001 (1991).

Beam-Foil Experiment of Neonlike Iron

K. Ando, Y. Zou, T. Kambara, Y. Kanai, M. Oura, Y. Nakai, and Y. Awaya

We continue to measure the decay curves of $2p^5 3s$-$2p^5 3p$ and $2p^5 3p$-$2p^5 3d$ transitions of the Ne-like iron after finishing the measurement of Ne-like Ti and Cr along isoelectronic sequence. The spectrum emitted from ion beams after passing carbon foil has many spectral lines as shown in Ref. 1. Among them, only restricted numbers of spectral lines are well isolated and allow a decay curve measurement. Moreover, in those transitions of Ne-like ions the lifetimes of 3p and 3d are almost similar, so that cascading transitions from 3d levels affect the estimation of a lifetime of 3p level. Therefore, the decay curves of the primary and the cascading transitions must be measured. The analysis of a decay curve which is affected by the cascading, is carried out by the ANDC (Arbitrary Normalized Decay Curve) method.[2)]

The measurement has not finished yet. An example of the decay curve of the $2p^5 3s\ (3/2,1/2)_2$-$2p^5 3p\ {}^3D_3$ transition at 350.58 Å is shown in Fig. 1. The distance 10 mm from the foil corresponds to the flight time of ion of 0.705 ns, since the velocity of iron ion is 14.18 mm/ns.

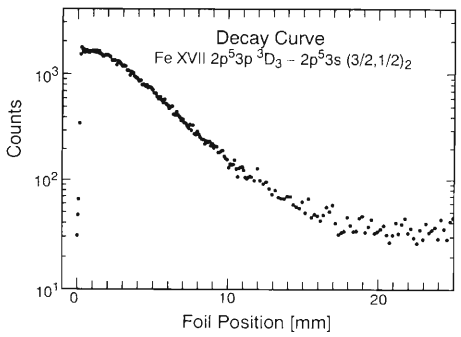

Fig. 1. A measured decay curve of the $2p^5 3s\ (3/2,1/2)_2$-$2p^5 3p\ {}^3D_3$ transition of Fe XVII at 350.58 Å. The velocity of iron ion is 14.18 mm/ns.

References

1) K. Ando, Y. Zou, T. Kambara, M. Oura, Y. Nakai, Y. Awaya, and T. Tonuma: *RIKEN Accel. Prog. Rep.*, **26**, 67 (1992).

2) L. Engström: *Nucl. Instrum. Methods*, **202**, 369 (1982).

Ejected Electron Spectra from $O^{4+**}(1s^2 3l3l')$

Y. Kanai, T. Kambara, Y. Awaya, N. Nakamura, M. Koide,
S. Ohtani, H. Suzuki, T. Takayanagi, and K. Wakiya

We carried out a high-resolution measurement of the electrons ejected from $O^{4+**}(1s^2 3l3l')$ produced by the double electron transfer collisions at 60 keV;

$$O^{6+}(1s^2) + T \longrightarrow O^{4+**}(1s^2 3l3l') + T^{2+}$$
$$(T = Ar, Ne, \text{ and } H_2)$$
$$\hookrightarrow O^{5+}(1s^2 2s) + e$$
$$\hookrightarrow O^{5+}(1s^2 2p) + e.$$

60 keV O^{6+} projectile ions were produced by the ECRIS (Electron Cyclotron Resonance Ion Source) for the RIKEN AVF cyclotron. Ejected electrons were measured by the zero-degree electron spectroscopy technique.[1)]

Ejected electron spectra from the doubly excited $O^{4+**}(1s^2 3l3l')$ ions are shown in Fig. 1. Vertical lines in the figure indicate theoretical values, which include a post collision interaction effect calculated from the lifetime.[2)] Solid and broken lines correspond to the transitions to the $O^{5+}(1s^2 2p)$ and $O^{5+}(1s^2 2s)$, respectively. Upper parts of the lines indicate the theoretical values for the ejected electron from the triplet states, and lower parts indicate those for the singlet states. Comparing the measured spectra with the theoretical results, we can notice following features; (1) The observed spectrum with the H_2 target has peaks only for the singlet states. On the other hand, (2) the observed spectrum with the Ne target has peaks only for the triplet states. (3) Observed spectrum with the Ar target has peaks for the singlet and the triplet states. These differences with the different targets must be explained by the double electron transfer processes from the target to O^{6+} ions.

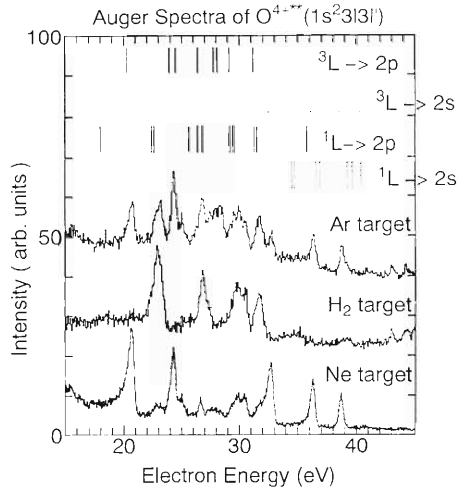

Fig. 1. High-resolution spectra of ejected electron from the doubly excited $O^{4+**}(1s^2 3l3l')$ ions produced in $O^{4+} + Ar$, H_2, Ne collisions. Solid and broken lines represent the theoretical energy for the transitions to the $O^{5+}(1s^2 2p)$ and $O^{5+}(1s^2 2s)$, respectively. Upper and lower parts of the lines are for the triplet and singlet states of the doubly excited states, respectively.

The feature (1) is due to that the electronic state of H_2 target is the singlet state and the spin flip does not occur in this collision. The difference between the feature (2) and the feature (3) may be related to the difference of the excitation energy from the ground state (triple state) to the lowest excited state (spin singlet state) of Ne^{2+} (or Ar^{2+}) ions. In the case of the Ne target, the ground state of Ne^{2+} is dominantly produced by the double electron transfer to the projectile ions, because of the large excitation energy (3.2 eV) from the ground state to the lowest excited state of Ne^{2+}. In the case of the Ar target, not only the ground state but also the lowest excited states of Ar^{2+} are produced, because of the small excitation energy (1.7 eV) of Ar^{2+}.

By using the target with many electrons, we can make the triplet state of the doubly excited ions, as shown in Fig. 1. Especially, the triplet state of $O^{4+**}(1s^2 3l3l')$ is made purely by using the Ne target. The detail of the spectroscopic study of the triplet state is in progress.

References

1) H. A. Sakaue et al.: *J. Phys.*, **B24**, 3787 (1990).
2) H. Bachau et al.: *Atom. Data Nucl. Data Tables*, **44**, 305 (1991).

Multiply Charged and Cluster Ions Produced from Gaseous and Frozen CF_4 under Energetic Heavy Ion Impact

H. Shibata, T. Tonuma, T. Matsuo, H. Kumagai, and H. Tawara

In the present work, we have observed multiply charged atomic and molecular ions and a variety of positively charged cluster ions produced from a complex molecular target, CF_4, in gaseous and frozen phases in collisions with energetic Ar^{13+} and Xe^{31+} ions ($\sim$ MeV/amu) from RILAC. Secondary ions produced were extracted, mass/charge-analyzed by a double focusing magnet and detected by a channeltron. Mass/charge spectra of atomic and molecular ions from frozen targets are found to be quite different from those from gaseous targets. For the first time, the parent molecular ions, CF_4^+, have been observed in the frozen gas experiment.

Figure 1(a) shows a typical mass/charge spectrum of ions from a gaseous CF_4 target in 1.5 MeV/amu Xe^{31+} ion impact. Singly charged CF_3^+ molecular ions are seen as a dominant peak, and singly charged CF_2^+, CF^+, doubly charged CF_3^{2+} and CF_2^{2+} molecular ions are also observed in the spectrum. All of these molecular ions are produced in dissociative ionization processes, and no parent molecular ions, CF_4^+ (expected by the arrow in the figure), are observed. In addition to these molecular ions, some multiply charged atomic ions such as C^{i+} (up to $i = 3$) and F^{i+} ($i = 1$ and 2) are observed. Relative production of doubly charged molecular ions and multiply charged atomic ions is found to be enhanced in ion impact compared with that in 500 eV electron impact.[1)]

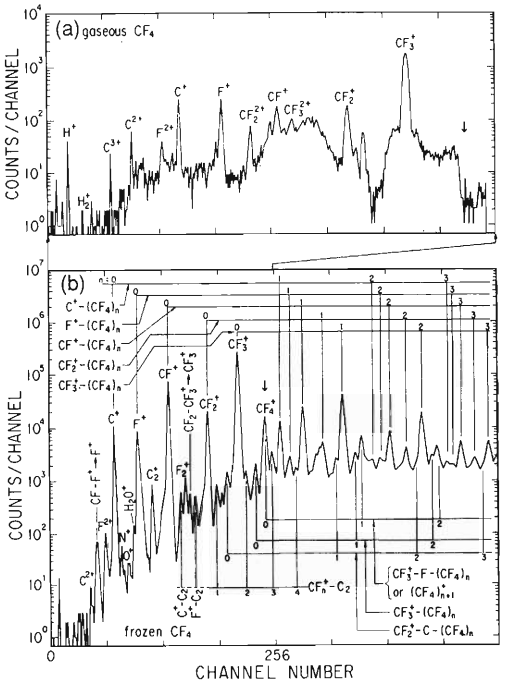

Fig. 1. Mass/charge spectra of ions from (a) gaseous and (b) frozen CF_4 targets under 1.5 MeV/amu Xe^{31+} and Ar^{13+} ion impact, respectively.

Figure 1(b) shows a typical mass/charge spectrum of ions from a frozen CF_4 target in 1.5 MeV/amu Ar^{13+} ion impact. The spectrum shows the production of multiply charged atomic ions in addition to dominant singly charged atomic, molecular and a variety of cluster ions. Atomic and molecular ions of C^{i+}, F^{i+} (up to $i = 2$), CF^+, CF_2^+ and CF_3^+ are observed as in the gaseous CF_4 target described above. It should be pointed out that the parent molecular ions, CF_4^+, are observed, which are not seen for the gaseous target. Cluster ions of C_2^+, F_2^+, $C^+(CF_4)_n$, $F^+(CF_4)_n$, $CF_m^+(CF_4)_n$ (m = 1–3, n = 1–3), $CF_2^+C(CF_4)_n$, $CF_3^+C(CF_4)_n$, $CF_3^+F(CF_4)_n$ or $(CF_4)_{n+1}^+$ and $C^+C_2F_n$ (up to n = 4) are also observed.

It is noted that there is a significant difference in multiply charged ion production between gaseous and frozen targets: in the gaseous target, the intensities of C^{i+} ($i > 1$) ions are generally larger than those of F^{i+} ions, whereas in the frozen target the intensities of C^{i+} ions are smaller than those of F^{i+} ions. This difference can be understood to be due to sharing of Coulomb dissociation energy of multiply charged molecular ions which results in large initial kinetic energies of multiply charged atomic ions. In CF_4 molecules, C atoms sit at the center among four F atoms and get only small kinetic energy. Thus, their intensities are reduced because of low escape probabilities from surfaces.

References

1) Ce Ma, M. R. Bruce, and R. A. Bonham: *Phys. Rev.*, **A44**, 2921 (1991).

Ions from C_{60}/C_{70} Fullerenes Deposited on Metallic Foil under Energetic, Heavy Ion Impact

H. Tawara, T. Tonuma, H. Kumagai, and T. Matsuo

A number of investigations on physical and chemical properties of carbon fullerences and also collision features are under way.[1] Recently in C_{60}^+ ions colliding with gas targets have observed many dissociation product ions resulting from the emission of a series of two carbon atoms (C_2).

In the present work, secondary ions from the layers of C_{60}/C_{70} mixtures deposited on metallic foil have been observed under 1.5 MeV/u Ar^{13+} ion impact. A thin fullerene target was prepared by dissolving C_{60}/C_{70} mixtures in toluene, putting a few droplets of them onto 1 μm Al foil and drying under normal air. Secondary ion mass spectrum has been obtained with a time-of-flight spectrometer. A typical secondary ion spectrum is shown in Fig. 1; in addition to the dominant peaks of the parent C_{60}^+ (also C_{70}^+ and C_{84}^+) fullerene ions, there are a series of peaks corresponding to dissociation product ions of these parent fullerenes: namely, C_{58}^+, C_{56}^+, C_{54}^+ and so on from C_{60} (similar ion peaks from C_{70} and C_{84}).

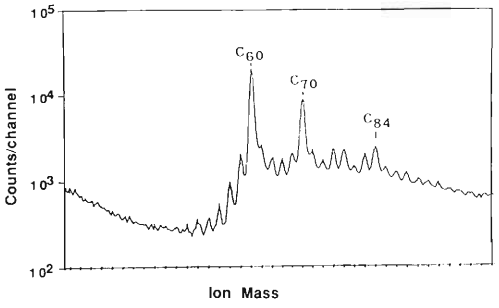

Fig. 1. Ion spectrum from C_{60}/C_{70} fullerene deposited on Al foil under 1.5 MeV/u Ar^{13+} ion impact.

It is interesting to compare relative intensities, R, of dissociation product ions over the parent fullerene ions, which may provide important information on the dissociation of fullerenes. The present results on R are shown in Fig. 2, together with data for 50 keV C_{60}^+ ions incident on H_2 targets.[2,3] The relative intensities observed by both groups can be fitted with the following form:

$$R \sim \exp(-a * n)$$

where n ($\leq$ represents the number of C_2 pairs emitted from fullerene and a depends a number of collision parameters.[3] Fitting the observed data gives $a = 0.53$ for the deposited C_{60} layers under 1.5 MeV/u Ar^{13+} impact in the present work and $a = 0.44$ for 50 keV

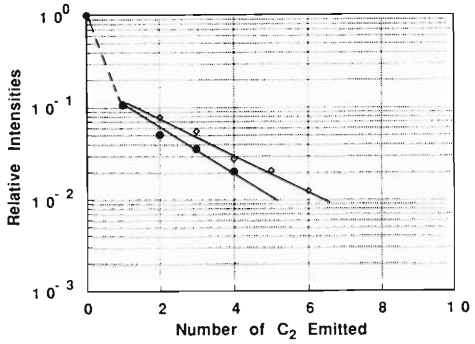

Fig. 2. Relative intensities of dissociation ions over the parent C_{60}^+ ions open square: 50 keV C_{60}^+ ions on H_2 gas.[3] solid circles: 1.5 MeV/u Ar^{13+} ions incident on deposited C_{60}.

C_{60}^+ ion collisions with H_2 targets. As the number of C_2 pairs emitted increases, the relative intensities decrease more slowly in low energy free C_{60}^+ ions colliding with H_2 than in energetic ion impact on C_{60}. This difference may be due to the presence of the excited C_{60}^{+*} ions, compared with the ground state C_{60}.

If the successive emission of C_2 pairs is independent of each other, the relative intensities of the dissociation ions can be given as follows:

$$R \sim P^n * (1 - P)^{(30-n)}$$

where P represent the emission probability of a single C_2 pair from the fullerene. As shown in Fig. 2, C_{58}^+/C_{60}^+ ratio is estimated to be the order of 0.1 in the present work (this ratio is 0.07 under 40.8 eV photon impact[4]) and we can assume $P \ll 1$ in the present collision processes. Thus,

$$P^n \sim \exp(-a * n).$$

The present analysis clearly supports an assumption[3] that the successive emission of C_2 pairs from fullerene is independent of each other.

References

1) R. F. Curl and R. E. Smalley: *Scientific American*, Oct. issue, p. 54 (1991).
2) A. B. Young, L. M. Cousin, and A. G. Harrison: *Rapid Comm. Mass Spectro.*, **5**, 226 (1991).
3) P. Hvelplund, L. H. Andersen, H. K. Haugen, J. Lindhard, D. C. Lorents, R. Malhotra, and R. Rouff: *Phys. Rev. Lett.*, **69**, 1915 (1992).
4) R. K. Yoo, B. Ruscic, and J. Berkowitz: *J. Chem. Phys.*, **96**, 911 (1992).

Muon Catalyzed Fusion in Thin Solid D_2 Layer

K. Nagamine, P. Strasser, and K. Ishida

The production of a slow μ^- beam using the re-emission method is not as easily accomplished as the production of a slow μ^+ beam, since negative muons injected into condensed matter are captured by atomic nuclei and form muonic atoms. We proposed a method of producing slow μ^- beams by using μCF phenomena occuring in a high density D_2/T_2 mixture.[1,2] After fusion inside a dtμ molecule, most of the μ^- do not stick to the α fusion product but are left free with a kinetic energy of several keV. This liberation process can be repeated up to 150 times during a μ^- lifetime and a significant fraction of μ^- can be expected to be re-emitted from the surface.

The study is now under way by using a D_2 layer, where ddμ fusion takes place although much slower than dtμ fusion in D_2/T_2. In order to greatly improve the re-emission efficiency, we have proposed the two-layer arrangement (Fig. 1), where the first thick ($\sim$ 1 mm) layer of H_2/D_2 ($C_d = 0.001$) is used for formation and efficient diffusion of $\sim$ 1 eV dμ atoms[3] with the help of Ramsauer-Townsend effect, and the second thin ($\sim$ 1 μm) layer of D_2 for the conversion of dμ into slow μ^-.

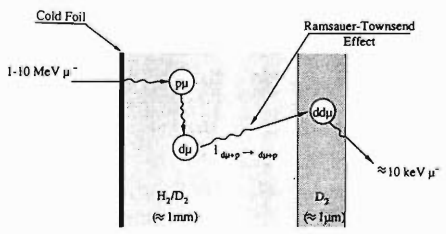

Fig. 1. Schematic of slow μ^- production using the two-layer arrangement.

As the first step, we carried out an experiment to confirm the efficient ddμ reaction in a thin D_2 layer by detecting 3-MeV protons from the dd fusion. The experiment was performed at the TRIUMF superconducting muon channel. High energy μ^- ($\sim$ 4 MeV) were injected into a target layer of solid hydrogen formed by freezing hydrogen gas (H_2 and D_2) onto 25-μm silver foil held at 3.5 K. An Si(Li) detector was used to measure the muonic hydrogen (pμ) K_α X-ray (1.9 keV) when μ^- were stopped in the H_2/D_2 layer. The μ^- stopping rate obtained at this target was $\sim$ 500 s^{-1}.

A Silicon Surface Barrier detector (SSB) was used to measure 3-MeV fusion protons. Typical SSB energy spectra are shown in Fig. 2 with 8 mg/cm^2 H_2/D_2 ($C_d = 0.001$) and about (a) 0.16 (b) 0.33, (c) 0.49, and (d) 0.82 mg/cm^2 D_2 added to it. The 3-MeV protons can clearly be seen when dd-μCF is produced in the D_2 layer. The center of the 3-MeV fusion proton peak is shifted to a lower energy as the D_2 layer thickness is increased due to the proton energy loss. The peak's width becomes also broader. The ddμ fusion yield in a 1 μm D_2 layer is expected to be around 1 s^{-1} from a very preliminary analysis of the SSB data. A careful analysis of these fusion proton data in thin solid deuterium films will bring us a precious understanding of μCF kinetics in the dd system, e.g., dμ thermalization process, ddμ mesomolecular formation and ddμ fusion.

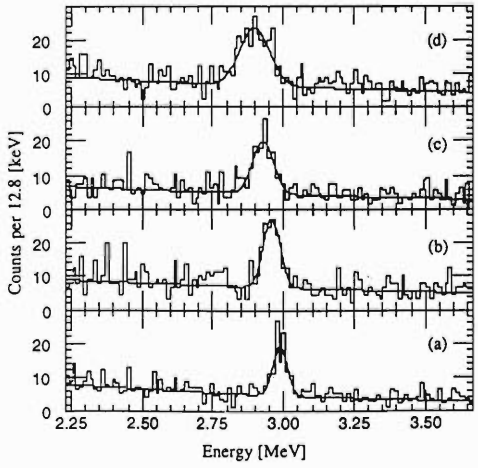

Fig. 2. Typical SSB spectra with 8 mg/cm^2 H_2/D_2 ($C_d = 0.001$) and (a) 0.16, (b) 0.33, (c) 0.49, and (d) 0.82 mg/cm^2 D_2 added to it.

As the next step, we are planning the detection of slow μ^- emission using a large-acceptance magnetic spectrometer. The slow μ^- released from the hydrogen target are collected and focused onto a Multichannel Plate (MCP) detector. If the production of slow μ^- beam is succesful, this would initiate a series of experiments which are today beyond our technical capabilities.

References

1) K. Nagamine: *RIKEN Accel. Prog. Rep.*, **23**, 25 (1989).
2) K. Nagamine, P. Strasser, and K. Ishida: *Muon Catalyzed Fusion*, **5/6**, 371 (1990/91).
3) B. M. Forster et al.: *Hyp. Int.*, **65**, 1007 (1990).

Resonance Ionization Spectroscopy of Fe

H. Katsuragawa, T. Minowa, S. Hashimoto,* and H. K. Uematsu**

Previously we have reported on resonance ionization spectroscopy (RIS) of Fe using a proportional counter.[1] In this work Fe atoms were supplied by a spark-discharge method. Mass separation of Fe isotopes was impossible because the resolving power of the TOF mass spectrometer was low.

We have carried out RIS of an Fe atomic beam to separate Fe isotopes and to observe isotope shifts with a narrow bandwidth dye laser and a high resolution mass spectrometer. The second harmonic radiation (532 nm) of a YAG laser was focused on an Fe target in a vacuum chamber to produce an Fe atomic beam. The laser pulse heated the Fe target up to 10^4 K and vaporized the target. The temperature was estimated by the velocity distribution of the Fe atomic beam. The dye laser was fired to ionized Fe atoms resonantly with a suitable delay after the YAG laser's firing.

A two-stage acceleration TOF mass spectrometer was used to separate isotopes of Fe (^{54}Fe, ^{56}Fe, ^{57}Fe, ^{58}Fe). Figure 1 shows a TOF spectrum of Fe^+. The spectrum shows asymmetric line shapes that are probably due to the non-uniform electric field in the accelerator. Relative intensity of each isotope peak is slightly different from the natural abundance of Fe isotopes. Although it is reported that ionization yields can depend on mass numbers of isotopes,[2] our result may be due to the time of flight which each isotope needs to reach the ionization volume. Irradiation of the dye laser beam with a suitable delay enables us to increase only one isotope species of Fe in a TOF spectrum because lighter species reach the detection area earlier.

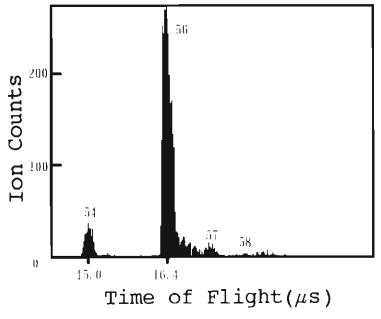

Fig. 1. Time-of-flight spectrum of Fe^+.

Ionization peak was observed at 385.590 nm which corresponds to the $z^5D_4^\circ$-a^5D_4 transition of Fe atom (Fig. 2). This line was observed in the previous work, too. The resolving power of the present work is improved by two orders of magnitude, which enables us to measure the isotope shift of Fe.

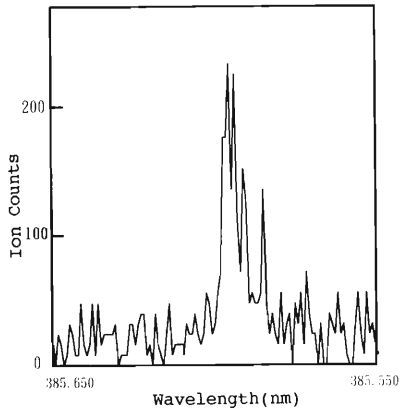

Fig. 2. Resonance ionization spectrum of Fe atomic beam. The ionization peak corresponds to the $z^5D_4^\circ$-a^5D_4 transition of Fe.

References

1) T. Minowa et al.: *Rev. Sci. Instrum.*, **60**, 3280 (1989).
2) P. Lambropoulos and A. Lyras: *Phys. Rev.*, **A40**, 2199 (1989).

* Faculty of Science, Toho University
** Tokyo Gakugei University

Laser Spectroscopy of Implanted Trace Atoms on a Metal Substrate: Application of Laser Ablation Ion Trap Method

Y. Matsuo, M. Wakasugi, H. Maeda, and M. Takami

Ion trap is an attractive technique that can confine ions for a long period of time and can easily be combined with laser cooling or other cooling techniques. The feasibility of ultra-high resolution spectroscopy in an ion trap has already been demonstrated.[1] Ion trap is also an effective tool for laser nuclear spectroscopy by means of the precision measurement of hyperfine structure of rare atoms with unstable nuclei.[2]

We have constructed an rf ion trap system which directly captures ions generated by laser ablation.[3] This method is useful for trapping the ions of heavy refractory metals, multiply-charged ions and implanted trace atoms on a metal substrate. However, it has been commonly accepted that ions should better be produced inside of ion trap electrodes because ions transferred from outside of the trap electrodes have excess kinetic energy so that these ions eventually come out of the trap electrodes. Thus, difficulties were originally anticipated for the direct capture of externally generated ions. On the other hand, under the presence of light buffer gases such as He, ions lose their excess kinetic energy through collisions with gases. We have applied this method to the ion trap system and obtained ion confining times in the range of a few minutes to a few hours depending on the ionic species.

We also expected that the ion trap with laser ablation method should be applied to the revaporization and ionization of implanted trace atoms. The atoms with relatively long-lived unstable nuclei are implanted on a metal substrate, which is then placed in an ion trap vacuum chamber, subjected to evaporation and injection for trapping. We here report a test experiment of the implantation of trace atoms using RIKEN IGISOL (ion guide isotope separator on line) at RIKEN Ring Cyclotron and the revaporization by laser ablation.

A sample was prepared by implanting heavy metallic ions onto a light metal target at RIKEN IGISOL, which was used as a mass analyzer with a dedicated ion source. Ba^+ ions were produced by the ion source, accelerated and separated by a magnet so that only the ions of ^{138}Ba were implanted onto an Al target within an area of approximately 50 mm^2. The density of Ba on the target was estimated to be about $10^{12}/mm^2$ for 120 minutes of implantation with 0.9 nA in current. Then the sample was placed in the vacuum chamber of an ion trap, revaporized and ionized by YAG laser ablation and subjected to the laser-induced-fluorescence (LIF) observation. Another important point in this scheme is that the substrate is aluminum (mass number 27) which has a quite different mass number from barium. Therefore, the stable condition of the ion trap for Ba^+ ions is unstable for Al^+ ions. Only Ba^+ ions can be selectively confined.

Figure 1 shows the LIF signal from the trapped Ba^+. LIF was observed after one YAG laser shot, but no LIF was observed after the second shot. This is because most Ba atoms in the laser spot ($\sim$0.3 mm^2) were vaporized after the first laser shot. The total number of trapped ions is estimated to be 10^4 from the LIF signal intensity.

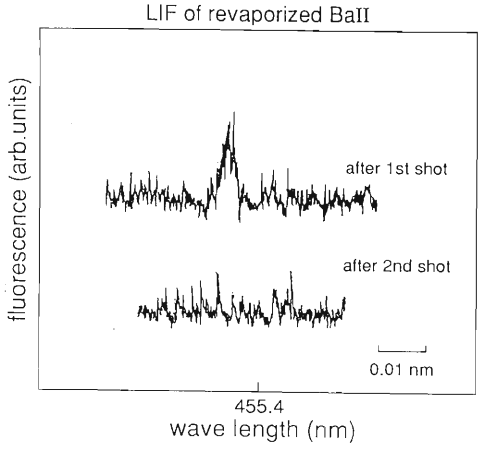

Fig. 1. LIF spectra from trapped Ba^+ ions which were implanted on an Al substrate and revaporized by the laser ablation method.

This method will be promising for the laser nuclear spectroscopy of rare atoms with unstable nuclei. The efficiency of trapping should be increased by the improvement of experimental arrangement.

References

1) W. M. Itano, J. C. Bergquist, and D. J. W. Winland: *Science*, **237**, 612 (1987).
2) H. Knab, M. Schupp, and G. Werth: *Europhys. Lett.*, **4**, 1361 (1987).
3) Y. Matsuo, H. Maeda, and M. Takami: *Hyp. Int.*, **74**, 269 (1992).

^{57}Fe Mössbauer Studies of $YBa_2Cu_{3.928}Fe_{0.072}O_8$ Oriented along the C Axis

T. Okada and K. Asai

A compound $YBa_2Cu_4O_8$ is a high-T_c superconductor (so-called 124 compound) with T_c = 80 K. It has two Cu sites (Cu(1): chain sites and Cu(2): plane sites) similar to a 123-superconductor, $YBa_2Cu_3O_7$. In a previous paper,[1] a ^{57}Fe Mössbauer study of $YBa_2(Cu_{1-x}Fe_x)_4O_8$ at various temperatures was reported. The spectrum was mainly composed of two doublets (a) and (b) at room temperatures and magnetically split into two sextets (A) and (B) at low temperatures. The hyperfine magnetic fields (H_{hf}) were observed at low temperatures below 40 K, meaning that the superconductivity and the magnetic order coexisted in that temperature region. By analyzing the spectra in the paramagnetic and magnetically ordered phases, in each iron ion site the two angles θ between the principal axis of the electric field gradient (*EFG*) and H_{hf} were obtained to be 90° or 35° at (A) sites and 66° or 45° at (B) sites, respectively. It has been known that in Cu(2) sites of the 123-compound the z axis of *EFG* was parallel to the crystalline c axis and that magnetic moments of Fe ions lay in the Cu-O plane (c plane). Since the local site symmetry of Cu(2) was identical in the 123- and 124-compounds, *EFG* and the magnetic anisotropy of Fe ions in Cu(2) sites were expected to be similar in both compounds. Then the angle θ of 90° was expected. The angle θ of 45° in (B) sites was expected if we assumed that quadrupole splitting (*QS*) was negative with the z axis of *EFG* lying along a fixed direction in the c plane and the directions of H_{hf} were oriented randomly within the c plane. The (B) site was expected to be Cu(1) sites. The above discussion is very reasonable but includes the assumption that the magnetic moments of iron ions lie in the c plane. The purpose of this paper is to clarify the direction of spin in each iron ion site and the site occupation of iron ions in the compound by using Mössbauer measurements of the powder specimen oriented.

Nobody has succeeded in growing a single crystal of $YBa_2Cu_4O_8$ yet. Then, in order to obtain the specimen oriented, at least, parallel to the c axis, the powder specimen was aligned along the c axis in epoxy by applying a high external magnetic field (14 T) and sliced into a thin plate of which the plane was confirmed to be the c plane by the x-ray analysis. Mössbauer spectra were obtained with transmission geometry where the incident γ ray is perpendicular to the c plane of the oriented specimen.

^{57}Fe Mössbauer spectra of the powder (a) and oriented (b) specimens of $YBa_2Cu_{3.928}Fe_{0.072}O_8$ at 4 K are shown in Fig. 1. Both spectra can be analyzed in terms of two magnetically split sextets denoted by (A) and (B), and one doublet (C) in the figure. Here, Fe ions in the doublet (C) are omitted from the discussion because of their small population. The values of H_{hf} can be derived to be 425 kOe in (A) and 245 kOe in (B), respectively. Mössbauer intensity ratio of each peak in the magnetically split sextet is determined by the angle between γ ray and the direction of spin. The intensity ratio is 3:2:1:1:2:3 when the direction of spin is random, and 3:4:1:1:4:3 when the incident γ ray is perpendicular to the direction of spin. As can be seen in Fig. 1, the difference of Mössbauer intensity ratio of spectra (a) and (b) is apparently observed. The ratio is obtained to be 3:2:1:1:2:3 in the powder specimen (a), and 3:4:1:1:4:3 in the specimen (b) oriented along the c axis, to which the incident γ ray is parallel. It means that the directions of spins of iron ion sites (A) and (B) are both in the c plane. The present result indicates that the major part of Fe ions occupies the Cu(2) sites and the minor the Cu(1) sites.

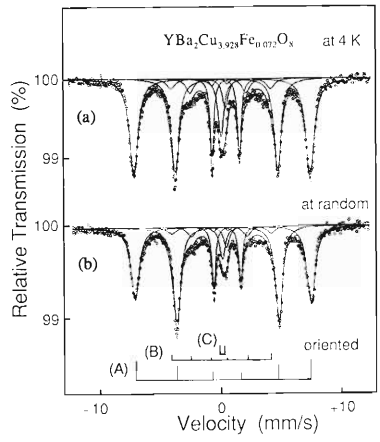

Fig. 1. ^{57}Fe Mössbauer spectra of the powder (a) and the oriented (b) specimens at 4 K.

References

1) T. Okada et al.: *Nucl. Instrum. Methods Phys. Res.*, **B76**, 338 (1993).

Charge State and Diffusivity of Hydrogenic Atom in GaAs with Si Donors

R. Kadono, S. Fujii,[*1] A. Matsushita, K. Nagamine, K. Nishiyama,[*2] and S. Tanigawa[*3]

Since the revelation in the early 1980s that hydrogen can form chemical complexes with impurities including carrier dopants to eliminate electronic states in silicon (i.e., hydrogen passivation), the structure and kinetics of hydrogen isotopes in semiconductors have been drawing much attention.[1)] However, while microscopic information on hydrogen-impurity complexes has been obtained by means of infra-red spectroscopy and channeling, relatively little is known about the isolated hydrogen state in semiconductors. It is noteworthy that μSR (Muon Spin Rotation, Relaxation, Resonance) has made a significant contribution to the latter by clarifying the electronic structure of isolated muonium state (a muonic analog of hydrogen atom in which proton is substituted by positive muon) in both elemental and compound semiconductors.[1,2)] Furthermore, the recent development of longitudinal spin relaxation technique for the muonium state has provided information on the diffusion property of isolated muonium in high-resistivity (HR) GaAs.[3)]

We report on the effect of silicon (Si) doping on the charge state ($Mu^{0,\pm}$) and kinetics of muonic states in GaAs. The μSR measurements were performed at UTMSL (Meson Science Laboratory, University of Tokyo) on two GaAs samples grown by the horizontal Bridgman method with different doping levels, having room temperature carrier concentration of 10^{12}–10^{14} cm^{-3} (GaAs:Si-A, non-metallic) and 9×10^{17} cm^{-3} (GaAs:Si-B, metallic), respectively.

The implanted positive muons are known to form two paramagnetic centers in GaAs discerned by the hyperfine structure, i.e., interstitial muonium (Mu) and bond-center muonium (Mu*). In addition, a diamagnetic muon ($Mu^{\pm}$) state is observed in doped GaAs, which is predominant in metallic samples. The current data indicate that the Mu state in non-metallic GaAs is replaced by $Mu^{\pm}$ in metallic GaAs probably due to the increased Fermi level, whereas Mu* state is only weakly affected by doping. Moreover, the change of the charge state was found to strongly influence the diffusion property of the muonic states as shown in Fig. 1. Namely, Mu is highly mobile in non-metallic GaAs with $D_\mu = a^2/32\tau_c \cong 10^{-8}$–$10^{-6}$ cm^2 s^{-1}, where the effect of weak doping is seen only below 30 K in GaAs:Si-A. Meanwhile, the jumping frequency of $Mu^{\pm}$ in GaAs:Si-B is less than 10^6 s^{-1} over the temperature range 4–300 K, being three orders of magnitude lower than that of Mu in non-metallic GaAs. Moreover, the $Mu^{\pm}$ state seems to be immobile at room temperature, suggesting that the state is deeply trapped or in a bound state with impurity atoms.

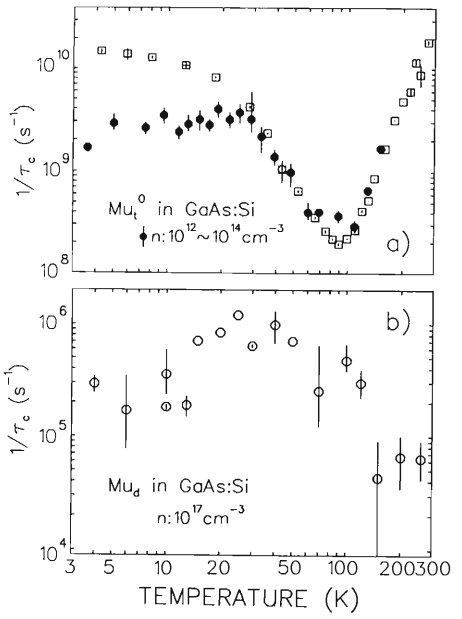

Fig. 1. The jumping frequencies of a) Mu in HR-GaAs (open squares, after Ref. 3 and in GaAs:Si-A (filled circles), and b) $Mu^{\pm}$ in GaAs:Si-B.

References

1) For a recent review, see, for example, J. I. Pankove and N. M. Johnson eds.: Hydrogen in Semiconductors, Academic, San Diego (1991).
2) For a recent review, see, for example, B. D. Patterson: *Rev. Mod. Phys.*, **60**, 69 (1988).
3) R. Kadono et al.: *Hyp. Int.*, **64**, 635 (1990).

*1 Sumitomo Electric Industries Ltd.
*2 Meson Science Laboratory, University of Tokyo
*3 Institute of Material Science, University of Tsukuba

Annealing Behaviour of Kr Atoms in Kr-Implanted Aluminium

M. Hacke and E. Yagi

It has been demonstrated that heavy inert gas atoms (Ar, Kr, and Xe) implanted into metals at ambient temperature precipitate into bubbles, and that for high implantation doses they are in a solid phase epitaxially aligned to matrices.[1-3)]

From previous channelling studies on the Kr-implanted Al, we obtained the following results. At the initial stage of implantation various types of complexes consisting of Kr atoms and vacancies (V) such as KrV_4, KrV_6 and larger ones are formed, and act as nucleation centres for the subsequent bubble formation.[4,5)] The formation of solid krypton is enhanced by the post-implantation irradiation.[6)] The objective of the present study is to investigate the behaviour of Kr atoms in aluminium for annealing and the stability of the Kr-vacancy complexes by the channelling method.

Kr^+ implantation was carried out at room temperature at 50 keV with a dose of 10^{15} Kr/cm^2 at a dose rate of about 2.2×10^{12} Kr/cm^2 s (specimen A) or 3.2×10^{12} Kr/cm^2 s (specimen B), The specimen A was isochronally annealed at 373, 433, 473, 523, and 593 K for 30 min. After each annealing treatment channelling analysis was performed at room temperature for <100>, <110>, and <111> channels with a 1.0 MeV He^+ beam accelerated by a tandem accelerator.

In the as-implanted state the Kr angular profile exhibits a shallow dip with nearly the same half-width as that of the corresponding channelling Al dip for the <100> and <111> channels, and a central peak superimposed on a shallow dip for the <110> channel. In the <100> Kr profile a very small central peak is superimposed on the dip. As previously reported,[4-6)] these profiles can be interpreted as showing that the Kr atoms are distributed over substitutional (S), tetrahedral (T) (Kr in KrV_4), octahedral (O) (Kr in KrV_6), and random (R) sites. The small <100> central peak originates from the T-site occupancy, and the <110> central peak from the T- and O-site occupancies.

Upon annealing at 433 K, the small <100> central peak disappears, and either of the <100> and <111> Kr profiles exhibits a shallower simple dip with nearly the same half-width as that of the corresponding Al dip. The <110> central peak is still observed. These results indicate that upon annealing at 433 K the T-site occupancy disappears but the O-site occupancy is still present. On annealing at 473 K a small portion of Kr atoms which have been located at the O sites are slightly displaced.

Upon annealing at 593 K the <110> central peak disappears, and any of the <100>, <110> and <111> Kr profiles exhibits a very shallow dip of the relative depth of approximately (3–8)% of the corresponding Al dip, indicating that the O-site occupancy disappears and most of Kr atoms ($\sim$ 95%) are located at R sites.

From the observed angular profiles the fractions of various site occupacies were estimated. They are shown in Fig. 1. The annealing stages at 433 and 593 K are explained in terms of the dissociation of KrV_4 and KrV_6 complexes, respectively.

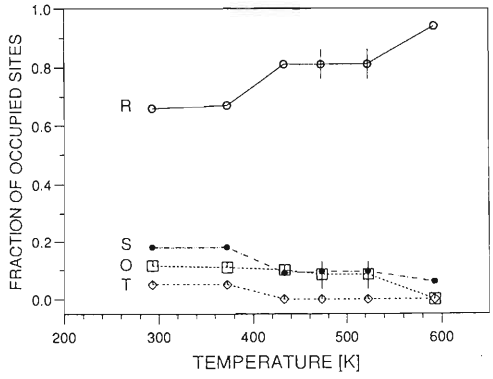

Fig. 1. The change of the fractions of various site occupancies with the annealing temperature. In two cases of annealing at 473 and 523 K the open squares represent the sum of the fractions of the O- and displaced O-site occupancies.

The specimen B was annealed at 683 K after similar isochronal annealing up to 593 K. The Kr profiles are significantly different from those obtained after annealing up to 593 K. For the <110> channel it exhibits a shallow dip approximately 1.5 times broader than the Al dip. This broader Kr dip can be explained by the channelling effect of the incident He^+ ions in an epitaxially aligned solid Kr crystal lattice, because the critical angle for channelling is larger for the Kr crystal than for the Al crystal. Therefore, on annealing at 683 K, solid krypton is formed.

References

1) A. vom Felde, J. Fink. Th. Müller-Heinzerling, J. Pflüger, B. Scheerer, G. Linker, and D. Kaletta: *Phys. Rev. Lett.*, **53**, 922 (1989).
2) C. Templier, C. Jaouen, J. -P. Rivière, J. Delafond, and J. Grilhé: *C. R. Acad. Sci., Ser. II*, **299**, 613 (1984).
3) J. H. Evans and D. J. Mazey: *J. Phys.*, **F15**, L1 (1985).
4) E. Yagi: *Nucl. Instrum. Methods Phys. Res.*, **B39**, 68 (1989).
5) E. Yagi, I. Hashimoto, and H. Yamaguchi: *J. Nucl. Mater.*, **169**, 158 (1989).
6) E. Yagi: *Phys. Rev. Lett.*, **67**, 3804 (1991).

High Energy Heavy Ion Irradiation of Superconductor $La_{2-x}Sr_xCuO_4$

M. Terasawa, T. Mitamura, T. Kohara, K. Ueda, H. Tsubakino, A. Yamamoto,*
Y. Awaya, T. Kambara, Y. Kanai, M. Oura, and Y. Nakai

Ion irradiation on oxide superconductors degrades the superconducting transition temperature (T_c) and decreases the critical current density (J_c) at a high ion fluence regime, where the material undergoes a superconducting-to-nonsuperconducting transition due to the defect accumulation. However, there is a possibility that the high energy heavy ions can enhance J_c at fairly low flunece through the interaction of ion-induced defects with the flux lattice.[1] In this work we investigated the effects of high energy and heavy ion irradiation on $La_{1.85}Sr_{0.15}CuO_4$.

Sintered polycrystalline specimens of $La_{1.85}Sr_{0.15}CuO_4$ were prepared by means of the conventional ceramic procedure. The specimen of 10 mm in diameter and 0.5 mm thick were thinned to less than 0.15 mm so that incident ions can penetrate throughout the specimen full depth. The specimens were irradiated with 3.5 GeV $^{136}Xe^{31+}$ ions from the RIKENRing Cyclotron. After the irradiation electrical resistivity measurements were made by a conventional four point probe method. The measurement was performed by applying a magnetic field in the way that the direction of incident heavy ions is parallel to the applied magnetic field.

From the I - V measurements by the four point probe method was decided a critical current density J_c at which a sharp increase in voltage was observable. Without application of the magnetic field, J_c was 35 A/cm^2 and 76 A/cm^2 for the unirradiated specimen and for the specimen irradiated to 1.2×10^{11} Xe/cm^2, respectively. With application of the magnetic field, the unirradiated specimen showed a drastic decrease of J_c, while the present Xe-ion-irradiated specimens showed no J_c change (1.2×10^{11} Xe/cm^2) or gradual decrease (3.0×10^{11} Xe/cm^2). Figure 1 shows J_c as a function of the applied magnetic field for the Xe irradiated and unirradiated specimens. The J_c data were normalized by the current densities at zero magnetic field for each specimen. Remarkable irradiation effect on the critical current density was observed.

High resolution transmission electron micrographs of the irradiated specimens revealed that the ion-induced damage comprises an amorphous columnar structure along the ion track. The columnar damage is about 5 nm in diameter on average, and the density is almost the same as that of the ion fluence.

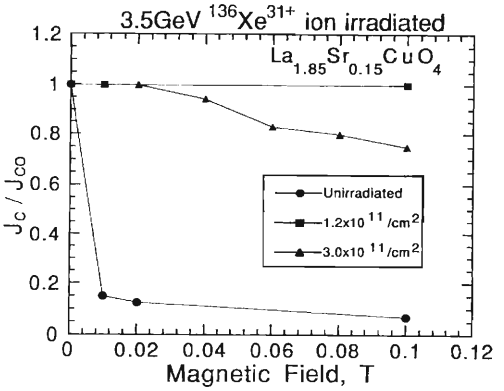

Fig. 1. Critical current density as a function of the applied magnetic field. The current density is normalized by the one, J_{co}, without magnetic field.

In conclusion, radiation effects of GeV heavy ions on $La_{1.85}Sr_{0.15}CuO_4$ were investigated for the first time. It is confirmed that the electron transport properties are improved and that the increase in J_c over 10 times the one before irradiation is obtainable with no degradation of the critical temperature T_c even in the magnetic field application. The columnar defects induced by the GeV heavy ions through an electronic stopping interaction may affect primarily for pinning the magnetic flux. Since the ion fluence is extremely low, deleterious effect against weak links between the superconducting grains, which has been a problem in the conventional neutron or proton irradiation resulting in T_c and J_c degradation, will be negligibly small in the GeV heavy ion irradiations.

References

1) L. Civale et al.: *Phys. Rev. Lett.*, **67**, 648 (1991).

* Himeji Institute of Technology

Single Event Effect in Power MOSFETs and CMOS ICs by High-Energy Heavy Ion

S. Matsuda, S. Kuboyama, T. Tamura, Y. Shimano, M. Nakajima, M. Uesugi, T. Kanno, J. Ohya, T. Ishii, H. Ohira, T. Kohno, N. Inabe, T. Nakagawa, M. Kase, A. Goto, and Y. Yano

Power MOSFETs and CMOS ICs are essential devices for power switching and digital processing, respectively. However, they have a possible catastrophic failure mode known as Single Event Burn-Out (SEB)/Single Event Latch-up (SEL) triggered upon incidence of high-energy heavy ions. Since this is an important phenomenon to be considered in space electronic applications, there is necessity to improve the immunity from these Single Event Effect (SEE) for the commercial devices.

To study the SEE mechanism, a spectrum of charge collected in the device was measured by a pulse-height analyzer system with a modified charge-sensitive amplifier. In previous work for Power MOSFETs,[1] it was suggested that SEB was triggered when a collected charge exceeded some threshold charge Q_{TH}. Figure 1 shows the charge spectra for several samples of different rated drain breakdown voltage (BV_{DS}). It is obvious that each sample has its own peculiar Q_{TH}. Detail of Q_{TH} is defined in reference.[2] It has been also identified that the 1st and 2nd peaks correspond to the collected charge from a drain junction and the injected charge from a source junction, respectively.

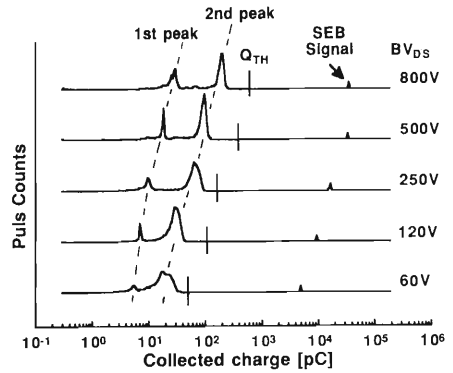

Fig. 1. Collected charge spectra by Xe ion irradiation for various rated voltage samples.[1]

High-energy heavy ions from RIKEN Ring Cyclotron were utilized this year to analyze the dependence of Q_{TH} on BV_{DS} and LET of ions. The parameters of heavy ions are shown in Table 1.

Table 1. Parameter of heavy ions.

Ion	Ar	Kr	Xe	Ni*
Energy [MeV/u]	95	10	26	4.3
LET in Si [Mev·cm^2/mg]	2	29	36	30
Range in Si [μm]	6000	104	240	32

* Data obtained in previous work

Calculated energy loss (ΔE) in the depletion region when SEB starts triggering is shown in Table 2. The depletion region was calculated based on the impurity density. Since no SEB was detected at the incidence of Ar ion, ΔE at the maximum rated voltage is shown in case of Ar ion. SEB is triggered when the energy loss ΔE in the depletion region gets beyond a certain value for each device.

Table 2. Energy loss in the depletion region of power MOSFET when SEB is triggered.

Device	A	B	C
Rated BV_{DS} [V_{DC}]	60	250	500
ΔE [MeV] by Xe ion	22	92	200
ΔE [MeV] by Kr ion	19	—*	194
ΔE [MeV] by Ni ion	20	90	200
ΔE [MeV] by Ar ion	(1.8)	(11)	(17)

* no test data

In the meantime, several CMOS ICs for space application including SRAM, Gate-Array, etc. were submitted to the experiment of SEL. Improvement of immunity from SEL was demonstrated by the experimental data. Moreover, it was suggested that the threshold LET of 64 Kbit SRAM for commercial use was 2 MeV·cm^2/mg.

For further study of Single Event Effect, more detailed analysis will be performed concerning the dependence of charge creation on supply voltage of devices.

References

1) S. Matsuda et al.: *RIKEN Accel. Prog. Rep.*, **26**, 75 (1992).
2) S. Kuboyama et al.: *IEEE Trans. Nucl. Sci.*, **NS-39**, 1698 (1992).

3. Radiochemistry and Nuclear Chemistry

Preparation of a Radioactive Multitracer Solution from Iron Foil Irradiated by 80 MeV/nucleon ^{16}O Ions

S. Chen, S. Ambe, and F. Ambe

We reported previously radiochemical procedures to prepare radioactive multitracer solutions free from carriers and salts by using Au, Ag, and Cu targets irradiated with a ^{12}C, ^{14}N, or ^{16}O beam.[1,2] The Cu target is suitable for preparing a multitracer solution of lighter elements. However, the preparation method from the Cu target takes a relatively long time to complete. Therefore, a more convenient method of preparing a radioactive multitracer solution from an Fe target irradiated with a heavy-ion beam has been developed.

Three sheets of Fe foil (24 mmø × 100 μm) mounted in a 40 mmø aluminum ball with a 20 mmø piercing hole were irradiated with an 80 MeV/nucleon ^{16}O beam in the falling ball irradiation system installed in a beam course of the RIKEN Ring Cyclotron.[1] The beam intensity was about 50 enA and the irradiation time was about one hour. The beam profile was roughly 10 × 10 mm.

The irradiated Fe foil (200 mg) containing various radioactive nuclides produced by the heavy-ion reactions was dissolved in 4 cm^3 of conc. HCl. Fe^{2+} in the solution was oxidized to Fe^{3+} with 1 cm^3 of hydrogen peroxide. Distilled water was added to the solution in order to adjust it to 6 mol dm^{-3} in HCl. The resultant solution was passed through a 10 mmø × 10 cm anion exchange column of Diaion SA#100, 100–200 mesh pretreated with 6 mol dm^{-3} HCl. Radionuclides were eluted with 6 mol dm^{-3} HCl. The first 40 cm^3 of the effluent was evaporated to 2 cm^3 under a reduced pressure of about 4 kPa in a rotary vacuum evaporater to yield a carrier- and salt-free multitracer solution.

The γ-ray spectra of the irradiated Fe foil, each effluent, and the multitracer solution were measured using pure Ge detectors. The spectra were analyzed with a version of the BOB code[3] on a FACOM M1800 computer at RIKEN.

The nuclides found in the multitracer solution were ^{7}Be, ^{24}Na, ^{28}Mg, ^{42}K, ^{43}K, ^{44m}Sc, ^{48}V, ^{48}Cr, ^{51}Cr, ^{52}Mn, and ^{54}Mn. No γ-rays due to the radionuclides of iron produced in the target foil (^{52}Fe etc.) were detected in the spectrum of the multitracer solution. This indicates that Fe was completely separated by the above anion exchange procedure.

Figure 1 shows representative elution curves through the anion exchange column with 6 mol dm^{-3} HCl. Their behavior agrees well with the distribution coefficients of those elements between an anion exchanger and 6 mol dm^{-3} HCl.[4]

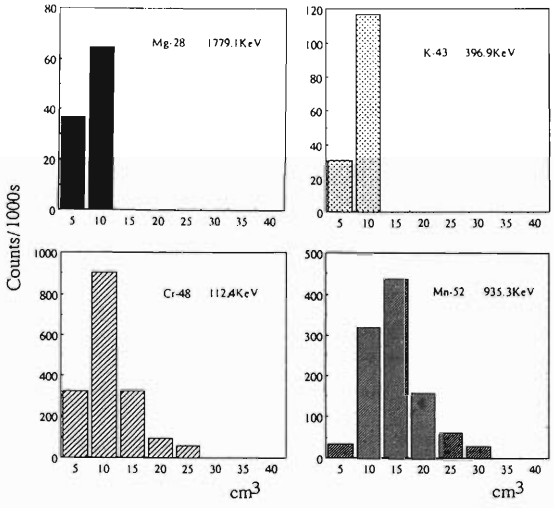

Fig. 1. The representative elution curves of radioactive nuclides produced in the iron target with 6 mol dm^{-3} HCl through an anion exchange column.

The present method of preparation of the multitracer solution from an Fe target by means of anion exchange takes only about 2 hours to complete. The useful radionuclides in the solution from an Fe target are essentially the same as those from a Cu target except for ^{52}Fe, ^{61}Co, and ^{62}Zn. Therefore, the present method using an Fe target is superior to that using a Cu target[2] and is especially profitable in studies of nuclides of a relatively short half-life.

References

1) S. Ambe et al.: *Chem. Lett.*, **1991**, 149.
2) S. Ambe et al.: *Anal. Sci.*, **7**, Suppl., p. 317 (1991).
3) H. Baba et al.: *J. Nucl. Sci. Technol.*, **8**, 1227 (1972).
4) K. A. Kraus and F. Nelson: *Proc. Int. Conf. Peaceful Uses Atomic Energy*, Geneva, **7**, 113 (1955).

Observation of Complex Formation of a Number of Metal Ions with Tea Extracts

W. Li, S. Ambe, Y. Ohkubo, M. Iwamoto, Y. Kobayashi, H. Maeda, and F. Ambe

Recently, the radioactive multitracer technique has been extensively applied to a variety of research fields due to its advantages over the conventional tracer techniques.[1] In this report, we brief results of a preliminary study on complex formation of metal ions with tea extracts using the technique. The results are significant in relation to the ingestion of metal elements by human being.

A portion of radioactive multitracer solution, obtained from irradiation of an Ag target with 80 MeV/nucleon ^{16}O ions, was twice evaporated gently to dryness in order to remove all the inorganic acid components. The residue was dissolved in diluted tea extracts prepared as described below. Four different kinds of tea, Japanese green tea (labeled as JG), Chinese green tea (CG), Chinese Wulon tea (CW), and Chinese black tea (CB), were used. Half a gram of each was added to 40 cm^3 distilled water. The suspension was heated to keep slightly boiling for 20 min. After filtration and centrifugation, the tea extracts (about 30 cm^3) were ready for the experiment. In case of studying the concentration dependence of distribution coefficients K_d, 2 g of Japanese green tea was treated in the same manner to yield a stock solution of the tea extract. We denote the concentration of the stock solution as C (arbitrary unit). The tea extracts with different concentrations were obtained by dilution of the stock solution with distilled water. For comparison, 0.1 mol dm^{-3} $HClO_4$ and 0.02 mol dm^{-3} DTPA solutions were also used. The pH values of these solutions were adjusted by NaOH to the values close to those of the tea extracts.

A conventional ion exchange method using Dowex 50W-X8 resin (100–200 mesh, Na-form) was employed to study the complex formation. About 30 mg of the resin (kept in equilibrium with a saturated NaCl solution) was added to 8 cm^3 of the tea extracts containing the multitracer. The suspension was shaken at 25 °C for 1 h. After centrifugation of the suspension, the supernatant solution was withdrawn for γ-ray spectroscopy with a pure Ge detector. The measurements of γ-ray spectra lasted for two weeks in order to cover a wide range of half-life of radioactive nuclides.

The adsorption percentages were determined for 14 elements in this experiment. Se(IV) and Tc(VII), existing generally in a form of negative ions, as well as Ru(III) or Ru(IV) and Rh(III) showed very low percentage of adsorption (typically less than 10%) for all of the solutions under study. The other metal ions, however, were adsorbed by the cation exchange resin to different extent. The adsorption percentages for selected metal elements are given in Table 1.

Table 1. Adsorption percentages by cation exchange resin.

Element (pH)	JG (5.9)	CG (5.8)	CW (5.2)	CB (5.2)	$HClO_4$ (5.7)	DTPA (5.9)
Be	7.1	3.2	3.8	8.7	26	3.6
Mn	52	55	44	48	49	27
Co	20	19	40	42	58	3.0
Rb	56	56	58	64	24	36
Sr	34	49	27	48	47	49
Y	31	27	37	34	40	2.0
Zr	10	18	5.0	11	51	0

The complex formation between the metal ions and $HClO_4$ is regarded to be negligible. From Table 1, we can see that the adsorption percentages of the majority of metal ions in the tea extracts are less than those in $HClO_4$ solution, indicating formation of certain kinds of complexes between these cations with the tea extracts. Rb can form a compound with $HClO_4$, leading to the decrease of the adsorption in a $HClO_4$ solution. Zr and Be formed more stable complexes with the tea extracts than Mn and Sr did. There is no much differece in the adsorption percentage among four kinds of tea extracts. The stability of the complexes of the tea extracts with the cations is not very large when compared with those of DTPA. Log-log plots of apparent Kd values versus the concentration of the extracts from Japanese green tea for Rb, Sr, and Co are shown in Fig. 1. As was expected, the Kd values decrease with increasing extract concentration.

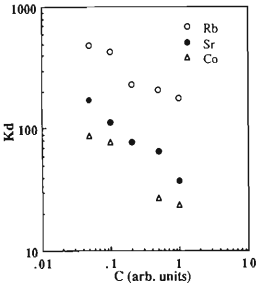

Fig. 1. Dependence of Kd values on the concentration of tea extracts.

References

1) S. Ambe et al.: *Chem. Lett.*, **1991**, 149; **1992**, 1059; S. Y. Chen et al.: *Anal. Sci.*, **7**, Suppl., 1105 (1991); S. Ambe et al.: *ibid.*, p. 317; M. Iwamoto et al.: *ibid.*, p. 313; S. Ambe et al.: *Appl. Radiat. Isot.*, **43**, 1533 (1992); S. Y. Chen et al.: *J. Radioanal. Nucl. Chem. Lett.*, in press.

Production of Multitracer Nuclides by Irradiation with a ^{84}Kr Beam

M. Iwamoto, S. Ambe, Y. Ohkubo, Y. Kobayashi, H. Maeda, and F. Ambe

We have been producing multitracers using C, N, O, and Ar ions accelerated by RIKEN Ring Cyclotron in these years. Separation of multitracers from targets is performed by radiochemical procedures or by heating under a reduced pressure.[1–5] In these methods, each target material requires a specific elaborate treatment. If much heavier ions are used as projectiles in combination with different targets and catcher foil for production of multitracer nuclides, it is expected that a large part of product nuclides are recoiled out of the target and can be collected by catcher foil placed behind the target. Using appropriate catcher foil of a common material, the same simple separation method is available for different targets. Some results of a preliminary experiment on this course is reported.

The target was Ti-, Cu-, Nb-, Ag-, Ta-, and Au-foil and the catcher was 25 mm-thick Al foil. The target assemblies were irradiated by 10.5 MeV/nucleon $^{84}Kr^{13+}$ ions using Falling Ball Irradiation System.[1] The average beam intensity was 10–30 enA and irradiation time was about 1 h. Details of experimental conditions for different targets are summarized in Table 1.

After the irradiation, the target and catcher foil were analyzed by direct γ-ray spectroscopy with pure Ge-detectors. Yield calculation of product nuclides was made by BOB code[6] and related programs. Assignment of the nuclides was performed on the basis of the energy of γ-rays and half-life.

Table 1. Experimental conditions.

Target	Thickness (μm)	Duration (h)	Total current (μC)
Ti	20	1.04	55.2
Cu	20	1.01	72.6
Nb	12.7	1.01	37.6
Ag	10	1.01	96.1
Ta	10	1.03	80.4
Au	25	0.98	26.4

Table 2 shows the fraction of various nuclides found in the catcher foil, that is the yield in catcher foil divided by the total yield. It is seen from Table 2 that all of the identified nuclides with a mass number exceeding that of the projectile (84) are exclusively found in the catcher foil. The high yield of ^{24}Na in the catcher foil is ascribed to fragmentation of ^{27}Al nuclei in the foil. These preliminary results already demonstrate the effectiveness of this catcher foil method. Analysis of the data on the other target assemblies is under way.

Table 2. Fractional yield in the catcher foil for the Ti target.

Nuclide	Fr. Yield	Nuclide	Fr. Yield
Na-24	0.91	Nb-90	1.0
K-43	0.22	Mo-93m	1.0
Sc-44m	0.21	Tc-95	1.0
Rb-81	1.0	Ru-97	1.0
Y-86	1.0	In-109	1.0
Zr-86	1.0	In-110m	1.0
Zr-89	1.0	In-111	1.0

References

1) S. Ambe et al.: *Chem. Lett.*, **1991**, 149.
2) S. Ambe et al.: *Anal. Sci.*, **7**, Suppl., p. 317 (1991).
3) M. Iwamoto et al.: *ibid.*, p. 313.
4) S. Ambe et al.: *Appl. Radiat. Isot.*, **43**, 1533 (1992).
5) S. Y. Chen et al.: *J. Radioanal. Nucl. Chem. Lett.*, in press.
6) H. Baba et al.: *J. Nucl. Sci. Technol.*, **8**, 1227 (1972).

Transport of Tc(VII) and Re(VII) through a Supported Liquid Membrane

S. Ambe, Y. Ohkubo, Y. Kobayashi, M. Iwamoto, M. Yanokura, H. Maeda, and F. Ambe

Technetium-99 with a long half-life ($T_{1/2} = 2.1 \times 10^5$ y) is widely distributed in both geo- and hydrosphere. Determination of ^{99}Tc in the environment is an important subject. For environmental samples, concentration of ^{99}Tc from a large volume is required for its exact determination.

Separation of metal ions by means of supported liquid membranes is now being viewed with keen interest as an efficient analytical tool. The method is considered to be especially suitable for preparation of radioactive tracer solutions because of (1) the simplicity of operation leading to facile automation, (2) the feasibility of concentrating tracers into a small volume of a solution, and (3) the necessity of a far smaller amount of extractants than in the case of conventional solvent extraction, resulting in little organic radioactive waste.

This paper describes the successful transport of Tc(VII) and Re(VII) from acid solutions to alkaline solutions by means of a TBP-decalin membrane supported on a microporous polytetrafluoroethylene sheet.

Tc* and Re* produced in the Au target irradiated with a 135 MeV/nucleon ^{14}N beam were used as tracers. After chemical treatment of the target, a solution containing Tc*(VII) and Re*(VII) was used as a feed solution which was 0.12 mol dm^{-3} NaCl and 0.04 mol dm^{-3} $NaNO_3$.

The microporous polytetrafluoroethylene sheet used as the support for TBP-decalin was Fluoropore FP-045 (Sumitomo Electric Ind.) with an average pore size of 0.45 μm, 75% porosity, and 0.08 mm thickness. A 24 mmϕ supported liquid membrane was prepared by impregnating the sheet with a TBP-decalin (3:1) solution. Distilled water or 0.5 mol dm^{-3} $NaHCO_3$ was used as a strip solution. The supported liquid membrane was fixed at the bottom of a Teflon vessel with a Teflon ring. The feed solution in an outer vessel was stirred at 400 rpm with a magnetic stirrer. The strip solution was circulated at a rate of 3 cm^3 min^{-1}, a given portion of the circulating solution being trapped in a Teflon vessel put on a pure-Ge detector for measurement of γ-rays. Measurement of 5000 s duration for the strip solution was automatically repeated, and the γ-ray spectra obtained were recorded on a disk.

The 0.5 mol dm^{-3} $NaHCO_3$ solution was shown to be better than distilled water as a strip solution giving higher rate of transport. Thereafter, the 0.5 mol dm^{-3} $NaHCO_3$ solution was used as a strip solution. Only slight difference in the initial transport rates of Tc(VII) was observed for the feed solutions at pH 0–1.36 as shown in Fig. 1. However, the transport of Tc(VII) from the feed solution at pH 0 showed signs of saturation soon after the start of permeation. Transport of Tc(VII) from the feed solution at pH 0.54 increased gradually with time. In the permeation using the feed solution at pH 0.74, the strip solution was replaced by a fresh 0.5 mol dm^{-3} $NaHCO_3$ solution 24 h after the start of transport. After replacement, the transport yield was enhanced as shown in Fig. 1. The transport behavior of Re(VII) is similar to that of Tc(VII); however, the amount of Re(VII) transported at a given time is smaller than that of Tc(VII).

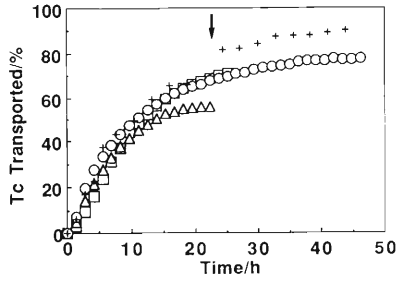

Fig. 1. Transport of Tc(VII) from feed solutions at pH 0–1.36. pH 0 (△), pH 0.54 (○), pH 0.74 (+), and pH 1.36 (2). An arrow indicates replacement of the strip solution with a fresh one in the permeation using the feed solution at pH 0.74.

It is concluded that both Tc(VII) and Re(VII) can be concentrated into a dil. $NaHCO_3$ solution from a large volume of solution adjusted to pH 1 by means of a supported liquid membrane impregnated with TBP-decalin. (Condensed from *Radiochim. Acta*, in press)

Determination of Stability Constants of Lanthanide-Humate Complexes with Multitracer Technique

Y. Minai, Y. Takahashi, M. Ishibashi,* S. Ambe, Y. Kobayashi, Y. Ohkubo, M. Iwamoto, M. Yanokura, H. Maeda, N. Takematsu, F. Ambe, and T. Tominaga

Humic substances (humic acid, fulvic acid, and humin) are a group of naturally-occurring organic polyacids, having various functional groups which can interact with metal cations in natural and artificially-modified environments. Laboratory studies on stability of actinide(III) complexes of humic substances have given relatively large values of stability constants suggesting that their complexes of humic substances can be dominant as their dissolved species in aqueous environments.[1,2] Similarity in chemical properties between actinide(III) and lanthanide(III) elements suggests that considerable amounts of lanthanide complexes with humic substances are also formed in hydrosphere. Laboratory study of stability of lanthanide-humic substance complexes would provide key knowledge to elucidate the role of humic substance complexation in the geochemical behavior of lanthanides.

As was shown in a previous report,[3] it has been revealed that the multitracer technique is quite useful to take information on complexation between lanthanide ions and humic substances. This report describes some preliminary results on the determination of stability constants of lanthanides with humic acid, using the multitracer technique.

A multitracer solution (3M HCl) was obtained from the gold foil target irradiated with ^{12}C beam accelerated in RIKEN Ring Cyclotron. The preparation procedure for the multitracer solution was given elsewhere.[4,5] After evaporation of the multitracer solution containing hydrochloric acid, 0.001 M perchloric acid was added to make the multitracer solution used for further experiments.

Solvent extraction with di(2-ethylhexyl)phosphate (DEHP) was used to determine the stability constants of lanthanide-humates.[1,2] Free lanthanide ions in the humic acid solutions containing the multitracer (I=0.1, $NaClO_4$) at pH 4–6, which was maintained by pH buffers, were extracted with DEHP in toluen. As noted in previous reports,[1,2] the observed distribution coefficient of each element is a function of the stability constant, the humic acid concentration, and the free ion concentration. The last term of this function was estimated by extrapolating the dependence of the distribution coefficient on pH and the DEHP concentration at pH 1–2, where hydrolysis is negligible, in the absence of the pH buffers.

The stability constants of the complexes of Eu, Gd, Tm, Yb, and Lu with the humic acid were determined, assuming the formation of the 1:1 complex for each lanthanide. The apparent stability constants of the Eu-humate $\log[\beta(eq^{-1})]$determined at pH4.0, 4.6, and 6.0 were approximately 8.5, 9.7, and 12.0, respectively. These values were identical with the reported values determined by solvent extraction using a single tracer of europium. The stability constants of the Gd-humate were also identical with those of the Eu-humate, whereas the stability constants of Tm-, Yb-, and Lu-humates (as β) were approximately 10 times higher than those of the Eu- and Gd-humates. Because of the small ionic radii of the heavier lanthanides (Tm, Yb, and Lu) relative to those of the middle lanthanides (Eu and Gd), the electrostatic interaction between their ions and the ligand molecule may be stronger in the heavier lanthanides than in the middle lanthanides.

Recent studies on abundance patterns of lanthanides in oceanic sediments suggested that heavier lanthanides migrate in the sediment column during diagenesis.[6] Although there has been no report on direct evidence for the occurrence of lanthanide-humic substance complexes in environments, higher stability of heavier lanthanide complexes with naturally-occurring organic substances (including humic substances) may relate to the higher mobility of heavier lanthanides reported.

References

1) Y. Minai et al.: Proc. 3rd. Int. Symp. Adv. Nucl. Energ. Res., p. 229 (1991).
2) Y. Takahashi et al.: *J. Radioanal. Nucl. Chem. Lett.*, in press.
3) Y. Minai et al.: *RIKEN Accel. Prog. Rep.*, **26**, 89 (1992).
4) S. Ambe et al.: *Chem. Lett.*, **1991**, 149.
5) S. Ambe et al.: *Anal. Sci.*, **7**, Suppl., p. 317 (1991).
6) Y. Minai et al.: *Proc. Ocean Drilling Program, Sci. Results*, **127/128**, 719 (1992).

* School of Science, University of Tokyo

Utilization of Multitracer Solutions for Studies on the Ion Exchange Behavior of a Strongly Acidic Resin NAFION

N. Aoki, H. Harakawa, Y. Saito, K. Kimura, S. Ambe, Y. Ohkubo, Y. Kobayashi, M. Iwamoto, H. Maeda, M. Yanokura, and F. Ambe

Radioactive multitracer solutions, in a carrier- and salt-free condition, prepared from silver[1,2] and gold[2-4] foil irradiated with 135 MeV/nucleon ^{12}C ions were used for the titled studies in a NAFION-HF system after being converted to a hydrofluoric acid solution. The NAFION-501 resin, manufactured by DuPont, is a perfluorinated polymer containing ~5 mmol g^{-1} sulfonic acid groups. Because of the strong acidity of the resin, a comparison of its exchange behavior with that of a common cation exchange resin attracts much attention.

The resin, commercially available as a cylindrical shape of ca. 1 mm$\phi \times 3$ mm, was crushed with a stamp mill at liquid nitrogen temperature, passed through a 50-mesh screen, and used. Into a small polyethylene bottle, 0.1 ml of the multitracer solution and 2.4 g of the resin were introduced, and the acidity of the system was adjusted to 0.1, 0.3, 1, 3, and 5 mol dm^{-3} with hydrofluoric acid by making the volume of the solution to 10 ml. The contents of the bottle were shaken vigorously at 25 °C with an 8-shape mode shaker. Time of the shaking was 16 hours for the silver-multitracer and 75 hours for the gold-multitracer. After filtration, γ-ray spectrometry was carried out for both phases. The γ-ray spectra were analyzed on a FACOM M1800 computer.

The distribution ratios (D) of Na, Ga, Rb, Sr, Y, Zr, Nb, Ru, Rh, and Pd were obtained from the silver-multitracer runs and those of Sc, Rb, Y, Ag, Ba, Ce, Eu, Gd, Tb and Lu from the gold-multitracer runs. The D's for Rb obtained from the silver and the gold runs showed that the equilibrium was almost attained by the 16 hours shaking. As shown in Fig. 1a, the slopes for alkali and alkaline earth metal ions in the log-log plotting were approximately -1 and -2, respectively, which is characteristic of the ion exchange. As for rare earth elements, the slope for Ce was approximately -3, whereas those for Y, Eu, Tb, and Lu ranged from -1 to -2 (Fig. 1b). It seems likely that there would be a relation between the slopes and ionic radii. D's for noble metals in the hydrofluoric acid system remained rather constant with increasing acidity and were not much different from those in a perchloric acid system.[5]

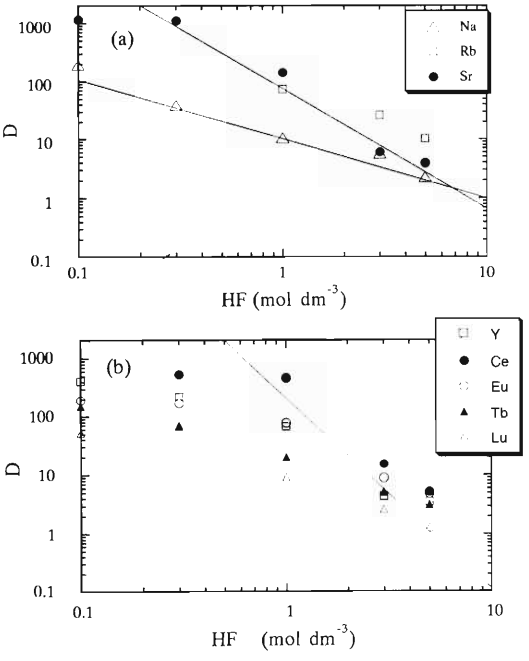

Fig. 1. Relationship between D and acidity. (a) Na, Rb, and Sr. (b) Y, Ce, Eu, Tb, and Lu.

References

1) S. Ambe, S. Y. Chen, Y. Ohkubo, Y. Kobayashi, M. Iwamoto, M. Yanokura, and F. Ambe: *RIKEN Accel. Prog. Rep.*, **25**, 95 (1991).
2) S. Ambe, S. Y. Chen, Y. Ohkubo, Y. Kobayashi, M. Iwamoto, M. Yanokura, and F. Ambe: *Anal. Sci.*, **7**, Suppl., p. 317 (1991).
3) S. Ambe, S. Y. Chen, Y. Ohkubo, Y. Kobayashi, M. Iwamoto, and F. Ambe: *RIKEN Accel. Prog. Rep.*, **24**, 73 (1990).
4) S. Ambe, S. Y. Chen, Y. Ohkubo, Y. Kobayashi, M. Iwamoto, M. Yanokura, and F. Ambe: *Chem. Lett.*, **1991**, 149.
5) T. Bamba, H. Harakawa, Y. Saito, K. Kimura, T. Yaita, S. Shibata, S. Ambe, Y. Ohkubo, M. Iwamoto, Y. Kobayashi, M. Yanokura, H. Maeda, and F. Ambe: *RIKEN Accel. Prog. Rep.*, **26**, 88 (1992).

Adsorption Behavior of Various Elements in Chloride Solutions on Activated Carbon Fiber and Non-ionic Macro-reticular Copolymer Using Multitracer

S. Shibata, K. Watari,* Y. Noda,* S. Ambe, Y. Ohkubo, M. Iwamoto, Y. Kobayashi, M. Yanokura, H. Maeda, and F. Ambe

Activated carbon and non-ionic macro-reticular (MR) copolymers have been reported to be effective adsorbents for a number of organic substances in aqueous solutions, but not enough attention has been paid to the adsorption of inorganic substances. These adsorbents have particularly high distribution ratios (*Kd*) for tetrachloro complex anions of Fe(III), Ga(III) and Au(III) in HCl solutions above 6 mol·dm^{-3} without any other organic ligands.[1,2] Such peculiar adsorption behavior has been observed in cation exchange resins,[3] too.

In the present work, the adsorption behavior of inorganic elements on Kynol ACF-1605-15 (novoloid-based activated carbon fiber) and Amberlite XAD-7 (non-ionic MR copolymer) was studied in 0.01–10 mol·dm^{-3} solutions of HCl and LiCl. The multitracer was prepared by the irradiation of 135 MeV/nucleon $^{12}C^{6+}$ onto Au or Ag foil.[4]

The retention of the elements was studied under static conditions (batch method). The multitracer solution was shaken with the adsorbent for 2 hours, and a half of the supernatant (fraction **s**) and the remaining half containing the adsorbent (fraction **r**) were divided. The radioactivities of fractions **s** and **r** were measured with a high-resolution gamma-ray spectrometer, and analyzed with the BOB code[5] on a SUN workstation. The radioactive nuclides in the multitracer were identified by the gamma-ray energies and half lives. *Kd* was calculated by

$$Kd = (A_r - A_s)/2A_s \cdot V/m$$

where A_s and A_r are the peak areas of fractions **s** and **r**, respectively, and V and m denote the volume of a suspension (cm^3) and the weight of an adsorbent (g), respectively.

Figure 1 shows the adsorption profiles of 36 elements in log-log plotting of *Kd* against the concentration of Cl^-. An important feature of these profiles is that the *Kd* of several elements increases with increasing Cl^- concentration above 5 mol·dm^{-3}. The authors are now studying adsorption behavior of other elements using the multitracer prepared from other targets.

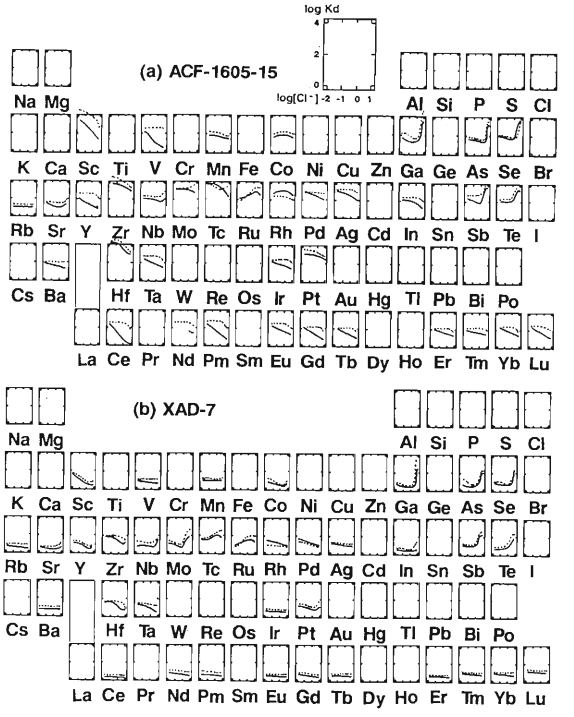

Fig. 1. Effect of Cl^- concentration in HCl (—) and LiCl (···) on *Kd* values of elements for ACF-1605-15 (a) and XAD-7 (b).

References

1) K. Watari, K. Imai, S. Shibata, and M. Miura: *J. At. Energy Soc., Japan*, **26**, 384 (1984).
2) S. Shibata, K. Watari, and K. Kaneko: *Radioisotopes*, **39**, 26 (1990).
3) F. Nelson, T. Murase, and K. A. Kraus: *J. Chromatog.*, **13**, 503 (1964).
4) S. Ambe, S. Y. Chen, Y. Ohkubo, Y. Kobayashi, M. Iwamoto, M. Yanokura, and F. Ambe: *Anal. Sci.*, **7**, Suppl., 317 (1991).
5) H. Baba, H. Okashita, S. Baba, T. Suzuki, H. Umezawa, and H. Natsume: *J. Nucl. Sci. Technol.*, **8**, 1227 (1972).

* Natl. Inst. Radiol. Sci.

Study of the Solvent Extraction of Various Elements with Diphosphine Dioxide (DPDO) by Use of the Multitracer

T. Yaita, S. Tachimori,* S. Ambe, M. Iwamoto, Y. Kobayashi,
H. Maeda, Y. Ohkubo, M. Yanokura, and F. Ambe

Diphosphine dioxides (DPDOs; Fig. 1) are one of neutral bidentates and show the highest extractability in these organophosphorous compounds for trivalent lanthanide and actinide elements from nitric acid solutions.

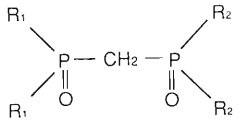

Fig. 1. Diphosphine dioxides R_1, R_2 = p-Tol, X=CH_2 (this work).

However, distribution coefficients of DPDO have not been obtained for most of elements except several lanthanide and actinide elements. Therefore, from the standpoint of the separation of lanthanide and actinide elements from the others, it is interesting and important to clarify the extraction properties of DPDO and to compare them with those of other bidentate extractants. In this work, the distribution coefficients (K_d) of DPDO for various elements were determined by using the multitracer.

Recently, a large number of radioactive nuclides have been produced as the multitracer by the high-energy heavy-ion irradiation on several targets in the RIKEN Ring Cyclotron.[1,2] The multitracer technique makes it possible to determine K_d values of various elements under the same condition, and has greater advantage than the single tracer technique in solvent extraction experiments.

Multitracer solutions were obtained from the Au targets irradiated with ^{12}C beam accelerated by RIKEN Ring Cyclotron. The irradiated target was dissolved in aqua regia. This solution was evaporated to dryness. After this residue was dissolved in 3 mol dm^{-3} HCl, Au was removed from the solution with diethyl ether solvent extraction and the aqueous phase was dried up again. Finally, the residue containing the multitracer was dissolved in 1–12 mol dm^{-3} HNO_3.

The nitric acid solution containing the multitracer was shaken with a 0.02 M DPDO-$CHCl_3$ solution for 20 min., and separated again by centrifugation for 10 min. Then, the radioactivity of organic and aqueous phases was measured. The distribution coefficient was calculated from the following formula:

$$K_d = [M]_{org}/[M]_{aq}$$

where $[M]_{org}$ and $[M]_{aq}$ denote the radioactivity of nuclides in the organic and aqueous aliquots, respectively. Figure 2 shows the dependence of K_d values for various elements on the nitric acid concentration. From this figure, it is clear that the trivalent elements (Y, Tm, In) can be separated from noble metal elements (Ru, Rh, Ir, Au) and the alkaline earth element (Ba). Furthermore, the variation patterns were classified into three categories: (1) two peaks with the maximum about 4 M HNO_3 and the minimum in the range of 8–10 M HNO_3, (2) no acidity dependence and (3) simple increase of K_d with HNO_3 concentration.

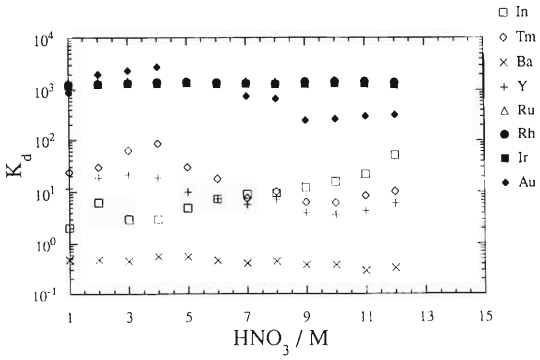

Fig. 2. The nitric acid dependence of K_d values for various elements.

References

1) S. Ambe, S. Y. Chen, Y. Ohkubo, Y. Kobayashi, M. Iwamoto, M. Yanokura, and F. Ambe: *Chem. Lett.*, **1991**, 149.
2) S. Ambe, S. Y. Chen, Y. Ohkubo, Y. Kobayashi, M. Iwamoto, M. Yanokura, and F. Ambe: *Anal. Sci.*, **7**, Suppl., p. 317 (1992).

* Japan Atomic Energy Res. Inst.

Yield Distributions of Hf Isotopes from the Reactions of Heavy Ions on W Target

W. Li, S. Ambe, Y. Ohkubo, M. Iwamoto, Y. Kobayashi, H. Maeda, and F. Ambe

Recently, the multinucleon transfer reaction has achieved great success in production of new neutron-rich nuclides above the classical fission product region (A > 170). In order to search for even more neutron-rich nuclides and to study decay properties of such exotic nuclei in this mass region, it is instructive to examine the general evolution of the yield distribution of the target residues produced from heavy ion reactions. For this purpose, we have carried out a series of yield measurements for Hf isotopes produced from the reactions of natural W targets with 135 MeV/nucleon ^{12}C, 80 MeV/nucleon ^{16}O, 40 MeV/nucleon ^{40}Ar, and 10.5 MeV/nucleon ^{84}Kr ions. In this report, we give the yield distribution of Hf isotopes produced from the 10.5 MeV/nucleon $^{84}Kr + W$ reaction. The results are compared with those from the 135 MeV/nucleon $^{12}C + W$ reaction.

Natural W metal foil (47 mg/cm^2) was irradiated for 20 min by 10.5 MeV/nucleon ^{84}Kr ions delivered from RIKEN Ring Cyclotron. After the end of irradiation, the target was immediately transferred to the hot laboratory by Falling Ball Irradiation System. The W foil was dissolved in a mixture of concentrated HF and HNO_3, containing 10 mg Hf carrier. An Sm^{3+} solution was added to remove the radioactive rare earth nuclides by co-precipitation with SmF_3. Hf was then precipitated in the form of $BaHfF_6$ by adding a Ba^{2+} solution. After the precipitate was dissolved in HNO_3 saturated with H_3BO_3, Hf was extracted from an about 10 mol dm^{-3} HNO_3 solution containing 1% H_2O_2 to a 25% HDEHP (di(2-ethylhexyl)phosphate)-toluene solution. A 1 mol dm^{-3} HF-1 mol dm^{-3} HNO_3 solution was used for back-extraction of Hf from the organic phase. Finally, Hf was precipitated once again as $BaHfF_6$, and was subjected to γ-ray spectroscopy. The chemical separation took only about 8 min and γ-ray counting began 11 min after the end of irradiation. Chemical yield of Hf was about 80% as determined in a cold experiment.

In this experiment, the cumulative yields were determined for 10 Hf isotopes ranging from 166 to 183 in mass number. The yield dependence on the mass number of the Hf isotopes is shown in Fig. 1. Although neutron-deficient nuclides are dominant among the radioactive Hf isotopes, neutron-rich Hf nuclides were also produced with non-negligible cross sections.

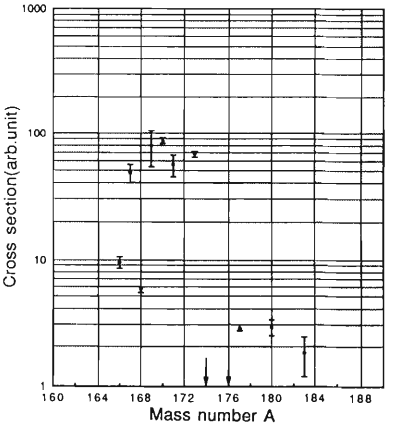

Fig. 1. The yield distribution of Hf isotopes for the reaction of a natural W target with 10.5 MeV/nucleon ^{84}Kr ions. The arrows show stable isotopes with no isomers.

When compared with similar measurements on the reaction of a W target with 135 MeV/nucleon ^{12}C ions (see Fig. 2), it is obvious that the low-energy ^{84}Kr ions are more favorable than the intermediate energy ^{12}C ions for efficient production of neutron-rich exotic nuclides relative to neutron-deficient nuclides resulting in improvement of S/N ratio in detection of the former. Data analysis is still in progress.

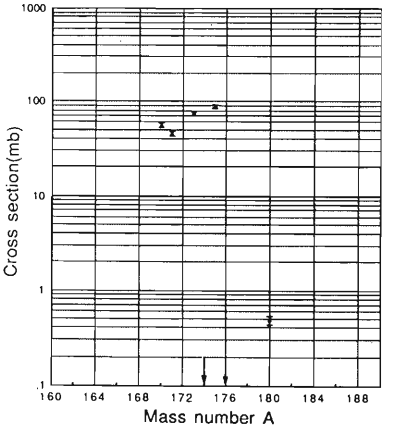

Fig. 2. The yield distribution of Hf isotopes for the reaction of a natural W target with 135 MeV/nucleon ^{12}C ions. The arrows show stable isotopes with no isomers.

Study on the Nuclear Reactions of ^{93}Nb, ^{181}Ta, and ^{197}Au Induced by Secondary Neutrons in 40 MeV/nucleon ^{40}Ar Ion Collisions

W. Li, Y. Ohkubo, S. Ambe, Y. Kobayashi, M. Iwamoto, H. Maeda, and F. Ambe

Shikata et al. and Nakajima et al. reported some measurements on the reactions induced by secondary neutrons produced by irradiation of a thick iron target with 135 MeV/nucleon ^{14}N ions.[1,2] In their experiments, emphasis was placed only on the (n, xn) reactions, where x is 2–5. It is necessary to carry out a full measurement for all of the reaction products in order to understand the secondary-neutron-induced reactions. As a first general survey, the present report gives the experimental results from study on nuclear reactions of ^{93}Nb, ^{181}Ta, and ^{197}Au targets with the secondary neutrons produced by irradiation of a thick stainless steel target with 40 MeV/nucleon ^{40}Ar ions.

The experiments were performed on the RIKEN Ring Cyclotron. Forty MeV/nucleon ^{40}Ar ions were stopped in a stainless steel Faraday cup with a thickness of 1.2 cm after traversing primary targets consisting mainly of 0.1 mm thick gold foil for a different experiment. A secondary target assembly used for neutron irradiation was placed immediately behind the Faraday cup. The target assembly consisted of ^{27}Al, ^{93}Nb, ^{181}Ta, and ^{197}Au foil. The irradiation lasted for about 23 h (with several interruptions). Following the irradiation, the secondary targets were analyzed by direct γ-ray spectroscopy for 4–5 weeks. Nuclidic assignment and yield calculation were done by conventional nuclear chemical techniques.

In this work, the yields for the reaction products were determined relative to that of ^{24}Na produced from the reference reaction of ^{27}Al(n, α)^{24}Na. The mass yield distributions obtained from the experimental data are shown in Fig. 1 as a function of mass loss ΔA from the target for the reactions of ^{93}Nb, ^{181}Ta, and ^{197}Au, respectively.

The mass yield distributions, as seen from Fig. 1, are approximately parallel with each other. The slopes were calculated to be 2.30 ± 0.27 u^{-1}, 2.29 ± 0.26 u^{-1}, and 2.48 ± 0.18 u^{-1} (u: mass unit) for the reactions of ^{93}Nb, ^{181}Ta, and ^{197}Au targets, respectively. These values are in good agreement within the experimental errors, indicating that the slope of the mass yield distribution is independent of the target species for the secondary-neutron induced reactions. The lightest products were found to be ^{86}Y^{g} and ^{86}Zr in the activated ^{93}Nb targets, which resulted from removal of 8 nucleons from the composite system of a target nucleus and a neutron. The separation energy of a neutron is about 8 MeV for the nuclides involved in this work and the kinetic energy of the neutrons emitted from the composite system is about 2 MeV on average. Thus, we can draw the conclusion that a significant fraction of the secondary neutrons had an energy larger than 70 MeV, which is much larger than the incident energy per nucleon of the ^{40}Ar ions. The estimation is supported by the neutron inclusive measurements with the time-of-flight method on the ^{14}N + Ag reaction at 35 MeV/nucleon.[3]

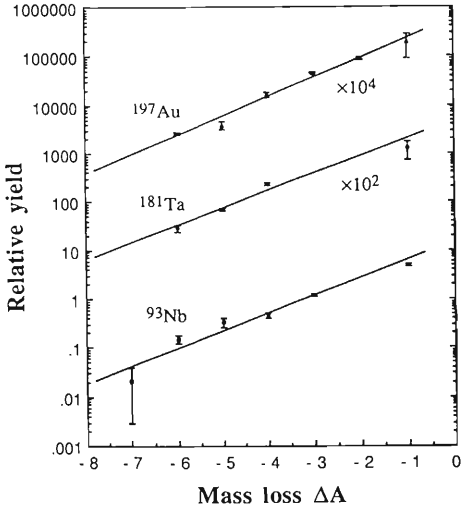

Fig. 1. The mass yield distributions as a function of mass loss ΔA from the target for the reactions of ^{93}Nb, ^{181}Ta, and ^{197}Au with the secondary neutrons produced from the irradiation of a thick stainless steel target with 40 MeV/nucleon ^{40}Ar ions. The solid lines are the linear regressions of the data.

References

1) T. Shikata et al.: *RIKEN Accel. Prog. Rep.*, **25**, 250 (1991).
2) S. Nakajima et al.: *ibid.*, **26**, 183 (1992).
3) H. R. Schelin et al.: *Phys. Rev.*, **C39**, 1827 (1989).

Limiting Behavior of the Recoil Velocities in the Heavy-Ion Reactions

H. Baba, M. Furukawa, Y. Ohkubo, T. Saito, A. Shinohara,
K. Takesako, S. Watanabe, and A. Yokoyama

Intermediate and high energy heavy-ion reactions mostly involve fragmentation of target nuclei. It has been demonstrated that the slope against A of the mass-yield curve for target-fragmentation products reaches a limiting value at projectile energies around 2 GeV, irrespective of light or heavy-ion projectiles. We found that the limiting fragmentation is manifested in the fragmentation of lanthanoid target nuclei induced by heavy ions with energies above 1 GeV.[1] Here we discuss the limiting behavior of the recoil velocities of the reaction products.

The experiments were carried out at the E3b beam course in RIKEN Ring Cyclotron. Sheets of Pr and Ho foil together with Al catchers were bombarded with heavy-ion beams as listed in Table 1. The irradiated foil was separately subjected to off-beam gamma-ray spectrometry with Ge detectors.

Table 1. The mean values of the recoil velocities of the reaction products.

Projectile	Energy (GeV)	Target	$\langle\beta_{\parallel}\rangle$ ($\times 10^{-2}$)
^{15}N	1.05	^{165}Ho	1.25±0.09
^{14}N	1.89	^{165}Ho	1.12±0.10
^{40}Ar	2.36	^{141}Pr	1.38±0.06
^{40}Ar	3.80	^{141}Pr	1.18±0.12

The mean projected recoil ranges are obtained as the product of the thickness of the target and the ratio of the radioactivities detected both in the target and the forward cather foil. The recoil velocities of the product nuclides, $\beta_{\parallel}$, were deduced from their recoil ranges by using the range-velocity relationship. It is seen in all systems that the recoil velocity inceases slightly as the product mass number decreases. The mean values of $\beta_{\parallel}$ in each reaction system are summarized in Table 1. The mean recoil velocities are practically the same within the error for the systems of different target-projectile combinations.

The results of the radiochemical experiments on target fragmentation are informative to examine the actual kinematics of the two-step process. This model has been successful in describing the fragmentation process. The properties of the recoil velocities can be understood on the basis of this model.[2] The recoil velocity of the excited target nucleus M_F is related to the excitation energy E^*. The product $M_F E^*$ is then expected to give a particular limiting value in a high-energy region. This is demonstrated in Fig. 1, together with the present results indicating that a transient type of the limiting behavior of the recoil velocity appears at the energy where the mass distribution attains the limiting behavior. Both may be ascribed to a phase transition of the collective motion of nucleons.

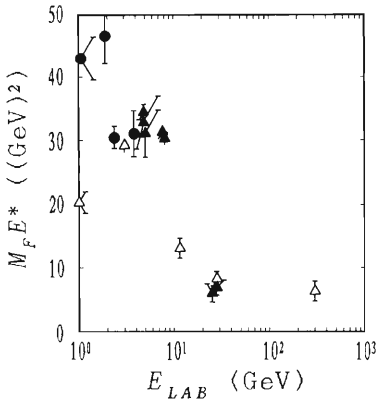

Fig. 1. The product $M_F E^*$ as a function of the projectile energy. Circles represent the data in this work and triangles those given in Ref. 2. Open and solid symbols correspond to the systems with light and heavy projectiles, respectively.

References

1) K. Takesako, T. Saito, H. Kusawake, A. Yokoyama, H. Baba, Y. Ohkubo, A. Shinohara, and M. Furukawa: *RIKEN Accel. Prog. Rep.*, **26**, 91 (1992).
2) E. M. Friedlander and H. H. Heckman: in Treatise on Heavy-Ion Science, edited by D. A. Bromley, Plenum, New York, **4**, 403 (1985).

Dependence of Mass Transfer in the Heavy Ion Reaction on the Mass Asymmetry at Entrance Channel

M. Kiriu, A. Yokoyama, K. Takesako,* S. Watanabe, N. Takahashi,
T. Saito, H. Baba, and Y. Ohkubo

Deep inelastic reaction is an important process in the heavy-ion-induced reaction especially for the energy region below 100 MeV/u. This is a dissipative process accompanying a large amount of kinetic energy loss and transfer of several dozens of nucleons at most. These features are explained by the model of formation and disintegration of a dinuclear system. The results of calculation for the deep inelastic process are, however, very much affected by the reaction time, namely, the life time of the dinuclear system. We measured the mass distribution of ^{51}V with ^{136}Xe ions and that of ^{175}Lu with ^{12}C ions to obtain information on the dinuclear life time. The results were subjected to the analysis based on a diffusion model[1] together with other data of nearly the same composite system with different mass asymmetry at the entrance channel in order to compare the feature of the mass distributions and deduce a systematics of the reaction time.

A sheet of vanadium foil with a thickness of 8.47 mg/cm^2 was bombarded with a ^{136}Xe beam (8.5 MeV/u) at the E3b beam course of RIKEN Ring Cyclotron. The Xe ions lose their kinetic energy down to 7.1 MeV at the target center. Two sheets of Al catcher foil (5.67 mg/cm^2 thick) were placed downstream of the target. Irradiation time of the stack was about 90 min. The carbon ion beam for bombarding ^{175}Lu targets was obtained from the AVF cyclotron of Research Center for Nuclear Physics, Osaka University. The target foil was sandwiched with catcher foil and irradiated with ^{12}C ions of 110MeV at the target center for 142 minutes. Identification and yield determination of the product nuclides were carried out by off-beam γ-ray spectrometry.

According to the prescription of the diffusion model, the relation between the reaction time of DIT and the dispersion of mass distribution (σ_{DIT}) can be described as

$$\sigma^2_{\mathrm{DIT}} = 2D_{\mathrm{A}}\tau_{\mathrm{ap}}, \qquad (1)$$

if dependence of evolution of the dinuclear system on the angular momentum is neglected for simplification. Moreover by using a calculated diffusion coefficient $D^{1)}_{\mathrm{A}}$ which applies very well to a large quantity of experimental data, the reaction time is deduced from the mass distribution. Obtained time is plotted in Fig. 1 versus mass asymmetry at entrance channel together with data obtained from references.[2] The figure demonstrates that the reaction time is independent of mass asymmetry except for a very asymmetric case of the present study. This consequence is clearly different from the linearly increasing reaction time deduced from the ejectile angular distribution by Agarwal[3] as indicated in Fig. 1. This implies that the apparent reaction time presently deduced involves the dispersion due to mass flow and fluctuation in the dinuclear system and therefore it is tenable to supply some information on the dynamics of mass flow in the dinuclear system. We like to point out that the presently deduced apparent reaction time appears to show clear-cut dependence on the direction of mass flow in the dinuclear system.

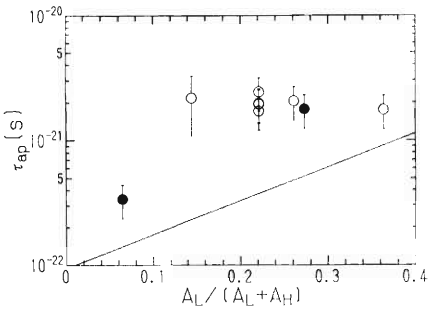

Fig. 1. Reaction time of deep inelastic process versus mass asymmetry at entrance channel. Closed and open circles represent the data from the present study and those from references, respectively.

References

1) S. Ayik et al.: *Z. Phys. A*, **277**, 299 (1976); S. Ayik et al.: *ibid.*, **279**, 145 (1976); G. Wolschin and W. Nörenberg: *ibid.*, **284**, 209 (1978).
2) H. Kusawake: Osaka Univ. Master Thesis, p. 13 (1990); J. V. Kratz et al.: *Phys. Rev.*, **C13**, 2347 (1976); J. V. Kratz et al.: *Phys. Rev. Lett.*, **33**, 502 (1976); R. J. Otto et al.: *ibid.*, **36**, 135 (1976).
3) S. Agarwal: *Z. Phys. A*, **297**, 41(1980).

* Fac. Sci., Osaka University

Competition between Fission and Spallation in the Reaction Induced by Intermediate Energy Heavy Ions

J. Kurachi, E. Taniguchi, A. Shinohara, M. Furukawa, S. Kojima, Y. Ohkubo, F. Ambe, K. Takesako, A. Yokoyama, T. Saito, H. Baba, and S. Shibata

Nuclear reactions induced by intermediate energy heavy ions have been extensively investigated. But heavy ion induced fission has not been clearly understood. We measured the product yields and linear momentum transfer in the interaction of gold with intermediate energy heavy ions to study the projectile dependence of the nuclear reactions including fission.

The targets were irradiated with heavy-ion beams at the falling ball irradiation facility[1] installed at the E3b course of the RIKEN Ring Cyclotron. The irradiation conditions are shown in Table 1. The target stack consisted of gold foil (20–48 mg/cm^2 thick) surrounded by Mylar, Kapton, carbon or aluminum catchers. After irradiation, the targets and the catcher foil were assayed by means of non-destructive γ-ray spectrometry. Formation cross sections were determined from measured disintegration rate of the products in the whole target stack. Mass yield distributions were deduced from the obtained formation cross sections. Linear momentum transfer and isotropic momentum components were calculated from the measured recoil ranges, 2W(F + B), and the forward-to-backward ratios, F/B, by means of a two step vector model.[2] Here, W is the target thickness, F and B are activity ratios of given products in the forward and backward catchers to the total activity, respectively.

Table 1. Irradiation conditions.

Projectile	Energy (MeV/u)	Irradiation time (sec)	Total flux (particles)	Target thickness (mg/cm^2)
^{14}N	35	3618	4.76×10^{14}	48.3
^{15}N	70	5730	8.95×10^{13}	43.3
^{14}N	135	8960	1.47×10^{14}	43.3
^{40}Ar	30	2400	1.05×10^{14}	20.6
^{40}Ar	38	3547	2.28×10^{13}	37.6
^{40}Ar	59	4056	3.06×10^{13}	43.5
^{40}Ar	95	4386	2.28×10^{13}	45.0

Spallation, fission and nucleon transfer reaction products were observed. The mass distribution of fission products was obtained by subtracting spallation component from mass yield in the range of A = 55–130. The spallation component was extrapolated from the mass yields in the range of A = 135–175. The fission cross sections were estimated from the mass distribution of fission products assuming that its shape is Gaussian. The angular momentum imparted to the excited nucleus was estimated, assuming that initial interaction is the fusion of target nucleus and the part of projectile that gives measured linear momentum transfer to the product.

The angular momenta decrease with increasing incident energy and seem to be constant at higher energies, as shown in Fig. 1. The variation of fission cross section is shown in Fig. 2. The fission cross section decreases with increasing incident energy per nucleon: its variation is similar to that of angular momentum.

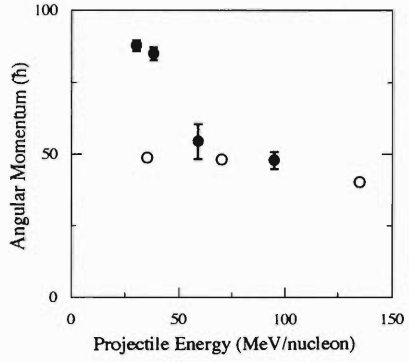

Fig. 1. Dependence of angular momentum imparted to excited nucleus on projectile energy. Symbols indicate different incident particles; ○: ^{14,15}N, ●: ^{40}Ar.

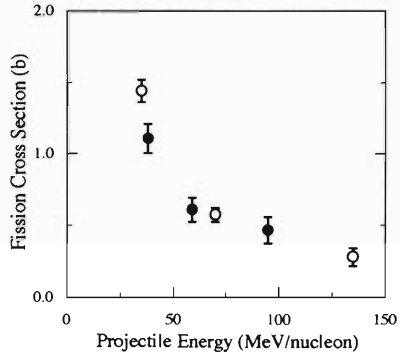

Fig. 2. Dependence of fission cross section on projectile energy. Symbols indicate different incident particles; ○: ^{14,15}N, ●: ^{40}Ar.

References
1) F. Ambe et al.: *Chem. Lett.*, **1991**, 49.
2) L. Winsberg: *Nucl. Instrum. Methods*, **150**, 465 (1978).

Time-Differential Perturbed-Angular-Correlation (TDPAC) of γ-Rays of ^{99}Ru in $YBa_2Cu_3O_{7-x}$ Using ^{99}Rh as a Source Nuclide

Y. Ohkubo, Y. Kobayashi, K. Harasawa, S. Ambe, T. Okada, S. Shibata, K. Asai, and F. Ambe

In a previous experiment[1] we first prepared $YBa_2Cu_3O_{7-x}$ ($x \lesssim 0.2$) containing ^{99}Rh, which decays to ^{99}Ru. All heating processes were done in flowing oxygen. Then, we prepared $YBa_2Cu_3O_{7-x}$ (^{99}Rh) ($x \approx 1$) by heating the $YBa_2Cu_3O_{7-x}$ (^{99}Rh) ($x \lesssim 0.2$) sample at 760 °C over 6 h, holding it at that temperature for 1 h, and cooling to room temperature over 16 h all the while under reduced pressure of about 3 Pa. By measuring TDPAC spectra for the 3/2+ level of ^{99}Ru in the two samples, we obtained results indicating that Rh ions occupy the Cu-1 site exclusively. We considered the reason for the result to be as follows: Rh ions prefer +3 valence. Since we first prepared $YBa_2Cu_3O_{7-x}$ (^{99}Rh) ($x \lesssim 0.2$) in oxygen and the average valence of the Cu ions at the Cu-1 site was close to +3 while that of the Cu-2 site was +2, Rh ions occupied the Cu-1 site. The temperature of 760°C needed to prepare $YBa_2Cu_3O_{7-x}$ (^{99}Rh) ($x \approx 1$) was not high enough for Rh ions at the Cu-1 site to move to the Cu-2 site.

In the present experiment we heated $YBa_2Cu_3O_{7-x}$ (^{99}Rh) ($x \lesssim 0.2$) in flowing nitrogen at several temperatures to attempt to prepare $YBa_2Cu_3O_{7-x}$ (^{99}Rh) ($x \approx 1$) following the heating process[2] employed by Smith, Taylor, and Oesterreicher, and then measured the TDPAC spectra of ^{99}Ru in those samples to see whether Rh ions at the Cu-1 site move to the Cu-2 site.

About 97% enriched ^{99}Ru was irradiated with 13-MeV protons available from the INS-SF cyclotron. A carrier-free solution containing $^{99}Rh^{3+}$ was obtained from the irradiated ruthenium target by radiochemical separation. CuO powder was added to the solution in order to let it adsorb $^{99}Rh^{3+}$. An essentially identical heating process to that used in Ref. 1 was employed to prepare $YBa_2Cu_3O_{7-x}$ (^{99}Rh) ($x \lesssim 0.2$). This material was heated in nitrogen at 770 °C for 2 days, quenched quickly to room temperature and subjected to TDPAC measurement. Similar processes were followed at 820, 870, and 920 °C on the same sample.

Measurements of the TDPAC spectra of ^{99}Ru in the sample heated in nitrogen at 820 °C were made at 10, 293, and 573 K. Those for the samples heated at other temperatures were made only at 293 K. Figure 1(a) shows the frequency spectra at 293 K of YBaCuO(^{99}Ru) prepared at 770, 820, 870, and 920 °C. Here, we use the notation YBaCuO, considering that a part of $YBa_2Cu_3O_{7-x}$ possibly decomposed into Y_2BaCuO_5 during the heating in nitrogen. Figure 1(b)

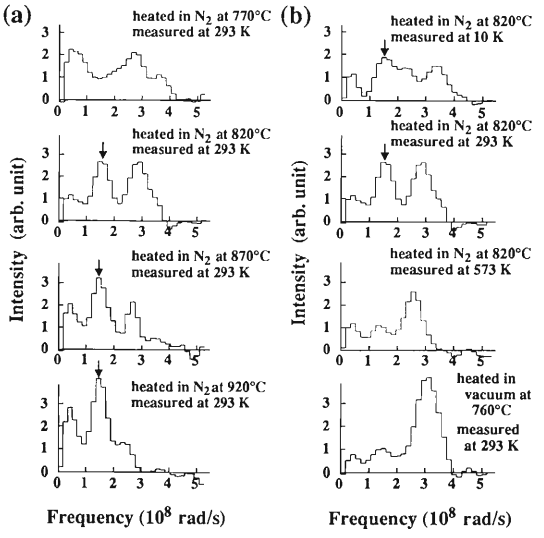

Fig. 1. (a) Frequency spectra at 293 K of ^{99}Ru in YBaCuO prepared by heating $YBa_2Cu_3O_{7-x}$ (^{99}Rh) ($x \lesssim 0.2$) in nitrogen. (b) Frequency spectra at 10, 293, and 573 K of ^{99}Ru in YBaCuO prepared in nitrogen at 820 °C. The frequency spectrum at 293 K of $YBa_2Cu_3O_{7-x}$ (^{99}Ru) ($x \approx 1$) prepared in the previous experiment[1] is also shown in the bottom for comparison.

shows those of the sample prepared at 820 °C and measured at 10, 293, and 573 K. The frequency spectrum at 293 K of $YBa_2Cu_3O_{7-x}$ (^{99}Ru) ($x \approx 1$) prepared in the previous experiment[1] is also shown in Fig. 1(b) for comparison. A new peak indicated with an arrow appears in the measurement at 293 K for the samples prepared at 820, 870, and 920 °C, but not for the sample prepared at 770 °C, as seen in Fig. 1(a). We can observe from Fig. 1(b) that this peak is considerably reduced at 573 K. It is reported that there is antiferromagnetic ordering with $T_N = 420$ K at the Cu-2 site of $YBa_2Cu_3O_{7-x}$ ($x \approx 1$). We are thus tempted to assign this peak to ^{99}Ru which moved to the Cu-2 site. However, we are not convinced of it yet. The peak assignments are under consideration.

References

1) Y. Ohkubo, Y. Kobayashi, K. Harasawa, S. Ambe, T. Okada, K. Asai, S. Shibata, S. Takeno, and F. Ambe: *RIKEN Accel. Prog. Rep.*, **26**, 95 (1992).
2) M. G. Smith, R. D. Taylor, and H. Oesterreicher: *Phys. Rev. B*, **42**, 4202 (1990).

Slow Positron Beam Production Using AVF Cyclotron

Y. Itoh, Y. Ito, I. Kanazawa, N. Ohshima, Y. Yamamoto, N. Nakanishi, A. Goto, and M. Kase

Experiments to produce an intense slow positron beam have been started from 1993. The method is to produce short lifetime β^+-decay radioisotopes by nuclear reactions, and then to stop the emitted high energy positrons in a moderator having a negative work function for positron. Since a fraction of the stopped positrons are re-emitted from the surface with very small emittance, they are collected and accelerated to a desired energy. The technique of using the negative work function moderator has become a common practice, and usually long lifetime radioisotope (^{22}Na) or electron linacs are used as the sources of fast positrons. However the intensity of the slow positrons obtained from the long lifetime radioisotopes is limited to less than 10^5 e^+/s. Intense slow positron beams can be obtained when electron linacs are used, but the pulsed nature of the beam (several ms) sets limitations to the applicability for practical purposes. Intense and constant wave slow positron beams are desirable for many experiments, and for this purpose the use of short lifetime β^+-decay radioisotopes produced by nuclear reactions is a promising method because the yield of isotope production is high. Due to the short lifetimes of the positron emitters, slow positron beams must be produced on-line with the operation of the accelerator. Reactions as ^{11}B(p,n)^{11}C, ^{14}N(p,α)^{11}C, ^{19}F(p,n)^{19}Ne, ^{23}Na(p,n)^{23}Mg, ^{12}C(d,n)^{13}N, ... etc. are considered to be efficient to produce intense positron emitters, and boron nitride, NaF, and carbon film are the candidate target materials. But the choice of the reactions and target materials is not straightforward since the yield and the characteristics (e.g. emittance) of the slow positron beam depend not only on the nuclear reactions but also on various factors like the distribution of the positron emitters in the target, emission of fast positrons from the target, geometry of the moderator with respect to the target, and so on. The first step of our experiments is to compare various target materials. For this purpose we have constructed a temporary target chamber and a slow positron beam guide (Fig. 1). A thin film or plate of target material is mounted on a water cooled holder at an angle of 30 degrees to the incident proton beam. As the moderator a tungsten film 10 μm thick and well annealed at about 2000 °C is placed 5 mm apart from the target, and the slow positrons re-emitted from the moderator are accelerated to 50–500 eV and are guided through the solenoid transport tube. The yield and the beam profile of the slow positrons are measured by MCPA (micro channel plate array).

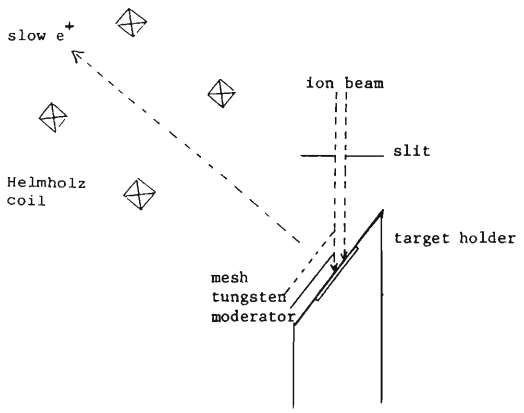

Fig. 1. Schematic diagram of slow positron beam production.

Positronium Formation and Annihilation in Porous Silicon

Y. Itoh, H. Murakami, and A. Kinoshita*

Porous silicon is an important electronic material in the current fabrication technology and its visible photoluminescence has attracted strong attention on development of a photo-electronic device. The physical and chemical properties of porous silicon are dominantly controlled by the surface state of a porous layer. Various techniques are utilized to study the surface states. Positron annihilation spectroscopy is also a powerful tool since it is very sensitive to holes or pores.

We have measured the positron annihilation in porous silicon, and reported that two lifetime components are very long and the Doppler broadened annihilation radiation is sharpened by magnetic field.[1] It is concluded that the efficient yield of positronium is formed in the porous silicon. In a present study, we report the results of temperature dependence of the positronium yield and lifetime in porous silicon, and of the effect of gas adsorption on the positronium states.

Figure 1 shows that the longest lifetime component is about 34 ns at 300 K, which increases to 45 ns as the temperature decreases to about 100 K and then levels off at about 45 ns from 100 K to about 10 K. The second lifetime component of about 0.55 ns is almost constant in the temperature range of 300 K to 10 K. The longest lifetime and the second one are considered to correspond to the positronium lifetime in free state in the pores and that trapped on the pore surfaces. The intensity of the longest lifetime component decreases while that of the 0.55 ns component increases with the temperature decrease to 100 K and both intensities level off below 100 K. It follows that the surface trapped positronium of 0.55 ns increases and the free positronium of the longest lifetime decreases with the temperature decrease. The changes of both intensities originate from the thermal activation of positronium emission from the pore surfaces. The adsorption effect of residual gas on the pore surface has also to be taken into account in order to explain the lifetime and intensity saturation below 100 K. Therefore, the effect of gas on the positron annihilation in the porous silicon was examined. Oxygen gas causes a drastic decrease in the intensity and lifetime of the longest lifetime component at 300 K. These decreases of lifetime and intensity have arisen from the spin conversion of ortho-positronium by an unpaired electron of oxygen. We are making the experiments on the temperature dependence of lifetime and intensity in porous silicon under a designated gas atmosphere such as oxygen, nitrogen and others. The saturation effect shall be clearly understood from the results on the gas adsorption on the pore surfaces.

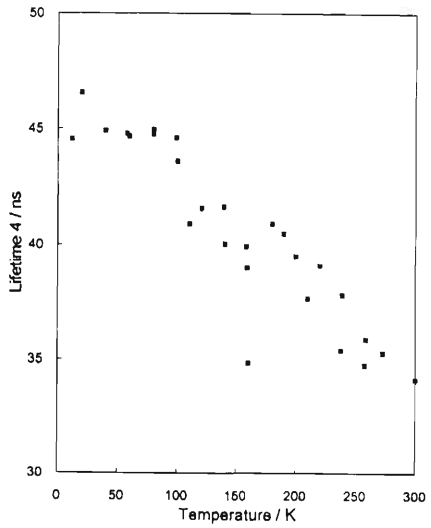

Fig. 1. Temperature dependence of the longest lifetime component.

With the aid of positron annihilation spectroscopy, it is possible to make the surface state of porous silicon clear and elucidate the photoluminescence mechanism.

References

1) Y. Itoh, H. Murakami, and A. Kinoshita: *Appl. Phys. Lett.*, **63**(20), 1 (1993).

* Physics Dept., Tokyo Denki University

Heavy Ion Beam Analysis for H-D Isotope Exchange in Glass Surface Layers

T. Kobayashi, T. Nozaki, M. Aratani, and M. Yanokura

Cations in surface layers of silicate glass are known to be replaced by hydrogen in hot water, and the hydrogen can be back-replaced by cations or submitted to H-D isotope exchange. We thought that the deuterated glass, made by dipping in hot D_2O for a week, could be used for time-integration monitoring of vapour pressure and cation contents of soil water. Various silicate glass plates were surveyed for the rates of the above three reactions under various conditions. Saturated solutions of highly soluble salts and hydroxide-oxide mixtures were used to give well reproducible vapour pressures. The sample surface was analyzed by the simultaneous measurement of heavy ion ERDA (Elastic Recoil Detection Analysis), RFS (Rutherford Forward Scattering) and RBS (Rutherford Back Scattering) under almost the same conditions as in our previous measurements.[1)]

The hydrogenation in harder glass proceeded more slowly but to a larger depths (mostly over 3 μm) than in softer glass (often under 1.5 μm) in prolonged dipping in hot water (several days, 130–180 °C). The hydrogenated layers of soft glass were dissolved gradually in hot water to be detected by the colorimetry of silica; this dissolution can be the cause of poorer reproducibility observed for softer glass in all the three reactions. Figure 1 shows the ERDA spectrum of the Pyrex glass deuterated and exposed to moisture. Under measurement conditions giving a nearly rectangular spectrum for homogeneously distributed deuterium, as in our present measurement, $K = (R - R_0)/(4 + R)$ is a reasonable and convenient measure of the degree of D-by-H replacement, where R_0 and R are the ratios of ROI A value to ROI B value for the deuterated glass without and after a moisture exposure, respectively. Figure 2 shows the K values for deuterated Pyrex glass chips heated with $La(OH)_3$-La_2O_3 in sealed tubes. At 250 °C, a considerable decrease of total hydrogen in the glass was also observed at the beginning, and this can be related with the lower exchange rates in the successive stages. The glass giving Fig.1 is one of the samples of our preliminary field experiment, in which deuterated glass chips were buried in a desert land for 5 months at depths from 10 to 165 cm; the K values found were from 1.66 to 1.77. We intend to prepare a set for moisture monitoring, utilizing micro-pore membranes in conjunction with the deuterated glass.

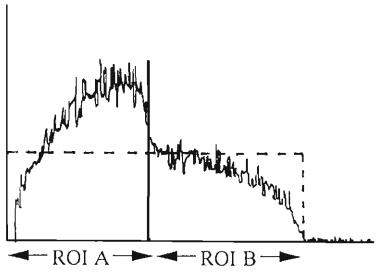

Fig. 1. An ERDA spectrum of the Pyrex glass deuterated and exposed to moisture. (Ordinate: Counts per channel in linear scale)

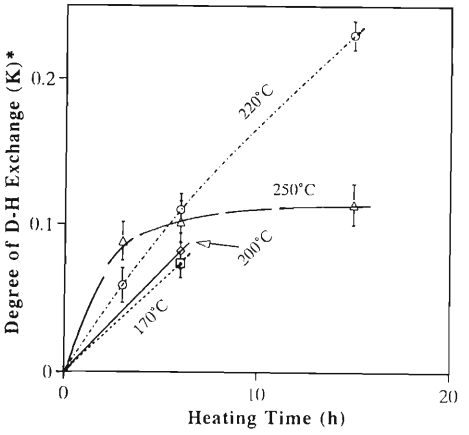

Fig. 2. Degree of D-by-H exchange in the Pyrex glass heated with $La(OH)_3$-La_2O_3. *See text.

References

1) H. Nagai, S. Hayashi, M. Aratani, T. Nozaki, M. Yanokura, I. Kohno, O. Kuboi, and Y. Yatsurugi: *Nucl. Instrum. Methods Phys. Res.*, **B28**, 59(1987).

4. Radiation Chemistry and Radiation Biology

Time and Depth Resolved Dynamics of Excited States in Ion Track in Condensed Matter

K. Kimura, Y. Sahara, K. Yokoo, and T. Shiba

(1) Dynamics of core excitons produced in ion irradiated BaF_2

Ion irradiated BaF_2 exhibits two kinds of luminescence with peak wavelengths at 220 and 310 nm, which can be observed also by vacuum-ultra-violet photoirradiation and electron irradiation with low LET. The 220 nm luminescence can be assigned to Auger-electron-free transitions of valence electrons to Ba^{3+} which is the hole of the outermost inner shell. Ion irradiations exhibited following characteristic phenomena about the Auger-electron-free luminescence which cannot be observed in low LET irradiation. (1) The decay curve is composed of two components. (2) The decay time of the fast component decreased with increasing LET, while the slow one was independent of LET. These LET effects were explained by competition kinetics between the Auger-electron-free radiative transition and the nonradiative annihilation of Ba^{3+} whose process originates from LET dependent dense free electrons. The kinetics enables us to obtain the lifetime and yields of the core excitons.[1,2]

The 310 nm luminescence can be assigned to the self-trapped exciton (STE) as well known in alkali halides. Ion irradiations showed drastic LET dependence of luminescence decay, as shown in Fig. 1. The figure shows

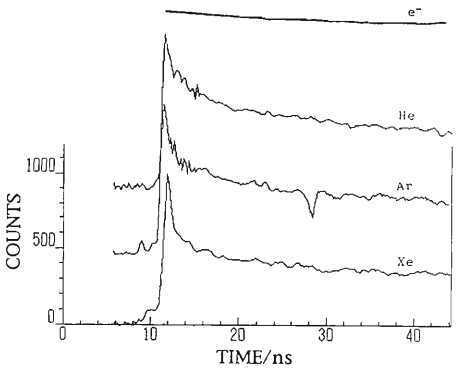

Fig. 1. Decay curves of 310 nm luminescence from ion- and electron-irradiated BaF_2 single crystals at room temperature. The curves are plotted in equal heights and with a given longitudinal shift.

that decay curves due to ion irradiations have fast decay components, in contrast with a simple exponential of electron irradiation. Also, the fast component decays more rapidly with increasing LET, i.e., increasing excitation density, while the decay curves after a few hundreds ns coincides with the curve for electron irradiation. This effect can be explained by the STE-STE exchange effect. Namely, the exchange interaction destroys STE nonradiatively. Such process would be the first finding.[2,3] The decay curves could be fitted by theoretical curves, which would be the first one to deal with distance-dependent rate constants. This may be useful in the photochemistry such as high density excitation as well as in the same problem in solid state physics.

(2) Track-depth resolved dynamics of excited states

In order to study depth-resolved radiation effects along the ion track in condensed matter, we have developed a micro track scope and measured luminescence spectra, luminescence intensity and its efficiency as a function of ion range, stopping power, and ion velocity. In case of near-liquid helium (helium cluster), it was reported that the luminescence bands originate from transitions between Rydberg states; these states are produced by bimolecular reactions of the lowest triplet excimers (^{3}a). Further, it was found that at the depth due to the maximum energy deposition, there occur the dissociative reactions of three ^{3}a. Near the termination of the ion track where the ion velocity is about 1.3 times larger than that of 1S orbital electron, the second Bragg peak for the luminescence efficiency was found, which was explained as caused by the charge exchange effect.[4,5]

References

1) K. Kimura and J. Wada: *Phys. Rev.*, **B48**, 15535 (1993).
2) K. Kimura: *Nucl. Instrum. Methods Phys. Res.*, **B** (1993) in press.
3) K. Kimura and H. Kumagai: *Rad. Eff. Def. Solids*, **126**, 45 (1993).
4) K. Kimura: *Phys. Rev.*, **A47**, 327 (1993).
5) K. Kimura: *Nucl. Instrum. Methods Phys. Res.*, **A327**, 34 (1993).

Beam End Point Measurement with Positron Emitting Secondary Beams

T. Tomitani, M. Kanazawa, M. Sudou, F. Soga, T. Kanai, Y. Sato,
N. Inabe, A. Yoshida, and Y. Watanabe

The accuracy of dose distribution in heavy ion therapy is much dependent on the range estimation of projectile ions in the target medium. Heavy ion range is a function of the electron density of the medium. Heavy ion range is estimated from the measured CT number by looking up a measured conversion table. Since CT number is a complicated function of electron density and Z-number, there are some ambiguities in the conversion and some sorts of experimental checking means are needed. With β^+ emitting ion beams, we can measure their end points by measuring annihilation pair γ rays with a positron emission tomography (PET). End point distribution provides us such a checking means. Preliminary experiments on the measurement of end points of β^+ emitter were done at the RIKEN Ring Cyclotron. ^{11}C was used, since its LET is close to ^{12}C which will be used for heavy ion therapy at NIRS, and its half life, 20.34 min., is appropriate for the measurement. A small PET device of high spatial resolution was used, which was originally developed for physiologic studies of animals.

The PET device used in the experiment consists of 128 bismuth germanate crystals of 4 mm wide by 10 mm high and by 20 mm deep coupled to 64 gridded photomultipliers of 12.7 mm square. The measured spatial resolution inside the tomographic plane is about 3 mm FWHM and that along axial direction is 2.5 mm FWHM. Since the PET device consists of a single ring, a target sample must be scanned to measure the three-dimensional distribution. Instead of moving the detector system, the sample was driven by a pulse motor controlled remotely by a microcomputer. A polymethyl methacrylate ($C_6H_8O_5$, Lucite) block was used as a target material. The Lucite sample was engraved with two sets of characters, i.e., 'RIPS' and 'NIRS'.

The line width of character sets was set to 2 mm which is comparable to the spatial resolution of the PET. The depths of the character sets were set to 4 mm and 5 mm, respectively, as shown in Fig. 1. To cover the pattern shown in Fig. 1, an ^{11}C beam was defocused to about 6 cm ϕ. Nonuniformity of the beam was corrected by a separate measurement of the beam profile with a flat disk.

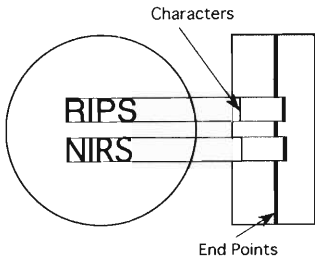

Fig. 1. Depth resolution test pattern made of Lucite engraved with two sets of characters.

The ^{11}C distributions corrected for the beam nonuniformity are shown in Fig. 2, in which the total number of ^{11}C particles was of the order of 10^9. Since beam intensity at the periphery of the field of view is weak and noise in the reconstructed images is enlarged enormously at the periphery, images only inside the region of 6 cm diameter are shown in the figure. End point distributions of ^{11}C were measured successfully. The spatial resolution is limited to 3 mm cube due to the PET resolution.

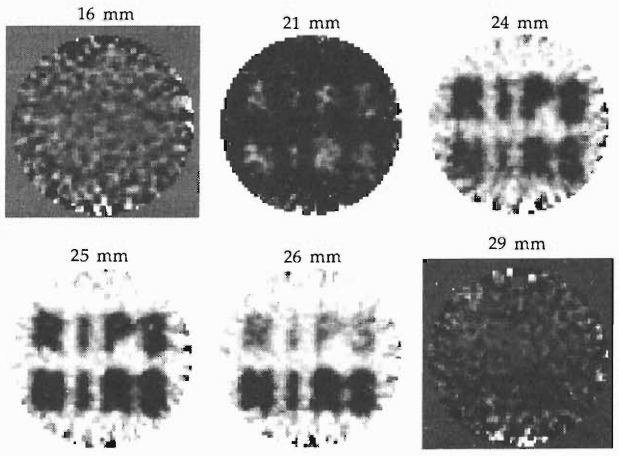

Fig. 2. Distribution of ^{11}C at various depths from the Lucite surface. Character line width is 2 mm and character height is 14 mm.

Initial Recombination in a Parallel Plate Ionization Chamber Exposed to Heavy-ion Beams

T. Kanai, M. Sudou, S. Minohara, and F. Yatagai

We have installed an irradiation system at E5 room of the RIKEN Ring Cyclotron Facility for studies of radiation biology using heavy-ion beams. The biological and physical data are used to modify the heavy-ion beams for the heavy-ion radiation therapy.[1] In the biological studies and radiation therapies using heavy-ion beams, an accurate determination of the absorbed dose is essential. Dosimetry for the heavy-ion beams was described in a separate paper.[2] Fluence of the uniform irradiation field was measured by a plastic scintillator, and dose at the entrance position of the depth dose distribution was obtained by multiplication of the fluence by the stopping power of the heavy ions at the position. Then, the depth dose distribution was normalized by the dose at the entrance position. The depth dose distributions are usually measured by a parallel plate ionization chamber. As discussed in a previous paper,[2] initial recombination plays an important role in measuring the ionization current of an air-filled parallel plate ionization chamber. The ion collection efficiency in the parallel plate ionization chamber is not 100% because of the initial recombination. The LET dependence of the ion collection efficiency was measured for several gases and differential W-values of the gases for the 135 MeV/u carbon and neon ions were deduced.

Two types of parallel plate ionization chamber were used for the measurements of the initial recombination. One has an entrance window of 2.5 μm thick aluminized polyester sheet and the other has an entrance window of 1 mm thick Lucite sheet. A signal electrode of 5 mm in diameter is surrounded by a guard ring that is against disturbance of electric field near the boundary of the signal electrode. A gap between the signal and the high voltage electrodes is 2 mm. Usual operating bias of the high voltage electrode is 400 V, which is 2000 V/cm electric field. The initial recombination of the parallel plate ionization chamber depends on an angle between the heavy-ion beam and the electric field of the chamber. The thin-window chamber was used for this angular dependence. Only air can be used as a gas of the cavity of the chamber. The gas in the thick-window chamber can be replaced. The recombination for several gases was measured by this thick-window chamber.

The chamber was irradiated by uniform heavy-ion beams at the irradiation site of the irradiation facility.[1] Ionization current was measured by an electrometer Keithley 617. The LETs of the heavy-ion beams were changed by changing absorber thickness of the irradiation facility.[1] Ionization currents of the parallel plate ionization chamber were measured by changing the voltage applied to the high voltage electrode. The inverses

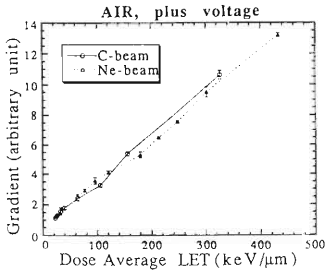

Fig. 1. Typical result of LET dependence of the slope of plots of the inverse of the ionization current against the inverse of the applied high voltage at V > 100.

of the ionization current were plotted against the inverse of the applied high voltage. The data corresponding to $1/V < 0.01$, that is, $V > 100$, can be fitted by a straight line. Decrease of the ion collection efficiency at such a high electric field can be regarded as the decrease due to the initial recombination.

The differential W-values of air, nitrogen, argon, carbon dioxide, and tissue equivalent gas for 135 MeV/u carbon and neon ions were measured by the same methods described in the previous report.[2] The ion currents were corrected by the recombination effect.

Figure 1 shows the results of LET dependence of the gradient of the slope at $V > 100$ for air. It can be said that the recombination depends only on the LET of the heavy-ion beams and increases roughly linearly with LET. The experimental data is now being analyzed using model calculation. For argon and nitrogen gases, the decreases of ion collection efficiency due to the initial recombination were not observed.

Table 1 summerizes the differential W-values of those gases for 135 MeV/u carbon and neon ions.

Table 1. Differential W-values for 135 MeV/u carbon and neon ions. The results in Refs. 2)–4) are also written for comparison.

	C 135MeV/u	Ne 135 MeV/u	Photon/Electron[3]
Air	33.5 eV	34.2 eV	33.85 eV
N_2	35.8 eV	36.6 eV	34.8 eV
Ar	23.6 eV	24.3 eV	23.8 ~ 26.4 eV
CO_2	21.4 eV	21.9 eV	33.0 eV
TEG	28.6 eV	29.3 eV	29.2 eV
	^{4}He 18.3 MeV/u[4]		
TEG	29.2 +/- 0.9 eV		
	C 129.4 MeV/u	^{3}He 10.3 MeV/u	C 6.7 MeV/u [2]
Air	33.7 +/- 0.9 eV	34.5 +/- 1.0 eV	36.5 eV +/- 1.0 eV

References

1) T. Kanai et al.: HIMAC report 004 (NIRS-M-91) NIRS publication, (1993).
2) T. Kanai et al.: *Radiat. Res.*, **135**, 293 (1993).
3) ICRU report 31 (International Commission on Radiation Units and Measurements, Washington) (1979).
4) T. Kanai and K. Kawachi: *Radiat. Res.*, **112**, 426 (1987).

Ionization Tracks Produced by Ar (95 MeV/u) Ions and their *Core-Penumbra* Structure

M. Suzuki, T. Takahashi, and K. Kuwahara

Since the ionization track structure produced by heavy ions is of great importance in radiobiology, many works have been done to answer the question whether the ionization track manifests the two distinctive distributions, i.e., "*core-penumbra*" structure,[1] or a single continuous distribution obeying, for instance, the $1/r^2$ law. Theoretical works based on Monte Carlo calculations claim that there is no evidence of an enhanced energy deposition in the center of the tracks.[2] Recent microdosimetric experiments are also in favor of the $1/r^2$ law.[3] However, the accuracies of the calculations and the experiments are limited by the availability of the electron-atom interaction cross sections and by the smallest feasible detection volume, respectively.

In order to finalize the issue, therefore, one needs new instruments or techniques which can reveal the ionization track structure in detail. As a promising instrument, we have proposed and constructed a proportional scintillation imaging chamber (*PSIC*) which provides high quality photographic images of the ionization tracks in real time.[4] The *PSIC* has been successfully operated at the E5A beam line of RIKEN Ring Cyclotron, detecting the ionization tracks produced by N (135 MeV/u) ions and Ar (95 MeV/u) ions.

Figure 1 displays the lateral brightness variation of the observed ionization track image produced by the Ar ion. The figure demonstrates that the ionization track has the *core-penumbra* structure. We have fitted the brightness curve to the double Gaussian electron density distribution function, $\rho(r)$, given as

$$\rho(r) = N_0 \left[\frac{f}{\pi b_1^2} \exp\left(-\frac{r^2}{b_1^2}\right) + \frac{1-f}{\pi b_2^2} \exp\left(-\frac{r^2}{b_2^2}\right) \right],$$

where r denotes the radial distance, N_0 a constant, b_1 the *core* radius, b_2 the *penumbra* radius, and f the relative fraction of the number of the secondary electrons in the *core* to the total number of the secondary electrons. The best fitted curve is shown by the solid curve in Fig. 1, and the best fitted values for f, b_1, and b_2 are listed in Table 1 together with those calculated by Magee and Chaterjee.[5]

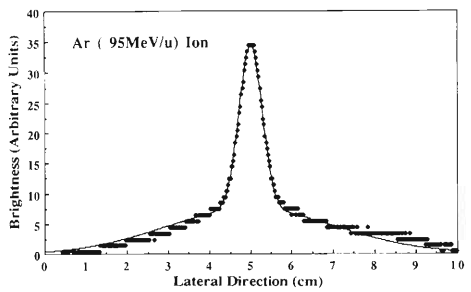

Fig. 1. Lateral brightness variation of the observed image of ionization track produced by Ar (95 MeV/u).

Table 1. Ionization track parameters.

	f	b_1 (mm)	b_2 (mm)
present	0.49 ± 0.1	3.7 ± 0.4	25 ± 3
theoretical[5]	0.5	0.003	23

As can be seen from Table 1, the f-value determined in the present work is very close to 0.5, indicating that the equipartition holds under the present experimental conditions. The b_2-value obtained is also in good agreement with the calculated one. Since b_2 corresponds to the typical δ-electron range in the medium, one could infer that the energy of the typical δ-electrons is 50 keV for the Ar ions.

The b_1-value determined in the present work is, on the other hand, three orders of magnitude larger than the calculated one. From a theoretical view point, it is natural to define b_1 as the radius of the cylinder about a heavy ion trajectory in which the resonant electronic excitation occurs. The secondary electrons created in the cylinder, however, will disperse by the random-walk process in background gas while thermalizing. At the time of the observation the electrons should have completed their thermalization process, so that the b_1-value determined experimentally includes the thermalization length, $L_{\rm th}$, which is much larger than the b_1-value defined theoretically. One could, therefore, interpret the experimental b_1-value as $L_{\rm th}$, which is about 4 mm for the present study. In order to verify our understanding, it would be worthwhile to compare the ionization track parameters among various high-energy heavy ions. Data analysis on the N ion images currently in progress will provide us with further information upon the *core-penumbra* model.

References

1) A. Chaterjee et al.: *Rad. Res.*, **54**, 479 (1973).
2) M. Kramer and G. Kraft: **GS/91-1**, 205 (1991).
3) N. F. Metting et al.: *Rad. Res.*, **116**, 183 (1988).
4) M. Suzuki et al.: *RIKEN Accel. Prog. Rep.*, **26**, 116 (1992).
5) J. Magee and A. Chaterjee: *J. Phys. Chem.*, **84**, 3529 (1980).

Calibration of CR-39 Track Detector for Space Radiobiological Studies and LET Measurements of Cosmic Ray Nuclei

K. Ogura, T. Doke, K. Kuwahara, M. Matsushima,* S. Nagaoka,**
K. Nakano, M. Suzuki, T. Takahashi, H. Yamada,* and F. Yatagai

In the complex radiation field in space, the so-called HZE (high Z and high energy) particles are of special concern to the space radiobiological studies. During the First Material Processing Test (FMPT) space shuttle mission in September 1992, Japanese Radiation Monitoring Container & Dosimeters (RMCD) accommodating biological samples and CR-39 track detectors were exposed to cosmic radiations while the space shuttle Endeavour stayed for about 7 days in the orbit at about 300 km altitude with the inclination of 57°.

Figure 1 shows the response curve of a CR-39 track detector, which was obtained by the irradiations of C, N, Ne ions with energies of 135 MeV/nucleon and 95 MeV/nucleon Ar ions from the RIKEN Ring Cyclotron. The low LET region of the response curve was obtained by 10 MeV proton exposure at the TIARA Cyclotron of JAERI, Takasaki.

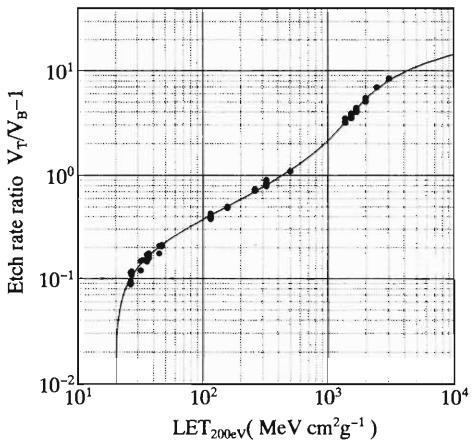

Fig. 1. Response curve of the detector : reduced etch rate ratio vs. LET_{200eV} in CR-39.

After the mission, CR-39 detectors were etched in a 7N-NaOH solution at 70 °C for 30 hours and analyzed by using an image processor. The LET_{200eV} value in CR-39 for individual particles was computed from the reduced etch rate ratio of the track using the response curve of the detector in Fig. 1. The measured data of LET_{200eV} in CR-39 were converted to the total energy loss LET_∞ in water. In Fig. 2 we present preliminary results of the measured integral LET spectra. The effective solid angle (Ω) of the detector is defined by

$$\Omega = \pi(1 - \cos^2\theta_c),$$

where θ_c is the maximum detectable zenith angle and depends on the LET value of the incident particle. The effective detection threshold of LET_∞ values in water was reduced down to about 4 keV/μm due to the high sensitivity of our CR-39 detector as shown in Fig. 2.

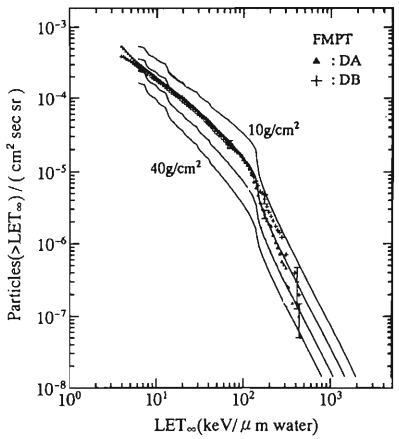

Fig. 2. Observed integral LET-spectra inside the RMCD on FMPT and calculated spectra (solid lines) behind shieldings of 10, 20, 30, and 40 g/cm^2 of CR-39 (Wiegel et al., 1988).

Figure 2 additionally shows the calculated LET spectra[1] behind different amounts of shieldings. These model spectra were calculated for the German Spacelab in a circular orbit at 324 km altitude with an inclination of 57°. These are almost the same mission parameters as for the FMPT mission. Taking account of the data of neutron monitor[2] and the intensities of protons observed in space,[3] the influence of solar modulation on galactic cosmic rays can be considered as almost the same in magnitude at the period of both missions. Our spectra are very similar to the calculated spectra over the entire LET range. Moreover, the shoulder position of the spectrum due to the minimum ionizing cosmic iron ions appeared around 130 keV/μm and agrees well with the model predictions. From Fig. 2 we can also estimate the total amount of the effective shieldings of the detectors inside the RMCD to be approximately 20 g/cm^2 of CR-39.

References

1) B. Wiegel et al.: in "Terrestrial Space Radiation and Its Biological Effects", edited by P. D. McCormack et al., Plenum Press, p. 795 (1988).
2) R. A. Mewaldt et al.: *Proc. 23rd ICRC* (Calgary), **3**, 404 (1993).
3) Z. Fujii and F.B. McDonald: *ibid.*, p. 477.

* College of Ind. Technol. Nihon Univ.
** Natl. Space Dept. Agency of Japan

Radiation Effects of Ion-particles on Various DNA Structures

S. Kitayama, M. Kikuchi, K. Nakano, M. Suzuki, T. Takahashi, and H. Watanabe

Ionizing radiation including accelerated particles induces various damages in DNA such as hydroxylation of base and sugar, disruption of phosphodiester bonds, etc. However, living cells repair the most of them except lethal damage which has not been clearly identified. From the technical limitation to analyze the change of molecular structure of long DNA in living cells, the biological effects of radiation have been studied mostly on the changes of DNA molecules whose molecular weights are less than $10^8 (\sim 1.5 \times 10^5$ base pairs). Recent technichal progress in the analysis of large DNA such as pulse field gel electrophoresis (PFGE) makes it possible to measure the molecular change of long DNA bigger than $\sim 10^7$ base pairs.

Even though prokaryotic cell has no nucleus its single molecule of double-stranded DNA, corresponding to one chromosome, is folded extensively within a small cell envelope. Many cellular constituents are thought to be associated with the folded DNA. It is still unknown whether any segments of chromosomal DNA molecule are evenly attacked by radicals produced by radiations or whether cell constituents protect it or enhance the radiation damages. As reported last year(1), we carried out the experiments to confirm the differrent radiation effecs on "naked", "folded" or "packaged" DNA. We found by electron-microscopic observation that DNA, after removals of RNA and proteins, is still enveloped in an agarose hole whose diameter is almost the same as that of intact cells. Therefore, it can be thought that the DNA in the "naked" sample is still folded in a small space corresponding to the single cell. Therefore, the name of "folded" must be changed to "cell wall and RNA free" sample as a more appropriate terminology.

In order to compare the radiation effects of N-ions ($\sim$135 MeV/μ) on these three folded forms of DNA, cells of *Deinococcus radiodurans* were solidified with agarose (DNA is still "packaged" in a cell with its constituents). Before the irradiation the cells were lysed with lysozyme in the presence of RNase ("cell wall & RNA free") followed by proteinase K treatments ("naked"). RNA and proteins were removed by the incubation with these enzymes following the ittadiation and DNA were digested with a restriction endonuclease, Not I. The digested fragments (Not I fragments) were analysed by PFGE as shown in Fig. 1. At least two conclusions can be drawn from the figure; (1) DNA in "cell wall & RNA free" sample is the most sensitive to N-ion bombardment, (2) Among the Not I fragments the biggest fragment (ca 480 kbp) is more sensitive to it than the others (400, 390, 360, 324, 255, 240, 225, 215, 109, 102, 100 kbp). After completing the more detailed experiments these results will be analyzed quantitatively using densitometer tracing and will be also compared with the effects of low LET radiation such as gamma-rays.

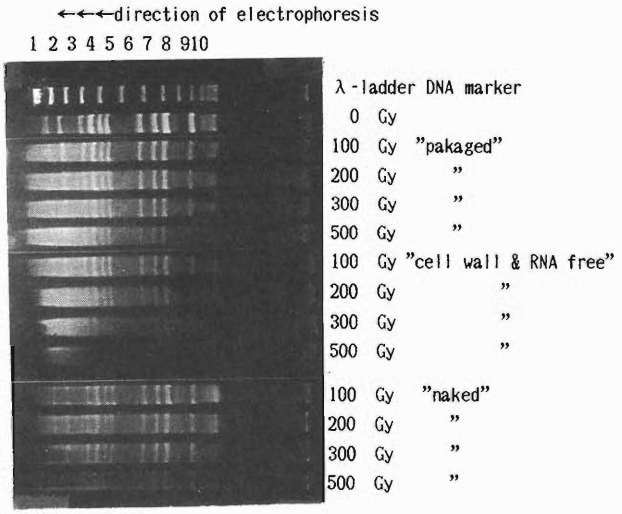

Fig. 1. Disappearance of Not I fragments in three different folded forms of DNA after the irradiation with N^+-ions. The molecular weights of λ-ladder DNA size standard shown in the figure are as follows (bp): 1 = 48.5k, 2 = 97.0k, 3 = 145.5k, 4 = 194.0k, 5 = 242.5k, 6 = 291k, 7 = 339.5k, 8 = 388.0k, 9 = 436.5k, 10 = 485.0k.

References

1) S. Kitayama et al.: *RIKEN Accel. Prog. Rep.*, **26**, 103 (1992).

Studies on Induced Mutations by Ion Beam in Plants

Induced Mutants of Rice Resistant to Bacterial Leaf Blight

H. Nakai, H. Watanabe, Y. Kobayashi, S. Kitayama, T. Takahashi, and T. Asai*

Bacterial leaf blight(BLB) of rice caused by *Xanthomonas campestris pv. oryzae* is one of the most important diseases seriously affecting the production of rice in rice growing areas all over the world.[1] M_3 (the third generation after mutagen treatment) lines of rice derived from the M_2 BLB resistant plants, which originated from the seeds irradiated by ion beams ($^{14}N^{+}$), thermal neutrons and gamma-rays, were grown in the experimental rice fields of Shizuoka University to be inoculated using the BLB isolate T7133.[2] The inoculated plants of every line were scored for disease severity by measuring the length of the lesions 3 weeks after inoculation and the lines which showed resistance to BLB were selected.

The results are presented in Table 1. In the table, frequency of the resistant mutants was calculated by number of resistant lines selected/number of total M_2 seedlings analyzed. It was noted that the frequency of BLB resistant mutants in the treatment of the ion beam as significantly higher than that in the other mutagen.

Table 1. Frequency of bacterrial leaf blight resistant mutants of rice in the mutagens of ion beam, thermal neutrons and gamma-rays.

Mutagen	Dose (krad)	Seed fertility in M_1 (%)	No. of M_2 Seedlings*	No. of Plants selected	Frequency of resistant mutant
Ion beam	10	52	30,000	8	2.6×10^{-4}
Thermal neutron	1.0–1.5	53	30,000	3	1.0×10^{-4}
Gamma-ray	30	49	15,000	3	2.0×10^{-4}

* No. of seeds sown

It can be concluded from the present experiment that ion beams could be very effective mutagen for induction of useful mutants for the plant breeding.

References

1) H. Nakai et al.: *J. of Agricultural Sci., Camb.*, **111**, 309 (1988); *ibid.*, **114**, 219 (1990).
2) H. Nakai et al.: *RIKEN Accel. Prog. Rep.*, **25**, 110 (1991).

* Shizuoka University

Effect of HZE Particles (Ar, N) on Hatching Rate and Occurrence of Pycnosis of *Artemia salina*

M. Ishikawa and F. Takashima*

This experiment was planned to obtain fundamental data for the establishment of a biological monitoring system of cosmic radiation in space; especially to examine the effect of HZE particles on biological activity. *Artemia salina* was chosen for its toughness to environmental change: the eggs can survive more than several months under dry condition.

Although *Artemia salina* is popular in radiation biology, the data of the effect of HZE particles on its biological activity is not available. In the present study, we examined the effect of the energy of Ar and N ions on the hatching rate and the occurrence of pycnoses of *Artemia salina*.

Eggs of *Artemia salina* were stuffed in holes of 9 mm diameter of plastic plates (1mm-thick, track detector) and sandwiched between appropriate number of the same plastic plates without holes (Fig. 1). In order to examine the effect of energy, the samples were stacked; the nearer the sample to the incidence surface, the higher the energy of the beam.

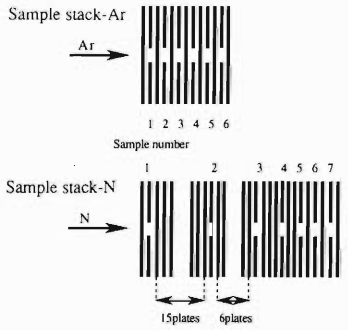

Fig. 1. Sample stacks.

After the exposure of Ar or N beam, the samples were kept at 3 °C before the deternination of hatching rate and occurrence of pycnoses. The hatching rate was determined after incubation at 25 °C for 48 hours in artificial sea water. The nauplii were dyed and served for microscopic observation to count the pycnoses.

The hatching rates of *Artemia salina* exposed to Ar ion beams were plotted against the dose in Fig. 2. The hatching rate decreased with increase of the dose except two groups of samples of which the beam energy was lower.

The occurrence of pycnoses of *Artemia salina* was depicted in Fig. 3. The occurrence of pycnoses correlated with the energy of the beam when the dose was

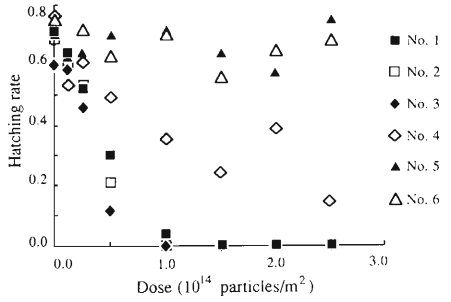

Fig. 2. Hatching rate of *Artemia salina*. Ar (88 MeV).

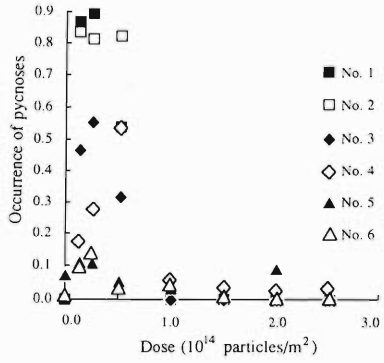

Fig. 3. The occurrence of pycnosis in *Artemia salina*. Ar (88 MeV).

less than 5×10^{13} (particles/m^2), however the occurrence of pycnoses of samples exposed to larger dose was small.

The hatching rates of *Artemia salina* exposed to N ion beam were shown in Fig. 4.

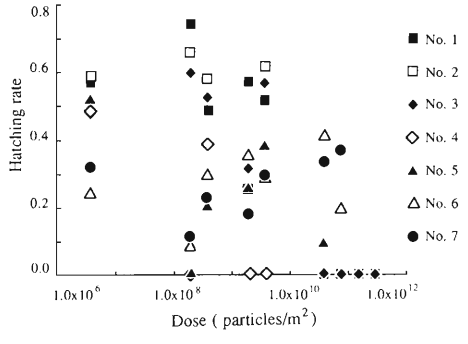

Fig. 4. Hatching rate of *Artemia salina* N (135 MeV).

* Dept. of Aquatic Biosciences, Tokyo Univ. of Fisheries

Chromosome Aberrations Induced by 135 MeV Carbon and Neon Beams of RIKEN Ring Cyclotron in Human Blood Cells

H. Ohara,* M. Minamihisamatu,** T. Kanai,** K. Eguchi-Kasai,**
K. Fukutsu,** H. Itsukaichi,** F. Yatagai, and K. Sato**

Chromosome aberrations,which were induced in human blood cells after irradiation with carbon and neon ions (135 MeV/n) produced by RRC, were examined at the first post irradiation mitosis in order to establish a dose response of the aberration frequencies/cell vs change in LET. Studies on the difference in frequencies of chromosome aberrations with ions as well as LETs might bring us some cell biological aspects of the radiation damage induced by high LET particle beams.

Figure 1 shows the data of dose responses for frequencies of dicentric plus ring type aberrrations per cell after irradiation with four different ion beams at different LETs. Among them, one is neon beams with 70 KeV/μm of LET (closed squares) and the other three curves are all with carbon beams at different LETs. All of the curves were obtained by fitting the aberration frequencies to the linear quadratic model of $y = \alpha D + \beta D^2 + c$. The results indicate that all curves were fitted well with high correlation coefficients (r = 0.88–0.99). Thus, following conclusions might be drawn from the present study. (1) As LET increases, an upward concave curve of dose response, which is seen typically for such a low LET beam, turns first into a downward concave curve and further into a linear type. Such a change of dose response was observed in the present study with high LET carbons and neons. Similar types of linear response have been already observed either with neutrons[1] or with such X-rays with absorption energy to cause high density of ionizations by kicking out of K-shell electrons.[2] A question, however, is whether the saturation of aberration that was observed in the curve of open squares for 41.5 KeV/μm of LET beam is true or not. The saturation in the production of aberrations somehow means that the cells which received the aberrations more than the saturated level cannot survive to pass the first mitosis after irradiation, i.e., they are definitely damaged to allow an interphase death. On the other hand, the two beams of neon and carbons with highest LET showed incrementally high frequencies of aberrations without saturation not like the one with low LET, which means that the cells are not definitely damaged at least for ability to enter the first division after irradiation. (2) The dose response for dicentric and ring aberrations was observed different with ion species though the dose-average LET was amost the same. It was clear that the neon curve showed a higher rate of aberration production than the carbon's with the same LET (69.9 KeV/μm). This result suggests that a high rate of aberration production may not always inhibit the ability of cells to enter mitosis. The response of the cells irradiated with neon beams is clearly due to the beam difference, probably being related to the track sturucture and the associated change in ionizing densities. (3) The RBEs which were estimated relative to the response of the lowest LET carbon ion beams, were 2.45 for neons, 1.67 for the highest LET carbons and 1.16 for the second carbons. These results indicate that biological effects of particle beams might be dependent on fluctuations in LET or ionizing density as well as those of track structures and other physical qualities of beams suggested in other report.[3] More detailed studies are in progress.

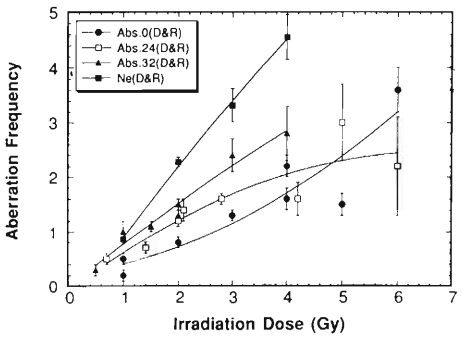

Fig. 1. Dose response curves of dicentric and ring types of chromosome aberrations against different LETs of particle radiations produced by RRC. Abs. 0, Abs. 24, and Abs. 32 refer to those carbon ion beams with LETs of 22.4, 41.5, and 69.9 KeV/μm, and Ne refers to the neon beams with 70.0 KeV/μm. All curves were fitted to linear-quadratic model equations.

References

1) Y. Matsuda, H. Ohara, and I. Tobari: *Mutation Res.*, **176**, 251 (1987).
2) H. Ohara, K. Shinohara, K. Kobayashi, and T. Ito: in "DNA Damage by Auger Emitters", ed. by K. F. Baverstock and D. E. Charlton, Taylor & Francis Ltd., London, p. 123 (1988).
3) G. Kraft, M. Kramer, and M. Scholz: *Radiat. Environ. Biophys.*, **31**, 161 (1992).

* Dept. General Education, Okayama University
** Natl. Inst. Radiol. Sci.

Molecular Characterization of Mutations in Human Cells Irradiated with Carbon Ions

M. Watanabe, M. Suzuki, Y. Kase, and F. Yatagai

Several studies have focused on the molecular structure of radiation-induced mutations and have found that the most common lesion is a large deletion of genetic information. However, only a few studies have been reported in the literature determining how the molecular structure of radiation-induced mutations is affected by heavy ions. We previously reported that heavy ions were generally more effective in cell killing, chromosome aberration induction, mutation induction and neoplastic cell transformation induction than gamma-rays in SHE cells.[1-6] It is clear from track structure studies that heavy ions can deposit large clusters of ionization in DNA which may produce qualitatively different types of initial damage from those produced by the sparsely-ionizing X- or gamma-rays. It is of considerable interest, therefore, to examine the nature of mutations induced by heavy ions in comparison to those induced by gamma-rays. In this study, we detected mutation induction at *hprt* locus in human cells irradiated with carbon and neon ions with several LET and examined the molecular characterization of mutations.

Primary human embryo (HE) cells were irradiated at confluence at room temperature (20 °C). The carbon ions were generated by the ring cyclotron at the Institute of Physical and Chemical Research (RIKEN) and the cyclotron at National Institute of Radiological Science (NIRS). The fluence of carbon ion beams was measured with a plastic scintillator and the value of LET was measured with a proportional counter filled with tissue equivalent gas. The energy of carbon ion beam was 135 MeV/n (RRC) and 12 MeV/n (NIRS). We changed LETs of beams by changing the Lucite absorber thickness. LET values at the sample position were estimated to be varied from 22 to 230 keV/μm. The dose rate was about 1 Gy/min in all beams.

The incidence of mutation in cells irradiated with carbon ions was higher than that in cells irradiated with ^{137}Cs gamma-rays. The RBEs, compared to ^{137}Cs gamma-ray, were between 2.7–7.2 for carbon ions when they were compared at the same absorbed dose level and the highest value was 7.2 for 124 keV/μm carbon ions. DNA isolated from 129 independently derived mutants was examined by the polymerase chain reaction (PCR). Primers for 8 exons of human *hprt* gene were used in a multiplex reaction to show rapidly whether the mutants carried deletions at these site. A few deletions were found among the spontaneous mutants, while 'total' gene deletions formed in about half the mutants found after irradiation. At equilethal doses little difference in mutant spectrum was found for the gamma-ray set compared to the carbon ion set. In the case of mutants induced by carbon ions, the proportion of complete deletion mutants was dependent on the LET of carbon ions. All mutants induced by 124 keV/μm carbon ions were whole gene deletions, while all of mutants induced by 230 keV/μm carbon ions were not deletions.

It is surprising that no deletion mutants were found after the irradiation of carbon ions at 230 keV/μm which gives the biggest track structure among all of carbon ions used in this study. In addition the 68 and 124 keV/μm carbon ions are inducing deletions of all 8 exons. It may be that for mutation endpoint, which requires cell viability for recovery, only moderate clusters of energy deposition in DNA from carbon ions are responsible; these damage events may overlap in severity with damage from gamma-ray track ends. Since large clusters of energy deposition from higher LET radiation may be dominantly lethal, it is likely that only low clusters of energy deposition from secondary electrons may be responsible for mutants induced by 230 keV/μm carbon ions.

In the present study we reported that different LETs of heavy ions have different mutation spectra. Such phenomena require critical examination using large numbers of independently-isolated mutants; it is clear that the methods introduced in this report may be used to examine the such aspects of comparative mutagenesis, also to examine the biological meaning of track structure of heavy ions, where many mutants need to be rapidly assessed at the molecular level.

References

1) M. Suzuki, M. Watanabe, K. Suzuki, K. Nakano, and I. Kaneko: *Radiat. Res.*, **120**, 468 (1989).
2) K. Suzuki, M. Suzuki, K. Nakano, I. Kaneko, and M. Watanabe: *Int. J. Radiat. Biol.*, **58**, 781 (1990).
3) M. Suzuki, M. Watanabe, K. Suzuki, N. Nakano, and K. Matsui: *ibid.*, **62**, 581 (1992).
4) M. Watanabe, V. M. Maher, and J. J. McCormick: *Mutation Res.*, **146**, 533 (1985).
5) M. Watanabe, M. Suzuki, K. Suzuki, and K. Watanabe: *In vitro Toxicol.*, **4**, 93 (1991).
6) M. Watanabe and K. Suzuki: *Mutation Res.*, **249**, 71 (1991).

RBEs of Various Human Monolayer Cells Irradiated with Carbon Beams

H. Ito, S. Yamashita, I. Nishiguchi,* N. Shigematsu,* W. J. Ka,* F. Yatagai, and T. Kanai

Most biological studies for carbon beams were performed with mice and rodent cells. However, irradiation effects of X-ray on human cells are something different from those on rodent cells; for example, smaller initial shoulders and smaller Do values for human cells. This study was performed to determine the RBEs of carbon beam irradiation on various human tumor cells in vitro.

Thirteen human tumor cell lines were used in this study (4 from squamous cell carcinoma and 9 from adenocarcinoma). They were maintained in the F-10 medium supplemented with 10% fetal calf serum by transferring cells into new vessels once a week. For irradiation experiments, RIKEN Ring Cyclotron and the Shimazu X-ray machine were used. A dose response of cell survivals was determined for carbon beams at various LETs, and the several parameters of cell inactivation were caluculated. The curve fitting was made by a multitarget model for Do, n and Dq.

There is a good correlation between the biological effects of heavy particle irradiation and LET. However, when LET is so high, this correlation cannot be maintained because of the overkill phenomenon. The biological experiments with carbon beams were performed at various LETs that do not make overkill. RBE of some test radiation compared with X-rays is defined by the ratio of the doses of standard X-rays and the test radiation required for the equal biological effect. In this sutdy, we have used 200 KVp X-rays as standard radiation. For convenience, doses required to produce surviving fractions of 0.1 or 0.01 have been used for RBE estimation and qualities of carbon beams at various LETs were compared. RBE can be determined easily if the relationship of biological effects v.s. irradiation dose is established.

Figure 1 showed the survival curves of two cell lines (TE 5 & A 43.1) irradiated with 200 KVp X-ray and carbon beams at various LETs. These cells had similar "n" values (1.7 vs. 1.5) but different radiosensitivities (Do: 1.38 Gy vs. 2.43 Gy) for X-rays. When they were irradiated with carbon beams, the survival curves became steeper and Do values decreased with increment of LETs in both cell lines. The initial shoulder of the TE 5 survival curve disappeared at a lower LET of 20 KeV/μm. On the other hand, A 43.1 cells showed the initial shoulder even at a higher LET of 80 KeV/μm. The TE 5 cells irradiated with 20 KeV/μm carbon beams showed RBE of 2.54, and the A 43.1 cells, 1.70. This result suggested that the irradiation effects of carbon beams on human tumor cells were

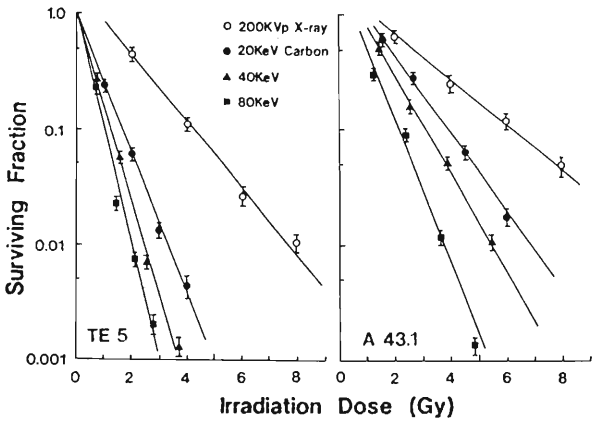

Fig. 1. Survival curves of TE 5 and A 43.1 cells.

different among each cell line. RBE values at 10% survivals irradiated with LET of 20 KeV/μm showed 1.31–2.54, and those with 80 KeV/μm, 2.24–4.07 (Fig. 2). Nine cell lines were established from adenocarcinoma and 4 from squamous cell carcinoma. There was no relationship between histology of tumor and RBE. It is necessary to analyse the relationship between RBEs and radiosensitivities of X-ray in the next step. When RBEs determined by in vitro experiments are applied to clinical radiotherapy, it is very difficult to determine the average single RBE value even for the some LET values in the heavy particle therapy, because the RBEs were different from one cell line to another.

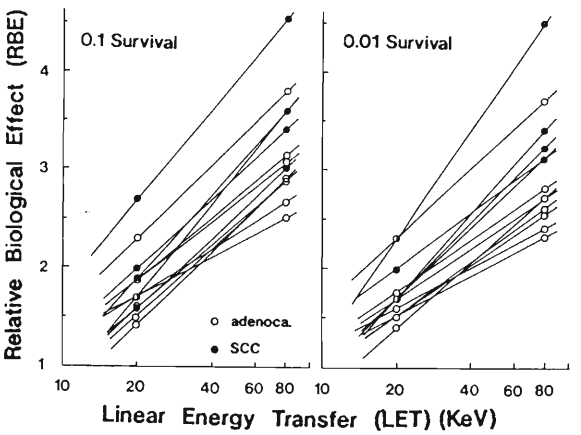

Fig. 2. Relationship between RBE and LET. RBEs of 13 human tumor cells were determined at 0.1 and 0.01 surviving fraction.

* Dept. of Radiology, Keio Univ., School of Medicine

Sensitivity of ts85 Mutant Strain from Mouse FM3A Cells to Heavy Ions

F. Yatagai, K. Nakano, T. Kanai, K. Saito, and F. Hanaoka

One of our interests in elucidating biological effects of heavy-ions is to get some insights into the induced DNA damages in mammalian cells. In *Saccharomyces cerevisiae*, *RAD 9*-dependent response detects potentially lethal DNA damages and causes arrest of cells in G2 until such damage is repaired.[1] The mutation in RAD 6, ubiquitin-conjugating enzyme E2, expresses the phenotype of G2 block through the lack of chromatin condensation. Interestingly, the *RAD 6* gene of *Saccharomyces cerevisiae* also plays a key role in postreplication repair of numerous chemical and physical DNA damages including UV- and X-ray induced lesions.[2] The ts85 mutant strain from mouse FM3A,[3] defective in ubiquitin-activating enzyme E1, represents the defects in the early step of chromatin condensation. The ts mutant cells as well as their wild-type were irradiated with ions of C and Ne to study the contribution of this gene product to the repair of heavy-ion damages.

The cell suspension was exposed to C- or Ne-ion. The irradiated cells were plated and incubated at 39 °C for 20 hrs for the induction of ts phenotype and then shifted down to 33 °C (developed by Dr. H. Ikehata). As the phenotypically non-expressed control, the plates were also incubated at 33 °C without the above shifting up to 39 °C. The survival curves for C-ions were shown in Fig. 1. In contrast to UV (data not shown), the survival curves for ts85 mutant, shifted up to 39 °C at the incubation, represent almost no sensitization compared to the curves of non-expressed cell, incubated at 33 °C following the irradiation. This characteristic was also observed with 63.3 KeV/μm Ne-ions (data not shown). The tendency of LET-dependent sensitization by the temperature shift would be observed even with this sort of limited experiments if this mutant cell was sensitized by the δ-ray effect. In fact, this mutant cell irradiated with X-rays did not show any sensitization (data not shown). Before getting the

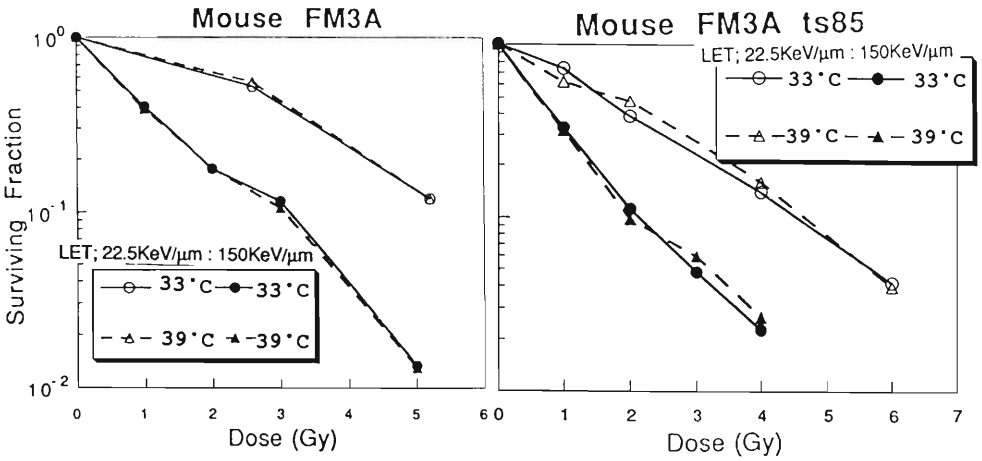

Fig. 1. The survival curves of FM3A and its ts mutant ts85 cells for carbon ion.

conclusion that the function of ts85 mutation is, if not all, different from that of RAD6 in yeast, we have to check the detailed experimental conditions, for example, recovery of the lethal damage due to the delay in starting the incubation at 39 °C, scavenging effect of the medium during the irradiation, etc. The present experimental results also suggest that DNA damages are, at least, different from UV damages.

References

1) T. A. Weinert and L. H. Hartwell: *Science*, **241**, 317 (1988).
2) L. Prakash: *Mol. Gen. Genet.*, **184**, 471 (1981).
3) T. Eki et al.: *J. Biol. Chem.*, **265**, 26 (1990).

PLD Repair in Tumor Cells after Carbon Beam Irradiation

N. Kubota, M. Kakehi,* S. Matsubara,* F. Yatagai, T. Kanai, and T. Inada**

It is well known that mammalian cells repair radiation damage by two known processes: Sublethal damage (SLD) repair and potentially lethal damage (PLD) repair.[1] Modification of SLD repair with increasing LET has been investigated extensively, but modification of PLD reapir with increasing LET has been studied only to a limited extent. The results of these PLD experiments, in contrast to the severely reduced repair of SLD, are uncertain and discrepant. Because recovery from PLD might significantly contribute to the ultimate therapeutic response of a solid tumor, we have investigated the ability of plateau phase human osteosarcoma cells (MG-63) to recover from PLD after irradiation with carbon ions, accelerated by the RIKEN Ring Cyclotron, with the spread-out Bragg peak (SOBP) and unmodulated plateau. The physical characteristics have been descrived in detail.[2] The reference radiation was Cs-137 γ-rays from the Gamma-Cell 40. Cell survival was measured by the standard colony-formation technique. Plateau phase cells were prepared by plating 5×10^5 cells in a T25 flask and incubated for 5 days without an intervening change of medium. For the PLD repair experiment, plateau phase cells were trypsinized at various times after the irradiation.

Cell survival was measured for plateau phase MG-63 cells at various depths (entrance, proximal, midpoint, and distal) in the SOBP of carbon beam. Dose-response curves measured by 24 hr delayed plating are given in Fig. 1. RBE values calculated at 10% survival level were 1.7, 2.5, 2.7, and 3.2 at entrance, proximal, midpoint, and distal within the SOBP. Corresponding RBE values at 1% survival level were 1.5, 1.9, 2.1, and 2.5.

Results of the PLD repair in plateau phase MG-63 cells at various depths in the SOBP of carbon beam and γ-rays are shown in Fig. 2. After γ-ray exposure, there was an increase in survival with time. The recovery ratio, measured by the ratio of cell survival by 24 hr delayed plating to immediate plating, was 7.0. After carbon beam irradiation, recovery was found to be reduced, and the ratios were 6.1, 3.2, 3.0, and 3.4 at the entrance, proximal, midpoint, and distal within the SOBP, respectively. Thus, our results clearly demonstrated that there was still detectable PLD repair when plateau phase MG-63 cells were exposed to carbon beam.

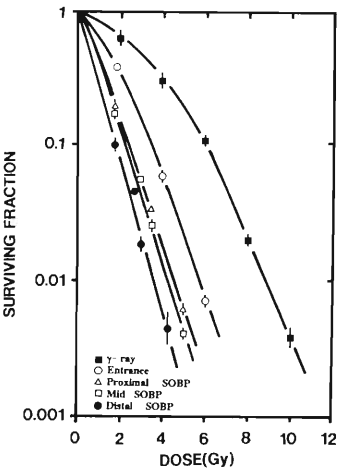

Fig. 1. Cell survival by 24 hr delayed plating of plateau phase cells afer carbon beam and γ-ray irradiation.

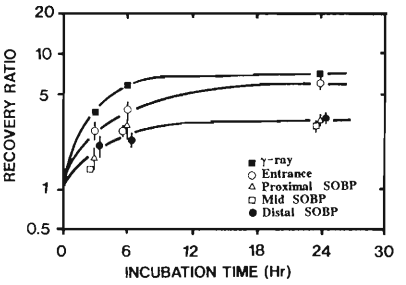

Fig. 2. PLD repair after irradiation with carbon beam and γ-rays.

References

1) N. Kubota et al.: *Int. J. Radiat. Biol.*, **54**, 221 (1988).
2) T. Kanai et al.: Proc. 2nd Workshop on Physical and Biological Research with Heavy Ions, p. 1 (1992).

* Yokohama City Univ.
** Univ. of Tsukuba

The Early Skin Reaction after Carbon Ion Slit-Beam Irradiation

H. Tatsuzaki, T. Okumura, H. Takahashi, T. Kanai, S. Minohara, M. Sudou, and F. Yatagai

The tolerance dose of an organ depends on many factors including LET (linear energy transfer) and irradiated volume. The effects of irradiated volume on a tolerance dose with different LET beams should be clarified to develop better radiation therapy. To study the above point, this experiment was performed using a skin of mouse as the target organ system.

Materials and methods

Twelve week old female C_3H/He Slc mice were used for this experiment. The animals are raised under a specific pathorgen free conditon.

All the irradiation was performed using RIKEN Ring Cyclotron. Two radiation beams with different LET were used. One was the entrance plateau portion of an original mono-peak beam of a 135 MeV/u C-ion beam and the other was the middle portion of three cm spread out Bragg peak (SOBP) from the same C-ion beam. This SOBP was produced by a rotating range modulator. The flatness of SOBP was adjusted biologically so as to get 10% survival of V79 cells uniformly.[1] The LET values of these beams at skin surface were around 22 keV/μ and 71 keV/μ, respectively. The beams were collimated to 25, 15, or 5 mm wide slit-shape with a copper final collimator (Fig. 1). In this way, irradiated volumes were changed. The lower hint legs of mice were irradiated under anesthesia using 65 mg/kg sodium pentobarbital i.p. injection.

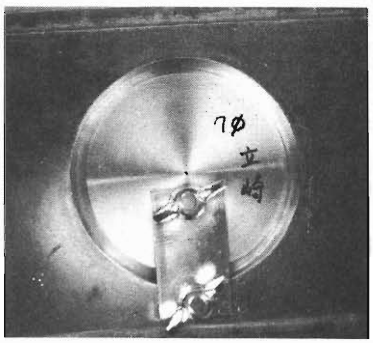

Fig. 1. Final collimator with a 5 mm slit made of copper.

Early skin reaction was observed to evaluate radiation effect. Seven days before irradiation, the lower hint leg of the mice was shaved using a razor blade for precise observation. The irradiated skins were observed every other day from the seventh post-irradiation day to the 35th post-irradiation day. An area independent skin score (Table 1) modified from Fowler's[2] or Aizawa's[3] one was used because the irradiated area was different among three groups. The peak score during observation periods was used for the analysis.

Table 1. Area independent skin score.

score	descriptions
0.5	minimal changes from normal /graying
1.0	slight reddening
1.5	definite reddening, dry desquamation (+−) /no hair with slight atrophy
2.0	severe reddening or dry desquamation (+)/atrophy
2.5	dry desquamation (++)/scales
3.0	moist desquamation (+−)
4.0	moist desquamation (+)
5.0	moist desquamation (++)

Results

The peak skin reaction increased with dose until a certain skin reaction level. Then it saturated above a certain dose level. The saturation level of skin score was different among each slit group: Score 4 for 25 mm slit, score 3.5 for 15 mm slit, and score 2.5 for 5 mm slit. These saturation levels were almost the same for the two LET beams. Volume dependence was more eminent in a higher dose region.

References

1) T. Kanai et al.: Proc. 2nd Workshop on Physical and Biological Research with Heavy Ions. NIRS-M-90, HIMAC-003, edited by K. Ando and T. Kanai, Natl. Inst. of Radiol. Sci., Chiba, Japan, p. 1 (1992).
2) J. F. Fowler et al.: *Int. J. Radiat. Biol.*, **9**, 241 (1965).
3) H. Aizawa: *Nippon Acta Radiol.*, **33**, 602 (1973).

5. Instrumentation

Computing Environment around the Accelerator Facility

T. Ichihara, Y. Watanabe, and A. Yoshida

A general description of the data acquisition system at the RIKEN accelerator research facility can be found elsewhere.[1] In this report, we will describe the recent improvement of the system.

(1) On-line data acquisition system

Currently, seven Micro VAX's are used for on-line experiments at the RIKEN accelerator research facility. The node names and locations are as follows:

RIKMV1::	Micro VAX II (1F)
RIKMV2::	Micro VAX II (B2F E3)
RIKMV3::	Micro VAX II (Linac)
RIKMV4::	Micro VAX II (B2F RIPS)
SMART::	VAX Station 3520 (B2F SMART)
SMARTF::	VAX Server 3300 (B2F SMART)
RIKLV2::	VAX Station 3100 M76 (1F)

Independent measurements and counter tests can be performed without interference. The current version of the data-taking program supports the CAMAC multi-crate parallel-readout using multi-J11's (starbursts). The throughput of the data acquisition is increased by using these parallel readout features. Digital audio tape (DAT) units of 2 GB capacity are used for the standard on-line data recording.

(2) Off-line data processing system-1

The following VAX/VMS and Alpha/VMS work stations are available for the off-line data analysis and for general purpose calculations.

RIKEN::	(virtual node name of the cluster)
RIKVAX::	VAX-6610 (Central)
RIKVS0::	VAX Station 4000-60 [Ring 1F]
RIKVS2::	VAX Station 4000-60 [Ring 2F]
RIKVS3::	VAX Station 4000-60 [Ring 1F]
RIK835::	VAX Station 4000-60 [Radiation lab.]
RIKLV1::	VAX Station 3100 M76 [Linac Lab.]
RIKAX1::	DEC 3000-400 (Ring 1F)
RIKAX2::	DEC 3000-400 (Ring 1F)
RIKAX3::	DEC 3000-400 (Ring 2F)
RIKAX4::	DEC 3000-300 (Linac lab.)
RIKAX5::	DEC 3000-300 (Atomic lab.)
RIKAX6::	DEC 3000-300 (Ring, nuclear theory)
RIKAX7::	DEC 3000-300 (Radiation lab.)
RIKSNA::	DECnet/SNA Gateway

Seven Open/VMS high-performance alpha work stations (RIKAX1-RIKAX7) have been newly installed mainly for the off-line data analysis.

Theses computers are connected by LAVC (Local Area VAX Clusters) via the ethernet. They are also connected to the HEPnet (DECnet) and TISN Internet (DECnet/IP) and reachable from all over the world.

(3) Off-line data processing system-2

Following FACOM main-frame computers have been also used for the off-line data analysis.

FACOM M-380	(RIKEN ring cyclotron)
FACOM M-1800/20	(RIKEN computing center)

These two computers are connected by the Network Job Entry (NE) and DSLINK via the ethernet. These two computers are also connected to the DECnet/SNA Gateway. Operation of the FACOM M-380 was terminated in the summer of 1993, because seven high performance work stations (Alpha/VMS) have been installed recently.

(4) Wide area computer network

The RIKEN accelerator research facility is connected to the world-wide network of HEPnet (High Energy Physics NETwork)/SPAN (Space Physics Analysis Network) as Area 40, which is a part of the DECnet Internet, and to the TISN internet (Todai International Science Network) which is a part of "The Internet" (NSFnet, ESnet, NSI, DDN etc.).

In order to support these wide area network connections, we are now supporting following 5 leased lines at the accelerator research facility.

512 kbps	to University of Tokyo
64 kbps	to KEK, Tsukuba
19.2 kbps	to RIKEN Komagome
9.6 kbps	to Tokyo Institute of Technology
9.6 kbps	to NTT X.25 (DDX-80)

The leased line between RIKEN-Wako and KEK was upgraded from 9.6 kbps to 64 kbps in August 1993.

(5) Address of the electric-mail

The address of the electric-mail for a general user of the RIKEN accelerator research facility is described as follows, where the userid should be replaced by a proper name.

(HEPnet/DECnet)
RIKEN::*USERID* (or 41910::*USERID*)
(Internet/Bitnet)
USERID@RIKVAX.RIKEN.GO.JP

References

1) T. Ichihara et al.: *IEEE Trans. on Nucl. Sci.*, **36**, 1628 (1989).

A GAL16V8A Programming Equipment

J. Fujita

A programmable logic device (PLD) is a newly-developed small scale gate array whose internal functions are designed and programmed by the users. The PLD can replace more than 90% of standard TTL parts. They reduce the number of IC packages used on a circuit board, and reduce the board space and the number of boards. This results in a lower system cost. Reduction of the number of packages reduces the interconnections between the packages which are the least reliable portions of a digital system, and therefore improves the reliability.

A generic array logic 16V8A (GAL16V8A) is one of many PLDs and is produced by LATTICE Semiconductor corporation. It is electrically erasable and 100 erase/write cycles are guaranteed.[1)]

The 16V8A has 36 unique row addresses accessible by the users. Each of 32 rows addressed from 0 to 31 contains 64 bits of input term data where the custom AND array pattern is programmed. The outputs of the AND array are fed into an output logic macrocell (OLMC), where each output can be individually set to active high or active low state, with either combinational or registered configurations. A common Output Enable (OE) can be connected to all outputs, or separate inputs or product terms can be used to provide individual output enable controls. The row with address 60 contains 82 bits of data which specify the architecture and output polarity for programming the OLMC. The row with address 63 is addressed to erase the bulk of the device and reset it to a generic state.

We have made and tested a programming equipment for GAL16V8A. The equipment consists of a PC-9801 personal computer, a DIO-3298BPC parallel input/output interface board on the I/O slot of the computer, and a programming circuit board with a 20-pins ZIF socket for inserting 16V8A. The programming board is shown in Fig. 1. The pins on the left end are directly connected to the parallel I/O board through a 50-pins flat cable of 20 cm long. A bit pattern mentioned above is written with an usual text editor on PC-9801 in a data format which is agreed by the Joint Electron Device Engineering Council (JEDEC). Each term point is expressed by '1' (fused) or '0' (not fused) in this JEDEC format.

The device is programmed in the following procedure. STR pin 11 is set to logically high, Vcc pin 20 is driven to 5.25 V, and Edit pin 2 is driven to 15.0 V. A row address number is selected by pins RAG0-RAG5 and the bit data to be programmed on the row are shifted into a register through the serial data input

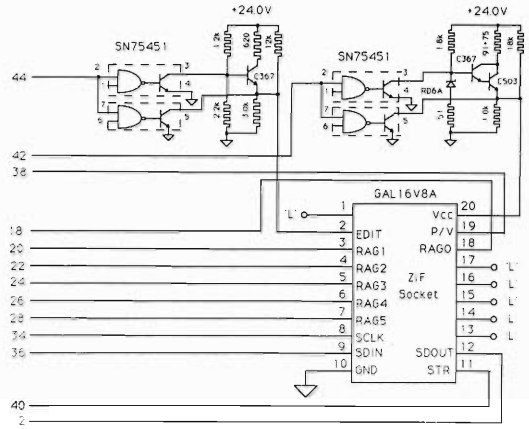

Fig. 1. A GAL16V8A programming board.

(SDIN) pin 9 with synchronous clock pulses on SCLK pin 8. Program/Verify (P/V) pin 19 selects between program and verify modes. When the P/V is set to high, the device enters the program mode. The data in the shift register are fused on the gate array when STR is brought to low for 10 msec. The device enters the verify mode when the P/V is set to low and STR is negated for 5 microsec. The fused data are shifted out from the serial data output (SDOUT) pin 12 with clock pulses on the SCLK. These program and verify steps are repeated for all necessary rows.

The program is developed in language C, except for the part written in an assembler to obtain a correct pulse width of 10 msec for STR.

An address decoder circuit shown in Fig. 2 is programmed by this equipment and expected functions are obtained on each pin.

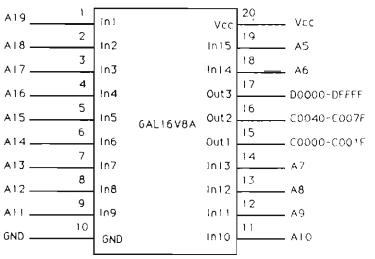

Fig. 2. An address decoder programmed in GAL16V8A.

References

1) GAL16V8 Data Sheet, LATTICE Semiconductor Corp.

In-beam Mössbauer Spectroscopy in RILAC (1)

Y. Kobayashi, Y. Yoshida,* H. Häßlein,* S. Nasu,** and F. Ambe

Implantation technique has been one of very powerful tools for materials characterization in detecting the probes in substances. This technique coupled with nuclear methods, like NMR, PAC, and Mössbauer spectroscopy provides important information for the physicochemical properties and complements the materials characterization. Particularly, implantation studies with Mössbauer spectroscopy have been carried out since 1965. A few years later an excellent method was developed with the evolution of accelerator performance.[1,2] This is the Mössbauer spectroscopy with the Coulomb excitation and recoil implantation by using time bunched beams from accelerators and it consists of the following three steps: (1) excitation of the 14.4 keV ^{57}Fe nuclear level (Mössbauer level) in the target (^{57}Fe foil) via the Coulomb interaction with a pulsed heavy-ion beam (^{40}Ar, E = 110 MeV); (2) ejection of ^{57}Fe atoms and recoil implantation into specimens; (3) measurement of a Mössbauer spectrum within 30 to 400 ns after implantation with use of parallel-plate avalanche counters, repeated after every beam burst. The in-beam Mössbauer experimental setup by using a heavy-ion beam (Ar- or Xe-beams) at RILAC is shown in Fig. 1.[3] It is a special version of Mössbauer spectroscopy, suitable to study local features of single probe atoms in host matrices. Via the hyperfine interaction s-electron densities, electric field gradients, and hyperfine magnetic fields can be measured. Such information can be obtained on an atomic level. The method of in-beam Mössbauer spectroscopy has been developed mainly at two accelerators, VICKSI in Hahn-Meitner-Institut-Berlin and UNILAC in GSI. Y. Yoshida, R. Sielemann and their co-workers have investigated the fast diffusion of Fe atoms in metals by means of the in-beam Mössbauer technique.[4,5] However, only a few applications to host substances except metals seem to have been reported until now.

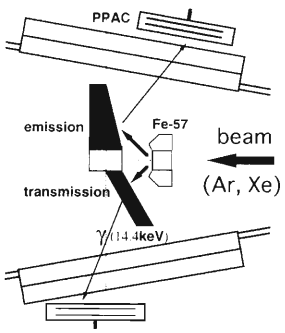

Fig. 1. The apparatus of the in-beam Mössbauer experiment with the Coulomb excitation and recoil implantation.

In the field of material science, the "in-beam Mössbauer method" possesses some characteristic advantages described as follows: (1) Single implanted atoms can be virtually observed because there is no restriction of solubility limits for probes in any host matrices. (2) The probes are directly detected after implantation within the lifetime of the Mössbauer excited state (τ = 140 ns for ^{57}Fe). Occupation probabilities for the lattice positions which are substitutional and/or interstitial sites can be also determined. (3) Since pulsed beams are employed in such experiments, it is also possible to study dynamic effects just after the implantation by time differential coincidence.

A new scattering chamber is going to be constructed and set at the beam-line D-1 in RILAC before February 1994. At the first beam time (March 1994), the performance of in-beam Mössbauer spectrometers will be checked with indium metal as a host matrix. Another scattering chamber will also be made, allowing coincident experiments involving a pulsed laser to create or anneal metastable electronic states in correlation to the recoil implantation in the systems of martensitic transformation of NiTi alloys, solidified rare gases (Ar, Kr, and Xe), and inorganic compounds showing spin-crossover and mixed-valence phenomena. Such experiments promise an increasing insight into the dynamics of out-of-equilibrium electronic systems on an atomic level. For this purpose, the most valuable would be an upgrading of RILAC concerning the beam intensity and the time-bunched beams. Higher intensity would allow us to routinely perform investigations in the time differential mode. With the beam intensity and pulsed beams available at present such an experiment seems impossible. The first step toward the development of such coincidence experiments could however be expected within the nearest future.

References

1) G. D. Sporouse and G. M. Kalvius: in Mössbauer Effect Methodology, edited by I. J. Gruverman, Plenum Press, New York, **4**, 37 (1968).
2) F. E. Obenshain: *ibid.*, p. 61.
3) S. Laubach, P. Schwalbach, M. Hartick, E. Kankeleit, B. Keck, and R. Sielemann: *Hyp. Int.*, **53**, 75 (1990).
4) M. Menningen, R. Sielemann, G. Vogl, Y. Yoshida, K. Bonde-Nielsen, and G. Weyer: *Europhys. Lett.*, **3**, 927 (1987).
5) P. Schwalbach, S. Laubach, M. Hartick, E. Kankeleit, B. Keck, M. Menningen, and R. Sielemann: *Phys. Rev. Lett.*, **64**, 1274 (1990).

* Shizuoka Institute of Science and Technology
** Faculty of Engineering Science, Osaka Univ.

Development of Low Energy Unstable Nuclear Beam Channel "SLOW"

T. Matsuzaki, R. Kadono, K. Ishida, A. Matsushita, I. Watanabe, and K. Nagamine

A low-energy radioisotope beam channel "SLOW" has been developed at RIKEN Ring Cyclotron. The SLOW beam line is not only for the study of emission mechanisms of various low-energy radioactive as well as stable ions from a characterized surface of the primary target, but also for the generation of useful radioactive ion beams for surface-physics studies of the secondary target. The detailed design, construction and performance are described in Ref. 1.

The development works of the beam line has been done to improve the vacuum, to decrease the background signals to a multi-channel plate (MCP) placed at the focusing point and to improve the mass resolution.

For the vacuum improvement, sheets of beryllium foil of 50 μm were placed at the entrance and exit of primary beam line connected to the SLOW beam line. The beryllium foil separates the vacuum spaces and avoids intruding impurity components from the beam dump line. In addition, an ion pump has been installed to improve the vacuum around the target.

The background to MCP during beam-on to the target originates from the beam dump, target itself and a switching magnet in the E7 experimental room. A radiation shield has been built around the downstream end of the SLOW beam line to reduce the background to MCP. The shield is composed of lead blocks and paraffin blocks with admixture of 10% boric acid. The primary beam dump line has been also redesigned and installed, which has a larger diameter to avoid the primary beam hitting the beam duct wall. The primary beam stops in a carbon cylinder enclosed by an evacuated stainless steel can and the produced outgas does not flow into the beam line vacuum. The background has been reduced to one seventh of the previous value after the above works.

After installation of new high-voltage power supplies for electric quadrupole lenses, the beam line tuning work has been performed. For this purpose, an ion-source system has been newly designed and constructed, and the mass spectra were observed for ions from air, argon and xenon gases. Alkaline ions generated from a hot tungsten-target surface were also used, where the alkaline atoms were contained in the target as impurities. To improve the mass resolution, two sets of slits are placed in the line; an adjustable four-jaw slit at the first focusing position (F1) and a fixed two-jaw slit just in front of MCP at the second focusing position (F2), see Ref. 1. A typical mass spectrum for xenon ions is shown in Fig. 1 and the mass resolution (m/Δm) is obtained to be about 550 in the mass region of 130–140, where the widths of F1 and F2 slits are 2 mm and 1 mm, respectively.

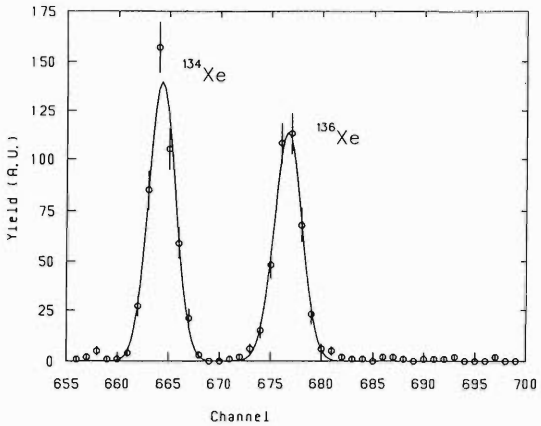

Fig. 1. A typical mass spectrum for xenon ions.

References

1) T. Matsuzaki, R. Kadono, K. Ishida, A. Matsushita, and K. Nagamine: *Nucl. Instrum. Methods Phys. Res.*, **B70**, 101 (1992).

New Detector System for the First Focal Plane of SMART

H. Okamura, S. Ishida, N. Sakamoto, H. Otsu, T. Uesaka, T. Wakasa, H. Sakai, T. Ichihara, T. Niizeki, K. Katoh, T. Yamamoto, T. Yamashita, Y. Hara, and H. Ohnuma

The first focal plane (FP-1) of the SMART spectrograph is primarily used to measure the $(d, {}^2\mathrm{He})$ charge exchange reaction.[1] The ^{2}He is efficiently measured by the coincidence detection of two protons emitted to close geometries. The large angular and momentum acceptance of FP-1, combined with the medium energy deuteron beam from the RIKEN Ring Cyclotron, greatly enhances the detection efficiency of the ^{2}He. The previous detector system, however, was inefficient in resolving trajectories of two protons since it gave information only on X and Y coordinates.[2] It also had a problem in the single-particle detection efficiency due to the lack of redundancy.

A new detector system has been constructed aiming for the ^{2}He detection with higher efficiency and better resolutions. It consists of two sets of multi-wire drift chambers (MWDC) and two layers of plastic-scintillator hodoscope. They are contained in a detector box which is filled with He gas to reduce the multiple scattering.

Each MWDC has six planes, X-X'-U-U'-V-V', consisting of cells 20 mm wide by 16 mm thick. The X', U', and V' planes are offset by 1/4 cell with respect to the X, U, and V planes, respectively, to resolve left-right ambiguities. The U-U' and V-V' wires are oriented at $+36.87°$ and $-36.87°$, respectively. The anode wires are 30 μm gold-plated tungsten and the field-shaping wires are 80 μm gold-plated molybdenum. The cathode planes are 50 μm gold-plated molybdenum wires spaced by 5 mm and are shared by neighboring anode planes. Each wire is held in place by delrin feedthroughs that are mounted in precisely drilled holes in an aluminum frame with a size of $174^W \times 64^H \times 25^D$ cm^3. The sensitive area is $112^W \times 40^H$ cm^2.

We employed the Ne + C_2H_6 (20:80) drift chamber gas as a compromise between the requirement to reduce the multiple scattering and the reasonably large signal.[3] The MWDCs are operated at -2.7 and -3.1 kV on the cathode and field-shaping wires, respectively, and the single-hit efficiency more than 99% is obtained.

Each layer of hodoscope consists of 16 plastic scintillators with a size of $8.5^W \times 40^H \times 0.5^t$ cm^3. Neighboring scintillators overlap by 5 mm. Two hodoscopes are offset by 4 cm to keep the effective cell size reasonably small. The ^{2}He event trigger is made by requiring that there are at least two scintillators hit in both of the hodoscopes. It should be noted that those scintillators can be neighboring ones. This trigger condition allows a simple electronics, the reasonably high efficiency at small p-p relative energies, and clean ^{2}He events, at the same time.

Currently the energy resolution of 700 keV is routinely observed in the $(d, {}^2\mathrm{He})$ reaction measurement. Further improvement is expected by optimizing the optics properties, for example, by making the fields of PQ1 and PQ2 stronger. The study of this new optics is in progress.

References

1) H. Ohnuma et al.: *Phys. Rev.*, **C47**, 648 (1993).
2) H. Okamura et al.: *RIKEN Accel. Prog. Rep.*, **25**, 128 (1991).
3) A. C. Betker et al.: *Nucl. Instrum. Methods Phys. Res.*, **294**, 549 (1990).

Measurement of the Fusion Cross Section of ^{27}Al + ^{197}Au Using MWPC and Multi-target System

A. Yoshida, T. Fukuda, T. Sekine, Y. Watanabe, K. Kimura, Y. Mizoi, M. Tanikawa, H. Sakurai, Y. Watanabe, H. Kobinata, Y. Pu, C. Signorini, G. Liu, and M. Ishihara

A system was designed to measure efficiently the fusion-fission cross section of neutron rich unstable nuclei. To gain a reaction yield, we used a multi-target system comprised of a stack of thin Au foil, and fission fragments were measured by two sets of Multi-Wire Proportional Chamber(MWPC) positioned both at left and right side of the targets. The first experiment using an unstable beam ^{29}Al was reported last year and the schematic view of this system has been shown.[1] In order to obtain a better knowledge of the detector performance, an experiment was performed by using a stable ^{27}Al beam with enough intensity and monochromatic energy.

The experiment was done at E7 hall by using a direct beam from AVF Cyclotron. The 6.5 MeV/u ^{27}Al beam, with intensity of 10^7 cps maximum, was bombarded to a stack of 20 thin Au targets with thickness of ~140 μg/cm^2 on an average. Those targets were supported by ~80 μg/cm^2 Mylar backing foil and were located in the MWPC filled with 10 mbar iso-butane plus 40 mbar He gas. A Micro Channel Plate detector (MCP) and an elastic scattering beam monitor were located at the entrance of the chamber to measure the beam current. The energy loss and the transmission of the ^{27}Al beam passing through each target were precisely measured by a Si detector. The transmission of the beam until the last 20th target was 93% and the total energy loss was 60 MeV. The energy deposits of the fission fragments in a wire plane vs. their ejected angles are shown in Fig. 1. The energy deposits of fission fragments were in good agreement with those of the ^{252}Cf fission source, and were sufficiently larger than those of elastically scattered particles, so that the fission was clearly separated from other backgrounds. 4-plane coincidence and the selections of the opening angle (155–180 deg. in labo.system) were used to get further reduction of the bakground. The efficiency of the detector was obtained by the simulation, which takes into account the angular distribution of the fusion-fission and the detector geometry.

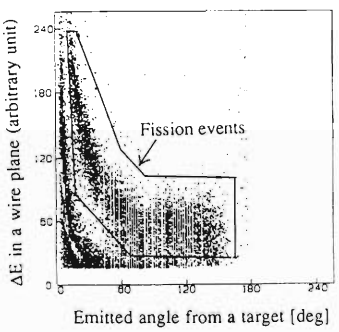

Fig. 1. The energy deposits of the fission fragments in a wire plane vs. their ejected angles from the Au target. Fission fragments show a larger energy deposit than other elastically scattered particles.

We got an excitation function of the fusion cross section as shown in Fig. 2. The X-error bars indicate the evaluated energy spread of the ^{27}Al beam on each Au target and Y-error bars include only statistical errors. The experimental data show a good agreement with the theoretical calculation by Stelson.[2]

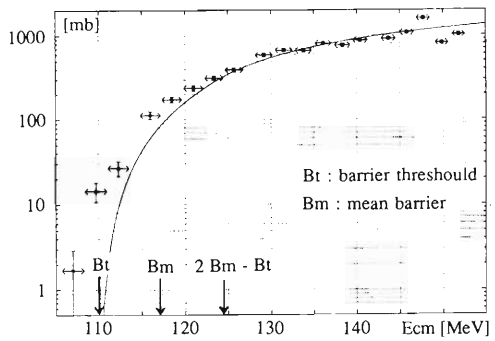

Fig. 2. The energy dependence of ^{27}Al+^{197}Au fusion-fission cross section. Each data point corresponds to one of the stacked Au target. The solid line indicates the theoretical calculation based on Stelson model.

From this result, we believe that our system has good capability of measuring the excitation function of the fusion-fission cross section until the sub-barrier region. We are planning to measure the fusion cross section of ^{29}Al and more neutron rich beams by using this system.

References

1) A. Yoshida et al.: *RIKEN Accel. Prog. Rep.*, **26**, 20 (1992).
2) P. H. Stelson: *Phys. Lett.*, **B205**, 190 (1988).

First Laser-rf Double Resonance Spectroscopy of Refractory Elements

M. Wakasugi, W. Jin, T. Inamura, T. Murayama, H. Katsuragawa,
T. Ishizuka, M. Koizumi,* and I. Sugai

A laser-rf double resonance (LRDR) spectroscopy technique is powerful for precise measurements of hyperfine structure (HFS) because the high sensitivity of laser-induced fluorescence detection is coupled to the high precision of radio-frequency spectroscopy technique in LRDR. This technique has been firstly applied to study molecular structure and HFS in atoms eighteen years ago.[1,2] A lot of information about atomic structure and nuclear properties have been deduced from experimental data measured by means of LRDR.[3] This technique, however, has never been applied to refractory elements because it is hard to produce the atomic beam.

We have constructed a high-resolution atomic-beam laser spectroscopy system for refractory elements using an argon-ion sputtering atomic-beam source,[4] and introduced a laser-rf double resonance technique to the system. We have succeeded in the precise measurements of the hyperfine structures of the ground state $^4F_{3/2}$ in ^{181}TaI and a low lying metastable state $^5D_2$ in ^{183}WI , which are typical refractory elements, for the first time using the LRDR technique.

An intense atomic beam of refractory elements was produced with argon-ion sputtering; we can get a collimated atomic beam of 10^{10} atoms/s. Two laser beams were crossed with the atomic beam perpendicularly. One was used as a pump laser and the other a probe laser. The pump laser was reflected to the opposite direction with a cubic mirror to increase the optical pumping effect. Fluorescence induced by the probe laser was detected with a single-photon counting photomultiplier. An rf field was produced with 2.5-cm long wire (rf loop) parallel to the atomic beam between two lasers; a synthesizer coupled to a power amplifier was used as an rf source; and the applied rf power was typically 30 mW at the terminal connected to the wire. To reduce the stray magnetic field in the rf region, Helmholtz coils were used in three dimensions.

First, we carried out laser-induced fluorescence spectroscopy with the 551.5-nm transition from the $^5D_2$ state of the $5d^46s^2$ configuration to the $^7D_1$ state of $5d^46s6p$ configuration in ^{183}WI. Three hyperfine transitions were observed in this spectrum because both the upper and the lower states were split into two hyperfine levels. When the laser frequency was fixed at one of the transitions, the fluorescence intensity was reduced to 10% of that without pump laser. We could clearly measure the change of the fluorescence intensity as a function of rf frequency. Figure 1 shows the rf resonance spectrum, and the center of the resonance frequency corresponds to the hyperfine splitting in the $^5D_2$ state.

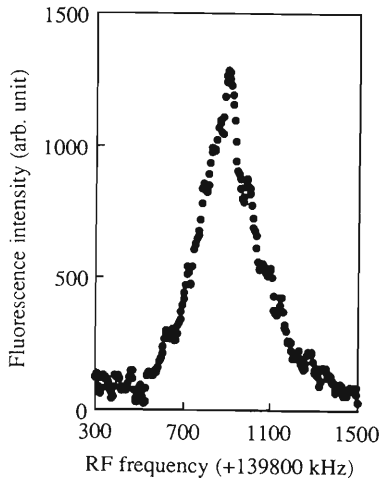

Fig. 1. RF resonance spectrum of $^5D_2$ state in ^{183}WI.

The hyperfine splitting in the $^5D_2$ state was determined to be 140670.3(20) kHz by making a least-squares fit to the experimental line shape with a Lorentzian function. The magnetic dipole hyperfine constant A was derived to be 56268.1(8) kHz. This value agrees with the previous one measured by means of atomic-beam magnetic resonance,[5] and the accuracy was by one order improved compared with it. The precise values of the hyperfine splittings of the $^4F_{3/2}$ state in ^{181}TaI were also determined with accuracy of 2 ppm.

In this experiment, we found that the heavy-ion sputtering is exceedingly useful for precise measurement of hyperfine structure of refractory elements.

References

1) S. D. Rosner, R. A. Holt, and T. D. Gaily: *Phys. Rev. Lett.*, **35**, 785 (1975).
2) W. Ertmer and B. Hofer: *Z. Phys.*, **A276**, 9 (1976).
3) W. J. Childs: *Phys. Rep.*, **211**, 113 (1992).
4) M. Wakasugi, W. G. Jin, T. T. Inamura, T. Murayama, T. Wakui, T. Kashiwabara, H. Katsuragawa, T. Ariga, T. Ishizuka, M. Koizumi, and I. Sigai: *Rev. Sci. Instrum.*, **64**, 3487 (1993).
5) S. Büttgenbach, R. Dicke, and F. Träber: *Phys. Rev.*, **A19**, 1383 (1977).

* Jpn. Atomic Energy Res. Inst.

Measurement of Attenuation Length of Scintillation Photons in Liquid Xenon Due to Heavy Ions

K. Masuda, N. Ishida, K. Kuwahara, H. Okada, T. Komiyama, K. Hasuike,
M. Suzuki, M. Kase, T. Takahashi, J. Kikuchi, and T. Doke

Liquid xenon has very good properties not only as ionization detectors, but also as scintillation detectors[1] because of its large scintillation yield (4×10^7 photons/GeV) and its fast scintillation decay time (5 ns and 20 ns). In good scintillators, the emitted photons should travel in the scintillator without attenuation and be detected by photo-detectors. In this experiment, the attenuation length of photons emitted in liquid xenon has been measured using a improved liquid xenon scintillation chamber.

Figure 1 shows a schematic diagram around photo-multiplier which was newly installed. The whole chamber schematic is shown elsewhere.[2] There are six beam windows that allow heavy ions to enter the inner chamber and excite liquid xenon. Each window is separated by 10 cm to each other. A cylindrical anti-reflector was installed in the chamber. This reflector was carefully designed (see the circle in Fig. 1) because only a few percent reflection at the wall would change the result remarkably. Therefore, a part of photons, corresponding to the solid angle for the Pyrex glass, should be observed. The wave length of emitted photons is shifted by a thin sodium salicylate layer deposited on the Pyrex glass and observed by photo-multiplier (Hamamatsu R329). The inner chamber containing liquid xenon was thermally insulated and cooled by dry ice blocks put into ethyl alcohol (see Fig. 1 of Ref. 2). The space between the inner and outer chamber (see Fig. 1) was evacuated by a turbo molecular pump (less than 1×10^{-6} Torr), and the inner chamber wrapped by aluminized mylar. The operating temperature and pressure was precisely kept at the temperature of -77 °C and at the pressure of 4.8 atm during the experiment. Liquid xenon was purified three times by molecular sieves and GAS CLEAN,[3] and reserved in the sampling cylinders before experiment.

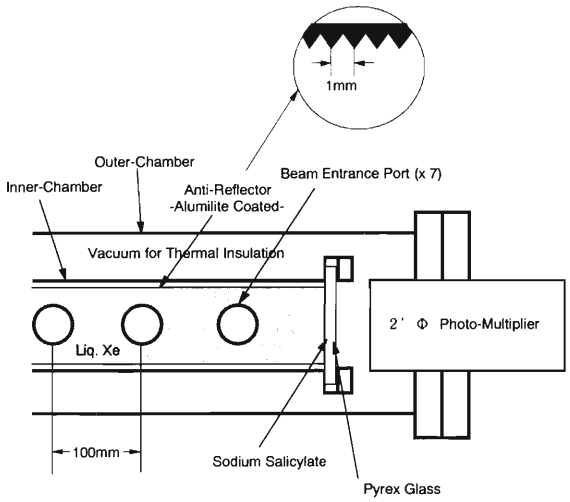

Fig. 1. A schematic diagram around the photo-multiplier and a magnified figure of the anti-reflector.

Figure 2 shows the experimental result. The light yields per solid angle were normalized at the distance of 137 mm that corresponds to the nearest beam window to the Pyrex glass. If scintillation photons travel without any loss, this value should be unity over the whole distance. The exponential fitting in Fig. 2 shows that the attenuation length is 304 mm. This result is consistent with experiments by other authors.[4,5] This value seems to be long enough when scintillation light is used for a timing signal of time projection chamber, but too short for a large scale calorimeter.

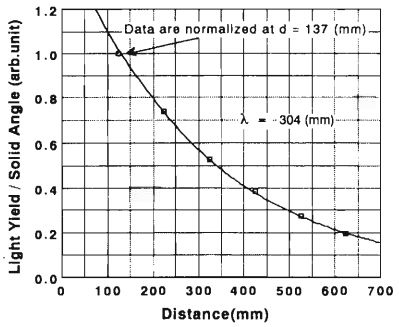

Fig. 2. The light yields per solid angle against the distance between the beam window and the Pyrex glass. Data are normalized at the distance of 137 mm.

References

1) T. Doke: *Portugal Phys.*, **12**, 9 (1981).
2) T. Doke et al.: *RIKEN Accel. Prog. Rep.*, **25**, 140 (1991).
3) Nikka Seiko Co., Ltd. GAS CLEAN GC-RX.
4) A. Braem et al.: *Nucl. Instrum. Methods Phys. Res.*, **A326**, 325 (1993).
5) M. Minerskjold et al.: *ibid.*, to be published.

Measurement of Response Functions of Organic Liquid Scintillator for Neutrons up to 133 MeV

T. Nakamura, N. Nakao, M. Takada, T. Shibata, Y. Uwamino, K. Shin,*
N. Nakanishi, S. Fujita, S. Nakajima, T. Ichihara, and T. Inamura

We have measured the response functions of a 12.7-cm-diameter by 12.7-cm-long BC501A organic liquid scintillator (BICRON Co.Ltd) for neutrons of energy up to about 133 MeV with the TOF method using RIKEN Ring Cyclotron.

H_2^+-ions accelerated to 135 MeV/u were injected to a 5 mm-thick natural Li target (1.25 MeV loss) and a 7 cm-thick ^{9}Be target with 2 cm-thick graphite (full stop). Semi-monoenergetic neutrons and white-spectral neutrons were generated from the Li target and the ^{9}Be + C target, respectively. In both cases, neutrons were generated at 0 degree to the beam axis and charged particles which penetrated through the target were swept out by the clearing magnet. The detector was placed at 13.47 m away from the target in the E4 beam course. In order to measure the response functions for neutrons of energy as lower as possible, pulsed beam was thinned out to 40 μsec pulsed beam interval with the beam chopper only in the ^{9}Be + C run, where the pile up of low energy neutrons (< 50 MeV) to high energy neutrons (> 50 MeV) was reduced to 1 to 2%. The neutron flight time, the pulse height and rise time of the detector light outputs were measured in the list mode and the list data was stored by a CAMAC data taking system.

The time resolution in this experiment was about 1.53 nsec which resulted in about 5.7 MeV energy resolution for the 133 MeV neutron energy. After eliminating γ-ray pulses from the rise time distribution, we have obtained the neutron response functions for energy range between 9 MeV and 133 MeV. Figure 1 shows the response functions for 74–78 MeV and 120–125 MeV neutron energy range as an example.

The measured response functions were compared with the response functions calculated with the Monte carlo codes, SCINFUL[1] and for neutrons up to 80 MeV. Some disagreements between measurement and calculation can be seen except the upper edge of the response functions, since the charged particle production reactions of ^{12}C are not well estimated. The absolute values of the measured response functions were obtained by normalizing them with respect to the calculated value around the upper edge of the response function, which enabled us to get the detector efficiency. Figure 2 shows the neutron spectra of p-Li and p-^{9}Be + C reactions obtained with the help of thus-obtained detector efficiency.

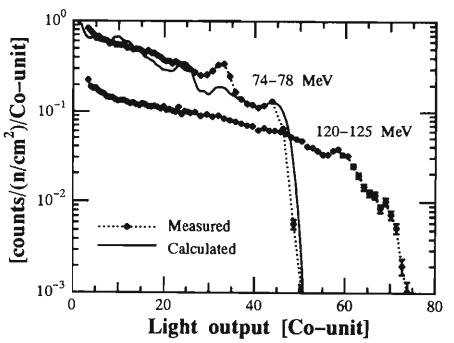

Fig. 1. Response functions of the scintillator.

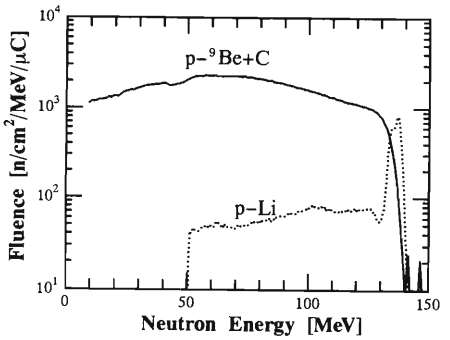

Fig. 2. Neutron spectra of 135 MeV p-Li and p-^{9}Be + C.

References

1) J. K. Dickens: *Computer in Phys.*, Nov./Dec., p. 62 (1989).

* Department of Nuclear Engineering, Kyoto University

Test of Inorganic Scintillators Using RIKEN Ring Cyclotron

K. Matsuzaki, T. Ichihara, Y. Saito, K. Suzuki, and T. Takahashi

We plan to study astronomical objects in the Hard X/gamma-ray band (30 keV–1 MeV) with a new detector on board a satellite. Expected flux in the hard X/gamma-ray region is low (10^{-5}–10^{-6} photons/cm^2/s/keV) and thus we need a detector with high sensitivity.

Sensitivity of the detector is limited by the background counts. In order to achieve the high sensitivity, we have developed a well-type phoswich counter.[1,2] The counter features a very tight active shield that surrounds a small detection part. A collimator and a shield of the counter are made of BGO : $Bi_4Ge_3O_{12}$ scintillators. The candidate for detection part of the phoswich counter is an inorganic scintillator YAP : $YAlO_3$(Ce) or GSO : Gd_2SiO_5(Ce) which possesses a shorter decay time than BGO (see Table 1).

Table 1. Characteristics of scintillators.

	NaI(Tl)	GSO	BGO	YAP
Decay time(ns)	230	60	300	30
Effective atomic number	50	59	74	35
Density(g/cm^3)	3.7	6.7	7.1	5.5
Radiation length(cm)	2.6	1.4	1.2	2.6
Peak emission(nm)	410	430	480	347
Light yield(NaI=100)	100	25	12	40
Index of refraction	1.85	1.9	2.15	1.94
Hygroscopic	Yes	None	None	None

Inorganic scintillators (e.g. NaI, CsI) have been used in space to date but the activity induced by the cosmic ray has been limiting the detectors' sensitivity.[3] We carried out this experiment to select a scintillator which would be least activated by the cosmic ray. We examined three scintillators, YAP, GSO and NaI(Tl). We used the NaI as a standard scintillator in our study.

In the orbital environment the typical energy of proton after passing through a BGO shield is expected to be ~100 MeV. Thus we placed the scintillators in 135 MeV proton beam line of the Riken Ring Cyclotron. Beam was extracted through a 5cm acrylic window and the energy of proton becomes ~100 MeV by the energy loss in the window. The number of protons was counted with three plastic scintillators in coincidence. The beam intensity had been set extremely low ($\sim 3 \times 10^4$ c/s/cm^2), so that scintillators could count each proton. Protons corresponding to three year's exposure in the orbit (about 3×10^8 protons) passed through each scintillator.

We have been measuring gamma-ray emitted from radio-isotopes produced in each scintillator. The level we are measuring is far below the room background, and we use a low background cave made of thick Pb and Cu for the measurement. Since the phoswich counter can reduce compton-scattered events in which some fraction of energy is deposited in the active shields, identification of the radio-isotope is important rather than net continuum level.

From the measurements of initial three months, the NaI shows many prominent peaks with lifetimes from one to a few days in the energy range 100–400 keV. Two lines with a longer decay time at around 60 keV and 100 keV still remain in the spectrum. The GSO also shows many peaks but the magnitudes are lower than those of the NaI by an order of magnitude. The YAP shows some peaks at around 45, 400, and 500 keV. The magnitudes of these peaks are of the same order as these of the GSO. However, the feature that no peaks are shown in the energy range 50–350 keV is very promising for our hard X-ray detector. If GSO or YAP is used, the background rate is estimated to be lower than the previous mission with an NaI scintillator.

References

1) T. Kamae et al.: *IEEE Trans. Nucl. Sci.*, **40-2**, 204 (1993).
2) T. Takahashi et al.: *ibid.*, **40-4**, 890 (1993).
3) A. C. Rester et al.: *AIP Conf. Proc.*, **186**, 223 (1987).

A New Method of Pulse Shape Discrimination for BaF_2 Scintillators

Y. Yanagisawa, H. Murakami, S. Moriya, T. Motobayashi, K. Furutaka, and Y. Futami

The pulse-shape analysis technique has been widely applied to particle-γ discrimination for BaF_2 scintillators.[1,2] The light output of BaF_2 has two components, the fast one with 0.6 ns decay constant and slow one with about 0.6 μs (Fig. 1). This allows the discrimination , because their relative intensities depend on the type of radiation detected. Usually the fast component is measured by a charge sensitive ADC with a narrow gate of several tens nanosecond duration, and is compared with the total light output measured with a wide gate of about 2μs.

We developed a new method based on the RC(CR)^4 shaping with a short time constant (2.1 ns) to pick up the negative fast component. This method has an advantage in experiments using many scintillators, because the ADC's can be operated with a wide gate common to all detectors. This makes the electronics system much simpler and cheeper than in the usual method, where the gate timing has to be adjusted for each detector to account for the different arrival time of the particle detected.

The performance of the present method was tested by using a shaping amplifier with about 2 ns shaping time constant. The shaping amplifier was composed of a hybrid IC (MA405) and a base time clamping circuit. The response of the amplifier to a BaF_2 signal is shown in Figs. 1 and 2. These figures demonstrate that the fast component was picked up with the amplifier. Eight amplifiers were set in a NIM one-span module to match experiments with many BaF_2 scintillators. BaF_2 scintillators were irradiated with various particles, and a good particle separation was obtained. The present method was successfully applied to a phoswich detector consisting of plastic and BaF_2 scintillators.

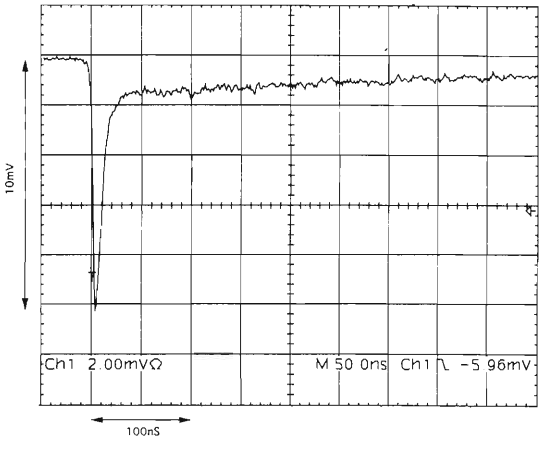

Fig. 1. The output signal of a BaF_2 scintillator with ^{137}Cs.

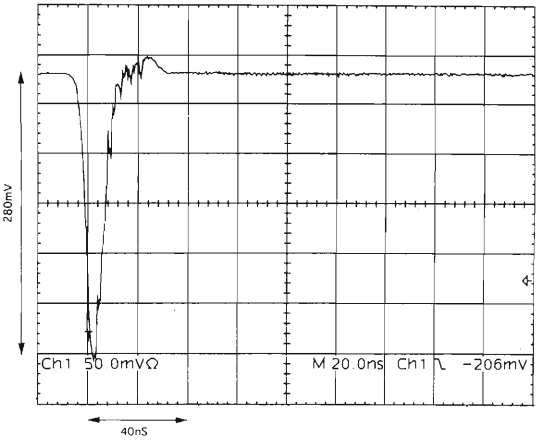

Fig. 2. The response of the amplifier to a BaF_2 signal (Fig. 1).

References

1) K. Wisshak and F. Käppeler: *Nucl. Instrum. Methods Phys. Res.*, **A227**, 91 (1984).
2) S. Kubota et al.: *ibid.*, **A242**, 291 (1986).

Development of Radiation Monitor in Space

T. Imai, H. Kato, and T. Kohno

Protons, electrons and alpha particles (we call them light particles hereafter) are major components of the space radiation environment. During recent several years we have developed a cosmic ray heavy ion telescope for the satellite observation.[1] The main target of this telescope is limited within the elemental range from Li to Fe because of its large dynamic range of pulse height information to be dealt with. But the flux data of the light particles in space are also necessary because they can be a very important reference such as solar flare events. Meanwhile, for identification of the light particles, we do not need a high resolution technique such as position sensitive detectors which are necessary for the heavy particle identification. Furthermore, since the flux of light particles is much higher than that of heavy particles, we can use relatively small detectors to get sufficient statistics. Therefore the observations of light particles should be done by a different telescope which is simpler than that for heavy particles. According to above consequence, we have developed another telescope for the observation of light particles. And these two telescopes are planned to be launched aboard the same satellite, ETS-VI (the sixth Engineering Test Satellite). This telescope is called DOM (DOse Monitor), althogh it observes not 'dose' but energy spectra of light particles. The reason for this name comes from the applicational point of view that the 'dose' in space is mainly caused by electrons, protons and alphas.

As shown in Fig. 1, the telescope consists of seven silicon solid state detectors. The first two and the last one detectors are PIN type photo-diodes with a thickness of 0.2 mm and an effective area of 10 mm $\times$ 10 mm. The other four detectors are lithium drifted type silicon detectors with a thickness of 3 mm and an effective diameter of 10 mm. The first two detectors (PIN1, PIN2) are used for coincidence measurement and PIN1 is used as a ΔE detector. The total energy E is defined as the sum of all detectors except anti-detector (PIN3). If we consider a quantity of

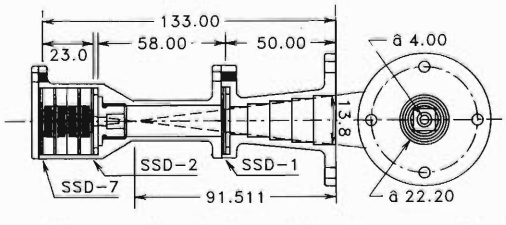

Fig. 1. Cross sectional view of detector assembly of DOM telescope.

$$\Delta E \times (E + k \times \Delta E)\,,$$

this value becomes nearly constant against energy and shows different values depending on the particle mass. (The value k is adjusted by experimental results.) According to this principle and by using combination of sum and multiplication circuits, we can identify electrons, protons, alphas and particles heavier than alphas. The energy regions to be observed for each particle are 0.5–5 MeV for electrons, 7–45 MeV for protons, 28–180 MeV for alphas and 80–330 MeV for particles heavier than alphas. All these energy regions are divided into 16 channels and the count number of all channels is telemetered to the ground in every 64 seconds.

In order to check the characteristics of each detector, we performed accelerator measurements using 95 MeV/u ^{40}Ar beam from RIKEN Ring Cyclotron. Seven samples of lithium drifted detectors were irradiated with a direct beam guided to the atmosphere through a myler film. In order to check the energy loss change in each detector five of them were also irradiated with a beam passed through a 2 mm aluminum plate to degrade the beam energy. The measured peak energies of each detector are shown in Table 1 in comparison with calculated values. The results show the tendency that the measured energies are 10% larger for the direct beam and 5% less for the energy degraded beam, respectively, than the calculated values. Since we do not need so high accuracy for the particle separation as written above the obtained results given in Table 1 are acceptable for practical use.

Table 1. Measured energy outputs of seven detector samples.

	MeV		obs/cal	
	no Al	Al 2mm	no Al	Al 2mm
1	1889	2496	1.09	0.95
2	1884	2502	1.09	0.96
3	1908	2490	1.11	0.95
4	1908	2477	1.11	0.95
5	1921	2480	1.11	0.95
6	1910	–	1.11	–
7	1915	–	1.11	–

References

1) T. Kohno et al.: *J. Phys. Soc. Jpn.*, **60**, 3967 (1991).

Segmented Germanium Detector

E. Ideguchi, Y. Gono, T. Morikawa, T. Kishida, and M. Ishihara

Gamma ray mesurements using heavy ion induced reactions are often suffered from the Doppler effect. This effect is especially serious when one uses, so called, inverse reactions. The use of high-spin isomer beams (HSIB) is one of such cases. High-spin isomers to be used as secondary beams are those of N = 83 isotones, ^{144}Pm, ^{145}Sm, ^{147}Gd, and ^{148}Tb. In these cases the secondary target may be light elements. Then one expects that recoil velocities of the reaction products become to be as high as 0.10 of light velocity, which is about a factor 3 larger than that of normal heavy ion induced reactions.

To correct the energy shifts originating from the Doppler effect, it is neessary to detect γ-rays to get information of directions of emitted γ-rays and to set each Ge detector having small solid angle. In order to achieve this aim, we designed a detector complex consisting of a segmented Ge and a cylindrical Ge counter as shown in Fig. 1. The segmented detector is a transmission type ΔE γ-ray counter. The cylindrical Ge detects Compton scattered γ-rays from the segmented Ge detector.

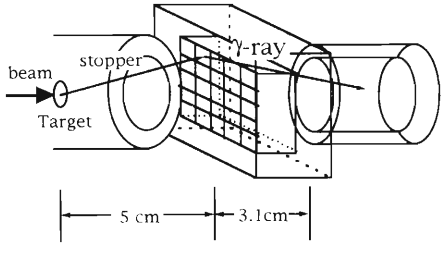

Fig. 1. The set-up of Ge detectors.

In order to estimate the performance of this detection system, we made simulation for the set-up of Ge detectors as shown in Fig. 1. In order to get good position sensitivity and large efficiency, one needs to increase both the number of segments and the thickness of the crystal. On the other hand, cross talk events increase with the thickness of the segmented detector. So we chose the size of each segment as 10 × 10 mm with 20 mm in thickness and the total number of segments as 25. The segmented Ge detector is used as a scatterer and gives directions of emitted γ-rays. Then the energy information should be obtained by summing signals from two detectors. Since multiply hit events in segmented Ge loose the direction information, only single hit events are taken. The resulting sum energy spectrum for a 1.33 MeV γ-ray is shown in Fig. 2. Continuum part of the spectrum is much reduced comparing with that of a spectrum taken by a single Ge detector.

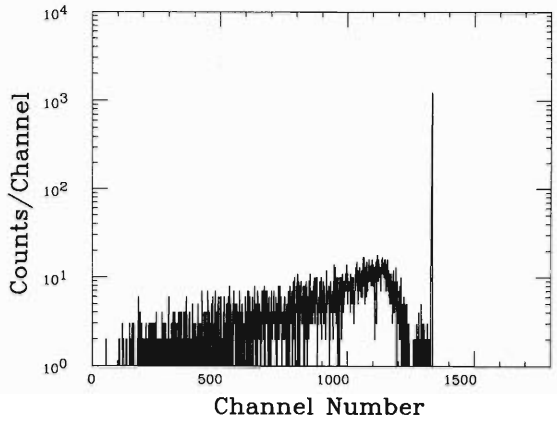

Fig. 2. Calculated sum energy spectrum for a 1.33 MeV γ-ray.

Figure 3 shows the total energy peak efficiency of various combinations of Ge detectors obtained by using Monte Carlo simulation program. In the figure, abbreviations, Cyl(C), Seg(S), Clv, mean a normal cylindrical Ge, a segmented Ge and a clover type detector,[1] respectively. The lowest efficiency curve, '1Cylat25cm', corresponds to a case where one cylindrical Ge is placed at 25 cm from a target which has the same solid angle as those of each segment placed at 5 cm from a target. A case of '1Seg1Cyl', which means one set of 25 segmented Ge is set at 5 cm from a target and one cylindrical Ge is set right back of the segmented Ge, has about a factor 3 larger efficiency comparing with a single cylindrical Ge at 25 cm. However, when one uses 1 segmented Ge with 7 cylindrical Ge's, '1Seg7Cyl', one gets only 2.5 times larger efficiency than '1Seg1Cyl'. This means that the dead space between Ge detectors is too large. And one can find that a single Ge at right back to the seg-

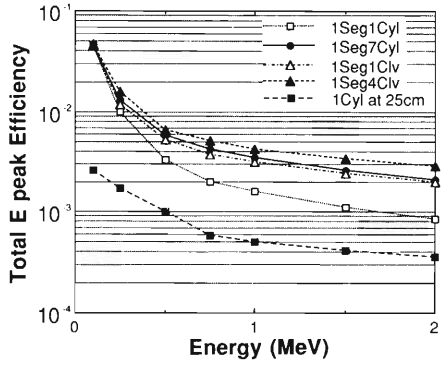

Fig. 3. Calculated total energy peak efficiency of various combinations of Ge detectors.

mented Ge is far more effective comparing to the other 6 cylindrical Ge's. A clover Ge has 4 Ge's in one cryostat so that the dead space between Ge detectors is minimized. So the segmented Ge can be used most effectively by combining it with a clover Ge detector. From our simulation for '1Seg1Clv', we got as large efficiency as '1Seg7Cyl', as shown in Fig. 3.

Finally it may be worth while to point out that the continuum part of the spectrum in Fig. 2 arises from the γ-rays escaped from the back detector. This can be further reduced if one uses an anti-Compton shield for the back detectors such as cylindrical Ge's or clover Ge's.

References

1) J. Gerl and R. M. Lieder: EUROBALL III, p. 52 (1992).

6. Material Analysis

In-situ Analysis of Liquid Samples by PIXE

K. Maeda and J. Kawai

PIXE (particle induced X-ray emission) is an attractive tool to study the dynamic processes in liquid such as diffusion and coagulation. PIXE analysis of liquid samples is, in general, carried out using solid targets prepared by preconcentration (e.g. evaporation of solvent), and there is little information available as to the direct analysis of liquid. We have examined appropriate experimental conditions and normalization parameters for the quantitative analysis by direct (i.e. in-situ) observation of liquid.

Aqueous solutions of nitrates of Cu, Fe and Cr (tens to thousands ppm) and their mixture (Cu 100 ppm, Fe 60 ppm) were used as model samples. Twenty ml of a sample solution was put in a polycarbonate bottle with a 7.5 μm-thick Kapton window. Each bottle was equipped with a Pt wire (0.5 mm in diameter) probe for beam current monitoring. A He ion beam of 8.0 MeV and 3 mm in diameter accelerated by RILAC was transported into air through a 6 μm-thick Al exit window. The sample solution was irradiated with the beam through the Kapton entrance window. Emitted X-rays were analyzed by a Si(Li) semiconductor detector with 30 mm^2 sensitive area. The distance between the Al window and the Kapton window was 6 mm. After passing the 6 μm Al, the 6 mm air gap and the 7.5 μm Kapton, the energy of the He ions decreased by 2.0 MeV, giving an incident beam energy of 6.0 MeV at the solution. The penetration depth of 6.0 MeV He in water was 44 mg/cm^2.

As a normalization parameter, (1) the integrated sample current (i.e. accumulated charge (Q)) measured through the Pt wire, (2) the background continuum intensity integrated from 10 to 15 keV, and (3) the Ar Kα X-ray intensity from Ar in air were found to be useful in the order of (1)–(3). We repeated the X-ray measurement twice or more for each target sample, irradiating the He beam continuously. When the total amount of accumulated charge throughout the experiment (denoted by 'total accumulated charge') did not exceed 1 μC, good proportionality (standard deviation S.D. = $\pm$12% for parameter (1)) was obtained between the CuKα intensity and the Cu concentration over the range of three orders (see Fig. 1). S.D. for parameters (2) and (3) were $\pm$14% and $\pm$15%, respectively. The minimum detection limit for Cu for Q = 1 μC was 4 ppm. The good proportionality was also obtained for Cr. But the proportionality was broken for tens ppm Fe solutions. Increasing the amount of incident beam is useless for improving the accuracy of analysis, since,

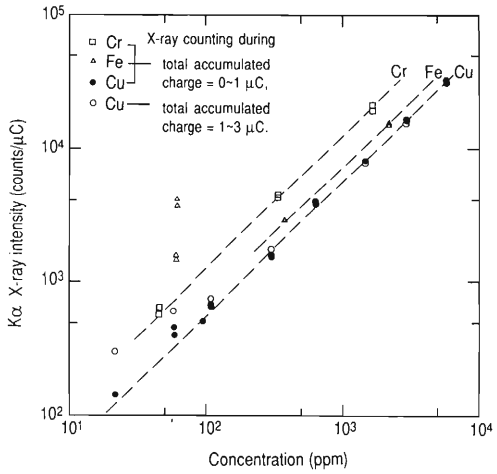

Fig. 1. Kα intensities of Cu, Fe and Cr normalized with the accumulated charge (Q). The gradients of the dotted lines are 1, showing that the X-ray intensity $\propto$ the metal element concentration. Q = 0.5–1 μC.

as seen from Fig. 2, the solute element tended to deposit on the Kapton window surface when the total accumulated charge exceeded ~2 μC. Bubbles due to beam irradiation were not found when the total accumulated charge was kept less than ~2 μC. From this study, we conclude that direct observation of dynamic phenomena in liquid phases by using PIXE is possible under moderate beam irradiation.

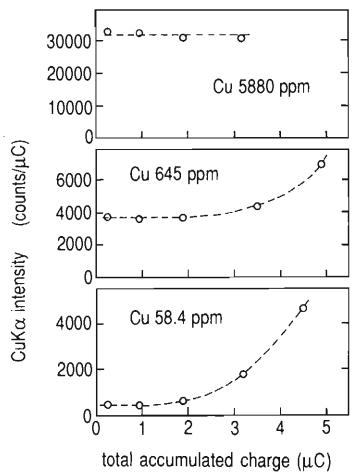

Fig. 2. Change of the Cu Kα intensity as a function of the total accumulated charge. Q = 0.5–1 μC.

Hydrogen Depth Profile of Al-alloy Vacuum Chamber Exposed to Synchrotron Radiation

K. Kanazawa, M. Yanokura, and M. Aratani

Neutral gas desorption due to synchrotron radiation is the main gas load for vacuum systems of electron storage rings. The main desorbed gases are H_2, CO and CO_2 for typical vacuum chamber materials such as aluminium, copper and stainless steel. The basic motive of this paper is to identify the gas source through the quantitative measurement of surface hydrogen, carbon and oxygen for samples exposed to synchrotron radiation. In this paper, hydrogen near the surface of aluminium is analysed by ERDA (Elastic Recoil Detection Analysis)[1] using RILAC.[2] Samples were prepared from a quadrupole magnet chamber of the TRISTAN accumulation ring which had been exposed to synchrotron radiation over 6 y (Fig. 1). The vacuum chamber of the TRISTAN is made of specially extruded aluminium of the type 6063 (ISO AlMgSi).

Every sample has a hydrogen concentrated layer on its surface, whose number density is from 0.42 to 5.4×10^{16} atoms cm^{-2}. The depth profile of hydrogen is shown in Fig. 2. Most of this hydrogen is considered to be contained in a surface oxide layer of aluminium. The surface irradiated directly with synchrotron radiation (sample 3-2) shows the least hydrogen content. The exposure to synchrotron radiation is well memorized as the depletion of the number of surface hydrogen. This means that H_2 desorption during exposure to synchrotron radiation originates from the observed hydrogen concentration. The result is imporant to understand the mechanism of the desorption due to synchrotron radiation.

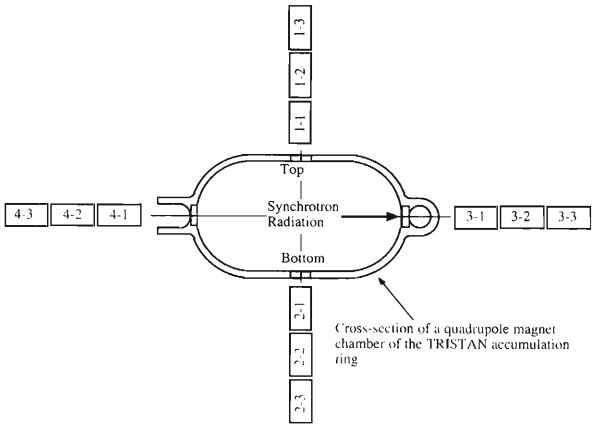

Fig. 1. The original location of samples in the quadrupole magnet chamber. Samples 3-1, 3-2, and 3-3 are cut from the area where the synchrotron light illuminated directly.

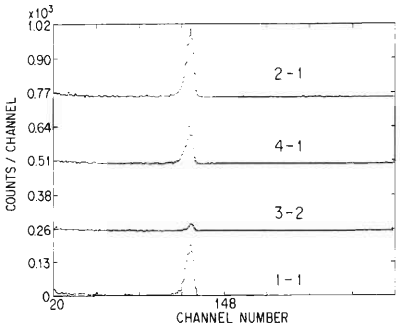

Fig. 2. Hydrogen depth profile of the first group of aluminium samples measured with detector-1 with a 20 μm aluminium absorber. Vertical scale is linear. Energy is lower toward the left. The peak corresponds to surface hydrogen. Hydrogen in metal, whose energy is lower than that of surface hydrogen, is hardly counted.

References

1) H. Nagai, S. Hayashi, M. Aratani, T. Nozaki, M. Yanokura, I. Kohno, O. Kuboi, and Y. Yatsurugi: *Nucl. Instrum. Methods Phys. Res.*, **B28**, 59 (1987).

2) E. Ikezawa, Y. Miyazawa, M. Hemmi, M. Kase, Y. Chiba, T. Chiba, T. Aihara, T. Ohki, and H. Hasebe: Proc. 14th Symp. on ISIAT '91, Tokyo, p. 151 (1991).

Simultaneous Depth Analysis of Deuterium and Helium in He^+-implanted YIG Annealed in D_2

K. Matsushita, T. Kikuchi,* K. Furuya, M. Yanokura, M. Aratani, and R. Imura**

Annealing of He^+-implanted magnetic bubble garnet films in a hydrogen atmosphere enhances the magnetic anisotropy field through the chemical effect of diffused hydrogen in the ion implanted lattice.[1] Recently, a photo-induced effect of ion-implanted YIG films has been found by Tsuchiya et al.[2] To elucidate both mechanisms, a study on the depth distribution change of helium and hydrogen in the film during annealing procedure by elastic recoil detection analysis (ERDA) has been carried out. The condition of simultaneous depth analysis of hydrogen, deuterium and helium has been developed and the change of depth distribution of these elements through annealing has been analyzed.

Samples were prepared as follows: After the growth of 1.6 μm thick $Y_3Fe_5O_{12}$ (YIG) films on both sides of 2 inches thick $Gd_3Ga_5O_{12}$ (GGG) substrate by a conventional liquid phase epitaxial method, He^+ ions were implanted on one side of the film with a dose of 1.2×10^{16} ions/cm^2 at 90 KeV. Specimens were annealed at 320 °C for 1 hr not in a hydrogen atmosphere but in a D_2 atmosphere at 1 atm as a tracer.

The depth profiles of hydrogen, deuterium and helium in this sample were measured simultaneously by ERDA using an Ar^+ beam from the RILAC, whose incident angle and energy were 30° and 50 MeV, respectively.[3] Forward recoiled ions were detected by an SSD at an angle of 35°. An aluminum foil filter of 15 μm was inserted in order to eliminate scattered Ar^+ and recoiled O^+ beams. The total ions were monitored by an SSD at an angle of 45°.

Figure 1 shows a measured energy spectrum of this sample. The positions of triangle marks indicate the equivalent energy of each element recoiled directly from the surface. In this condition, the largest measurable depths of He, D and H were calculated to be as large as 0.53 μm, 0.8 μm and 0.73 μm, respectively.

Figure 2 shows the measured depth distributions of He and D, together with the theoretical distribution

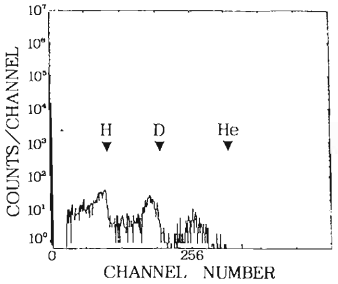

Fig. 1. Energy spectrum of H, D, and He.

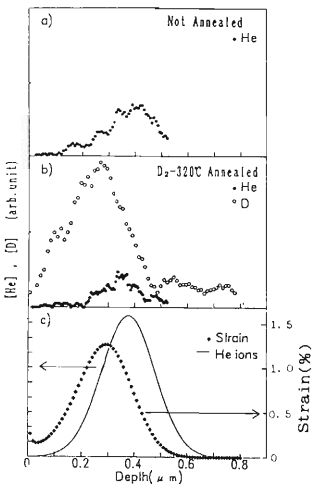

Fig. 2. Depth distribution of He and D in YIG by ERDA ((a) and (b)) and calculated distribution of implanted He and lattice strain (c).

of implanted helium and defect-induced lattice strain calculated by the LSS theory. In Fig. 2(a), the helium depth distribution in an as-implanted sample has a peak at 0.4 μm from the surface, which coincides with the calculated one. While, the peak position of helium in the annealed sample shifted toward the position of the strain distribution peak in Fig. 2(b). The shift toward the peak position of strain from implanted sites has been reported by Gerard et al[4] and Byoung-gon et al.[5] When the specimen was kept in a deuterium atmosphere at 320 °C for 1 hour, deuterium diffused into the sample and concentrated at the sites of strain distribution, differently from a homogeneous sample in which the deuterium distribution can be expected to be exponential.

From the ERDA results, it is concluded that both helium and deuterium diffused to the defect-induced strained region through annealing and that the concentration of these two species at the strained lattice in YIG may increase photosensitive sites which bring an effective magnetic anisotropy field change.

* Dept. Appl. Chem., Fac. Sci., Sci. Univ. Tokyo
** Cent. Res. Lab., Hitachi Ltd.

References

1) O. Okada: *J. Magn. Soc. Jpn.*, **8**, 153 (1984).
2) T. Tsuchiya and K. Uematsu: *Jpn. J. Appl. Phys.*, **25**, L357 (1986).
3) K. Yano, H. Oyama, M. Yanokura, M. Aratani, and M. Minami: *RIKEN Accel. Prog. Rep.*, **24**, 64 (1990).
4) Ph. Gerard, P. Martin, and M. T. Delaye: *J. Appl. Phys.*, **57**, 4058 (1985).
5) Y. Byoung-gon, E. Arai, and R. Imura: *Jpn. J. Appl. Phys.*, **30**, 290 (1991).

IV. NUCLEAR DATA

Status Report of the Nuclear Data Group

Y. Tendow, A. Yoshida, Y. Ohkubo, A. Hashizume, and K. Kitao

The Nuclear Data Group have been continuing the following data activities since previous years.[1)]

(1) Nuclear reaction cross-section data (EXFOR)

Compilation of nuclear reaction cross sections induced by charged particles into the exfor format has been continued. We had originally restricted our scope of compilation to the production cross section of only twenty radioisotopes commonly used in the biomedical application field; ^{11}C, ^{13}N, ^{15}O, ^{18}F, ^{28}Mg, ^{52}Fe, ^{67}Ga, ^{68}Ge, ^{74}As, ^{77}Br, ^{82}Br, ^{77}Kr, ^{81}Rb, ^{82m}Rb, ^{111}In, ^{123}Xe, ^{127}Xe, ^{123}I, ^{124}I, and ^{125}I. We are now not necessarily adhering to the above-mentioned isotopes, but expanding our choice to a wider scope of variety. We are also picking up old data not contained in the EXFOR master file yet.

A transmission magnetic tape R008 containing newly compiled EXFOR entries R0040 through R0050 with a total of 56 subentries or 63 excitation functions has been sent to the IAEA Nuclear Data Section (NDS) this year.

Cross section data for the production of radioxenon isotopes, especially other isotopes than ^{123}Xe, were surveyed extensively.[2)] ^{123}Xe is the parent to produce ^{123}I isotope which is one of very useful labels for radiopharmaceuticals and we have reviewed elsewhere.[3)] Other radioxenon isotopes are also useful in medical diagnosis and applications.

(2) Evaluated nuclear structure data file (ENSDF)

We have been participating in the ENSDF compilation network coordinated by the Brookhaven National Nuclear Data Center (NNDC). The evaluation and compilation of A = 129 mass chain has been completed and now under the editorial review at NNDC for print in the Nuclear Data Sheets. Mass chains of A = 127 and 118 have also been evaluated and sent to NNDC by the other members of the Japanese group this year. New evaluation of A = 120 mass chain is now in progress.

(3) Nuclear structure reference file (NSR)

We are engaged in collection and compilation of secondary references (annual reports, conference proceedings, etc.) published in Japan since previous year into the Nuclear Structure Reference (NSR) file and sending it to NNDC. The NSR file is offered for the on-line retrieval service by NNDC and also published periodically as the Recent References.

The compilations of 1991 and 1992 annual reports have been completed and sent to NNDC. Secondary sources surveyed this year are the following annual reports (in code name in NSR); RIKEN (RIKEN Accel. Prog. Rep.), JAERI-TLV (JAERI Tandem, Lin. & V.D.G.), INS (INS Univ. Tokyo), UTTAC (Univ. Tsukuba Tandem Accel. Center), RCNP (Res. Center Nucl. Phys. Osaka Univ.) and CYRIC (Cyclo. Radioisot. Center, Tohoku Univ.).

References

1) Y. Tendow, A. Yoshida, Y. Ohkubo, A. Hashizume, and K. Kitao: *RIKEN Accel. Prog. Rep.*, **26**, 135 (1992).
2) Y. Tendow, A. Hashizume, and K. Kitao: This report p. 128.
3) A. Hashizume and Y. Tendow: *RIKEN Accel. Prog. Rep.*, **19**, 163 (1985).

Production Cross Sections of Radioxenon Isotopes

Y. Tendow, A. Hashizume, and K. Kitao

Among radioxenon isotopes, ^{123}Xe has extensively been studied as the parent of ^{123}I which is a commonly used label for *in vivo* functional imaging in diagnosis and biomedical studies.[1] Other radioxenon isotopes than ^{123}Xe may act as impurities in the case, but each of them also can well be used separately e.g. as a generator of an iodine isotope or in diagnosis of ventilation function of lungs and blood flow. Cross section data for ^{123}Xe have been reviewed elsewhere.[1] We will review here the production cross sections for the other radioxenon isotopes through charged particle nuclear reactions.

Radioxenon isotopes are mainly produced through (p, xn), (d, xn) reactions on ^{127}I targets or spallation reactions with high energy protons on Cs, Ba or La targets. Cross section data except for the spallation reactions are summarized in Table 1 and examples of the excitation curves for the (p, xn) reactions[2] are shown in Fig. 1.

Table 1. Production cross sections for Xe isotopes.

Product	Reaction	Energy (MeV)	σ max (mb)	Ref.
^{127}Xe	^{127}I (p, n)	8 - 67	178	2 - 4)
	^{127}I (d, 2n)	6.5 - 89.8	470	5)
^{125}Xe	^{127}I (p, 3n)	21 - 67	760	2,3,6,7)
	^{127}I (d, 4n)	24.2 - 89.2	800	5)
	^{126}Te (^{3}He, 4n)	8 - 40	120	8)
	^{125}Te (α, 4n)	10 - 40	50	8)
^{122}Xe	^{127}I (p, 6n)	51 - 67	> 200	2,3)
	^{127}I (d, 7n)	62.5 - 89	190	5)
^{121}Xe	^{127}I (p, 7n)	62 - 67	> 80	2,6,9)
	^{127}I (d, 8n)	76 - 89	45	5)

^{127}Xe (36.4 d, EC) is produced through ^{127}I (p, n), (d, 2n) reactions with low energy protons or deuterons and convenient for the diagnosis of respiration function.

^{125}Xe (17.1 hr EC, β^+) is a main contaminant in ^{123}Xe produced by (p, 5n) and (d, 6n) but the daughter ^{125}I (59.4 d, EC) in the extracted ^{123}I may not seriously interfere because it emits a 35 keV γ-ray only.

Although ^{122}Xe is also one of the contaminants in the ^{123}Xe production, it can be used as a generator system providing ^{122}I for the positron emission tomography (PET). Spallation reactions with very high energy protons are also utilized for routine production of

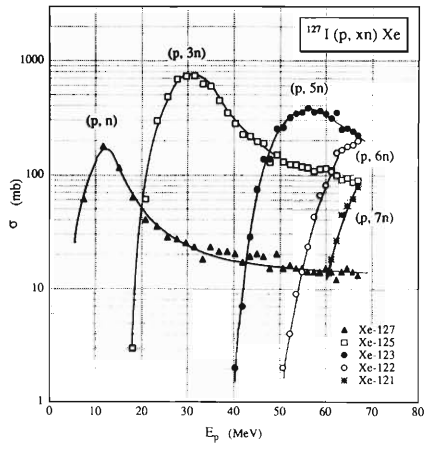

Fig. 1. Excitation functions for ^{127}I (p, xn) reactions (Ref. 2).

radioxenon isotopes.[10-12]

References

1) A. Hashizume and Y. Tendow: *RIKEN Accel. Prog. Rep.*, **19**, 163 (1985).
2) M. C. Lagunas-Solar, O. F. Carvacho, Bo-Li Liu, Yutai Jin, and Zhao Xiang Sun: *Int. J. Appl. Radiat. Isot.*, **37**, 823 (1986).
3) M. Dikšić and L. Yaffe: *J. Inorg. Nucl. Chem.*, **39**, 1299 (1977).
4) R. Collé and R. Kishore: *Phys. Rev.*, **C9**, 2166 (1974).
5) R. Weinreich, O. Schult, and G. Stöcklin: *Int. J. Appl. Radiat. Isot.*, **25**, 535 (1974).
6) D. B. Syme, E. Wood, I. M. Blair, S. Kew, M. Perry, and P. Cooper: *ibid.*, **29**, 29 (1978).
7) S. R. Wilkins, S. T. Shimose, H. H. Hines, J. A. Jungerman, F. Hegedus, and G. L. DeNardo: *ibid.*, **26**, 279 (1975).
8) Y. Homma and Y. Murakami: *ibid.*, **28**, 738 (1977).
9) M. C. Lagunas-Solar, O. F. Carvacho, L. J. Harris, and C. A. Mathis: *ibid.*, **37**, 835 (1986).
10) M. Adilbish, V. G. Chumin, V. A. Khalkin, O. Knotek, M. Ja. Kuznetsova, Ju. V. Norseev, V. I. Fominykh, and N. G. Zaitseva: *ibid.*, **31**, 163 (1980).
11) N. F. Peek and F. Hegedüs: *ibid.*, **30**, 631 (1979).
12) R. Michel, P. Dragovitsch, P. Englert, F. Peiffer, R. Stück, S. Theis, F. Begemann, H. Weber, P. Signer, R. Wieler, D. Filges, and P. Cloth: *Nucl. Instrum. Methods*, **B16**, 61 (1986).

V. DEVELOPMENT OF ACCELERATOR FACILITIES

1. Ion Accelerator Development

Status of the RIKEN 10 GHz ECR Ion Source

T. Kageyama, T. Nakagawa, A. Goto, M. Kase, and Y. Yano

Table 1 lists the ions that were produced with the ECR ion source (ECRIS) from November 1992 to October 1993. We delivered 13 kinds of ion species for the last one year in a total operation time of 184.5 days. Of those days, 180 days were devoted to delivering beams to the AVF cyclotron, and the remaining 8 days to stand-alone use of the ECRIS in atomic physics study. Recent upgrade of the ECRIS[1,2] has allowed us to get high beam intensity as well as to do easy and stable operation.

Table 1. Ions produced with the RIKEN 10 GHz ECRIS from November 1992 to October 1993.

Particle	Operation Time (days)	Rate (%)	Maximum Current (eμA)
P	4.5	2.4	200
H_2^+	7.5	4.1	200
d	4	2.1	200
$^{11}B^{3+}$	5	2.7	35
$^{12}C^{4+}$	40.5	22.0	60
$^{13}C^{4+}$	8.5	4.6	30
$^{14}N^{5+}$	2	1.1	120
$^{16}O^{6+}$	8.5	4.6	125
$^{18}O^{6+}$	44.5	24.1	100
$^{20}Ne^{7+}$	14.5	7.9	55
$^{22}Ne^{7+}$	15	8.1	50
$^{27}Al^{9+}$	6	3.3	20
$^{40}Ar^{11+}$	24	13.0	50
Total	184.5		

Because the number of kinds of ions demanded by users has increased, we have installed a new gas-feed system as shown in Fig. 1. The system consists of nine main-gas reservoirs, two mixing-gas reservoirs, and one reservoirs for an expensive gas such as an enriched isotope gas.

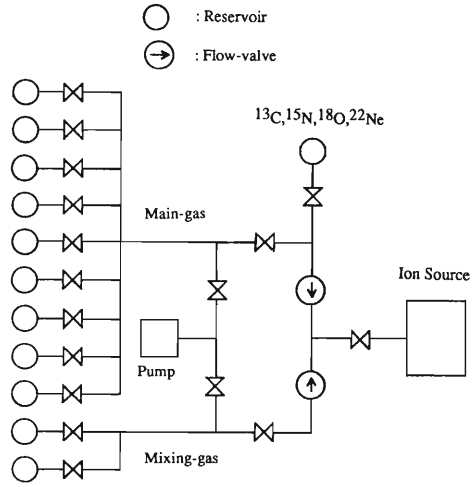

Fig. 1. Block diagram of the new gas-feed system.

References

1) T. Nakagawa et al.: *RIKEN Accel. Prog. Rep.*, **26**, 137 (1992).
2) T. Nakagawa et al.: *Jpn. J. Appl. Phys.*, **32**, L1335 (1993).

Development of the RIKEN Polarized Ion Source

H. Okamura, N. Sakamoto, T. Uesaka, H. Sakai, K. Hatanaka, K. Ikegami,
J. Fujita, M. Kase, A. Goto, T. Kubo, N. Inabe, and Y. Yano

The polarized ion source has been improved in many ways and is now ready for experimental use.[1] Several physics programs using the polarized deuteron beam are currently under way.[2,3]

One of the major difficulty in the ion source operation was the short lifetime of the dissociator nozzle. The white powder which was analyzed to be SiO_2 accumulates on the wall of cold nozzle and reduces the beam intensity very rapidly. It sometimes plugs the nozzle orifice after a few days operation. This was remedied by keeping the RF power as low as possible, typically at 60–80 W. Also the nozzle has been made longer so that the white deposits accumulate far away from the nozzle, expecting that the surface near the orifice will be kept clean. In this way, no reduction of intensity is observed for at least one week.

Also a -20 °C alcohol circulation system has been introduced for cooling the discharge tube in place of the water cooling system. This was reported to be very effective in reducing the white powder at IUCF.[4] We found, however, the amount of white deposits showed no dependence on the temperature of alcohol.

The performance of the dissociator was studied by using a compression tube installed downstream of the second sextupole magnet. The maximum beam flux into the 25 mm aperture is routinely observed to be 2.6×10^{16} atoms/sec at 37 K nozzle temperature. The N_2-layer technique to prevent the strong recombination at the nozzle works very reliably. Still the considerable effort is devoted to improve the performance of the dissociator.

The second major difficulty was concerned with the ECR ionizer. In the early design of the ionizer, the sextupole magnet was electrically isolated and biased to +7.5 kV operation voltage while the vacuum chamber remained at the ground potential. The ions were extracted axially to the upstream direction as well as radially through the gap of the sextupole magnet. As a result, the ions hit the RF transition units, the waveguide and the wall of vacuum chamber, which inhibits a long-term operation. The best performance of this ionizer was 20 μA with 60% polarization of the ideal value.

We have modified the design of the ionizer close to the one at PSI. A quartz plasma chamber is installed inside the sextupole magnet which is kept at the ground potential. The plasma region is pumped through the 5 cm aperture of three-stage extraction electrodes. A Ti sublimation pump is installed to amend the pumping power. The waveguide comes into contact with the sextupole magnet so that the 2.45 GHz microwave is efficiently directed. The plasma is ignited typically at a power of 30–40 W. The stable and long-term operation of the new ionizer allowed us extensive searches of optimum conditions. Currently the ion intensity of 140 μA is routinely observed with 65% polarization of the ideal value. It should be noted that the polarization is reduced to 50% without the Ti sublimation pump. Further improvement on the ionizer is going to be made aiming for the better pumping of the plasma region which will lead to the better polarization. Also some modifications are being made to the strong- and weak-field RF transition magnets to increase the polarization degree.

The beam polarization is monitored both at the exit of the AVF cyclotron ($E_d = 14$ MeV) and at the exit of the ring cyclotron ($E_d = 270$ MeV). The spin direction is freely controlled by using the Wien filter downstream of the ion source. While the beam is injected and accelerated with its spin axis inclined to the cyclotron magnetic field, a single turn extraction does not lead to a loss in the amplitude of polarization. According to this principle, we have succeeded in rotating the spin direction without reducing the polarization or the intensity.

References

1) H. Sakai et al.: *RIKEN Accel. Prog. Rep.*, **25**, 162 (1991); N. Sakamoto et al.: *ibid.*, **26**, 138 (1992).
2) N. Sakamoto et al.: This report, p. 39.
3) T. Uesaka et al.: This report, p. 40.
4) V. Derenchuk et al.: *IUCF Scientific and Technical Report*, p. 190 (1992).

Basic Study of Polarized He-3 Ion Source for the RIKEN AVF Cyclotron

A. Minoh, K. Ogiwara, T. Fujisawa, and T. Nakagawa

The polarized He-3 ion source based on optical pumping and electron cyclotron resonance (ECR) has been studied.[1-3] A principle of the ion source is presented in Ref. 1 and a block diagram of the source also shown. Now we plan to test our concept using the ECR ion source of the RIKEN AVF cyclotron. This report shows the present status of the development of the laser system, performance of vacuum system of the ECR ion source, and investigation of the optical pumping region. The output power of the LNA laser developed for pumping He-3 atoms was 20 mW and the spectral width was 30 GHz.[2] Nacher et al.[4-5] showed that the pumping power is more than 100 mW and the spectral width about 2 GHz to generate the sufficient nuclear polarization. Such low output power is caused by low power (1.5 W) of the Ar laser pumping LNA laser, and the spectral width was so wide because the etalon installed in the cavity to reduce the width disturbed laser oscillation in such low pumping power. Then we try to increase the pumping power by adding a diode laser (800 nm) to Ar laser because the diode laser is very compact and cheap comparing to Ar laser. Figure 1 shows a schematic view of the double pumping system. The pumping Ar laser beam is focused on one side of the laser rod by a focusing lens and the additional diode laser beam is focused on the other side of the lod. Then the laser cavity axis is bent 90 degree by the inserted mirror(s). The laser beam is linearly polarized in the plane of the paper by the mirror. An air gap etalon and an electrically controlled etalon are set between the lens and the end mirror of the cavity. The LNA laser pumped by a diode laser is studied with the system as shown in Fig. 2. The LNA laser cavity consists of the flat end mirrors (M1, M2) and intra-cavity lens (L). The output beam of the diode laser is collimated by ananamorphic prisms and focused on the position of 2–3 mm from the end of the laser rod by the focusing lens (F2). The maximum output power of the diode laser (SONY Co. 304V) is 1 W. The output beam of the diode laser has a large divergence angle comparing with the Ar laser. Then the spot size of the diode laser at the focusing point is five times greater than that of the Ar laser. Our preliminary experiment shows that the absorption coefficient of the LNA laser for the 794 nm light is ten times larger than that of 514 nm light of the Ar laser.

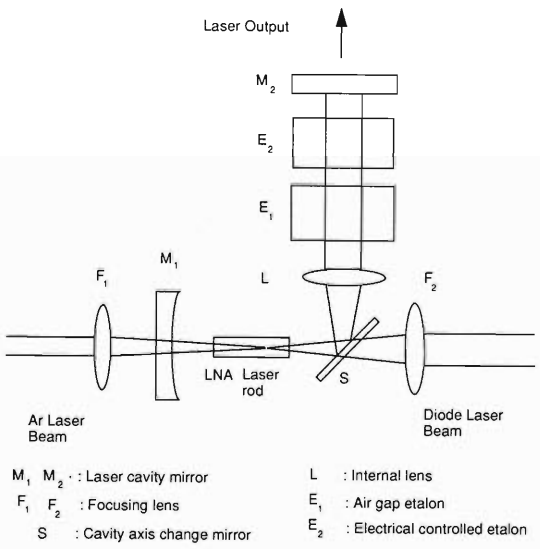

Fig. 1. LNA laser system pumped by the Ar laser and the diode laser.

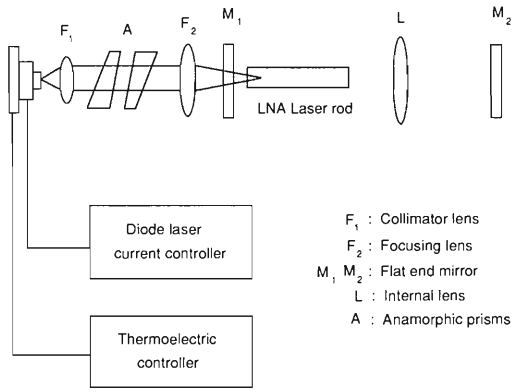

Fig. 2. LNA laser pumped by a diode laser for study.

These facts suggest that the beam of the diode laser should be focused on the LNA laser rod by the focusing lens whose focal length is about one third of the focal length for the Ar laser beam. In this case, the axial length of the gain medium is about one third of that with the Ar laser. The absorption coefficient of the LNA laser material rapidly varies arround the 800 nm wavelength region. The wavelength of the diode laser beam is strongly dependent on the temperature of the diode and the temperature of the diode laser is dependend on the output power of the laser. Then the temperature of the diode laser is controlled automatically with thermo-electric controller to keep the best laser oscillation. Figure 3 shows the pumping power dependence of the laser output. The output power for the focal length of 18 mm is higher than that of 30 mm.

The He-3 gas pressure in the pumping region should be between 0.1 Torr and 1 Torr to obtain the good nuclear polarization.[6] However, the ECR ion source should be operated under pressure of 10^{-5} to 10^{-7}

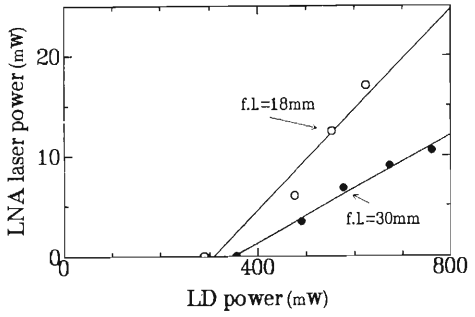

Fig. 3. The pumping power dependence of the diode laser pumped LNA laser.

Torr. Figure 4 shows the Pyrex tube for the pumping region and ECR ion source. The exit channel aperture of the tube is about 0.1 mm and the length 10 mm to hold the gas for a long time in the tube and keep a good vacuum of the ECR ion source. We measured the pressure of each section by feeding He-4 gas. The result shown in Fig. 5 is satisfactory. In the pumping region, the magnetic field of 0.01 T is enough to hold the nuclear polarization. However, the diagonal component of the magnetic field against z-axis should be less than 0.3×10^{-5} T to obtain good polarization.[7] Furthermore, the magnetic field of the ECR ion source is about 0.3 T. Thus, in the pumping region, the magnetic field have to be carefully adjusted. The measured magnetic field in the pumping region leaked from the ECR ion source was less than that of the earth. Then we plan to generate the magnetic field of the optical pumping region with a usual solenoid coil surrounded

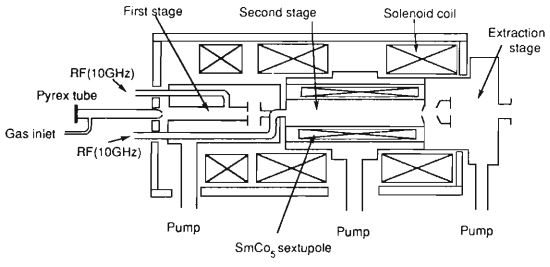

Fig. 4. Optical pumping region and ECR ion source.

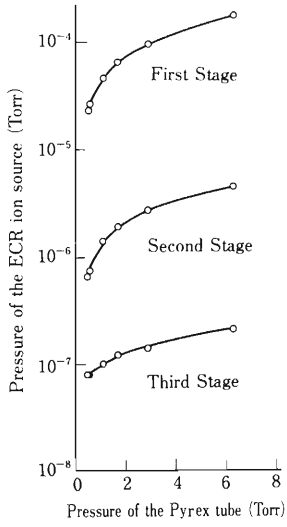

Fig. 5. Vacuum pressure of the ECR ion source.

by an iron cylinder. The magnetic field of 0.3 T in the ECR ion source is just the critical strength to hold the nuclear spin,[7] so a higher field as 1 T is desirable to hold perfectly the nuclear spin. However, it is of enough strength in order to see whether our concept is good or not. We test the whole system in the near future.

References

1) T. Fujisawa, A. Minoh, Y. Taniguchi, S. Ishii, K. Hatanaka, and Y. Oshiro: *RIKEN Accel. Prog. Rep.*, **22**, 222 (1988).
2) A. Minoh, K. Ogiwara, and T. Fujisawa: *ibid.*, **23**, 113 (1989); **24**, 136 (1990); **25**, 103 (1991); **26**, 139 (1992).
3) T. Fujisawa, A. Minoh, Y. Taniguchi, and K. Hatanaka: Int. Workshop on Polarized Ion Source and Polized Gas-Jet, Tukuba, Feb., p. 12 (1990).
4) P. J. Nacher and M. Leduc: *J. Physique*, **46**, 2057 (1985).
5) M. Leduc, S. B. Crampton, P. J. Nacher and F. Laloe: *Nucl. Sci. Appl.*, **1**, 1 (1983).
6) F. D. Colegrove, L. D. Schearer, and G. K. Walters: *Phys. Rev.*, **132**, 6, 2561 (1963).
7) T. B. Clegg: Workshop on Polarized ^{3}He Beams and targets, Princeton, New Jersey, p. 25 (1984).

Development of a New Type of Single-Bunch Selector

N. Inabe, M. Kase, T. Kawama,* M. Hemmi, O. Kamigaito,
M. Nagase, I. Yokoyama, A. Goto, and Y. Yano

A new type of single-bunch selector has been developed and installed on the beam transport line between the ECR ion source (ECRIS) and the AVF cyclotron. Figure 1 shows a schematic drawing of the single-bunch selector system. Electrodes are connected to a DC power supply via a switching module. A pulse for switching on/off is created by a function generator and sent to the module. Characteristics of the single bunch selector are summarized in Table 1. In the present method, the single-bunched beam is obtained

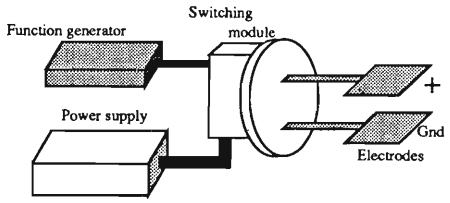

Fig. 1. Systematic drawing of the single-bunch selector.

Table 1. Characteristics of single bunch selector.

Gap between electrodes	60 mm
Length of electrodes in beam direction	80 mm
Width of electrodes	100 mm
Voltage	0–3 kV (DC)
Repetition rate	0–25 kHz
Rise time	20 ns
Duration time (T_{off})	> 150 ns

from a continuum beam of the ECRIS before entering the AVF cyclotron, while in a usual method a single-bunch selection is made from a bunched beam after a cyclotron. Since the single-bunch selection is made at low energy in the present method, the whole system can be small and of low cost.

Figure 2 shows how to make the single-bunch selection. A discrete beam can be produced from the beam of the ECRIS using an electric field which is switched off for a duration of T_{off}. The duration of the discrete beam picked up by the selector (T_{bon}) is given by subtracting a traveling time through the electric field from T_{off}. To get the single-bunched beam, T_{bon} is necessary to be as short as possible so as not to overlap the previous and the next bunches of the AVF cyclotron. To get as high-intensity single-bunched beam

* Sumijyu Accel. Service, Ltd.

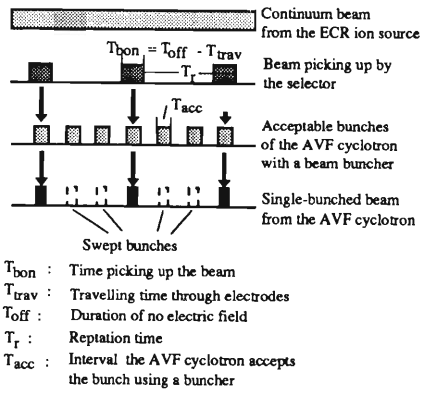

Fig. 2. Production scheme of a single-bunched beam with the selector.

as possible for a given repetition time (T_r), on the other hand, T_{bon} should be longer than T_{acc} (a duration that the AVF cyclotron can accept the bunch when using the beam buncher). In the system, unnecessary beam kicked away by an electric field is swept out at some places of the beam transport line to the AVF cyclotron.

A performance study of the single-bunch selector was carried out for the 7.45 KeV H_2^+ beam from the ECRIS which is accelerated to 7 MeV/nucleon by the AVF cyclotron with an RF frequency of 16.3 MHz. The setup is shown in Fig. 3. Time structure of the beam after the AVF cyclotron was measured by using a time of flight (TOF) between a reduced RF signal and a timing signal of a micro channel plate (MCP) with a target.[1] Beam current was measured with a Faraday cup.

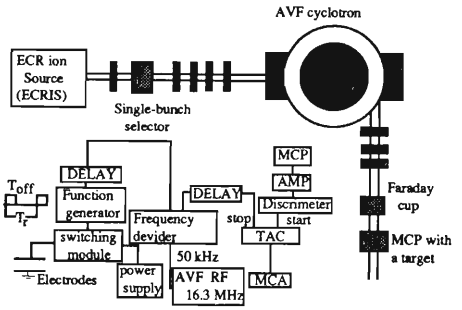

Fig. 3. Setup for a performance test of the single-bunch selector.

Figures 4a and 4b show typical examples of the TOF spectra. The T_{off} is 200 ns (T_{bon} = 106 ns) in Fig. 4a and 400 ns (T_{bon} = 306 ns) in Fig. 4b. The T_r is

50 μs and a voltage between the electrodes is 350 V in the both figures. The two peaks in Fig. 4a do not mean that the selector failed to make a single-bunch selection but they mean that the same single-bunch inside the AVF cyclotron is extracted with two-turns. The four peaks in Fig. 4b whose strengths change alternately mean that the single-bunch selection was not completed due to long T_{off} compared with the case of Fig. 4a. Production mechanism of those peaks is explained in Fig. 5. In the case of Fig. 4a, the time structure was measured for several positions of the target of the MCP to cover the whole region of the beam and it was ensured that no other peak existed. This shows that the single-bunched beam can be obtained

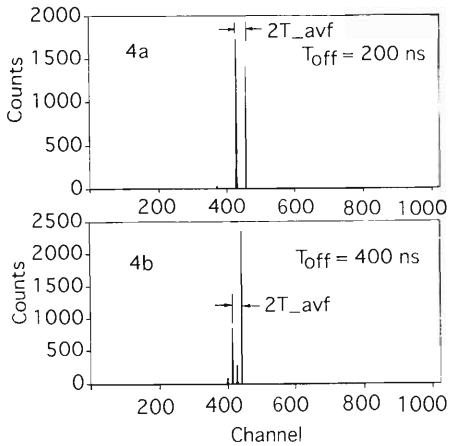

Fig. 4. Examples of time spectra of the beam: 4a, in the case of T_{off} = 200 ns; and 4b, in the case of T_{off} = 400 ns. T_avf means the RF period of the AVF cyclotron.

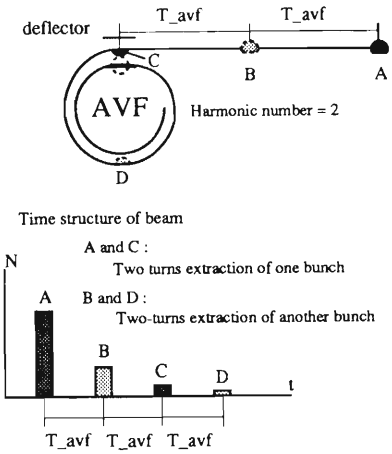

Fig. 5. Time structure of the beam from the AVF cyclotron for two bunches with two-turns extraction.

if the beam inside the AVF cyclotron can be extracted with the single turn. In fact, the careful tuning of the AVF cyclotron can realize the single-turn extraction.[2] Current of the single-bunched beam was 2.7 enA and this value was almost equal to that calculated by the current of continuum beam divided by the number of bunches during T_r. This shows that almost all fraction of the part selected with the single-bunch selector is accepted by the AVF cyclotron.

To get more intense single-bunched beams, we plan to increase the repetition rate up to as high as 1 MHz ($T_r \sim 1$ μs) using a higher speed semi-conductor device.

References

1) T. Kawama et al.: This report. p. 135.
2) A. Goto et al.: This report. p. 6.

Development of a Beam Phase Monitor with a Micro-Channel Plate

T. Kawama,* M. Kase, T. Nakagawa, N. Inabe, I. Yokoyama, A. Goto, and Y. Yano

A new beam monitor with a micro-channel plate (MCP) has been developed[1] for the measurement of time structure of various kinds of ion beams from the RIKEN Ring cyclotron (RRC) and the AVF cyclotron (AVF). This probe has a good sensitivity with a large dynamic range of beam intensities, compared with a conventional phase monitor with a capacitive pick-up electrode.

The structure of the new phase probe is shown in Fig. 1. An MCP is set parallel to the beam axis. A small target of 0.3 mmϕ tungsten wire is strung in parallel with the MCP surface. The target intersects

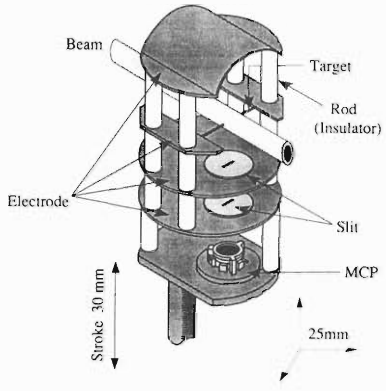

Fig. 1. Structure of the new phase probe with an MCP. All electrodes are made of stainless steel and supported by ceramic insulator rods. Each electrode is based so that a uniform field is produced from the wire to the MCP.

only a small fraction of a beam (a few percents at the maximum). Electrons and/or photons (considered to be mainly X ray) produced on the target by ion beams are introduced to the MCP through double slits. There are four sets of electrodes for producing an electric field for the electron acceleration. The whole electrodes including the target and the MCP can be moved remotely in perpendicular to the beam axis, keeping a constant distance (50 mm) between the wire and the MCP. In this way the position of wire with respect to the beam is selectable in order to adjust a signal rate (0.1–10 kcps) from the MCP. Fast and large signals with a rise time less than 1 ns and with a gain larger than 10^7 are obtained from the tapered coaxial shaped anode of the MCP. The timing of these signals with respect to the time origin determined by an RF master oscillator is measured with a time-to-analog converter and analyzed by a multi-channel analyzer. The device is installed inside beam-diagnostic chambers located in the extracted beam line of the RRC and the AVF.

Figure 2 shows a typical example of time spectrum obtained for 100 MeV/u ^{18}O beam from the RRC operated with the AVF. Beam bunches appear with time intervals of an RF period of the AVF (T_{AVF}) which is equal to 2 × T_{RRC} (an RF period of RRC). The time spread of a beam bunch was measured to be 940 ps in FWHM, corresponding to an RF phase spread of about 10 degrees.

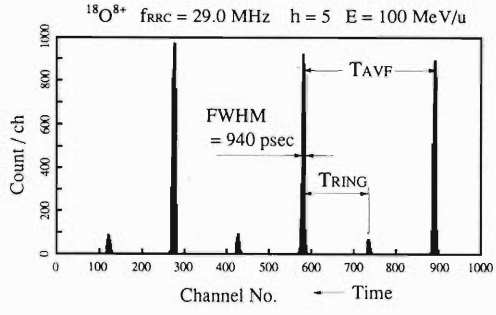

Fig. 2. Example of time spectrum of signals from the MCP for 100 MeV/u ^{18}O beam. Large peaks are due to a main beam, and small peaks are due to the effect of multi-turn extraction.

The position of peak in Fig. 2 is always relating to a beam phase to an RF phase. This allows the device to work as a phase probe. Figure 3 shows that the change of magnetic field in the RRC causes a shift of the peak. We can detect a deviation less than 10 ppm of a magnetic field from the isochronous one. An operator can

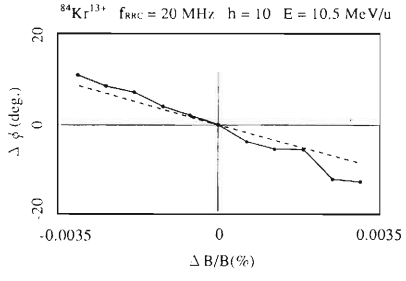

Fig. 3. The peak shift (that is, beam phase) vs. the change of magnetic field in the RRC. When ΔB/B is zero, the magnetic field is isochronous. A dashed line results from the following calculation.

* Sumijyu Accelerator Service, ltd.

stabilize the magnetic field by adjusting a magnetic current to keep this peak at the same position.

$$\varphi = -360 \times \Delta B/B \times \text{Nturn} \times \text{Nh}$$

ΔB : the change of magnetic field

B : a magnetic field

Nturn : a number of turn in the cyclotron

Nh : a harmonic number

This phase monitor also works as a monitor which gives information about the single turn extraction. In case of the RRC coupled with AVF, a harmonic number of the RRC is an odd number of five, and $T_{AVF} = 2 \times T_{RRC}$. Considering these conditions, we conclude that small peaks,which are observed at the middle points between large main-beam peaks as shown in Fig. 2, are due to the multi-turn extraction of the RRC. In other cases (e.g. for the AVF or for the RRC coupled with RILAC), we can also observe the peaks which are due to the multi-turn extraction by use of an electric chopper.[2] Figure 4 shows an example of the time spectrum obtained, when a beam is chopped for the duration of 1.2 μs, for the case of the RRC harmonic number of 11. In case of the multi-turn extraction, after a beam is switched off at A, eleven small peaks still remain and, after switched on at B, another group of eleven peaks appears first and full height peaks follow it. The number of peaks in each group corresponds to a harmonic number of the RRC. The details were reported in Ref. 1. In this way, we can observe to what degree the single-turn extraction is achieved for cyclotrons.

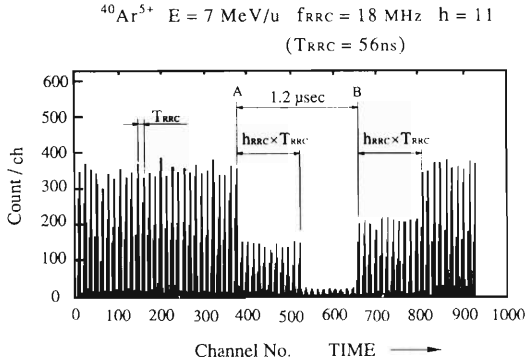

Fig. 4. A time spectrum of beam bunches when the beam is cut partially (1.2 μsec) by the beam chopper installed in the RILAC injection line.

References

1) M. Kase, T. Kawama, T. Nakagawa, N. Inabe, I. Yokoyama, A. Goto, and Y. Yano: Proc. the 9th Symp. on Accel. Sci. and Technol. in Japan, 1993 Tsukuba, p. 474 (1993).

2) M. Hemmi, H. Kumagai, and Y. Miyazawa: Proc. Linear Accel. Meet. in Japan, 1992, Sendai, p. 309 (1992).

Development of the Second-Harmonic Buncher for the RILAC

S. Kohara, A. Goto, Y. Miyazawa, T. Chiba, M. Hemmi,
Y. Chiba, E. Ikezawa, M. Kase, and Y. Yano

The second-harmonic buncher was constructed and installed on the injection beam line of the RILAC in March 1993 to increase beam intensity. It has been in routine operation since then. It has good impedance matching to a power feed line without adjusting device in the required wide frequency range. Beam intensity was increased by 50% with both the fundamental-frequency and the second-harmonic bunchers. The details of the design and the structure of the second-harmonic buncher were reported elsewhere.[1,2] The test results for the completed buncher are presented in this report.

A cross sectional view of the new buncher is shown in Fig. 1. Position of the movable shorting plate and capacitance of the variable capacitor are the two parameters determining a resonant frequency. Optimum combinations of these parameters, which realize the best impedance matching, are determined from measurements (as shown in Fig. 4).

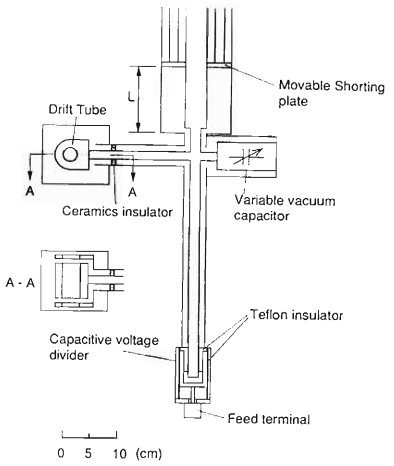

Fig. 1. Cross sectional view of the second-harmonic buncher.

The frequencies of the fundamental and higher modes measured with a nearly optimum parameter set are shown in Fig. 2 as a function of position of the movable shorting plate. The resonator has a parasitic resonance in the vicinity of 150 MHz for every position of the movable shorting plate. This is a half-wave-length mode standing on between the drift tube and the other open end terminal and having a node near the position of the capacitor. The measured Q-values are shown in Fig. 3. They are from 1000 to 1600. Figure 4-A shows input impedances at the feed point measured with the optimum parameter combinations

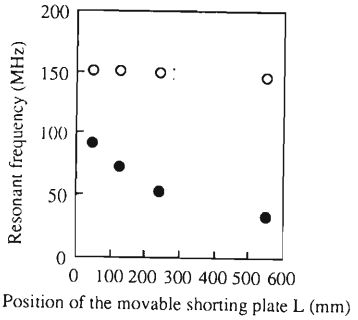

Fig. 2. Measured resonant frequencies as a function of position of the movable shorting plate for fundamental (•) and higher (○) modes with a nearly optimum parameter set.

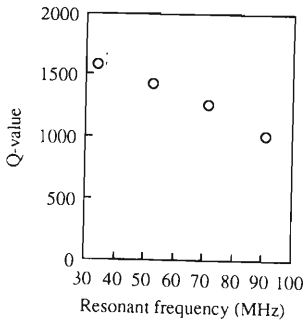

Fig. 3. Measured Q-values as a function of resonant frequency with a nearly optimum parameter set.

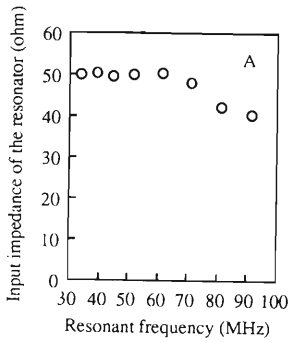

Fig. 4-A. Measured input impedances at the feed point as a function of resonant frequency with the optimum parameter set in Fig. 4-B. The imaginary parts of the impedances are zero.

shown in Fig. 4-B. The input voltage standing wave ratio (VSWR) increases to 1.25 at 90 MHz, but gives practically no problem.

The drift-tube voltage was measured by a calibrated capacitive voltage pickup. The results of the power test under atmospheric pressure are shown in Fig. 5.

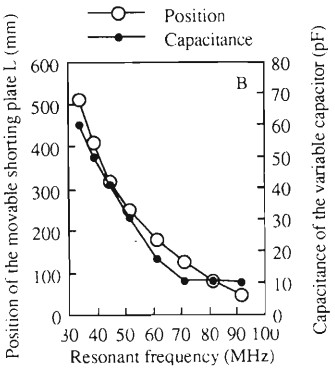

Fig. 4-B. Optimum combination of positions L of the movable shorting plate and capacitances of the variable capacitor.

The required peak drift-tube voltage of 1.5 kV (3kV/2 gaps) was obtained in the whole frequency range. Reflected power from the resonator to the amplifier was less than 1.2W. Stability of the drift-tube voltage was better than $\pm 1 \times 10^{-3}$ and stability of the phase $\pm 0.5°$.

Amplitudes of the higher mode were observed at high power levels. They are about 3% of the fundamental ones in the worst case and cause negligible effect on performance of the buncher.[2)]

Multipactoring phenomenon occurred in the power test under vacuum, but it was easily overcome by a pulse operation.

Results of the beam test with Ar^{6+} ion are listed in Table 1. The beam intensity at the exit of the RILAC was increased from 1.7 to 2.5 μA.

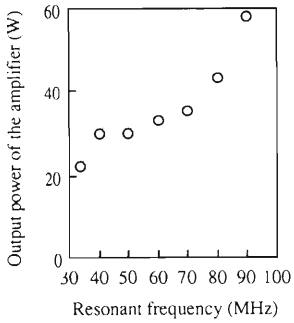

Fig. 5. Measured output powers of the amplifier for the required peak drift-tube voltage of 1.5 kV.

Table 1. Results of the beam test.

RILAC	28 MHz	28 MHz
Cockcroft	283 kV	283 kV
Fund. buncher	28 MHz	28 MHz
	1.3 kV	2.0 kV
Second buncher	no use	56 MHz
	no use	1.0 kV
Intensity	1.7 μA	2.5 μA

References

1) S. Kohara et al.: *RIKEN Accel. Prog. Rep.*, **26**, 142 (1992).
2) S. Kohara et al.: Proc. of the 9th Symp. on Accel. Sci. and Technol., KEK, p. 157 (1993).

Design of a Variable Frequency RFQ Linac for RILAC

O. Kamigaito, A. Goto, Y. Miyazawa, T. Chiba, M. Hemmi, M. Kase, and Y. Yano

A variable frequency RFQ has been designed as a new injector for RILAC. It will accelerate ions with a range of M/q = 7–28 up to 450 keV/q in the CW mode. The operational frequency will be varied between 17 MHz and 35 MHz. This RFQ and the 18 GHz-ECRIS, which is also under design,[1] are expected to greatly increase the heavy ion beams for RILAC in the near future.

One of the most important problems to be solved in the design is the frequency-tunability in the RILAC frequency range. As discussed below, we have proposed the "folded coaxial" structure for the cavity to solve the problem.

Figure 1 shows a schematic drawing of the RFQ cavity. The horizontal vanes are supported by the cavity wall on their ends. The vertical vanes are fixed on the inner surfaces of a rectangular tube which surrounds the horizontal vanes. This tube is settled on the ceramic insulators placed on the bottom of the cavity. A stem suspended from the top of the cavity is in contact with the rectangular tube. A moving short is put around the stem, which varies the resonant frequency.

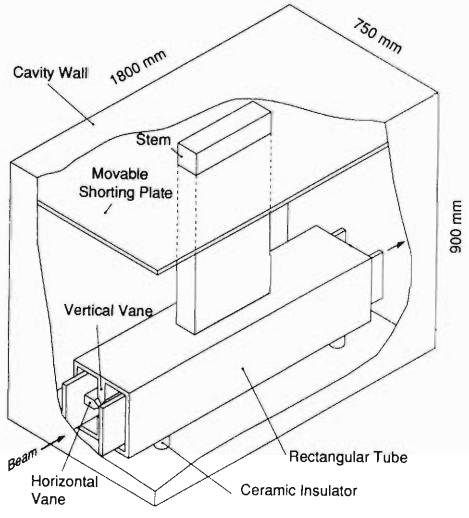

Fig. 1. Schematic drawing of the RFQ cavity.

The magnetic field of the fundamental mode is described in Fig. 2. The magnetic flux surrounds the stem, the rectangular tube, and the horizontal vanes in the tube. The direction of the flux is reversed at the middle of the vanes, and the magnetic field vanishes there. Figure 3(a) shows a conceptual drawing of the half of the cavity with the magnetic flux. As shown in the figure, this structure is equivalent to a "folded" coaxial cavity: If it is unfolded, it becomes a "normal" coaxial cavity illustrated in Fig. 3(b). In our design, the characteristic impedance of the short-end side is much larger than that of the open-end side.

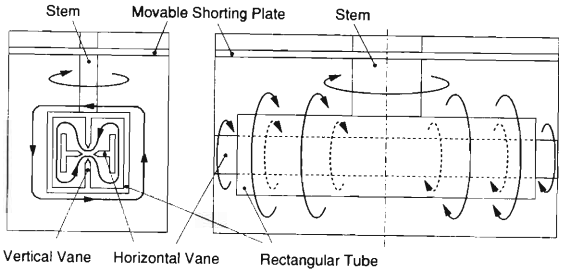

Fig. 2. Magnetic flux of the fundamental mode.

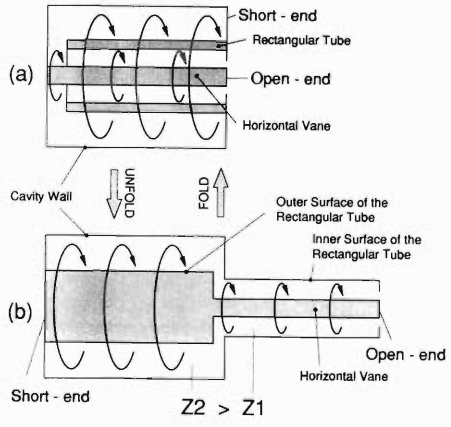

Fig. 3. (a) Conceptual drawing of the half of the RFQ cavity. (b) "Unfolded" $\lambda/4$-coaxial cavity. Z1 is the characteristic impedance of the open-end side and Z2 is that of the short-end side. In our design, Z2 is much larger than Z1.

This "folded coaxial" structure has the following advantages. The first one is the compactness of the cavity even for the low frequency. In addition to the folded structure, the difference of the characteristic impedance plays a significant role for it. Such cavities as shown in Fig. 3(b) are known to provide lower resonant frequencies than those having the same characteristic impedance over the whole length. The other one is the wide frequency-tunable range of the cavity. Since the shorting plate moves within the short-end side, where the characteristic impedance is large, the electric length of the cavity changed by the plate is longer than the actual stroke.

The calculation using the computer code MAFIA has shown that the resonant frequency of the fundamental mode can be varied between 17 MHz and 35 MHz, by changing the position of the shorting plate by 575 mm. In the calculation, no modulation was

added to the vane having the mean bore radius listed in Table 1. The calculated Q-values are 9700 at 17 MHz and 4800 at 35 MHz. Although there appears asymmetry of the electric field between the upper and the lower half in the rectangular tube, it is 2% at the largest and would yield negligible effects on the acceleration. Further analysis of the asymmetry and the method to eliminate it are under progress.

Using a simple cavity as shown in Fig. 4, we have measured the resonant frequency and the field distribution of the folded coaxial structure. The measured resonant frequency was in very good agreement with the MAFIA calculations.

Table 1. Key parameters of the RFQ.

Vane length	142 cm
Frequency	16.9–35.0 MHz
M/q	7–28
Incident energy	10 keV/q
Output energy	450 keV/q
Intervane voltage (V)	33.6 kV
Normalized emittance	145 π mm-mrad
Minimum bore radius	0.417 cm
Mean bore radius	0.770 cm
Maximum modulation	2.7
Focusing strength (B)	6.80
Max. defocusing strength	−0.30
Final synchronous phase	−25 deg.
Transmission (0 mA)	96%

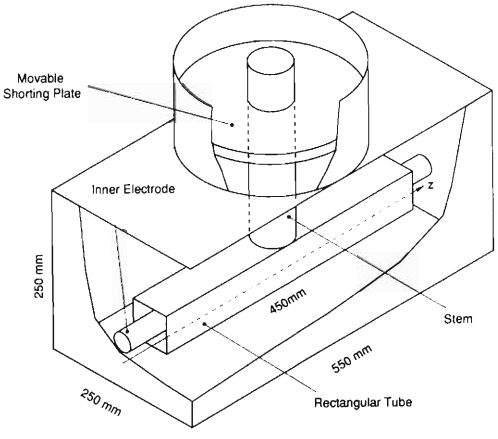

Fig. 4. Schematic drawing of the test cavity.

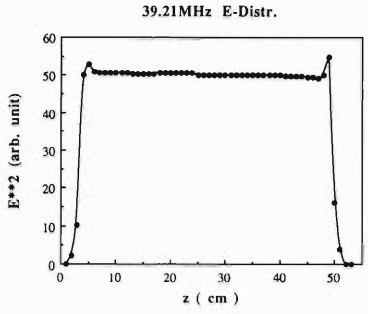

Fig. 5. Electric field distribution between the inner and the outer electrode of the test cavity. The abscissa (z) is indicated in Fig. 4.

The electric field distribution of the fundamental mode is flat along the acceleration axis as shown in Fig. 5. Thus this structure would be suitable for the RFQ cavity.

The vanes are designed in the usual way: they are divided into six sections according to the designing method developed at INS.[2] By use of the computer codes GENRFQ and the modified version of PARMTEQ, the vane parameters have been optimized to get the high beam-transmission efficiency and the short vane length.

The key parameters are listed in Table 1. The extraction voltage of the ion source is assumed to be 10 kV. A considerably small value of the intervane voltage V = 33.6 kV is sufficient to get the final energy of 450 keV/q. The calculated power losses are 4 kW at 17 MHz and 15 kW at 35 MHz.

Now a half-scaled model for the cold test of the cavity is under fabrication. It will be also used for the study of the vane alignment.

References

1) T. Nakagawa et al.: Proc. of the 9th Symp. on Accel. Sci. and Technol., p. 98 (1993).
2) T. Nakanishi, N. Ueda, S. Arai, T. Hattori, T. Fukushima, Y. Sakurada, T. Homma, N. Tokuda, S. Yamada, A. Mizobuchi, and Y. Hirao: *Particle Accel.*, **20**, 183 (1987).

RIKEN Accel. Prog. Rep. **27** (1993)

Construction of RIKEN-RAL Muon Research Facility

K. Nagamine, T. Matsuzaki, K. Ishida, and I. Watanabe

By using intense and high quality negative muons, many interesting and important experimental researches in the field of interdisciplinary science will become realised; some significant examples are muon catalyzed fusion, muonic X-ray element analysis and negative muon spin rotation/relaxation/resonance studies for condensed matter.

The high intensity and rapid-cycling proton synchrotron of the ISIS accelerator of Rutherford Appleton Laboratory (RAL), which had been constructed for a spallation neutron source, is most suited for the pulsed muon generation. The ISIS can produce 800 MeV protons with 70 ns width and 340 ns separation and 50 Hz repetition at an average current of 170 μA. In order to promote science research with pulsed negative as well as positive muons, an agreement has been established between RIKEN and SERC for RIKEN to construct muon facility at the north-side opposite to the existing surface positive muon channel at ISIS.

As the best beam channel for the negative muon production, we have adopted the beam channel with a decay section of superconducting solenoid like PSI or UTMSL/KEK. The design and construction of the advanced superconducting muon channel was started in 1990.

(1) Production target and pion injector

The production target presently in use for the south-side surface muon channel will also be used as the production target for the present channel, where one of three graphite targets with 2 mm, 5 mm, and 10 mm thickness can be selected. Proton beam-line vacuum from the ISIS accelerator is separated by a 100 μm thick Al window before the first quadrupole magnet. A radiation-resistant mineral-insulating conductor is used for the front-end quadrupole (Q1). In order to gain a large solid angle, a large aperture quadrupole with an aperture of 14 inches is used for the Q2. After the momentum analyzing first bend, a momentum selecting slit and a vacuum valve are placed. At the straight downstream after the bender, the Cerenkov counter is placed for the timing pulse for the pulsed muon experiment.

(2) Superconducting solenoid

The basic parameters for the superconducting solenoid are quite similar to those installed by the UTMSL Group either at UTMSL/KEK or at TRIUMF; a total length of 5.5 m, a bore diameter of 12 cm and a field of 5 T. The solenoid is cooled indirectly by a forced flow of a supercritical ^{4}He of 4.6 K and 10 atm through a cooling tube tightly wound around the coil. The cold bore of solenoid stays in the common vacuum space of the muon channel separated by the Al foil placed before the front-end quad and the foil placed at the vacuum duct ends for three experimental ports. The solenoid and its cryostat were completed in May 1993 and installed at ISIS in early fall of 1993.

(3) Helium refrigeration system

The system is composed of a Linde TCF 50 turbine cold box and a MYCOMP screw compressor. It can produce simultaneously (a) a supercritical helium for the solenoid, (b) an intermediate temperature helium flow for 100 K shield of the solenoid cryostat, (c) a liquid helium flow for power-lead cooling and (d) a two-phase helium flow for the experimental magnet. The system was installed at ISIS in May 1993 and a test of the unit performance was completed.

Theoretical Study of the Relativistic Cyclotron Maser Cooling

H. Suganuma, H. Toki, and I. Tanihata

Very recently, Ikegami proposed a new concept on the beam cooling; it is named as Cyclotron Maser Cooling (CMC). The CMC utilizes the relativistic effect on the cyclotron oscillation of the beam around the beam axis due to the magnetic field applied in the beam direction. The particles are cooled down to the microwave frequency provided by an external oscillating electric field which is applied perpendicular to the beam direction. This new method was claimed to cool down beams of various kinds in the matter of microseconds.[1,2] This is an extremely exciting finding and it would be very important to pay attention from the theoretical side to its feasibility and also to the applicability. We would like to study the CMC purely from a theoretical view point. In particular, we would like to derive the cooling condition and the cooling time in the laboratory frame, paying attention to the relativistic effect on the beams.

The details of the derivation of cooling conditions are provided in Ref. 3. We comment here only the comparison of our results with those of Ikegami.[1] All the results would coincide with the corresponding ones of Ikegami, if we put m in place of m^* in various places. This difference originates from the fact that, in the derivation of Ikegami,[1] the 'transverse γ factor', γ_T, defined as $\gamma T = 1 + i\omega_c/m$ in the beam rest frame remains unchanged by the Lorentz transformation to the laboratory frame. One should, however, change γ_T to $\gamma T^* = 1 + i\omega_c/m^*$ in the Lorentz transformation.

We summarize here the calculated results of the cooling condition and the cooling time. As reasonable parameters for the non-relativistic electron, we set the magnetic field H = 0.1 Tesla (1k Gauss) and the power eAo = 1 keV. The life time of electrons in the Landau orbit due to the electromagnetic transitions is $\tau \sim 10^{-8}$ sec. These values provide the radius R $\sim$ 5 cm and the cooling time T $\sim 2 \times 10^{-9}$ sec. The cooling time is an extremely small number, which agrees with that of Ikegami. What then happens if the beam velocity becomes relativistic? Let us consider the case $P_z \sim 5$ MeV, which corresponds to $\gamma_z \sim 10$. With the same parameters for the all the devices, we find that R $\sim$ 50 cm and T $\sim 2 \times 10^{-6}$ sec. Hence, the CMC is still powerful even in this case. Even the energy would become ultra-relativistic, if we can use stronger electric and magnetic fields and bigger size devises accordingly available in the present technology, we are able to cool down the electron beam up to an extremely ultra-relativistic energy. This statement is due to the dependence of the cooling conditions on the magnetic field as $R \propto H^{-1.5}$ and $T \propto H^{-3}$ as can be derived from the expressions in Ref. 3. As for the power of the oscillating electric field, it changes the cooling time to $T \propto (eAo)^{-2}$, while other quantities are unaffected.

The situation becomes severe for protons due to the large rest mass. In fact, in order to achieve the CMC cooling, we have to use much more powerful electromagnetic fields. Taking H = 10 Tesla and eAo = 1 MeV, we find that the radius and cooling time are (use $\tau \sim 10^{-5}$ sec): R $\sim$ 12 cm and T $\sim 7 \times 10^{-11}$ sec for non-relativistic protons. This result agrees with that of Ikegami.[1] As the beam energy increases, the radius of the magnetic field goes as γ_z and the cooling time as γ_z^3. Hence, even for $\gamma_z \sim 10$; $P_z \sim 10$ GeV, R $\sim$ 1.2 m and T $\sim 7 \times 10^{-8}$ sec. The cooling time is still impressive. However, the radius R $\sim$ 1.2 m may be close to the present technical limit. Concerning the length of the cooling devise, the length of the magnetic field L would be L $\sim$ 20 m in this case, which may be of the order or less of the circulation length of the cooler ring.

In conclusion, we have studied theoretically the cooling conditions and the cooling time of the CMC for various non-relativistic and relativistic beams. We have reproduced the results of Ikegami for the non-relativistic case. As for the relativistic case, however, we have found significant relativistic effects on the cooling conditions, which deviate largely from those of Ikegami. The radius of the Landau orbit to be cooled down increases like $R \propto \gamma_z$ with γ_z being defined as $m^* = \gamma_z$ m. The cooling time also increases like $T \propto \gamma_z^3$. As a consequence, the cooling conditions of the CMC become progressively severe as the beam energy increases. We conclude therefore that the CMC is a promising cooling mechanism for beams which are not very relativistic.

References

1) H. Ikegami: *Phys. Rev. Lett.*, **64**, 1737; 2593 (1990).
2) F. Kullander: Doctor thesis "Cyclotron Maser Cooling, a first experiment study", Osaka Univ. (1992).
3) H. Suganuma, H. Toki, and I. Tanihata: to be published.

2. Synchrotron Radiation Source Development

Correction of Emittance Modulation by Linear Coupling

H. Tanaka and A. Ando

The vertical emittance of the SPring-8 storage ring is mainly given by linear coupling of betatron oscillations and varies along the ring. The coupling should be reduced to around 1% to keep very high brilliance.

The behavior of coupling motion is completely described in normal mode. In this flame, oscillation amplitudes of each particle oscillate sinusoidally. The envelopes of these amplitudes for all the particles are constant along a ring. The emittances in the laboratory flame are obtained by the projection from the normal mode. This projection is a kind of the coordinate rotation. The rotation angle depends on the fact how many and how strong skew quadrupoles are, and then varies along a ring. This causes the modulation of the maximum emittance. Radiation damping and excitation cannot smear out this modulation because the damping time is about 100 times as large as the period of coupling motion.

The analytical formulae of the maximum emittance modulations are derived by a perturbation approach[1] and the correction method to reduce not only the coupling coefficient but also the maximum modulation along a whole ring is also obtained.

Figure 1 shows a typical example of the maximum variation of the vertical emittance, where the vertical alignment errors of sextupoles are assumed to be 0.1 mm in rms. Triangles and open circles show tracking results and analytical estimates, respectively, when the initial amplitudes are set to the predicted ones by the linear coupling resonance. The real line shows the average emittance given by this resonance.

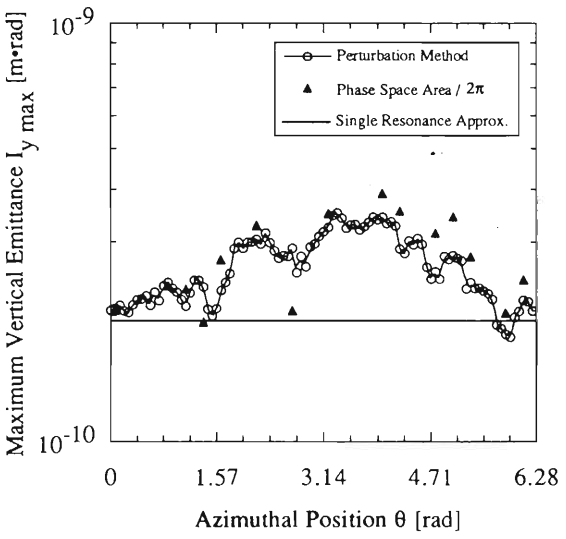

Fig. 1. Modulation of the max. vertical emittance.

The correction scheme is simulated as follows. Shaking the beam coherently in the horizontal direction, vertical oscillations are observed at 20 BPMs along the ring. At every BPM the most effective skew quadrpole magnet is selected and excited at the 20% level of the necessary strength to reduce the coupling oscillation amplitude at this point. The iteration is continued until the residual coupling oscillation becomes smaller than about 12% of the horizontal one (i.e. 1.5% coupling). In Fig. 2, some examples obtained by particle tracking are shown. Open symbols and real lines show the modulations before correction, and closed and dotted ones show after the correction. The different shapes of symbols correspond to the different rms values of alignment errors.

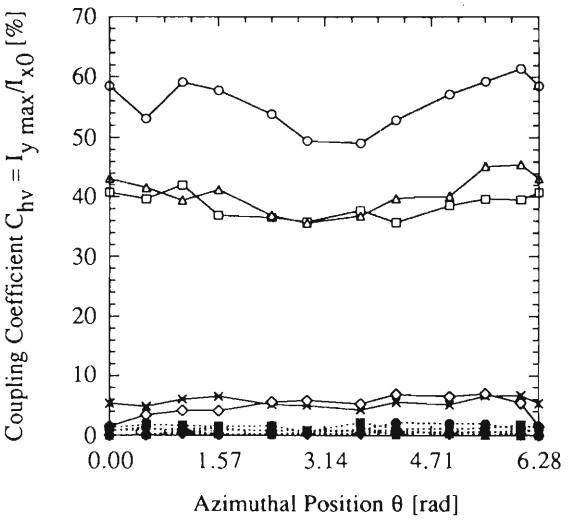

Fig. 2. Correction simulation.

References

1) A. Ando: *Particle Accelerators*, **15**, 177 (1984).

Survey for SPring-8 Storage Ring

S. Matsui, I. Takeshita, and K. Kumagai

A 1.4 km circumference of the SPring-8 surrounds Mihara-Kuriyama Hill which is 50 m higher than the storage ring level. In order to set many magnets precisely, the reference points for magnet alignment are necessary. Thus we made monuments around the ring. We surveyed 12 reference points (outside the ring) and 15 monuments (on the ring) in January 1993 to determine the monument position before the ring building is constructed. The number of measurements is 114 for angle and 106 for distance. Figure 1 shows the error ellipses of this survey result.

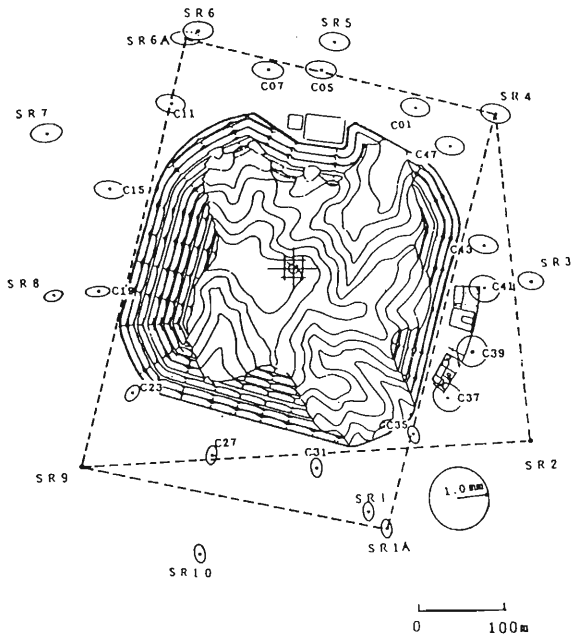

Fig. 1. Error ellipses.

Ten geodetic points (SR1–SR10) and sub-points (SR1A and SR6A) are positioned outside the ring. We cannot surround the Hill by a triangle. However, by setting the sub-points SR1A and SR6A, the circumference is surrounded by a quadrangle, which has a fewer sides (Fig. 1).

We made concrete monuments similar to a Japanese tomb stone. While surveying, a 1m high stand mounted on a monument was used for setting the survey instrument or the target. These 15 monuments (C01–C47) for the magnets alignment are placed at the intersected points of the straight lines on both sides of the bending magnet. These monuments are also used to construct the concrete tunnel.

An automatic plummet (WILD NL) was used for tripod setting.

The measurments of the distance and angle were made using Kern Mekometer ME5000 and WILD T3000, respectively.

The line between SR2 and SR9 was chosen to be a "baseline".

The program for analysis is written with BASIC language for a personal computer. Main part of the program is cited from the survey textbook. This program was so modified that we can calculate the many positions by using a small memory.

All error ellipses are smaller than the circles of radius 1 mm. However, including the error accompanied with setting of the tripod and the stand, the center coordinates of the seal on the monuments agree with the adjusted values within the error of ± 2 mm.

Concluding remarks are as follows: 1) The survey should be carried out before the building construction; 2) The concrete pillar on which a survey instrument is put is suitable for the fiducial point. Much time was used for setting the tripod at the Japanese fiducial point; 3) When the survey network is dense, the distance measurements are easy if using several reflectors. Many exchanges of reflectors are necessary when using a few reflectors; 4) A stand of height 1–1.5 m is necessary if the construction has started.

We made the second survey in October 1993. Now this data are being analyzed.

Field Measurements of SPring-8 Dipole Magnets

J. Ohnishi and M. Kawakami*

Eighty-eight dipole magnets will be installed in the Spring-8 storage ring. Forty dipoles of them have already been delivered to Nishi-Harima SPring-8 construction site and their field measurements have finished except two to inspect the field performance. The dipole magnet is iron-dominated one and has a length of 3090 mm and a gap height of 61 mm.[1] The field measurements were done by measuring the integrated magnetic fields $\int$Bds with an instrument called "Long Flip Coil". It has a two turns coil with a length of 3855 mm and a width of 15 mm. The integrated fields were measured by integrating the induced voltage during flipping the coil in about 0.7 seconds in the magnet gap.[2] Figure 1 shows a photograph of a dipole magnet being measured with Long Flip Coil.

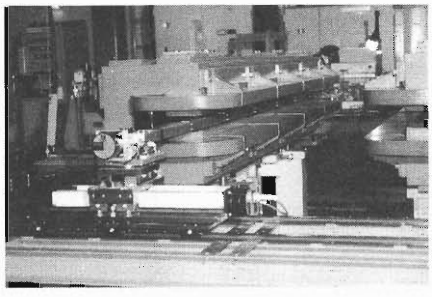

Fig. 1. A photograph of the SPring-8 dipole magnet measured with "Long Flip Coil".

Figure 2 shows a horizontal distribution of the integrated magnetic fields on the median plane as an example. A sextupole field found as a parabolic curve in this figure was presented systematically for all dipoles and its strength was smaller than the tolerant value (7×10^{-4} at x = 20 mm).

In the measurements of fluctuation of the integrated field strengths between magnets, a sample magnet and a reference magnet were powered in series and measured alternately to confirm the stability of the measurements. As the temperature of the measuring coil was found to affect the measured values in pre-measurement, the temperature of cooling water of magnet was decreased near the temperature of the measurement room to suppress a temperature rise of the measuring coil and the measuring time was kept

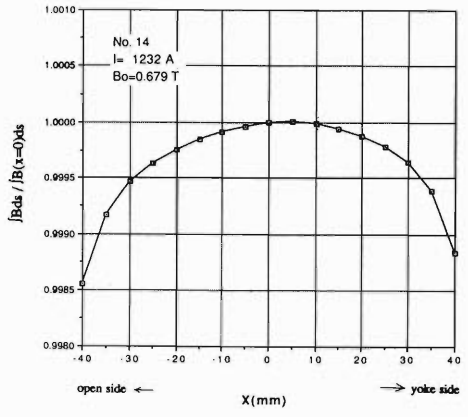

Fig. 2. Horizontal distribution of integrated fields along beam direction. Average of the field strength was a nominal value of 0.679 T.

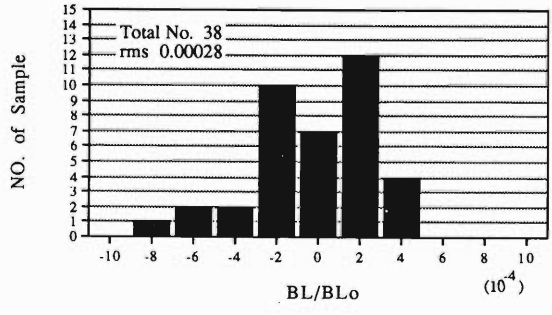

Fig. 3. Histogram of integrated field strength for 38 dipoles.

constant. As a result, the stability of the measured values of the reference magnet was better than $\pm 5 \times 10^{-5}$ during measurements of 38 dipoles. Figure 3 shows a histogram of the integrated field strengths normalized by the measured value of the reference magnet. The fluctuation was 2.8×10^{-4} in rms and small enough compared with the tolerant value of 5×10^{-4}.

References

1) SPring-8 Project Team: SPring-8 Project Part I, Facility Design (1991). [Revised]
2) J. Ohnishi, H. Takebe, and S. Motonaga: *RIKEN Accel. Prog. Rep.*, **23**, 167 (1989).

* Ishikawajima Kogyo Co. Ltd.

Field Measurements of SPring-8 Quadrupole Magnets

J. Ohnishi and N. Kumagai

The SPring-8 storage ring contains 480 quadrupole magnets. All the quadrupoles will be measured with respect to excitation curves, magnetic field lengths, multipole fields, and positions of magnetic center.

An equipment called "Harmonic Coils" was designed and manufactured. The principle of the measurement and experimental results with a prototype were described in Ref. 1. Figure 1 shows a photograph of the newly developed equipment. Harmonic coils are fixed inside a cylinder made of fiberglass reinforced epoxy resin which has a diameter of 80 mm and a length of 1600 mm. Two kinds of coil configuration of four manufactured cylinders are shown as cross-sectional views of the cylinders in Fig. 2. The coil cylinder is inserted in the magnet gap and fixed with bearing supports at both sides. Magnetic fields are obtained by Fourier analysis of the induced voltages measured while the coils rotate with a speed of 30 rpm.

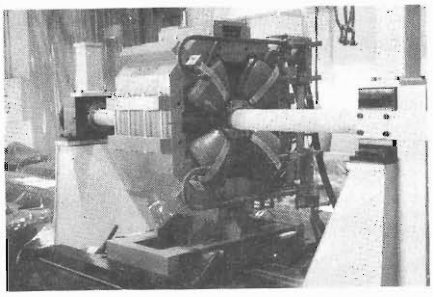

Fig. 1. Harmonic Coil and SPring-8 quadrupole magnet.

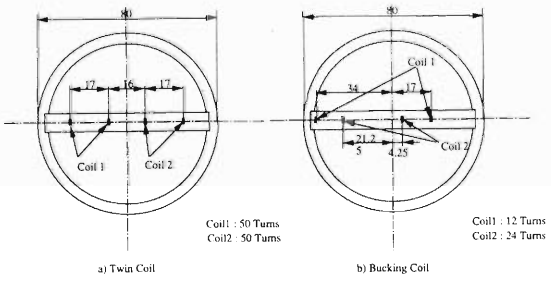

Fig. 2. Cross sections of two types of coil cylinders. Coil 1 and coil 2 are connected in series for both types.

The strength of quadrupole field must be measured in high reproducibility of better than 10^{-4} to measure the fluctuations between magnets. As the rotating radius of coil is changed due to the deformation in fixing the coil cylinder, it is not easy to achieve this high reproducibility when a magnet is exchanged. In the twin coil configuration in Fig. 2(a), changes of the output from the two coils were canceled out and the reproducibility was reached as good as about 5×10^{-5}.

Multipole components appearing from error of the magnet production are measured with the bucking coil configuration in Fig. 2(b).[2] As this configuration of coils cancels the output from the main quadrupole field, which is thousand times stronger than higher multipole fields, accuracy of the measurement of the multipoles is improved. The suppression ratio of the main term was 4% in the produced coil.

The magnetic center is also measured with this measurement equipment. The accuracy should be better than 20 μm. The method of measurement of the magnetic center is as follows. The dipole component induced from the harmonic coil is in proportion to the displacement of rotating axis of the coil from the magnetic center, and the phase of the dipole component against the quadrupole component presents the direction of the displacement. Calculating the position of the displacement from the strength and the phase, the rotating axis and the magnetic center are made coincided by moving the magnet with a computer controlled stage. Then the position of the magnetic center is obtained from the deviation between reference points of the measurement equipment and the magnet.

Presently, development of the measurement device for the displacement of coil axis from the reference point in magnets and adjustment for improvement of the accuracy are in progress.

References

1) J. Ohnishi and N. Kumagai: *RIKEN Accel. Prog. Rep.*, **26**, 155 (1992).
2) "Magnetic Measurement and alignment", CERN Accelerator School Proc. edited by S. Turner (1992).

Construction of Power Supplies for SPring-8 SR Magnet

H. Takebe, N. Kumagai, J. Ohnishi, K. Kumagai, S. Matsui, and S. Motonaga

Ten power supplies for quadrupole magnets (QP) and one power supply for sextupole magnets (SxP) were made in March 1993 for the SPring-8 Storage Ring. These PSs are set in the experimental hall until the PS-room A is completed.[1)]

The cable routes between the magnets and cable rack and a cooling water distributing header system for the magnets were designed. A proto-type cabling system for them was made in the previous 1 cell magnets in the experimental hall this autumn (Fig. 1). Test operation of QP with four Q-magnets was done and current ripple was measured. The stability was better than 3×10^{-5}.

A control sequence and interfaces for the power supply (PS) system were decided. Connection and control test of the RIO-B for the PSs was done also.[2,3)] A pin assignment example of the interface between RIO (type-B) and power supply is listed in Table 1.

Power supply's control command sequences and timing flow are also decided. The cyclic time for ADC read out strobe must be within 0.6 ms $\sim$ 20 ms and those for a DAC set will be within 0.4 ms $\sim$ 100 ms. The ADC data is transferred to the RIO card via a 16 bits parallel signal.

A block diagram of the SxP is shown in Fig. 2. A 33.3 kHz MOS-FET switching regulator system is piggy-backed by the 6th phase thyrister regulator. A VME controlled remote I/O card is connected to this PS using an optical fiber cable.[2)]

Table 1. Status read pin assignment of the PS control.

pin	a/b	status	contents
12	a	DI-Com	+5 $\sim$ 15 V
	b	DI-Com	+5 $\sim$ 15 V
13	a	DI0	ADC Data (LSB)
	b	DI1	.
.	.	.	ADC Data
.	.	.	.
.	.	.	.
21	a	DI6	.
	b	DI7	ADC Data (MSB)
22	a	DI-Com	+5 $\sim$ 15 V
	b	DI-Com	+5 $\sim$ 15 V
23	a	DI0	On/off
	b	DI1	Line Input
24	a	DI2	Local/Remote
	b	DI3	Fault/Fuse
25	a	DI4	Over Curr.
	b	DI5	Over Volt
26	a	DI6	Temp.Err (Fan)
	b	DI7	Mag.InterLck
27	a	DI-Com	+5 $\sim$ 15 V
	b	DI-Com	+5 $\sim$ 15 V
28	a	DI8	Water Flow
	b	DI9	Transistor/Fuse
29	a	DI10	Oven Error
	b	DI11	Polarity+
30	a	DI12	Fire/ Smoke
	b	DI13	Grounded
31	a	DI14	
	b	DI15	ADC Strobe
32	a	DI-Com	+5 $\sim$ 15 V
	b	DI-Com	+5 $\sim$ 15 V

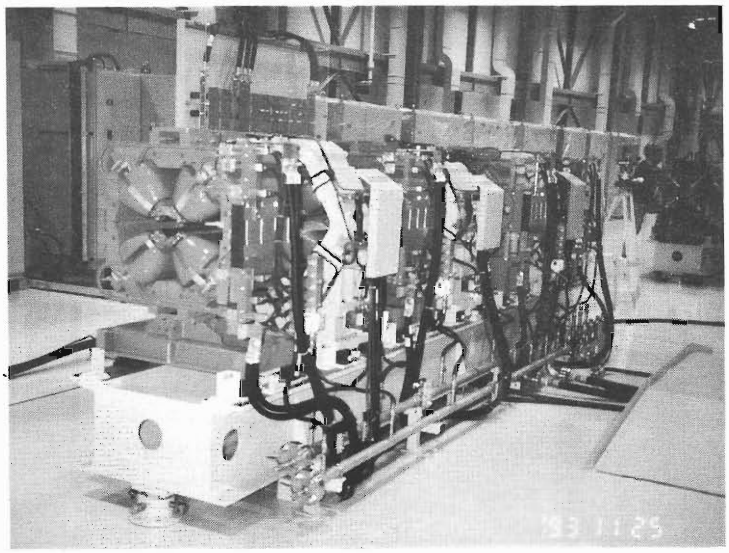

Fig. 1. Combination test of Q and S magnets, cabling and water header system. Q-PS and SxP are seen behind.

A bending magnet PS (BP) is being constructed and will be completed until next spring. An input transformer for 6.6 kV for this BP is located in an outer yard and connected by four sets of bus ducts for 24 phase rectifiers.

Twelve sets of steering magnet PS's are made and tested. Each steering magnet(St) is connected to one PS. Thirty-six sets of the St-PS are mounted in one cubicle and a DC source is supplied by one AC-DC converter.[1] Total number of the St-PS is 576.

Auxiliary (QA) PSs are designed and will be made in this winter.

Thirty-eight sets of skew Q-magnet power supply (SkP) system are now being designed. Ten or eight SkP sets will be located in each of the A, B, C, D PS rooms.

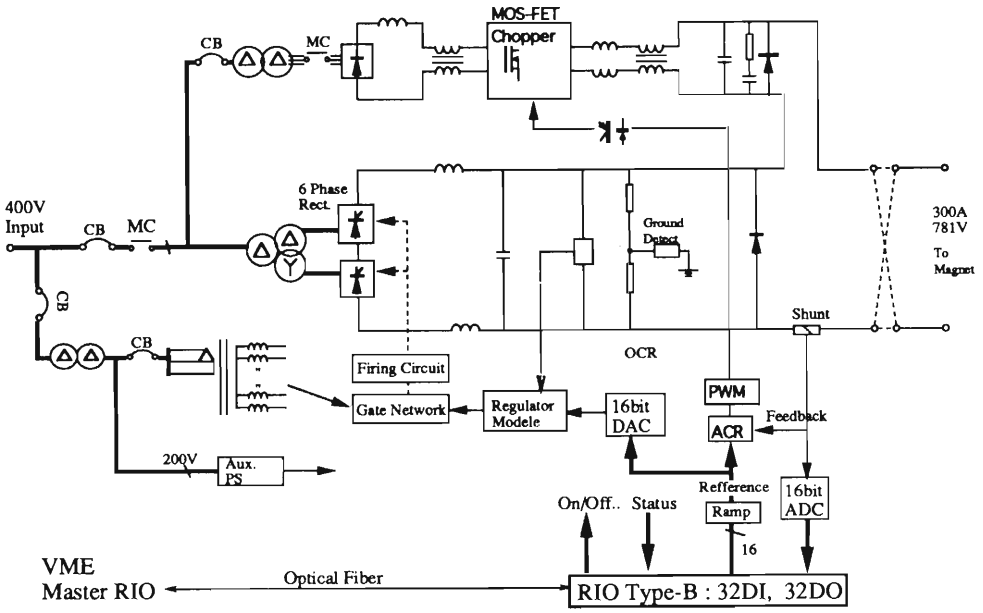

Fig. 2. Block diagram of the SxP.

References

1) H. Takebe et al.: *RIKEN Accel. Prog. Rep.*, **26**, 157 (1992).
2) H. Takebe et al.: *ibid.*, p. 176.
3) H. Takebe et al.: *ibid.*, **25** 209, (1991).

Preliminary Network for SPring-8 Machine Group

H. Takebe, I. Kobayashi, T. Masuda, T. Nakamura, S. Fujiwara, and T. Wada

A preliminary network system was made for the SPring-8 group (40 people) in the Harima construction site in April 1993.

Ten workstations, thirty personal computers and six VME[1,2] computers are connected as the first step to the (temporary) SPring-8 Local Area Network (LAN)

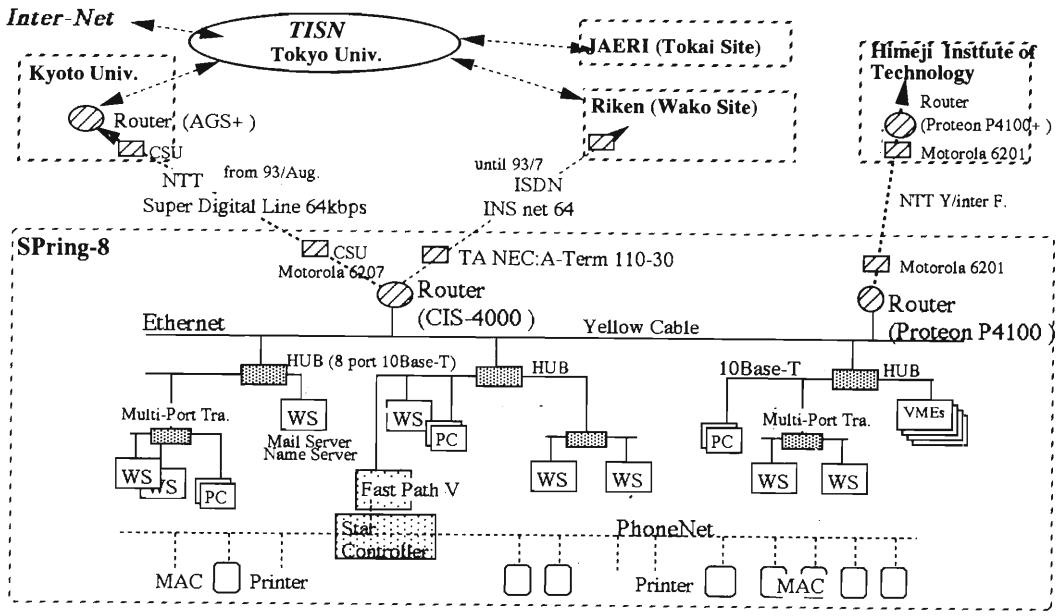

Fig. 1. Computer network of the SPring-8 storage ring building (Tentative stage).

using Ethernet TCP/IP protocol. Before end of July 1993, this LAN was connected to the RIEKN Wako site through INS-64K (NTT) using a Router (CISCO: CIS4000) as seen in the Fig. 1. In August 1993, this LAN was connected to the RIKEN and JAERI Tokai site via Kyoto University (Uji) and TISN[3] using NTT's SD-64K line.

Three sets of 8-port 10Base-T HUB were connected to the Yellow cable. This 10Base-T HUB's 8 ports were led to a modular jack (RJ-45) through 4 pairs of UTP cable (EIA: Category-5, 1061A). A PDS[4] patch panel system was introduced to an IDF box. From the IDF patch panel to each room wall consent, two pairs of the UTP cables were used for the 10Base-T, one pair for the telephone line, and one pair for the Macintosh Phone-net. Three RJ-45 jacks were assigned as shown in Fig. 2 and mounted in one consent panel. Each room has two wall jack consents. Four or six ports of 10Base-T HUB can be adopted to the Wall jack inside a room, if it was necessary. These rooms will be used by experiment user's groups in future.

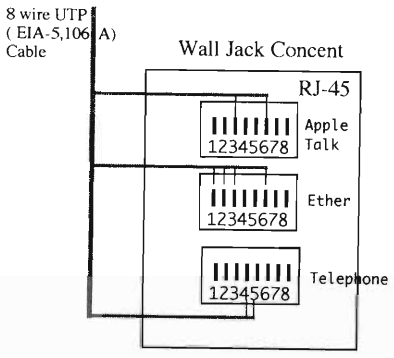

Fig. 2. 10Base-T HUB, Macintosh Phone-net and telephone cables are used.

References

1) T. Masuda et al.: *RIKEN Accel. Prog. Rep.*, **26**, 174 (1992).
2) H. Takebe et al.: *ibid.*, p. 177.
3) Tokyo Univ. Int. Sci. Network.
4) Premises Distribution System (Sanki Co. and AT&T).

Measurement of Temperature Dependence of HOM Frequencies in a Bell-shaped Cavity

H. Ego, M. Hara, Y. Kawashima, Y. Ohashi, T. Ohshima,
H. Suzuki,* I. Takeshita, and H. Yonehara*

Quality and current value of the beam in the storage ring of SPring-8 depend on beam instabilities. Intrinsic higher order modes (HOMs) in an RF cavity excited by the beam are likely to cause coupled-bunch instabilities.[1] Then characteristics of HOMs in a bell-shaped RF cavity[2] were measured and field distributions of them have been obtained with the bead perturbation technique.[3,4] Detuning HOM resonances from the instability conditions is one of methods for suppressing the instabilities. HOMs with high coupling impedances have the high Q-value and the frequency shift by more than 100 kHz is needed. Figure 1 shows a schematic diagram of controlling HOM frequencies with two movable plungers.[4] The plunger 1 on the side of the cavity is used for shifting HOM frequencies and the plunger 2 tunes the cavity to the accelerating frequency, 508.58 MHz, within ±0.5 KHz.

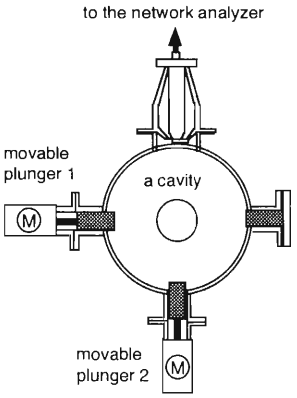

Fig. 1. A schematic diagram of the two-plunger system.

The temperature of the cavity increased by about 20°C in operation of 100 kW RF power.[5] HOM frequencies change in accordance with the temperature. The two-plunger system was tested for a prototype cavity at various temperatures. We heated up the cavity with mantle heaters instead of RF power, since it is difficult to measure HOM frequencies while feeding the RF power into the cavity.

The temperature of the cavity was set to 30, 40, 50, and 60 °C and controlled within ±0.5 °C. The cavity was evacuated to about 10^{-5} Pa to prevent oxidation. Resonant frequencies of the cavity were measured with a network analyzer. The network analyzer and the plungers were controlled by a computer with the GPIB interface.

Data of TM110 mode was shown in this report since those of other HOMs were similar to each other.

Figure 2 shows frequency shifts of the TM110 mode as a function of the position of the plunger 1. The frequency of TM110 mode changed at the rate of 12 KHz °C when the position of the plunger 1 was fixed. Then the frequency was very sensitive to the position of the plunger 1 and the shift at the rate of about 50 KHz/mm was attained. The amount of frequency shift was independent of the cavity temperature in this measurement. Similar data were obtained when the roles of two plungers were exchanged with each other.

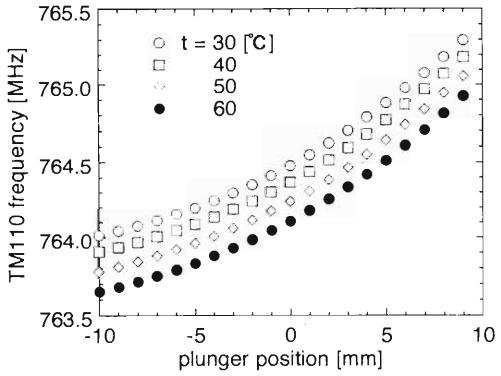

Fig. 2. Frequency shifts of TM110 mode as a function of the position of the plunger 1. The accelerating frequency was tuned to 508.580 MHz within ±0.5 KHz by the plunger 2. The origin of the abscissa shows the position of the inner surface of the cavity.

References
1) Y. Yamazaki, K. Takata, and S. Tokumoto: *IEEE Trans. Nucl. Sci.*, **28**, 2915 (1981).
2) K. Inoue et al.: *RIKEN Accel. Prog. Rep.*, **24**, 162 (1990).
3) H. Ego et al.: *ibid.*, **26**, 159 (1992).
4) H. Ego et al.: Proc. of 9th Symp. Accel. Sci. Technol., p. 249 (1993).
5) H. Ego et al.: Proc. of 17th Linear Accel. Meet. in Japan, p. 180 (1992).

* Japan Atomic Energy Research Institute

Test of Dummy Loads

Y. Ohashi, H. Ego, M. Hara, Y. Kawashima, T. Ohshima,
H. Suzuki,* I. Takeshita, N. Tani,* and H. Yonehara*

Four 1.2 MW klystrons (E3786) from Toshiba Co. are used to generate 508.58 MHz RF power to the storage ring cavities in the SPring-8. Figure 1 shows one section of the RF station. The RF power from a klystron is fed to the eight bell shape single-cell cavities through a circulator and three stage magic-tees. Reflected RF power is absorbed in two types of dummy loads, 300 and 50 kW ones. The 300 kW load is installed at the port #3 of a circulator which prevents the harmful reflected power from going back into a klystron. Four of them are to be used to absorb full power up to 1.2 MW in a klystron test. It is also used to absorb power to a particular cavity, which is inoperable by some trouble (we plan to disconnect this cavity from the system and terminate by two loads). Seven of the 50 kW loads are installed at the magic-tees, and it is also used to absorb coming back power directly from the cavity as described in the next paragraph. These dummy loads consist of water-cooled-coaxial loads and waveguide-to-coaxial transitions.

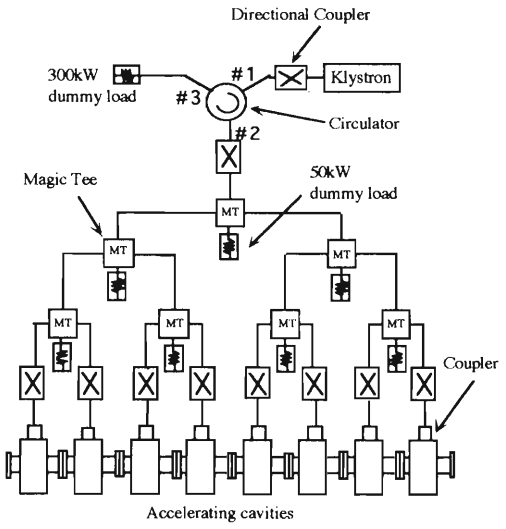

Fig. 1. RF transmission system.

We estimate the RF powers absorbed in these loads by considering only stationary reflection in the following two cases. Suppose we set a coupling coefficient β corresponding to the designed stored beam current of 100 mA. The reflected power is about 4 kW from each cavity without beam loading. This reflected power decreases with increasing beam current up to 100 mA. In another case, if the klystron power is not fed to a particular cavity which is inoperable, the reflected power induced by the beam loading becomes about 14 kW.

* Japan Atomic Energy Research Institute

We chose 50 kW loads at the magic-tees and 300 kW one at the circulator in consideration of above cases. They are operational even for the beam current up to 200 mA. These loads should stand, of course, for much higher transient reflected power.

We regards the RF leakage as a most important criterion in the selection process. In consideration of reliability and good shielding against RF leakage of the 300 kW loads, we selected them uniquely from the Premier Microwave of California, U.S.A. In order to examine performance, we purchased three different 50 kW loads from Premier, Bird Electronic Co., U.S.A., and Nihon Koshuha Co.

Table 1. Specification.

param.\ maker (kW)	Premier (300)	Premier (50)	Bird (50)	N. K. (50)
VSWR(max)	1.2	1.1	1.1	1.1
Weight (kg)	50	34	7	54
Length (cm)	380	92	50	86
Water flow (l/min)	45	230	42	50
Max. coolant press.(kgf/cm^2)	4.2	7	N.A. (~ 7)	10
Max RF leakage (dBc)	-80	-80	N.A.	-80
# of flanges	5	10	3	5

A specification of loads is listed in Table 1. Preceding to the installation, we examined all the loads at the RIKEN-Wako test stand. Tests include low power measurements of characteristics and high power measurements of temperature distribution, power reflection, and RF leakage. The reflected power from cavities has higher frequencies, so VSWR should be good not only at 508 MHz but also at higher ones. Since a low power measurement was done with a network analyzer through a coaxial-to-waveguide transition, it provided the characteristics of only two transitions near 508 MHz. Obtained VSWR of all the loads are less than 1.1. The result of high power measurements is listed in Table 2.

The 50 kW load from Premier shows very high temperature rise on the outer case. This is because water flows inside the resistor but not between the resistor and the outer case. Since this particular load has 10 flanges, a chance of RF leaking might be high because of the uneven tightening. A regulation on the RF leakage requires that electric field is to be 40 dBμV/m or below at 100 m away from the source or on the site boundary. A measurement should be done to map

Table 2. Result of high power measurement.

Parameter /company	Premier	Premier	Bird	N. K.
Power (kW)	300	50	50	50
Max temp rise (℃)	36(load),61 (transition)	80	18	13
Reflected power (kW)	.1	<.025	<.025	<.025
RF leak (dBm)	-60	-40	-40	-50

the electric field with an antenna and a spectrum analyzer. In this measurement we used a close-field probe (Hewlett Packard 11940A) to get a reasonable estimate. Observed power of -40 dBm can be converted to electric field, and the corresponding value is 152 dBμV/m on the surface. Leakage was observed fairly locally, so the active area (1.9 cm^2) of the probe is a good measure to estimate the field strength at a certain distance. We expect about 20 dB below the limit in the worst case with all the loads installed. Preceding to the high power measurement a similar test was attempted at low power of 10 W, however, a fairly large leak from an N-type connector interfered the meaningful measurement.

One practical problem arose in the 300 kW load that we could supply only 200 l/min in the test stand because of a big pressure loss in the water line. This is avoided by enlarging a diameter of the water connectors. Care also must be paid in the design of water lines to minimize the pressure loss.

In conclusion all the tested loads satisfied our requirements in the short term test. A long term operation for a reliability check is to be done next.

Test of 1.2 MW Circulator

T. Ohshima, H. Ego, M. Hara, Y. Kawashima, Y. Ohashi,
H. Suzuki,* I. Takeshita, N. Tani,* and H. Yonehara*

In a storage ring of SPring-8, four 1 MW klystrons are used to feed 508.58 MHz RF to the accelerating cavities. Each klystron drives eight cavities. A circulator is inserted between the klystron and cavities to protect the klystron from the reflected RF power. Circulator transfers an RF power circularly from the port-1 to the port-2, from the port-2 to the port-3 and so on. A klystron is connected to the port-1, the port-2 is connected to cavities, and the port-3 is terminated by a dummy load.

We tested two 1.2 MW Y-type circulators made by ANT corporation in Germany. A structure of the circulator is shown in Fig. 1. It has ferrite disks cooled by water at the junction of three wave guides. A static magnetic field is applied to the ferrite for its premagnetization. This field is generated by two permanent magnets mounted top and bottom of the wave guide of the circulator. Each permanent magnet is surrounded by a coil which is used for compensating the effects of the fluctuation of temperatures of the cooling water and/or the ambience. The specification of the circulator is shown in Table 1.

The RF characteristic of the circulator was measured with a calibrated network analyzer. The results were as follows: The insertion loss was less than 0.1 dB, the isolation was better than −25 dB, and the reflection was less than −25 dB, i.e. VSWR was less than 1.12.

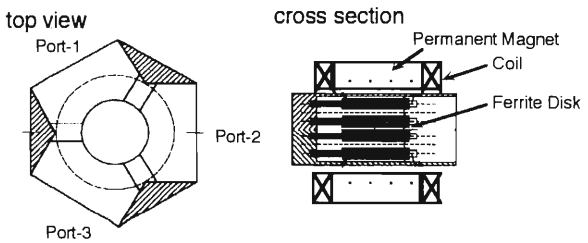

Fig. 1. A top view and a cross section of the circulator.

Table 1. The specifications of the circulator.

frequency	508.58MHz
20dB bandwidth	±2%
insertion loss	<0.15dB
forward power(CW)	max.1.2MW
reverse power(CW)	max.600kW
VSWR	<1.2
flange	WR1800

The high power tests were done with a set-up as shown in Fig. 2. The 1.2 MW klystron was connected to the circulator port-1 through a directional coupler (D.C.1). The port-2 was shorted with a short plate. The port-3 was terminated by a 1.2 MW dummy load.

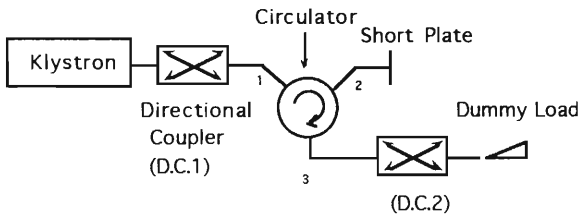

Fig. 2. A setup for the high power experiment.

Another directional coupler (D.C.2) was inserted between the port-3 and the dummy load. The worst phase condition is that the H-fields of the forward 1.2 MW wave and the reflected 600 kW wave are summed up in phase, which results in a largest energy loss at the ferrites. In this case the loss P_{loss} in the circulator is proprtional to the square of H-field, $P_{loss} \propto (\sqrt{P_{fwd}} + \sqrt{P_{rfl}})^2$, where P_{fwd} is a forward RF power and P_{rfl} is a reflected power. We measured the power loss in a condition of the total reflection of 875 kW at the port-2, which is equivalent to the forward 1.2 MW and reflected 600 kW. The loss was measured as a function of the distance between the short plate and the port-2. The step size was about 10 cm which corresponds to about 40 degrees of the RF phase. The insertion loss was determined by measuring the dissipated energy in the circulator, i.e. a temperature rise of its cooling water.

Figure 3 shows the power of the reflected wave from the circulator measured at the D.C.1. The ratio of

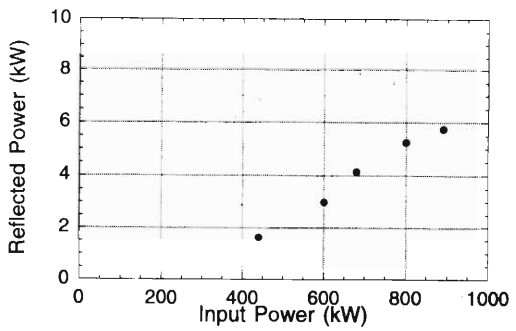

Fig. 3. The reflected power from the circulator.

* Japan Atomic Energy Research Institute

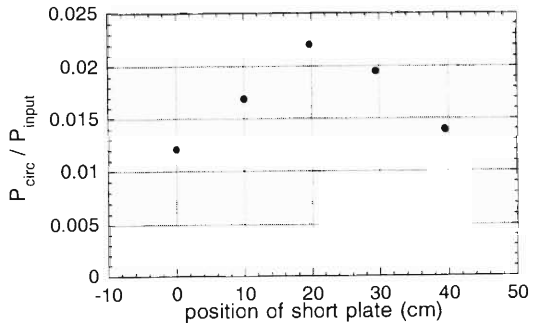

Fig. 4. The ratio of the dissipated power at the circulator (Pcirc) to the input power (Pinput) as a function of the short plate.

the reflected wave to the input power was less than 0.65%, which corresponds to that VSWR was 1.18. Figure 4 shows the ratio of the dissipated power in the circulator to the input power as a function of the position of the short plate. The maximum power loss at the circulator was observed when the short plate was set at a distance of 24 cm from the port-2. The insertion loss was less than 2.5%, i.e. 0.11 dB.

In conclusion, performance of the two circulators satisfied our requirements.

A Phase Lock System of 508.58 MHz Reference Line

Y. Kawashima, H. Ego, M. Hara, Y. Ohashi, T. Ohshima,
H. Suzuki,* I. Takeshita, N. Tani,* and H. Yonehara*

Fundamental radio frequency (RF) of 508.58 MHz generated by a synthesizer is delivered to four RF-stations located in a storage ring and also to one RF-station in a synchrotron ring.[1] Instability of the phase seriously affects the beam; therefore the phase must be kept as precisely as possible in all RF-stations. We are going to control the precision of phase within $\pm 1°$ of which value almost comes from the precision of a phase the total system. The phase lock system and obtained results are described here briefly.

First of all we explain the mechanism of a phase lock system. An RF is transmitted from station (A) to (B) through a transmission line, for example, as shown in Figs. 1 and 2. The RF signal received in the station (B) is divided into two. One is used there as a reference signal, and the other is returned to the station (A)

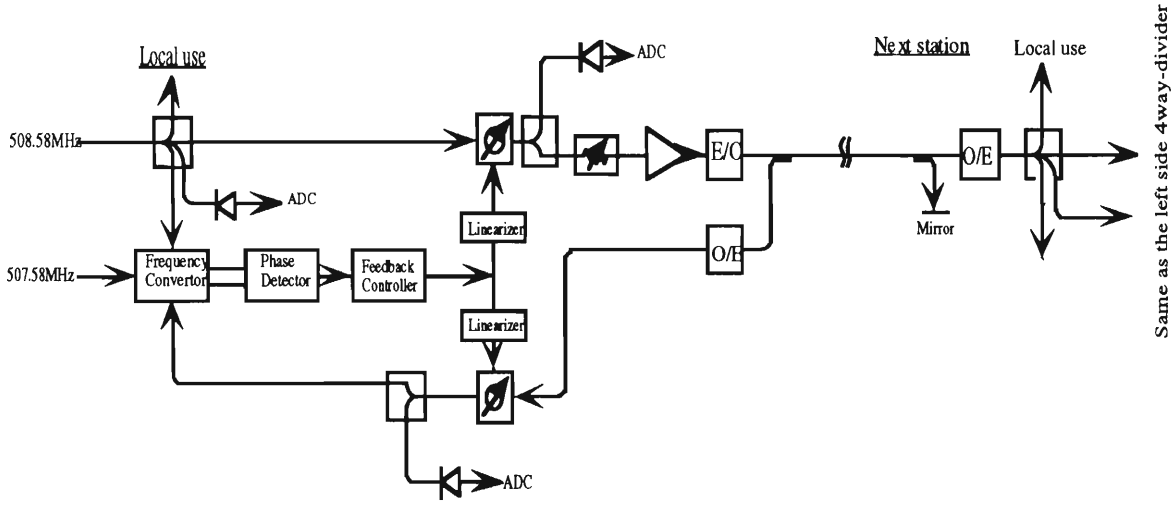

Fig. 1. Diagram of 508.58 MHz reference line.

through the same line. The transmission line is shrunk or expanded depending on the ambient temperature. Consequently, the phase change of a returned 508.58 MHz-RF signal is amplified just twice, because the returned RF signal passes through the same transmission line. A phase lock loop (PLL) at the station (A) detects these phase variations by observing the phase difference between the original and the returned signals, and adjusts a relative phase of the signal sent to (B) to keep the same reference phases at both stations (A) and (B). Thus the phases at the station (A) and (B) are always kept at almost the same angles. This is the phase lock system.

A coaxial cable has been used for a transmission line, for example, TRISTAN at KEK.[2] In case of TRISTAN, 508.58 MHz-RF in the station (B) is divided into two. One is used there, and the other is converted to detector currently existing. We have assembled various tools to confirm the phase lock system and tested just half-frequency to identify a returned signal from an original one. Then the converted RF signal is returned to the station (A) through the same coaxial

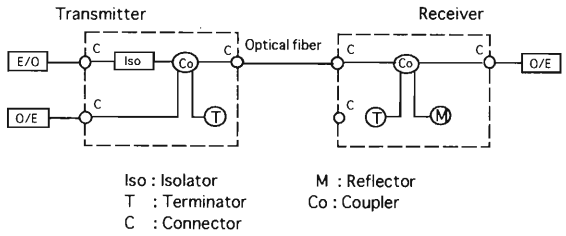

Fig. 2. Detail of the parts of transmitter and receiver.

cable. The returned RF signal is reconverted to the original frequency with an RF doubler and compared with original one. In our case, the transmission line uses an optical fiber instead of a coaxial cable. There are two merits to use it. One is very small attenuation and the other is less interference between forward and backward optical signals. So that we can deal with only 508.58 MHz-RF and the total system becomes simpler.

Our phase lock system consists of a PLL part, RF transmitter part, transmission line and receiver part,

* Japan Atomic Energy Research Institute

as shown in Fig. 1. Every part of PLL comprises NIM modules and the other consists of an electrical to optical (E/O) converter and an optical to electrical (O/E) converter, and an optical fiber. This performance was already reported elsewhere.[3] The RF optical signal from an E/O passes through an isolator which protects the E/O from the damage due to reflected light. The RF optical signal is divided into two. One is used there and the other is reflected by a mirror, as shown in Fig. 2. The PLL detects the phase difference between the transmitted and reflected RF signals and makes the difference small. Thus the total system is more compact compared to an old system with a coaxial cable.

We have tested the phase lock system with optical devices and had various troubles. For example, the terminators shown in Fig. 2 are connected with I-type connectors where phase is largely changed according to the temperature. Thus we connected an optical fiber to a terminator by the method of melting bonding, and then the phase variation got negligible small in this part. The other trouble is that the ratio of optical division at a transmitter and receiver parts in Fig. 2 is 50% in each branch and the total light returned to the transmitter is decreased largely. Consequently, S/N ratio got bad. In order to improve the S/N ratio, in particular, in the returned RF-signal, we changed the optical division ratio to 20% and 80% in the part of coupler, so that signal levels from O/Es in Fig. 2 become the same. We are improving these points and the phase stabilization is kept within $\pm 0.5^\circ$ as long as the change of room temperature at the location of a PLL is maintained at the level of $\pm 1^\circ$C.

References

1) Y. Ohashi et al.: *RIKEN Accel. Prog. Rep.*, **26**, 178 (1992).
2) M. Ono et al.: KEK Int. 87-6 (1987) and references therein.
3) Y. Kawashima et al.: *RIKEN Accel. Prog. Rep.*, **26**, 179 (1992).

A Direct Counter of 508.58 MHz

Y. Kawashima, H. Ego, M. Hara, Y. Ohashi, T. Ohshima, H. Suzuki,*
I. Takeshita, N. Tani,* and H. Yonehara*

In the SPring-8, 508.58 MHz radio frequency used in both storage and synchrotron rings is a fundamental frequency. A direct counter for 508.58 MHz has been required for beam handling, setting single-bunch mode for storage and synchrotron rings, beam monitoring, and so on. The technical difficulty has so far prohibited the realization of a fast counter. But we have recently realized a fast counter running in the region below 600 MHz. We briefly describe the performance of the 508.58 MHz-counter.

The requirements to the 508.58 MHz-counter are as follows;

(1) a direct counter of 508.58 MHz,

(2) a non-stop counter which counts from one to a preset value (A) set manually, then automatically resets and restarts without miscount, because 508.58 MHz is a continuous wave,

(3) generation of a single output pulse as a timing signal at the point of preset value (B), which is set with an external computer (Preset number (B) must be smaller than or equal to the number (A)).

Unfortunately there has been no commercialized ICs which work stably over 600 MHz. Even if a fast counter was required, one had to order special integrated cir cuits (ICs) made of GaAs to a semiconductor production company. The price of such ICs would become very expensive. Fortunately, commercialized ICs are recently produced by MOTOROLA, we can easily get them. We found an 8-bit synchronous binary counter, MC10E016, which counts up to 700 MHz and designed a direct counter of 508.58 MHz with it. Its block diagram is shown in Fig. 1. The most difficult point in the design is that the counter has to be made a reset every 2436 counts which correspond to the harmonic number of the storage ring. The number, of course, is different in case of the synchrotron. After reset, the counter must be restarted within a very short time of 1.966 nsec which comes from one count of 508.58 MHz. Total propagation delay time as to various gates including reset and recovery time is estimated to be 1.775 nsec. Next pulse comes only 191 psec later (1.966 nsec − 1.775 nsec = 191 psec). An actual circuit board consists of 6 layers to suppress an oscillation due to high frequency of 508.58 MHz. To make paths between ICs as short as possible, ICs were placed on both surfaces of a board. After various troubles, we could construct a 508.58 MHz-counter. It was very difficult to check such a fast counter. We invented a sophisticated method to check it.[1] It was verified that the 508.58 MHz-counter worked well up to 600 MHz without any trouble such as miscount.

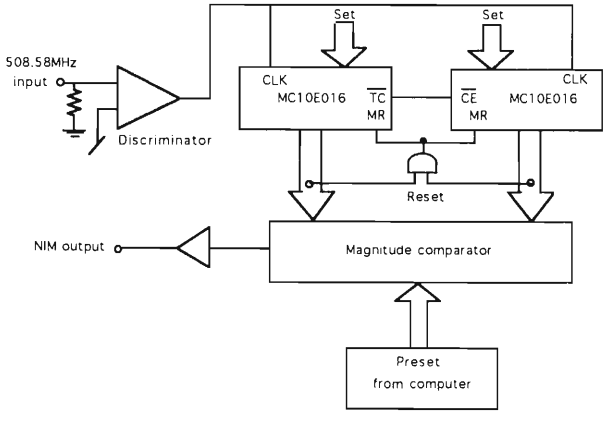

Fig. 1. Block diagram of a 508.58 MHz-counter.

This counter is not a final version. Final one will have to be equipped with an input port for external reset by a computer control to make a set time zero to all 508.58 MHz-counters used in the SPring-8. It is impossible to add an external reset-port in the present 508.58 MHz-counter. Because the extra gate of IC must be added in the circuit for an external reset-port, total propagation delay time becomes longer than one cycle of 508.58 MHz. Our solution to overcome this problem is to utilize a newly available IC instead of MC10E016. In the very near future a new version of 508.58 MHz-counter will be constructed.

References

1) H. Suzuki et al.: 9th Symp. on Accel. Sci. and Tech., p. 252 (1993).

* Japan Atomic Energy Research Institute.

Transmission Test of the Timing Signal for the SPring-8

H. Suzuki,* H. Ego, M. Hara, T. Hori,* Y. Kawashima, Y. Ohashi,
T. Nagafuchi,* T. Ohshima, N. Tani,* and H. Yonehara*

To operate the accelerator complex of the SPring-8 facilities, two systems for the timing coordination are necessary. The first system is associated with beam transfer from the linac to the synchrotron. The second system is associated with beam transfer from the synchrotron to the storage ring. The RF system of the linac is operated by an oscillator at the frequency of 2856 MHz. The RF systems of the synchrotron and the storage ring are operated by another oscillator at the frequency of 508.58 MHz and at the harmonic number of 672 and 2436, respectively. Since the width of short pulsed beam from the gun of the linac is 1 nsec at full width half maximum (FWHM) and the time width of each RF bucket in the two rings is 2 nsec, the timing accuracy required for beam transfer from the linac to the synchrotron and the synchrotron to the storage ring must be less than 100 psec to suppress the beam loss due to the synchrotron oscillation of the injected beam. For single bunch beam operation, it is necessary to select any one of the 2436 buckets as the single filled bucket in the storage ring into which the bunched beam from the synchrotron is transferred. Two concepts for the timing systems are being considered. One concept uses a synchronous timing table which has low jitters (lower than 100 psec) and the other utilizes a phase control loop which has the accuracy of lower than 1°. We had to choose the synchronous timing table, because there was no correlation between both frequencies of 2856 MHz and 508.58 MHz. The transfer line of the timing signal consists of an optical fiber and EO/OE (electrical to optical/vice versa) transmitter and receiver which have low jitters and low dependence on temperature. The time jitter is a serious problem in transmitting a beam effectively, because the beam is transported in the rigid beam line at the speed of light and the timing accuracy from the linac to the synchrotron almost depends on the jitters of the transfer line and the gun of the linac. And the timing accuracy of the synchrotron to the storage ring is easily achieved by comparing the RF phase between the two rings.

The jitters of a short-pulsed beam were measured with the gun of the linac. Obtained results are described.

(1) Optical Fiber and EO/OE

The timing signal generator for the gun trigger is situated in the control station of the synchrotron. The transfer line from the synchrotron to the gun is about 200 m long. Because the jitters of the timing signal are required to be less than 100 psec, the optical fiber and EO/OE which have low jitters are used for the timing system. The optical fiber (DTS-M02) which has low dependence on temperature is made by Sumitomo Electric Industries. The EO/OE (model 3510A and 4510A) which have high performance at high frequencies up to 3 GHz are made by ORTEL corporation.

(2) Old Transfer System of the Timing Signal

Figure 1 shows a block diagram of the old timing system for the prototype linac of SPring-8. The time jitters between the trigger signal (pulse generator, DG535 in Fig. 1) and the electron beam emitted from the gun following the signal (wall-current monitor, C.T. in Fig. 1) were measured by using the old timing system. The electron beam from the gun was measured by the wall-current monitor. This system made by Mitsubishi Electric corporation is a black box. The optical fiber and the EO/OE are used in this system. But DTS-M02, 3510A and 4510A are not used in this system.

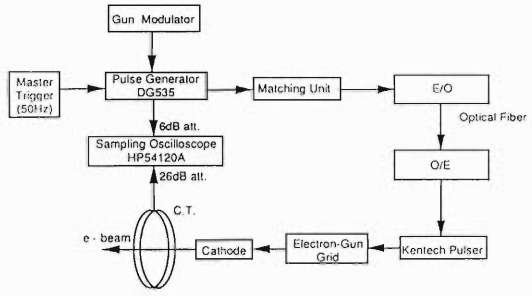

Fig. 1. The block-diagram of the old timing system.

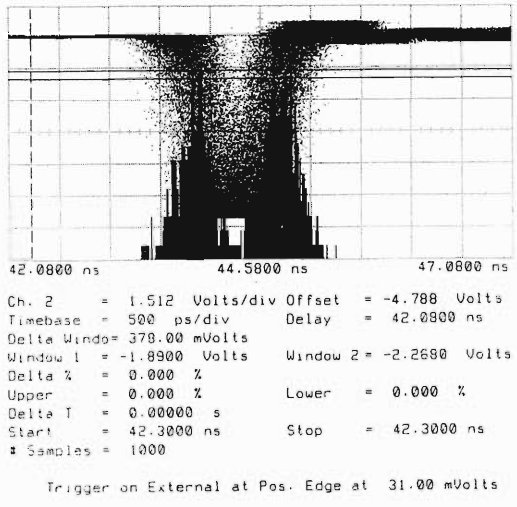

Fig. 2. The jitters of the old timing system.

* Japan Atomic Energy Research Institute

Figure 2 shows the jitters of the old timing system. Standard deviation of the jitters is 170 psec.

(3) New Transfer System of the Timing System

Figure 3 shows a block diagram of the new timing system. The optical fiber and the EO/OE are replaced with DTS-M02, 3510A and 4510A. To reduce the jitters caused by the dependence of the pulse height, a constant fraction discriminator (CFD:ORTEC model 935) is used after the E/O receiver. To minimize the jitters, the external delay, the threshold voltage and the walk voltage of the CFD were optimized to 2 nsec, −20.3 mV and 0.3 mV, respectively. The jitters at this point were reduced from 77 psec to 27 psec by the CFD. After this signal is amplified to a level of 9 V, the 9-V signal is used for the trigger of the grid pulser of the gun. Figure 4 shows the jitters of the beam current wave form for the trigger signal. Standard deviation of the jitter is 30 psec.

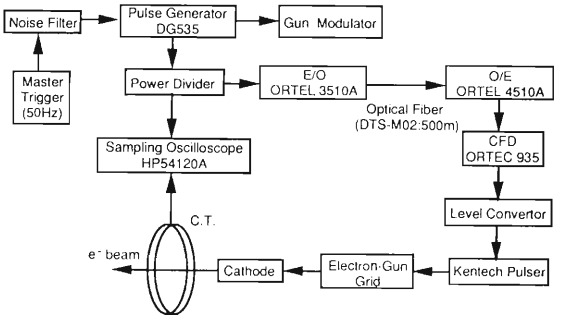

Fig. 3. The block-diagram of the new timing system.

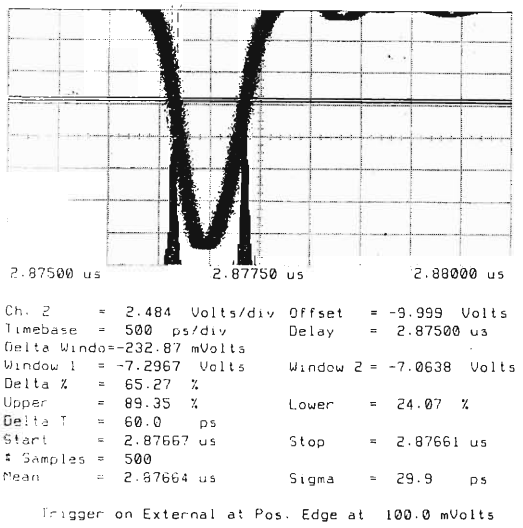

Fig. 4. The jitters of the new timing system.

The old and new timing systems for the gun of the linac were tested. The new timing system meets the specification of low jitters which must be less than 100 psec. A test using a pulse generator which has a faster risetime will be planned in the next year, and the jitters will be lower than 30 psec.

Control of SPring-8 SR Klystron Test Bench

S. Fujiwara, T. Masuda, and T. Wada

A VME system with LynxOS[1] is planned to be used in the control system of the SPring-8 storage ring (SR). We tested the VME system for the control of the klystron test bench and evaluated its hardware and software. We also examined the influence of noise on the VME system.

The test bench of the klystron is similar to that designed by KEK[2] and it has an interface with CAMAC. The VME system was connected to the klystron test bench through Interface (I/F) Box (Signal Conditioner) which conforms signal levels of VME I/O boards to those of the interface of the klystron test bench. The VME system is Motorola Delta LA. The CPU board is MVME147SA-1 with MC68030. Three DI boards (PENTLAND MPV910), a DO board (Digital DOUT2) and an ADC board (PENTLAND MPV906) were inserted into the VME system. The operating system is LynxOS. Test programs were written in C language. Figure 1 shows a schematic

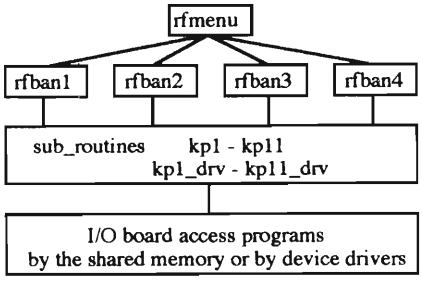

Fig. 1. Schematic diagram of the test programs.

diagram of the test programs. Programs rfban1 (to watch status), rfban2 (to measure analog), rfban3,4 (to control) and rfmenu (to select menu) are application programs. Programs kp1-kp11 (corresponding to connectors for using the shared memory) and kp1_drv-kp11_drv (corresponding to connectors for using device drivers) are sub_routine programs. Programs dout2 (DO set), mpv910 (DI read) and mpv906 (AI read) are I/O board access programs by the shared memory. Programs dout2drv.o (DO), m910drv.o (DI) and m906drv.o (AI) are I/O board access programs by device drivers.[3]

The test programs using the shared memory successfully controlled the klystron test bench except for the pulse-train control by rfban3,4. When the VME system sent pulse-train signals for increasing the voltage of the klystron test bench, the voltage increased and decreased alternately. We checked the followings to get the causes for this: Firstly, we thought that the LED in the I/F Box did not radiate light as current was small. We measured the current of the I/F Box and found that the current was right as designed. Next, we thought that the cables between the I/F Box and the klystron test bench got out of order. Those cables are made of flat cables which are bent like an S-word. The ends of the cables are furnished with the LED's. We found that a cross-talk happened when using the cables. We checked the cables and confirmed that they had no short circuit. We then thought that this cause was that signal lines were too close to each other. When the signal line for decrease was not connected, the increase signal had no problem; the increase of the voltage corresponded to the number of transmitted pulses. But when we sent the decrease signal under the same condition as above, the voltage of the klystron test bench was increased. The phenomenon showed no change either by separating the signal lines from each other or by exchanging the flat cables for twisted pair cables which were successfully used in the CAMAC system.

We verified the followings by this test. The klystron test bench was successfully controlled by the VME system using either of device drivers and the shared memory, except for the pulse-train control. We concluded that the I/F Box had a problem of way about DO (pulse-train). We have not yet figured out the causes of this problem. The VME system was not influenced by either noises from the IVR (inductive voltage regulator) or those that were generated when the interlock for off of a high-tension occurred.

References

1) T. Masuda, T. Nakamura, T. Wada, and Z. Wang: *RIKEN Accel. Prog. Rep.*, **25**, 240 (1991).
2) National Laboratory for High Energy Physics.
3) T. Masuda, T. Nakamura, H. Takebe, and T. Wada: *RIKEN Accel. Prog. Rep.*, **26**, 174 (1992).

Performance Test of Energy Analyzer for Photoelectrons Produced by SR Irradiation

K. Yano, K. Watanabe, H. Sakaue, and S. H. Be

We have successfully done measurement of the photodesorption yields of gases desorbed from an OFC (oxygen-free copper) model chamber by using photon beams with the critical energy of 26 keV from the accumulating ring (AR) of TRISTAN at KEK.[1] Measurements of energy distributions of photoelectrons are also planned at KEK to investigate desorption mechanisms. The plan of outline has been reported in Ref. 2. For that purpose an apparatus is prepared, which consists of an energy analyzer, a magnetically shielded vacuum chamber with mumetal sheets and a pumping system. This magnetic shielding reduces the geomagnetic field of ca. 0.03 mT to nearly zero and enables us to analyze electrons of lower energy less than a few eV. The energy analyzer is a double focusing electrostatic type. Previous to energy analysis of photoelectrons the performance test of the energy analyzer was performed by passing secondary electrons which were emitted from a silicon surface by electron bombardments. Figure 1 shows the sectional plan of the hemispherical analyzer with the mean sphere radius of 36.5 mm. Other dimensions are given in Fig. 1. Main specifications of the analyzer are as follows;

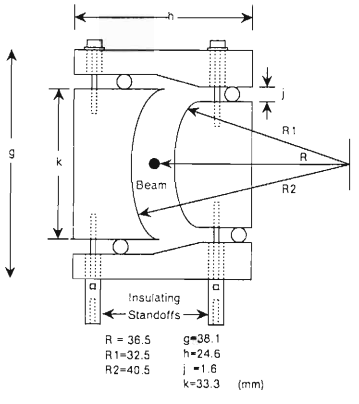

Fig. 1. Sectional plan of electrostatic energy analyzer.

Acceptance angle 0.002 sr
Resolution 0.4% for 0.05 cm diameter aperture
0.8% for 0.1 cm diameter aperture
Operating Temperature ambient, bakable to 400 °C
Construction materials oxygen-free copper, sapphire, stainless steel, alumina.

The electric connections of the analyzer and a microchannel plate charged particle detector (MCP) are schematically illustrated in Fig. 2. A three-element, cylindrical einzel lens, whose focal length is adjustable to ca. 10 cm, is mounted to the entrance aperture of the analyzer in oder to image a point source of electrons directly into the analyzer entrance aperture without alteration of the original electron energy spectrum. To obtain an energy spectrum in this experiment, the analyzer is operated in the constant transmission energy mode, that is to say, input energy range is scanned with some predetermined $\Delta \mathbf{V}$, where $\Delta \mathbf{V}$ is the potential difference between the sector electrodes. Potential of the middle electrode of the einzel lens has to be adjusted to compensate the chromatic aberration of the electrostatic lens in this mode. Energy-analyzed electrons are measured by the MCP composed of dual channel plates, the gain of each plate being several thousand. By the way, the above-mentioned operation and data acquisition will be controlled by a computer at a remote place in the experiment at KEK. The assembly of the analyzer including the einzel lens and the MCP is put in an electrostatic shielding box and then installed in the magnetically shielded measurement chamber.[2]

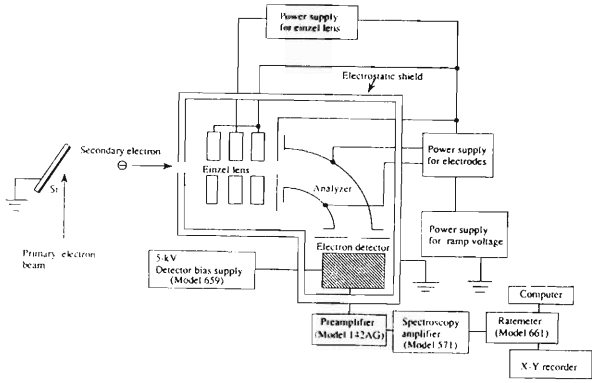

Fig. 2. Schematic diagram of measurement system.

An example of energy spectra of secondary electrons obtained by a performance test of the analyzer is demonstrated in Fig. 3 when energies of bombarding primaries are 200, 300, and 400 V. In conclusion we confirmed from this result that the analyzer works normally up to the energy less than a few eV without suffering from the geomagnetic field. In addition we can analyze the energy of photoelectrons up to 600 eV using our present apparatus.

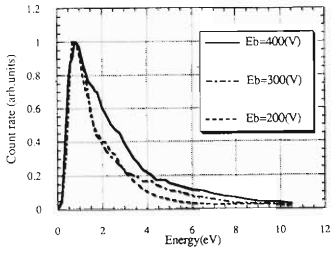

Fig. 3. Energy spectra of secondary electrons emitted from Si surface by electron bombardment.

Computer-controlled operation and a data acquisition system are in preparation.

References

1) K. Watanabe, T. Hanasaka, Y. Hirano, H. A. Sakaue, K. Yano, S. Yokouchi, and S. H. Be: *RIKEN Accel. Prog. Rep.*, **26**, 163 (1992).
2) H. A. Sakaue, K. Watanabe, K. Yano, T. Hanasaka, and S. H. Be: *ibid.*, **25**, 233 (1991).

Outgassing Rate Measurement of Braided Wire

K. Watanabe, K. Hayashi, and S. H. Be

We measured the outgassing rate of a braided wire before and after baking for about 24 hours by means of a so-called throughput method.

The measurement apparatus is schematically shown in Fig. 1.[1] The surface area of a sample chamber is 0.196 m^2. The conductance of the orifice between the sample chamber and pump side chamber is 2.15×10^{-3} m^3/s for N_2 at 22 °C.

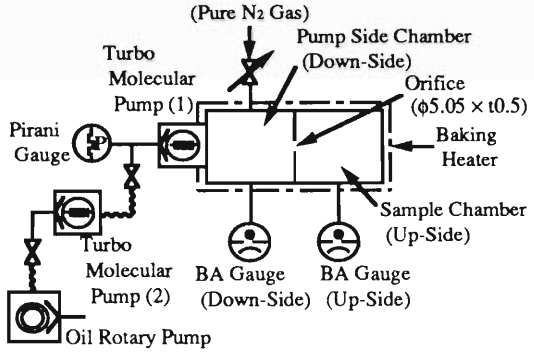

Fig. 1. Measurement apparatus.

The braided wire, made of OFHC (oxygen free copper), consists of three cylindrical strata woven from wires of 0.18 mm in diameter (Fig. 2) and its length is 3.2 m. The total surface area of wires is 2.0 m^2. The braided wire was cleaned using freon in an ultrasonic cleaner. The measurement procedure has been described elsewhere.[1]

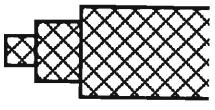

Fig. 2. Structure of braided wire.

Experimental results of the outgassing rates as a function of pumping time are shown in Fig. 3. The origins of the pumping time before and after baking are the starting point of evacuation of chambers and that of cool down. Because the outgassing rate is strongly influenced by temperature, the rate after baking is decreased with an increase of time. The cooling time required to reach room temperature after baking is a few hundred minutes.

The outgassing rates before and after baking are approximately 1×10^{-6} Pa·m^3/s and 5×10^{-10} Pa·m^3/s, respectively.

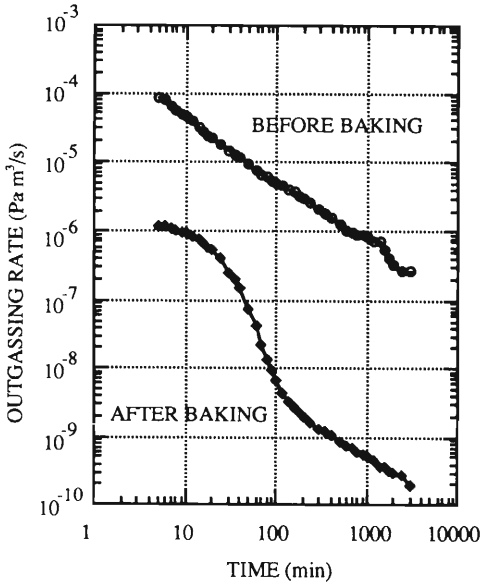

Fig. 3. Outgassing rate of braided wire.

References

1) T. Hanasaka et al.: *RIKEN Accel. Prog. Rep.*, **26**, 167; 169; 171 (1992).

Design of Beam Position Feedback Systems for SPring-8 Storage Ring

K. Kumagai

The stability of the photon beams is one of the critical parameters for the low emittance ring, SPring-8. The main disturbing sources affecting beam stability are: (1) machine floor deformation induced by sunlight and temperature; (2) deformation of magnets and girders due to the temperature change of cooling water or air; (3) ground vibrations induced by seismic motion, compressors, cooling water pressure, etc.; (4) power supply ripples and drift. In order to stabilize the photon beam, the electron (positron) beam must be stabilized in a few μm. For this purpose, two types of feedback system will be equipped in the SPring-8 storage ring: static closed orbit feedback and fast local bump feedback.

The static closed orbit feedback system is used for the reduction of the long term drift or rather low frequency vibrations of the beam position. The 288 beam position monitors (BPM) are installed in the ring and the same numbers of vertical and horizontal correctors are provided. The resolution of the BPM is about 10 μm and the maximum kick angles of correctors are 1.0 mrad for horizontal plane and 0.5 mrad for vertical. The orbit motion will be corrected in every minute.

For the beamlines with the tight beam stability requirement, a fast local bump feedback system will be added (Fig. 1). In each beamline the system has two or three photon beam position monitors which measure the deviation in angle and position of the beam and two sets of four corrector magnets that create the bumps for the horizontal and vertical plane. With a four-magnet bump it is possible to independently control both the position and the angle of the beam. The resolution of the photon-BPM will be about 1 μm and the kick angles of correctors are about 50 μrad. The frequency range of the feedback system will be up to 70 Hz. As the fast response is needed for the feedback loops, digital signal processor (DSP) boards are used to give the proper corrector strengths from the photon-BPM information. The systems also provide the cancellation of the deviations of beam position induced by changes of magnet gap width of insertion devices.

Detailed design of the feedback circuit is now in progress.

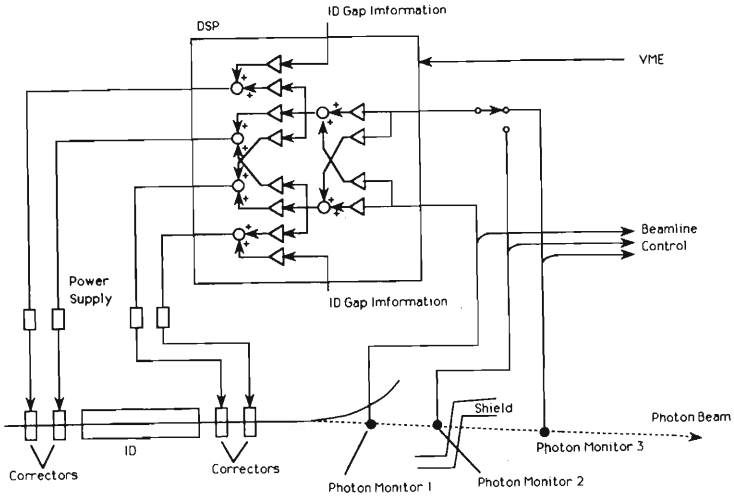

Fig. 1. Diagram of local bump feedback system.

VI. RADIATION MONITORING

Measurement of Activities Induced by 135 MeV/u ^{20}Ne Incident on an Iron Target with the Activation Method

N. Nakanishi, S. Nakajima, S. Fujita, K. Tanaka,* T. Takagi,** and M. Watanabe*

In designing accelerator facilities, it is indispensable to have accurate data for the neutron flux produced by high energy beams and/or neutron production cross sections. Therefore, a series of measurements for the neutron yield have been carried out for 135 MeV/u various incident particles on a thick iron target with the activation method.

Here, the activity induced in metals by neutrons produced by 135 MeV/u ^{20}Ne beams incident on a thick iron target is briefly presented. Seven metals of C, Al, Fe, Co, Ni, In, and Au were used as neutron detectors. These metal detectors were placed at scattering angles of 0, 30, 60, 90, 120, and 140 degs. Gamma rays were measured after irradiation. Details of experiment are described elsewhere.[1)]

Figure 1 shows the angular dependence of induced activities in the detector by various nuclear reactions. The activity basically represents the product of a neutron-activation cross section and the neutron number produced by an incident particle. The reactions and characteristics of detectors are also given in Ref. 1.

Hereafter, the activity will be unfolded using reaction cross sections, and the neutron flux will be evaluated and a further mechanism producing neutrons in the target will be examined.

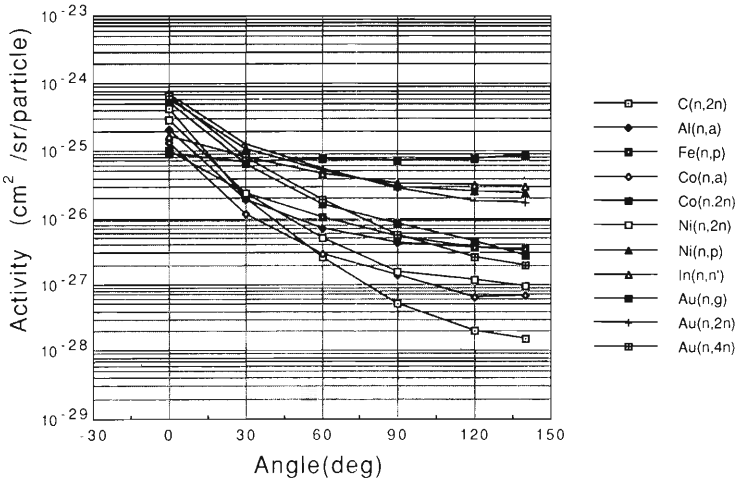

Fig. 1. Angular distributions of activities by neutron induced reactions. The neutrons are produced by 135 MeV/u ^{20}Ne beams incident on a thick iron target.

References

1) N. Nakanishi et al.: Proc. 9th Symp. on Accel. Sci. and Tech., Tsukuba, p. 425 (1993).

* Faculty of Science and Technology, Chuo Univ.
** Fukuda Giken

γ-ray Spectrum from Iron Targets Bombarded by Accerelated Ions

S. Nakajima, N. Nakanishi, S. Fujita, K. Tanaka,* and T. Takagi**

A series of experiments with activation foil has been continued to obtain secondary neutron spectra from iron targets bombarded by various accelerated ions.[1] A lot of γ-ray spectra from the activated foil were obtained in these experiments. We could get from these spectra information about produced neutrons. As an example, we showed in the last issue that significant presence of neutrons with energies larger than 40 MeV was easily observed in the reaction of 135 MeV/u nitrogen ions with an iron target.[2] There is also a report that neutrons whose enegy is up to 220 MeV were identified by the γ-ray analysis in the similar experiments.[3]

In those experiments iron targets were used only to produce neutrons, and so γ rays from them were not measured. But expecting that γ-rays from the targets offer some information about nuclear reactions, we measured them incidentally after each experiment. In the case of above experiment with 135 MeV/u nitrogen ions, we used an iron target of 12 mm in thickness and obtained a specrum as shown in Fig. 1. From the figure we could identify various nuclei such as Sc, V, Cr, Mn, and Co. Similar spectra were obtained with 135 MeV protons and 135 MeV/u deuterons as incident particles, and nuclei of V, Cr, Mn, and Co were also observed. The spetra were slightly different among the cases of protons, deutrons, and nitrogen ions, but the discrepancy was small.

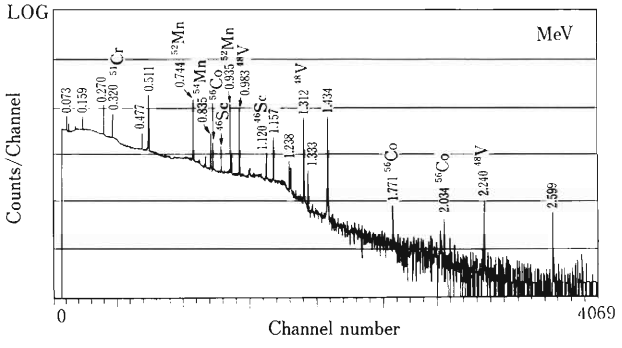

Fig. 1. γ-ray spectrum from an iron target irradiated by 135 MeV/u nitrogen.

In the case of the experiment using proton beam, we used a stack of iron foil and blocks for the target as shown in Fig. 2. We expected that we could get information from the γ-ray spectra of each foil or block about what reactions took place and what radioactive nuclei were produced in each part, or how was

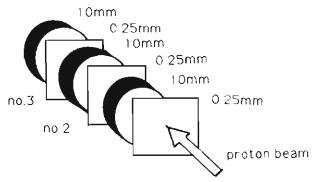

Fig. 2. Schematic diagram of target array used in the case of proton incident.

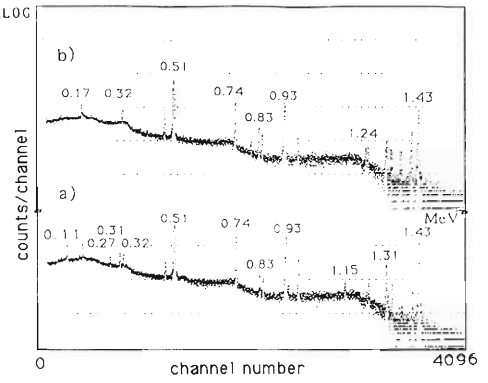

Fig. 3. γ-ray spectra from a) an iron target no. 2 and b) no. 3.

distribution of a dose rate along the iron target, and so on. Slight difference was seen, for example, between Fig. 3(a) and 3(b). But this experiment was a preliminary one and we measured the γ-rays from the target after long-hour irradiation that was necessary for the activation-foil experiment. Therefore intensities of radiations from each iron foil and block were strong. Consequently, the dead time of the counting system was long and then the energy resolution was poor. γ-rays from a nucleus having a short life-time disappear if we wait until the time when the intensity of radiation becomes week enough. Then, it is difficult to observe a difference in detail among these spectra with this experimental set up.

A rivised experiment, optimizing parameters such as counting rate, irradiation time, beam intensity, target's thickness and its number, is necessary to be done to clearly identify the difference of these spectra.

* Faculty of Science and Engineering, Chuo Univ.
** Fukuda Giken

References

1) N. Nakanishi et al.: This report, p. 165.
2) S. Nakajima et al.: *RIKEN Accel. Prog. Rep.*, **26**, 183 (1992).
3) O. Wenxin Li et al.: Private comunication.

Shielding Effect of the Concrete Wall between E1 and E2 Rooms

S. Nakajima

There are a neutron and a γ dose monitoring detectors in every radiation laboratory in the Nishina memorial building. Data of radiation level observed with these detectors in each room are transported to a computer every moment and stored in its disk memory.

In order to get some information about radiation shielding, I examined the data stored during experiments to measure neutron flux in the E1 radiation room. The experiments had been done in a scattering chamber set almost in the center of the room.[1] An iron target was put at the center of the chamber and bombarded by accelerated beams.

At an upper position of a side wall of the E1 room, there are a neutron and a γ dose monitors as shown in Fig. 1. When equipments and instruments arranged in the room are neglected, this room is considered to be symmetric in right and left with regard to the direction of the accerelated beams. Therefore, I can assume that these monitors are located on the opposite wall, that is, at a point A in Fig. 1. After all there would be a concrete wall of 1.5 m thick between two sets of monitors in E1 and E2 rooms. A difference between the simultaneously observed values with monitors in E1 and E2 can be considered approximately to denote directly a shielding effect of the concrete wall.

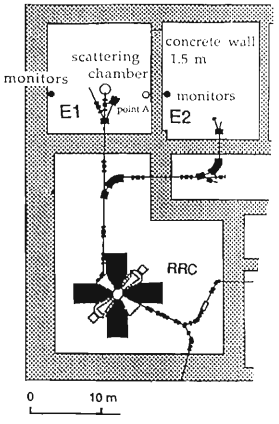

Fig. 1. A diagram showing a settled position of monitors and the scattering chamber.

Table 1 shows that neutron and γ dose rates decrease to $\sim 10^{-4}$ with the concrete wall. According to calculations using a program ANISN, the neutron dose rate decreases to $3.7 \cdot 10^{-3}$ with this wall in the case of 135 MeV/u nitrogen,[2] about one order of magnitude larger than the observed value.

Table 1. Dose rate (μSv/h) observed by the area monitors in E1 and E2 together with a ratio E2/E1. The numbers of the incident particles are not the same in three cases.

Incident particle (135 MeV/u)	Proton	Deutron	Nitrogen
Neutron dose rate			
E1 vault	30000	10000	6000
E2 vault	4	2	1.5
ratio E2/E1	$1.3 \cdot 10^{-4}$	$2 \cdot 10^{-4}$	$2.5 \cdot 10^{-4}$
γ dose rate			
E1 vault	15000	3000	900
E2 vault	3	1.5	0.8
ratio E2/E1	$2 \cdot 10^{-4}$	$5 \cdot 10^{-4}$	$9 \cdot 10^{-4}$

There are two problems. First, the neutron monitors have almost no sensitivity to the neutrons whose energies are more than $\sim$ 20 MeV. But in this case the difference between the observed and calculated ratios E2/E1 becomes larger if corrections of this effect are done, because its contribution to the observed value of a neutron level in E1 is larger than that in E2. Next, a reflection from the walls and a floor was considered in the calculation but the effect of various equipments was not included. In the case of 135 MeV nitrogen, measurements had been done to see the contribution of reflection using a rem counter. The result was that it became nearly 60% of total neutron dose rate at a right angle from the target in E1 room.[2] Then, even if the component of reflection is excluded assuming that it is completely from the equipments in the room, monitored values in E1 decrease only by a factor of about 2.

Above estimation is very rude, to be sure, but it is necesarry to try the calculation by ANISN again by changing an adopted model and parameters.

References

1) for instance, T. Shikata et al.: *RIKEN Accel. Prog. Rep.*, **25**, 250 (1991).
2) T. Shikata: Private communication.

Leakage Radiation Measurements in the Ring Cyclotron Facility

S. Fujita, N. Nakanishi, S. Nakajima, T. Takagi,* K. Tanaka,** M. Watanabe,** and T. Inamura

The radiation safety control system has worked steadily this year, so as to enable us to make radiation monitoring continuously and automatically.

From March 22 to 23 and from July 28 to 29, experiments were carried out with 135 MeV/u H_2^+ and $^{20}Ne^{10+}$ beams (highest energy/nucleon) at intensities of about 7 and 60 pnA. The beams were stopped at the target point A in the experimental vault E1. Leakage radiation of neutrons from E1 was measured with four neutron dose rate meters, TPS-451S's (Aloka). The beam current was read at the target A and recorded with a personal computer through a beam integrator ORTEC 439. Dose rates were normalized with respect to that at 1 pμA. Figures 1-(a), (b), and (c) show the target point A and positions where leakage radiation was measured in this experiment. Results

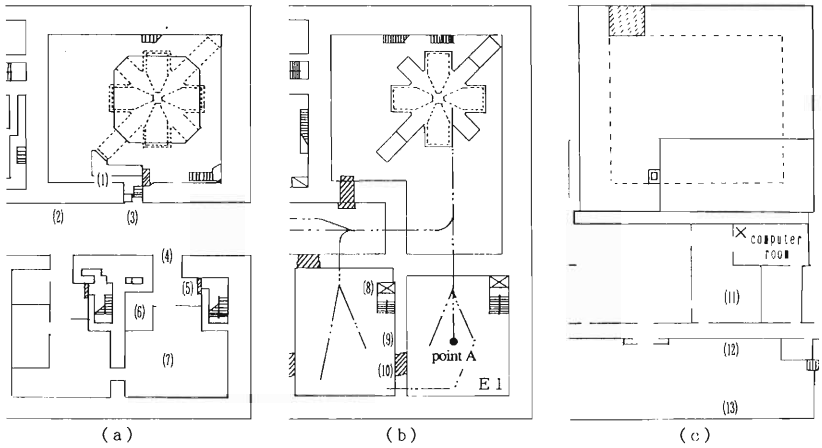

Fig. 1. Partial layout of the RIKEN Ring Cyclotron facility where the leakage radiation measurement was made. (a) Part of basement 2nd floor; (b) Part of basement 1st floor; (c) Part of ground floor. Leakage-radiation-dose measuring points are denoted by the number in parentheses. The monitoring position in the computer room is denoted by ×.

Table 1. Dose rates of neutron leakage radiation from a target point A in the experimental vault E1. (see Figs. 1-(a), (b), and (c)).

Measuring date	Sep.28,1991	Oct. 4,1991	Oct. 5,1992	Mar.23,1993	Jul.28,1993
Accelerated particle	$^{12}C^{6+}$	$^{14}N^{7+}$	Deuteron	Proton	$^{20}Ne^{10+}$
Measured position					
(1)	1017	-----	2432	242	25.4
(2)	0.51	-----	0.86	0.012	0.51
(3)	11.8	-----	18.5	0.61	12.3
(4)	56.5	-----	139	5.82	21.3
(5)	70.2	81.8	692	35.1	89.8
(6)	62.8	81.2	109	13.2	31.4
(7)	431	530	541	50.9	327
(8)	87.5	79.6	188	18.9	39.9
(9)	465	427	1054	88.6	211
(10)	460	560	626	67.8	367
(11)	2.49	2.32	3.73	2.14	1.59
(12)	6.33	5.38	6.62	0.3	3.93
(13)	1.95	2.22	2.29	0.09	1.81

are summarized in Table 1 together with a previous report.[1)]

This year, the radiation level in the controlled area has been much less than the safety limit (0.3 mSv/week). Leakage of neutrons has been recorded with a monitor in a ground-floor computer room just above a bending magnet that guides beams from the Ring Cyclotron vault to the distribution corridor. This radiation level, however, is far less than the safety limit (50 μSv/year) required at the boundary of the facility. No leakage of γ rays and neutrons was detected with environmental monitors set outside the building in this period.

References

1) S. Fujita, N. Nakanishi, T. Shikata, K. Ikegami, T. Takagi, I. Sakamoto, and T. Inamura: *RIKEN Accel. Prog. Rep.*, **25**, 284 (1991).

* Fukuda Giken
** Faculty of Science and Technology, Chuo University

Residual Activities in the Ring Cyclotron Facility

S. Fujita, K. Tanaka,* M. Watanabe,* N. Nakanishi, and T. Inamura

Residual activities were measured at various points in the Ring Cyclotron facility after almost every beam time and during the overhaul throughout the year. In the following we describe significant residual activities observed.

From August 5 to 8, the last experiment in the spring term was carried out with an $^{11}B^{5+}$ beam of 70 MeV/u in the experimental vault E6.

A routine overhaul was made in August, and the dose rates due to residual activities of the Ring Cyclotron and the injector AVF cyclotron were measured on Aug. 4 and 24. Those results are shown in Figs. 1 and 2 together with detection points. The residual activities at the Ring Cyclotron and injector AVF cyclotron have increased compared with those of a previous report[1] because beam intensity has been increased since last year.

In the period from Oct. 16, 1992 to Sep. 30, 1993, residual activities were measured along the beam lines with a portable ionization chamber. The detection points above 20 μSv/h are shown in Fig. 3. Table 1 summarizes the detected dose rates with measured dates. The maximum dose rate was 350 μSv/h at the point j (the production target chamber of RIPS) in the beam distribution corridor. We could not measure the dose rate there immediately after the beam time this year.

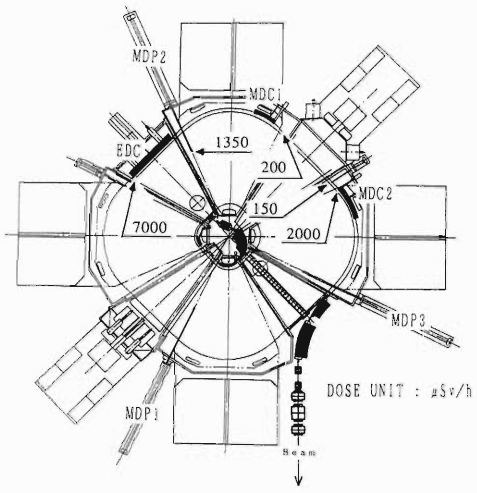

Fig. 1. Detection points around the RIKEN Ring Cyclotron: an electrostatic deflection channel, EDC; a magnetic deflection channel 1, MDC1; a magnetic deflection channel 2, MDC2; a main differential probe 1, MDP1; a main differential probe 2, MDP2; a main differential probe 3, MDP3. Indicated numerals are dose rates in units of μSv/h.

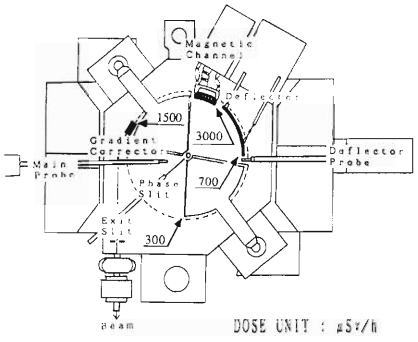

Fig. 2. Dose rates detected inside the injector AVF cyclotron. They are given in units of μSv/h.

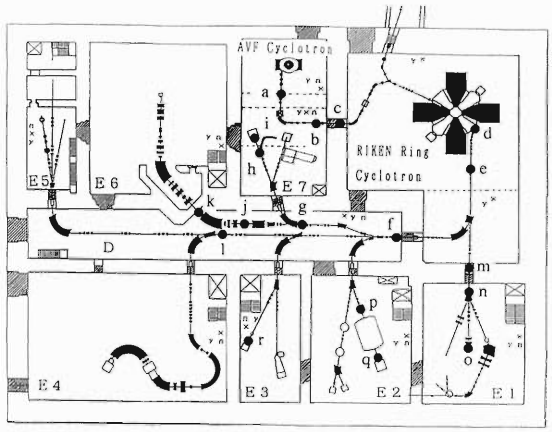

Fig. 3. Layout of the RIKEN Ring Cycrotron facility as of 1993. Monitoring positions are denoted by ×. Detection points of residual activities on the beam lines are denoted by alphabets.

Table 1. Summary of the residual activities measured along the beam lines with an ionization chamber survey meter. Alphabets indicate the detection points in Fig. 3.

Detection point	Detected dose rate (μSv/h)	Date	Detection point	Detected dose rate (μSv/h)	Date
a	65	Feb. 1,1993	j	350	Sep. 9,1993
b	33	Feb. 1,1993	k	72	Sep. 9,1993
c	27	Oct.19,1992	l	43	Sep. 9,1993
d	85	Oct.19,1992	m	28	Oct.19,1992
e	90	Oct.19,1992	n	48	Sep. 9,1993
f	130	Sep. 9,1993	o	250	Mar.26,1993
g	200	Sep. 9,1993	p	60	Oct.26,1992
h	100	Nov. 2,1992	q	60	Oct.26,1992
i	85	Nov. 2,1992	r	100	Feb. 1,1993

* Faculty of Science and Technology, Chuo University

References

1) S. Fujita, S. Okamoto, H. Matsumoto, K. Tanaka, N. Nakanishi, and T. Inamura: *RIKEN Accel. Prog. Rep.*, **26**, 186 (1992).

VII. LIST OF PUBLICATIONS

1. Accelerator development and accelerator physics

M. Hara and Y. Miyahara: "Large Synchrotron Facility SPring-8", *Engineering*, No. 60, p. 18 (1993).

J. L. Laclare, A. Ropert, L. Farvacque, H. Tanaka, J. Payet, P. Nghiem, and A. Tkatchenko: "Study of the Emittance Reduction in the ESRF Storage Ring", ESRF/MACH-LAT-93-08 (1993).

H. Ego, M. Hara, K. Inoue, Y. Kawashima, Y. Ohashi, H. Suzuki, I. Takeshita, and H. Yonehara: "Status of the SPring-8 RF System", *Int. J. Mod. Phys. A* (Proc. Suppl.), **2A**, 709 (1992).

H. Ego, M. Hara, K. Inoue, Y. Kawashima, Y. Ohashi, H. Suzuki, I. Takeshita, and H. Yonehara: "High Power Test of RF System for SPring-8", *ibid.*, p. 712.

M. Hara: "4th Int. Conf. on Synchrotron Radiation Instrumentation", *J. Atomic Energy Soc. Jpn.*, **34**, 58 (1992).

T. Nakagawa, T. Kageyama, M. Kase, A. Goto, and Y. Yano: "Upgrade of RIKEN 10 GHz Electron Cyclotron Resonance Ion Source Using Plasma Cathode Method", *Jpn. J. Appl. Phys.*, **32L**, 1335 (1993).

T. Kubo, M. Ishihara, N. Inabe, H. Kumagai, I. Tanihata, K. Yoshida, T. Nakamura, H. Okuno, S. Shimoura, and K. Asahi: "The RIKEN Radioactive Beam Facility", *Nucl. Instrum. Methods Phys. Res.*, **B70**, 309 (1992).

Y. Yano: "Recent Achievements at the RIKEN Ring Cyclotron", Proc. 13th Int. Conf. on Cyclotrons and Their Applications, Vancouver, p. 102 (1992).

T. Nakagawa, T. Kageyama, M. Kase, A. Goto, and Y. Yano: "Plasma Cathode Method for RIKEN ECRIS", *ibid.*, p. 365.

Y. Yano: "RIKEN Accelerator Research Facility (RARF)", Proc. Joint Italian-Japanese Meet. on Perspectives in Heavy Ion Physics, Catania, p. 1 (1993).

H. Ego, M. Hara, K. Inoue, Y. Kawashima, Y. Ohashi, H. Suzuki, I. Takeshita, and H. Yonehara: "Status of the SPring-8 RF System", Proc. 3rd Joint Symp. Synchrotron Radiation Sources, Pohang, Korea, p. 293 (1992).

H. Ego, M. Hara, K. Inoue, Y. Kawashima, Y. Ohashi, H. Suzuki, I. Takeshita, and H. Yonehara: "High Power Test of Single Cell Cavities for SPring-8", Proc. 17th Linear Accelerator Meeting in Japan, Sendai, p. 180 (1992).

M. Hara: "Characteristics of Photon at SPring-8", Proc. SPring-8 Workshop on Atomic Physics at High Brilliance Synchrotron Radiation Facilities, March, 1992, Himeji, p. 203 (1992).

Y. Yano: "Current Status and Future Scope on the RIKEN Accelerator Research Facility", Proc. 9th Symp. on Accel. Sci. and Technol., Tsukuba, KEK, p. 23 (1993).

A. Goto, T. Kageyama, M. Kase, S. Kohara, M. Nagase, T. Nakagawa, K. Ikegami, O. Kamigaito, N. Inabe, I. Yokoyama, J. Fujita, T. Kawama, and Y. Yano: "Status of the RIKEN AVF Cyclotron", *ibid.*, p. 59.

T. Masuda, S. Fujiwara, T. Nakamura, H. Takebe, and T. Wada: "Development of Device Drivers Embedded in Real Time OS for SPring-8 SR Control System", *ibid.*, p. 79.

T. Nakagawa, T. Kageyama, Y. Miyazawa, E. Ikezawa, M. Hemmi, M. Kase, A. Goto, M. Nagase, and Y. Yano: "Status of the RIKEN ECRIS's", *ibid.*, p. 95.

T. Nakagawa, T. Kageyama, A. Goto, N. Inabe, O. Kamigaito, M. Nagase, T. Chiba, M. Hemmi, M. Kase, Y. Miyazawa, E. Ikezawa, and Y. Yano: "Design of an 18 GHz ECRIS for the RILAC", *ibid.*, p. 98.

S. Kohara, A. Goto, Y. Miyazawa, T. Chiba, M. Hemmi, Y. Chiba, E. Ikezawa, M. Kase, and Y. Yano: "Development of a Second-Harmonic Buncher for the RILAC", *ibid.*, p. 157.

K. Ikegami, J. Fujita, T. Kubo, N. Inabe, T. Kageyama, M. Kase, A. Goto, Y. Yano, H. Sakai, H. Okamura, N. Sakamoto, T. Uesaka, S. Ishida, H. Otsu, T. Wakasa, and K. Hatanaka: "Development of the RIKEN Atomic Beam Type Polarized Ion Source", *ibid.*, p. 214.

O. Kamigaito, A. Goto, Y. Miyazawa, T. Chiba, M. Hemmi, M. Kase, and Y. Yano: "Design of a Variable Frequency RFQ Linac for the RILAC", *ibid.*, p. 220.

H. Ego, M. Hara, Y. Kawashima, Y. Ohashi, T. Ohshima, H. Suzuki, I. Takeshita, and H. Yonehara: "Higher Order Modes of the Single Cell Cavity for the SPring-8", *ibid.*, p. 249.

H. Suzuki, Y. Kawashima, Y. Ohashi, H. Yonehara, H. Ego, N. Tani, T. Nagafuchi, T. Hori, T. Oshima, and M. Hata: "Characteristics of RF Reference and Timing Signal Distribution for SPring-8", *ibid.*, p. 252.

N. Nakanishi, S. Nakajima, S. Fujita, H. Matsumoto, K. Tanaka, and T. Takagi: "Measurement of Neutron Yield Produced by 135 MeV/nucleon H_2 and ^2D Beams Incident on a Thick Iron Target with the Activation Method", *ibid.*, p. 425.

M. Kase: "Development of a Beam Phase Monitor with a Micro-Channel Plate for the RIKEN Ring Cyclotron", *ibid.*, p. 474.

M. Hara: "Synchrotron Radiation", *The Reviews of Laser Engineering*, **21**, 126 (1993).

M. Hara, T. Nakamura, T. Takada, and H. Tanaka: "Use of Long Straight Sections of SPring-8", *Rev. Sci. Instrum.*, **63**, 355 (1992).

M. Hara, S. H. Be, I. Takeshita, and T. Nanba: "Extraction of Infrared Radiation from SPring-8", *ibid.*, p. 1543.

T. Kusaka, K. Inoue, and M. Hara: "Design of RF Cavities for the 8 GeV Synchrotron Radiation Facility I. Design, Fabrication, and RF Measurements of Model Cavities", *Sci. Papers I.P.C.R.*, **68**, 28 (1992).

T. Kusaka, T. Yoshiyuki, K. Inoue, I. Takeshita, and M. Hara: "Design of RF Cavities of the 8 GeV Synchrotron Radiation Facility II. Design of RF Cavities for the SPring-8 Storage Ring", *ibid.*, p. 35.

M. Hara: "Light Source Performance of SPring-8", *SR Science and Technology Information*, **3**, No. 9, p. 2 (1993).

M. Hara: "SPring-8, A Challenge to Highly Brilliant Photon Source", Symp. on Charged Particle Optics-Data of 119th Meeting, July, 1992, Tsukuba, p. 1 (1992).

S. H. Be: "8 GeV Synchrotron Facility", *Vac. J.*, **29**, 6 (1993).

2. Nuclear physics and nuclear instrumentation

H. Sato: "Systematics of Isotope Production Rates: Fission Products and Their Barrier Penetration", in Abstact of the Second Meeting on Nuclear Incineration JAERI-memo 05-191, p. 46 (1993).

H. Kudo, M. Fujie, T. Tanase, M. Kato, K. Kurosawa, H. Sugai, H. Umezawa, T. Matsuzaki, and K. Nagamine: "Preparation of Pure Tritium for a Liquid D_2/T_2 Target of Muon Catalyzed Fusion Experiments", *Appl. Radiat. Isot.*, **43**, 577 (1992).

H. Toki, D. Hirata, and I. Tanihata: "Nuclear Properties Far from the Stability Line in the Relativistic Mean Field Theory", *Hyperfine Interact.*, **74**, 113 (1992).

K. Asahi, H. Okuno, H. Ueno, H. Sato, J. Kura, T. Kubo, T. Nakamura, N. Inabe, A. Yoshida, Y. Ohkubo, M. Adachi, T. Ichihara, M. Ishihara, T. Shimoda, H. Miyatake, N. Takahashi, D. Beaumel, D. J. Morrissey, and W. -D. Schmidt-Ott: "Spin-oriented Projectile Fragments: the First Application to g-Factor Measurement", *ibid.*, **75**, 101 (1992).

K. Asahi: "Fragment Spin Polarization and Its Application", *Inst. Phys. Conf. Ser.*, No. 132, p. 183 (1993).

K. Matsuta, A. Ozawa, Y. Nojiri, T. Minamisono, M. Fukuda, S. Momota, T. Ohtsubo, S. Fukuda, K. Sugimoto, I. Tanihata, K. Yoshida, K. Omata, J. R. Alonso, G. F. Krebs, and T. J. M. Symons: "NMR on Beta-emitting Fragment ^{43}Ti", *ibid.*, p. 229.

T. Takeda, K. Nagamine, Y. Yamazaki, R. Kadono, K. Ishida, M. Kamimura, Y. Yamazaki, and M. Mizumoto: "Progress of Muon Science", *J. Atomic Energy Soc. Jpn.*, **34**, 1098 (1992).

K. Nagamine: "Muon Catalyzed Nuclear Fusion and Cold Nuclear Fusion", *ibid.*, **35**, 27 (1993).

A. Ferragut, Y. Gono, T. Murakami, T. Morikawa, Y. H. Zhang, K. Morita, A. Yoshida, M. Oshima, H. Kusakari, M. Sugawara, M. Ogawa, M. Nakajima, S. Mitarai, A. Odahara, E. Ideguchi, T. Shizuma, M. Kidera, J. G. Kim, S. J. Chae, B. J. Min, and H. Kumagai: "A New High-Spin Isomer in ^{145}Sm", *J. Phys. Soc. Jpn.*, **62**, 3343 (1993).

H. T. Duong, C. Ekstrom, M. Gustafsson, T. T. Inamura, P. Juncar, P. Lievens, I. Lindgren, S. Matsuki, T. Murayama, R. Neugart, T. Nilsson, T. Nomura, M. Pellarin, S. Penslin, J. Persson, J. Pinard, I. Ragnarsson, O. Redi, H. H. Stroke, J. L. Vialle, and the ISOLDE Collaboration: "Atomic Beam Magnetic Resonance Apparatus for Systematic Measurement of Hyperfine Structure Anomalies (Bohr-Weisskopf Effect)", *Nucl. Instrum. Methods Phys. Res.*, **A325**, 465 (1993).

Y. Futami, T. Mizota, Y. H. Pu, Y. Honjo, K. Yuasa-Nakagawa, H. Toyokawa, S. M. Lee, K. Furutaka, T. Murakami, J. Kasagi, K. Yoshida, and T. Nakagawa: "Performance of a Phoswich Detector Composed of Thin Plastic and Thick BaF_2 Scintillators", *ibid.*, **A326**, 513 (1993).

Y. Hasegawa, H. Yuta, F. Suekane, T. Kondo, Y. Unno, H. Iwasaki, Y. Sakai, Y. Watanabe, T. Tanimori, K. Kaneyuki, L. Soso, T. Doke, A. Hitachi, T. Ito, K. Hasuike, K. Masuda, E. Shibamura, and T. Takahashi: "Photoionization of Dopants in Liquid Argon-Xenon Mixture", *ibid.*, **A327**, 57 (1993).

N. Ishida, T. Doke, J. Kikuchi, K. Kuwahara, T. Kashiwagi, M. Ichige, K. Hasuike, K. Ito, S. Ben, A. Hitachi, Y. H. Qu, K. Masuda, M. Suzuki, M. Kase, T. Takahashi, M. Chen, S. Sumorok, M. Gaudreau, and E. Aprile: "Measurement of Attenuation Length of Scintillation Light in Liquid Xenon", *ibid.*, p. 152.

M. Suzuki, T. Takahashi, H. Kumagai, M. Ishihara, and H. Kobayashi: "A Single-Neutron Sensitive Camera Based upon a Proportional Scintillation Imaging Chamber", *ibid.*, **A333**, 484 (1993).

M. Tohyama and E. Suraud: "Stochastic and Deterministic Solutions of the 2-D Boltzmann Equation", *Nucl. Phys.*, **A549**, 461 (1992).

W. Q. Shen, J. Peter, G. Bizard, R. Brou, D. Cussol, M. Louvel, J. P. Patry, R. Regimbart, J. C. Steckmeyer, J. P. Sullivan, B. Tamain, E. Crema, H. Doubre, K. Hagel, G. M. Jin, A. Peghaire, F. Saint-Laurent, Y. Cassagnou, R. Legrain, C. Lebrun, E. Rosato, R. MacGrath, S. C. Leong, S. M. Lee, Y. Nagashima, T. Nakagawa, M. Ogihara, J. Kasagi, and T. Motobayashi: "Components of Collective Flow and Azimuthal Distributions in $^{40}Ar + ^{27}Al$ and $^{40}Ar + ^{58}Ni$ Collisions below 85 MeV/u", *ibid.*, **A551**, 333 (1993).

M. Kato, W. Bentz, K. Yazaki, and K. Tanaka: "A Modified Nambu-Jona-Lasino Model for Mesons and Baryons", *ibid.*, **A551**, 541 (1993).

S. Hirenzaki, H. Toki, and I. Tanihata: "Proton Elastic Scattering with ^{9}Li and ^{11}Li and its Halo Structure", *ibid.*, **A552**, 57 (1993).

K. Sumiyoshi, D. Hirata, H. Toki, and H. Sagawa: "Comparison of Relativistic Mean Field Theory and Skyrme Hartree-Fock Theory for Finite Nuclei and

Nuclear Matter", *ibid.*, p. 437.

I. Tanihata: "Radioactive Beam Facilities and Their Physics Program", *ibid.*, **A553**, 361 (1993).

J. Chiba, D. Ashery, H. Ito, K. Kimura, T. Yu. Kiselev, S. Koda, K. Miyano, T. Murakami, T. Nagae, Y. Nakai, M. Nomachi, S. Sawada, M. Sekimoto, T. Suzuki, K. H. Tanaka, M. K. Viasov, and Y. Yoshimura: "Enhancement of Subthreshold Antiproton Production in Deuteron Induced Reactions", *ibid.*, p. 771c.

K. Tanaka, W. Bentz, and A. Arima: "EOS and Fermi-Liquid Properties in the 1/N Expansion of a Relativistic Many-Body Theory", *ibid.*, **A555**, 151 (1993).

S. Kox, J. Carbonell, C. Furget, T. Motobayashi, C. Perrin, C. Wilkin, J. Arvieux, J. P. Bocquet, A. Boudard, G. Gaillard, M. Garçon, L. Ghedira, G. Guillaume, F. Merchez, D. Rebreyend, and J. Yonnet: "Cross Section and Deuteron Analyzing Powers of the ^{1}H(d,2p)n Reaction at 200 and 350 MeV", *ibid.*, **A556**, 621 (1993).

Y. Gono, T. Murakami, T. Morikawa, A. Ferragut, Y. H. Zhang, K. Morita, A. Yoshida, H. Kumagai, M. Oshima, H. Kusakari, M. Sugawara, M. Ogawa, M. Nakajima, S. Mitarai, A. Odahara, E. Ideguchi, T. Shizuma, M. Kidera, J. C. Kim, S. J. Chae, and B. J. Min: "High-Spin Isomers and High-Spin Isomer Beams", *ibid.*, **A557**, 341c (1993).

D. Cussol, G. Bizard, R. Brou, D. Durand, M. Louvel, J. P. Patry, J. Péter, R. Regimbart, J. C. Steckmeyer, J. P. Sullivan, B. Tamain, E. Crema, H. Doubre, K. Hagel, G. M. Jin, A. Péghaire, F. Saint-Laurent, Y. Cassagnou, R. Legrain, C. Lebrun, E. Rosato, R. MacGrath, S. C. Jeong, S. M. Lee, Y. Nagashima, T. Nakagawa, M. Ogihara, J. Kasagi, and T. Motobayashi: "Charged-Particle Calorimetry of ^{40}Ar + ^{27}Al Reactions from 35 to 65 MeV/u", *ibid.*, **A561**, 298 (1993).

K. Nagamine: "Experiments on Muon Catalyzed Fusion", in Perspectives of Meson Science, eds. T. Yamazaki, K. Nakai, and K. Nagamine, North Holland, Amsterdam, p. 383 (1992).

K. Nagamine and K. Ishida: "Towards Advanced Muon-Beam Production", *ibid.*, p. 441.

C. -B. Moon, M. Fujimaki, S. Hirenzaki, N. Inabe, K. Katori, J. C. Kim, Y. K. Kim, T. Kobayashi, T. Kubo, H. Kumagai, S. Shimoura, T. Suzuki, and I. Tanihata: "Measurement of ^{11}Li + p and ^{9}Li + p Elastic Scatterings at 60 MeV", *Phys. Lett.*, **B297**, 39 (1992).

G. Bizard, R. Bougault, R. Brou, J. Colin, D. Durand, A. Genoux-Lubain, J. L. Laville, C. Le Brun, J. F. Lecolley, M. Louvel, J. Peter, J. C. Steckmeyer, B. Tamain, A. Badala, T. Motobayashi, G. Rudolf, and L. Stuttge: "From Binary Fission to Multifragmentation in the Decay of Heavy Excited Nuclei", *ibid.*, **302B**, 162 (1993).

H. Ejiri and H. Toki: "Search for Exotic Nuclear Transitions with Nuclear Instability," *ibid.*, **B306**, 218 (1993).

T. Shigetani, K. Suzuki, and H. Toki: "Pion Structure Function in the Nambu and Jona-Lasino Model", *ibid.*, **B308**, 383 (1993).

B. M. Young, D. Bazin, W. Benenson, J. H. Kelly, D. J. Morrissey, N. A. Orr, R. Ronningen, B. M. Sherrill, M. Steiner, M. Thoennessen, J. A. Winger, S. J. Yennello, I. Tanihata, X. X. Bai, N. Inabe, C.-B. Moon, S. Shimoura, T. Suzuki, R. N. Boyd, and K. Subotic: "Strong Isomer Production in Fragmentation Reactions", *ibid.*, **B311**, 22 (1993).

J. Miller, G. F. Krebs, J. Panetta, L. S. Schroeder, P. N. Kirk, Z.-F. Wang, W. Bauer, W. Benenson, D. Cebra, M. Cronqvist, B.-A. Li, R. Pfaff, T. Reposeur, J. Stevenson, A. Vander Molen, G. Westfall, J. S. Winfield, B. Young, T. Murakami, T. Suzuki, and I. Tanihata: "Mass Dependence of Pion Production in Heavy Ion Collisions Near, but Below Threshold", *ibid.*, **B314**, 7 (1993).

D. Hirata, H. Toki, I. Tanihata, and P. Ring: "Systematic Study of Sr Isotopes in the Relativistic Mean Field Theory", *ibid.*, p. 168.

A. A. Korsheninnikov, K. Yoshida, D. V. Aleksandrov, N. Aoi, Y. Doki, N. Inabe, M. Fujimaki, T. Kobayashi, H. Kumagai, C.-B. Moon, E. Yu. Nikolskii, M. M. Obuti, A. A. Ogloblin, A. Ozawa, S. Shimoura, T. Suzuki, I. Tanihata, Y. Watanabe, and M. Yanokura: "Experimental Study of ^{8}He + p Elastic and Inelastic Scattering", *ibid.*, **B316**, 38 (1993).

O. Kamigaito, H. Sakaguchi, M. Nakamura, S. Hirata, H. Togawa, T. Nakano, M. Yosoi, M. Ieiri, T. Ichihara, H. M. Shimizu, Y. Nakai, and S. Kobayashi: "Inelastic Scattering of Protons, ^{3}He, and ^{4}He at 30 MeV/Nucleon from ^{166}Er and ^{176}Yb and Quadrupole Moments of the Optical Potential", *Phys. Rev. C*, **45**, 1533 (1992).

T. Ohnuma, K. Hatanaka, S. I. Hayakawa, M. Hosaka, T. Ichihara, S. Ishida, S. Kato, T. Niizeki, M. Ohura, H. Okamura, H. Orihara, H. Sakai, H. Shimizu, Y. Tajima, H. Toyokawa, H. Yoshida, and M. Yosoi: "(d,^{2}He) Reactions at Ed=260 MeV as a Possible Probe to Nuclear Spin-excitation", *ibid.*, **47**, 648 (1993).

T. Suzuki, M. Fujimaki, S. Hirenzaki, N. Inabe, T. Kobayashi, T. Kubo, T. Nakamura, Y. Watanabe, and I. Tanihata: "Search for a Bound State of a Negative Pion and Neutrons in ^{18}O + Be Collisions", *ibid.*, p. 2673.

N. Fukunishi, T. Otsuka, and I. Tanihata: "Neutron-Skin and Proton-Skin Formations in Exotic Nuclei Far from Stability", *ibid.*, **48**, 1648 (1993).

S. Kim and S. Ohta: "QCD Thermodynamics with Eight Staggered Quark Flavors on a $16^3 \times 6$ Lattice", *Phys. Rev. D*, **46**, 3607 (1992).

H. Toki, D. Hirata, I. Tanihata, K. Sumiyoshi, and Y. Sugahara: "Relativistic Many Body Theory for Un-

stable Nuclei", Proc. China-Japan Joint Nucl. Phys. Symp. on Recent Topics on Nuclear Physics, Nov. 1992, Tokyo, p. 206 (1992).
H. Suganuma and T. Tatsumi: "Chiral Symmetry and Quark-Antiquark Pair Creation in the Strong Color-Electromagnetic Field", *Prog. Theor. Phys.*, **90**, 379 (1993).
K. Nagamine: "Slow μ^+ and μ^- Beam Production and the Next Generation of Muon Science", *Springer Proc. Phys.*, **59**, 55 (1992).
K. Nagamine: "Condensed Matter Studies with Polarized Bound Negative Muons", *ibid.*, p. 73.
H. Sato: "An Application of Multi-Precision Arithmetic in Physics: Nucleus as a Canonical Ensemble", *Trans. Inf. Proc. Soc. Jpn.*, **34**, 391 (1993).
T. Murakami, Y. Gono, A. Ferragut, Y. H. Zhang, K. Morita, A. Yoshida, M. Ogawa, M. Nakajima, B. J. Min, J. Kumagai, M. Oshima, T. Morikawa, M. Sugawara, and H. Kusakari: "High-spin Isomeric State in ^{144}Pm", *Z. Phys.*, **A345**, 123 (1993).
K. Nagamine: "Muon Science Research with Pulsed Muons at UT-MSL/KEK", *ibid.*, **C56**, 215 (1992).
K. Ishida and K. Nagamine: "Muon Facility Plans Towards JHP", *ibid.*, p. 296.

3. Atomic and solid-state physics

Y. Kanai, H. Sakaue, T. Kambara, Y. Awaya, N. Nakamura, S. Kitazawa, M. Nagata, S. Ohtani, H. Suzuki, T. Takayanagi, T. Nabeshima, T. Negishi, and K. Wakiya: "Doubly-Excited States of He-like and Be-like Ions in Highly-Charged Ions", AIP Conf. Proc., **274**, (6th Int. Conf. on the Physics of Highly Charged Ions), p. 63 (1993).
Y. Kanai, T. Kambara, M. Oura, Y. Zou, S. Kravis, and Y. Awaya: "Binary Encounter Peaks for 0° Electrons in Collisions of 0.8 MeV/amu Bi^{q+} with H_2 and He", *ibid.*, p. 135.
H. Shibata, T. Tonuma, T. Matsuo, H. Kumagai, and H. Tawara: "Multiply Charged Ions from Gaseous and Frozen CF_4 and SF_6 Produced by Energetic Heavy Ion Impact", *ibid.*, p. 335.
Y. Matsuo, H. Maeda, and M. Takami: "Gas Phase Ion-Molecule Reaction in an RF Ion Trap: Reactivity of the 5d Transition Series of Metal Ions (Lu^+, Hf^+, Ta^+, and W^+) with O_2", *Chem. Phys. Lett.*, **201**, 341 (1993).
R. Kadono and R. F. Kiefl: "Muon Diffusion in Solids", *Defect and Diffusion Forum*, **95/98**, 279 (1993).
E. Yagi: "Solid Krypton Precipitates in Kr-Implanted Aluminium", *ibid.*, p. 381.
Y. Matsuo, H. Maeda, and M. Takami: "High Resolution Laser Spectroscopy of Metallic Atoms and Molecules: Storage of Singly and Double Charged Ions Transferred from Externally Generated Laser Plasmas", *Hyperfine Interact.*, **74**, 269 (1992).
Y. Awaya and T. Kambara: "Studied of Atomic Physcis at RIKEN", *Int. J. PIXE*, **2**, 233 (1993).
N. Toshima: "Role of Projectile Continuum States in the Ionization of Atomic Hydrogen by High-Energy Ion Impact", *J. Phys.*, **B25**, L635 (1992).
H. Tawara, T. Hayaishi, T. Koizumi, T. Matsuo, K. Shima, T. Tonuma, and A. Yagishita: "Production of Multiply Charged Xe^{i+} Ions via Photoionization and Exitation in L-edge Region", *ibid.*, p. 1467.
N. Toshima: "Convergence of the Perturbation Series for High-Energy Electron Capture", *ibid.*, **B26**, L281 (1993).
K. Ando, Y. Zou, S. Kohmoto, T. Kambara, Y. Awaya, T. Tonuma, T. Niizeki, and S. Tsurubuchi: "Lifetimes of $2p^53p$ and $2p^53d$ Levels in Ti XIII", *J. Spectrosc. Soc. Jpn.*, **41**, 370 (1992).
T. Minowa, H. Katsuragawa, and H. Komatsu: "Resonance Ionization Spectroscopy of Molybdenum and its Application to a Pure Ion Source", *Nucl. Instrum. Methods Phys. Res.*, **B72**, 255 (1992).
T. Okada, K. Asai, N. Yamada, T. Matsumoto, Y. Yamada, and Y. Kodama: "^{57}Fe Mössbauer Studies of YBa_2 $(Cu_{1-x}Fe_x)_4O_8$", *ibid.*, **B76**, 338 (1993).
M. Sataka, M. Imai, Y. Yamazaki, K. Komaki, K. Kawatsura, Y. Kanai, and H. Tawara: "Binary Peak Electrons Observed at 0° for 2–4 MeV/u F^{q+}, Si^{q+} and Ni^{q+} Ions in Collisions with a He Target", *ibid.*, **B79**, p. 81.
R. Kadono: "Progress in Experimental Studies of Muon Diffuion", in Perspectives of Meson Science, eds. T. Yamazaki, K. Nakai, and K. Nagamine, North Holland, Amsterdam, p. 113 (1992).
H. Qui, A. Kosuge, H. Nakai, S. Yugo, M. Hashimoto, G. Safran, B. Pecz, B. Barna, E. Yagi, and H. Maruyama: "Effect of Bias-Voltage on Structural and Physical Properties of Ni Film DC Sputter-Deposited on Si(100) and SiO_2", Proc. 2nd Int. Symp. on Sputtering and Plasma Processes, ed. E. Kusano and H. Kitahara, ISSP'93 Committee, Tokyo, p. 207 (1993).
E. A. G. Armour, D. M. Lewis, and S. Hara: "Calculations of the Deexcitation Rate of $dt\mu$ within the Muonic Quasimolecule $(dt\mu)dee$", *Phys. Rev. A*, **46**, 6888 (1992).
H. Tawara, T. Tonuma, H. Kumagai, and T. Matsuo: "Ions Produced from Condensed CO Target under Energetic Ion Impact", *ibid.*, **47**, 1528 (1993).
A. Igarashi and N. Toshima: "Second-Order Born Cross Sections for Positronium Formation in Positron-Hydrogen Collisions", *ibid.*, p. 2386.
K. Hino: "Double Photoionization of He by High-Energy Photon Impact", *ibid.*, p. 4845.
K. Hino, T. Ishihara, F. Shimizu, N. Toshima, and J. H. McGuire: "Double Photoionization of Helium Using Many-Body Perturbation Theory", *ibid.*, **48**, 1271 (1993).
T. Kambara, Y. Awaya, and Y. Kanai: "Multiple Inner-Shell Ionization of Target Atoms by High-Energy Heavy-Ion Impact", *Radiat. Eff. Def. Solids*, **126**, 41 (1993).

Y. Zou, Y. Awaya, T. Kambara, Y. Kanai, M. Oura, K. Ando, A. Hitachi, and S. Kravis: "Foil Target Element and Incident Energy Dependence of Multiple Inner Shell Vacancy Production of Projectile Ar Ions", *ibid.*, p. 87.

H. Katsuragawa, M. Kubota, T. Minowa, and H. Komatsu: "A Simple and Efficient Pulsed-Heating Atomic Beam Source for Resonance Ionization Spectroscopy", *Rev. Sci. Instrum.*, **64**, 265 (1993).

4. Radiochemistry, radiation chemistry, and radiation biology

Y. Itoh and H. Murakami: "Defect Study on Electron Irradiated GaAs by Means of Positron Annihilation", *Appl. Phys.*, **A57**, 1 (1993).

Y. Itoh, H. Murakami, and A. Kinoshita: "Positron Annihilation in Porous Silicon", *Appl. Phys. Lett.*, **63**, 15 (1993).

T. Kanai, S. Minohara, T. Kohno, M. Sudou, E. Takada, F. Soga, K. Kawachi, A. Fukumura, and F. Yatagai: "Irradiation of 135 MeV/u Carbon and Neon Beams for Studies of Radiation Biology", HIMAC004 CNIRS-M-91, p. 1 (1993).

K. Kimura: "Depth and Time Resolved Dynamics for Excited States in Ion Track", KEK Proc. 7th Rad. Detect. Use, 93-8, p. 153 (1993).

K. Kimura: "Depth Resolved Dynamics of Ion-Tracks: Correlation between VUV- and UV-Luminescences from Near-liquid and Liquid Helium Irradiated with 4 MeV/amu N-ions", *Nucl. Instrum. Methods Phys. Res.*, **A327**, 34 (1993).

K. Nakagawa, K. Kimura, and A. Ejiri: "Photoionization Quantum Yield of TMAE (tetrakisdimethylaminoethylene) in Supercritical Xenon Fluid", *ibid.*, p. 60.

K. Kimura: "Track-Depth Resolved Dynamics of Helium Excimers in 4 MeV/amu N-ion Tracks in Near-liquid and Liquid Helium", *Phys. Rev. A*, **47**, 327 (1993).

Y. Ohkubo, Y. Kobayashi, K. Asai, T. Okada, and F. Ambe: "Time-Differential Perturbed-Angular-Correlation and Emission Mössbauer Studies on ^{99}Ru Arising from ^{99}Rh in Fe_3O_4", *Phys. Rev. B*, **47**, 11954 (1993).

K. Kimura and J. Wada: "LET-dependent Competition between Radiative and Nonradiative Annihilations of Core Holes Produced by Ion Irradiation of BaF_2 Single Crystal", *ibid.*, **48**, 15535 (1993).

M. Matsushima, T. Kojima, K. Ogura, H. Yamada, T. Takahashi, T. Doke, and S. Nagaoka: "Determination of Cosmic HZE Particle' Trajectories Using Image Analysis", Proc. 8th Symp. on Image Sensing Technologies on Industry in Japan, p. 63 (1993).

K. Kimura and H. Kumagai: "Lifetime Shortening and Quenching of Excitons of BaF_2 Single Crystal Created by Heavy-Ion Induced High-Density Excitation", *Rad. Eff. Def. Solids*, **126**, 45 (1993).

T. Kanai, T. Kohno, S. Minohara, M. Sudou, E. Takada, F. Soga, K. Kawachi, and A. Fukumura: "Dosimetry and Measured Differential W Values of Air for Heavy Ions", *Radiat. Res.*, **135**, 293 (1993).

5. Material analysis

J. Kawai, K. Nakajima, K. Maeda, and Y. Gohshi: "L X-Ray Line Shape of Copper(II) Compounds and Their Covalency", *Adv. in X-Ray Analysis*, **35**, 1107 (1992).

J. Kawai, K. Maeda, and T. Yamane: "Imaging Plate X-Ray Spectrometer for High Resolution PIXE", *Anal. Sci.*, **9**, 179 (1993).

S. Adachi, K. Takemoto, Y. Sasa, and K. Maeda: "PIXE Analysis of Hilar Gland for the Evaluation of Personal History of Exposure to Environmental Contaminant", *Int. J. PIXE*, **2**, 453 (1992).

T. Hanada, M. Mogi, J. Kawai, K. Maeda, Y. Sasa, and M. Uda: "Nickel Lα Spectra Measured by a High Resolution Particle Induced X-Ray Emission Spectrometer", *Nucl. Instrum. Methods Phys. Res.*, **B75**, 35 (1993).

K. Ishii, K. Maeda, M. Takami, Y. Sasa, M. Uda, and S. Morita: "Continuous Background in Heavy-Ion Induced X-ray Emission", *ibid.*, p. 73.

Y. Nishide, E. Hayashi, K. Maeda, Y. Sasa, and M. Uda: "PIXE Analysis of Calcified Tissue by Use of a Combined X-Ray Absorber", *ibid.*, p. 200.

K. Suzuki, K. Maeda, Y. Sasa, A. Okada, K. Sakamoto, and T. Ozawa: "Application of PIXE to Source Identification of Kosa Aerosol", *ibid.*, p. 317.

M. Uda, T. Tsunokami, R. Murai, K. Maeda, I. Harigai, Y. Nakayama, S. Yoshimura, T. Kikuchi, K. Sakurai, and Y. Sasa: "Quantitative Analysis of Ancient Egyptian Pigments by External PIXE", *ibid.*, p. 476.

K. Kakihara, S. Gohhara, T. Nishijima, S. Matsuo, S. Itoh, and K. Maeda: "Metal Analysis by PIXE in the Liver Tissure from Patients with Liver Diseases", *ibid.*, p. 521.

K. Maeda, Y. Sasa, M. Takami, and M. Uda: "Determination of X-Ray Take-off Angle from the L/K X-Ray Take-off Angle from the L/K X-Ray Intensity Ratio PIXE Analysis of a Nonflat Target", *ibid.*, **B77**, 137 (1993).

K. Kanazawa, M. Yanokura, and M. Aratani, and H. Akiyama: "Hydrogen Depth Profile of Al-alloy Vacuum Chamber Exposed to Synchrotron Radiation", *Vacuum*, **44**, 7 (1993).

VIII. LIST OF PREPRINTS

1993

RIKEN-AF-NP

141 S. Hirenzaki, T. Suzuki, and I. Tanihata: "A General Formula of the Coalescence Model"

142 V. A. Chrchin and V. A. Tsarev: "On a Nonstationary Quantum Mechanical Origin of Cold Nuclear Fusion"

143 V. A. Tsarev: "Cold Fusion Researches in Russia"

144 V. A. Tsarev: "Lebedev Physical Institute Group Researches in the Field of Long-baseline Neutorinos"

145 S. Ohta: "Large Scale Numerical Simulation of the Three-state Potts Model"

146 T. Ichihara, Y. Fuchi, K. Hatanaka, M. Hosaka, S. Ishida, S. Kato, H. Kawashima, S. Kubono, S. Miyamoto, T. Niizeki, H. Ohnuma, H. Okamura, H. Orihara, N. Sakamoto, S. Takaku, Y. Tajima, M. H. Tanaka, H. Toyokawa, T. Yamamoto, M. Yosoi, and M. Ishihara: "^{12}C(^{12}C, ^{12}N) ^{12}B Charge-exchange Reaction at E/A = 135 MeV"

147 K. Tanaka, W. Bentz, and A. Arima: "EOS and Fermi-Liquid Properties in the 1/N Expansion of a Relativistic Many-body Theory"

148 A. A. Korsheninnikov and T. Kobayashi: "Main Mechanisms in Fragmentation of the Exotic Nucleus ^{6}He"

149 M. Oshima, T. Morikawa, H. Kusakari, N. Kobayashi, M. Sugawara, Y. H. Zhang, A. Ferragut, S. Ichikawa, N. Shinohara, Y. Nagame, M. Shibata, Y. Gono, and T. Inamura: "Double-gamma Vibrational States in ^{168}Er and ^{192}Os"

150 Y. Gono, T. Murakami, T. Morikawa, A. Ferragut, Y. H. Zhang, K. Morita, A. Yoshida, H. Kumagai, M. Oshima, H. Kusakari, M. Sugawara, M. Ogawa, M. Nakajima, S. Mitarai, A. Odahara, E. Ideguchi, T. Shizuma, M. Kidera, J. C. Kim, S. J. Chae, and B. J. Min: "High-Spin Isomers and High-Spin Isomer Beams"

151 M. Mizoguchi, S. Hirenzaki, and H. Toki: "Microscopic Kaonic Atom Optical Potential in Finite Nuclei with Lambda(1405) and Sigma(1385) Resonances"

152 D. Hirata: "Study of Unstable Nuclei with the Relativistic Mean Field Theory"

153 N. Fukunishi, T. Otsuka, and I. Tanihata: "Neutron-Skin and Proton-Skin Formations in Exotic Nuclei Far From Stability"

154 S. Ohta: "Phases of the Three-state Potts Model in Three Spatial Dimensions"

155 A. A. Korsheninnikov, K. Yoshida, D. V. Aleksandrov, N. Aoi, Y. Doki, N. Inabe, M. Fujimaki, T. Kobayashi, H. Kumagai, C. -B. Moon, E. Yu. Nikolskii, M. M. Obuti, A. A. Ogloblin, A. Ozawa, S. Shimoura, T. Suzuki, I. Tanihata, Y. Watanabe, and M. Yanokura: "Observation of ^{10}He"

156 A. A. Korsheninnikov, K. Yoshida, D. V. Aleksandrov, N. Aoi, Y. Doki, N. Inabe, M. Fujimaki, T. Kobayashi, H. Kumagai, C. -B. Moon, E. Yu. Nikolskii, M. M. Obuti, A. A. Ogloblin, A. Ozawa, S. Shimoura, T. Suzuki, I. Tanihata, Y. Watanabe, and M. Yanokura: "Experimental Study of the ^{8}He + p Elastic and Inelastic Scattering"

157 I. Tanihata: "Study of Light Exotic Nuclei Using Radioactive Nuclear Beams"

158 T. Kobayashi: "Projectile Fragmentation of Exotic Nuclear Beams"

A. A. Korsheninnikov, K. Yoshida, D. V. Aleksandrov, N. Aoi, Y. Doki, N. Inabe, M. Fujimaki, T. Kobayashi, H. Kumagai, C. -B. Moon, E. Yu. Nikolskii, M. M. Obuti, A. A. Ogloblin, A. Ozawa, S. Shimoura, T. Suzuki, I. Tanihata, Y. Watanabe, and M. Yanokura: "Experimental Study of Neutron Rich Helium Isotopes"

D. Hirata, H. Toki, I. Tanihata, K. Sumiyoshi, Y. Sugahara, and R. Brockmann: "Relativistic Mean Field Theory for Unstable Nuclei"

A. Ozawa, T. Kobayashi, H. Sato, I. Tanihata, O. Yamakawa, K. Omata, K. Sugimoto, N. Takahashi, T. Shimoura, D. Olson, W. Christie, and H. Wieman: "Interaction Cross Sections and Radii of Mass Number A = 17 Isobars (^{17}N, ^{17}F, and ^{17}Ne)"

T. Nakamura, T. Kobayashi, M. Fujimaki, N. Inabe, T. Kubo, T. Suzuki, I. Tanihata, Y. Watanabe, A. Yoshida, T. Teranishi, N. Aoi, Y. Doki, M. Ishihara, S. Shimoura, N. Iwasa, K. Katori, and K. Abe: "Coulomb Dissociation of ^{11}Be"

159 T. Ichihara, T. Niizeki, H. Okamura, H. Ohnuma, H. Sakai, Y. Fuchi, K. Hatanaka, M. Hosaka, S. Ishida, K. Kato, S. Kato, H. Kawashima, S. Kubono, S. Miyamoto, H. Orihara, N. Sakamoto, S. Takaku, Y. Tajima, M. H. Tanaka, H. Toyokawa, T. Uesaka, T. Yamamoto, T. Yamashita, M. Yosoi, and M. Ishihara: "Spin-Isospin Resonances Observed in the (d, ^{2}He) and (^{12}C, ^{12}N) Reactions at E/A = 135 MeV"

160 K. Tanaka: "Quasiparticle Properties and the Dynamics of High-density Nuclear Matter"

IX. PAPERS PRESENTED AT MEETINGS

1. Accelerator development and accelerator physics

M. Hara: "Photon Beam Characteristics from Insertion Device Sources of the SPring-8", JASRI Microbeam Formation Subcommittee 7th Study Meeting, Tokyo, Jan. (1992).

M. Hara: "Characteristics of Photon at SPring-8", SPring-8 Workshop on Atomic Physics at High Brilliance Synchrotron Radiation Facilities, Himeji, Mar. (1992).

M. Hara: "SPring-8, A Challenge to Highly Brilliant Photon Source", Symp. on Charged Particle Optics, Tsukuba, July (1992).

H. Ego, M. Hara, K. Inoue, Y. Kawashima, and Y. Ohashi: "RF System of the Storage Ring for SPring-8", 15th Int. Conf. on High Energy Accelerators, Hamburg, Germany, July (1992).

H. Ego, M. Hara, K. Inoue, Y. Kawashima, and Y. Ohashi: "High Power Test of the Storage Ring RF System for SPring-8", *ibid.*

M. Hara: "SPring-8 Project", Seminar at Synchrotron Trieste, Trieste, Italy, July (1992).

H. Ego, M. Hara, K. Inoue, Y. Kawashima, Y. Ohashi, H. Suzuki, I. Takeshita, and H. Yonehara: "High Power Test of Single Cell Cavities for SPring-8", 17th Linear Accelerator Meet. in Japan, Sendai, Sept. (1992).

H. Ego, M. Hara, K. Inoue, Y. Kawashima, Y. Ohashi, H. Suzuki, and H. Yonehara: "On the Performances of an Optical Fiber and Related Modules for the Timing System of the SPring-8", Fall Meet. Phys. Soc. Jpn., Niigata, Oct. (1992).

H. Ego, M. Hara, K. Inoue, K. Kawashima, Y. Ohashi, H. Suzuki, I. Takeshita, and H. Yonehara: "RF System for the SPring-8 Storage Ring", APS Meet. on RF System for RF Workshop, Argonne, U.S.A., Sept. (1992).

M. Hara: "RF System for the SPring-8 Storage Ring", Int. Advisory Committee of the SPring-8, Himeji, Nov. (1992).

H. Ego, M. Hara, K. Inoue, Y. Kawashima, Y. Ohashi, H. Suzuki, I. Takeshita, and H. Yonehara: "Status of the SPring-8 RF System", 3rd Joint Symp. on Synchrotron Radiation Sources, Pohang, Korea, Nov. (1992).

M. Hara: "Light Source Performance of SPring-8", JASRI 7th Subcommittee of Microbeam Formation, Tokyo, Mar. (1993).

A. Goto: "RIKEN Cyclotron", 2nd Meet. on Biological Effect of High LET Particle Beams, Tokyo, Mar. (1993).

H. Okamura, H. Sakai, N. Sakamoto, T. Uesaka, S. Ishida, H. Otsu, T. Wakasa, K. Hatanaka, T. Kubo, N. Inabe, K. Ikegami, J. Fujita, M. Kase, A. Goto, and Y. Yano: "Development of the RIKEN Polarized Ion Source", Int. Workshop on Polarized Ion Sources and Polarized Gas Targets, Madison, U.S.A., May (1993).

K. Watanabe, S. H. Be, Y. Oikawa, H. A. Sakaue, C. Y. Xu, S. Yokouchi, Y. Wang, S. Takahashi, M. Tsuchiya, and Y. Yanagi: "Vacuum Chamber and Crotch Absorber for the SPring-8 Storage Ring Vacuum System", Particle Accel. Conf., Washington, D.C., U.S.A., May (1993).

H. Ego, M. Hara, Y. Kawashima, Y. Ohashi, T. Ohshima, H. Suzuki, I. Takeshita, and H. Yonehara: "Higher Order Modes of the Single Cell Cavity for the SPring-8", 9th Symp. on Accelerator Sci. Tech., Tsukuba, Aug. (1993).

K. Kumagai and S. Matsui: "The Injection Septum Magnets of the SPring-8 Storage Ring", 13th Int. Conf. on Magnet Technology, British Columbia, Canada, Sept. (1993).

H. Ego, M. Hara, Y. Kawashima, Y. Ohashi, H. Suzuki, and H. Yonehara: "Phase Stabilized Fiber Optic Links for the SPring-8 RF Reference Distribution", Fall Meet. Phys. Soc. Jpn., Kochi, Oct. (1993).

Y. Yano: "Present Status and Future Project of RARF (RIKEN)", 5th China-Japan Joint Symp. on Accel. for Nucl. Sci. and Their Applications, Osaka, Oct. (1993).

A. Goto, Y. Miyazawa, O. Kamigaito, T. Nakagawa, M. Hemmi, T. Chiba, M. Kase, N. Inabe, and Y. Yano: "Upgrade Project of the RILAC", *ibid.*

K. Watanabe, K. Hayashi, T. Hanasaka, K. Yano, and S. H. Be: "Outgassing of Stainless Steel and Copper Due to Electron-Stimulated Desorption", Vacuum Conf., Tokyo, Oct. (1993).

Y. Yano: "The Present Status and Future Plan of RIKEN Accelerator Research Facility, Japan", 3rd Natl. Seminar on Phys. and Technol. of Particle Accelerators and Their Applications, Calcutta, India, Nov. (1993).

2. Nuclear physics and nuclear instrumentation

S. Takagi, T. Nakamura, F. Makino, T. Kohno, and N. Shiono: "Observation of Damage on IC Devices in the Earth's Radiation Belt", 18th ISTS, Kagoshima, May (1992).

K. Nagamine and P. W. Williams: "Muon Science Program in RIKEN-RAL Collaboration", Japan-U.K. Seminar on Science and Technology, London, U.K., Oct. (1992).

K. Asahi: "Nuclear Moments Measured with Polarized Projectile Fragments", RIKEN Symp. on Nuclear Spectroscopy with Unstable Nuclear Beams, Wako, Nov. (1992).

K. Yoshida, J. Kasagi, H. Hama, M. Sakurai, M. Kodama, K. Furutaka, K. Ieki, W. Galster, T. Kubo, M. Ishihara, and A. Galonsky: "Disappearance of

the Giant Dipole Resonance in Hot Nuclei Produced in ^{40}Ar Induced Reaction", Japan-China Joint Nuclear Physics Symp. on Recent Topics on Nuclear Physics, Tokyo, Nov./Dec. (1992).

H. Toki, D. Hirata, I. Tanihata, K. Sumiyoshi, and Y. Sugahara: "Relativistic Many Body Theory for Unstable Nuclei", *ibid.*

S. Hirenzaki and H. Toki: "Structure and Formation of Deeply Bound Pionic Atoms", *ibid.*

K. Asahi, H. Okuno, H. Ueno, H. Sato, M. Adachi, T. Kubo, T. Nakamura, N. Inabe, A. Yoshida, Y. Ohkubo, T. Ichihara, M. Ishihara, T. Shimoda, H. Miyatake, and N. Takahashi: "Spin Polarization by Abrasion Process in Intermediate-energy Heavy-ion Collision and Its Application", *ibid.*

T. Matsuzaki and K. Ishida: "Present Status of Construction of RIKEN-RAL Muon Facility", RIKEN Symp. on Muon Science 1992, Wako, Dec. (1992).

K. Tanaka: "Fermi-Liquid Properties of Nuclear Matter in a Relativistic Many-Body Theory", Workshop on Relativistic Many-Body Methods for Bound Systems of Hadrons, Kyoto, Dec. (1992).

T. Ichihara: "RIKEN SMART Spectrograph: Overview, Detector and Recent Experiment", S800 Workshop on Focal Plane Detectors, Michigan, U.S.A., Jan. (1993).

K. Nagamine: "Present and Future of Muon Catalyzed Nuclear Fusion", Workshop on Nuclear Waste Transmutation Using Particle Beams, Tokai, Jan. (1993).

H. Sato: "Systematics of Isotope Production Rates: Fission Products and Their Barrier Penetration", 2nd Meet. on Nuclear Incineration, Tokai, Jan. (1993).

T. Matsuzaki: "Present Status of SLOW Facility", RIKEN Symp. on Non Nucl. Phys. Res. by RRC, Wako, Jan. (1993).

K. Nagamine: "Production and Application of Low-Energy Nuclear and Elementary Particle Beams", *ibid.*

I. Tanihata: "Physics with Radioactive Nuclear Beams", Brasilian Summer Seminar on Nuclear Physics, Sao Paulo, Brasil, Jan./Feb. (1993).

T. Matsuzaki: "R & D in International Collaboration on Muon Facility at High-Intensity Proton Accelerator-RIKEN-RAL", Workshop on Research and Developments for JHP and Related Scientific Topics, Tanashi, Mar. (1993).

K. Furutaka, J. Kasagi, T. Murakami, A. Yajima, Y. Akeboshi, K. Matsuda, Y. Futami, K. Yuasa-Nakagawa, T. Nakagawa, T. Murakami, S. Sawada, Y. Nakai, T. Motobayashi, A. Galonsky, and G. Bizard: "Measurements of Neutrons Emitted in Heavy-Ion Fusion Reaction", RCNP Workshop on Hot and Dense Nuclear Matter Produced in Heavy-Ion Reactions, RCNP, Osaka Univ., Osaka, Mar. (1993).

K. Asahi, H. Okuno, H. Ueno, H. Sato, H. Izumi, T. Sekine, M. Doi, M. Adachi, T. Kubo, T. Nakamura, N. Inabe, A. Yoshida, Y. Ohkubo, M. Ishihara, T. Shimoda, H. Miyatake, and N. Takahashi: "Spin Polarized Radioactive Nuclear Beam and Its Application", STA Forum for Multi-Disciplinary Researches, Kobe, Mar. (1993).

I. Tanihata: "Usage of High Energy Radioactive Nuclear Beams", *ibid.*

A. A. Korsheninnikov: "Study of Nuclei beyond the Dripline", *ibid.*

I. Tanihata: "Production and Use of Radioactive Beams for Nuclear Structure and Astrophysical Studies", JSPS-INS Spring School, Shimoda, Mar. (1993).

H. Sato: "Systematics of Isotope Production Rates: Mass Excess Dependence of Fission Products", RIKEN Int. Workshop on Heavy-Ion Reactions with Neutron-Rich Beams, Wako, Mar. (1993).

I. Tanihata: "Neutron Skins and Neutron Halos", 48th Ann. Meet. of Phys. Soc. Jpn., Sendai, Mar./Apr. (1993).

S. Hirenzaki, T. Suzuki, and I. Tanihata: "A General Formula of the Coalescence Model", *ibid.*

S. Ohta: "Large-Scale Numerical Simulation of Thermodynamic Systems with Global Z(3) Symmetry", *ibid.*

K. Tanaka and W. Bentz: "Quasiparticle Properties and the Dynamics of High-Density Matter in a Relativistic Many-Body Theory", *ibid.*

T. Murakami, Y. Gono, Y. H. Zhang, A. Ferragut, T. Morikawa, E. Ideguchi, K. Morita, A. Yoshida, M. Oshima, H. Kusakari, M. Sugawara, M. Ogawa, J. C. Kim, S. J. Chae, B. J. Min, S. Mitarai, A. Odahara, T. Shizuma, M. Kidera, and M. Shibata: "High Spin Isomer Beams", *ibid.*

T. Uesaka: "The Development of Polarized Deuteron Ion Source in RIKEN", *ibid.*

A. Yoshida, T. Fukuda, T. Sekine, Y. Watanabe, K. Kimura, H. Okuno, H. Ueno, H. Izumi, Y. Mizoi, M. Tanikawa, I. Nomura, K. Asahi, M. Ishihara, S. Shimoura, T. Nakamura, T. Kubo, and H. J. Kim: "Subbarrier Fusion with Neutron-Rich Nuclear Beams", *ibid.*

M. Tohyama: "Diffusion Coefficient for Nuclear Deformations", *ibid.*

K. Hasuike, H. Okada, T. Doke, J. Kikuchi, K. Masuda, and M. Suzuki: "Energy Resolution of TMA Doped Liquid Xe Pulsed Ionization Chamber", *ibid.*

M. Suzuki, T. Takahashi, H. Kumagai, K. Agata, N. Takahashi, S. Kamiya, S. Hirasawa, S. Sugawara, and H. Kobayashi: "On the Development of a Single Neutron Sensitive Camera", *ibid.*

M. Wakasugi, W. G. Jin, T. T. Inamura, T. Murayama, T. Wakui, T. Kashiwabara, H. Katsuragawa, T. Ariga, T. Ishizuka, M. Koizumi, and I. Sugai: "Quadrupole Moment of ^{180}Ta", *ibid.*

K. Nagamine: "Construction of RIKEN-RAL Muon Facility", Workshop on Low Energy Muon Science,

Santa Fe, U.S.A., Apr. (1993).

I. Tanihata: "Study of Nuclei Far from the Stability Using Radioactive Nuclear Beams", Flerov Laboratory School-Seminar, Dubna, Russia, May (1993).

A. Ozawa, T. Kobayashi, H. Sato, I. Tanihata, O. Yamakawa, K. Omata, K. Sugimoto, N. Takahashi, T. Shimoda, D. Olson, W. Christie, and H. Wieman: "Interaction Cross Sections and Radii of Mass Number A=17 Isobars (^{17}N, ^{17}F, and ^{17}Ne)", 3rd Int. Conf. on Radioactive Nuclear Beams, Michigan, U.S.A., May (1993).

A. A. Korsheninnikov, K. Yoshida, D. V. Aleksandrov, N. Aoi, Y. Doki, N. Inabe, M. Fujimaki, T. Kobayashi, H. Kumagai, C.-B. Moon, E. Yu. Nikolskii, M. M. Obuti, A. A. Ogloblin, A. Ozawa, S. Shimoura, T. Suzuki, I. Tanihata, Y. Watanabe, and M. Yanokura: "Experimental Study of Neutron Rich Helium Isotopes", *ibid.*

D. Hirata, H. Toki, I. Tanihata, K. Sumiyoshi, Y. Sugahara, and R. Brockmann: "Relativistic Mean Field Theory for Unstable Nuclei", *ibid.*

K. Matsuta, A. Ozawa, Y. Nojiri, T. Minamisono, M. Fukuda, S. Momota, T. Ohtsubo, S. Fukuda, K. Sugimoto, I. Tanihata, K. Yoshida, K. Omata, J. R. Alonso, G. F. Krebs, and T. J. M. Symons: "Production and Polarization of Beta-emitting ^{43}Ti", *ibid.*

T. Nakamura, S. Shimoura, T. Kobayashi, T. Teranishi, H. Okuno, Y. Watanabe, A. Yoshida, N. Inabe, T. Suzuki, M. Fujimaki, K. Abe, N. Iwasa, T. Kubo, K. Katori, I. Tanihata, and M. Ishihara: "Coulomb Dissociation of ^{11}Be", *ibid.*

H. Toki: "Pion Absorption and the Properties of Delta in Nuclei", Int. Symp. on Delta Excitation in Nuclei at RIKEN, Tokyo, May (1993).

K. Nagamine: "RIKEN-RAL Muon Facility and Advanced μSR Research", Int. Conf. on Muon Spin Rotation, Maui, U.S.A., June (1993).

T. Kohno: "Observation of Large Proton Intensity Gradient at Geosynchronous Orbit on October 27–31, 1991 According to GMS-4 and GOES-7 Measurements", Int. Workshop on Space Radiation Environment: Empirical and Physical Models, Dubna, Russia, June (1993).

S. Hirenzaki and H. Toki: "Formation of Deeply Bound Pionic Atoms by (d, ^{3}He) Reactions", Particle and Nuclei XIII Int. Conf. (PANIC), Perugia, Italy, June/July (1993).

I. Tanihata: "Future Use of Radioactive Nuclear Beams", Gordon Conf. on Nuclear Chemistry, New Hampsure, U.S.A., July (1993).

T. Kohno and A. Struminsky: "Peculiarities of Solar Proton Spectrum in Stratosphere and Geostationary Orbit on 2–3 November 1992", 23rd Int. Cosmic Ray Conf., Calgary, Canada, July (1993).

K. Nagamine: "Science Research with Pulsed Muons–the First 12 Years and Next Future–", PSI Colloquim, Zurich, Swiss, Aug. (1993).

T. Ichihara: "Spin-isospin Resonances Observed in the (d, ^{2}He) and (^{12}C, ^{12}N) Reactions at E/A = 135 MeV", Gull Lake Nuclear Physics Conf. on Giant Resonances, Gull Lake, Michigan, U.S.A., Aug. (1993).

K. Nagamine: "Recent Muon Science Research in Japan", Heidelberg University Physics Colloquim, Heidelberg, Germany, Sept. (1993).

M. Suzuki, T. Takahashi, Y. Awaya, M. Oura, and T. Mizogawa: "A Gas Scintillation Proportional X-ray Imaging Chamber", 3rd London Conf. on Position-Sensitive Detectors, Brunel, U.K., Sept. (1993).

K. Nagamine: "Towards Ultra-High Fusion Density Muon Catalyzed Fusion", ICENES '93, Makuhari, Sept. (1993).

K. Nagamine: "Advanced Muon Catalyzed Fusion Research Program at RIKEN-RAL Facility", *ibid.*

K. Nagamine: "Overview of Muon Catalyzed Fusion Experiment", RIKEN Symp. on Muon Sci. 1993 (Muon Catalyzed Nuclear Fusion), Wako, Sept. (1993).

K. Nagamine: "Plans for μCF Experiment at RIKEN-RAL Muon Facility", *ibid.*

K. Nagamine: "Slow Muon Source Using μCF", *ibid.*

T. Motobayashi: "Comments on the Coulomb Dissociation", Workshop on Selected Topics in Nuclear Astrophysics, Tokyo, Sept. (1993).

I. Tanihata: "Physics with Radioactive Nuclear Beams", Int. School of Heavy Ion Physics, 3rd Course: Probing the Nuclear Paradigm, Erice-Sicily, Italy, Oct. (1993).

I. Tanihata: "How Well Did We Understand the Dripline?", 9th High-Energy Heavy-Ion Study, Berkeley Ca., U.S.A., Oct. (1993).

T. Motobayashi: "Multi-step Excitation Effects in the ^{14}O Coulomb Dissociation"; "Preliminary Results of the ^{8}B Coulomb Dissociation Related to the Reaction ^{7}Be(p,γ)^{8}B Producing Solar Neutrinos"; "Nuclear Breakup Contribution in the ^{16}O $\rightarrow^{12}$ C + α Dissociation", Workshop on Coulomb Dissociation of Light Nuclei, Strasbourg, France, Oct. (1993).

T. Nakamura: "Coulomb Dissociation of a Halo Nucleus", *ibid.*

S. Ohta: "First-Order Phase Transition with Global Z(3) and Z(4) Symmetry", 1993 Int. Symp. on Lattice Field Theory 'Lattice 93', Dallas, U.S.A., Oct. (1993).

T. Motobayashi: "Determination of Astrophysical Reaction Rates through the Coulomb Dissociation Method", 1993 Fall Meet. Phys. Soc. Jpn., Kochi, Sept./Oct. (1993).

N. Fukunishi: "Excitation of ^{9}Li Core in ^{11}Li", *ibid.*, Kochi, Oct. (1993).

K. Yoshida, I. Tanihata, T. Kobayashi, T. Suzuki, S. Shimoura, K. Sugimoto, K. Matsuta, S. Fukuda, H. Wieman, W. Christie, and D. Olson: "Coincidence Measurements for Neutrons and α Particles from the

Fragmentation of ^{6}He at 800 A MeV", *ibid.*

Y. Futami, S. Tomita, Y. Honjo, T. Mizota, H. Toyokawa, K. Matsuda, K. Furutaka, K. Yuasa-Nakagawa, J. Kasagi, T. Nakagawa, S. M. Lee, and W. Q. Shen: "Correlation between Fission Fragments and Light Particles in the Reactions ^{84}Kr + ^{27}Al, ^{56}Fe (E_L = 10.5 MeV/u)", *ibid.*

A. Odahara, Y. Gono, S. Mitarai, H. Tomura, E. Ideguchi, T. Shizuma, M. Kidera, M. Shibata, T. Morikawa, T. Kishida, Y. H. Zhang, A. Ferragut, K. Morita, A. Yoshida, T. Murakami, M. Oshima, H. Kusakari, M. Sugawara, B. J. Min, C. J. Kim, and S. J. Chae: "High Spin Isomer and Level Structure of ^{145}Sm", *ibid.*

T. Morikawa, T. Kishida, Y. H. Zhang, A. Ferragut, K. Morita, A. Yoshida, Y. Gono, S. Mitarai, A. Odahara, E. Ideguchi, T. Shizuma, M. Kidera, M. Shibata, T. Murakami, M. Oshima, H. Kusakari, M. Sugawara, B. J. Min, C. J. Kim, S. J. Chae, and S. A. Shin: "High Spin Isomer Beams", *ibid.*

E. Ideguchi, Y. Gono, T. Morikawa, and T. Kishida: "Simulation of a γ-ray Spectrum for a Segmented Ge Detector", *ibid.*

T. Ariga, M. Wakasugi, W. G. Jin, T. T. Inamura, T. Murayama, T. Wakui, H. Katsuragawa, T. Ishizuka, M. Koizumi, and I. Sugai: "Precise Measurement of Hyperfine Structure in ^{183}W with Laser-rf Double Resonance", *ibid.*

M. Suzuki, T. Takahashi, T. Mizogawa, M. Oura, and Y. Awaya: "On the Development of a Proportional Scintillation X-ray Imaging System", *ibid.*

A. Ozawa, I. Tanihata, T. Kobayashi, O. Yamakawa, K. Omata, H. Sato, D. Hirata, N. Takahashi, T. Shimoda, K. Sugimoto, D. Olson, W. Christie, and H. Wieman: "Interaction Cross Sections and Radii of Mass Number A = 17 Isobars (^{17}N, ^{17}F, and ^{17}Ne)", *ibid.*

N. Iwasa, T. Motobayashi, S. Shimoura, M. Gai, T. Delbar, Y. Watanabe, T. Kubo, N. Inabe, Y. Futami, K. Furutaka, M. Kurokawa, H. Murakami, Y. Ando, T. Teranishi, K. Harn, Z. Zhao, R. France, S. Shirato, J. Ruan, and M. Ishihara: "Measurement of the Reaction Cross Section of ^{7}Be(p,γ)^{8}B with ^{8}B Coulomb Dissociation Method", *ibid.*

T. Ichihara, T. Niizeki, H. Ohnuma, S. Ishida, T. Uesaka, H. Ogami, H. Okamura, H. Orihara, K. Kato, S. Kubono, M. Tanaka, Y. Fuchi, T. Yamamoto, T. Yamashita, and M. Ishihara: "Spin-Isospin Resonances Observed in the (^{12}C, ^{12}N) Reactions at E/A = 135 MeV", *ibid.*

T. Uesaka, H. Sakai, H. Okamura, S. Ishida, N. Sakamoto, H. Ohtsu, T. Wakasa, T. Ichihara, Y. Yano, K. Hatanaka, H. Ohnuma, T. Niizeki, and T. Yamamoto: "Analyzing Power Measurements for Deuteron Elastic Scatering (Ed = 270 MeV)", *ibid.*

T. Niizeki: "Spin-Isospin Excitation in Light Nuclei", *ibid.*

K. Matsuzaki: "Activation of Inorganic Scintillator YAP, GSO, and NAI", *ibid.*

M. Tohyama: "Giant Resonances in a Neutron Rich Nucleus", *ibid.*

H. Izumi, K. Asahi, H. Okuno, H. Ueno, K. Nagata, Y. Hori, M. Adachi, A. Yoshida, G. Liu, N. Nori, T. Sekine, H. Sato, M. Doi, M. Harada, and M. Ishihara: "Measurement of Electric Quadrupole Moments for Neutron-rich Nuclei ^{14}B and ^{15}B", *ibid.*

H. Kitagawa, Y. Nishino, S. Tadokoro, and T. Suzuki: "Distribution of Perturbative Gluon in the MIT Bag Model", *ibid.*

H. Kitagawa, A. Ozawa, and I. Tanihata: "Reaction Cross Sections of Light Mirror Nuclei (A = 17) in the Glauber Model", *ibid.*

K. Furutaka, J. Kasagi, T. Murakami, A. Yajima, Y. Akeboshi, K. Matsuda, Y. Futami, K. Yuasa-Nakagawa, T. Nakagawa, T. Murakami, S. Sawada, Y. Nakai, T. Motobayashi, A. Galonsky, and G. Bizard: "Measurements of Neutrons Emitted in ^{40}Ar + ^{116}Sn Reactions at E/A = 30, 37 MeV/u", *ibid.*

K. Tanaka: "Quasiparticle Properties and the Dynamics of High-Density Matter in a Relativistic Many-Body Theory II", *ibid.*

T. Nakamura, T. Teranishi, N. Aoi, Y. Doki, M. Ishihara, T. Kobayashi, M. Fujimaki, N. Inabe, T. Kubo, T. Suzuki, I. Tanihata, Y. Watanabe, A. Yoshida, S. Shimoura, N. Iwasa, K. Katori, and K. Abe: "Coulomb Dissociation of ^{11}Be", *ibid.*

S. Hirenzaki, N. Fukunishi, D. Hirata, and H. Kitagawa: "(^{3}He, t) Reactions on Unstable Nuclei", *ibid.*

H. Suganuma, H. Monden, S. Sasaki, and H. Toki: "Influence of the Abelian Monopole Condensation on the Chiral Condensate", *ibid.*

T. Horihata and N. Onishi: "Wobbling Motion by the Constrained HFB", *ibid.*

J. Chiba, D. Ashery, H. Ito, K. Kimura, Yu. T. Kiselev, S. Kouda, K. Miyano, T. Murakami, T. Nagae, Y. Nakai, M. Nomachi, S. Sawada, M. Sekimoto, Y. Sugaya, T. Suzuki, K. H. Tanaka, M. K. Vlasov, and Y. Yoshimura: "Subthreshold Antiproton Production in pA and dA Collisions III", *ibid.*

Y. Yoshimura, D. Ashery, H. Ito, J. Chiba, K. Kimura, Yu. T. Kiselev, S. Kouda, K. Miyano, T. Murakami, T. Nagae, Y. Nakai, M. Nomachi, S. Sawada, M. Sekimoto, Y. Sugaya, T. Suzuki, K. H. Tanaka, and M. K. Vlasov: "Subthreshold Antiproton Production in pA and dA Collisions IV", *ibid.*

H. Sato: "Systematics of Alpha Q-values: Potential Dependence of the Alpha Decay Life Time", Symp. on Science of Beams of Short Life Nuclei '93, Tokyo, Dec. (1993).

3. Atomic and solid-state physics

H. Katsuragawa, T. Minowa, M. Kubota, and H. Komatsu: "Resonance Ionization Spectroscopy of a Mo Atomic Beam Generated by a Laser Ablation", Fall Meet. Opt. Soc. Jpn., Kyoto, Nov. (1992).

K. Asahi: "Polarization Using the Projectile Fragmentation Reaction and Its Application to Solid State Physics", INS Symp. on Science with Short-lived Nuclear Beams, Tanashi, Jan. (1993).

A. Hitachi, J. A. LaVerne, and J. L. Kolata: "High Resolution Measurements of Heavy Ions by Allene-added Liquid Argon Ionization Chamber", Radiation Detection and Its Application, Tsukuba, Jan. (1993).

Y. Matsuo, H. Maeda, and M. Takami: "Ion-molecule Interaction and Spectroscopy in an rf Ion Trap", RIKEN Symp. on Laser Science (15th), Wako, Feb. (1993).

T. Kambara: "New Beams and Atomic Physics", STA Forum for Multi-Disciplinary Researches–Exploring New Researches with Radioactive Nuclear Beams and Muon Beams, Kobe, Mar. (1993).

Y. Awaya: "Summary Reports of Atomic Physics Session", *ibid.*

R. Kadono: "A Prospect of μSR in Condensed Matter Physics", *ibid.*

M. Sataka, M. Imai, Y. Yamazaki, K. Komaki, K. Kawatsura, Y. Kanai, and H. Tawara: "Ion Charge Dependence of Binary Encounter Electrons Peak", 48th Ann. Meet. Phys. Soc. Jpn., Sendai, Mar. (1993).

E. Yagi: "Introductory Talk to the Symposium on the Application of Nuclear Methods to the Studies of Defects and Impurities in Solids", *ibid.*

T. Okada, K. Asai, N. Yamada, T. Matsumoto, Y. Yamada, and Y. Kodama: "Mössbauer Study of $YBa_2(Cu_{1-x}Fe_x)_4O_8$ II", *ibid.*

R. Kadono, A. Matsushita, K. Nishiyama, and K. Nagamine: "Muon-induced Excition Luminescence in RbBr", *ibid.*

R. Kadono: "Anomalous Muonium State and Radiolysis", *ibid.*

Y. Matsuo, M. Wakasugi, H. Maeda, and M. Takami: "RF Ion Trap of Surface Implanted Elements Using Laser Ablation Method", *ibid.*

R. Kadono: "A Prospect of μSR in Condensed Matter Physics", *ibid.*

H. Qui, E. Yagi, and M. Hashimoto: "Effect of Bias-Voltage on Structure and Resistivity of Ni Films Prepared by DC Sputter-Deposition Method", 40th Ann. Meet. Jpn. Soc. Appl. Phys., Tokyo, Mar. (1993).

H. Qui, A. Kosuge, H. Nakai, S. Yugo, M. Hashimoto, G. Safran, B. Pecz, P. B. Barna, E. Yagi, and H. Maruyama: "Effect of Bias-Voltage on Structural and Physical Properties of Ni Films DC-Sputter-Deposited on Si(100) and SiO_2", 2nd Int. Symp. on Sputtering and Plasma Processes, Tokyo, May (1993).

R. Kadono, A. Matsushita, K. Nishiyama, and K. Nagamine: "Muon Radiolysis in Alkali Halides", Int. Conf. Muon Spin Rotation/Relaxation/Resonance, Maui, Hawaii, June (1993).

R. Kadono, S. Fujii, A. Matsushita, K. Nagamine, K. Nishiyama, and S. Tanigawa: "Quantum Diffusion of Muonium in GaAs with Shallow Donor Impurities", *ibid.*

R. Kadono, J. H. Brewer, K. Chow, S. R. Kreitzman, Ch. Niedermayer, T. M. Riseman, J. W. Schneider, and T. Yamazaki: "Critical Behavior of Electric Field Gradient in MnSi Probed by Muon Level-Crossing Resonance", *ibid.*

R. Kadono: "Muon Diffusion in Crystalline Solids", *ibid.*

Y. Kanai: "Status of Atomic Physics Research in Foreign Countries", RIKEN Symp. on Atomic Physics with Accelerators XII, Wako, June (1993).

H. Tawara, T. Tonuma, H. Kumagai, and T. Matsuo: "Multiply Charged Secondary Ions from Condensed Molecular Gas Targets under Highly Ionized Heavy Projectile Impact-Molecular Structure Effect", 18th Int. Conf. on Phys. of Electronic and Atomic Collisions, Aarhus, Denmark, July (1993).

T. Tonuma, H. Kumagai, T. Matsuo, H. Shibata, and H. Tawara: "Positively and Negatively Charged Clusters Produced from Frozen Oxygen, Nitrogen and Carbon Monoxide Molecules under Energetic Heavy Ion Impact", *ibid.*

H. Takagi, S. Hara, and H. Sato: "Off-the-energy-shell Effects in Dissociative Recombination of $H_2^+ + e$, H", *ibid.*

M. R. Harston, S. Hara, M. Kamimura, and I. Shimamura: "Corrections on Resonance Energies of Muonic Molecules $[(d+\mu)^+ - d^+]e^-e^-$ and $[(dd\mu)^+ - d^+]e^-e^-$", *ibid.*

E. G. Armour, C. P. Franklin, D. M. Lewis, and S. Hara: "Auger De-excitation within the Muonic Molecule, $[(dt\mu)dee]$", *ibid.*

T. Kambara, Y. Kanai, S. Kravis, Y. Nakai, M. Oura, and Y. Awaya: "Scattering Angle Dependent Measurements of Charge States of Projectile and Recoil Ions in 47 MeV Ar-Ar Collisions", *ibid.*

J. Z. Tang, S. Watanabe, and M. Matsuzawa: "Very Narrow Doubly Excited States of He by HSCC and MQDT Methods", *ibid.*

M. Oura, T. Kambara, Y. Kanai, S. Kravis, Y. Nakai, Y. Awaya, and B. D. DePaola: "Measurement of Radiative Electron Rearrangement X-rays from Projectile Ions Excited by a Carbon Foil", *ibid.*

H. Tawara, T. Tonuma, H. Kumagai, and T. Matsuo: "Secondary Ions Produced from Condensed Rare Gas Targets under Energetic Ion Impacts", 5th Workshop on Fast Ion-Atom Collisions, Debrecen, Hungary, July (1993).

Y. Awaya: "JAERI-RIKEN 8 GeV Synchrotron Radiation Facility–SPring-8", *ibid.*

M. Oura, Y. Awaya, T. Koizumi, Y. Itoh, S. Kravis, T. M. Kojima, M. Sano, M. Kimura, and K. Okuno: "Research and Development for Photoionization of Multiply Charged Ions at SPring-8", *ibid.*

T. Kambara: "Target Multiple Ionization in Hard and Soft Ion Atom Collisions", 18th Int. Seminar on Ion-Atom Collisions, Stockholm, Sweden, July (1993).

J. Z. Tang: "Doubly Excited States in the Photodetachment Spectra of H^-", 4th UK-Japan Seminar on the Theory of Atomic Collisions, Belfast, U.K., July (1993).

Y. Matsuo, M. Wakasugi, H. Maeda, and M. Takami: "Laser Spectroscopy of Trace Atoms in an Rf Ion Trap: Storage of Ions Produced by Laser Ablation of Implanted Atoms", Int. Symp. on Atomic Frequency Standards and Coherent Quantum Electronics, Nara, Aug. (1993).

M. Terasawa, T. Mitamura, T. Kohara, K. Ueda, H. Tsubakino, A. Yamamoto, Y. Awaya, T. Kambara, Y. Kanai, M. Oura, and Y. Nakai: "High Energy Heavy Ion Irradiation Effects on Electron Transport Property in $La_{2-x}Sr_xCuO_4$", 3rd IUMRS Int. Conf. on Advanced Materials, Tokyo, Aug. (1993).

S. Kravis, M. Oura, Y. Awaya, and K. Okuno: "An EBIS for Use with Synchrotron Radiation", 5th Int. Conf. on Ion. Sources, Beijing, China, Aug. (1993).

Y. Kanai: "Experiments by Low-velocity Highly Charged Ions", 18th Meet. Soc. for Atomic Collision, Koganei, Aug. (1993).

M. Suzuki, T. Takahashi, Y. Awaya, M. Oura, and T. Mizogawa: "A Proportional Scintillation X-ray Imaging Chamber and Its Performance", 3rd London Conf. on Positron-Sensitive Detectors, London, U.K., Sept. (1993).

H. Qui, H. Nakai, M. Hashimoto, H. Maruyama, E. Yagi, G. Safran, M. Adamik, and P. B. Barnas: "Effect of Bias-Voltage on Epitaxial Growth and Physical Properties of Ni Films DC-Sputter-Deposited on MgO(100)", 1993 Fall Meet. Jpn. Soc. Appl. Phys. Related Soc., Sapporo, Sept. (1993).

M. Hacke and E. Yagi: "Annealing Behaviour of Kr-Implanted Aluminium", 8th Int. Conf. on Surface Modification of Metals by Ion Beams, Kanazawa, Sept. (1993).

S. Sakamoto and K. Ishida: "Muon Transfer Experiment", RIKEN Symp. on Muon Science, Wako, Sept. (1993).

M. Kimura, N. Shimakura, N. F. Lane, S. Kravis, I. Shimamura, Y. Awaya, and K. Okuno: "Single- and Double Electron Capture in Collisions of Multiply Charged Ions, He^{2+}, $C^{q+}(q = 4, 5)$, and $Ar^{q+}(q = 6, 8)$ Ions with H_2 Molecules at eV Collision Energies", 46th Gaseous Electronics Conf., Montreal, Canada, Oct. (1993).

R. Kadono: "Dynamics of Hydrogenic Impurity (Muonium) in GaAs", 3rd Lattice Defect Forum on Frontier of Physics on Defects, Kurashiki, Oct. (1993).

R. Kadono, A. Matsushita, K. Nishiyama, K. Nagamine, S. Fujii, and S. Tanigawa: "Quantum Diffusion of Muonium in GaAs: Effect of Shallow Donor Impurities", 1993 Fall Meet. Phys. Soc. Jpn., Okayama, Oct. (1993).

E. Yagi and M. Hacke: "Annealing Behaviour of Kr-Implanted Aluminium", *ibid.*

T. Okada, K. Asai, N. Yamada, T. Matsumoto, Y. Yamada, and Y. Kodama: "Mössbauer Study of Oriented 124 Compound", *ibid.*

S. Hashimoto, T. Minowa, H. Komatsu, and H. Katsuragawa: "Resonance Ionization Spectroscopy of Fe", *ibid.*

Y. Matsuo and M. Takami: "Lifetimes of Lu^+ Excited and Meta-stable States in an rf Ion Trap", *ibid.*

M. Terasawa, T. Mitamura, T. Kohara, K. Ueda, H. Tsubakino, A. Yamamoto, Y. Awaya, T. Kambara, Y. Kanai, M. Oura, and Y. Nakai: "High Energy Heavy Ion Irradiation Effects on Electron Transport Property in $La_{1.85}Sr_{0.15}CuO_4$", *ibid.*

Y. Yamazaki, K. Komaki, T. Azuma, K. Kuroki, Y. Kakutani, K. Kawatsura, T. Kambara, Y. Kanai, M. Oura, Y. Nakai, and Y. Awaya: "Inverse Mott Scattering of Conduction Electrons in Ferromagnets by Fast Heavy Ions", *ibid.*

M. Sataka, M. Imai, Y. Yamazaki, K. Komaki, K. Kawatsura, Y. Kanai, H. Tawara, and D. R. Shultz: "Binary Peak Electrons at 0° for Multiple Charged Gold Ion in Collisions with He-atom", *ibid.*

Y. Kanai, T. Kambara, M. Oura, S. Kravis, Y. Awaya, and Y. Zou: "Ion Charge Dependence of Peak Energy for Binary Encounter Electrons", *ibid.*

T. Kambara, Y. Kanai, S. Kravis, Y. Nakai, M. Oura, and Y. Awaya: "Multiple Ionization of Target Ar Atom by 42 MeV Ar-Ion Collision", *ibid.*

M. Oura, T. Kambara, Y. Kanai, S. Kravis, Y. Nakai, Y. Awaya, and B. D. DePaola: "Study of Radiative Electron Rearrangement X-rays from Ti Ions", *ibid.*

M. Oura, S. Kravis, Y. Awaya, K. Okuno, and M. Kimura: "R&D of EBIS for Experiments Using Synchrotron Radiation", *ibid.*

T. Koizumi, T. Itoh, M. Oura, S. Kravis, M. Sano, M. Sekioka, T. Yamashita, and Y. Awaya: "Photoionization with 4d Electron Excitation of Ba^+", *ibid.*

K. Nagamine, K. Nishiyama, and R. Kadono: "Solid State Physics and Wide Applications Using Muons", RIKEN Symp. on Researches on Solid State Physics and Materials, Atomic Physics, Nuclear Chemistry, Biology and Medicine Using RIKEN Ring Cyclotron VII, Wako, Oct. (1993).

T. Kambara: "Future Possibilities in Atomic Physics with Heavy Ions", *ibid.*

M. Suzuki, T. Takahashi, Y. Awaya, M. Oura, T. Mizogawa: "On the Development of a Proportional Scintillation X-ray Imaging Chamber", Int. Workshop on Area Detectors, Harima Science Garden City, Hyogo, Nov. (1993).

M. Terasawa, T. Mitamura, T. Kohara, K. Ueda, H. Tsubakino, A. Yamamoto, Y. Awaya, T. Kambara, Y. Kanai, M. Oura, and Y. Nakai: "GeV Energy Heavy Ion Irradiation on Oxide Superconductor", Workshop for High Temperature Superconductivity, Tokai, Dec. (1993).

J. Z. Tang: "Spectra of Highly Excited States of He", Workshop for Quantum Chaos, Highly Excited Atom, and Highly Excited Molecule, Nagoya, Dec. (1993).

E. Yagi: "Research Activities by Using a Small Tandem Accelerator in RIKEN", Symp. Nucl. Research Lab. Fac. Eng., Univ. Tokyo, Tokyo, Dec. (1993).

E. Yagi: "Behaviour of Kr Atoms in Aluminium", IMR Tohoku Univ. Symp. on Behaviour of Hydrogen and Helium in Metals under Particle Irradiation, Sendai, Dec. (1993).

4. Radiochemistry, radiation chemistry, and radiation biology

A. Yokoyama, K. Takesako, T. Saito, H. Kusawake, H. Baba, Y. Ohkubo, A. Shinohara, and M. Furukawa: "Limiting Behavior in the Medium Energy Heavy-Ion Nuclear Reactions", Specialists' Meet. on Science and Engineering of Fission, Kumatori, Dec. (1992).

F. Yatagai: "Analysis of Biological Damages Induced by Heavy Ions", RIKEN Symp. on Researches on Solid State Physics and Materials, Atomic Physics, Nuclear Chemistry, and Biology and Medicine Using RIKEN Ring Cyclotron, Wako, Jan. (1993).

K. Kimura: "Depth and Time Resolved Dynamics for Excited States in Ion Track", Symp. on Radiation Detectors and Their Uses, Tsukuba, Jan. (1993).

S. Ambe, Y. Ohkubo, Y. Kobayashi, M. Iwamoto, M. Yanokura, H. Maeda, and F. Ambe: "Transport of Tc and Re through a Supported Liquid Membrane", Topical Symp. on the Behavior and Utilization of Technetium '93, Sendai, Mar. (1993).

K. Kimura: "Depth and Time Resolved Dynamics of Ion Tracks by Means of Luminescence Measurements", 48th Ann. Meet. Phys. Soc. Jpn., Sendai, Mar. (1993).

S. Ambe, Y. Ohkubo, Y. Kobayashi, M. Iwamoto, H. Maeda, M. Yanokura, and F. Ambe: "Study on Distribution of Radioactive Nuclides in Plants", 1993 Ann. Meet. Atomic Energy Soc., Kyoto, Mar. (1993).

Y. Minai, Y. Takahashi, M. K. Kubo, S. Toyoda, M. Ishibashi, H. Ohtsuka, S. Ambe, Y. Kobayashi, Y. Ohkubo, M. Iwamoto, M. Yanokura, H. Maeda, S. Shibata, N. Takematsu, F. Ambe, and T. Tominaga: "Multitracer Study on Dependence of Humate-Complex Stability on Ionic Radii and Charge of Metal Ion", 65th Natl. Meet. Chem. Soc. Jpn., (Spring), Tokyo, Mar. (1993).

Y. Kobayashi, S. Ambe, Y. Ohkubo, M. Iwamoto, H. Maeda, M. Yanokura, and F. Ambe: "Preparation of a Multitracer from Gold Foils Irradiated with Heavy Ions by Solvent Extraction", *ibid.*

K. Takesako, S. Watanabe, M. Kiriu, T. Saito, H. Kusawake, A. Yokoyama, H. Baba, Y. Ohkubo, A. Shinohara, E. Taniguchi, and M. Furukawa: "Study on Low- and Intermediate-Energy Heavy-Ion Induced Nuclear Reactions by Radiochemical Methods", *ibid.*

M. Watanabe, M. Suzuki, K. Suzuki, K. Nakano, F. Yatagai, and T. Kanai: "LET Dependency of Mutation Induction at the HGPRT Locus and Molecular Characterization of Mutations in Human Cells Irradiated with Accelerated Carbon Ions", Int. Seminar on Molecular Mechanisms in Radiation Mutagenesis and Carcinogenesis, Doorwerth, The Netherlands, Apr. (1993).

Y. Itoh, H. Murakami, and A. Kinoshita: "Characterization of Porous Silicon by Positron Annihilation", 4th Int. Workshop on Positron and Positronium Chemistry, Strasburg, France, June (1993).

K. Ando, S. Koike, S. Furukawa, M. Kimoto, M. Iizuka, T. Kiuchi, W. Shimizu, T. Sugita, C. C. Koo, T. Kanai, S. Matsushita, and F. Yatagai: "Saturation of Skin Damage after Accelerated Carbon Particles", Int. Congr. of Radiation Oncology, Kyoto, June (1993).

K. Kimura: "LET-dependent Competition between Radiative and Nonradiative Annihilations of Core Holes Produced by Ion Irradiation of BaF_2, Single Crystal", 15th Int. Conf. Atom. Phys. Sol., London, Canada, July (1993).

F. Ambe: "Usefulness of Multitracers", 30th Ann. Meet. Radioisot. Phys. Sci. Ind., Tokyo, July (1993).

M. Furukawa, A. Shinohara, E. Taniguchi, J. Kurachi, S. Kojima, T. Saito, Y. Ohkubo, and F. Ambe: "Production of Multitracer Nucleids by Intermediate-Energy Heavy-Ion Nuclear Reactions", *ibid.*

H. Harakawa, J. Kawarada, T. Bamba, Y. Saito, K. Kimura, S. Ambe, Y. Ohkubo, Y. Kobayashi, M. Iwamoto, H. Maeda, M. Yanokura, and F. Ambe: "Determination of Elements Distribution for NAFION Resin by Using Multitracer Solution", *ibid.*

S. Shibata, K. Watari, Y. Noda, S. Ambe, Y. Ohkubo, M. Iwamoto, Y. Kobayashi, M. Yanokura, H. Maeda, and F. Ambe: "Adsorption Behavior of Various Elements in Chloride Solutions of Multitracer Prepared from Ag Target on Non-ionic Macro-reticular Copolymer and Activated Carbon Fiber", *ibid.*

Y. Minai, Y. Takahashi, H. Ohtsuka, M. Ishibashi, S. Ambe, Y. Kobayashi, Y. Ohkubo, M. Iwamoto, M. Yanokura, H. Maeda, S. Shibata, N. Takematsu, F. Ambe, and T. Tominaga: "Multitracer Study on Interaction between Humic Substance and Metal Ions", *ibid.*

S. Ambe, Y. Ohkubo, Y. Kobayashi, M. Iwamoto, H. Maeda, M. Yanokura, and F. Ambe: "Multitracer Study on Transport and Distribution of Metal-Ions in Plants", *ibid.*

H. Tatsuzaki, T. Okumura, H. Takahashi, M. Miyakawa, T. Kanai, S. Minohara, M. Sudou, and F. Yatagai: "The Irradiated Volume Dependency of Early Skin Reaction after Carbon Ion Beam Irradiation", 3rd Workshop on Physical and Biological Research with Heavy Ions, Chiba, Sept. (1993).

F. Yatagai, K. Nakano, T. Kanai, K. Saito, and F. Hanaoka: "Sensitivity of ts85 Mutant Strain from Mouse FM3A Cells to Heavy Ions", *ibid.*

K. Ogura, T. Doke, T. Hayashi, T. Kojima, M. Matsushima, S. Nagaoka, K. Nakano, T. Takahashi, H. Yamada, and F. Yatagai: "Tracking and LET Measurements of Cosmic Ray Nuclei for Space Radiobiological Studies", *ibid.*

T. Doke, T. Hayashi, R. Takeuchi, K. Ogura, and S. Nagaoka: "LET-Distribution on Space Shuttle IML-1 and FMPT Missions", 1993 Fall Meet. Jpn. Soc. Appl. Phys., Sapporo, Sept. (1993).

Y. Itoh, H. Murakami, and A. Kinoshita: "Characterization of Porous Silicon by Means of Positron Annihilation II", *ibid.*

Y. Minai, Y. Takahashi, M. Ishibashi, T. Ohta, S. Ambe, Y. Kobayashi, Y. Ohkubo, M. Iwamoto, M. Yanokura, H. Maeda, N. Takematsu, F. Ambe, and T. Tominaga: "Application of Multitracer Technique to Evaluation of Complexation Ability of Humic Acid", Ann. Meet. Geochem. Soc. Jpn., Osaka, Sept. (1993).

T. Kobayashi, T. Nozaki, M. Yanokura, and M. Aratani: "Ion Beam Analysis and RI Tracer Method of the Observation of Cation Exchange in Glass Surface Layers", 37th Symp. on Radiochemistry, Kanazawa, Oct. (1993).

J. Kurachi, E. Taniguchi, A. Shinohara, M. Furukawa, S. Kojima, Y. Ohkubo, F. Ambe, K. Takesako, T. Saito, H. Baba, and S. Shibata: "Competition between Fission and Spallation in the Reactions Induced by Intermediate Energy Heavy Ions", *ibid.*

K. Takesako, T. Saito, S. Watanabe, A. Yokoyama, H. Baba, Y. Ohkubo, A. Shinohara, E. Taniguchi, and M. Furukawa: "Transition to Limiting Behavior in Heavy-Ion Reactions Exhibited at Intermediate Energies", *ibid.*

M. Kiriu, A. Yokoyama, K. Takesako, S. Watanabe, N. Takahashi, T. Saito, H. Baba, and Y. Ohkubo: "Dependence of Mass Transfer in the Heavy Ion Reaction on the Mass Asymmetry at Entrance Channel", *ibid.*

S. Ambe, K. Takeshita, Y. Ohkubo, Y. Kobayashi, H. Maeda, M. Iwamoto, M. Yanokura, and F. Ambe: "Study of Adsorption of Metal Ions on α-Fe_2O_3 Using a Multitracer", *ibid.*

N. Aoki, T. Bamba, H. Harakawa, Y. Saito, K. Kimura, S. Ambe, Y. Ohkubo, Y. Kobayashi, M. Iwamoto, H. Maeda, M. Yanokura, and F. Ambe: "Study on the Ion Exchange Adsorption of Various Elements on Superacid Resin NAFION Using a Multitracer III", *ibid.*

S. Shibata, K. Watari, Y. Noda, S. Ambe, Y. Ohkubo, M. Iwamoto, Y. Kobayashi, M. Yanokura, H. Maeda, and F. Ambe: "Adsorption Behavior of Various Elements on Non-ionic Macro-reticular Copolymer in Chloride Solutions Using Radio-active Multitracer", *ibid.*

W. Li, Y. Ohkubo, S. Ambe, Y. Kobayashi, M. Iwamoto, H. Maeda, and F. Ambe: "Study of the Products from Reactions Induced by Secondary Fast Neutrons in Intermediate Energy Heavy Ion Collisions", *ibid.*

Y. Kobayashi, Y. Yoshida, R. Sielemann, L. Wende, and F. Ambe: "Chemical Behavior of ^{57}Fe Atoms in Polytetrafluoroethylene by in-beam Mössbauer Spectroscopy", *ibid.*

Y. Itoh, H. Murakami, and A. Kinoshita: "Positronium Formation in Porous Silicon", *ibid.*

M. Iwamoto, S. Ambe, Y. Ohkubo, Y. Kobayashi, M. Yanokura, and F. Ambe: "Production of Multitracer Nuclides by Irradiation with ^{84}Kr Beam", *ibid.*

H. Ohtsuka, Y. Minai, S. Ambe, Y. Takahashi, M. Ishibashi, Y. Kobayashi, Y. Ohkubo, M. Iwamoto, M. Yanokura, H. Maeda, F. Ambe, and T. Tominaga: "Group Separation of Lanthanides from Multitracer Solution", *ibid.*

Y. Kobayashi, S. Ambe, K. Takeshita, Y. Ohkubo, H. Maeda, M. Iwamoto, M. Yanokura, and F. Ambe: "Application of a Multitracer to Solvent Extraction", *ibid.*

T. Yaita, S. Tachimori, S. Ambe, Y. Kobayashi, Y. Ohkubo, H. Maeda, M. Iwamoto, M. Yanokura, and F. Ambe: "Study on the Solvent Extraction of Various Elements with Diphosphine Dioxide (DPDO) from Nitric Acid Solution by Use of Multitracer", *ibid.*

N. Kubota et al.: "Response of Human Tumor Cells Grown as Plateau Phase and Multicellular Spheroids to Carbon Beam Irradiation", 36th Ann. Meet. Jpn. Radiat. Res. Soc., Hiroshima, Oct. (1993).

H. Ohara, M. Minamihisamatsu, K. Fukutsu, H. Itsukaichi, K. Kasai, T. Kanai, F. Yatagai, and K. Sato: "Effects of 135 MeV/n of Carbon Ion Beams Produced by RIKEN Ring Cyclotron on Human Blood Chromosomes", *ibid.*

H. Tatsuzaki, T. Okumura, H. Takahashi, M. Miyakawa, T. Kanai, S. Minohara, M. Sudou, F. Yatagai: "The Effects of Irradiated Volume on Early Skin Reaction after Carbon Ion Beam Irradiation", *ibid.*

K. Ando, S. Koike, K. Fukutsu, T. Aruga, M. Iizuka, N. Hori, T. Kanai, and K. Shirasuna: "Increase of Mitotic Indices in a Human Salivary Gland Tumor Xenograft after Irradiation with Particle Beams", *ibid.*

M. Suzuki, M. Watanabe, Y. Kase, T. Kanai, F. Yatagai, T. Kato, and S. Matsubara: "The Effects of Cell Death and Mutation Induction Irradiated with Accelerated Carbon Ion Beams with Spread out Bragg Peak", *ibid.*

Y. Kase, M. Suzuki, T. Kanai, H. Yatagai, T. Katoh, and M. Watanabe: "LET Dependence of Biological Effects in Normal Human Cells Irradiated with Accelerated Neon Ions", *ibid.*

F. Yatagai: "Analysis of Biological Damages Induced by Heavy Ions", RIKEN Symp. on Researches on Solid State Physics and Materials, Atomic Physics, Nuclear Chemistry, and Biology and Medicine Using RIKEN Ring Cyclotron VII. The Next Heavy-Ion Accelerator Project, Wako, Oct. (1993).

Y. Kobayashi, H. Maeda, and Y. Ohkubo: "Study on Hyperfine Interaction by Means of Unstable-nuclei Beam with High Intensity", *ibid.*

S. Tsubouchi, F. Yatagai, H. Oohara, and E. Kano: "Relative Biological Effectiveness (RBE) of 30 MeV Neutron and 135 MeV Carbon Beams as Observed by Acute Cell Death (Pyknosis) of Pancreatic Islet of Golden Hamster", 52nd Ann. Meet. of Japanese Cancer Research, Sendai, Oct. (1993).

K. Kimura, T. Shiba, and Y. Sahara: "Effect of the High-density Excitation on Luminescence of the Self-trapped Exciton in BaF_2", 1993 Fall Meet. Phys. Soc. Jpn., Okayama, Oct. (1993).

K. Kimua, T. Shiba, and Y. Sahara: "Lifetime Shortening of STE Luminescence in BaF_2 Excited at High Density and STE-STE Distance-dependent Kinetics", *ibid.*

H. Murakami, Y. Itoh, and A. Kinosita: "Positronium Formation in Porous Silicon", *ibid.*

K. Kimura, Y. Sahara, and T. Shiba: "Quenching Processes of Self-trapped Excitons in BaF_2, Excited at High Density", 36th Conf. Radiat. Chem., Tokyo, Oct. (1993).

Y. Kobayashi: "Exotic Chemistry by Unstable-nuclei Beams", KUR Symp. on Material Science by Short-lived RI, Kumatori, Nov. (1993).

S. Ambe, K. Takeshita, Y. Ohkubo, Y. Kobayashi, H. Maeda, M. Iwamoto, M. Yanokura, and F. Ambe: "Multitracer Study of Adsorption of Metal Elements on α-Fe_2O_3", 7th General Meet. Jpn. Soc. Adsorption, Chiba, Nov. (1993).

S. Shibata, K. Watari, Y. Noda, S. Ambe, Y. Ohkubo, M. Iwamoto, Y. Kobayashi, M. Yanokura, H. Maeda, and F. Ambe: "Adsorption Behavior of Various Elements on Activated Carbon Fiber in Chloride Solutions Using Radioactive Multitracer", *ibid.*

N. Kubota et al.: "Response of Human Tumor Cells to Carbon Beam", 6th Ann. Meet. Jpn. Soc. Ther. Radiol. Oncol., Fukuoka, Nov. (1993).

S. Koike, K. Ando, M. Iizaka, T. Aruga, T. Kanai, S. Minohara, M. Sudo, N. Hori, C. C. Koo, and F. Yatagai: "Tumor Growth Delay and Tumor Cell Kills after Single Doses of Carbon-12", *ibid.*

5. Material analysis

K. Matsushita, A. Hirotsune, T. Kikuchi, and K. Furuya: "Evaluation of Thermal Stability and States of Deuterium and Herium in He^+ Implanted YIG Annealed in D_2", 41st Ann. Meet. of Jpn. Soc. Anal. Chem., Kyoto, Sept. (1992).

K. Kanazawa, M. Yanokura, and M. Aratani: "Quantitative Measurement of Light Elements on the Surface of Vacuum Chamber Materials for Electron Storage Rings", 36th Symp. on Radiochemistry, Hachioji, Oct. (1992).

J. Kawai and K. Maeda: "Chemical Effects on the Intensity of Ti Kη (Radiative Auger Satellite) X-Ray Fluorescence Spectra", 28th Colloq. Spectroscopicum Internationale, York, U.K., June (1993).

J. Kawai and K. Maeda: "Imaging Plate PIXE Spectrometer for Chemical State Analysis", 11th Int. Conf. on Ion Beam Analysis, Balatonfured, Hungary, July (1993).

K. Maeda and J. Kawai: "K-LL Radiative Auger Satellite of Ca $\sim$ Zr (Z = 20 $\sim$ 40)", 16th Int. Conf. on X-Ray and Inner-Shell Processes, Debrecen, Hungary, July (1993).

K. Maeda and J. Kawai: "Chemical Effects on the Ca Kη and KLβ X-Ray Spectra", *ibid.*

K. Maeda and J. Kawai: "In-situ Analysis of Liquid Sample by PIXE", 11th PIXE Symp., Tsukuba, Oct. (1993).

X. LIST OF SYMPOSIA

(Jan.–Dec. 1993)

1) 1st Symp. on Theory of Atomic and Molecular Processes
13, 14 Jan., Wako, RIKEN, Atomic Physics Lab.

2) Atomic Physics with Accelerator XII
1 June, Wako, RIKEN, Atomic Physics Lab.

3) Muon 1993 – Muon Catalyzed Fusion
28, 29 Sept., Wako, RIKEN, Metal Physics Lab.

4) Researches on Solid State Physics and Materials, Atomic Physics, Nuclear Chemistry, and Biology and Medicine Using RIKEN Ring Cyclotron VII – The Next Heavy-Ion Accelerator Project
25 Oct., Wako, RIKEN, Nuclear Chemistry Lab., Metal Physics Lab., Atomic Physics Lab., and Cellular Physiology Lab.

5) Muon Science 1993 – Medical and Biological Application of Non-destructive Element Analysis Using Muons
10 Dec., Wako, RIKEN, Metal Physics Lab.

6) 2nd Symp. on Theory of Atomic and Molecular Processes
23, 24 Dec., Wako, RIKEN, Atomic Physics Lab.

7) Int. Workshop on Area Detectors for Synchrotron Radiation Research
24–26 Nov., Harima Science Garden City, SPring-8 Project Team

XI. LIST OF SEMINARS

(Jan.–Dec. 1993)

Radiation Lab., Cyclotron Lab., and Linear Accelerator Lab.

1) E. Suraud, Toulouse Univ. (France), 20 Jan.
"On Stochastic Approaches of Nuclear Dynamics"

2) P. Möller, Los Alamos Natl. Lab. (USA), 25 Jan.
"Recent Nuclear Mass Calculations and Their Use in r-Process"

3) Y. Fujita, Osaka Univ. (Osaka), 9 Feb.
"Experiments Using FRS and ESR at GSI"

4) A. Bonasera, LNS, INFN (Italy), 3 Mar.
"Challenges in Heavy Ion Collisions"

5) D. Stoll, Univ. of Tokyo (Tokyo), 12 May
"Continuum Limit and Background Field in QED (1+1)"

6) T. Suomijarvi, Univ. of Paris (France), 25 May
"The Study of the Giant Dipole Resonance Built on the Continuum States with the MEDEA Multidetector"

7) R. Wada, Texas A&M Univ. (USA), 11 June
"Reaction Dynamics in Cu+Au at 35 A MeV"

8) T. Marumori, Sci. Univ. of Tokyo (Tokyo), 23 June
"Microscopic Theory of Collective Motion in One Particle Level Crossing Region"

9) Y. Nishino, RCNP, Osaka Univ. (Osaka), 28 June
"Structure Functions of Hadrons in the QCD Sum Rules"

10) J. Janecke, Univ. of Michigan (USA), 29 June
"Study of Giant Resonances with (^{3}He,t) and (^{7}Li,^{7}Be) Charge Exchange Reactions"

11) A. Sakai, Yamagata Univ. (Yamagata), 5 July
"Quark Confinement and Number of Flavors in a Lattice QCD with Wilson Quarks"

12) R. Boyd, Ohio State Univ. (USA), 26 July
"Radioactive Beam Measurements in Astrophysics"

13) J. Kolata, Univ. of Notre-Dame (USA), 27 July
"Elastic Scattering and Fragmentation of ^{12,14}Be"

14) T. Maruyama, Kyoto Univ. (Kyoto), 23 Aug.
"Study of High Energy Heavy Ion Reactions by Relativistic BUU"

15) T. Otsuka, Univ. of Tokyo (Tokyo), 6 Sept.
"Laboratory-Frame View of Nuclear Rotation"

16) R. Brockmann, Mainz Univ. (Germany), 20 Sept.
"Relativistic Many Body Theory of Nuclei"

17) G. M. Zinovjev, Acad. Sci. of Ukraine (Ukraine), 22 Sept.
"Dissipative Processes in an Expanding Massive Gluon Gas"

18) H. Nakada, Juntendo Univ. (Chiba), 18 Oct.
"E2 Properties of Nuclei Far from Stability and the Proton-Halo Problem of ^{8}B"

20) R. Casten, BNL (USA), 25 Oct.
"Universal Correlations of Nuclear Observables: A Possible Synthesis of Structural Evolution"

21) D. Youngblood, Texas A&M Univ. (USA), 4 Nov.
"Nuclear Compressibility from the Giant Monopole Resonance"

22) J. Galin, GANIL (France), 12 Nov.
"Hot Nuclei Close to Their Limit of Stability"

23) A. Zilges, Univ. of Köln (Germany), 15 Nov.
"Photon Scattering Experiments – A New Approach to Low Lying Collective Excitations"

24) M. Petrascu, IAP (Rumania), 25 Nov.
"Projectile Breakup Mechanism in Light Nuclear Systems"

25) S. Okabe, Hokkaido Univ. (Sapporo), 29 Nov.
"Visualization of Nuclear Reactions – A Computer Simulation of Quantum Systems by Molecular Dynamics"

26) J. N. De, VECC (India), 13 Dec.
"Limiting Temperature in Finite Nuclei"

27) D. Beaumel, ORSAY (France), 27 Dec.
"Neutron Decay Studies of Giant States with the EDEN Multidetector"

Atomic Physics Lab.

1) B. D. DePaola, Kansas State Univ. (USA), 12 Jan.
"Charge Transfer Experiments Using Laser-Excited Targets"

2) V. I. Zoran, Inst. Phys. Nucl. Eng. (Rumania), 21 Jan.
"'Defreezing' the Target Electron Wave Function in Swift Asymmetric Collision (Breathing, Rotation, Coupling, ...)"

3) M. Kimura, ANL (USA), 12 Mar.
"Chemical Effects in Molecular Photoabsorption and Photoemission"

4) R. Schuch, MSI (Sweden), 19 Mar.
"Experiments with Cold Ions and Electrons in the Stockholm Storage Ring"

5) L. Spielberger, Univ. of Frankfurt (Germany), 7 Apr.
"First Result in the Impact Parameter Dependent Investigation of Ionization and Charge Transfers in 1.05 MeV/amu $O^{6+} \rightarrow$ Ar Collisions"

6) V. McKoy, Dept. of Chemistry, Cal. Tech. (USA), 26 May
"Studies of Electron-Molecule Collisions on Highly Parallel Computers"

7) W. Eissner, The Queen's Univ. (UK), 2 June
"Inner-Shell Photoionization Calculations –Applications to Be and Na–"

8) Y. Azuma, ANL (USA), 13 Sept.
"The Trend of Atomic Physics by Synchrotron Radiation in the U.S."

9) I. Martinson, Univ. of Lund (Sweden), 28 Oct.
"Spectroscopy of Highly Charged Ion at University of Lund"

10) Z. G. Zhi, Univ. of Electro-Communications (Tokyo), 28 Oct.
"No-Linear Optical Process Using Electro-Magnetically Induced Transparency"

11) J. Z. Tang, RIKEN, (Saitama), 16 Dec.
"Photoionization of He from Excited States"

Nuclear Chemistry Lab.

1) W. Li, Inst. Modern Phys. (China), 4 Mar.
"Radiochemical Study of Heavy-Ion Reactions in IMP"

2) A. Shinohara, Nagoya Univ. (Nagoya), 4 Mar.
"Nuclear Chemical Studies on Intermediate-Energy Heavy-Ion Reactions"

3) K. H. Lieser, T. H. Darmstadt (Germany), 15 Mar.
"Speciation, a Challenge to Analytical Chemistry"

4) G. F. Hermann, Mainz Univ. (Germany), 15 Oct.
"Super heavy Elements – Could We Still Find Them?"

5) K. Morita, RIKEN, (Saitama), 15 Oct.
"A Search for Super Heavy Elements with Use of (HI,αxn) Reactions"

6) H. Häßlein, Shizuoka Inst. Sci. Tech. (Shizuoka), 19 Nov.
"Intrinsic Defect in Germanium Studied by Perturbed-Angular-Correlation"

Synchrotron Radiation Facility Design Group

1) H. Hama, UVSOR (Aichi), 25 June
"A Control System of UVSOR-Ring and Its Application for the Low α Operation"

2) T. Kawakubo, KEK (Ibaragi), 19 July
"A Profile Monitor with MCP"

3) H. Sumiyoshi, Matsusho-Gakuen Junior College (Nagano), 10 Aug.
"A New Simulation Code for High-Energy Multiple Collisions"

4) M. Tejima, KEK (Ibargi), 2 Sept.
"Single Pass Monitor"

5) A. Taketani, Fermi Nat. Acc. Lab. (USA), 10 Sept.
"Measurement of Asymmetry Rate of Muons from W-Bosons in Proton-Antiproton Collisions at 1.8 TeV"

6) C. Zhang, NSRL (China), 16 Sept.
"Alignment Networks for NSRL and the Magnets' Planar Position"

7) T. Nagae, UVSOR (Aichi), 30 Sept.
"Development of Micro-Strip Gas Chamber"

8) Y. Tsusaka, Nagoya Univ. (Aichi), 15 Oct.
"Development of an X-Ray Telescope for Astronomical Observations"

9) N. Liu, NSRL (China), 8 Nov.
"Status of Hefei National Synchrotron Radiation Laboratory"

XII. LIST OF PERSONNEL

RIKEN Accelerator Research Facility

ISHIHARA Masayasu 石原正泰 (Facility Director)
AWAYA Yohko 粟屋容子 (Vice Facility Director)
YANO Yasushige 矢野安重 (Vice Facility Director)

Linac Division

CHIBA Toshiya 千葉利哉
HEMMI Masatake 逸見政武
KASE Masayuki 加瀬昌之
MIYAZAWA Yoshitoshi 宮沢佳敏*
CHIBA Yoshiaki 千葉好明
IKEZAWA Eiji 池沢英二
KOHARA Shigeo 小原重夫

Ring Cyclotron Division

FUJITA Jirou 藤田二郎
IKEGAMI Kumio 池上九三男
KAGEYAMA Tadashi 影山 正
KASE Masayuki 加瀬昌之
KUBO Toshiyuki 久保敏幸
NAKAGAWA Takahide 中川孝秀
YOKOYAMA Ichiro 横山一郎
GOTO Akira 後藤 彰*
INABE Naohito 稲辺尚人
KAMIGAITO Osamu 上垣外修一
KOHARA Shigeo 小原重夫
NAGASE Makoto 長瀬 誠
OGIWARA Kiyoshi 荻原 清

Experimental Support Division

ICHIHARA Takashi 市原 卓
KANAI Yasuyuki 金井保之
KUMAGAI Hidekazu 熊谷秀和
MORITA Kosuke 森田浩介
WATANABE Yasushi 渡邊 康
YATAGAI Fumio 谷田貝文夫
KAMBARA Tadashi 神原 正
KOBAYASHI Toshio 小林俊雄*
MATSUZAKI Teiichiro 松﨑禎市郎
OHKUBO Yoshitaka 大久保嘉高
YANOKURA Minoru 矢野倉 実

Radioisotope Facilities Division

AMBE Fumitoshi 安部文敏*
KOBAYASHI Yoshio 小林義男
IWAMOTO Masako 岩本正子

Radiation Protection Group

FUJITA Shin 藤田 新
NAKANISHI Noriyoshi 中西紀喜*
NAKAJIMA Shunji 中島諄二

Secretariat

NAKAMURA Toshiko 中村とし子
YOSHIDA Tohru 吉田 徹**

Steering Committee

AMBE Fumitoshi 安部文敏
CHIBA Yoshiaki 千葉好明
HANAOKA Fumio 花岡文雄
ISHIHARA Masayasu 石原正泰
KATSUMATA Koichi 勝又紘一
KOBAYASHI Toshio 小林俊雄
MATSUOKA Masaru 松岡 勝
NAGAMINE Kanetada 永嶺謙忠
TAKAMI Michio 高見道生
YAGI Eiichi 八木栄一
AWAYA Yohko 粟屋容子
GOTO Akira 後藤 彰
INAMURA Takashi T. 稲村 卓
KAMITSUBO Hiromichi 上坪宏道
KIRA Akira 吉良 爽
KUMAGAI Noritaka 熊谷教孝
MIYAZAWA Yoshitoshi 宮沢佳敏
TAKAHASHI Tan 高橋 旦
TANIHATA Isao 谷畑勇夫***
YANO Yasushige 矢野安重

---

* Group Leader, ** Manager, *** Chairperson

Scientific and Engineering Personnel

Cosmic Radiation Laboratory

IMAI Takashi 今井 喬　　KOHNO Tsuyoshi 河野 毅

(Visitors)
HASEBE Nobuyuki 長谷部信行 (Fac. Gen. Educ., Ehime Univ.)
KASHIWAGI Toshisuke 柏木利介 (Fac. Eng., Kanagawa Univ.)
KATO Chihiro 加藤千尋 (Fac. Sci., Shinshu Univ.)
MUNAKATA Kazuoki 宗像一起 (Fac. Sci., Shinshu Univ.)
MURAKAMI Hiroyuki 村上浩之 (Fac. Sci., Rikkyo Univ.)
NAGATA Katsuaki 永田勝明 (Fac. Eng., Tamagawa Univ.)
NAKAMOTO Atsushi 中本 淳 (Fac. Sci., Rikkyo Univ.)
YANAGIMACHI Tomoki 柳町朋樹 (Fac. Sci., Rikkyo Univ.)

(Students)
FUJIKI Kenichi 藤木謙一 (Fac. Sci., Ehime Univ.)
ITO Tomoyuki 伊藤朋行 (Fac. Sci. Eng., Waseda Univ.)
ITSUMI Norifumi 逸見憲史 (Fac. Sci. Eng., Waseda Univ.)
SHINO Tomoaki 篠 智彰 (Fac. Sci. Eng., Waseda Univ.)

Cyclotron Laboratory

FUJITA Jirou 藤田二郎
GOTO Akira 後藤 彰***
INABE Naohito 稲辺尚人
KAGEYAMA Tadashi 影山 正
KITAGAWA Hisashi 北川 尚
KUBO Toshiyuki 久保敏幸
NAGASE Makoto 長瀬 誠
NAKAJIMA Shunji 中島諄二
OGIWARA Kiyoshi 荻原 清
OTSUKA Takaharu 大塚孝治**
SUZUKI Toshio 鈴木敏男**
WAKASUGI Masanori 若杉昌徳
YANO Yasushige 矢野安重*
FUJITA Shin 藤田 新
IKEGAMI Kumio 池上九三男
JIN Weiguo 金 衛国
KAMIGAITO Osamu 上垣外修一
KOHARA Shigeo 小原重夫
MORITA Kosuke 森田浩介
NAKAGAWA Takahide 中川孝秀
NAKANISHI Noriyoshi 中西紀喜
OHTA Shigemi 太田滋生
SUGANUMA Hideo 菅沼秀夫
UESAKA Tomohiro 上坂友洋
YAMAJI Shuhei 山路修平***
YOKOYAMA Ichiro 横山一郎

---

* Chief Scientist, ** Visiting Advisory Scientist, ***Senior Scientist

(Visitors)
ABE Yasuhisa 阿部恭久 (Uzi Res. Cent., Yukawa Inst. Theor. Phys., Kyoto Univ.)
AOKI Shirou 青木司郎 (NASDA)
ARAI Eiichi 新井栄一 (Res. Lab. Nucl. Reactors, Tokyo Inst. Technol.)
ARAKAWA Kazuo 荒川和夫 (JAERI, Takasaki)
EJIRI Hiroyasu 江尻宏泰 (Dept. Phys., Osaka Univ.)
ENYO Hideto 延与秀人 (Dept. Phys., Kyoto Univ.)
FUJIOKA Manabu 藤岡 学 (Cyclotron Radioisot. Cent., Tohoku Univ.)
FUJISAWA Takashi 藤沢高志 (Denki Kogyo Co. Ltd.)
FUJITA Yoshitaka 藤田佳孝 (Dept. Phys., Osaka Univ.)
FUJIWARA Mamoru 藤原 守 (RCNP, Osaka Univ.)
FUKUDA Mitsuhiro 福田光宏 (JAERI, Tokai)
FUKUMOTO Sadayoshi 福本貞義 (Univ. Tsukuba)
FURUNO Kohei 古野興平 (Inst. Phys. Tandem Accel. Cent., Univ. Tsukuba)
HAMA Hiroyuki 浜 広幸 (I.M.S.)
HASHIMOTO Osamu 橋本 治 (Inst. Nucl. Study, Univ. Tokyo)
HATA Kazuo 秦 和夫 (Fac. Eng., Kyoto Univ.)
HATANAKA Kichiji 畑中吉治 (RCNP, Osaka Univ.)

HATSUKAWA Yuichi 初川雄一 (JAERI, Tokai)
HATTORI Toshiyuki 服部俊幸 (Res. Lab. Nucl. Reac., T.I.T.)
HAYANO Ryugo 早野龍五 (Dept. Phys., Univ. Tokyo)
HEIGUTI Kazuhiko 平口和彦 (Graduate Sch. Sci. Technol., Niigata Univ.)
HIRAO Yasuo 平尾泰男 (NIRS)
HONMA Toshihiro 本間寿広 (Cyclotron Radioisot. Cent., Tohoku Univ.)
HORIBATA Takatoshi 堀端孝俊 (Fac. Eng., Aomori Univ.)
HORIGUTI Takayoshi 堀口隆良 (Dept. Phys., Hiroshima Univ.)
HORIUCHI Hisashi 堀内ひさし (Dept. Phys., Kyoto Univ.)
HOSONO Kazuhiko 細野和彦 (RCNP, Osaka Univ.)
IGARASHI Toshio 五十嵐敏雄 (NASDA)
IKEDA Kiyomi 池田清美 (Dept. Phys., Niigata Univ.)
IKEDA Nobuo 池田伸夫 (Inst. Nucl. Study, Univ. Tokyo)
IKEGAMI Hidetsugu 池上栄胤 (RCNP, Osaka Univ.)
IKEZOE Hiroshi 池添博 (JAERI, Tokai)
IMAI Kenichi 今井憲一 (Dept. Phys., Kyoto Univ.)
INOUE Makoto 井上信 (Inst. Chem. Res., Kyoto Univ.)
ISHII Takayuki 石井孝幸 (NASDA)
ISHIZUKA Takeo 石塚武男 (Dept. Phys., Saitama Univ.)
IWAMOTO Akira 岩本昭 (JAERI, Tokai)
IWASHITA Yoshihisa 岩下芳久 (Inst. Chem. Res., Kyoto Univ.)
KAJI Harumi 鍛冶東海 (Fac. Eng., Tohoku Univ.)
KAMEYAMA Hirobumi 亀山浩文 (Dept. Phys., Chiba Keizai Jr. Coll.)
KAMIMURA Masayasu 上村正康 (Dept. Phys., Kyushu Univ.)
KANAZAWA Mitsutaka 金沢光隆 (NIRS)
KANMURI Tetsuo 冠哲夫 (Dept. Phys., Osaka Univ.)
KANNO Tooru 菅野徹 (NASDA)
KATAYAMA Ichirou 片山一郎 (Inst. Nucl. Study, Univ. Tokyo)
KATAYAMA Takeshi 片山武司 (Inst. Nucl. Study, Univ. Tokyo)
KATO Kiyoshi 加藤幾芳 (Dept. Phys., Hokkaido Univ.)
KATORI Kenji 鹿取謙二 (Dept. Phys., Osaka Univ.)
KATOU Shouhei 加藤昌平 (Dept. Phys., Osaka Univ.)
KATSURAGAWA Hidetsugu 桂川秀嗣 (Dept. Phys., Toho Univ.)
KAWAI Mitsuji 河合光路 (Dept. Phys., Kyushu Univ.)
KIKUCHI Fumio 菊池文男 (Coll. Arts Sci., Univ. Tokyo)
KOHMOTO Toshiro 河本敏郎 (Dept. Phys., Kyoto Univ.)
KONDOU Michiya 近藤道也 (RCNP, Osaka Univ.)
KOSAKO Toshiso 小佐古敏荘 (Atomic Energy Res. Cent., Univ. Tokyo)
KOTAJIMA Hisaya 古田島久哉 (Fac. Eng., Tohoku Univ.)
KUBOYAMA Tomoji 久保山智司 (NASDA)
KUDO Hisaaki 工藤久昭 (Dept. Chem., Niigata Univ.)
KUROYANAGI Tokihiro 黒柳登喜大 (Dept. Phys., Kyushu Univ.)
LEE Sang Moo 李相茂 (Inst. Phys., Univ. Tsukuba)
MARUMORI Toshio 丸森寿夫 (Fac. Sci. Technol., Sci. Univ. Tokyo)
MATSUDA Sumio 松田純夫 (NASDA)
MATSUI Yoshiko 松井芳子 (Fac. Tech., Tokyo Univ. Agri. Tech.)
MATSUKI Seishi 松木征史 (RCNP, Osaka Univ.)
MATSUSE Takehiro 松瀬丈浩 (Dept. Phys., Shinshu Univ.)
MATSUYANAGI Kenichi 松柳研一 (Dept. Phys., Kyoto Univ.)
MIAKE Yasurou 三明康郎 (Inst. Phys., Univ. Tsukuba)
MIDORIKAWA Shouichi 緑川章一 (Dept. Market, Meiji Univ.)
MINAMISONO Tadanori 南園忠則 (Dept. Phys., Osaka Univ.)
MIURA Iwao 三浦岩 (RCNP, Osaka Univ.)
MIYAMURA Osamu 宮村修 (Fac. Sci., Osaka Univ.)
MIYATAKE Hiroari 宮武宇也 (Fac. Sci., Osaka Univ.)
MIZOTA Takeshi 溝田武志 (Inst. Phys., Univ. Tsukuba)
MIZUNO Yoshiyuki 水野義之 (RCNP, Osaka Univ.)
MORI Yoshiharu 森義治 (KEK)

MURAKAMI Tetsuya 村上哲也 (Dept. Phys., Kyoto Univ.)
MURAOKA Mitsuo 村岡光男 (Dept. Educ., Chiba Univ.)
MURAYAMA Toshiyuki 村山利幸 (Tokyo Univ. Mercantile Marine)
MUROTANI Shin 室谷 心 (Sch. Sci. Eng., Waseda Univ.)
NAGAI Yasuki 永井泰樹 (Dept. Appl. Phys., Tokyo Inst. Technol.)
NAITOU Ichirou 内藤一郎 (NASDA)
NAKAHARA Hiromichi 中原弘道 (Dept. Chem., Tokyo Metrop. Univ.)
NAKAI Koji 中井浩二 (KEK)
NAKAJIMA Masato 中島真人 (NASDA)
NAKAMURA Ichiro 中村市郎 (Dept. Phys., Saitama Univ.)
NAKAMURA Takashi 中村尚司 (Cyclotron Radioisot. Cent., Tohoku Univ.)
NIITA Koji 仁井田浩二 (Dept. Phys., Univ. Giessen, Germany)
NODA Akira 野田 章 (Inst. Nucl. Study, Univ. Tokyo)
NODA Kouji 野田耕司 (NIRS)
NOMURA Toru 野村 亨 (Inst. Nucl. Study, Univ. Tokyo)
OGATA Hiroshi 小方 寛 (RCNP, Osaka Univ.)
OGAWA Kengo 小川健吾 (Fac. Educ., Chiba Univ.)
OKABE Shigetou 岡部成玄 (Center Inf. Proc. Educ., Hokkaido Univ.)
OKAMURA Hiroyuki 岡村弘之 (Dept. Phys., Univ. Tokyo)
OKUMURA Susumu 奥村 進 (JAERI, Takasaki)
ONISHI Naoki 大西直毅 (Dept. Phys., Coll. Arts Sci., Univ. Tokyo)
OOHIRA Hideharu 大平秀春 (NASDA)
OOTSUKI Tsutomu 大槻 勤 (Lab. Nucl. Sci., Tohoku Univ.)
OOURA Akio 大浦昭夫 (NASDA)
OOYA Jirou 大矢次郎 (NASDA)
OSUGA Toshiaki 大須賀敏明 (Coll. Arts Sci., Chiba Univ.)
PU Yuehu 蒲 越虎 (Inst. Nucl. Study, Univ. Tokyo)
SAGARA Kenji 相良建至 (Dept. Phys., Kyushu Univ.)
SAKAI Hideyuki 酒井英行 (Dept. Phys., Univ. Tokyo)
SASAGAWA Tatsuya 笹川辰弥 (Dept. Phys., Tohoku Univ.)
SATO Yukio 佐藤幸夫 (NIRS)
SATOU Kenichi 佐藤憲一 (Dept. Phys., Tohoku Coll. Pharm.)
SATOU Kenji 佐藤健次 (NIRS)
SEKINE Toshiaki 関根俊明 (JAERI, Tokai)
SHIBATA Tokushi 柴田徳思 (Inst. Nucl. Study, Univ. Tokyo)
SHIKAZONO Naoki 鹿園直基 (JAERI, Tokai)
SHIMANO Yosuke 嶋野洋介 (NASDA)
SHIMIZU Akira 清水 昭 (RCNP, Osaka Univ.)
SHIMOMURA Koichiro 下村浩一郎 (Meson Sci. Lab., KEK Brunch, Univ. Tokyo)
SHINOZUKA Tsutomu 篠塚 勉 (Cyclotron Radioisot. Cent., Tohoku Univ.)
SHIRAI Toshiyuki 白井敏之 (Res. Inst. Fundam. Phys., Kyoto Univ.)
SUEKI Keisuke 末木啓介 (Inst. Nucl. Study, Univ. Tokyo)
SUGAI Isao 菅井 勲 (Inst. Nucl. Study, Univ. Tokyo)
SUGIYAMA Hiroki 杉山大樹 (NASDA)
SUMIYOSHI Hiroyuki 住吉広行 (Matsusho-Gakuen Jr. Coll.)
TAGISHI Yoshihiro 田岸義宏 (Tandem Accel. Cent., Univ. Tsukuba)
TAKADA Kenjiro 高田健次郎 (Dept. Phys., Kyushu Univ.)
TAKEMASA Tadashi 武政尹士 (Dept. Phys., Saga Univ.)
TAKEUCHI Suehiro 竹内末広 (JAERI, Tokai)
TAKIGAWA Noboru 滝川 昇 (Dept. Phys., Tohoku Univ.)
TAMAGAKI Ryozo 玉垣良三 (Dept. Phys., Kyoto Univ.)
TAMURA Takashi 田村高志 (NASDA)
TANAKA Jinichi 田中仁市 (Inst. Nucl. Study, Univ. Tokyo)
TOKI Hiroshi 土岐 博 (Dept. Phys., Tokyo Metrop. Univ.)
TOMIMASU Takio 富増多喜夫 (FEL Res. Inst. Inc.)
TOMITANI Takehiro 富谷武浩 (NIRS)
TOMOTA Toshiaki 友田敏章 (Fac. Eng., Aomori Univ.)
TORIYAMA Tamotsu 鳥山 保 (Dept. Appl. Phys., Tokyo Inst. Technol.)

TSUNEMOTO Hiroshi 恒元 博 (NIRS)
UESUGI Masato 上杉正人 (NASDA)
UWAMINO Yoshitomo 上蓑義朋 (Inst. Nucl. Study, Univ. Tokyo)
WADA Michiharu 和田道治 (Dept. Phys., Tohoku Univ.)
WAKAI Masamichi 若井正道 (Dept. Phys., Osaka Univ.)
WAKUTA Yoshihisa 和久田義久 (Fac. Eng., Kyushu Univ.)
WANG Zhen 王 真 (Inst. Modern Phys., Acad. Sinica, China)
YAMANOUCHI Mikio 山内幹雄 (Tandem Accel. Cent., Univ. Tsukuba)
YAMADA Taiichi 山田泰一 (Dept. Phys., Kochi Women's Univ.)
YAMAMOTO Yasuo 山本安夫 (Tsuru Univ.)
YAMAZAKI Takashi 山崎 魏 (RCNP, Osaka Univ.)
YAZAKI Koichi 矢崎紘一 (Dept. Phys., Univ. Tokyo)
YOSHIDA Nobuaki 吉田宣章 (Dept. Phys., Univ. Tokyo)
YOSHIDA Shiro 吉田思郎 (Dept. Phys., Ishinomaki Senshu Univ.)
YOSHINAGA Naotaka 吉永尚孝 (Dept. Phys., Saitama Univ.)
YOSHIOKA Yasuhiro 吉岡康弘 (NASDA)
YOSHIZAWA Yasukazu 吉沢康和 (Coll. Ind. Technol.)

(Students)
AOKI Yuka 青木由香 (Dept. Phys., Tohoku Univ.)
ARIGA Takehiro 有賀健博 (Dept. Phys., Saitama Univ.)
FURUYA Shinji 古谷信司 (Dept. Appl. Phys., Tokyo Inst. Technol.)
FUTAMI Yasuyuki 二見康之 (Dept. Phys., Univ. Tsukuba)
HAMADA Shingo 濱田真悟 (Dept. Nucl. Eng., Kyoto Univ.)
HIRAI Masahide 平井政秀 (Dept. Phys., Sophia Univ.)
HONMA Hiroyuki 本間裕之 (Dept. Phys., Tokyo Inst. Technol.)
INOUE Jirou 井上次郎 (Dept. Phys., Sophia Univ.)
KASHIWABARA Taketo 柏原健人 (Dept. Phys., Toho Univ.)
KATOU Haruhiko 加藤治彦 (Dept. Phys., Chuo Univ.)
KIYONO Satoshi 清野 聡 (Dept. Appl. Phys., Tokyo Inst. Technol.)
KUMAGAI Kenji 熊谷健二 (Dept. Phys., Hiroshima Univ.)
MABUCHI Hideyuki 馬渕英之 (Dept. Phys., Kounan Univ.)
MARUYAMA Toshiki 丸山敏毅 (Dept. Phys., Kyoto Univ.)
MATSUMOTO Norihiro 松本典洋 (Dept. Phys., Kounan Univ.)
MINEMURA Toshiyuki 峯村俊行 (Dept. Phys., Chuo Univ.)
MOTOGI Yoshio 本城義夫 (Dept. Phys., Univ. Tsukuba)
NAKAGAWA Keiko 中川恵子 (Dept. Phys., Tohoku Univ.)
NAKAO Noriaki 中尾徳晶 (Dept. Phys., Tohoku Univ.)
OGAWA Izumi 小川 泉 (Dept. Phys., Kyoto Univ.)
OOSAKI Toshiro 大崎敏郎 (Dept. Appl. Phys., Tokyo Inst. Technol.)
SASAKI Reiji 佐々木玲仁 (Dept. Phys., Tohoku Univ.)
SATOU Hideko 佐藤英子 (Dept. Phys., Univ. Tsukuba)
SENOO Kenichi 妹尾賢一 (Dept. Appl. Phys., Tokyo Inst. Technol.)
SHINOZAKI Akihisa 篠崎章久 (Dept. Phys., Tohoku Univ.)
SUNAOSHI Hitoshi 砂押 仁 (Dept. Phys., Tohoku Univ.)
TAKADA Shinji 高田真志 (Dept. Phys., Tohoku Univ.)
TAKAHASHI Takumi 高橋琢巳 (Dept. Phys., Chuo Univ.)
TAKEDA Kenji 竹田賢志 (Dept. Appl. Phys., Tokyo Inst. Technol.)
TANIGAWA Masashi 谷川勝至 (Dept. Phys., Tokyo Metrop. Univ.)
TOMITA Shigeo 富田成夫 (Dept. Phys., Univ. Tsukuba)
TOMOHISA Yasuhiko 友久保彦 (Dept. Phys., Univ. Tsukuba)
UMETSU Youichirou 梅津陽一郎 (Dept. Phys., Tohoku Univ.)
WAKUI Takashi 湧井崇志 (Dept. Phys., Toho Univ.)
WATANABE Koutarou 渡辺康太郎 (Dept. Appl. Phys., Tokyo Inst. Technol.)

Linear Accelerator Laboratory

CHIBA Toshiya 千葉利哉
CHIBA Yoshiaki 千葉好明
FUJIMAKI Masaki 藤巻正樹
HEMMI Masatake 逸見政武
HIRENZAKI Satoru 比連崎悟
IKEZAWA Eiji 池沢英二
KASE Masayuki 加瀬昌之
KOBAYASHI Toshio 小林俊雄**
KUMAGAI Hidekazu 熊谷秀和
MIYAZAWA Yoshitoshi 宮沢佳敏
OZAWA Akira 小沢顕
SUZUKI Takeshi 鈴木健
TANIHATA Isao 谷畑勇夫*
TONUMA Tadao 戸沼正雄
YANOKURA Minoru 矢野倉実
YOSHIDA Koichi 吉田光一

* Chief Scientist, ** Senior Scientist

(Visitors)
ALEKSANDROV D. V. (Kurchatov Inst., Russia)
BOLBOT Michael D. (Notre Dame Univ., U.S.A.)
BOYD Richard (Ohio State Univ., U.S.A.)
BROCKMANN Rolf (Inst. Phys. Univ. Mainz, Germany)
CARLSON Brett (CTA, Inst. Estudos Avancados, Brasil)
CHLOUPEK Frank (Ohio State Univ., U.S.A.)
DEMYANOVA Alla S. (Kurchatov Inst. Atomic Energy, Russia)
FENG Jun 馮軍 (Shanghai Inst. Nucl. Res., China)
FUJIWARA Mamoru 藤原守 (RCNP, Osaka Univ.)
FURUYA Keiichi 古谷圭一 (Fac. Sci., Sci. Univ. Tokyo)
HIRATA Daisy (CTA, Inst. Estudos Avancados, Brasil)
ITO Noriaki 伊藤憲昭 (Dept. Cryst. Mater., Nagoya Univ.)
KANAZAWA Kenichi 金澤健一 (KEK)
KATORI Kenji 鹿取謙二 (Fac. Sci., Osaka Univ.)
KIKUCHI Jun 菊池順 (Sci. Eng. Res. Lab., Waseda Univ.)
KIMURA Kikuo 木村喜久雄 (Fac. Eng., Nagasaki Inst. Appl. Sci.)
KOLATA James (Notre Dame Univ., U.S.A.)
KORSHENINNIKOV A. A. (Kurchatov Inst., Russia)
MATSUTA Kensaku 松多健策 (Osaka Univ.)
MATUOKA Nobuyuki 松岡伸行 (Res. Cent. Nucl. Phys., Osaka Univ.)
MOCHIZUKI Keiko 望月けい子 (Osaka Univ.)
MOON Chang-Bun (Seoul Natl. Univ., Korea)
MURAOKA Mitsuo 村岡光男 (Coll. Arts Sci., Chiba Univ.)
NIKOLSKI Evgenini Y. (Kurchatov Inst., Russia)
NOJIRI Yoichi 野尻洋一 (Osaka Univ.)
OGAWA Kengo 小川建吾 (Coll. Arts Sci., Chiba Univ.)
OGLOBLIN Alexei A. (Kurchatov Inst., Russia)
OJIMA Minoru 小嶋稔 (Osaka Univ.)
OMATA Kazuo 小俣和夫 (Inst. Nucl. Study, Univ. Tokyo)
RAIMANN Gerhard (Ohio State Univ., U.S.A.)
SAGAWA Hiroyuki 佐川弘幸 (Fac. Sci., Univ. Tokyo)
SAKAI Hideyuki 酒井英行 (Fac. Sci., Univ. Tokyo)
SUDA Toshimi 須田利美 (Fac. Sci., Tohoku Univ.)
SUGAWARA Masahiko 菅原昌彦 (Fundam. Sci., Chiba Inst. Technol.)
SUZUKI Yasuyuki 鈴木宣之 (Fac. Sci. Niigata Univ.)
TOKI Hiroshi 土岐博 (Tokyo Metrop. Univ.)
WADA Takahiro 和田隆宏 (Osaka Dentist Univ.)
YAMAGUCHI Hiromi 山口裕美 (Sci. Eng. Res. Lab., Waseda Univ.)
ZAHAR Mohamed (Notre Dame Univ., U.S.A.)

(Students)
FUKUDA Moichi 福田茂一 (Fac. Sci., Osaka Univ.)
HARADA Akihiko 原田昭彦 (Fac. Sci., Osaka Univ.)
IZUMIKAWA Takuji 泉川卓司 (Fac. Sci., Osaka Univ.)
MATSUSHITA Kenichi 松下健一 (Fac. Sci., Sci. Univ. Tokyo)

MIHARA Mototsugu 三原基嗣 (Fac. Sci., Osaka Univ.)
MIYAKE Toru 三宅 徹 (Fac. Sci., Osaka Univ.)
MIYAMOTO Shinya 宮本真哉 (Fac. Sci., Tokyo Metrop. Univ.)
MOCHIZUKI Keiko 望月圭子 (Fac. Sci., Osaka Univ.)
NAKAZATO Masahisa 中里真久 (Fac. Sci., Osaka Univ.)
OBUTI Marcia (Sci. Technol., Saitama Univ.)
ONISHI Takashi 大西 崇 (Fac. Sci., Osaka Univ.)
SASAKI Makoto 佐々木 誠 (Fac. Sci., Osaka Univ.)
TANIGAKI Minoru 谷垣 実 (Fac. Sci., Osaka Univ.)
YAMAGUCHI Takayuki 山口貴之 (Fac. Sci., Osaka Univ.)

Radiation Laboratory

FUKUNISHI Nobuhisa 福西暢尚
ISHIHARA Masayasu 石原正泰*
KISHIDA Takashi 岸田 隆
MORIKAWA Tsuneyasu 森川恒安
SUZUKI Masayo 鈴木昌世
TANAKA Kazuhiro 田中和廣
WATANABE Yasushi 渡邊 康
ICHIHARA Takashi 市原 卓
IZUMO Koichi 出雲光一
KONNO Satoshi 金野 智
NAKAMURA Takashi 中村隆司
TAKAHASHI Tan 高橋 旦
TENDOW Yoshihiko 天道芳彦
YOSHIDA Atsushi 吉田 敦

* Chief Scientist

(Visitors)
ABE Yasuhisa 阿部恭久 (Res. Inst. Fundam. Phys., Kyoto Univ.)
ADACHI Minoru 足立 實 (Dept. Appl. Phys., Tokyo Inst. Technol.)
ANDO Yoshiaki 安藤嘉章 (Dept. Phys., Rikkyo Univ.)
APRILE Elena (Columbia Univ., U.S.A.)
ASAHI Koichiro 旭 耕一郎 (Fac. Sci., Tokyo Inst. Technol.)
BECK F. A. (Groupe RSN, Strasbourg, France)
BROGLIA R. (Milano Univ., Italy)
CASTEN Rick (Brookhaven Natl. Lab., U.S.A.)
DOKE Tadayoshi 道家忠義 (Sci. Eng. Res. Lab., Waseda Univ.)
FLOCARD Hubert (Inst. Phys. Nucl., Orsay, France)
FUCHI Yoshihide 渕 好秀 (Inst. Nucl. Study, Univ. Tokyo)
FUJIOKA Manabu 藤岡 学 (Dept. Phys., Tohoku Univ.)
FUKUDA Mitsunori 福田光順 (Fac. Sci., Osaka Univ.)
FUKUDA Tomokazu 福田共和 (Inst. Nucl. Study, Univ. Tokyo)
GONO Yasuyuki 郷農靖之 (Dept. Phys., Kyushu Univ.)
GUY Y. Bizard (CAEN Univ., France)
HASEGAWA Takeo 長谷川武夫 (Fac. Eng., Miyazaki Univ.)
HASHIZUME Akira 橋爪 朗 (Japan Atomic Energy Relations Organ.)
HITACHI Akira 月出 章 (Kochi Med. Sch.)
ICHIMURA Munetake 市村宗武 (Coll. Arts Sci., Univ. Tokyo)
IEKI Kazuo 家城和夫 (Fac. Sci., Rikkyo Univ.)
IJIRI Kenichi 井尻憲一 (Radioisot. Cent., Univ. Tokyo)
ISHIDA Nobumichi 石田伸道 (Seikei Univ.)
ISHIKAWA Masanobu 石川雅紀 (Tokyo Univ. Fisheries)
IWASAKI Hiroyuki 岩崎博行 (KEK)
KANEYUKI Kenji 金行健治 (Fac. Sci., Tokyo Inst. Technol.)
KASAGI Jirohta 笠木次郎太 (Lab. Nucl. Sci., Tohoku Univ.)
KASAI Kiyomi 笠井清美 (Natl. Inst. Radiol. Sci.)
KATAYAMA Ichiro 片山一郎 (Inst. Nucl. Study, Univ. Tokyo)
KATO Seigo 加藤清吾 (Fac. Educ., Yamagata Univ.)
KATORI Kenji 鹿取謙二 (Fac. Sci., Osaka Univ.)
KAWAKAMI Hirokane 川上宏金 (Inst. Nucl. Study, Univ. Tokyo)
KAWASHIMA Hideo 川島英雄 (Inst. Nucl. Study, Univ. Tokyo)
KIKUCHI Jun 菊池 順 (Sci. Eng. Res. Lab., Waseda Univ.)

KIM Hee J. (Oak Ridge Natl. Lab., U.S.A.)
KIM Jong Chan 金 鐘 贊 (Seoul Natl. Univ., Korea)
KITAHARA Yoshitaka 北 原 義 孝 (Hoya Corp.)
KITAO Kensuke 喜多尾憲助 (Natl. Inst. Radiol. Sci.)
KOMAGATA Kazuyuki 駒 形 和 行 (Asahi Glass Co., Ltd.)
KONDO Takahiko 近藤敬比古 (KEK)
KUBONO Shigeru 久保野 茂 (Inst. Nucl. Study, Univ. Tokyo)
KUBOTA Shinzou 窪 田 信 三 (Fac. Sci., Rikkyo Univ.)
KUSAKARI Hideshige 草 刈 秀 榮 (Fac. Educ., Chiba Univ.)
LEE Sang Mu 李 相 茂 (Inst. Phys., Univ. Tsukuba)
LIU Guanhua 劉 冠 華 (Inst. Mod. Phys., Acad. Sinica, China)
MAEDA Kazushige 前 田 和 茂 (Coll. Gen. Educ., Tohoku Univ.)
MASUDA Kimiaki 増 田 公 明 (Saitama Coll. Health)
MATSUDA Takeshi 松 田 武 (KEK)
MATSUYANAGI Kenichi 松 柳 研 一 (Dept. Phys., Kyoto Univ.)
MIN Byung Joo 閔 丙 珠 (Korea At. Energy Res. Inst., Korea)
MITARAI Shiro 御手洗志郎 (Dept. Phys., Kyushu Univ.)
MIYACHI Takashi 宮 地 孝 (Inst. Nucl. Study, Univ. Tokyo)
MIYATAKE Hironari 宮 武 宇 也 (Coll. Gen. Educ., Osaka Univ.)
MORINOBU Shunpei 森 信 俊 平 (Dept. Phys., Kyushu Univ.)
MOTOBAYASHI Tohru 本 林 透 (Fac. Sci., Rikkyo Univ.)
MOTTELSON Ben R. (NORDITA, Denmark)
MUKERJEE Reshmi (Columbia Univ., U.S.A.)
MURAKAMI Takeshi 村 上 健 (Natl. Inst. Radiol. Sci.)
NAGAI Yasuki 永 井 泰 樹 (Fac. Sci., Tokyo Inst. Technol.)
NAGASHIMA Yasuo 長 島 泰 夫 (Dept. Phys., Univ. Tsukuba)
NAKAJIMA Mitsuo 中 島 充 夫 (Graduate Sch. Nagatsuda, Tokyo Inst. Technol.)
NAKAMURA Syougo 中 村 正 吾 (Fac. Educ., Yokohama Natl. Univ.)
NAKAYAMA Shintaro 中山信太郎 (Coll. Gen. Educ., Tokushima Univ.)
NEUGART Rainer (Mainz Univ., Germany)
NIIZEKI Takashi 新 関 隆 (Fac. Sci., Tokyo Inst. Technol.)
NORO Tetsuo 野 呂 哲 夫 (RCNP, Osaka Univ.)
OGAWA Masao 小 川 雅 生 (Graduate Sch. Nagatsuda, Tokyo Inst. Technol.)
OGURA Koichi 小 倉 紘 一 (Coll. Ind. Technol., Nihon Univ.)
OHNUMA Hajime 大 沼 甫 (Fac. Sci., Tokyo Inst. Technol.)
OKAMURA Hiroyuki 岡 村 弘 之 (Fac. Sci., Univ. Tokyo)
ORIHARA Hikonojo 織原彦之丞 (Cyclotron Radioisot. Cent., Tohoku Univ.)
OSHIMA Masumi 大 島 眞 澄 (Japan Atomic Energy Res. Inst.)
OSHIRO Takashi 尾 城 隆 (Tokyo Univ. Fisheries)
OTSUKA Takaharu 大 塚 孝 治 (Fac. Sci., Univ. Tokyo)
OYAIZU Michihiro 小柳津充広 (Inst. Nucl. Study, Univ. Tokyo)
RUAN (GEN) Jianzhi 阮 建 治 (Dept. Phys., Rikkyo Univ.)
SAKAGUCHI Harutaka 坂 口 治 隆 (Dept. Phys., Kyoto Univ.)
SAKAI Mitsuo 坂 井 光 夫 (Inst. Nucl. Study, Univ. Tokyo)
SAKAI Yoshihide 堺 井 義 秀 (KEK)
SAKURAGI Hiroyuki 桜 木 弘 之 (Fac. Sci., Osaka City Univ.)
SAKURAI Hiroyoshi 桜 井 博 義 (Fac. Sci., Univ. Tokyo)
SATO Hiroshi 佐 藤 竑 (Seikei Univ.)
SCARLASSARA Fernando (Univ. di Padova, Italy)
SHIBAMURA Eido 柴 村 英 道 (Saitama Coll. Health)
SHIMIZU Hajime 清 水 肇 (Fac. Educ., Yamagata Univ.)
SHIMIZU Yoshifumi 清 水 良 文 (Dept. Phys., Kyushu Univ.)
SHIMODA Tadashi 下 田 正 (Coll. Gen. Educ., Osaka Univ.)
SHIMOURA Susumu 下 浦 享 (Dept. Phys., Rikkyo Univ.)
SHIRATO Shoji 白 土 釣 二 (Dept. Phys., Rikkyo Univ.)
SHIROYAMA Masaki 城 山 正 樹 (Asahi Glass Co., Ltd.)
SUEKANE Fumihiko 末 包 文 彦 (Fac. Sci., Tohoku Univ.)
SUGAWARA Masahiko 菅 原 昌 彦 (Chiba Inst. Technol.)

SUZUKI Yasuyuki 鈴木宜之 (Dept. Phys., Niigata Univ.)
TAKADA Eiichi 高田栄一 (Natl. Inst. Radiol. Sci.)
TAKAHASHI Noriaki 高橋憲明 (Coll. Gen. Educ., Osaka Univ.)
TAKAHASHI Tadayuki 高橋忠幸 (Fac. Sci., Univ. Tokyo)
TAKAKU Shinsaku 高久清作 (Inst. Nucl. Study, Univ. Tokyo)
TAKIGAWA Noboru 滝川 昇 (Dept. Phys., Tohoku Univ.)
TANAKA Masahiko 田中雅彦 (Inst. Nucl. Study, Univ. Tokyo)
TANIMORI Tohru 谷森 達 (Fac. Sci., Tokyo Inst. Technol.)
TANOKURA Atsushi 田野倉 敦 (Fac. Sci. Technol., Sophia Univ.)
TAO Kazuyuki 垰 和之 (Radioisot. Cent., Univ. Tokyo)
TERAKAWA Atsuki 寺川貴樹 (Cyclotron Radioisot. Cent., Tohoku Univ.)
TLUSTY Pavel (Inst. Nucl. Study, Univ. Tokyo)
TOKI Hiroshi 土岐 博 (Dept. Phys., Tokyo Metrop. Univ.)
TOYOKAWA Hidenori 豊川秀訓 (RCNP, Osaka Univ.)
UNNO Yoshinobu 海野義信 (KEK)
UNO Masahiro 宇野正宏 (The Ministry of Education)
WATANABE Yasushi 渡辺靖志 (Fac. Sci., Tokyo Inst. Technol.)
YAMAMOTO Sukeyasu 山本祐靖 (Fac. Sci. Technol., Sophia Univ.)
YAMAYA Takashi 山屋 尭 (Dept. Phys., Tohoku Univ.)
YATO Osamu 矢頭 治 (Kagoshima Agr. Exp. Stn.)
YOSHIDA Kazuo 吉田和夫 (Hoya Corp.)
YOSHINAGA Naotaka 吉永尚孝 (Saitama Univ.)
YOSOI Masaru 與曽井 優 (Dept. Phys., Kyoto Univ.)
YUTA Haruo 湯田春雄 (Fac. Sci., Tohoku Univ.)
ZHANG Yuhu 張 玉虎 (Inst. Mod. Phys., Acad. Sinica., China)

(Students)
AKEBOSHI Yoshihiro 明星慶洋 (Fac. Sci., Tokyo Inst. Technol.)
AOI Nori 青井 考 (Fac. Sci., Univ. Tokyo)
CHAE Soo-Joh (Seoul Natl. Univ., Korea)
DOI Masashi 土井雅史 (Fac. Sci., Tokyo Inst. Technol.)
DOKI Yasuhiro 土記康博 (Fac. Sci., Univ. Tokyo)
FUJITA Tetsushi 藤田哲史 (Fac. Sci., Univ. Tokyo)
FURUTAKA Kazuyoshi 古高和禎 (Fac. Sci., Tokyo Inst. Technol.)
FUTAMI Yasuyuki 二見康之 (Inst. Phys., Univ. Tsukuba)
GUIMARAES Valdir (Inst. Nucl. Study, Univ. Tokyo)
HANAKI Hidenobu 花木秀信 (Fac. Sci., Tokyo Inst. Technol.)
HARA Yousuke 原 洋介 (Fac. Sci., Tokyo Inst. Technol.)
HARADA Masaki 原田昌樹 (Fac. Sci., Tokyo Inst. Technol.)
HASUIKE Katsuhito 蓮池勝人 (Sch. Sci. Eng., Waseda Univ.)
HIRAI Masaaki 平井正明 (Fac. Sci., Univ. Tokyo)
HONJO Yoshio 本城義夫 (Inst. Phys., Univ. Tsukuba)
HORI Yoichi 堀 陽一 (Fac. Sci., Tokyo Inst. Technol.)
HOSAKA Masahito 保坂将人 (Cyclotron Radioisot. Cent., Tohoku Univ.)
ICHIGE Masayuki 市毛正之 (Sch. Sci. Eng., Waseda Univ.)
IDEGUCHI Eiji 井手口栄治 (Dept. Phys., Kyushu Univ.)
IKEDA Yasufumi 池田泰文 (Dept. Phys., Rikkyo Univ.)
INOUE Masahiro 井上昌宏 (Dept. Phys., Rikkyo Univ.)
ISHIDA Satoru 石田 悟 (Fac. Sci., Univ. Tokyo)
ITO Tomoyuki 伊藤朋行 (Sci. Eng. Res. Lab., Waseda Univ.)
IWASA Naohito 岩佐直仁 (Dept. Phys., Rikkyo Univ.)
IWATA Yoshiyuki 岩田佳之 (Dept. Phys., Rikkyo Univ.)
IZUMI Hideaki 出水秀明 (Fac. Sci., Tokyo Inst. Technol.)
KAMIMURA Kazuto 上村和人 (Dept. Phys., Rikkyo Univ.)
KATOH Kenichi 加藤健一 (Fac. Sci., Tokyo Inst. Technol.)
KAWAGUCHI Tsutomu 川口 勉 (Dept. Phys., Rikkyo Univ.)
KIDERA Masanori 木寺正憲 (Dept. Phys., Kyushu Univ.)
KIKUCHI Tadashi 菊地 正 (Dept. Phys., Rikkyo Univ.)

KOBAYASHI Misaki 小林美咲 (Sch. Sci. Eng., Waseda Univ.)
KOBINATA Hideo 小日向秀夫 (Fac. Sci., Univ. Tokyo)
KOGANEMARU Kenichi 小金丸健一 (Graduate Sch. Nagatsuda, Tokyo Inst. Technol.)
KOMIYAMA Tatsuto 込山立人 (Sch. Sci. Eng., Waseda Univ.)
KUBO Madoka 久保 円 (Fac. Sci. Technol., Sophia Univ.)
KUROKAWA Meiko 黒川明子 (Dept. Phys., Rikkyo Univ.)
KUWAHARA Kota 桑原宏太 (Sch. Sci. Eng., Waseda Univ.)
MATSUDA Kiyohide 松田清秀 (Fac. Sci., Tokyo Inst. Technol.)
MATSUZAKI Keiichi 松崎恵一 (Fac. Sci., Univ. Tokyo)
MIYAMOTO Shouichi 宮本昭一 (Cyclotron and Radioisot. Cent., Tohoku Univ.)
MIZOI Yutaka 溝井 浩 (Coll. Gen. Educ., Osaka Univ.)
MOCHINAGA Kensuke 持永建介 (Fac. Sci., Univ. Tokyo)
MORIYA Shingo 守屋真吾 (Dept. Phys., Rikkyo Univ.)
MURATA Tomoki 村田知樹 (Fac. Sci. Technol., Sophia Univ.)
NAGANUMA Masayuki 永沼正行 (Graduate Sch. Nagatsuda, Tokyo Inst. Technol.)
NAGATA Kazuhiko 長田和彦 (Fac. Sci., Tokyo Inst. Technol.)
NAKAMURA Tadashi 中村 正 (Sci. Eng. Res. Lab., Waseda Univ.)
NISHIO Teiji 西尾禎治 (Dept. Phys., Rikkyo Univ.)
NUNOYA Yoshihiko 布谷嘉彦 (Dept. Phys., Rikkyo Univ.)
ODAHARA Atsuko 小田原厚子 (Dept. Phys., Kyushu Univ.)
OGAMI Hiroshi 尾上博司 (Fac. Sci., Tokyo Inst. Technol.)
OGAWA Hiroshi 小川博嗣 (Fac. Sci., Tokyo Inst. Technol.)
OGAWA Shinsuke 小川真資 (Dept. Phys., Rikkyo Univ.)
OHNISHI Hiroko 大西裕子 (Coll. Agric. Vet. Med., Nihon Univ.)
OHSAKI Yoshinori 大嵜美紀 (Graduate Sch. Nagatsuda, Tokyo Inst. Technol.)
OKADA Hiroyuki 岡田宏之 (Sch. Sci. Eng., Waseda Univ.)
OKUNO Hiroki 奥野広樹 (Fac. Sci., Univ. Tokyo)
OTSU Hideaki 大津秀暁 (Fac. Sci., Univ. Tokyo)
SAITO Tomoki 斎藤知樹 (Seikei Univ.)
SAITO Yoshitaka 齋藤芳隆 (Fac. Sci., Univ. Tokyo)
SAKAMOTO Naruhiko 坂本成彦 (Fac. Sci., Univ. Tokyo)
SASAKI Mitsuru 佐々木 充 (Coll. Gen. Educ., Osaka Univ.)
SATO Hiromi 佐藤広海 (Fac. Sci., Tokyo Inst. Technol.)
SATO Hiroyasu 佐藤弘康 (Seikei Univ.)
SATOU Yoshiteru 佐藤義輝 (Fac. Sci., Univ. Tokyo)
SAWADA Shinya 澤田真也 (Dept. Phys., Kyoto Univ.)
SEKINE Takashi 関根 隆 (Fac. Sci., Tokyo Inst. Technol.)
SHIBATA Masataka 柴田雅隆 (Dept. Phys., Kyushu Univ.)
SHINODA Morihiko 篠田守彦 (Sci. Eng. Res. Lab., Waseda Univ.)
SHIRAKI Tadashi 白木正志 (Dept. Phys., Rikkyo Univ.)
SHIRAKURA Tetsuya 白倉徹也 (Coll. Gen. Educ., Osaka Univ.)
SHIMURA Masakatsu 志村正勝 (Fac. Sci. Technol., Sophia Univ.)
SHIZUMA Toshiyuki 静間俊行 (Dept. Phys., Kyushu Univ.)
SUEMATSU Shigeyuki 末松繁行 (Dept. Phys., Kyushu Univ.)
SUZUKI Kiyoshi 鈴木清詞 (Fac. Sci., Univ. Tokyo)
TAJIMA Yasuhisa 田島靖久 (Fac. Sci., Tokyo Inst. Technol.)
TAKEDA Kenji 竹田賢志 (Fac. Sci., Tokyo Inst. Technol.)
TERANISHI Takashi 寺西 高 (Fac. Sci., Univ. Tokyo)
TOMITA Shigeo 冨田成夫 (Inst. Phys., Univ. Tsukuba)
TOMURA Hiromi 外村浩美 (Dept. Phys., Kyushu Univ.)
TUCHIDA Hideo 土田英夫 (Fac. Sci., Tokyo Inst. Technol.)
UCHIBORI Takeshi 内堀武司 (Fac. Sci. Technol., Sophia Univ.)
UENO Hideki 上野秀樹 (Fac. Sci., Tokyo Inst. Technol.)
UESAKA Tomohiro 上坂友洋 (Fac. Sci., Univ. Tokyo)
WAKASA Tomotsugu 若狭智嗣 (Fac. Sci., Univ. Tokyo)
WATANABE Yutaka 渡辺 裕 (Fac. Sci., Univ. Tokyo)
YAMAMOTO Takuhisa 山本琢久 (Fac. Sci., Tokyo Inst. Technol.)
YAMASHITA Toshiyuki 山下利幸 (Fac. Sci., Tokyo Inst. Technol.)

YAMAZAKI Hiroshi 山崎弘詞 (Fac. Sci., Tokyo Inst. Technol.)
YANAGISAWA Yoshiyuki 柳澤善行 (Dept. Phys., Rikkyo Univ.)
YOON Chong Cheol 尹 鐘哲 (Fac. Sci., Tokyo Inst. Technol.)

Atomic Physics Laboratory

ANDO Kozo 安藤剛三
KAMBARA Tadashi 神原 正**
KRAVIS Scott (STA-fellow)
NISHIDA Masami 西田雅美
SHIMAMURA Isao 島村 勲**
WATANABE Naoki 渡部直樹
AWAYA Yohko 粟屋容子*
KANAI Yasuyuki 金井保之
NAKAI Yoichi 中井陽一
OURA Masaki 大浦正樹
TANG Jianzhi 唐 建志
YOSHIDA Takashi 吉田高志

* Chief Scientist, ** Senior Scientist

(Visitors)
AZUMA Toshiyuki 東 俊行 (Coll. Arts Sci., Univ. Tokyo)
DANJO Atsunori 壇上篤徳 (Dept. Phys., Niigata Univ.)
DEPAOLA Brett D. (Kansas State Univ., U.S.A.)
FUJIMA Kazumi 藤間一美 (Fac. Eng., Yamanashi Univ.)
FUKUDA Hiroshi 福田 宏 (Sch. Administration and Informatics, Univ. Shizuoka)
HARA Shunsuke 原 俊介 (Dept. Gen. Educ., Tsukuba Coll. Technol.)
HARSTON Michael R. (Dept. Math., Univ. Nottingham, U.K.)
HINO Kenichi 日野健一 (Dept. Appl. Phys. Chem., Univ. Electro-Commun.)
HITACHI Akira 月出 章 (Sci. Eng. Res. Lab., Waseda Univ.)
HUTTON Roger (Univ. Lund, Sweden)
ISHII Keishi 石井慶之 (Dept. Eng. Sci., Kyoto Univ.)
ISOZUMI Yasuhito 五十棲泰人 (Inst. Chem. Res., Kyoto Univ.)
ITO Shin 伊藤 真 (Radioisot. Res. Cent., Kyoto Univ.)
ITOH Akio 伊藤秋男 (Fac. Eng., Kyoto Univ.)
ITOH Yoh 伊藤 陽 (Fac. Sci., Josai Univ.)
KARASHIMA Shosuke 唐島照介 (Dept. Electron. Eng., Tokyo Univ. Sci.)
KAWATSURA Kiyoshi 川面 澄 (Kyoto Inst. Technol.)
KIMURA Mineo 季村峯生 (Argonne Natl. Lab., U.S.A.)
KOBAYASHI Nobuo 小林信夫 (Dept. Phys., Tokyo Metrop. Univ.)
KOHARA Takao 小原孝夫 (Fac. Sci., Himeji Inst. Technol.)
KOIKE Fumihiro 小池文博 (Sch. Med., Kitasato Univ.)
KOIZUMI Tetsuo 小泉哲夫 (Dept. Phys., Rikkyo Univ.)
KOMAKI Kenichiro 小牧研一郎 (Coll. Arts Sci., Univ. Tokyo)
KOWARI Kenichi 小割健一 (Dept. Chem., Tokyo Inst. Technol.)
KUROKI Kenro 黒木健郎 (Natl. Res. Inst. Police Sci.)
MARTINSON Indrek (Univ. Lund, Sweden)
MATSUO Takashi 松尾 崇 (Dept. Pathol., Tokyo Med. Dent. Univ.)
MATSUZAWA Michio 松澤通生 (Dept. Appl. Phys. Chem., Univ. Electro-Commun.)
MITAMURA Tohru 三田村 徹 (Fac. Eng., Himeji Inst. Technol.)
MIZOGAWA Tatsumi 溝川辰巳 (Nagaoka Coll. Technol.)
MUKOYAMA Takeshi 向山 毅 (Inst. Chem. Res., Kyoto Univ.)
NYSTROEM Bosse (Univ. Lund, Sweden)
OHTANI Shunsuke 大谷俊介 (Inst. Laser Sci., Univ. Electro-Commun.)
OKUNO Kazuhiko 奥野和彦 (Dept. Phys., Tokyo Metrop. Univ.)
O'ROURKE Franceska (Dept. Appl. Math., Queen's Univ. Belfast, U.K.)
SATO Hiroshi 佐藤浩史 (Dept. Phys., Ochanomizu Univ.)
SCHMIDT-BÖCKING Horst (Univ. Frankfurt, Germany)
SEKIOKA Tsuguhisa 関岡嗣久 (Fac. Eng., Himeji Inst. Technol.)
SHIBATA Hiromi 柴田裕美 (Res. Cent. Nucl. Sci., Univ. Tokyo)
SHIMA Kunihiro 島 邦博 (Tandem Accel. Cent., Univ. Tsukuba)
SHIMAKURA Noriyuki 島倉紀之 (Coll. Gen. Educ., Niigata Univ.)
SPIELBERGER Lutz (Univ. Frankfurt, Germany)

SUGER Jack (Natl. Inst. Stand. Technol., U.S.A.)
SUZUKI Hirosi 鈴木 洋 (Inst. Laser Sci., Univ. Electro-Commun.)
TAKAYANAGI Toshinobu 高柳俊暢 (Dept. Phys., Sophia Univ.)
TAWARA Hiroyuki 俵 博之 (Natl. Inst. Fusion Sci.)
TERASAWA Mititaka 寺澤倫孝 (Fac. Eng., Himeji Inst. Technol.)
TOSHIMA Nobuyuki 戸嶋信幸 (Inst. Appl. Phys., Univ. Tsukuba)
TSURUBUCHI Seiji 鶴淵誠二 (Fac. Technol., Tokyo Univ. Agric. Technol.)
WAKIYA Kazuyoshi 脇谷一義 (Dept. Phys., Sophia Univ.)
WATANABE Shinichi 渡辺信一 (Dept. Appl. Phys. Chem., Univ. Electro-Commun.)
YAMAZAKI Yasunori 山崎泰規 (Coll. Arts Sci., Univ. Tokyo)
YOSHINO Masuhiro 吉野益弘 (Lab. Phys., Shibaura Inst. Technol.)
ZORAN I. Valeriu (Inst. Phys. Nucl. Eng., Romania)
ZOU Yaming 邹 亚明 (Jiao Tong Univ., China)

(Students)
KAKUTANI Nobukazu 角谷暢一 (Coll. Arts Sci., Univ. Tokyo)
KASUGA Masahito 春日真人 (Coll. Arts Sci., Univ. Tokyo)
KOIDE Michi 小出美知 (Dept. Phys., Meisei Univ.)
KYOH Suigen 姜 帥現 (Fac. Eng., Kyoto Univ.)
NAKAMURA Nobuyuki 中村信行 (Inst. Laser Sci., Univ. Electro-Commun.)
NEGISHI Tomoo 根岸智夫 (Dept. Phys., Sophia Univ.)
SANO Mutsumi 佐野 睦 (Dept. Phys., Rikkyo Univ.)
YAMAGATA Masahiro 山形昌広 (Coll. Arts Sci., Univ. Tokyo)
YAMASHITA Tetsurou 山下徹郎 (Dept. Phys., Rikkyo Univ.)

Metal Physics Laboratory

ISHIDA Katsuhiko 石田勝彦
KINO Yasushi 木野康志
MATSUNO Shunichi 松野俊一
NAGAMINE Kanetada 永嶺謙忠*
YAGI Eiichi 八木栄一**
KADONO Ryosuke 門野良典
KOYAMA Akio 小山昭雄
MATSUZAKI Teiichiro 松﨑禎市郎
WATANABE Isao 渡邊功雄

* Chief Scientist, ** Senior Scientist

(Visitors)
AKAISHI Yoshinori 赤石義紀 (Fac. Sci., Hokkaido Univ.)
FUJIOKA Manabu 藤岡 学 (Cyclotron Radioisot. Cent., Tohoku Univ.)
JONES E. Steven (Dept. Phys. Astronomy, Brigham Young Univ., U.S.A.)
KAMIMURA Masayasu 上村正康 (Fac. Sci., Kyushu Univ.)
KUMAGAI Kenichi 熊谷健一 (Fac. Sci., Hokkaido Univ.)
MATSUSHITA Akira 松下 明 (Res. Dev. Co. Ltd., Japan)
MINAMISONO Tadanori 南園忠則 (Fac. Sci., Osaka Univ.)
MIYAKE Yasuhiro 三宅康博 (Meson Sci. Lab., Univ. Tokyo)
MORITA Masato 森田正人 (Fac. Sci., Josai Univ.)
TORIKAI Eiko 鳥養映子 (Fac. Eng., Yamanashi Univ.)
WATANABE Tsutomu 渡部 力 (ICU)

(Students)
DAWSON Wayne (Fac. Sci., Univ. Tokyo)
STRASSER Partrick (Fac. Eng., Univ. Tokyo)

Magnetic Materials Laboratory

OKADA Takuya 岡田卓也**

** Senior Scientist

Plasma Physics Laboratory

OYAMA Hitoshi 大山 等　　YANO Katsuki 矢野勝喜

(Visitors)
SAKAMOTO Yuichi 坂本雄一 (Electr. Eng. Dept., Toyo Univ.)

Microwave Physics Laboratory

MINOH Arimichi 箕曲在道

Earth Sciences Laboratory

TAKEMATSU Noburu 竹松 伸

Inorganic Chemical Physics Laboratory

AMBE Shizuko 安部静子　　MAEDA Kuniko 前田邦子
MATSUO Yukari 松尾由賀利　　TAKAMI Michio 高見道生*

* Chief Scientist

(Visitors)
ISHII Keizo 石井慶造 (Cyclotron Radioisot. Cent., Tohoku Univ.)
KAWAI Jun 河合 潤 (Dept. Metallurgy, Kyoto Univ.)

Nuclear Chemistry Laboratory

AMBE Fumitoshi 安部文敏*　　ARATANI Michi 荒谷美智
ITOH Yoshiko 伊東芳子　　IWAMOTO Masako 岩本正子
KOBAYASHI Yoshio 小林義男　　MAEDA Haruka 前田はるか
OHKUBO Yoshitaka 大久保嘉高

* Chief Scientist

(Visitors)
ASAI Kichizo 浅井吉蔵 (Univ. Electro-Commun.)
BABA Hiroshi 馬場 宏 (Fac. Sci., Osaka Univ.)
CHEN Shaoyong 陳 紹勇 (South China Sea Inst. Oceanol.)
ENDO Kazutoyo 遠藤和豊 (Showa Coll. Pharm. Sci.)
FURUKAWA Michiaki 古川路明 (Fac. Sci., Nagoya Univ.)
HARAKAWA Hiroaki 原川裕章 (Coll. Sci. Eng., Aoyamagakuin Univ.)
HIRUNUMA Rieko 蛭沼利江子 (Showa Coll. Pharm. Sci.)
ITO Yasuo 伊藤泰男 (Res. Cent. Nucl. Sci. Technol., Univ. Tokyo)
KANAZAWA Ikuzo 金沢育三 (Fac. Educ., Gakugei Univ.)
KIMURA Kan 木村 幹 (Coll. Sci. Eng., Aoyamagakuin Univ.)
KOBAYASHI Takayuki 小林貴之 (Sch. Hygien. Sci., Kitasato Univ.)
KOJIMA Sadao 小島貞男 (Nucl. Med. Cent., Aichi Medical Univ.)
MINAI Yoshitaka 薬袋佳孝 (Fac. Sci., Univ. Tokyo)
MURAKAMI Hideoki 村上英興 (Tokyo Gakugei Univ.)
NOZAKI Tadashi 野崎 正 (Sch. Hygien. Sci., Kitasato Univ.)
OKADA Shigenobu 岡田繁信 (R/D Eng., Shimazu Corp.)
SAITO Kazuo 斉藤和男 (Toshiba Corp., R&D Cent.)
SAITO Tadashi 斎藤 直 (Fac. Sci., Osaka Univ.)
SHIBATA Sadao 柴田貞夫 (Natl. Inst. Radiol. Sci.)
SHIBATA Seiichi 柴田誠一 (Inst. Nucl. Study, Univ. Tokyo)
SHINOHARA Atsushi 篠原 厚 (Fac. Sci., Nagoya Univ.)
SUGAI Isao 菅井 勲 (Inst. Nucl. Study, Univ. Tokyo)
TANAKA Akira 田中 章 (Showa Coll. Pharm. Sci.)

TAZAKI Kazue 田崎和江 (Fac. Sci., Shimane Univ.)
TOMINAGA Takeshi 富永 健 (Fac. Sci., Univ. Tokyo)
YAITA Tsuyoshi 矢板 毅 (JAERI, Tokai)
YANAGA Makoto 矢永誠人 (Jikei Univ. Sch. Med.)
YOKOTA Yuko 横田裕子 (Coll. Sci. Eng., Aoyamagakuin Univ.)
YOKOYAMA Akihiko 横山明彦 (Fac. Sci., Osaka Univ.)
YUKAWA Masae 湯川雅枝 (Natl. Inst. Radiol. Sci.)

(Students)
AOKI Naoki 青木尚樹 (Coll. Sci. Eng., Aoyamagakuin Univ.)
BAMBA Takehiro 番場丈博 (Coll. Sci. Eng., Aoyamagakuin Univ.)
FURUTA Riko 古田理子 (Showa Coll. Pharm. Sci.)
HARUTA Hiroshi 春田博司 (Showa Coll. Pharm. Sci.)
KASUGA Ryouichi 春日良一 (Fac. Sci., Osaka Univ.)
KIRIU Masaru 桐生 大 (Fac. Sci., Osaka Univ.)
KURACHI Junji 倉知淳史 (Fac. Sci., Nagoya Univ.)
MUKAI Kazuhiko 向 和彦 (Fac. Sci., Osaka Univ.)
MUROYAMA Toshiharu 室山俊浩 (Fac. Sci., Nagoya Univ.)
NAKAMURA Jin 中村 仁 (Univ. Electro-Commun.)
ODA Hirotaka 小田寛貴 (Fac. Sci., Nagoya Univ.)
OHTSUKA Hiroshi 大塚博史 (Fac. Sci., Univ. Tokyo)
OTA Tomoko 太田知子 (Fac. Sci., Univ. Tokyo)
SATO Yoshihiko 佐藤嘉彦 (Fac. Sci., Nagoya Univ.)
TAKAHASHI Yoshio 高橋嘉夫 (Fac. Sci., Univ. Tokyo)
TAKESAKO Kazuhiro 竹迫和浩 (Fac. Sci., Osaka Univ.)
TAKESHITA Kazutaka 竹下和孝 (Fac. Sci., Toho Univ.)
TANAKA Shigeo 田中茂男 (Fac. Sci., Toho Univ.)
TANIGUCHI Eugene 谷口勇仁 (Fac. Sci., Nagoya Univ.)
WATANABE Seiya 渡辺誠也 (Fac. Sci., Osaka Univ.)
YAMAGUCHI Takayuki 山口貴行 (Fac. Sci., Osaka Univ.)
YANO Daisaku 矢野大作 (Fac. Sci., Osaka Univ.)

Chemical Dynamics Laboratory
KIMURA Kazuie 木村一宇

(Visitors)
ITO Yasuo 伊藤泰男 (Res. Cent. Nucl. Sci. Technol., Univ. Tokyo)

(Students)
SAHARA Yasumori 佐原靖盛 (Dept. Phys., Chuo Univ.)
SHIBA Takayuki 柴 貴之 (Dept. Phys., Chuo Univ.)
YOKOO Keiichi 横尾啓一 (Dept. Phys., Chuo Univ.)

Cellular Physiology Laboratory
HANAOKA Fumio 花岡文雄*
KITAYAMA Shigeru 北山 滋
YATAGAI Fumio 谷田貝文夫**

* Chief Scientist, ** Senior Scientist

(Visitors)
ANDO Koichi 安藤興一 (Natl. Inst. Radiol. Sci.)
FUKUMURA Akifumi 福村明史 (Natl. Inst. Radiol. Sci.)
FURUSAWA Yoshiya 古沢佳也 (Natl. Inst. Radiol. Sci.)
HASHIMOTO Shozo 橋本省三 (Fac. Med., Keio Univ.)
HOSHINO Kazuo 星野一雄 (Natl. Inst. Radiol. Sci.)
IIZUKA Masayuki 飯塚正之 (Natl. Inst. Radiol. Sci.)

ITO Hisao 伊東久夫 (Fac. Med., Keio Univ.)
ITOH Hiroko 伊藤浩子 (Natl. Inst. Radiol. Sci.)
ITSUKAICHI Hiromi 五日市ひろみ (Natl. Inst. Radiol. Sci.)
KANAI Tatsuaki 金井達明 (Natl. Inst. Radiol. Sci.)
KAWACHI Kiyomitsu 河内清光 (Natl. Inst. Radiol. Sci.)
KIKUCHI Masahiro 菊地正博 (JAERI, Takasaki)
KIMOTO Masafumi 木元正史 (Natl. Inst. Radiol. Sci.)
KOBAYASHI Yasuhiko 小林泰彦 (JAERI, Takasaki)
KOHNO Toshiyuki 河野俊之 (Natl. Inst. Radiol. Sci.)
KOIKE Sachiko 小池幸子 (Natl. Inst. Radiol. Sci.)
KOJIMA Eiichi 小島栄一 (Natl. Inst. Radiol. Sci.)
KOSAKA Toshifumi 小坂俊文 (Dept. Vet. Radiol., Nihon Univ.)
KUBOTA Nobuo 窪田宣夫 (Fac. Med., Yokohama City Univ.)
McINTYRE Cindy L. (Radiobiol. Unit, Med. Res. Counc., U.K.)
MINOHARA Shinichi 簑原伸一 (Natl. Inst. Radiol. Sci.)
MIYAHARA Nobuyuki 宮原信幸 (Natl. Inst. Radiol. Sci.)
MURAISO Chidori 村磯知採 (Natl. Inst. Radiol. Sci.)
MURAKAMI Masahiro 村上正弘 (Natl. Inst. Radiol. Sci.)
NAKAI Hirokazu 中井弘和 (Dept. Agric., Shizuoka Univ.)
OHARA Hiroshi 大原 弘 (Dept. Gen. Cult., Okayama Univ.)
OKUMURA Toshiyuki 奥村敏之 (Fac. Med., Univ. Tsukuba)
SOGA Fuminori 曽我文宣 (Inst. Nucl. Study, Univ. Tokyo)
SUDO Michio 須藤美智雄 (Natl. Inst. Radiol. Sci.)
TAGUCHI Yasuko 田口泰子 (Natl. Inst. Radiol. Sci.)
TAKATUJI Toshihiro 高辻俊宏 (RI Cent., Nagasaki Univ.)
TANAKA Kaoru 田中 薫 (Natl. Inst. Radiol. Sci.)
TATSUZAKI Hideo 立崎英夫 (Fac. Med., Univ. Tsukuba)
TOMURA Hiromi 外村浩美 (Natl. Inst. Radiol. Sci.)
TSUBOI Atsushi 坪井 篤 (Natl. Inst. Radiol. Sci.)
TSUBOUCHI Susumu 坪内 進 (Suzuka Med. Technol. Univ.)
WATANABE Hiroshi 渡辺 宏 (JAERI, Takasaki)
WATANABE Masami 渡辺正己 (Fac. Pharm., Nagasaki Univ.)
YAMASHITA Shoji 山下昌次 (Natl. Saitama Hospital)

(Students)
FUJI Hiroshi 藤 浩 (Fac. Med., Univ. Tsukuba)
KAWASHIMA Mitsuhiko 河島光彦 (Fac. Med., Univ. Tsukuba)
TAKAHASHI Hideyuki 高橋英幸 (Fac. Med., Univ. Tsukuba)

Safety Center

HARASAWA Kaoru 原沢 薫
INOUE Yoshio 井上義夫
KATOU Hiroko 加藤博子
MATSUZAWA Yasuhide 松沢安秀
SAKAMOTO Ichiro 坂本一郎
TAKI Kenro 滝 剣朗
INAMURA Takashi T. 稲村 卓*
KAGAYA Satoru 加賀屋 悟
KOTOU Takeo 加藤武雄
MIYAGAWA Makoto 宮川真言
SHINOHARA Shigemi 篠原茂己
USUBA Isao 薄葉 勲

* Head

Surface Characterization Center

IWAKI Masaya 岩木正哉*
KOBAYASHI Takane 小林 峰

* Head

Radioisotope Technology Division

NAKANO Kazushiro 中野和城　　YATAGAI Fumio 谷田貝文夫*

---

* Head

(Visitors)
MAEZAWA Hiroshi 前澤 宏 (Fac. Med., Tokai Univ.)
SUZUKI Masao 鈴木雅雄 (Fac. Pharm., Nagasaki Univ.)

(Students)
KASE Youko 加瀬陽子 (Fac. Pharm., Nagasaki Univ.)

Synchrotron Radiation Facility Design Group

ANDO Ainosuke 安東愛之輔
BE Suck Hee 裵 碩喜
CHEN Limen 陳 利民
DATE Schin 伊達 伸
EGO Hiroyasu 恵郷博文
FUJIWARA Shigeki 藤原茂樹
HARA Masahiro 原 雅弘
KAMITSUBO Hiromichi 上坪宏道
KAWASHIMA Yoshitaka 川島祥孝
KUMAGAI Keiko 熊谷佳子
KUMAGAI Noritaka 熊谷教孝
MASUDA Takemasa 増田剛正
MATSUI Sakuo 松井佐久夫
MOTONAGA Shoshichi 元永昭七
NAKAMURA Takeshi 中村 剛
OHASHI Yuji 大橋裕二
OHKUMA Haruo 大熊春夫
OHNISHI Junichi 大西純一
OHSHIMA Takashi 大島 隆
OIKAWA Yoshifumi 老川嘉郁
OUCHI Tetsuya 大内徹也
SAEKI Hiroshi 佐伯宏氏
SAKAUE Hiroyuki 坂上裕之
SASAKI Shigeki 佐々木茂樹
SOUTOME Kouichi 早乙女光一
TAKANO Shirou 高野史郎
TAKEBE Hideki 武部英樹
TAKESHITA Isao 竹下勇夫
TANAKA Hitoshi 田中 均
WADA Takahiro 和田隆宏
WADA Takeshi 和田 雄
WANG Yong 王 勇
WATANABE Kowashi 渡邊 剛
XU Choyin 徐 朝銀
XU Weimin 徐 為民
ZHAN Chao 張 超

(Visitors)
GOHSHI Yohichi 合志陽一 (Dept. Ind. Chem., Univ. Tokyo)
HANASAKA Takao 花坂孝雄 (Shimazu Co.)
HAYAKAWA Shinjiro 早川慎二郎 (Dept. Ind. Chem., Univ. Tokyo)
HAYASHI Katsuyuki 林 勝之
HIRANO Yoshiki 平野芳樹 (Anelva Co.)
INOUE Kouji 井上浩司 (Kobe Steel. Ltd.)
SATO Seiichi 佐藤誠一 (IHI Co.)
SHIBUYA Keiichi 渋谷敬一 (SMC Ltd.)
TAKAHASHI Sunao 高橋 直 (Kobe Steel. Ltd.)
TSUCHIYA Masao 土屋将夫 (IHI Co.)
YANAGI Yoshihiko 柳 義彦 (Hitachi, Ltd.)
YOKOUCHI Shigeru 横内 茂 (Osaka Vacuum Ltd.)

(Students)
IGARI Sinichi 猪狩真一 (Coll. Hum. Sci., Nihon Univ.)
KATO Haruhiko 加藤治彦 (Fac. Eng. Sci., Chuo Univ.)
SUGANUMA Kenji 菅沼健治 (Coll. Hum. Sci., Nihon Univ.)
TAMURA Kazuhiro 田村和宏 (Fac. Sci., Hiroshima Univ.)

AUTHOR INDEX

ABE Ryo 阿部 亮 3, 6
ADACHI Minoru 足立 實 42
AIHARA Toshimitsu 藍原利光 5
AKAGI Hiroyasu 赤木宏安 3, 6
AKEBOSHI Yoshihiro 明星慶洋 35, 36, 37
ALEKSANDROV D. V. 50, 51
AMBE Fumitoshi 安部文敏 77, 78, 79, 80, 81, 82, 83, 84, 85, 86, 89, 90, 111
AMBE Shizuko 安部静子 77, 78, 79, 80, 81, 82, 83, 84, 85, 86, 90
ANDO Ainosuke 安東愛之輔 143
ANDO Kozo 安藤剛三 65
ANDO Yoshiaki 安藤嘉章 43
AOI Nori 青井 考 42, 46, 47, 50, 51, 82
AOKI Naoki 青木尚樹 82
ARATANI Michi 荒谷美智 93, 124, 125
ASAHI Koichiro 旭 耕一郎 42
ASAI Kichizo 浅井吉蔵 72, 90
ASAI Tatsuo 浅井辰夫 101
AWAYA Yohko 粟屋容子 59, 60, 61, 62, 63, 64, 65, 66, 75
AZUMA Toshiyuki 東 利行 60
BABA Hiroshi 馬場 宏 87, 88, 89
BAUER W. 48
BE Suck Hee 裵 碩喜 161, 163
BEHR K. H. 52
BELBOT Michael D. 46
BENENSON W. 48
BERGSTROM Jr. P. M. 56
BIZARD Guy 36
BOYD Richard N. 45
BROCKMANN Rolf 19
BURKARD K. 52
CEBRA D. 48
CHAE Soo Joh 蔡 洙祚 31, 32, 33
CHEN Shaoyong 陳 紹勇 77
CHIBA Toshiya 千葉利哉 5, 137, 139
CHIBA Yoshiaki 千葉好明 5, 137
CHLOUPEK Frank 45
CHRISTIE William 34, 44
CRONQVIST M. 48
DELBAR Thierry 43
DEPAOLA Brett 63
DOKE Tadayoshi 道家忠義 99, 116
DOKI Yasuhiro 土記康博 47, 50, 51
EGO Hiroyasu 恵郷博文 150, 151, 153, 155, 157, 158
EGUCHI-KASAI Kiyomi 江口（笠井）清美 103
FERRAGUT Alain 31, 32, 33
FRANCE Jr. Ralph Hayward 43
FUCHI Yoshihide 渕 好秀 41
FUJII Satoshi 藤井 知 73
FUJIMAKI Masaki 藤巻正樹 45, 47, 50, 51
FUJIOKA Manabu 藤岡 学 30
FUJISAWA Takashi 藤岡高志 131
FUJITA Jirou 藤田二郎 3, 6, 110, 130
FUJITA Shin 藤田 新 117, 165, 166, 168, 169
FUJITA Yoshitaka 藤田佳孝 30
FUJIWARA Shigeki 藤原茂樹 149, 160
FUKUDA Shigekazu 福田茂一 34
FUKUDA Tomokazu 福田共和 114
FUKUNISHI Nobuhisa 福西暢尚 15, 16
FUKUTSU Kumiko 福津久美子 103
FURUKAWA Michiaki 古川路明 87, 89
FURUNO Kohei 古野興平 32
FURUTAKA Kazuyoshi 古高和禎 35, 36, 37, 43, 119
FURUYA Keiichi 古谷圭一 125
FUTAMI Yasuyuki 二見康之 35, 36, 37, 43, 119
GAI Moshe 43
GALONSKY Aaron 36
GEISSEL Hans 52
GONO Yasuyuki 郷農靖之 31, 32, 33, 121
GOTO Akira 後藤 彰 3, 6, 76, 91, 129, 130, 133, 135, 137, 139
HÄßLEIN Helmut 111
HACKE Marcus 74
HANAOKA Fumio 花岡文雄 106
HARA Masahiro 原 雅弘 150, 151, 153, 155, 157, 158
HARA Shunsuke 原 俊介 57, 58
HARA Yousuke 原 洋介 113
HARAKAWA Hiroaki 原川裕章 82
HARASAWA Kaoru 原沢 薫 90
HARN Kevin I. 43
HARSTON Michael R. 57, 58
HASEBE Hiroo 長谷部裕雄 5
HASHIMOTO Satoshi 橋本 知 70
HASHIZUME Akira 橋爪 朗 127, 128
HASUIKE Katsuhito 蓮池勝人 116
HATANAKA Kichiji 畑中吉治 39, 40, 130
HAYASHI Katsuyuki 林 勝之 163
HEMMI Masatake 逸見政武 5, 133, 137, 139
HINO Kenichi 日野健一 54, 56
HIRAI Masaaki 平井正明 46
HIRATA Daisy 20, 21, 44
HIRENZAKI Satoru 比連崎 悟 24

HOFMANN Helmut 12
HONJO Yoshio 本城義夫 35
HONMA Takayuki 本間隆之 3, 6
HORBATSCH Marko 59
HORI Toshihiko 堀 利彦 158
HORI Yoichi 堀 陽一 42
HORIBATA Takatoshi 堀端孝俊 14
HOSAKA Masahito 保坂将人 41
ICHIHARA Takashi 市原 卓 38, 40, 41, 109, 113, 117, 118
ICHIKAWA Ryuji 市川龍二 3, 6
IDEGUCHI Eiji 井出口栄治 31, 33, 46, 121
IKEDA Nobuo 池田伸夫 30
IKEGAMI Kumio 池上九三男 3, 6, 130
IKEZAWA Eiji 池沢英二 5, 137
IMAI Takashi 今井 喬 120
IMURA Ryo 井村 亮 125
INABE Naohito 稲辺尚人 3, 6, 43, 47, 50, 51, 76, 96, 130, 133, 135
INADA Tetsuo 稲田哲雄 107
INAMURA Takashi 稲村 卓 115, 117, 168, 169
IRNICH H. 52
ISHIBASHI Mie 石橋美絵 81
ISHIDA Katsuhiko 石田勝彦 69, 112, 141
ISHIDA Nobumichi 石田伸道 116
ISHIDA Satoru 石田 悟 38, 39, 40, 41, 113
ISHIHARA Masayasu 石原正泰 41, 42, 43, 46, 47, 114, 121
ISHII Takayuki 石井孝幸 76
ISHIKAWA Masanobu 石川雅紀 102
ISHIZUKA Takeo 石塚武男 115
ISSHIKI Hiroshi 一色 博 3, 6
ITO Hisao 伊藤久夫 105
ITO Yasuo 伊藤泰男 91
ITOH Yoshiko 伊東芳子 91, 92
ITSUKAICHI Hiromi 五日市ひろみ 103
IWAKI Masaya 岩木正哉 8
IWAMOTO Masako 岩本正子 78, 79, 80, 81, 82, 83, 84, 85, 86
IWASA Naohito 岩佐直仁 43, 47
IZUMI Hideaki 出水秀明 42
JENSEN Aksel S. 12
JIN Weiguo 金 衛国 115
KA Wei Jei 柯 偉傑 105
KADONO Ryosuke 門野良典 73, 112
KAGEYAMA Tadashi 影山 正 3, 6, 129
KAKEHI Masae 筧 正兄 107
KAKUTANI Nobukazu 角谷暢一 60
KAMBARA Tadashi 神原 正 59, 60, 61, 62, 63, 64, 65, 66, 75
KAMIGAITO Osamu 上垣外修一 3, 6, 133, 139
KAMIMURA Masayasu 上村正康 57, 58
KANAI Tatsuaki 金井達明 96, 97, 103, 105, 106, 107, 108
KANAI Yasuyuki 金井保之 59, 60, 61, 62, 63, 64, 65, 66, 75
KANAZAWA Ikuzo 金沢育三 91
KANAZAWA Kenichi 金澤健一 124
KANAZAWA Mitsutaka 金澤光隆 96
KANNO Tooru 菅野 徹 76
KASAGI Jirohta 笠木治郎太 35, 36, 37
KASE Masayuki 加瀬昌之 3, 5, 6, 76, 91, 116, 129, 130, 133, 135, 137, 139
KASE Youko 加瀬陽子 104
KATAYAMA Ichiro 片山一郎 30
KATO Hiroshi 加藤 博 120
KATO Seigo 加藤静吾 38, 41
KATOH Kenichi 加藤健一 38, 39, 41, 113
KATORI Kenji 鹿取謙二 47
KATSURAGAWA Hidetsugu 桂川秀嗣 70, 115
KAWAI Jun 河合 潤 123
KAWAKAMI Minoru 川上 稔 145
KAWAMA Tetsuo 川間哲雄 3, 6, 133, 135
KAWASHIMA Hideo 川島英雄 41
KAWASHIMA Yoshitaka 川島祥孝 150, 151, 153, 155, 157, 158
KAWATSURA Kiyoshi 川面 澄 60
KIDERA Masanori 木寺正憲 31, 33
KIKUCHI Jun 菊池 順 116
KIKUCHI Masahiro 菊地正博 100
KIKUCHI Tadashi 菊地 正 125
KIM Jong Chan 金 鐘賛 31, 32, 33
KIMURA Kan 木村 幹 82
KIMURA Kazuie 木村一宇 95
KIMURA Kikuo 木村喜久雄 45, 114
KIMURA Mineo 季村峯生 54
KINOSHITA Akira 木下 彬 92
KIRIU Masaru 桐生 大 88
KIRK P. N. 48
KISHIDA Takashi 岸田 隆 31, 46, 121
KITAGAWA Hisashi 北川 尚 9, 26, 27
KITAO Kensuke 喜多尾憲助 127, 128
KITAYAMA Shigeru 北山 滋 100, 101
KOBAYASHI Iwao 小林磐雄 149
KOBAYASHI Takayuki 小林貴之 93
KOBAYASHI Toshio 小林俊雄 34, 44, 45, 47, 50, 51, 52
KOBAYASHI Yasuhiko 小林泰彦 101

KOBAYASHI Yoshio 小林義男 78, 79, 80, 81, 82, 83, 84, 85, 86, 90, 111
KOBINATA Hideo 小日向秀夫 114
KOHARA Shigeo 小原重夫 3, 6, 137
KOHARA Takao 小原孝夫 75
KOHNO Tsuyoshi 河野 毅 76, 120
KOIDE Michi 小出美知 66
KOIZUMI Mitsuo 小泉光生 115
KOJIMA Sadao 小島貞男 89
KOLATA James J. 45, 46
KOMAKI Kenichiro 小牧研一郎 60
KOMATSUBARA Tetsuro 小松原哲郎 32
KOMIYAMA Tatsuto 込山立人 116
KORSHENINNIKOV A. A. 50, 51
KRAVIS Scott D. 59, 61, 62, 63, 64
KREBS G. F. 48
KUBO Toshiyuki 久保敏幸 43, 47, 130
KUBONO Shigeru 久保野 茂 30, 38, 41, 45
KUBOTA Nobuo 窪田宜夫 107
KUBOYAMA Satoshi 久保山智司 76
KUDO Hisaaki 工藤久昭 30
KUMAGAI Hidekazu 熊谷秀和 31, 32, 33, 50, 51, 67, 68
KUMAGAI Keiko 熊谷桂子 144, 147, 164
KUMAGAI Noritaka 熊谷教孝 146, 147
KURACHI Junji 倉知淳史 89
KUROKAWA Meiko 黒川明子 30, 43
KUROKI Kenro 黒木健郎 60
KUSAKARI Hideshige 草刈英栄 31, 32, 33
KUWAHARA Kota 桑原宏太 98, 99, 116
LEE Sang Moo 李 相茂 35
LENCINAS Sergio 59
LI B.-A. 48
LI Wenxin 李 文新 78, 85, 86
LIU Guanhua 劉 冠華 42, 46, 114
LU Jun 呂 駿 32
MACEK Joseph H. 56
MAEDA Haruka 前田 はるか 71, 78, 79, 80, 81, 82, 83, 84, 85, 86
MAEDA Kuniko 前田邦子 123
MAIE Takeshi 真家武士 3, 6
MASUDA Kimiaki 増田公明 116
MASUDA Takemasa 増田剛正 149, 160
MATSUBARA Sho 松原 升 107
MATSUDA Kiyohide 松田清秀 35, 36, 37
MATSUDA Sumio 松田純夫 76
MATSUI Sakuo 松井佐久夫 144, 147
MATSUO Takashi 松尾 崇 67, 68
MATSUO Yukari 松尾由賀利 71
MATSUSHIMA Masanao 松島正直 99
MATSUSHITA Akira 松下 明 73, 112
MATSUSHITA Kenichi 松下健一 125
MATSUTA Kensaku 松多健策 34
MATSUZAKI Keiichi 松崎恵一 118
MATSUZAKI Teiichiro 松﨑禎市郎 112, 141
MATSUZAWA Michio 松澤通生 54, 55
MILLER J. 48
MIN Byung Joo 閔 丙珠 31, 32, 33
MINAI Yoshitaka 薬袋佳孝 81
MINAMIHISAMATU Masako 南久松真子 103
MINOH Arimichi 箕曲在道 131
MINOHARA Shinichi 蓑原伸一 97, 108
MINOWA Tatsuya 箕輪達哉 70
MITAMURA Tohru 三田村 徹 75
MITARAI Shiro 御手洗志郎 31, 33
MIYAMOTO Shouichi 宮本昭一 41
MIYATAKE Hiroari 宮武宇也 30, 46
MIYAZAWA Yoshitoshi 宮沢佳敏 5, 137, 139
MIZOI Yutaka 溝井 浩 114
MIZOTA Takeshi 溝田武志 35
MOLEN A. Vander 48
MOON Chang Bum 文 昌範 50, 51
MORIKAWA Tsuneyasu 森川恒安 31, 32, 33, 121
MORISHITA Toru 森下 享 54
MORITA Kosuke 森田浩介 30, 31, 32, 33
MORIYA Shingo 守屋真吾 119
MOTOBAYASHI Tohru 本林 透 10, 30, 43, 119
MOTONAGA Shoshichi 元永昭七 147
MUKAI Junko 向 淳子 32
MÜNZENBERG Gottfried 52
MURAKAMI Hideoki 村上英興 92
MURAKAMI Hiroyuki 村上浩之 30, 43, 119
MURAKAMI Takeshi 村上 健 31, 32, 33, 36, 48
MURAYAMA Toshiyuki 村山利幸 115
NAGAFUCHI Teruyasu 永渕照康 158
NAGAI Yasuki 永井泰樹 30
NAGAMINE Kanetada 永嶺謙忠 69, 73, 112, 141
NAGAOKA Shunji 長岡俊治 99
NAGASE Makoto 長瀬 誠 3, 6, 133
NAGASE Mamoru 長瀬 守 54
NAGATA Kazuhiko 長田和彦 42
NAKAGAWA Takahide 中川孝秀 3, 6, 35, 36, 37, 76, 129, 131, 135
NAKAHARA Hiromichi 中原弘道 30
NAKAI Hirokazu 中井弘和 101
NAKAI Yoichi 中井陽一 60, 61, 62, 63, 64, 65, 75
NAKAJIMA Masato 中島真人 76
NAKAJIMA Mitsuo 中島充夫 31

NAKAJIMA Shunji 中島諄二 117, 165, 166, 167, 168
NAKAMURA Nobuyuki 中村信行 66
NAKAMURA Takashi 中村隆司 43, 46, 47
NAKAMURA Takashi 中村尚司 117
NAKAMURA Takeshi 中村 剛 149
NAKANISHI Noriyoshi 中西紀喜 91, 117, 165, 166, 168, 169
NAKANO Kazushiro 中野和城 99, 100, 106
NAKAO Noriaki 中尾徳晶 117
NASU Saburo 那須三郎 111
NICKEL F. 52
NIIZEKI Takashi 新関 隆 38, 39, 40, 41, 113
NIKOLSKII E. Yu. 50, 51
NISHIGUCHI Iku 西口 郁 105
NISHINAKA Ichiro 西中一朗 30
NISHINO Yoshinori 西野吉則 26
NISHIYAMA Kusuo 西山樟生 73
NODA Yutaka 野田 豊 83
NOMURA Toru 野村 亨 30
NOZAKI Tadashi 野崎 正 93
OBUTI M. M. 50, 51
ODAHARA Atsuko 小田原厚子 31, 33
OGAWA Masao 小川雅生 31, 32, 33
OGIWARA Kiyoshi 荻原 清 131
OGLOBLIN A. A. 50, 51
OGURA Koichi 小倉紘一 99
OHARA Hiroshi 大原 弘 103
OHASHI Yuji 大橋祐二 150, 151, 153, 155, 157, 158
OHIRA Hideharu 大平秀春 76
OHKI Tomonori 大木智則 5
OHKUBO Yoshitaka 大久保嘉高 78, 79, 80, 81, 82, 83, 84, 85, 86, 87, 88, 89, 90, 127
OHNISHI Junichi 大西純一 145, 146, 147
OHNUMA Hajime 大沼 甫 38, 40, 41, 113
OHSHIMA Nagayasu 大島永康 91
OHSHIMA Takashi 大島 隆 150, 151, 153, 155, 157, 158
OHTA Shigemi 太田滋生 29
OHTANI Shunsuke 大谷俊介 66
OHYA Jiro 大矢次郎 76
OKADA Hiroyuki 岡田宏之 116
OKADA Takuya 岡田卓也 72, 90
OKAMOTO Hiroyuki 岡本博行 54
OKAMURA Hiroyuki 岡村弘之 38, 39, 40, 41, 113, 130
OKUMURA Toshiyuki 奥村敏之 108
OKUNO Hiroki 奥野広樹 42, 46
OLSON Douglas 34, 44
OMATA Kazuo 小俣和夫 44
ONISHI Naoki 大西直毅 13, 14
ORIHARA Hikonojo 織原彦之丞 38, 41
OSHIMA Masumi 大島真澄 31, 32, 33
OTSU Hideaki 大津秀暁 38, 39, 40, 113
OTSUKA Shozo 大塚省三 3, 6
OTSUKA Takaharu 大塚孝治 16
OURA Masaki 大浦正樹 59, 60, 61, 62, 63, 64, 65, 75
OZAWA Akira 小沢 顕 9, 44, 45, 50, 51
PANETTA J. 48
PFAFF R. 48
PU Yuehu 蒲 越虎 30, 114
RAIMANN Gerry 45
REPOSEUR T. 48
RING Peter 20
RUAN (GEN) Jian Zhi 阮 健治 43
SAHARA Yasumori 佐原靖盛 95
SAITO Keiko 斉藤恵子 106
SAITO Tadashi 斎藤 直 87, 88, 89
SAITO Yoshitaka 斎藤芳隆 118
SAITO Yuko 斎藤裕子 82
SAKAI Hideyuki 酒井英行 38, 39, 40, 113, 130
SAKAMOTO Naruhiko 坂本成彦 38, 39, 40, 41, 113, 130
SAKAUE Hiroyuki 坂上裕之 161
SAKURAI Hiroyoshi 桜井博義 46, 114
SASAKI Shoichi 佐々木勝一 28
SATO Hiromi 佐藤広海 42
SATO Hiroshi 佐藤 竑 17, 18, 25, 44
SATO Kohki 佐藤弘毅 103
SATO Yukio 佐藤幸夫 96
SATOU Yoshiteru 佐藤義輝 39
SCHMIDT-BÖCKING Horst 59, 61
SCHROEDER L. S. 48
SCHWAB W. 52
SEKINE Takashi 関根 隆 42, 114
SHEN Wenqing 35
SHIBA Takayuki 柴 貴之 95
SHIBATA Hiromi 柴田裕実 67
SHIBATA Masataka 柴田雅隆 33
SHIBATA Sadao 柴田貞夫 83
SHIBATA Seiichi 柴田誠一 89, 90
SHIBATA Tokushi 柴田徳思 117
SHIGEMATSU Naoyuki 茂松直之 105
SHIMAMURA Isao 島村 勲 55, 57, 58
SHIMANO Yosuke 嶋野洋介 76
SHIMODA Tadashi 下田 正 30, 44
SHIMOURA Susumu 下浦 享 34, 43, 46, 47, 50, 51
SHIN Kazuo 秦 和夫 117
SHINOHARA Atsushi 篠原 厚 87, 89

SHINOZUKA Tsutomu 篠塚 勉 30
SHIRAKURA Tetsuya 白倉 徹也 46
SHIRATO Shoji 白土鈔二 43
SHIZUMA Toshiyuki 静間俊行 31
SIGNORINI Cosimo 114
SOGA Fuminori 曽我文宣 96
SPIELBERGER Lutz 61
STEVENSON J. 48
STRASSER Patrick 69
SUDOU Michio 須藤美智雄 96, 97, 108
SUEKI Keisuke 末木啓介 30
SUGAI Isao 菅井 勲 115
SUGANUMA Hideo 菅沼秀夫 28, 142
SUGAWARA Masahiko 菅原昌彦 31, 32, 33
SUGIMOTO Kenzo 杉本健三 34, 44
SUZUKI Hiromitsu 鈴木寛光 150, 151, 153, 155, 157, 158
SUZUKI Hirosi 鈴木 洋 66
SUZUKI Kiyoshi 鈴木清詞 118
SUZUKI Masao 鈴木雅雄 104
SUZUKI Masayo 鈴木昌世 98, 99, 100, 116
SUZUKI Takeshi 鈴木 健 24, 34, 47, 48, 50, 51, 52
SUZUKI Toru 鈴木 徹 26, 27
SÜMMERER Klaus 52
TACHIMORI Shoichi 館盛勝一 84
TADOKORO Satoru 田所 智 26, 27
TAJIMA Yasuhisa 田島靖久 41
TAKADA Masashi 高田真志 117
TAKAGI Tetsuya 高城徹也 165, 166, 168
TAKAHASHI Hideyuki 高橋英幸 108
TAKAHASHI Katsuhiko 高橋克彦 3, 6
TAKAHASHI Naruto 高橋成人 88
TAKAHASHI Noriaki 高橋憲明 44
TAKAHASHI Tadayuki 高橋忠幸 118
TAKAHASHI Tan 高橋 旦 98, 99, 100, 101, 116
TAKAHASHI Yoshio 高橋嘉夫 81
TAKAKU Shinsaku 高久清作 41
TAKAMI Michio 高見道生 71
TAKASHIMA Fumio 隆島史夫 102
TAKAYANAGI Toshinobu 高柳俊暢 66
TAKEBE Hideki 武部英樹 147, 149
TAKEMATSU Noburu 竹松 伸 81
TAKESAKO Kazuhiro 竹迫和浩 87, 88, 89
TAKESHITA Isao 竹下勇夫 144, 150, 151, 153, 155, 157
TAMURA Takashi 田村高志 76
TANAKA Hitoshi 田中 均 143
TANAKA Kazuhiro 田中和廣 22, 23
TANAKA Kinya 田中欽也 165, 166, 168, 169
TANAKA Masahiko 田中雅彦 41
TANG Jianzhi 唐 建志 55
TANI Norio 谷 教夫 151, 153, 155, 157, 158
TANIGAWA Shoichiro 谷川庄一郎 73
TANIGUCHI Eugene 谷口勇仁 89
TANIHATA Isao 谷畑勇夫 9, 16, 20, 21, 24, 34, 44, 45 47, 48, 49, 50, 51, 52, 142
TANIKAWA Masashi 谷川勝至 30, 114
TATSUZAKI Hideo 立崎英夫 108
TAWARA Hiroyuki 俵 博之 67, 68
TENDOW Yoshihiko 天道芳彦 127, 128
TERANISHI Takashi 寺西 高 43, 46, 47
TERASAWA Mititaka 寺澤倫孝 75
TOHYAMA Mitsuru 遠山 満 11
TOKI Hiroshi 土岐 博 19, 20, 21, 28, 142
TOMINAGA Takeshi 富永 健 81
TOMITA Shigeo 富田成夫 35
TOMITANI Takehiro 富谷武浩 96
TONUMA Tadao 戸沼正雄 67, 68
TOSHIMA Nobuyuki 戸嶋信幸 53
TOYOKAWA Hidenori 豊川秀訓 35, 38, 41
TSUBAKINO Harushige 椿野晴繁 75
TSUKADA Kazuaki 塚田和明 30
TSUKIORI Noritoshi 月居憲俊 3, 6
UEDA Kohichi 上田光一 75
UEMATSU Haruko K. 植松晴子 70
UENO Hideki 上野秀樹 42
UESAKA Tomohiro 上坂友洋 38, 39, 40, 41, 113, 130
UESUGI Masato 上杉正人 76
UNO Masahiro 宇野正宏 17
URAI Teruo 浦井輝夫 8
UWAMINO Yoshitomo 上簀義朋 117
WADA Michiharu 和田道治 30
WADA Takeshi 和田 雄 149, 160
WAKABAYASHI Yoshihiro 若林由浩 55
WAKASA Tomotsugu 若狭智嗣 38, 39, 40, 113
WAKASUGI Masanori 若杉昌徳 71, 115
WAKIYA Kazuyoshi 脇谷一義 66
WANG Z.-F. 48
WATANABE Hiroshi 渡辺 宏 100, 101
WATANABE Isao 渡辺功雄 112, 141
WATANABE Kowashi 渡邊 剛 161, 163
WATANABE Masaki 渡辺眞樹 165, 168, 169
WATANABE Masami 渡辺正己 104
WATANABE Seiya 渡辺誠也 87, 88
WATANABE Shinichi 渡辺信一 55
WATANABE Yasushi 渡辺 康 43, 45, 46, 47, 50, 51, 96, 109, 114
WATANABE Yutaka 渡辺 裕 114

WATARI Kazuo 渡利一夫 83
WESTFALL G. 48
WIEMAN Haward 34, 44
WINFIELD J. S. 48
YAGI Eiichi 八木栄一 8, 74
YAITA Tsuyoshi 矢板 毅 84
YAJIMA Akira 矢嶋 亨 36
YAMADA Hiroaki 山田博章 99
YAMAJI Shuhei 山路修平 12
YAMAKAWA Osamu 山川 修 44
YAMAMOTO Atsushi 山本厚之 75
YAMAMOTO Sukeyasu S. 山本祐靖 46
YAMAMOTO Takuhisa 山本琢久 38, 40, 41, 113
YAMAMOTO Yoshiaki 山本悦章 91
YAMASHITA Shoji 山下昌次 105
YAMASHITA Toshiyuki 山下利幸 38, 39, 41, 113
YAMAUCHI Hiromoto 山内啓資 5
YAMAZAKI Yasunori 山崎泰規 60
YANAGISAWA Yoshiyuki 柳澤善行 119
YANO Katsuki 矢野勝喜 161
YANO Yasushige 矢野安重 3, 6, 40, 76, 129, 130, 133, 135, 137, 139
YANOKURA Minoru 矢野倉 実 5, 50, 51, 80, 81, 82 83, 84, 93, 124, 125
YATAGAI Fumio 谷田貝文夫 97, 99, 103, 104, 105, 106, 107, 108
YOKOO Keiichi 横尾啓一 95
YOKOYAMA Akihiko 横山明彦 87, 88, 89
YOKOYAMA Ichiro 横山一郎 3, 6, 133, 135
YONEHARA Hiroto 米原博人 150, 151, 153, 155, 157, 158
YOSHIDA Atsushi 吉田 敦 30, 31, 32, 33, 42, 46, 47, 96, 109, 114, 127
YOSHIDA Koichi 吉田光一 34, 36, 37, 45, 50, 51, 52
YOSHIDA Yutaka 吉田 豊 111
YOSOI Masaru 与曽井 優 38, 41
YOUNG B. 48
YUASA-NAKAGAWA Keiko 湯浅 (中川) 恵子 35, 36, 37

ZAHAR Mohamed 46
ZHANG Yuhu 張 玉虎 31, 32, 33
ZHAO Zhiping 43
ZOU Yaming 邹 亚明 65

RIKEN Accelerator Progress Report

理化学研究所加速器年次報告　第27巻　(1993)

印　刷　平成6年 (1994) 3月23日
発　行　平成6年 (1994) 3月31日

発行者　理化学研究所
代表者　有馬朗人
〒351-01　埼玉県和光市広沢2番1号
電話　(048) 462−1111

編集者　理化学研究所加速器研究施設
運営委員会

印刷所　株式会社ユニバーサル・アカデミー・プレス
〒113　東京都文京区本郷6丁目16番2号BR本郷5ビル

定価5,000円
(消費税別)

理化学研究所

埼玉県　和光市　広沢